

**The nature and origin of PGE mineralization in the Rooipoort  
area, northern Bushveld Complex, South Africa.**

Jennifer Williamina Smith

Thesis submitted for the degree of Doctor of Philosophy at the University of Leicester,  
Department of Geology

February 2014



---

# **The nature and origin of PGE mineralization in the Rooipoort area, northern Bushveld Complex, South Africa**

Jennifer Williamina Smith

## **Abstract**

The Grasvally Norite-Pyroxenite-Anorthosite (GNPA) member within the northern limb of the Bushveld Complex is a PGE-Ni-Cu mineralized, layered package of mafic cumulates. This magmatic sulfide deposit is developed at the equivalent stratigraphic position to the Platreef, being overlain by Main Zone gabbro-norites and in places resting unconformably on metasediments from the Transvaal Supergroup.

Parental magmas to the GNPA member were of a 'hybrid' composition containing both B1 and B2/B3 type magma components which were strongly crustally contaminated and S saturated at the time of emplacement. At depth, the assimilation of crustal S was crucial for ore genesis. Although parental magma(s) experienced a second localised contamination event, interaction with the local footwall at the time of emplacement, did not have any control on the genesis of sulfide mineralization. A single primary sulfide liquid, enriched in PGE, Ni, Cu and semi-metals was distributed throughout the succession during multiphase emplacement of the GNPA member.

The distribution and mineralogy of platinum-group and chalcophile elements results from the complex behaviour of these elements during both sulfide fractionation and hydrothermal processes. The primary assemblage is characterised by IPGE-rich pyrrhotite, IPGE-, Rh, and Pd-rich pentlandite, chalcopyrite, and associated Pt-As and Pd-Bi-Te minerals. Secondary assemblages in addition contain Pd- and Rh-rich pyrite and millerite, and discrete minerals including Pd antimonides and arsenides.

Whilst correlations between the GNPA/Platreef and Upper Critical Zone remain relatively speculative, the northern limb deposits are thought to have formed from compositionally similar or related magmas, which were poorer in Mg, richer in Ca and Fe and Pd dominant relative to the magma(s) that formed the Upper Critical Zone. It is proposed that with depth the Platreef may progressively transform into a layered succession that is exposed south of the Ysterberg-Planknek Fault and represented by the GNPA member. The Platreef can therefore possibly be viewed as a marginal facies of the GNPA member, and sulfide-rich magma which escaped up the margins of the northern limb chamber.

---

## Acknowledgements

To start, I wish to thank Dave Holwell, not only for his committed supervision of the project, but also for all his support, advice and encouragement over the last few years and for giving me the freedom to explore the areas I was most interested in. My most sincere thanks also go to Iain McDonald who helped conceive the project, and who has been actively involved from the early stages, providing technical expertise and constructive discussion throughout.

Many thanks also to the stable isotope team at SUERC who were very welcoming and accommodating. Adrian Boyce supervised all the isotope work, providing valuable guidance on data interpretation, and constructive discussion during preparation of Chapter Five. A special thank you also goes to Alison and Terry for their guidance, assistance and patience in analysis of isotopes.

At Leicester, thank you to the department administrative and technical staff. In particular I would like to thank Rob Wilson, Nick Marsh, Rob Kelly, Cheryl Haidon and Colin Cunningham, for their assistance in sample preparation and geochemical analysis. My fellow postgraduate students, especially Sam and Nyree are thanked for keeping me relatively sane during my time in Leicester and encouraging me to the end.

This project is funded by NERC (NE/1528426/1), with additional funding obtained from the SEG and IOM<sup>3</sup>. Caledonia Mining Corporation and in particular Trevor Pearton, provided logistical support and access to drill-core, without which the PhD would not have been possible.

A massive thank you to mum, dad, Yvonne and Joanna for all their support over the last few years and for taking a holiday in Leicester! And finally thank you to David, for putting up with my PhD ramblings and encouraging me to the very end.

---

## Table of Contents

Abstract .....	i
Acknowledgments .....	ii
List of Figures .....	vii
List of Tables.....	ix
<b>Chapter One: Introduction</b>	
1.1 The distribution of PGE within the Earth’s crust .....	2
1.2 Formation of magmatic sulfide deposits .....	4
1.2.1 Generation and emplacement of parental magma.....	5
1.2.2 Inducing sulfur saturation and the concentration of PGE .....	7
1.3 Behaviour of PGE during sulfide fractionation .....	8
1.4 Aims and Objectives .....	11
1.5 Thesis organization.....	12
<b>Chapter Two: Regional Geological Setting</b>	
2.1.The Bushveld Complex.....	16
2.2. Rustenburg Layered Suite.....	17
2.2.1. Overview of Bushveld Stratigraphy .....	17
2.2.2. The Critical Zone .....	19
2.2.3. Evolution of the Bushveld Complex .....	22
2.2.4. Age of the Bushveld Magmatic Province.....	23
2.3. Northern limb.....	23
2.3.1. Structure .....	26
2.3.2. Stratigraphy of the northern limb.....	26
2.3.3. Genesis of the Platreef .....	30
2.4. The GNPA member.....	32
2.4.1. Stratigraphy.....	33
2.4.2. Mineralization.....	35
2.4.3. Origin of the GNPA member and Platreef .....	36
<b>Chapter Three: The mineralogy and petrology of sulfide mineralization</b>	
3.1 Abstract .....	39
3.2 Introduction.....	40
3.3 Regional Geology.....	42

---

3.4 Samples and Methods .....	45
3.5 Petrology.....	47
3.5.1 Footwall lithologies .....	47
3.5.2 GNPA member lithologies.....	49
3.6 Platinum–group element mineralization .....	53
3.7 Sulfide mineralogy .....	54
3.7.1 Primary textured sulfide assemblages .....	56
3.7.2 Secondary textured sulfide assemblages .....	58
3.7.3 Footwall sulfide assemblages.....	60
3.8 Discussion.....	61
3.8.1 Regional context of the GNPA member .....	61
3.8.2 Sulfide mineralogy and distribution.....	62
3.8.3 Implications for PGE mineralization.....	66
3.9 Conclusions.....	66
3.10 Acknowledgements .....	67

#### **Chapter Four: Precious and base–metal geochemistry and mineralogy**

4.1 Abstract .....	69
4.2 Introduction.....	71
4.3 Regional Geological Setting .....	73
4.4 Samples and methods.....	75
4.5 Platinum–group mineralogy.....	79
4.5.1 PGM assemblage .....	79
4.6 PGE and base metal geochemistry .....	84
4.6.1 Non chromitiferous rocks and quartzites.....	89
4.6.2 Chromitiferous rocks .....	91
4.6.3 Chondrite normalized PGE patterns .....	92
4.7 PGE concentrations in BMS .....	93
4.7.1 Non chromitiferous rocks.....	95
4.7.2 Chromitiferous rocks .....	98
4.8 Mass balance .....	99
4.8.1 Primary sulfide assemblages .....	100
4.8.2 Secondary sulfide assemblages .....	101
4.9 Discussion.....	101

---

4.9.1 Primary magmatic signature.....	102
4.9.2 Hydrothermal interaction.....	104
4.9.3 Evaluation of ore forming processes .....	105
4.10 Conclusions .....	109
4.11 Acknowledgements .....	110

## **Chapter Five: S isotopes and S/Se ratios**

5.1 Abstract .....	112
5.2 Introduction.....	114
5.3 Processes determining and modifying S/Se ratio.....	116
5.4 Processes determining and modifying S isotope composition.....	117
5.5 Geological Setting of the GNPA member .....	118
5.5.1 Sulfide mineralogy .....	120
5.5.2 Justification as a case study .....	121
5.6 Samples and Methods .....	121
5.7 Results.....	124
5.7.1 Sulfur isotopes.....	128
5.7.2 Bulk S/Se ratios .....	133
5.7.3 <i>In situ</i> S/Se ratios .....	135
5.8 Comparison of S/Se ratios and S isotopes.....	138
5.8.1 Primary sulfide assemblage .....	139
5.8.2 Secondary sulfide assemblage.....	140
5.8.3 Footwall sulfide assemblages.....	141
5.9 Discussion.....	141
5.9.1 Primary partitioning behaviour and secondary mobility of Se in sulfides .....	141
5.9.2 Implications for interpretation of S/Se ratios and S isotopes .....	146
5.10 Acknowledgements .....	153

## **Chapter Six: Geochemical characteristics of the GNPA member**

6.1 Abstract .....	155
6.2 Introduction.....	157
6.3 Samples and Methods .....	157
6.4 Major element geochemistry.....	158
6.4.1 Geochemical variations with depth.....	159

---

6.4.2 Cr/MgO ratios .....	163
6.5 Trace element geochemistry.....	166
6.5.1 Rare earth element geochemistry.....	166
6.5.2 Spidergrams .....	170
6.6 Mineral Chemistry.....	172
6.6.1 Plagioclase composition .....	172
6.6.2 Pyroxene composition .....	174
6.6.3 Comparison of mineral and whole rock chemistry .....	178
6.7 Discussion.....	179
6.7.1 Crustal contamination.....	181
6.7.2 Emplacement of the GNPA member.....	181
6.7.3 Magmatic lineage of the GNPA member .....	184
6.8 Conclusions.....	187
<b>Chapter Seven: Conclusions</b>	
7.1 Conclusions.....	189
7.1.1 Chapters 3 and 4.....	189
7.1.2 Chapter 5.....	189
7.1.3 Chapter 6.....	190
7.2 Implications for our understanding of the northern limb .....	191
7.2.1 Formation of the GNPA member .....	191
7.2.2 Ore genesis .....	196
7.2.3 Relationship of the GNPA member with the Platreef .....	198
7.3 Summary .....	201
7.4 Recommendations for future work.....	202
<b>References</b> .....	204
<b>Appendix 1: Whole Rock Geochemistry</b> .....	233
<b>Appendix 2: LA-ICP-MS data</b> .....	254
<b>Appendix 3: Mass Balance</b> .....	272
<b>Appendix 4: Sulfur Isotopes</b> .....	274
<b>Appendix 5: Electron Microprobe data</b> .....	279

---

## List of Figures

### Chapter One

Figure 1.1 Locations of PGE mineralization within mafic and ultramafic intrusions .....	3
Figure 1.2 PGE resources of the world.....	4
Figure 1.3 Formation of a Ni-Cu-PGE deposit.....	5
Figure 1.4 Concentrations of elements in a partial melt.....	6
Figure 1.5 Fractionation of sulfide liquid.....	9

### Chapter Two

Figure 2.1 Geological map of the Bushveld Complex.....	16
Figure 2.2 Stratigraphy of the eastern and western limbs of the Bushveld Complex.....	18
Figure 2.3 Geological map of the northern limb of the Bushveld Complex.....	25
Figure 2.4 Stratigraphy of the northern limb of the Bushveld Complex.....	29
Figure 2.5 Detailed map of the GNPA member in the Rooipoort-Grasvally region.....	33
Figure 2.6 Stratigraphy of the GNPA member .....	34
Figure 2.7 'Pudding basin' model .....	37

### Chapter Three

Figure 3.1 Geological map of the northern limb of the Bushveld Complex.....	41
Figure 3.2 Detailed map of the GNPA member.....	44
Figure 3.3 Stratigraphic logs of boreholes RP05.45 and RP04.23.....	46
Figure 3.4 Photomicrographs of mineralogy and igneous textures.....	48
Figure 3.5 Photomicrographs of mineralogy and igneous textures .....	52
Figure 3.6 Reflected light images of sulfide mineralogy and textures.....	55
Figure 3.7 Alteration of sulfides.....	58
Figure 3.8 Paragenetic sequence .....	65

### Chapter Four

Figure 4.1 Geological map of the northern limb of the Bushveld Complex .....	72
Figure 4.2 Detailed map of the GNPA member in the Rooipoort-Grasvally region.....	75
Figure 4.3 Detailed stratigraphic logs of boreholes RP04.23 and RP05.45.....	78
Figure 4.4 Backscattered electron photomicrographs of PGM.....	81
Figure 4.5 Whole rock PGE geochemistry .....	90
Figure 4.6 Chalcophile ratios with depth.....	92
Figure 4.7 Chondrite normalized PGE profiles .....	93
Figure 4.8 TRA spectra.....	96
Figure 4.9 PGE contents of sulfide minerals.....	97
Figure 4.10 Mass Balance.....	100

### Chapter Five

Figure 5.1 Geological map of the northern limb of the Bushveld Complex .....	119
--	-----

---

Figure 5.2 Sulfide assemblages.....	120
Figure 5.3 S isotopes.....	130
Figure 5.4 Sulfur in wt% versus Se (ppm).....	133
Figure 5.5 PGE tenor (Pt + Pd in 100% sulfide), versus bulk S/Se ratio).....	133
Figure 5.6 Whole rock Se and PGE.....	134
Figure 5.7 TRA spectra of sulfides.....	136
Figure 5.8 S/Se ratio of sulfide phases.....	138
Figure 5.9 S isotope versus bulk S/Se ratios.....	139
Figure 5.10 Comparison of bulk and <i>in situ</i> S/Se ratios.....	140
Figure 5.11 Genetic model.....	152

## Chapter Six

Figure 6.1 Composition of the GNPA member.....	159
Figure 6.2 Major element variations with depth.....	161
Figure 6.3 Trace element variations with depth.....	163
Figure 6.4 Whole rock Cr (ppm) and MgO (wt%). .....	164
Figure 6.5 Chondrite normalized rare earth element plots for the GNPA member.....	167
Figure 6.6 Chondrite normalized rare earth element fields for the Bushveld Complex.....	169
Figure 6.7 Ce vs Sm.....	170
Figure 6.8 Primitive mantle-normalized trace element patterns.....	171
Figure 6.9 $(\text{Nb}/\text{Th})_{\text{PM}}$ vs $(\text{Th}/\text{Yb})_{\text{PM}}$ .....	172
Figure 6.10 An content of plagioclase.....	174
Figure 6.11 Compositions of pyroxenes.....	176
Figure 6.12 Pyroxene compositions within the Platreef.....	177
Figure 6.13 Pyroxene composition with depth.....	178
Figure 6.14 Genetic model.....	186

## Chapter Seven

Figure 7.1 Genetic model.....	193
Figure 7.2 The Platreef on Turfspruit.....	199
Figure 7.3 Relationship between the GNPA member and Platreef.....	200

---

## List of Tables

### Chapter Three

Table 3-1 Sulfide assemblage and degree of alteration .....	57
---	----

### Chapter Four

Table 4-1 Platinum group minerals .....	80
Table 4-2 Proportions of PGM types. ....	82
Table 4-3 Textural associations of PGM.....	82
Table 4-4 Whole rock PGE geochemistry .....	86
Table 4-5 Compositions of base metal sulfides.....	94

### Chapter Five

Table 5-1 In situ S isotopes and S/Se ratios.....	125
Table 5-2 Whole rock S and Se.....	132
Table 5-3 Se concentrations of sulfides.....	143
Table 5-4 Se concentrations of sulfides within Jinchuan intrusion, China.....	144

### Chapter Six

Table 6-1 Element Ratios.....	165
Table 6-2 Mineral compositions. ....	172

# Chapter One

## Introduction

## 1.1 The distribution of PGE within the Earth's crust

The Earth's mantle is the principal reservoir from which platinum-group element (PGE) concentrations in the crust are derived. The PGEs represent a geochemically coherent group of six siderophile metals (ruthenium (Ru), rhodium (Rh), palladium (Pd) osmium (Os), iridium (Ir) and platinum (Pt)), which commonly occur together in nature at concentrations of a few parts per billion or less, in most rocks. There are very few major occurrences of PGE in the Earth's crust, with economic concentrations (1–10 parts per million (ppm)) almost exclusively found in association with mafic and/or ultramafic rocks. The majority of the world's PGE resources occur in two types of deposits, both of which are intimately associated with Ni-Cu sulfides or chromite (Misra 2000; Naldrett 2004; Arndt et al. 2005; Maier 2005). Type I represents stratiform or stratabound deposits in large igneous layered intrusions. The most significant of these is the Bushveld Complex in South Africa which is host to the vast preponderance of accessible PGE, with the Great Dyke in Zimbabwe and the Stillwater Complex in Montana, USA being minor contributors. Type II represent massive Ni-Cu sulfide deposits, from which PGE and in particular Pd, are significant by-products. The most important of these deposits are Noril'sk in Russia and the Sudbury igneous complex in Canada.

A schematic diagram illustrating the geological setting of the different types of PGE-Ni-Cu deposits in mafic and/or ultramafic intrusions is shown in Figure 1.1. In addition, a comprehensive summary of intrusion related PGE deposits and their key characteristics is available in Maier (2005). These types of intrusions and conduits/feeders account for around 98% of the world's identified PGE resources (Misra 2000). From Figure 1.2, which provides a compilation of the Earth's known resources of Pt, Pd and Rh in terms of the geological formations in which they occur, it is immediately apparent that the Bushveld Complex accounts for the majority of the world's PGE reserves.

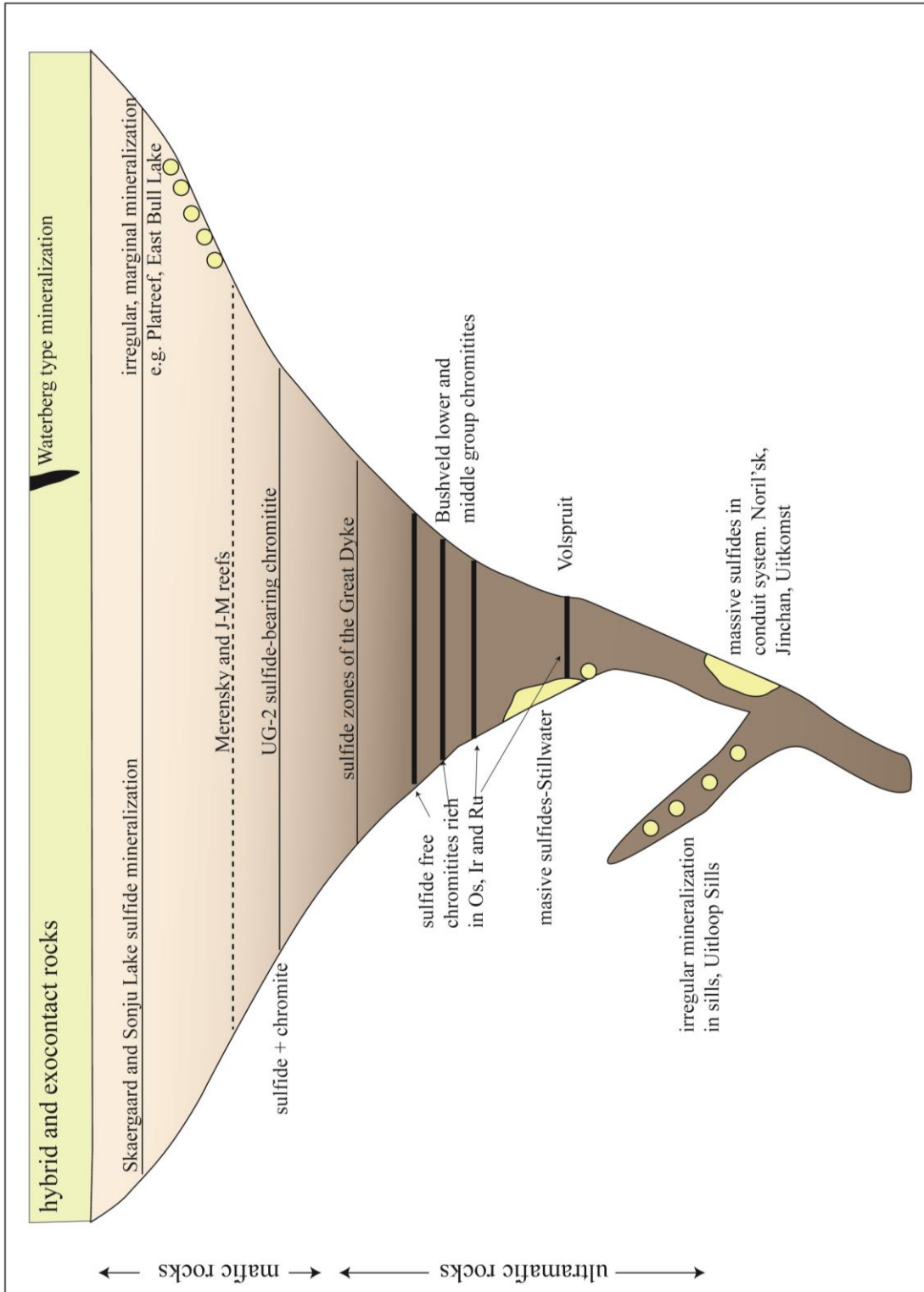


**Figure 1.1** Schematic diagram showing the occurrences and expected locations of PGE mineralization within mafic and ultramafic intrusions and their feeder conduits. Note that no single intrusion is likely to contain all of the styles of mineralization shown. Modified from Maier (2005) and Naldrett (2011).

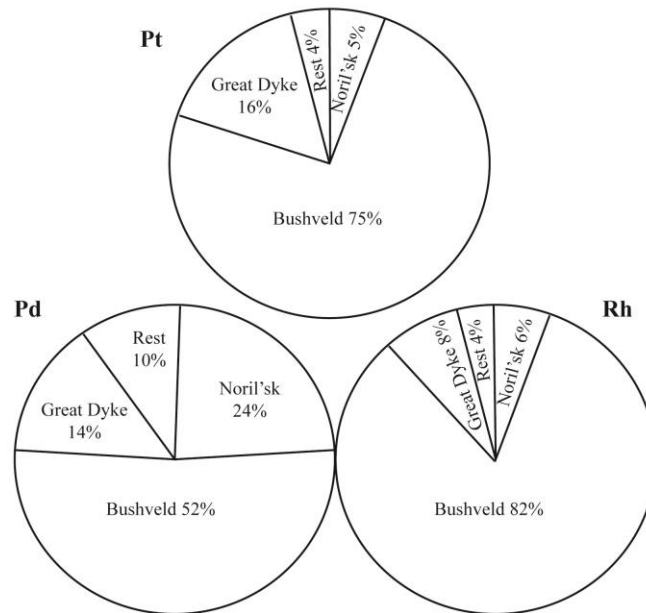


**Figure 1.2** Pt, Pd and Rh resources of major mining areas of the world (from Naldrett et al. 2008)

## 1.2 Formation of magmatic sulfide deposits

The transfer of PGE from the mantle into the crust is accomplished by two main methods: 1) through the development of mantle partial melts and their intrusion into the crust; and 2) through the emplacement of mantle slabs in subduction/collision zones (Naldrett et al. 2009). The first mechanism is by far the most important as it is responsible for the generation of both PGE-Ni-Cu layered intrusions and Ni-Cu sulfide deposits. These deposits are believed to result from the interplay of a very specific and unique combination of circumstances which operated both within the mantle and in the crust (Naldrett et al. 2009).

The formation of magmatic sulfide PGE-Ni-Cu deposits is considered to be dependent on five critical processes/stages (Arndt 2005; Maier 2005; Naldrett et al. 2009; Naldrett 2011). These are: (1) the development of a metal-bearing parental melt through partial melting of the mantle; (2) that the melt ascends into the crust without reaching S saturation; (3) the magma becomes saturated in S resulting in the segregation of an immiscible sulfide liquid; (4) the sulfide liquid interacts with a much larger mass of silicate magma, increasing its PGE tenor; and (5) finally the metal-rich sulfide liquid needs to be concentrated so that the sulfides can be mined economically. These key requirements are expanded on in the following sections and summarised in Figure 1.3.

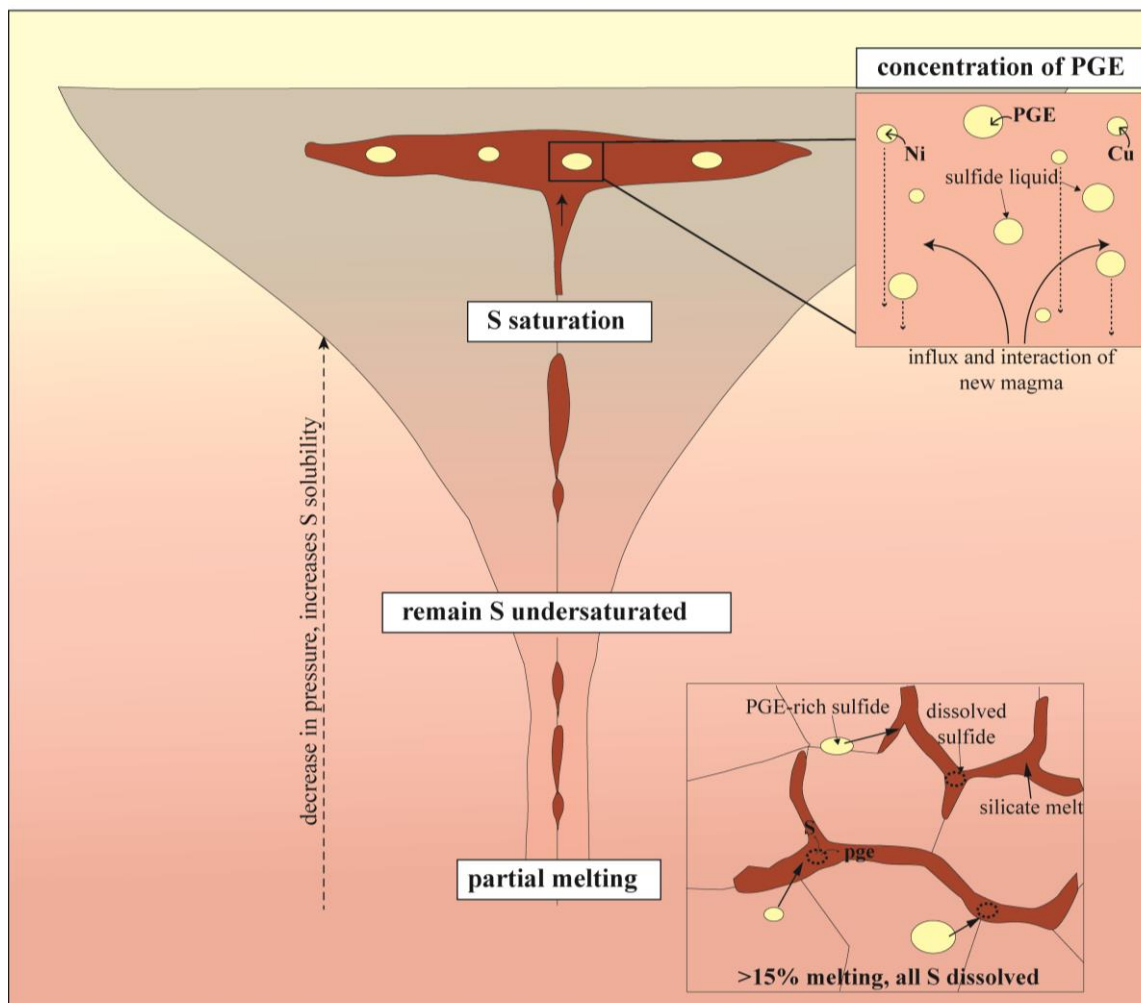


**Figure 1.3** Summary of the processes essential in the formation of a Ni-Cu-PGE deposit. See text for explanation.

### 1.2.1 Generation and emplacement of parental magma

In order to produce a PGE fertile magma, the PGE which are believed to reside within sulfides in the upper mantle are required to partition into the magma through partial melting. Sulfides are among the first phases to melt, and as the degree of partial melting increases they progressively dissolve into the silicate liquid (Fig. 1.3). When melting exceeds 15 to 25% (depending on the S content of the peridotite and depth of melting), sulfide is completely dissolved (Figure 1.4a; e.g. Wendlandt 1982; Naldrett and Barnes 1986; Keays 1995; Rehkämper et al. 1999). The high sulfide/silicate melt partition coefficients ( $D_{\text{sul/sil}}$ ) of the PGE (values of 17,000–92,000; Naldrett 2011 and references therein), mean that PGE will largely be retained in the sulfide until it melts completely, and it is therefore only at this amount of melting that they will be transferred into the silicate melt (see Figure. 1.3; 1.4b). The principal control over a magmas metal content is therefore the degree of partial melting attained. At low degrees of melting (ca 10%) PGE are retained within the un-

dissolved sulfide that forms a dense residue that remains within the upper mantle during extraction of the silicate magma. The PGE contents of the silicate melt are therefore low and uneconomic (Arndt et al. 2005; Maier 2005).

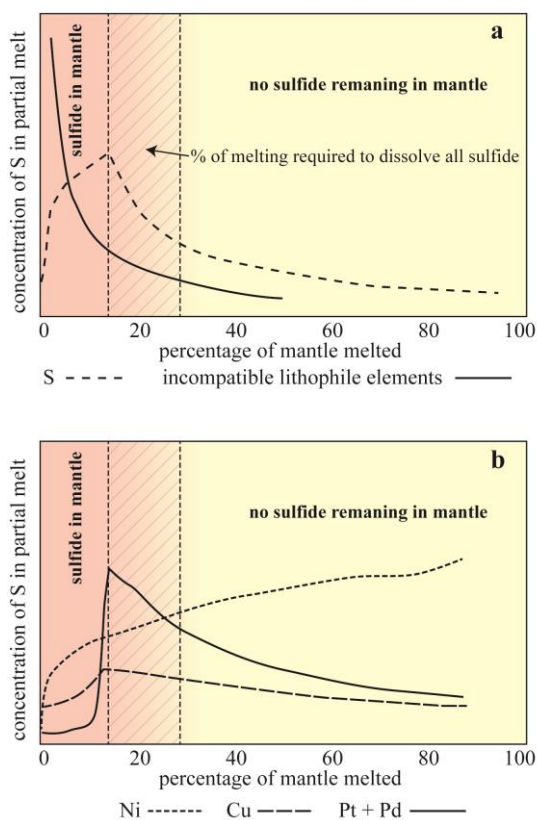


**Figure 1.4** Schematic trends showing the variations in the concentrations of a) sulfur and incompatible lithophile elements and b) Ni, Cu and Pt+Pd in the partial melt. Note that the Ni contents of the melt increases continuously with degree of partial melting, whilst that of Cu, PGE and S peak at the stage of complete sulfide dissolution and then decrease as they are diluted from continued melting with no further addition of these elements. The range in the percentage of melting required to dissolve all sulfide is also highlighted. Modified from Naldrett (2011) and Arndt et al. (2005)

To develop PGE deposits that can be exploited economically it is essential that the parental magma does not become saturated in S and thus loses its PGE component during ascent into the upper crust. Mavrogenes and O'Neill (1999) highlighted that it is actually unlikely that any mafic and/or ultramafic melt will arrive into the crust saturated in S, resulting from the significant increase in S solubility imposed by a decrease in pressure. To illustrate, for a 13.5% partial melt (i.e. the partial melt that was just sufficient to dissolve all mantle S; see Naldrett 2011 and references therein) rising from a depth equivalent to 20 kbars (assuming constant temperature and composition), the amount of sulfide the melt can dissolve increases from 0.45 to 0.68 wt% (Naldrett 2011). Thus even though magma was saturated in the upper mantle, it is far from saturated as it approaches the surface. Although a decrease in temperature has the opposite effect on the S solubility, the effect of

pressure is considered to be far more significant (Wendlandt 1982; Mavrogenes and O'Neill 1999).

### 1.2.2 Inducing sulfur saturation and the concentration of PGE

Many consider the development of an immiscible sulfide liquid to be the most effective and important mechanism by which PGE are concentrated. Although chromite and hydrothermal fluids are also known to concentrate PGE (Boudreau and McCallum 1992; McDonald et al. 1995; McDonald et al. 1999; Naldrett et. al 2008 and references therein), these processes are considered rather insignificant in the formation of economic, intrusion related PGE deposits. As mafic and/or ultramafic magmas are emplaced into the upper crust undersaturated in S (Mavrogenes and O'Neill 1999; Naldrett 2011), a sulfide melt can only segregate if the solubility of S is reduced or significant quantities of S are added into the system (Maier 2005). Important processes that may trigger sulfide saturation include the following:

- (i) Sulfur saturation may be reached through fractional crystallization either by: (1) increasing S content of the magma through crystallizing oxides and silicates which S is not incorporated into; or (2) by fractionating Fe-rich minerals such as olivine, pyroxenes, chromite and magnetite which decreases the  $\text{Fe}^{+2}$  content of the magma and the S solubility as S is bonded to  $\text{Fe}^{+2}$  in the magma (Haughton et al. 1974; Shima and Naldrett, 1975; Li et al. 2001).
- (ii) The assimilation of crustal S is considered by many as being essential in inducing S saturation (Leshner and Groves 1986), and is thus believed to be the most practical mechanism for producing the extraordinary quantities of sulfide required to form giant magmatic ore deposits such as Voisey's Bay, Noril'sk and the Bushveld Complex (e.g. Naldrett 1999; Li et al. 2002). Sulfur saturation may also be triggered by the addition of silica through assimilation of felsic country rocks which lowers the sulfur solubility of the magma (Irvine 1975; Li and Naldrett 1993). Furthermore, an increase in oxygen fugacity through contaminating with oxygen-bearing country rocks can result in the precipitation of chromite and magnetite and/or a lowering of the FeO content of the magma, both of which act to decrease a magma's sulfur carrying capacity (Haughton et al. 1974; Buchanan and Nolan 1979).

- (iii) It has also been suggested that mixing of compositionally contrasting, S undersaturated magmas could result in S saturation (e.g. Naldrett and von Gruenewaldt 1989; Li et al. 2001).

The ability of a sulfide liquid to then become highly enriched in PGE is then dependent on the presence of a high R factor (R factor refers to sulfide to silicate ratio) and the sulfide melt equilibrating with a large volume of magma (Arndt et al. 2005; Maier 2005; Naldrett 2011). Where R is in the range of 10,000 to 100,000 the Ni and Cu contents will not be much higher than at lower R values (100 to 2,000) which is typical of most Ni sulfide ores, however the Pt (and other PGE) concentration will be significantly increased in the range of those characterizing the Merensky Reef (Naldrett 2011). In large intrusions such as the Bushveld Complex, high PGE tenors may also be attained through the settling of the dense sulfide droplets through a large magma column, from which they scavenge PGE. Alternatively where conduit systems are present, sulfides can become progressively enriched in PGE through interaction with multiple batches of S undersaturated magma in a similar manner to that proposed by Kerr and Leitch (2005). Examples where upgrading of sulfides has been important in terms of PGE tenors include; Noril'sk- Talnakh ores (Naldrett et al. 1996), Voisey's Bay deposits (Naldrett et al. 2000); the Platreef (McDonald and Holwell 2007; Holwell et al. 2007; McDonald et al. 2012); the Merensky Reef (Naldrett et al. 2009) and the Platinoe Reef of the Skaegaard intrusion (Holwell and Keays 2014).

Finally, in order to develop an economic PGE deposit, the PGE-rich sulfide liquid must accumulate in sufficient quantities. Within deposits such as the Bushveld Complex and the Stillwater Complex, the sulfide melt accumulates either at the base of the magma chamber or above an impermeable layer (e.g. chromitite layer) to form a highly concentrated stratiform deposit.

### **1.3 Behaviour of PGE during sulfide fractionation**

An understanding of the behaviour of PGE during fractionation of a sulfide liquid has only been gained (Fig. 1.5) within the last decade through detailed comparison of the partitioning behaviour of PGE within natural sulfide systems (revealed by laser ablation-inductively coupled plasma-mass spectrometry (LA-ICP-MS) studies; see review by Holwell and McDonald 2010, and references therein) with earlier constrained experimentally derived data (Fleet et al. 1993; Li et al. 1996; Barnes et al. 1997; Ballhaus et al. 2001; Mungall et al. 2005). Knowledge of the concentration of PGEs in sulfide minerals and their

preference for a particular sulfide mineral is fundamental, especially when evaluating the economic potential of a deposit and designing efficient metal recovery systems (Barnes et al. 2006; Holwell and McDonald 2010).

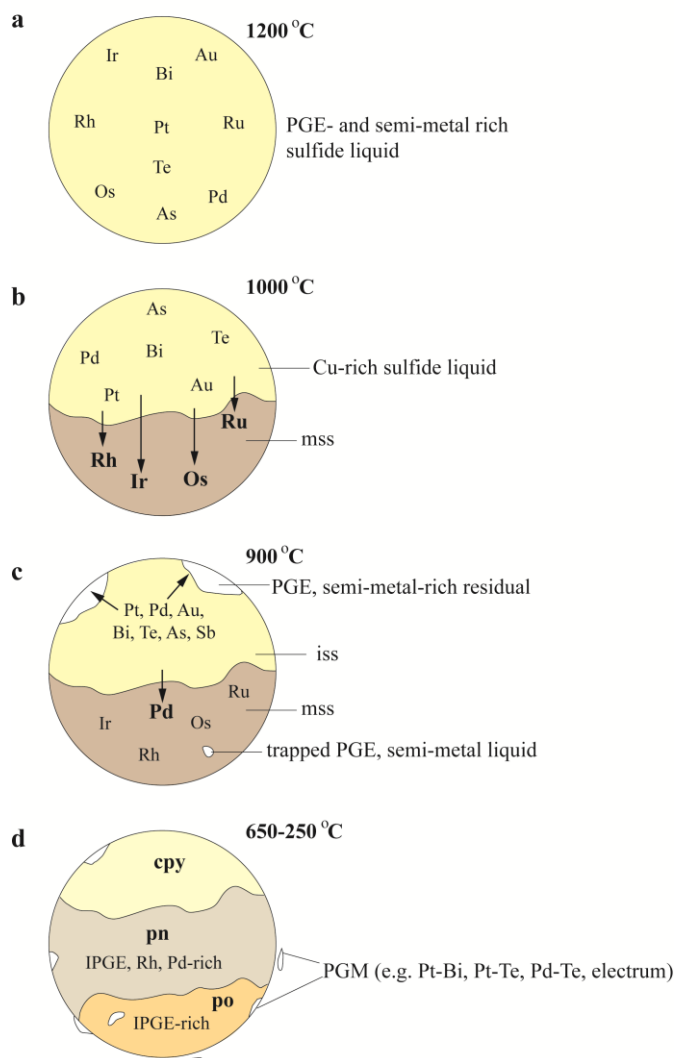


**Figure 1.5** Schematic representation of a fractionating, PGE-rich sulfide liquid droplet (see text for detailed explanation). Major partitioning behaviour at each temperature controlled stage (a-c) is highlighted by larger text. Modified from Holwell and McDonald 2010.

Figure 1.5 provides a summary of the behaviour of PGEs in natural sulfide systems as revealed by experimental and LA-ICP-MS studies. Following the separation of a PGE-rich sulfide liquid from a silicate melt (Fig. 1.5a), experimental studies have shown that the Fe-Ni-Cu sulfide liquid begins to fractionate with decreasing temperature. At around 1000°C the Fe-rich portion crystallizes as monosulfide solid solution (mss), leaving a Cu-rich residual liquid which subsequently crystallizes as intermediate solid solution (iss) at 900°C (Fig. 1.5b-c). Experimental work has shown that the partitioning behaviour of most of the

chalcophile elements into mss is negatively dependent on the S/metal ratio and  $fS_2$  of the sulfide system, which in turn is controlled by the  $fO_2$  (Li et al. 1996; Barnes et al. 2001; Ballhaus et al. 2001; Sinyakova et al. 2001; Mungall et al. 2005). In magmatic sulfide systems where the  $fO_2$  is close to fayalite-magnetite-quartz (FMQ), the  $fS_2$  should be in the range -2 to 0 (Wallace and Carmichael 1992). At these  $fS_2$  the iridium group PGEs (IPGEs; Os, Ir, Ru) and Rh preferentially partition into mss, whilst Pt, Pd, Au and the semi-metals are retained within the Cu-rich sulfide residual. Nickel also becomes compatible with mss (Li et al. 1996; Barnes et al. 2001).

Experimental data has shown that Pt, Pd and Au are also incompatible within iss (Fleet et al. 1993; Li et al. 1996; Peregoedova 1998). Thus, rather than partitioning into iss when it crystallises, it seems Pt, Pd and Au are preferentially concentrated into a late-stage immiscible semimetal-rich melt (Fig. 1.5c; Fleet et al. 1993; Helmy et al. 2007; Helmy et al. 2010; Tomkins 2010). Where semi-metals are in abundance (particularly Sb and As), typically through crustal contamination at high temperatures (e.g. Platreef at Turfspruit; Hutchinson and Kinnarid 2005; Hutchinson and McDonald 2008), virtually all the Pt and Pd can be accommodated for within the semimetal-rich melt. In contrast where semi-metals are scarce (e.g. Platreef at Overysel; Holwell and McDonald 2006; 2007) the late-stage melt preferentially scavenges Pt over Pd (Fleet et al. 1993; Helmy et al. 2007). Consequently the resulting high Pd:semimetal ratio causes the excess Pd that cannot be accommodated for by the semimetal melt to partition into mss (Fig. 1.5c; Helmy et al. 2007). The control exerted by semimetals appears to be the most fundamental factor in terms of affecting the partitioning behaviour and thus mineralogical characteristics of magmatic sulfide-hosted Pt and Pd ores.

As the temperature falls further mss exsolves into pyrrhotite and pentlandite between 250°C and 650°C. Whilst the IPGE remain in solid solution within both sulfide phases, Rh and any Pd present appear to preferentially partition into pentlandite over coexisting pyrrhotite. The iss recrystallizes to chalcopyrite with no PGE in solid solution (Fig. 1.5d). During cooling and crystallization of the semimetal-rich melt Pt and Pd combine with the semimetals to form discrete platinum-group element minerals (PGM; e.g. Hutchinson and McDonald 2008). As the late-stage semimetal melt is thought to be expelled to grain boundaries during crystallization of iss, PGM are often observed around the margins of sulfides. Later replacement, focussed around the margins of the sulfide blebs by secondary

actinolite, tremolite and chlorite, isolates the PGMs as satellite grains within secondary silicates.

#### **1.4 Aims and Objectives**

In terms of layered mafic intrusions the Bushveld Complex is one of a kind, both in terms of its overall size and PGE resources. For these reasons since its discovery in 1924, it has been a highly active area for exploration, mining and scientific research. The eastern and western limbs which are host to the two largest PGE deposits in the world: the Merensky Reef and UG2 chromitite have in the past been the focus of numerous studies. Consequently, the conditions and processes responsible for their genesis are considered to be well constrained although some aspects are to this day, still debated. Until relatively recently (prior to 1990s), the northern limb of the Bushveld Complex had received very little scientific attention in comparison to the eastern and western limbs. However Anglo Platinum currently operate five open-pit mines within the northern limb of the complex which are collectively referred to as the Mogalakwena Platinum Mines. The success of their low-cost, high tonnage approach has since renewed interest in the northern limb and in particular the huge PGE reserves of the Platreef. With continued exploration and research on the Platreef and new discoveries being made within the Main Zone rocks (Maier and Barnes 2010; McDonald and Harmer 2011; Lombard 2012; Kinnaird et al. 2012; Holwell et al. 2013) the northern limb remains highly exciting and prospective.

The premise of this thesis is to constrain the nature and origin of PGE mineralization within the Grasvally Norite-Pyroxenite-Anorthosite (GNPA) member, an ore body in the northern limb of the Bushveld Complex which has previously seen little scientific interest resulting from its proximity to the more economical Platreef. Although this project contributes further to our understanding of the magmatic history of the northern limb of the Bushveld Complex, it rather more importantly presents implications for our understanding of the Platreef and its relationship with the rest of the complex. This project set out with the following three objectives:

- Determine the role of magmatism, contamination and hydrothermal processes in the development of PGE mineralization within the GNPA member.
- Establish the geochemical characteristics of the GNPA member to place constraints on its relationship with the Platreef and the Upper Critical Zone of the eastern and western limbs.

- Develop a holistic genetic model for the GNPA member and associated mineralization.

In addition to these three main objectives this thesis also addresses several fundamental questions regarding how we determine the source of S responsible for ore formation:

- Are S isotopes and S/Se ratios reliable indicators of the initial source of S?
- Are S/Se ratios of sulfide determined *in situ* capable of tracing the S source?
- What magmatic and low temperature processes are capable of modifying the S isotope signature and the S/Se ratio?

Not only do these findings have implications for the interpretation of S isotopes and S/Se ratios and thus the ore genesis of magmatic sulfide deposits they also provide an insight into the primary partitioning behaviour and secondary mobility of Se in sulfides during high temperature fractionation and low temperature alteration.

## 1.5 Thesis organization

This thesis is presented as four ‘journal-style’ chapters with each chapter investigating one or more of the aims and objectives described above.

### **Chapter 2:** *The Bushveld Complex*

This chapter provides an introduction to the Bushveld Complex, summarizing key aspects of the extensive literature available. It focusses primarily on: the genesis of both Critical Zone and Platreef mineralization; introducing the GNPA member; and proposals on how these three deposits relate to each other.

### **Chapter 3:** *The mineralogy and petrology of sulfide mineralization within the GNPA member*

Chapter 3 provides a detailed account on the petrography and mineralogy of silicates, oxides and base metal sulfides (BMS) within the GNPA member. We begin to explore the importance of magmatic and hydrothermal processes in the development of mineralization within the GNPA member. Chapter three is published within the journal Applied Earth Science (Transactions of the Institute of Mining and Metallurgy B; 120: B158–B174). I completed detailed logging, sample collection, microscope analysis, figure production and wrote the chapter. Dave Holwell and Iain McDonald were involved in discussion during preparation of the manuscript.

**Chapter 4:** *Precious and base–metal geochemistry and mineralogy of: implications for a multistage emplacement*

This chapter sets out to investigate the precise distribution and mineralogy of PGE within the GNPA member. This was done to establish: the role played by sulfide liquid in the concentration of PGE; and the effects of post-magmatic fluids on the mineralogy and distribution of PGE. We also explore the processes involved in ore genesis, with particular interest on constraining the timing of S saturation relative to emplacement, by comparing the GNPA mineralization with its nearest analogue the Platreef and more widely with the Merensky Reef. This chapter is published within the journal *Mineralium Deposita*. I completed all sample collection, sample preparation, analysis using the SEM, figure production, data synthesis, data interpretation and wrote the chapter. Dave Holwell and Iain McDonald assisted with data interpretation. Iain McDonald also processed the LA-ICP-MS data and assisted in the writing of the laser ablation methodology.

**Chapter 5:** *The combined use of in situ S isotope and S/Se analysis in assessing ore genesis of magmatic sulfide PGE-Ni-Cu deposits*

In the study of magmatic Ni-Cu-PGE sulfide deposits, S isotopes and S/Se ratios have long been used to determine the source of S and thus the role of crustal contamination in achieving S saturation. In this chapter through presenting isotope and S/Se data for the GNPA member I assess the ability of both indicators to retain the initial S signature in dynamic settings where magmatic, contamination and hydrothermal processes have been critical in terms of ore genesis. Our findings have important implications for: the use and interpretation of such data in the study of magmatic sulfide deposits; the genesis of the GNPA member; and the behaviour of Se during both high temperature sulfide fractionation and low temperature alteration processes. This chapter is to be submitted to a peer-reviewed journal that has yet to be decided. I completed all sample preparation, figure production, S isotope analysis, data synthesis, data interpretation and wrote the chapter. Iain McDonald processed LA-ICP-MS data. Dave Holwell and Adrian Boyce assisted in data interpretation and were involved in discussion during preparation of this manuscript.

**Chapter 6:** *Geochemical characteristics of the GNPA member*

Chapter 6 provides further constraints on the genesis of the GNPA member through studying variations in the major/trace element and mineral chemistry of the succession. Here I utilize geochemical characteristics to determine: (i) the magmatic lineage of the rocks and if the GNPA member is geochemically similar to the Platreef and Upper Critical

Zone; and (ii) the nature in which the GNPA succession was emplaced. This chapter also constrains further the degree and timing of crustal contamination relative to emplacement and S saturation.

**Chapter 7:***Conclusions*

This chapter summarizes the key findings of chapters 3 to 6 and explores the implications of the results presented in this thesis for our understanding of the northern limb ore-bodies and their relationship with the rest of the complex.

# Chapter Two

## Regional Geological Setting

## 2.1. The Bushveld Complex

The 2.06 Ga (Walraven et al. 1990) Bushveld Complex located in the north-eastern region of South Africa (Fig. 2.1) is the world's largest mafic layered intrusion, covering an area of ca. 65,000 km<sup>2</sup>. It represents the Earth's largest repository of magmatic ore deposits and currently accounts for 86% and 35% of the annual global production of Pt and Pd, respectively (Butler 2011). The huge reserves of platinum-group elements (PGE) are hosted primarily in three deposits; the Merensky Reef, the UG-2 chromitite and the Platereef.

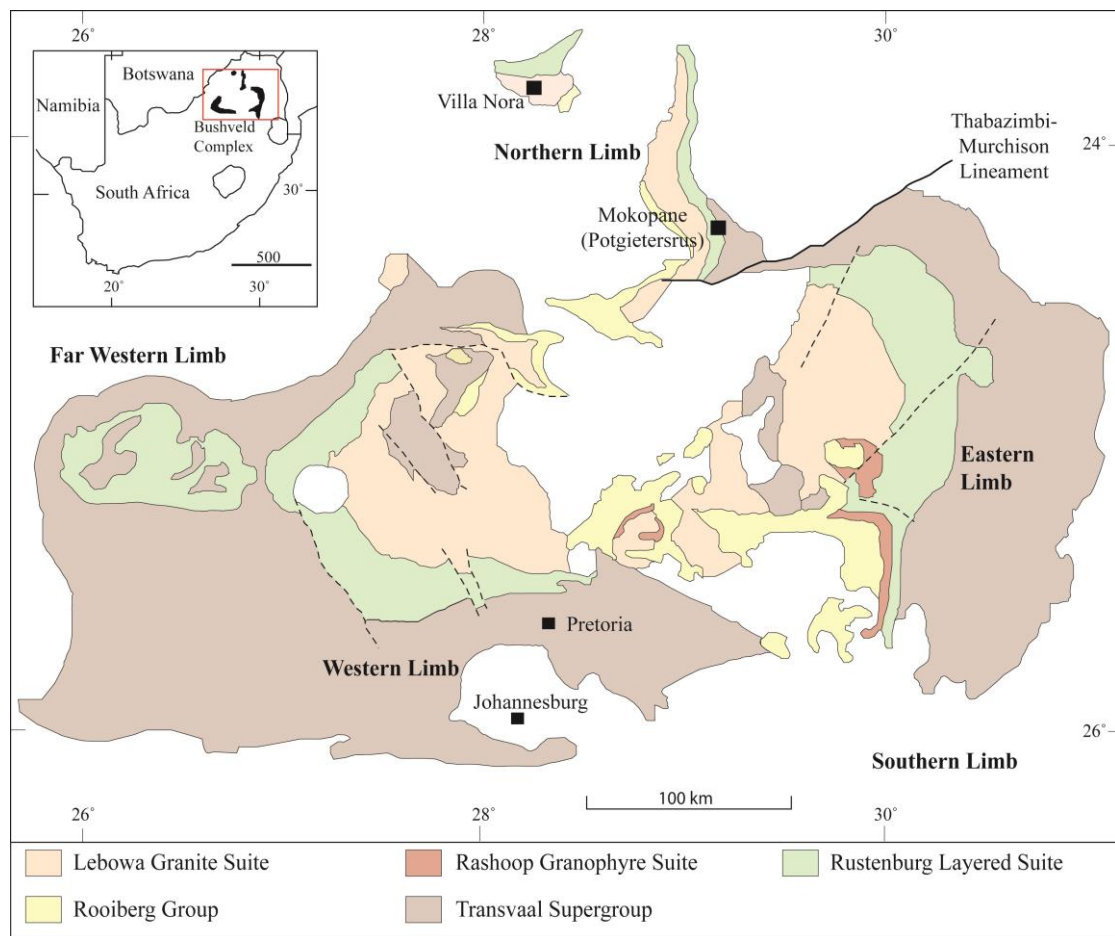


**Figure 2.1** Geological map of the Bushveld Complex. Inset map showing its location within South Africa. Adapted from Eales and Cawthorn (1996).

The Bushveld Magmatic Province as a whole comprises five major magmatic suites: the felsic volcanics of the Rooiberg Group (Twist 1985; Buchanan et al. 2002), the mafic-ultramafic layered rocks of the Rustenburg Layered Suite (RLS), the Rashoop Granophyre Suite (Walraven 1985), the Lebowa Granite Suite (Walraven and Hattingh 1993) and a set of marginal pre- and syn- Bushveld sills (Cawthorn et al. 1981; Fig. 2.1)

## 2.2. Rustenburg Layered Suite

In most of the scientific literature and in this study also, the term Bushveld Complex refers solely to the economically important part of the complex known as the Rustenburg Layered Suite (RLS). The RLS consists of a 7–8 km thick layered package of ultramafic and mafic cumulates, host to world class chromium, vanadium and PGE deposits. Emplacement of the RLS into the northern region of the Kaapvaal Craton occurred along a regional unconformity between the preceding Rooiberg Group volcanics, and the Transvaal Supergroup. The mafic/ultramafic cumulates were intruded at variable stratigraphical levels into Transvaal sediments ranging in age from 2.20 to 2.55Ga and Archaean basement granites and gneisses (Bekker et al. 2001, 2004; Hannah et al. 2004). The Bushveld Complex has been spatially divided into five limbs (Fig. 2.1): the near symmetrical western and eastern limbs; a southern limb, partially hidden by younger sediments; a heavily eroded far western limb; and a northern limb (Eales and Cawthorn 1996).

The interconnectivity of the eastern and western limbs has been the subject of debate. Petrologically they are remarkably similar with correlation of numerous distinctive layers, sequences and PGE horizons possible (Lee 1996; Barnes and Maier 2002a). Such similarities combined with geophysical models led to the original assumption that the limbs were connected at depth (Hall 1932). Based on the absence of a positive gravity anomaly between the two limbs however, Cousins (1959) challenged the connectivity of the limbs with Meyer and de Beer (1987) later arguing that they represent two discrete, inward-dipping sheets that terminate at depth. More recent geophysical models presented by Cawthorn and Webb (2011) and Webb et al. (2004) support connectivity between the two limbs, as through accounting for isostatic readjustment the observed gravity anomaly can be produced. They therefore envisage that the limbs represent a single downwrapped lopolithic intrusion with similar magmas and processes operating concurrently in both limbs. This interpretation is consistent with the much earlier proposal of Hall (1932).

### 2.2.1. Overview of Bushveld Stratigraphy

In the eastern and western limbs the RLS is conventionally divided into five stratigraphic zones based on modal mineralogy: Marginal Zone norites, Lower Zone pyroxenites and harzburgites, Critical Zone chromitite-pyroxenite-norite cyclic units, Main Zone gabbro-norites, and Upper Zone anorthosites, ferrogabbros and magnetites (Fig. 2.2).

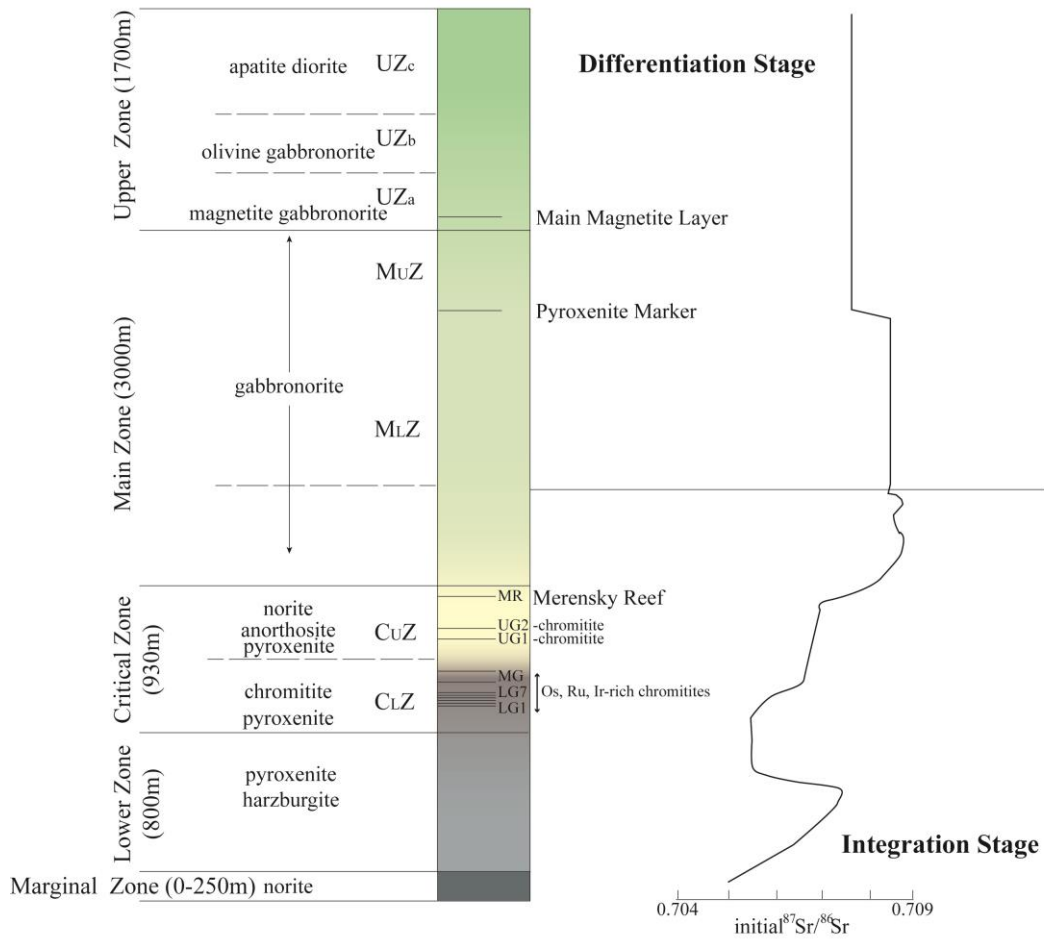


**Figure 2.2** Generalised stratigraphy of the eastern and western limbs of the Bushveld Complex showing major subdivisions, dominant rock type and thickness of each zone. Position of PGE-bearing lower (LG), middle (MG) and upper group (UG) chromitites and the Merensky Reef are indicated with initial  $^{87}\text{Sr}/^{86}\text{Sr}$  ratio for whole-rock and plagioclase separates (from Kruger 1994) also shown. Modified from Eales and Cawthorn (1996) and Kruger (2005).

The thickness of each zone and position of PGE-bearing chromitites are provided in Figure 2.2. A complete succession is only observed in the northern sectors of both the eastern and western limbs. In the eastern limb, for example, the full sequence is exposed north of Steelpoort, but to the south the Lower, Critical, and Main Zones successively abut and terminate against the sedimentary floor rocks; a similar geometry is recorded in the northern limb and will be presented in section 2.3.

### 2.2.2. The Critical Zone

The Critical Zone which is divided into a lower ( $C_LZ$ ) and an upper Critical Zone ( $C_UZ$ ) is host to world class chromium and PGE deposits (Fig. 2.2). The  $C_LZ$  is entirely ultramafic characterized by orthopyroxenitic cumulates whilst the  $C_UZ$  is recognised by the appearance of cumulus plagioclase and contains chromite, pyroxenite, norite and anorthosite cyclic units. Although subjective, nine cyclic units are generally recognised in the  $C_LZ$  and eight within the  $C_UZ$ . The economically important UG-2 chromitite and Merensky Reef are located at the base of cyclic units 5 and 7 within the  $C_UZ$ . The base of each cycle is characterized by a reversal in the trend of Fe enrichment, interpreted to indicate magma replenishment (e.g. Kruger and Marsh 1982; Eales and Cawthorn 1996).

#### 2.1.1.1 Chromitites

Within the Critical Zone chromitite layers identified at the base of cyclic units form three stratigraphical groupings referred to as the lower (LG), middle (MG) and upper (UG) groups (Fig. 2.2; Cousins and Feringa 1964). Seven LG chromitites (LG-1 to -7), four MG chromitites (MG-1 to -4) and two UG chromitites (UG-1 and -2) are normally identified, although the number of chromitite occurrences does vary significantly, with considerable lateral variation also observed (Hatton and von Gruenewaldt 1987). The chromitites range from 0.15 to 2 m in thickness and may consist of single or multiple seams. The chromium content of the chromitite layers and thus the Cr/Fe ratio decreases upwards through the succession (Kinnaird et al. 2002). The prevailing intercumulus phase also changes from chiefly orthopyroxene in the LG, to orthopyroxene and plagioclase in the MG and plagioclase in the UG chromitites. Naldrett et al. (2012) provides more detail on the geochemical variations characteristic of each chromite group.

Numerous models attempt to account for the formation of the chromitite layers which include: (i) contamination by a siliceous component (Irvine 1975); (ii) mixing between resident and new magma (Irvine 1977; Irvine et al. 1983); and (iii) pressure changes (Cameron 1977). Although a single model is yet to be agreed on, Sr isotopic data indicates that each chromitite layer is associated with a new influx of magma (Kinnaird et al. 2002). A decrease in the  $(Pt + Pd)/(Ru + Ir + Os)$  ratio over the Lower Zone and subsequent increase over the  $C_LZ$  suggests a gradual increase in the primitiveness of the resident magma (Eales et al. 1990). The olivine associated chromitites (LG-1 to LG-4) are therefore thought to result from the mixing between a primitive and an evolved magma (Kinnaird et al. 2002). The overlying chromitites associated with orthopyroxene (LG-5 to MG-1) or

orthopyroxene and plagioclase (MG-2 and above) however, are thought to have formed from mixing of two compositionally distinct magmas (Irvine 1977; Irvine et al. 1983). The magmas involved are thought to include an  $\text{Al}_3\text{O}_3$  poor but MgO, Cr and  $\text{SiO}_2$  rich U-type and a tholeiitic in composition A-type (Harmer and Sharpe 1985; Irvine and Sharpe 1986). The latter is now termed T-type in the current literature.

#### *2.1.1.2 PGE mineralization*

PGE mineralization occurs in well-defined layers in association with the chromite layers. The UG-2 and Merensky Reef represent the most economically important (Fig. 2.2) with grades (3PGE+Au) typically ranging between 5 and 7 g/t, locally exceeding 10 g/t (Kinnaird et al. 2002). The Merensky Reef is bounded by an upper and lower chromitite layer (2 to 40 mm thick), separated by a texturally heterogeneous feldspathic pyroxenite, which is pegmatoidal in places (Lee 1996, Naldrett et al. 2009) and varies in thickness from 0 to 10 m. Other than the chromite layers, PGE-bearing sulfides may also occur in the anorthositic footwall, up to 1 m below the lower chromitite (Leeb-du Toit 1986; Barnes and Maier 2002a and b), throughout the interval between the two chromitites and <1 m above the upper chromite layer. In addition to the UG-2 and Merensky Reef, all other chromitites contain lower, but significant concentrations of PGE even though they are poor in BMS (Lee and Parry 1988; Teigler and Easles 1993; Scoon and Teigler 1995). Within these chromitites there does appear to be a notable variation in PGE proportion according to the host rock. Whilst the IPGE group (Ru, Os, Ir) occurs consistently, there is a low abundance of Pt-Pd-Rh in the pyroxenite-hosted LG, MG-1 and MG-2 (Lee and Parry 1988; Scoon and Teigler 1995). In contrast, those chromitites associated with plagioclase-bearing rocks (MG-3, MG-4 and UG-1) are more enriched in Pt-Pd-Rh (Lee and Parry 1988; Scoon and Teigler 1995). The Pt-rich chromitites of the Critical Zone are dominated by the PGE sulfides laurite, braggite and cooperite together with antimonides, arsenides, bismuthides, tellurides and alloys (Kinloch 1982).

#### *2.1.1.3 Genesis of mineralization*

In recent years, many authors have attempted to address the origin of PGE mineralization within the  $C_UZ$  (e.g. Ballhaus and Sylvester 2000; Barnes and Maier 2002a, b; Wilson and Chunnnett 2006; Naldrett et al. 2009). Many agree that the  $C_UZ$  and associated mineralization resulted from the mixing of a resident (T-type) magma present within the Bushveld chambers crystallizing orthopyroxene and plagioclase with a more primitive magma (U-type; orthopyroxene-olivine and/or chromite) that was enriched in PGE and

characterized by low Cu/Pd ratios (Naldrett et al. 2009). Rare earth element concentrations presented by Maier and Barnes (1998) further confirms that the Bushveld Complex crystallized from at least two compositionally distinct magmas.

Mixing of highly energetic influxes of the T-type magma, injected along the cumulate-magma interface (Naldrett et al. 2009), with resident magma is thought to have resulted in sulfide immiscibility, consequently depleting the overlying magma of its metals (Campbell et al. 1983; Maier and Barnes 1999; Li and Ripley 2005; Naldrett et al. 2009). The ability of magma mixing to induce sulfur saturation has in the past been questioned, however existing sulfur solubility data (which has significantly improved over the last 20 years) shows that various proportions of mixing of these magmas can give rise to sulfide immiscibility, provided both magmas are close to sulfide saturation at the time of mixing (Naldrett and von Gruenewaldt 1989; Li et al. 2001; Cawthorn et al. 2002; Li and Ripley 2005). In the case of the C<sub>v</sub>Z it has been proposed that the pre-Merensky and Merensky influxes of U-type magma were so enriched in PGE through the complete dissolution of sulfides in a staging chamber. Naldrett et al. (2009) have postulated that earlier batches of magma en route to the complex deposited sulfides within a staging chamber. Interaction of these sulfides with subsequent S undersaturated magma dissolved FeS, resulting in the progressive enrichment of the sulfides in highly chalcophile elements such as PGE, Ni and Cu. The Merensky magma pulses then become PGE enriched (ca. 200 ppb Pt as compared with 10–20 ppb) through the complete dissolution of these highly enriched sulfides (Naldrett et al. 2009).

It has been argued that mixing of magmas is not necessary to induce sulfur saturation, for example Cawthorn (2005) believes sulfide segregation and the formation of chromite layers are best explained through the negative effect of an increase in pressure on sulfide solubility (Mavrogenes and O'Neill 1999). Further, through utilizing Boudreau and Meurer (1999) vapour refining model in which volatiles released in a cooling pile of igneous cumulates ascend, dissolving amongst other elements, S, the PGE, Ni and Cu, Wilmore et al. (2000) suggested that the addition of a S- and PGE-rich vapour to a crystallizing magma at the top of a cumulate pile could result in sulfide immiscibility, and the subsequent concentration of PGE within sulfides.

### 2.2.3. Evolution of the Bushveld Complex

The filling of the Bushveld magma chamber occurred over a period of ca. 75,000 years (Cawthorn and Walraven 1998). Breaks in the initial  $^{87}\text{Sr}/^{86}\text{Sr}$  ratios ( $R_o$ ) in conjunction with mineral composition reversals demonstrate the multiple intrusive nature of the Bushveld Complex (Fig. 2.2; Kruger 1994). Furthermore, they also highlight the close association of magma addition with mineralization which is particularly apparent at the level of the Merensky Reef (Kruger and Marsh 1982; Kruger 1992). Kruger (1994) views the RLS as having three main magmatic lineages: the Lower and Critical Zone (with low  $R_o$  0.705 to 0.7064); the Main Zone gabbro-norite lineage (high  $R_o$  ca. 0.7082); and the Upper Zone Fe-rich gabbro-norite lineage ( $R_o$  ca. 0.7075).

The evolution of the Bushveld magma chamber is thought to have occurred in two major stages, with a lower, open-system 'Integration stage' and an upper-closed system, 'Differentiation stage' (Figure 2.2; Kruger 2005). The Lower, Critical and Lower Main ( $M_LZ$ ) Zones are represented in the initial evolutionary phase and are characterized by multiple influxes of magma, contrasting in isotopic composition. The progressive mixing of new and residual fractionated magmas resulted in the crystallization from harzburgite in the Lower Zone ( $R_o$  0.705), to orthopyroxenite in the  $C_LZ$ , norite and anorthosite in the  $C_UZ$  ( $R_o$  0.7064) and finally, norite and gabbro-norite in the  $M_LZ$  ( $R_o$  0.7064–0.709; Kruger 2005). The addition of magma and its interaction with pre-existing hot cumulates, residual magma and roof melts, is considered crucial in the evolution and development of unique PGE bearing horizons within the Critical Zone such as the Merensky Reef, UG-2 chromitite, LG-2 and other chromitite layer cumulates (Kruger and Marsh 1982; Campbell et al. 1983; Kruger 1999, 2003; Kinnaird et al. 2002).

The flux of magma at the Merensky Reef level differed significantly in composition from that which produced the preceding cumulate rocks (Eales and Cawthorn 1996). Post precipitation of the Merensky and Bastard cyclic units, the  $M_LZ$  crystallized simultaneously with the continued addition of magma. Once the influx of magma ceased, the chamber evolved in a closed system. Fractional crystallization proceeded in the Upper Main Zone ( $M_UZ$ ) which was disturbed by the final and largest injection of magma at the Pyroxenite Marker (Cawthorn et al. 1991). Isotopic data indicates that the Upper Zone differentiated from a single influx of magma.

#### **2.2.4. Age of the Bushveld Magmatic Province**

The emplacement age of the Bushveld Complex is considered well constrained at 2.06 Ga ( $\pm 3$  Ma Kruger et al. 1986;  $\pm 27$  Ma Walraven et al. 1990). More recent U-Pb dating of titanite within a calc-silicate from within the eastern limb RLS, which preserves the crystallization age rather than the cooling age, provides a tight constraint on the minimum age of Bushveld emplacement of  $2058.9 \pm 0.8$  Ma (Buick et al. 2001). This together with the  $2061 \pm 2$  Ma age of the Rooiberg Group roof rocks (Walraven 1997) tightly brackets the emplacement of the RLS to the interval 2059–2061 Ma. However, recent high precision U-Pb zircon dating of the Merensky Reef within the eastern limb indicates a significantly younger crystallization age of  $2054.4 \pm 1.3$  Ma (Scoates and Friedman 2008). The same study also attained a U-Pb rutile age of  $2055.0 \pm 1.3$  Ma which they interpret as the cooling age. These younger ages are more consistent with the Hutchinson et al. (2004) minimum age of the Platreef at  $2053.7 \pm 3.2$  Ma. Given the size of the Bushveld Complex, and the uncertainties surrounding the intrusion sequence between the limbs, notable discrepancies in the age of the Critical Zone within the eastern and western limbs and the slightly younger age of the Platreef within the northern limb could indicate that crystallization of the RLS was not synchronous between the limbs.

In addition to the RLS, the Lebowa Granite Suite has been dated at  $2052 \pm 2$  Ma whilst the Rashoop Granophyre Suite is slightly older at 2054 Ma (Walraven and Hattingh 1993). Therefore regardless of the age discrepancies of the RLS, all the Bushveld magmatism both intrusive and extrusive is believed to have occurred within a relatively short time interval between 2052–2061 Ma, with much of the magmatism considered to have been synchronous.

### **2.3. Northern limb**

The northern limb of the Bushveld Complex has a N-S trending, WSW-dipping sinuous outcrop which varies in thickness from 4 to 15 km over a strike length of 110 km. The total areal extent of the RLS in the northern limb was estimated at 7275 km<sup>2</sup> by van der Merwe (1978). South of Mokopane (previously known as Potgietersrus), the RLS is NE trending with a westward dip between 15° and 27°. In the north the strike changes to northwest and eventually to due north, with westward dips decreasing upwards through the layered cumulates from 45° to 10° (van der Merwe 2008). The limb is truncated in the south by the NE trending Zebediela Fault (Fig. 2.3) which juxtaposes the RLS with the Phanerozoic Karoo sedimentary sequence from the upper Transvaal Supergroup. The Zebediela Fault

along with the Ysterberg-Planknek Fault represent near surface expressions of the Thabazimbi-Murchison Lineament (TML) which separates the northern limb from the eastern and western limbs. The TML represents a pre-Bushveld collisional suture zone (ca. 2.9 Ga) between the Pietersberg and Kaapvaal terranes which has experienced repeated reactivation (Good and de Wit 1997; McDonald et al. 1999; Armitage et al. 2007). Although not clearly understood it is thought that the TML exercised some control over the emplacement of the Bushveld Complex either by acting as a feeder (Kinnaird et al. 2005) or through forming a permanent/temporary barrier to the movement of Bushveld magmas (Kruger 2005). Van der Merwe (1978) also proposed that the emplacement of the northern limb was principally controlled by the intersection point of three major tectonic lineaments, located west of Mokopane.

A characteristic feature of the northern limb is the pronounced transgression of the mafic succession northwards from the TML, through the Palaeoproterozoic Transvaal Supergroup (Sharman-Harris et al. 2005; van der Merwe 2008). The footwall units, northwards, consist of: interbedded quartzites and shales of the Magaliesberg Quartzite Formation, quartzites and shales of the Timeball Hill Formation, shales of the Duitschland Formation, the Penge banded iron formation, the Malmani Subgroup dolomites and Archean basement granites and gneisses (e.g. Sharman-Harris et al. 2005; Holwell and McDonald 2006; van der Merwe 2008; Fig. 2.3).

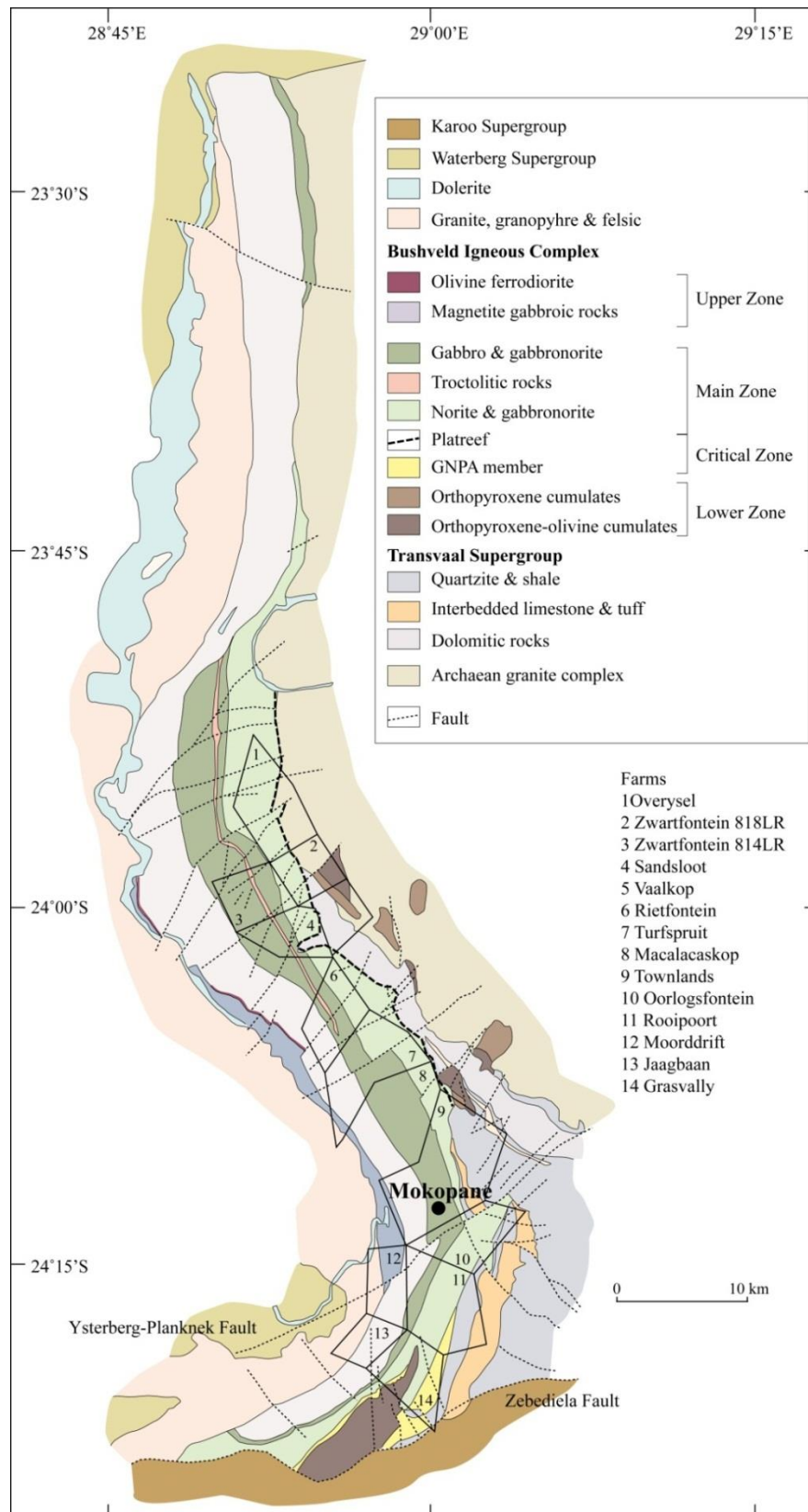


**Figure 2.3** Geological map of the northern limb of the Bushveld Complex (after Ashwal et al. 2005). Boundaries of farms mentioned in text are shown.

### 2.3.1. Structure

Within the northern limb, the RLS has been disturbed by several phases of faulting, all of which are thought to post-date emplacement and consolidation of the intrusion. Truter (1947), van Rooyen (1954) and de Villiers (1967) recognised E to ENE, N to NNW and NW fault trends. Hulbert (1983) recognised four phases of fault deformation. The earliest phase generated N trending reverse faults such as the Grasvally Fault. The second and third phases of deformation are represented by WNW and NE striking faults respectively, with the latter occurring post-Waterberg. The north easterly trending Zebediela and Ysterberg-Planknek Faults are considered to mark the final episode of faulting within the southern sector of the northern limb which occurred in post-Karoo times (van der Merwe 1978).

The sediments of the Transvaal Supergroup display a series of small synclines which in areas are also evident in the overlying RLS. In total five synclines exist termed the: Tsamahaans, Townlands, Kleinmeid, Moorddrift and Vaalkop synclinal structures (van der Merwe 2008). The NNE trending, northwards plunging Kleinmeid syncline observed within the RLS east of the Grasvally Fault, is thought to have developed from drag associated with movement of this fault (Verbeek and Lomborg 2005).

### 2.3.2. Stratigraphy of the northern limb

The mafic succession (summarised in Fig. 2.4) deviates from the conventional Bushveld stratigraphy of the eastern and western limbs shown in Figure 2.2. This limb is divided into four principal zones, with notable variations in the stratigraphy also observed north and south of the Ysterberg-Planknet Fault (Fig. 2.3 and 2.4).

Lower Zone cumulates are developed locally south of Mokopane and as satellite bodies beneath the Platreef (Fig. 2.3; van der Merwe 1976; Yudovskaya et al. 2012). The Lower Zone in the northern limb is unusually thick (800–1600 m) comprising a sequence of pyroxenites and harzburgites which contain 37 cyclic units, many of which are incomplete or beheaded (Hulbert and von Gruenewaldt 1982; 1985). Hulbert (1983) defined three subzones: the Volspruit pyroxenite; the Drummonlea harzburgite chromitite; and the Moorddrift Harzburgite pyroxenite (Fig. 2.4). The Drummonlea harzburgite chromitite contains two economically important chromitite seams (Fig. 2.4) which crop out over a strike length of 5 km (Hulbert and von Gruenewaldt 1985). The Lower Zone is considered unique from the rest of the complex on the basis of its; extreme thickness, superior quality

of chromite ore and mineral compositions (e.g. higher Mg content in orthopyroxene and olivine; van der Merwe 1976).

The Platreef and GNPA member represent the northern limb equivalent of the Critical Zone of the eastern and western limbs. To the north of the Ysterberg–Planknek Fault, the PGE-bearing Platreef forms the base of the RLS (Fig. 2.3) developed from the farms Townlands to Dorstland (Fig. 2.3). The Platreef represents a 10–400 m thick package of sill-like intrusions (Kinnaird 2005), which are dominated by variably altered and texturally heterogeneous feldspathic pyroxenites, with norite, peridotites and gabbros. Zones of intense serpentinisation may occur, along with country rock xenoliths typically <1500 m long. The ore-body is irregularly mineralized with PGE, Ni and Cu over a strike length of 30 km, with the highest and most consistent grades associated with the central sector between the farms Tweefontein and Overysel (McDonald and Holwell 2011). In detail, the Platreef is a highly complex zone of igneous and hybrid lithologic units, that vary significantly along strike which in part is directly related to contamination of the Platreef magma through assimilation of differing floor rocks (e.g. Harris and Chaumba 2001; Armitage et al. 2002; Manyeruke 2003; Hutchinson and Kinnaird 2005; Kinnaird 2005; Kinnaird et al. 2005; Manyeruke et al. 2005; Sharman-Harris et al. 2005; Holwell and McDonald 2006; Holwell et al. 2006; Holwell and McDonald 2007; Holwell et al. 2007; Hutchinson and McDonald 2008). The footwall variability has also been shown to exert a strong control over the PGE and BMS mineralization style developed, affecting most significantly the platinum-group mineralogy (e.g. Holwell et al. 2006; Hutchinson and McDonald 2008).

Within the Platreef, PGE generally reside in close association with BMS (primarily pyrrhotite, pentlandite, chalcopyrite and minor pyrite). Where hydrothermal fluids have significantly interacted with the ore-body, decoupling of PGE from BMS is common (e.g. at Turfspruit and Sandsloot; Kinnaird et al. 2005; Hutchinson and McDonald 2008; Holwell et al. 2006). Platreef mineralization is characterized by Pt/Pd ratios of around unity or lower and PGE grades (3PGE+Au) between 1–4 g/t although rare intersections of up to 26 g/t are also observed (Hutchinson and Kinnaird 2005). The Platreef is dominated by Pt-As and Pd-Bi-Te-bearing PGM. The ubiquity of this sulfide associated PGM assemblage along strike in conjunction with its prevalence in the most unaltered rocks indicates a common initial mineralization style. Hydrothermal redistribution and local contamination have in places, modified the PGM assemblage to varying degrees, through introducing Sb

and S-bearing PGM (see Holwell et al. 2006; Hutchinson and McDonald 2008). The presence and abundance of antimonides and sulfides relates directly to footwall lithology. The primary distribution of PGE in BMS and associated Bi-Te-As-dominant assemblage is consistent with the concentration and subsequent fractionation of a sulfide liquid (Holwell and McDonald 2007; 2010).

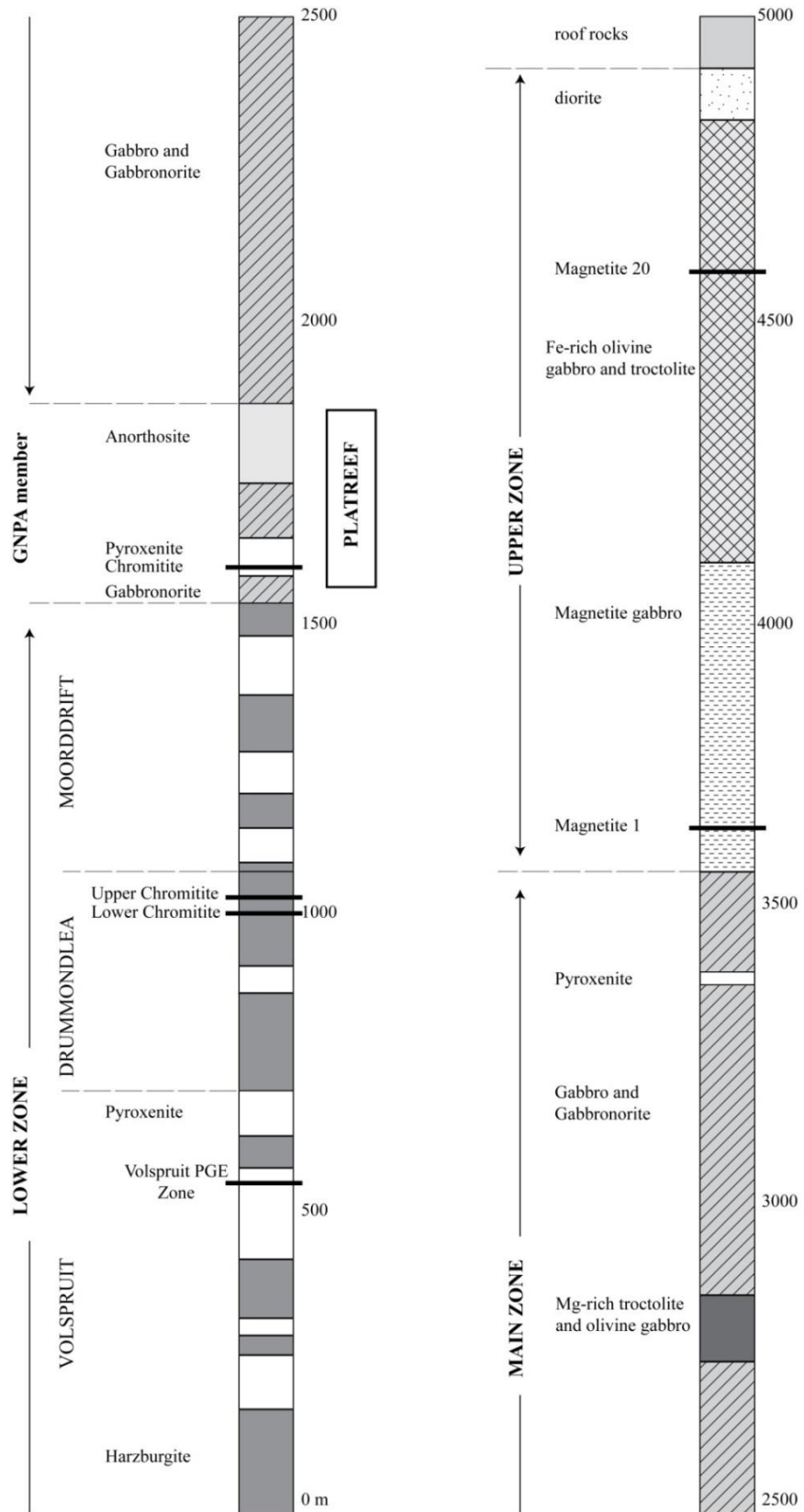


**Figure 2.4** Stratigraphy of the northern limb of the Bushveld Complex. Modified from McDonald et al. (2005).

To the south of the Ysterberg–Planknek Fault, the mafic succession differs significantly hosting a distinct layered package of PGE-bearing mafic cumulates which Hulbert (1983) termed the Grasvally Norite-Pyroxenite-Anorthosite (GNPA) member (Fig. 2.5 and 2.6). The GNPA member is developed at a similar stratigraphical position to the Platreef, being overlain by Main Zone gabbronorites and resting directly on both Lower Zone ultramafic/mafic cumulates and the Magaliesberg Quartzite Formation from the Palaeoproterozoic Transvaal Supergroup (Fig 2.5 and 2.6). The GNPA member is discussed in greater detail in section 2.4.

The Main Zone within the northern limb attains a maximum thickness of 2200 m, in comparison to the 4400 m thickness observed elsewhere in the complex (van der Merwe 1976). In the south of the limb this zone, dominated by homogeneous gabbros and gabbronorites is poorly developed reaching <1200 m in thickness (van der Merwe 2008). Within the Main Zone up to seven mottled anorthosite and two pyroxenite layers have been identified (van der Merwe 1976, 1978; Hulbert 1983). It is generally accepted that intrusion of Main Zone gabbronorites occurred significantly after the emplacement of the Platreef (Holwell et al. 2005; Holwell and Jordaan 2006). In the eastern and western limbs of the complex, the Main Zone has long been proven to be barren of PGE, due to depletion of its metals during formation of the underlying Merensky Reef (e.g. Maier and Barnes 1999). Within the northern limb however, a number of PGE enriched zones have been identified including: (i) Pt-rich sulfide mineralization in in the Upper Main Zone on Moorddrift (Maier and Barnes 2010; Holwell et al. 2013); (ii) at the base of the Main Zone within the Aurora project to the far north of the limb (McDonald and Harmer 2011); and on the Waterberg project which is north of the exposed northern limb (Lombard 2012; Kinnaird et al. 2012). The Upper Zone is marked by the first appearance of cumulus magnetite and apatite and consists of a 1500 m thick succession of cyclic units of magnetite, magnetite gabbro, gabbro and anorthosite (van der Merwe 1976).

### **2.3.3. Genesis of the Platreef**

Although the relationship of the Platreef with the Merensky Reef is still debated there is a general consensus that Platreef mineralization resulted from primary orthomagmatic processes involving: (i) separation of a sulfide liquid prior to intrusion; (ii) enrichment and upgrading of the sulfide melt through repeated interaction with large volumes of magma in a staging chamber; and (iii) entrainment and transport of the PGE enriched sulfides into the Platreef (Lee 1996; McDonald and Holwell 2007; Holwell et al. 2007).

#### 2.1.1.4 Staging chamber model

It is generally agreed that the Merensky Reef sourced its high PGE content from the overlying body of Main Zone magma (c.f. Cawthorn et al. 2002). This mechanism of PGE enrichment is not feasible for the Platreef as field observations suggest intrusion of Main Zone occurred significantly after the emplacement of the Platreef (Holwell et al. 2005; Holwell and Jordaan 2006). This also introduces the mass balance problem of generating high PGE concentrations from a small volume package of magma such as the Platreef. McDonald and Holwell (2007) and Holwell et al. (2007) developed Lee's (1996) original notion further proposing PGE-rich sulfides were introduced into the Platreef from a deeper, pre-existing magma chamber that supplied the pre-Platreef Lower Zone. This model plausibly accounts for the Platreef mass balance paradox as sulfides contained within the staging chamber were able to acquire very high PGE tenors while producing a corresponding volume of metal-depleted Lower Zone cumulates (McDonald and Holwell 2007).

Within the staging chamber, it is thought an early-formed sulfide liquid became progressively enriched in PGE, Ni and Cu through reacting with multiple later batches of silicate magma at low R factors. Metal concentrations were most probably further increased through partial dissolution of the pre-existing sulfides as described by Kerr and Leitch (2005). This is confirmed by McDonald et al.'s (2012) discovery that the early sulfide liquid exhibited lower than mantle S/Se ratios (<2000; Eckstrand and Hulbert 1987). A major pulse of magma (Main Zone magma) later breached the established Lower Zone magmatic system remobilizing the PGE-rich sulfides and injecting them within a silicate crystal mush which ultimately crystallized to form the Platreef. The localised addition of crustal S and semi-metals into the Platreef, controlled by footwall lithology, modified the sulfide droplets *in situ* resulting in metallurgical variations along strike.

#### 2.1.1.5 Source of sulfur

Sulfur saturation and the development of an immiscible sulfide liquid is fundamental processes for concentrating economic volumes of PGE, Ni and Cu within a magmatic system. The assimilation of crustal S is considered by many as being essential in inducing S saturation (Leshner and Groves 1986), and thus is believed to be the most practical mechanism for producing the extraordinary quantities of sulfide required to form giant magmatic ore deposits such as the Bushveld Complex (e.g. Li et al. 2002). In low-S systems like the Bushveld Complex, sulfur saturation can also be achieved through a number of

other mechanisms, these include; contamination by silica through assimilation of felsic rocks; increasing the  $fO_2$  through assimilation of oxygen bearing rocks, both contamination processes lower FeO content and thus the S-carrying capacity of the magma; low pressure fractionation; and mixing of compositional distinct undersaturated magmas (see review by Maier 2005).

The role of externally derived S in the formation of magmatic sulfides can be independently assessed utilizing either S isotopes or S/Se ratios. Holwell et al. (2007) suggested a purely magmatic origin for Platreef mineralization as primary sulfides exhibit  $\delta^{34}S$  values consistent with mantle derived S ( $0 \pm 2\text{‰}$ ; Omhoto and Rye 1979), attributing higher  $\delta^{34}S$  values (up to  $+11\text{‰}$ ) to local contamination of S which acted only to modify pre-existing sulfides. Penniston-Dorland et al. (2008) argued on the basis of  $\Delta^{33}S$  signatures that all of the Platreef S was magmatic in origin and confirmed that the Platreef magma was sulfide-saturated prior to emplacement. Ihlenfeld and Keays (2011) used the dominance of high S/Se ratios to challenge the importance of mantle S, proposing that S saturation was driven by early stage, pre-emplacement crustal contamination, with localised *in situ* contamination occurring during emplacement (see also Holwell et al. 2007).

#### **2.4. The GNPA member**

The GNPA member, which is unique to the northern limb, crops out only to the south of the Ysterberg-Planknek Fault where it strikes NE for 30 km (Fig. 2.3 and 2.5; Verbeek and Lomborg 2005). To the south of the limb, the Zebediela Fault truncates and juxtaposes the GNPA member with the Phanerozoic Karoo sedimentary sequence from the upper Transvaal Supergroup (Armitage et al. 2002; Kinnaird 2005). To the east of the N-S trending Grasvally Fault (Fig. 2.5) the GNPA member forms a southwards plunging syncline directly overlying interbedded quartzites and shales of the Magaliesberg Quartzite Formation. West of the Grasvally Fault Lower Zone lithologies underlie the GNPA member (Fig. 2.5). The contact is characterized by a chilled margin up to 7m in thickness with calc-silicate xenoliths also occasionally present (de Klerk 2005; Maier et al. 2008).

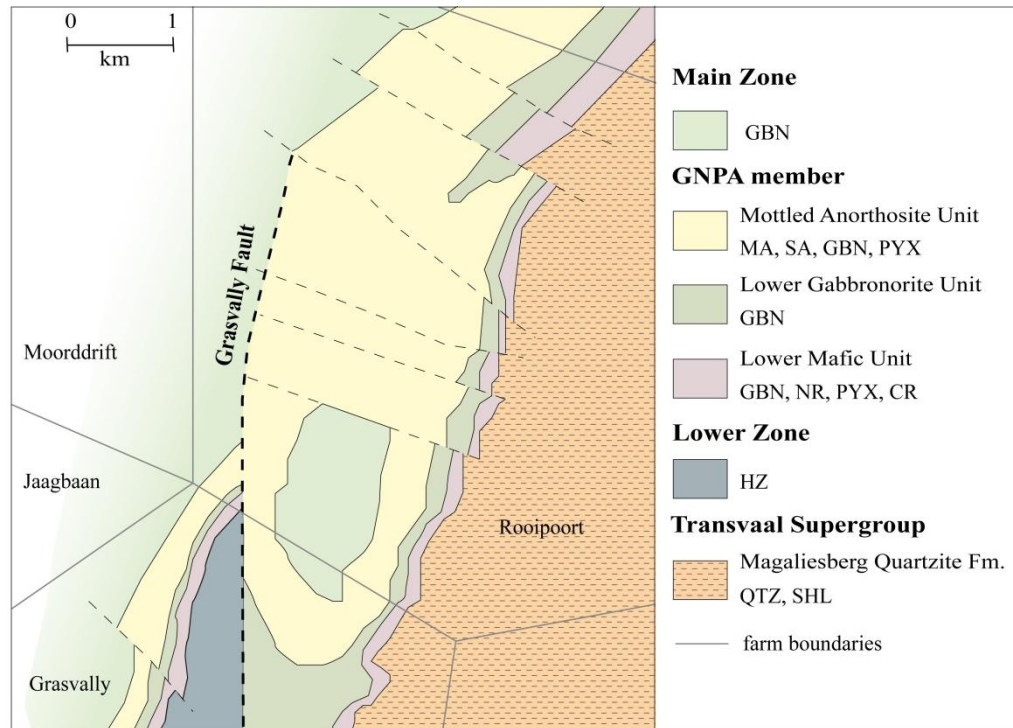


**Figure 2.5** Detailed map of the GNPA member in the Rooipoort-Grasvally region. Adapted from Maier et al. (2008). Lithological abbreviations *SA* spotted anorthosite, *MA* mottled anorthosite, *GBN* gabbronorite, *PYX* pyroxenite, *NR* norite, *CR* chromitite, *HZ* harzburgite, *QTZ* quartzite and *SHL* shale.

#### 2.4.1. Stratigraphy

The 400–800 m thick layered succession comprises varied textured gabbronorites, norites, anorthosites, pyroxenites and a PGE-bearing chromitite. Hulbert (1983) originally divided the GNPA member into a lower pyroxenitic sub-zone 1 and an upper noritic sub-zone 2. De Klerk (2005) introduced new terminology subdividing the succession into three stratigraphic units (Fig. 2.6); the Lower Mafic Unit (LMF); the Lower Gabbronorite Unit (LGN); and the Mottled Anorthosite Unit (MANO).

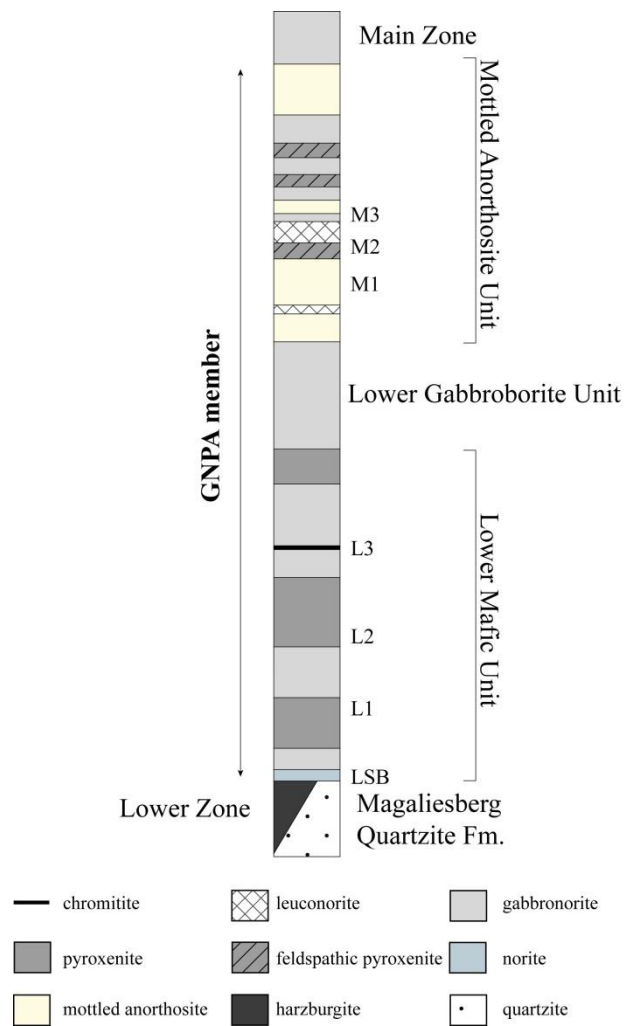


**Figure 2.6** Stratigraphy of the GNPA member, highlighting dominant rock type and position of de Klerks (2005) seven PGE and BMS-bearing horizons

The basal LMF unit is dominated by melanorite, feldspathic pyroxenite, gabbronorite and pyroxenite and contains orthopyroxene-clinopyroxene, unique orthopyroxene-clinopyroxene-chromite and orthopyroxene cumulates (Hulbert 1983; Verbeek and Lomborg 2005). It was recognised by de Klerk (2005) that the LMF and MANO units are separated by a zone of fine- to medium-grained gabbronorites, termed the LGN unit. The upper and lower contacts of this unit vary considerably, with chilled zones, gradational and sheared contacts all observed. On the basis of the uniform nature of this unit in conjunction with the presence of occasional chilled margins, de Klerk (2005) suggested that it represents a sill of Main Zone rocks which preferentially intruded along the original LMF-MANO contact. The MANO unit is most readily distinguished from the underlying LGN and LMF units by a marked increase in the proportion of plagioclase cumulates present and the dominance of mottled and spotted anorthosites. The crystallization order for this part of the sequence appears to be governed by the liquidus order plagioclase-

orthopyroxene-clinopyroxene (Hulbert 1983). A transitional contact is generally evident between the upper MANO unit mottled anorthosites and gabbro-norites of the overlying Main Zone. The GNPA stratigraphy is discussed in greater detail in Chapter 3.

#### **2.4.2. Mineralization**

The GNPA member is Pd-rich and characterized by Pt/Pd ratios of  $<1$  (McDonald and Holwell 2011, and references therein). The PGE and BMS mineralization is not lithologically bounded and is developed as wide but irregular zones throughout the LMF and MANO units. Hulbert (1983) and de Klerk (2005) both identified seven PGE- and BMS-bearing horizons on the farms Grasvally and Rooipoort, respectively (Fig. 2.6). Correlation of these horizons is complicated by their discontinuous nature and lack of marker horizons, with the exception of a PGE-bearing chromitite developed within the basal LMF unit (Fig. 2.6, L3 horizon). The stratigraphic position of the chromitite varies throughout the region being developed near the base of the LMF on Grasvally (Hulbert 1983) and over 100m from the footwall contact on Rooipoort. East of the Grasvally Fault, the chromite layer (0.2 to  $>1$  m thick) contains two seams which are correlated easily throughout the Rooipoort and Grasvally region and characterized by Pt/Pd ratios of  $<1$ . To the west of the Grasvally Fault, the chromitite shows less lateral continuity, forming thinner impersistent schlieren and lenses with Pt/Pd ratios reaching  $>2$ .

PGE grades associated with sulfide enriched regions reach up to 2 ppm (2PGE+Au), with localised intersections of 5 ppm (2PGE+Au) (Verbeek and Lomborg 2005; Maier et al. 2008). The chromitites carry significant and consistent PGE concentrations, typically around 4 ppm throughout the Rooipoort and Grasvally region. Sulfides are disseminated to blebby in texture, comprised primarily of pyrrhotite, pentlandite, chalcopyrite and pyrite with minor millerite. The work of Smith et al. (2011b; 2012) (Chapter 3 and 4) provides the most detailed account to date of the BMS and PGE mineralization within the GNPA member, thus they will not be discussed in detail here.

To the north of Rooipoort the GNPA member exhibits less laterally variability, enabling correlation of the succession throughout Warpsings. In this region, three PGE reefs referred to as the A, B and C reef are consistently recognised which range in thickness from  $<1$  to  $>5$  m (Muller 2008). The upper C reef is associated with mottled anorthosites, the middle B reef with pyroxenites and the A reef with a chromitite layer developed near the base of the succession. PGE grades are slightly lower than observed further south on

Rooipoort, ranging from <1 to <4 ppm (3PGE+Au). The well-developed chromitite on Warsprings, contains significantly lower grades (<1 ppm) than on Rooipoort (Muller 2008).

### **2.4.3. Origin of the GNPA member and Platreef**

The GNPA member, based primarily on the development of a UG2-'like' chromitite, has been regarded by both Hulbert (1983) and van der Merwe (1978; 2008) as an upper Critical Zone equivalent. This notion however has been contested due to the silicate and PGE geochemistry being distinct in the GNPA chromitites to that observed in the UG2-chromitite (von Gruenewaldt et al. 1989; McDonald et al. 2005). The GNPA member is considered by many to form part of the same succession as the Platreef. Whilst Maier et al. (2008) and van der Merwe (2008) believe that the GNPA member merges laterally with the Platreef, van der Merwe (1978) previously positioned the Platreef at the base of the Main Zone thus equating the GNPA member with the Upper Critical Zone. The latter is favoured by Kruger (2005) who believes that the Platreef represents a time equivalent of the Merensky Reef formed from the southwards migration of Main Zone magma, which initially entered the complex to the north of the TML (Fig. 2.1).

Justifiably the correlation of the GNPA/Platreef with the Critical Zone of the eastern and western limbs has been questioned. On the basis of rather significant and unaccounted for geochemical differences McDonald et al. (2005) view the Platreef and GNPA member as being distinct from the Critical Zone, resulting from the mixing of Lower and Main Zone magmas. The viability of this theory has been questioned as evidence exists to suggest that the Lower Zone cumulates were consolidated, significantly cooled and tilted prior to emplacement of a later magma (van der Merwe 1978; Kinnaird et al. 2005).

Although the GNPA member and Platreef have long been assumed to correlate with the Critical Zone, Ivanplats recent discovery of corresponding Merensky Reef cyclic units on the farm Turfspruit (Fig. 2.3; Dunnnett et al. 2012; Grobler et al. 2012) provide the first convincing stratigraphic correlations between the Platreef/GNPA member and the rest of the complex. A model similar to that proposed by Naldrett et al. (2008) is now rather favourable for the origin of the Platreef. Naldrett et al. (2008) suggest that the Platreef formed from a mixture of Critical and Main Zone-type magmas that moved outward and escaped up the margins of the limb, resulting from the injection of Upper Critical Zone magma into the chamber. Naldrett (2008) illustrates this using the concept of nesting pudding basins to represent the floor and roof of the chamber (Fig. 2.7). Each limb is

suggested to contain a similar distribution of layered cumulates with stratiform reefs in the centre (e.g. Merensky Reef and UG2-chromitite) and complex injections of melt and sulfides along the margins (e.g. Platreef; Fig. 2.7a). Contrasting levels of erosion in each limb, then determine how much of the Rustenburg layered suite is preserved. Thus Naldrett (2008) suggests the northern limb has suffered much less erosion than the eastern and western limbs thus preserving the escaped magma which formed the Platreef (Fig. 2.7b).

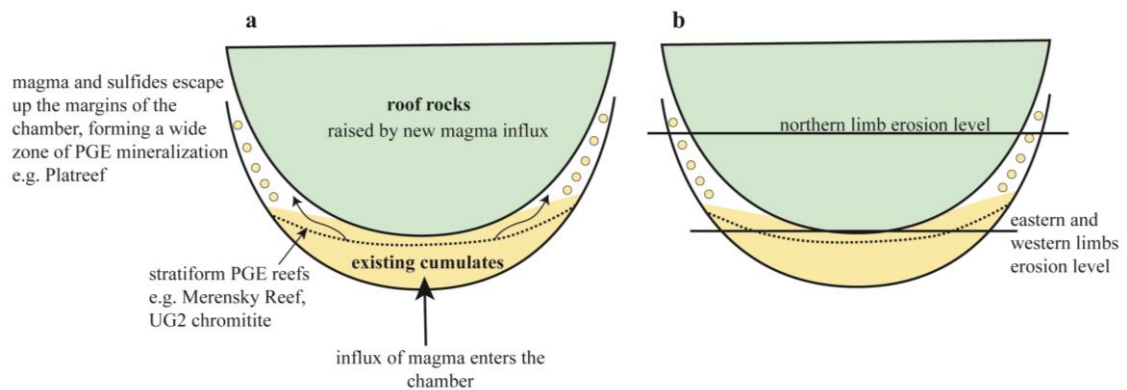


**Figure 2.7** ‘Pudding basin’ model after Naldrett et al. (2008) with a) showing the concept of nested pudding bowls to represent the floor and roof of the Bushveld chamber. New injections of magma raise the roof and/or squeeze up along the margins and b) showing the different levels of erosion required to expose the Platreef in the northern limb and the Critical Zone in the eastern and western limbs.

If such a model is correct, then as highlighted by McDonald and Holwell (2011) the Platreef should be laterally transformed into something representative of the Upper Critical Zone and a thicker, more complete Critical Zone sequence should also be developed downdip towards the centre of the northern limb. Although the GNPA member may represent the lateral transition of the Platreef into Upper Critical Zone, the latter can only be tested when deeper drilling and/or seismic data becomes available. This model is also yet to explain several key distinctions including: (1) the presence of a magmatic break between the Platreef and Main Zone (Holwell et al. 2005; Holwell and Jordaan 2006) with evidence of continued interaction of Critical and Main Zone magmas in the eastern and western limbs (Seabrook et al. 2005); (2) the more evolved compositions of silicates within the GNPA member; and (3) the significantly lower Pt/Pd ratios associated with Platreef and GNPA member (McDonald et al. 2005).

## Chapter Three

### The mineralogy and petrology of sulfide mineralization within the GNPA member

**Chapter 3 is published within the journal Applied Earth Science**

Smith JW, Holwell DA, McDonald I (2011) The mineralogy and petrology of platinum-group element-bearing sulfide mineralization within the Grasvally Norite–Pyroxenite–Anorthosite (GNPA) member, south of Mokopane, northern Bushveld Complex, South Africa. *Applied Earth Science (Transactions of the Institute of Mining and Metallurgy B)* 120: B158–B174.

I completed detailed logging, sample collection, microscope analysis, figure production and I wrote the entire paper. The co-authors were involved in discussion during preparation of the manuscript.

### 3.1 Abstract

The Grasvally Norite–Pyroxenite–Anorthosite (GNPA) member is a 400 to 800 m thick cumulate package located in the northern limb of the Bushveld Complex, south of the town of Mokopane. On the farm Rooipoort it forms the lowermost unit of the magmatic stratigraphy, overlying Transvaal Supergroup sediments, whereas further south on the farm Grasvally it overlies Lower Zone rocks of the Bushveld Complex. The GNPA member is divided into three units; the Lower Mafic Unit (LMF), the Lower Gabbro-norite Unit (LGN) and the Mottled Anorthosite Unit (MANO). Platinum–group element (PGE) mineralization is closely associated with base metal sulfides (BMS) and is confined to the LMF and MANO where PGE grades range from 1–4 ppm (3PGE+Au). A number of distinct BMS assemblages are observed throughout the area and are interpreted to be the result of a combination of primary magmatic processes and low temperature alteration. In areas where the GNPA member is underlain by Lower Zone rocks, a pyrrhotite–chalcopyrite–pentlandite sulfide assemblage dominates, representing initial orthomagmatic sulfide mineralization. Late-stage low temperature alteration has significantly altered much of the sulfide mineralogy, producing two secondary pyrite–chalcopyrite–pentlandite±pyrrhotite±millerite and pyrite–pentlandite±millerite sulfide assemblages. The primary assemblage was variably altered by crystallization of pyrite and millerite from pyrrhotite and pentlandite at temperatures below 230°C. Sulfide replacement was associated with the precipitation of quartz and secondary silicates. This replacement of sulfides is more prevalent towards the base of the unit where the GNPA member is underlain by quartzites. These features suggest a strong footwall control over the low temperature alteration and thus the extent of the development of the secondary sulfide assemblages.

## 3.2 Introduction

The 2.06 Ga Bushveld Complex in South Africa is the world's largest layered igneous intrusion covering an area of ca. 65,000 km<sup>2</sup> (Fig. 3.1). It represents the Earth's largest repository of magmatic ore deposits and currently accounts for 86% and 35% of the annual global production of Pt and Pd, respectively (Butler 2011). These huge platinum–group element (PGE) reserves are hosted primarily in three deposits; the Merensky Reef, the UG2-chromitite and the Platreef. Within the northern limb of the Bushveld Complex, PGE mineralization is developed in four distinct mafic/ultramafic bodies, (1) the Platreef, north of the town of Mokopane (previously known as Potgietersrus); (2) within a sequence of layered cumulates referred to as the Grasvalley Norite–Pyroxenite–Anorthosite (GNPA) member developed only to the south of Mokopane; (3) within Lower Zone cumulates on the farm Volspruit, also south of Mokopane; and (4) within Main Zone rocks on Moorddrift farm (Maier and Barnes 2010), on the Aurora project to the far north of the limb (McDonald and Harmer 2011) and on the Waterberg project which is north of the exposed northern limb (Kinnaird et al. 2012). At present, the Platreef is being mined by Anglo Platinum in four open-pit mines opened between 1992 and 2006, collectively referred to as the Mogalakwena Mine (McDonald and Holwell 2011). The success of this low-cost, high-tonnage PGE mining has since led to increased exploration along the entire strike of the Platreef and facilitated an expanding number of geochemical and mineralogical studies, revealing the true complexity of the unit (e.g. Armitage et al. 2002; Hutchinson and Kinnaird 2005; Kinnaird 2005; Kinnaird et al. 2005; Sharman-Harris et al. 2005; Holwell and McDonald 2006; Holwell et al. 2006; Hutchinson and McDonald 2008). In contrast, south of Mokopane, exploration has been far less extensive with Caledonia Mining Corporation and Platinum Group Metals being the only companies at present prospecting the GNPA member mineralization. Consequently, only limited mineralogical and geochemical studies have been undertaken on this ore body (e.g. van der Merwe 1976 and 1978; Hulbert 1983; McDonald et al. 2005; Maier et al. 2008; van der Merwe 2008), thus the GNPA member remains poorly constrained and understood in comparison to other PGE-bearing units of the Bushveld Complex.

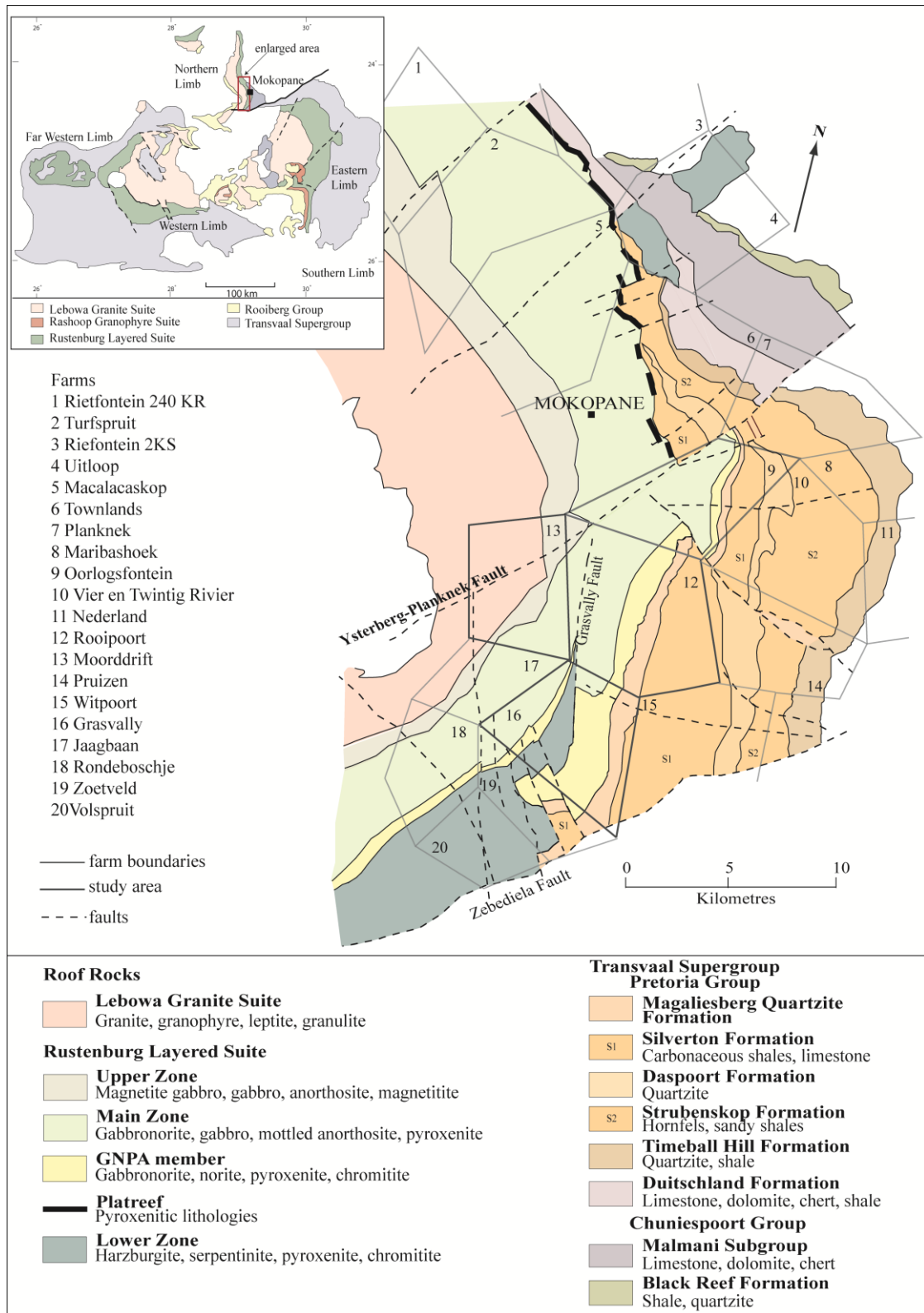


**Figure 3.1** Geological map of the northern limb of the Bushveld Complex, highlighting the location of the GNPA member and the location of the study area on the farms Rooipoort, Grasvally and Moorddrift (thicker farm boundaries). Inset map adapted from Eales and Cawthorn (1996) and main map modified from van der Merwe (2008).

This study provides the first detailed account since the original work of Hulbert (1983) that focuses on the petrography and mineralogy of silicates, oxides and base metal sulfides (BMS) in the GNPA member, and the first that utilizes the wealth of information provided by drilling since 2003. Thus this study covers a greater geographical area than Hulbert's (1983) previous work and also extends down dip and in doing so presents the most extensive description of PGE mineralization-hosting GNPA member rocks to the south of the Platreef.

### **3.3 Regional Geology**

The ultramafic–mafic portion of the Bushveld Complex is referred to as the Rustenburg Layered Suite and has been spatially divided into five limbs (Fig. 3.1): the near symmetrical western and eastern limbs; a southern limb, partially hidden by younger sediments; a heavily eroded far western limb; and a northern limb (Eales and Cawthorn 1996). The Rustenburg Layered Suite is also conventionally divided into five stratigraphic zones based on modal mineralogy: Marginal Zone norites, Lower Zone pyroxenites and harzburgites, Critical Zone chromitite-pyroxenite-norite cyclic units, Main Zone gabbronorites, and Upper Zone anorthosites, ferrogabbros and magnetites.

The northern limb is characterised by the local development of unusually thick (800–1600m) sequences of Lower Zone lithologies; the apparent absence of the Critical Zone, which is so obviously developed in the eastern and western limbs; and the variation of the mafic succession along strike (McDonald et al. 2005; Fig. 3.1). To the north of the Ysterberg–Planknek Fault, the PGE- and BMS-bearing Platreef forms the base of the Rustenburg Layered Suite (Fig. 3.1) and is developed as a 10–400 m thick package comprising texturally heterogeneous and variably altered pyroxenitic lithologies (e.g. Hutchinson and Kinnaird 2005; Kinnaird 2005; Holwell and McDonald 2006; Hutchinson and McDonald 2008). Although Lower Zone cumulates have been identified beneath the Platreef (Yudovskaya et al. 2012) it remains unclear as to whether these represent isolated satellite bodies or a continual layer as in van der Merwe's (1976) original cross-sections. To the south of the Ysterberg–Planknek Fault the magmatic succession differs significantly (Fig. 3.1). This region contains locally developed Lower Zone harzburgites on and west of the farm Grasvally, a unique layered package termed the GNPA member, and overlying Main Zone gabbronorites and Upper Zone rocks. A characteristic feature of the northern limb is the pronounced transgression of the mafic succession northwards from the Thabazimbi–Murchison Lineament (Fig. 3.1) through the Palaeoproterozoic Transvaal

Supergroup (van der Merwe 2008). Northwards, the footwall consists of interbedded quartzites and shales of the Magaliesberg Quartzite Formation, quartzites and shales of the Timeball Hill Formation, shales of the Duitschland Formation, the Penge Banded Iron Formation, the Malmani Subgroup dolomites and Archean basement granites and gneisses (e.g. Sharman-Harris et al. 2005; Holwell and McDonald 2006; van der Merwe 2008).

The north-east striking GNPA member crops out over a distance of 30 km (Verbeek and Lomberg 2005), reaching a maximum thickness of 800 m. The GNPA member was originally divided into two major sub-units by Hulbert (1983) but more recently has been divided into three by de Klerk (2005); the Lower Mafic Unit (LMF), the Lower Gabbronorite Unit (LGN) and the Mottled Anorthosite Unit (MANO). The LMF is distinguished from the unmineralized, homogeneous gabbronorites of the LGN by an increase in melanocratic lithologies, the development of two chromitites and elevated chromium values. The MANO is recognised by a substantial increase in plagioclase cumulates and the development of lithologies such as mottled and spotted anorthosites. It is suggested that the unmineralised LGN represents a sill of Main Zone rocks (de Klerk 2005; Maier et al. 2008) however this is yet to be confirmed. The main structural control over the magmatic succession in the area is the N–S trending Grasvally Fault (Fig. 3.2a and b). East of this fault the GNPA member forms a plunging synform which directly overlies interbedded quartzites and shales of the Magaliesberg Formation (Fig. 3.2b). In contrast, west of the fault Lower Zone cumulates comprise the footwall to the GNPA member. Hulbert (1983) and de Klerk (2005) both identified nine PGE and BMS mineralised horizons, all of which are confined within the LMF and MANO on the farms Grasvally and Rooipoort. These reefs are highly discontinuous and sporadic in nature with the exception of the PGE- and BMS-bearing chromitites which are laterally persistent throughout Grasvally and Rooipoort (Verbeek and Lomberg 2005). PGE grades associated with sulfide enriched regions reach up to 2 ppm (Pd+Pt+Au), with localised intersections of 5 ppm (2PGE+Au; Verbeek and Lomberg 2005; Maier et al. 2008).

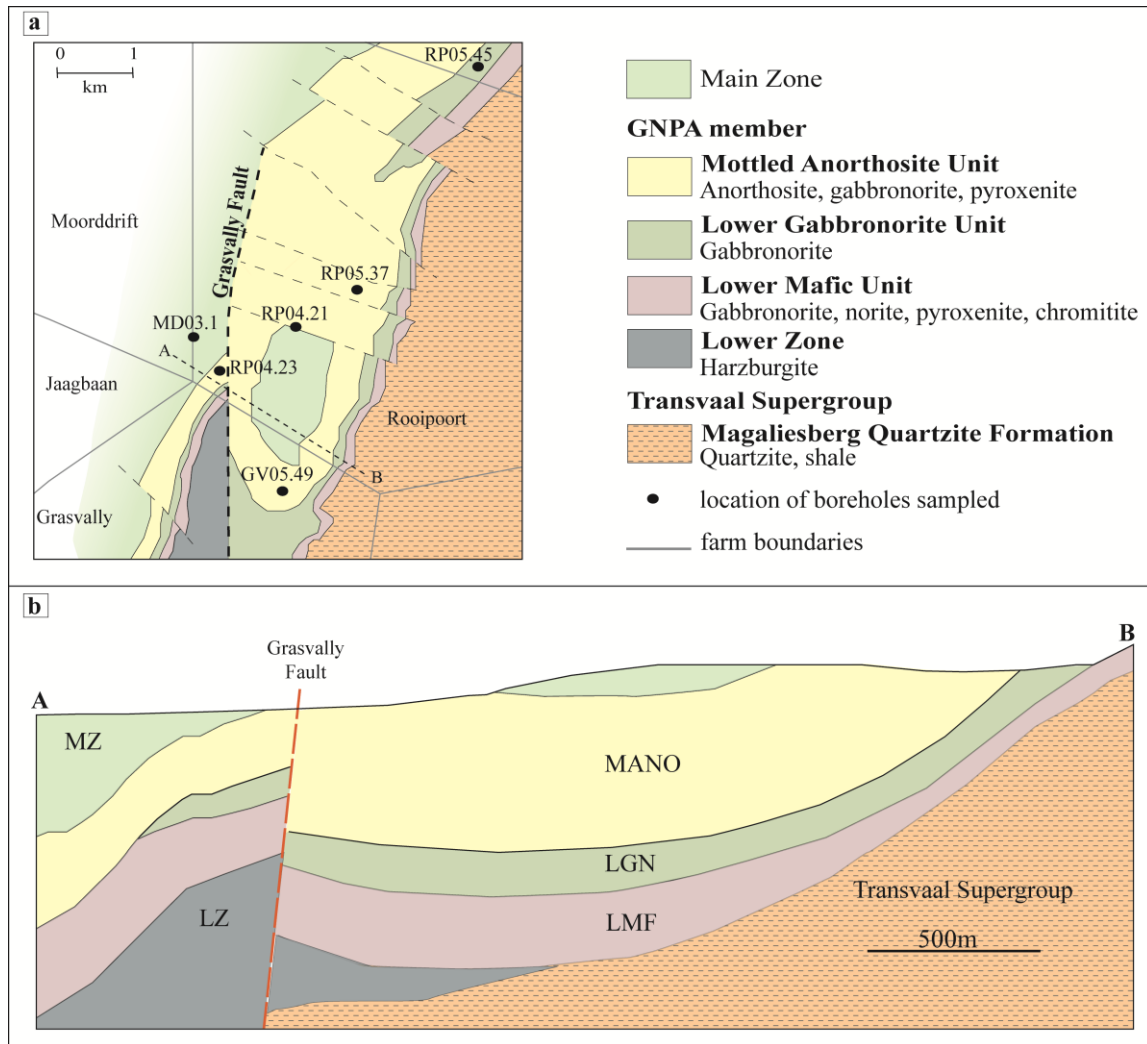


**Figure 3.2** a) Map showing the geology of the GNPA member, on the farms Rooipoort, Grasvally, Moorddrift and Jaagbaan, b) cross section with the same horizontal and vertical scales through Rooipoort, showing the outcrop pattern of the Main Zone (MZ), Mottled Anorthosite Unit (MANO), Lower Gabbronorite Unit (LGN), Lower Mafic Unit (LMF) and the Lower Zone (LZ). Adapted from Maier et al. (2008).

At present the relationship of the GNPA member with the rest of the Bushveld Complex remains poorly constrained and controversial (von Gruenewaldt et al. 1989; McDonald et al. 2005; Maier et al. 2008; van der Merwe 2008; McDonald and Holwell 2011). The GNPA member is assumed by numerous authors (Hulbert 1983; Maier et al. 2008; van der Merwe 2008) to correlate with the Upper Critical Zone of the eastern and western limbs with the two chromitites believed to directly correspond to the Merensky Reef and UG2 chromitite. In addition it has also been proposed that the GNPA member represents a lateral facies of the Platreef with the two bodies suggested to merge at the Ysterberg–Planknek Fault (van der Merwe 2008). These correlations however are primarily based on the presence of PGE grade and vague lithological associations. In contrast, McDonald et al. (2005) suggested that the northern limb ore-bodies are distinct from the Upper Critical Zone and propose

they resulted from the mixing of Lower and Main Zone magmas. The viability of this theory has been questioned as evidence exists to suggest that the Lower Zone cumulates were consolidated, significantly cooled and tilted prior to emplacement of a later magma (van der Merwe 1978; Kinnaird et al. 2005). The relationship (if any) between the northern limb and the Upper Critical Zone and also the GNPA member and the Platreef currently remains unclear.

### 3.4 Samples and Methods

Samples have been obtained from six boreholes drilled by Caledonia Mining Corporation on the farms Rooipoort, Grasvally and Moorddrift (Fig. 3.1) where the GNPA member overlies Lower Zone and metasedimentary quartzites. The location of all these boreholes is shown in Figure 3.2a. Stratigraphic logs of boreholes RP04.23 and RP05.45 are provided in Figure 3.3 as representative sections from the eastern and western parts of the area. These logs also highlight mineralized zones identified by the presence of visible BMS. The depths in Figure 3.3 reflect borehole depth in metres and not true thickness as boreholes were drilled vertically. Within the Rooipoort area dips vary from 5 to 30° with the variation largely due to the presence of a syncline directly adjacent to the Grasvally Fault. Steeper values correspond to the eastern limb of the syncline and to the west of the Grasvally Fault (Fig. 3.2b).

In total, 52 polished thin sections were analysed under transmitted and reflected light microscopy. All the samples highlighted in Figure 3.3 were examined in thin section. The additional 9 samples analysed were obtained from a number of other boreholes (Fig. 3.2) and are representative of the MANO. Mineral identification of the sulfide occurrences was performed at the University of Leicester using a Hitachi S-3600N Environmental Scanning Electron Microscope, coupled to an Oxford Instruments INCA 350 energy dispersive X-ray analysis system. Overall 34 sections were examined on the scanning electron microscope.

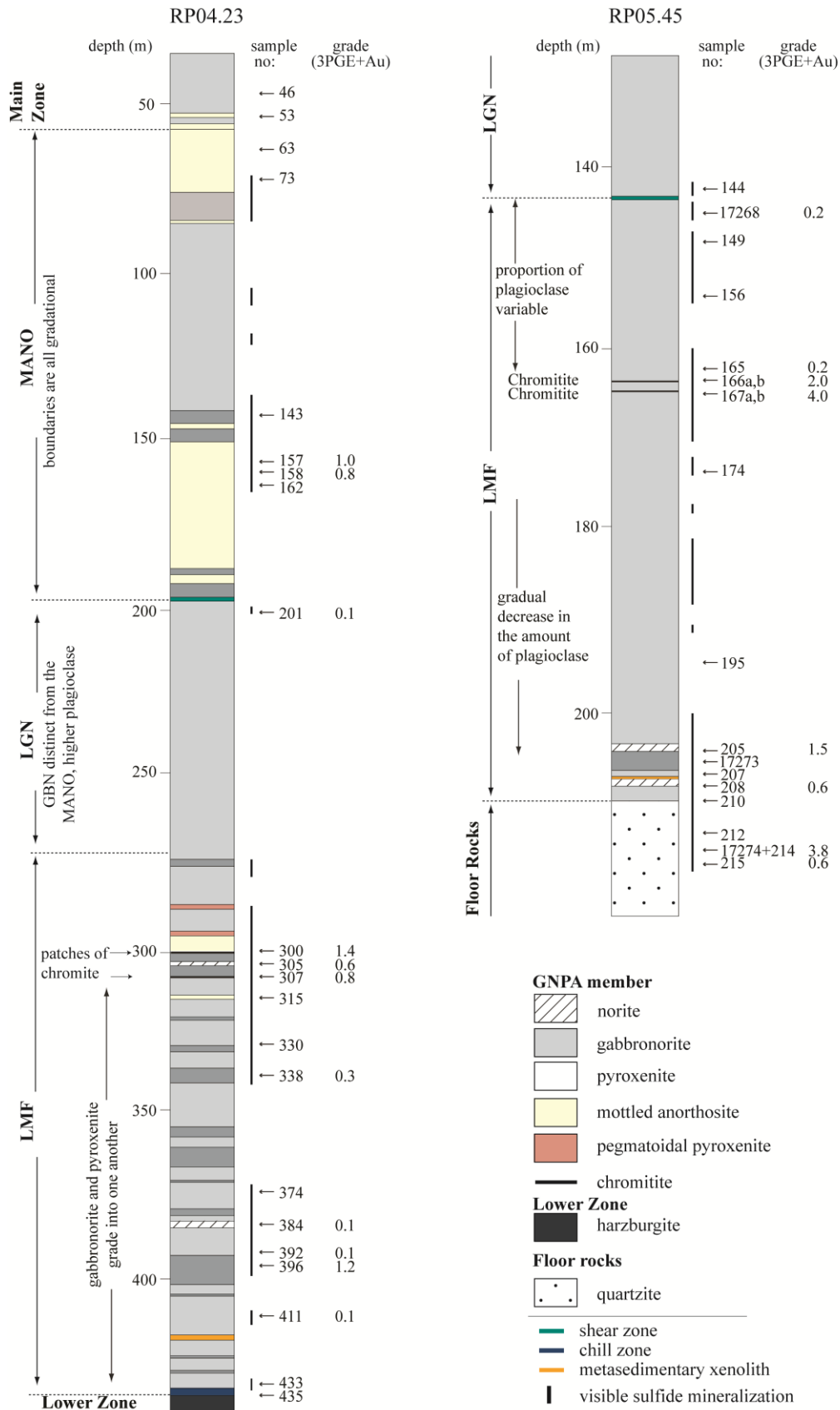


Figure 3.3 Stratigraphic logs of boreholes RP05.45 and RP04.23, showing the position of samples and zones of visible sulfide mineralization and indication of PGE grades.

### 3.5 Petrology

Rock names have mostly been assigned using the IUGS (Streckeisen) scheme and are distinguished typically by the modal percentage of plagioclase, orthopyroxene and clinopyroxene. Under the IUGS classification a rock containing >10 modal % plagioclase and < 90 modal % orthopyroxene would be termed a norite. However, in keeping with Bushveld nomenclature, if the plagioclase is intercumulus to the orthopyroxene, the rock is classified as a feldspathic pyroxenite. Where plagioclase or pyroxenes total > 90% of the modal mineralogy the rock is referred to as an anorthosite or pyroxenite, respectively. The term pegmatoidal is used when grains are interlocking and >2 cm in diameter.

#### 3.5.1 Footwall lithologies

##### 3.5.1.1 *Transvaal Supergroup*

To the east of the Grasvally Fault quartzites from the Magaliesberg Quartzite Formation directly underlie the GNPA member. Calc-silicate xenoliths are also occasionally observed between the contact of the LMF with floor quartzites and Lower Zone harzburgites. The fine- to medium-grained quartzites consist of poorly sorted and poorly rounded grains which have a high sphericity (Fig. 3.4a). Individual quartz grains have irregular and embayed edges (Fig. 3.4a) and are generally separated by a very fine matrix. A coarser plagioclase-rich matrix containing secondary chlorite is also developed but appears to be confined to thin, inconsistent layers occurring in association with the sulfide bearing zones. Coarse-grained amphibole is found in association with interstitial sulfides.

##### 3.5.1.2 *Bushveld Complex Lower Zone*

West of the Grasvally Fault, in the south-west of Rooipoort and in the north-west of Grasvally, Lower Zone harzburgites underlie the GNPA member. In this area, the Lower Zone reaches a minimum thickness of 1600 m, comprising 37 cyclic units (Hulbert 1983) which range from <10 to 140 m in thickness. Detailed petrographical descriptions of the entire Lower Zone unit are provided in Hulbert and von Gruenewaldt (1982), Hulbert (1983), Hulbert and von Gruenewaldt (1985) and von Gruenewaldt et al. (1989). The Lower Zone cumulates in contact with the GNPA member consist of serpentinised, poikilitic harzburgites which contain olivine-chromite cumulates with minor orthopyroxene and secondary chlorite (Fig. 3.4b). The harzburgites are interlayered with orthopyroxenites (Verbeek and Lomborg 2005). These rocks equate to Hulbert's (1983) uppermost Lower Zone division, the Moorddrift harzburgite-pyroxenite subzone.

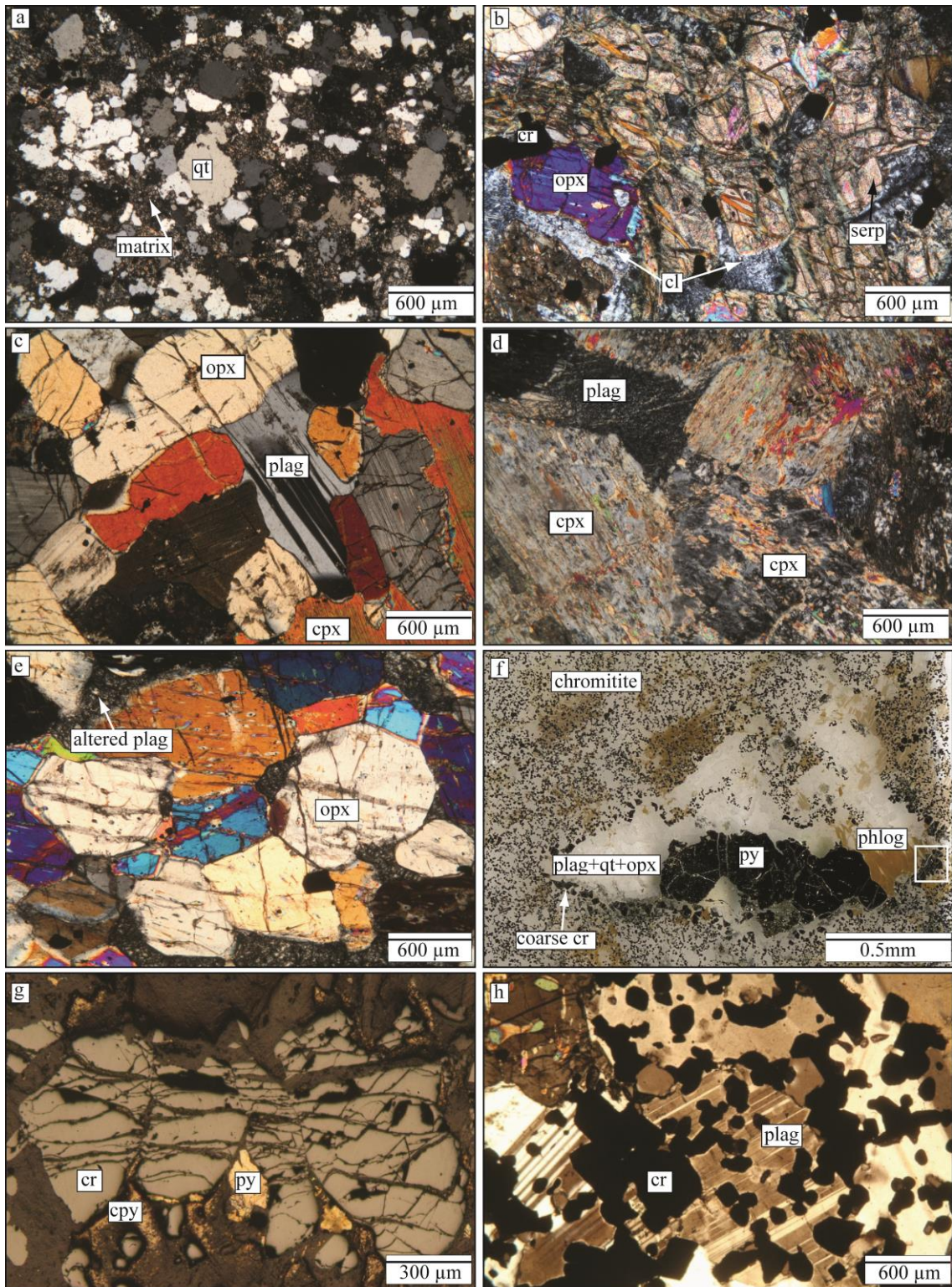


**Figure 3.4** Thin section photographs of some of the petrographical relationships within the LMF and footwall lithologies; f represents a scan of a thin section, and g is taken in reflected light, all others are in cross-polarised light. a) Footwall quartzites containing poorly sorted quartz (qt) grains and a fine-grained matrix; b) Lower Zone harzburgite containing serpentinised (serp) cumulus olivine, with secondary chlorite (cl), orthopyroxene (opx) and minor chromite (cr); c) gabbronorite with cumulus orthopyroxene and intercumulus plagioclase (plag) and clinopyroxene (cpx); d) clinopyroxenite with intercumulus plagioclase; e) LMF-Lower Zone contact represented by a pyroxenite chill zone. Orthopyroxene forms the cumulus phase. Granoblastic texture is developed; f) chromitite from east of the Grasvally Fault showing the pyrite (py) bearing chromite free pockets which are rimmed by coarse chromite grains (boxed). The pyrite bleb is surrounded by cumulus plagioclase with minor quartz, orthopyroxene and phlogopite (phlog); g) expanded

view of box highlighted in f showing heavily fractured, coarse chromite grains with minor pyrite and chalcopyrite (cpy); h) chromitite from west of the Grasvally Fault showing the euhedral to anhedral nature of the chromite grains.

### 3.5.2 GNPA member lithologies

#### 3.5.2.1 Lower Mafic Unit (LMF)

The presence of a fine-grained chilled margin at the base of the LMF regardless of underlying lithology (Hulbert 1983; de Klerk 2005) indicates that the Lower Zone cumulates cooled significantly prior to the emplacement of the GNPA member. The chilled margins range in thickness from a few centimetres up to 20m. Where the LMF is in contact with Lower Zone harzburgites, a granoblastic texture is developed within the orthopyroxenite chilled zone (Fig. 3.4d) which contains minor euhedral chromite. Although the cumulus orthopyroxene crystals are not altered they exhibit rounded and embayed margins. The chill zone developed over the quartzites is generally thicker, heavily altered and hosted typically by a gabbronorite.

The LMF is dominated by fine- to coarse-grained mafic lithologies such as gabbronorites, (Fig. 3.4c) norites, pyroxenites (Fig. 3.4d) and feldspathic pyroxenites. Pegmatitic occurrences are relatively rare and are restricted to pyroxenites and feldspathic pyroxenites. The LMF is characterised by orthopyroxene-clinopyroxene, orthopyroxene-clinopyroxene-chromite, clinopyroxene and orthopyroxene cumulates (Hulbert 1983; McDonald et al. 2005). Plagioclase bearing cumulates are also present but are less common. Throughout the unit, clinopyroxene is ubiquitous forming >10–30 modal %. The association of cumulus clinopyroxene with chromite and the presence of orthopyroxene-clinopyroxene-chromite cumulates originally identified by Hulbert (1983) are features unique to the GNPA member.

Although mottled anorthosites are rare in the LMF, within borehole RP04.23 approximately 20 cm below the LMF–LGN contact the upper chromitite is overlain by an anorthosite (Fig. 3.3) that grades into the overlying pegmatitic feldspathic pyroxenite and the underlying chromite-bearing pyroxenite. Granitic dykes and <10 cm to >1 m thick calc-silicate xenoliths are common throughout the LMF. Minor chilled margins (1–2 cm thick) are frequently developed around calc-silicate xenoliths.

The LMF is characterised throughout Grasvally and Rooipoort by the development of two laterally continuous PGE- and BMS-bearing chromitites that are consistently present within the upper LMF and have been observed over 100 m from the basal contact on Rooipoort. In contrast, on Grasvally Hulbert (1983) found the lower chromitite to occur near to the base of the LMF. The chromitites developed east and west of the Grasvally Fault are texturally and mineralogically distinct and thus will be discussed in detail separately. The chromitites to the east of the fault are separated by up to 1 m of gabbronorites, are sulfide-bearing (5–10 modal % and up to 1 wt% S), and range in thickness from 0.2–1 m. Chromite forms approximately 60 modal % with intercumulus plagioclase (30 modal %), clinopyroxene and orthopyroxene (<10 modal %). Chromite grains have not amalgamated to form large aggregations and are small (0.1 to 0.3 mm) and euhedral. The corners of the chromite grains are often seen to be slightly rounded. Phlogopite and quartz are relatively common within these chromitites (Fig. 3.4f). Sulfides are generally disseminated in nature and interstitial to the chromite, however polyphase blebs >1 cm in length are also common (Fig. 3.4f). No sulfides were found as inclusions within chromite grains.

The chromitites to the east of the Grasvally Fault contain irregular-shaped chromite free areas or pockets that also host the majority of the larger sulfide blebs (>1 cm; Fig. 3.4f). These pockets are coarser than the surrounding chromitite and contain heavily altered cumulus plagioclase, minor, less altered orthopyroxene and secondary silicates, primarily secondary chlorite, tremolite and actinolite. Accessory quartz and phlogopite are spatially related to sulfides and typically surround large sulfide blebs which are situated at the base of the chromite-poor regions, juxtaposed to cumulus chromite (Fig. 3.4f). It is currently unclear what these chromite-poor regions represent, with plausible possibilities including either micro-xenoliths or small pockets of trapped melt containing sulfide droplets. Contacts between chromitites and sulfide-rich, chromite-free regions are characterised by texturally distinct chromite grains that are relatively large, heavily fractured and anhedral (Fig. 3.4g). These unique shaped grains could be the result of the *in situ* reaction of cumulus chromite crystals with silicates and an interstitial liquid as described in Henderson and Suddaby (1971).

The two chromitites to the west of the Grasvally Fault are considerably thinner than those to the east of the fault. The chromitites range in thickness from 2–5 cm and are separated by norite, gabbronorite and pyroxenite ranging between 4 cm to 7 m in thickness. These

chromitites appear patchy and disseminated in nature with chromite forming only 25–45 modal %, and are also significantly poorer in sulfide (<1 modal % and <0.3 wt% S). The chromitites are characterised by chromite-clinopyroxene-plagioclase cumulates, with relatively coarse cumulus clinopyroxene constituting approximately 25–30 modal % of the rock. The clinopyroxene crystals are generally devoid of any chromite. Although the chromite is occasionally observed as small (0.3 to 0.4 mm), individual euhedral grains the majority exist as anhedral, polygonal aggregates (Fig. 3.4h). Both phlogopite and quartz are completely absent from these chromitites.

#### 3.5.2.2 *Lower Gabbronorite Unit (LGN)*

The LGN consists predominantly of homogenous, fine- to medium-grained gabbronorites which contain variable proportions of cumulus plagioclase (Fig. 3.5a). Petrographically these rocks appear comparable to those typical of the Main Zone. Pyroxenitic xenoliths derived from the MANO and LMF with occasional sheared contacts are common. The upper and lower contacts of this unit vary considerably, with chilled zones up to 8 cm thick, gradational and sheared contacts all observed. On the basis of the uniform nature of this unit in conjunction with the presence of occasional chilled margins, de Klerk (2005) suggested that it represents a sill of Main Zone rocks which preferentially intruded along the original LMF-MANO contact. The LGN is generally sulfide-free, barring rare occurrences near the upper and lower contacts.

#### 3.5.2.3 *Mottled Anorthosite Unit (MANO)*

The MANO is most readily distinguished from the underlying LGN and LMF by the marked increase in the proportion of plagioclase cumulates present and the dominance of mottled and spotted anorthosites (Fig. 3.5b). Clinopyroxene typically forms less than 10 modal % in comparison to up to 30 modal % in the LMF. Cyclic units with gradational boundaries, on a scale of tens of metres, of orthopyroxenite, norite, gabbronorite and anorthosite are common within the MANO. Hulbert (1983) recognised that the basal layers of all these cyclic units consist of plagioclase-only cumulates.

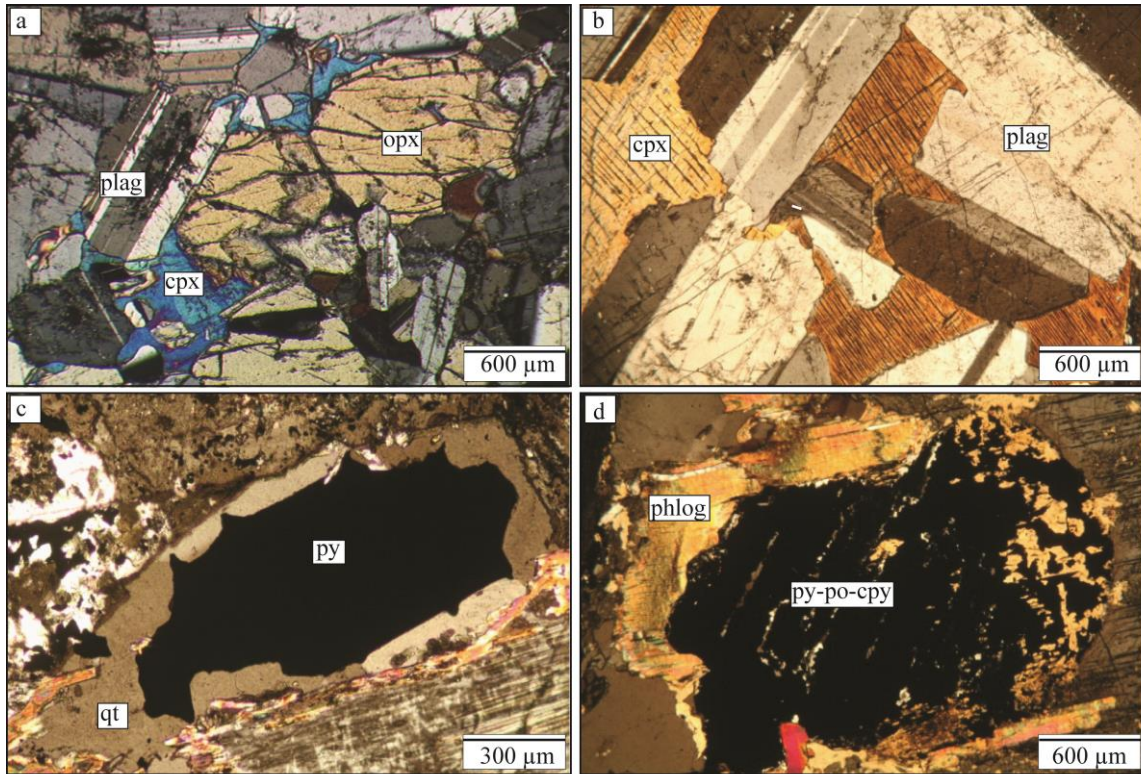


**Figure 3.5** Cross-polarised light images showing petrographical relations within the LGN and MANO a) LGN gabbronorite, with cumulus plagioclase (plag) and orthopyroxene (opx) with intercumulus clinopyroxene (cpx); b) mottled anorthosite with oikocrysts of clinopyroxene; c) association of quartz (qt) with pyrite, within the MANO; d) association of phlogopite with sulfide consisting of pyrite, pyrrhotite (po) and chalcopyrite (cpy) also in the MANO.

Within the prevailing rock type, mottles exist as large (2–10 cm in diameter) oikocrysts of orthopyroxene and occasionally clinopyroxene, whereas spots of orthopyroxene and clinopyroxene typically range from <1–2 cm. Where BMS and PGE mineralization is developed, quartz is often present within the host lithologies. Quartz occurs either as an interstitial phase that often surrounds and is closely associated with the sulfides (Fig. 3.5c) or veins through the larger sulfides. In addition, phlogopite also constitutes a minor phase which is also preferentially associated with sulfides (Fig. 3.5d). An anomalous feature of the MANO, which has only been observed within borehole MD03.1 (Fig. 3.2) <5 m from the MANO-LGN contact, is the association of accessory chromite with rare occurrences of pegmatoidal orthopyroxenite. Shear zones and PGE-poor quartz veins contain zones of abundant sulfides (around 1 cm thick) comprising chalcopyrite, pentlandite and galena. Within the shear zones the original mineralogy has been completely replaced by very fine secondary silicates and quartz which constitutes >50 modal %.

#### 3.5.2.4 *Main Zone*

The Main Zone south of Mokopane is characterised by an 1120 m sequence of gabbro and gabbro with three to four mottled anorthosite layers (Hulbert 1983; van der Merwe 2008). In summary the Main Zone constitutes an alternating sequence of pigeonite-free and pigeonite-bearing gabbroic rock, with the crystallization order plagioclase, orthopyroxene, clinopyroxene (Hulbert 1983). The gabbros are comparable to those of the LGN shown in Figure 3.5a. On Grasvally, Hulbert (1983) noted that the contact between the Main Zone and MANO is distinguished by a chilled margin. Where the Platreef is developed to the north of the Ysterberg–Planknek Fault, a chilled margin is developed at the base of the Main Zone rocks (Holwell et al. 2005; Weise et al. 2008). In contrast, on Rooipoort in borehole RP04.23 (Fig. 3.2) the contact with the GNPA member is characterised by a small shear zone approximately 12 cm in thickness which separates Main Zone gabbros from mottled anorthosites typical of the MANO. Furthermore, on Moorddrift although a sharp transition exists between leuconorites of the Main Zone and the MANO mottled anorthosites there is no evidence of a chilled contact.

### **3.6 Platinum–group element mineralization**

Initial results show that throughout the GNPA member, a strong correlation exists between PGE and Ni, Cu and S, thus high Ni and Cu values are generally indicative of high PGE grades. Throughout the Rooipoort area, a positive correlation between both Ni and Cu and S and Cu is evident which was also noted by Maier et al. (2008). Platinum–group element and BMS mineralization, identified by visible sulfide, is typically confined to three to five zones that range in thickness from a few metres to  $\geq 50$  m (Fig. 3.3) and is hosted within all rock types, including chromitites. Mineralization also extends for several metres into the footwall quartzites to the east of the Grasvally Fault. With the exception of the chromitite-hosted mineralization, these BMS and PGE enriched zones cannot be correlated with confidence along strike. Although PGE concentrations are highly variable (Fig. 3.3) the highest grades of 4 ppm (Pd+Pt+Rh+Au) are associated with the chromitites developed east of the Grasvally Fault and the floor quartzites. The GNPA member, like the Platreef, is noticeably Pd-dominant with Pt/Pd ratios typically  $< 1$ . Platinum–group mineral (PGM) assemblages are dominated by Pt arsenides, Pd bismuthotellurides, Pd tellurides, Pd antimonides and Au/Ag minerals (Smith et al. 2010, 2011b). There is a noticeable lack of PGE sulfides and alloys. In agreement with the geochemical data, the PGM are associated with the sulfides, typically occurring included within or as satellite grains around the

sulfides. The nature and distribution of PGE mineralization within the GNPA member will be addressed in more detail in a companion paper.

### 3.7 Sulfide mineralogy

The sulfide content within the GNPA member is highly variable with sulfide minerals typically constituting 3 to 10 modal % of the rock. The highest sulfide contents are found in the dense chromitites developed to the east of the Grasvally Fault, within the MANO and within floor quartzites close to the contact with the mafic rocks. The sulfide minerals present within the GNPA member are pyrrhotite (po), pentlandite (pn), chalcopyrite (cpy), pyrite (py) and millerite (mil). Three principal sulfide assemblages were found to exist throughout the GNPA member which include; 1) po–cpy–pn, 2) py–cpy–pn±po±mil and 3) py–pn±mil. These three distinct assemblages, in conjunction with textural features, enabled the sulfide occurrences to be categorised into; 1) primary textured sulfides, 2) secondary textured sulfides and 3) footwall sulfides. The latter two exhibit complex textural associations between individual sulfide phases and are characterised by the dominance of pyrite.

The sulfide textures are highly diverse and vary considerably in complexity (Fig. 3.6a-j). Textures include irregular shaped, complexly intergrown sulfides >1 cm in length; spherical, centimetre sized blebs; and intergranular and disseminated assemblages. Cross-cutting PGE-poor quartz veins up to 4 cm in thickness containing cores of massive chalcopyrite with minor pyrrhotite were also observed within the MANO.

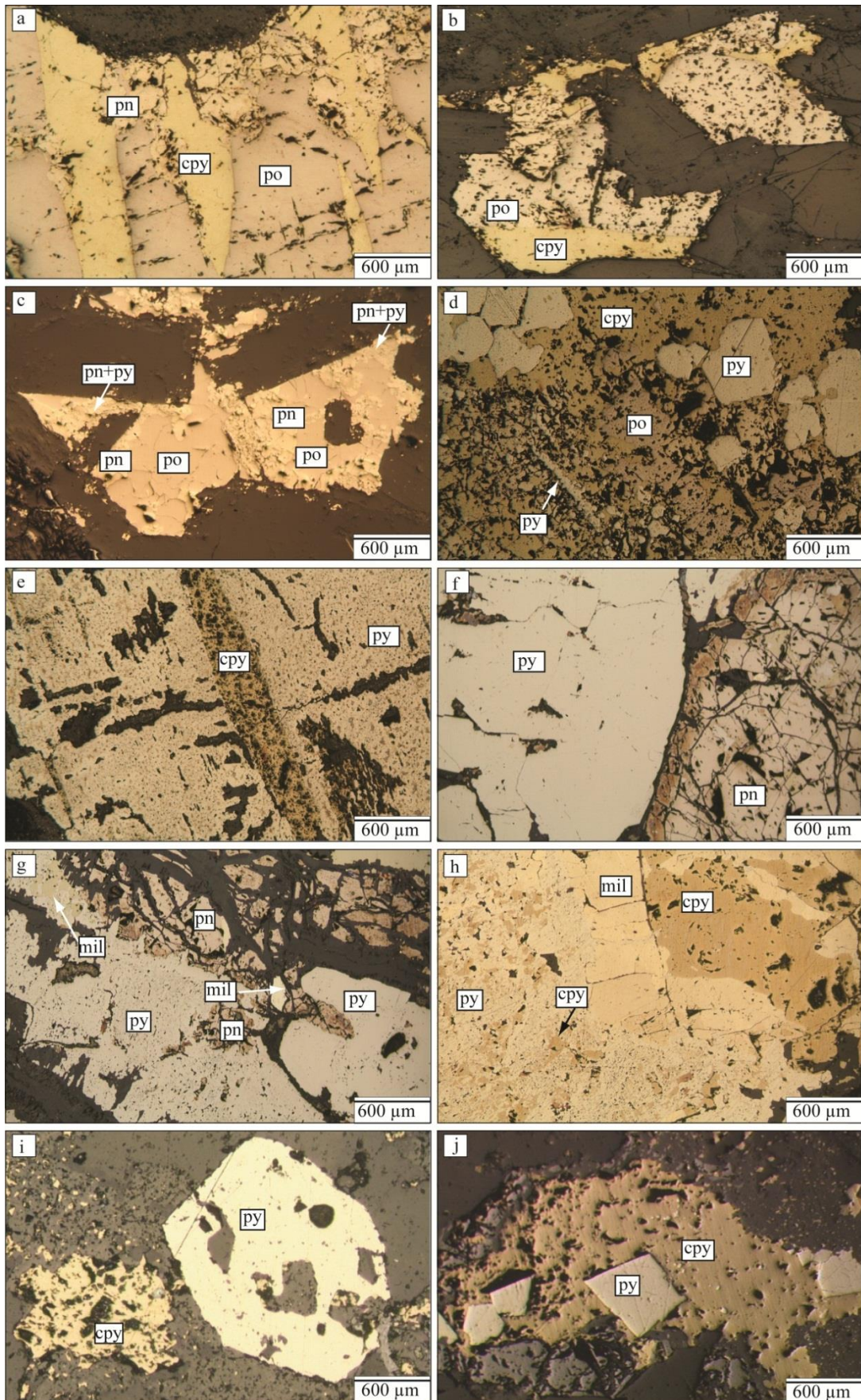


**Figure 3.6** Reflected light images of primary, secondary and footwall sulfides; a) typical primary sulfide assemblage showing exsolution flames of chalcopyrite (cpy) surrounded by pyrrhotite (po), with pentlandite (pn) confined to the margins; b) primary assemblage dominated by pyrrhotite with chalcopyrite around the

margins; c) pyrrhotite dominated assemblage although see minor replacement of pyrrhotite and pentlandite by pyrite (py); d) secondary sulfide assemblage, subhedral-anhedral pyrite overprinting and replacing chalcopyrite, pyrrhotite and pentlandite; e) secondary sulfide dominated by pyrite, with primary chalcopyrite exsolution flames preserved; f) moderately replaced sulfide, pentlandite is confined to the margins but is not being replaced by pyrite; g) advanced stages of alteration, pyrrhotite replaced entirely by pyrite and pentlandite by pyrite and millerite (mil); h) extensive alteration, pyrite and millerite replacing chalcopyrite; i) footwall quartzites containing large pyrite porphyroblast with interstitial chalcopyrite; j) footwall quartzites with euhedral pyrite overprinting interstitial chalcopyrite.

### 3.7.1 Primary textured sulfide assemblages

Primary textured sulfides are defined as those which exhibit magmatic textures and contain the assemblage po–cpy–pn. Primary textures include fractionated blebs of sulfide comprising a core of pyrrhotite with pentlandite and chalcopyrite generally confined to the margins (Fig. 3.6a and b); flame exsolution of chalcopyrite within pyrrhotite (Fig. 3.6a) and, more rarely, pentlandite within pyrrhotite; and single-phase micron to millimetre sized, disseminated interstitial grains.

To the west of the Grasvally Fault, primary sulfide textures dominate throughout the LMF and are also present in restricted layers within the MANO (Table 3.1). Within the basal section of the GNPA member, specifically below the upper chromitite, BMS enrichment is generally restricted to coarse norites, gabbro-norites and clinopyroxenites. The sulfides are characterised by intergranular polyphase blebs and large ( $\geq 1$  cm in length), spherical, fractionated blebs, which are often surrounded by coarse cumulus plagioclase and clinopyroxene crystals. In contrast, where primary sulfide assemblages are developed in the MANO, sulfides are typically more intergranular and disseminated in nature (micrometre to millimetre scale) and are hosted by pyroxenite, mottled anorthosite, pegmatoidal pyroxenite and gabbro-norite. Large primary sulfide blebs ( $\geq 1$  cm) are rarer than within the LMF. Where present, alteration of these primary sulfides by secondary silicates such as tremolite, actinolite, talc, amphibole and chlorite is minimal and confined to thin halos around the margins of the sulfides (Fig. 3.7a, Table 3.1), typical of many magmatic sulfide assemblages (e.g. Li et al. 2004; Hutchinson and Kinnaird 2005; Holwell et al. 2006; Li et al. 2008).

Sample no	unit	rock type	fresh/ altered	sulfides	replacement	assemblage	quartz	silicate alteration
<b>RP04.23</b>								
63	MANO	MA	fresh	Primary	n/a	po-pn-cpy	yes	none
157	MANO	MA	fresh	Secondary	moderate	py-pn-cpy	yes	<b>moderate</b> - confined to cpy and pn. Euhedral py overprints alteration
158	MANO	MA	fresh	Secondary	moderate	py-pn-cpy	yes	<b>moderate</b> - confined to cpy and pn
162	MANO	MA	altered	Secondary	moderate	py-pn-cpy	yes	<b>extensive</b> - relicts of cpy and pn remain
191	MANO	PYX	altered	Primary	n/a	pn-cpy		<b>moderate</b> - tremolite needles protrude pn
201	LGN	GBN	fresh	Secondary	moderate	py-pn-cpy		<b>moderate</b> - confined to margins
300	LMF	CR	fresh	Primary	n/a	po-pn-cpy		none
305	LMF	NR	fresh	Primary	n/a	po-pn-cpy		<b>minor</b> - confined to margins
307	LMF	CR	fresh	Primary	n/a	po-pn-cpy		none
315	LMF	GBN	fresh	Primary	n/a	po-pn-cpy		none
330	LMF	GBN	fresh	Primary	n/a	po-pn-cpy		<b>minor</b> - halo around interstitial sulfides
338	LMF	CPX	fresh	Primary	n/a	po-pn-cpy		none
374	LMF	GBN	fresh	Primary	n/a	po-pn-cpy		none
384	LMF	NR	fresh	Primary	n/a	po-pn-cpy	minor	<b>minor</b> - halo around interstitial sulfides
392	LMF	GBN	fresh	Primary	n/a	po-pn-cpy		<b>minor</b> - confined to margins of po blebs
396	LMF	GBN	fresh	Primary	n/a	po-pn-cpy		<b>minor</b> - confined to margins
411	LMF	GBN	fresh	Primary	n/a	po-pn-cpy		<b>minor</b> - around margins of bleb replacing po, pn and cpy
<b>RP05.45</b>								
146	LMF	GBN	altered	Secondary	advance	py-mil-cpy	minor	<b>moderate</b> - confined to margins of py bleb and within fractures
149	LMF	GBN	fresh	Secondary	advance	py-mil-cpy-pn	yes	<b>high</b> - relicts of cpy and pn remain, py not affected
156	LMF	GBN	altered	Secondary	moderate	py-cpy-pn	yes	<b>high</b> - cpy and pn within blebs
165	LMF	GBN	altered	Secondary	moderate	py-mil-cpy-pn	yes	<b>high</b> - within bleb only minor replacement of py. Cpy replaced extensively
166	LMF	CR	altered	Secondary	advance	py-mil-cpy-pn	yes	<b>high</b> - relicts of cpy and pn. No alteration of py
167	LMF	CR	fresh	Secondary	advance	py-mil-cpy-pn	yes	<b>high</b> - relicts of cpy and pn. Minor alteration of py around the margins
205	LMF	NR	altered	Secondary	advance	py-mil-cpy	yes	<b>moderate</b> - restricted to cpy
17273	LMF	PYX	fresh	Secondary	moderate	py-mil-cpy		<b>moderate</b> - restricted to cpy
208	LMF	NR	fresh	Secondary	advance	py-pn-mil	yes	<b>minor</b> - confined to margins of bleb replacing only pn
212	FLR	QTZ		Secondary	moderate	py-mil-cpy	n/a	<b>high</b> - only cpy replaced
214	FLR	QTZ		Secondary	moderate	py-mil-cpy	n/a	<b>high</b> - focussed on cpy, minor alteration of py
215	FLR	QTZ		Secondary	moderate	py	n/a	none
<b>RP04.21</b>								
448	MANO	MA	fresh	Secondary	moderate	py-mil-cpy	yes	<b>high</b> - restricted to cpy and pn
679	MANO	GBN	altered	Secondary	minor	po-cpy-pn-py	yes	<b>high</b> - cpy, pn and po, overprinting py not replaced
681	MANO	MA	fresh	Secondary	moderate	py-pn-cpy		<b>moderate</b> - confined to cpy and pn
17262	MANO	GBN	fresh	Primary	n/a	po-pn-cpy		<b>minor</b> - confined to margins
693	MANO	NR	altered	Secondary	minor	po-pn-cpy-py	yes	<b>moderate</b> - cpy and po around the margins of bleb
<b>RP05.37</b>								
69	MANO	NR	altered	Secondary	minor	py-pn-cpy-po	yes	<b>minor</b> - confined to margins
71	MANO	PYX	fresh	Secondary	minor	py-pn-cpy-po	yes	none
<b>MD03.1</b>								
552	MANO	Peg OPX	fresh	Secondary	moderate	pn-py-cpy	yes	<b>moderate</b> - protrude through cpy and pn

**Table 3-1** List of samples from the Rooipoort area highlighting the type of sulfide assemblage present and the degree of secondary replacement by pyrite and millerite. Also indicates the extent of secondary silicate replacement of the sulfides. Rock types: *MA* mottled anorthosite, *PYX* pyroxenite, *GBN* gabbronorite, *NR* norite, *CR* chromitite, *CPX* clinopyroxenite, *Peg OPX* pegmatoidal orthopyroxenite. *QTZ* quartzite. For sulfide abbreviations see Figure 3.6.

### 3.7.2 Secondary textured sulfide assemblages

Secondary textured sulfide assemblages are compositionally and texturally more complex and variable (Fig. 3.6c-h) and are dominated either by py–cpy–pn±po±mil (Fig. 3.3.c, d, e and h) or by py–pn±mil (Fig. 3.6f and g) assemblages. The secondary textures evident are due to the replacement of the primary sulfide phases, chalcopyrite, pentlandite and pyrrhotite by later pyrite and millerite at low temperatures. The degree of replacement by pyrite and millerite is variable throughout the succession (Table 3.1; Fig. 3.6c-h) thus resulting in the diverse range of secondary textures observed in these sulfides. Secondary sulfides lack the well-defined phase zonation observed in the primary occurrences and although pyrrhotite, pentlandite and chalcopyrite remain abundant, they are joined by significant quantities of pyrite and millerite (Fig. 3.6c-j).

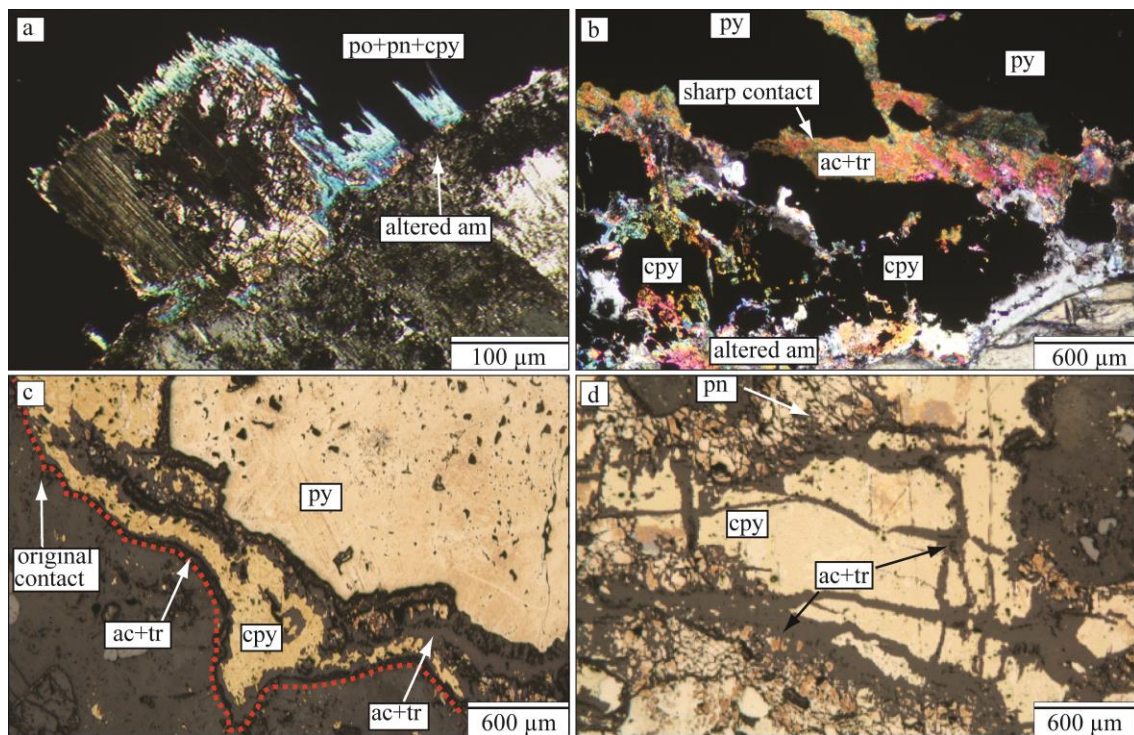


**Figure 3.7** a and b are cross-polarised light images, a) primary sulfide comprised of pyrrhotite (po), pentlandite (pn) and chalcopyrite (cpy) being replaced around the margins by altered amphibole (am); b) secondary sulfide with extensive replacement of chalcopyrite by actinolite (ac) and tremolite (tr). The pyrite (py) although in contact with secondary silicates is not being replaced by them. c and d are reflected light images c) extensive replacement of chalcopyrite by actinolite and tremolite, with the original boundary highlighted. Primary pyrrhotite has been completely replaced by pyrite; d) replacement of chalcopyrite and pentlandite by actinolite and tremolite within a secondary sulfide assemblage. Replacement of chalcopyrite is focussed along cracks.

Secondary assemblages are present as finely disseminated sulfides, intergranular polyphase sulfides and spherical to irregular shaped centimetre sized blebs. These sulfide assemblages dominate throughout the succession to the east of the Grasvally Fault and are also common west of the Grasvally Fault within much of the MANO. These sulfides are not

stratiform and are hosted by a wide range of lithologies including gabbro-norite, pyroxenites, mottled anorthosites and chromitites.

The degree of replacement of the original primary sulfides by pyrite and millerite varies considerably throughout the succession (Table 3.1) and can be considered to be a continuum from a purely magmatic assemblage such as those described in the section above to almost completely replaced sulfides. Figure 3.6 shows this progressive replacement style as preserved in various parts of the GNPA member. The sulfides which have experienced only minor replacement by low temperature pyrite retain the textures typical of primary assemblages and are still dominated by pyrrhotite (Fig. 3.6c and d). In these cases, pyrite forms only a minor phase and is seen to either replace chalcopyrite, pentlandite and pyrrhotite (Fig. 3.6c) or be confined to the margins where it overprints these primary phases (Fig. 3.6d). Millerite is not observed within these assemblages. Such textures are observed in both disseminated, interstitial assemblages and in large ( $\geq 1$  cm), irregular shaped blebs, however they are relatively uncommon and have only been observed within the MANO in boreholes RP04.21 and RP05.37 (Fig. 3.2; Table 3.1).

Sulfides which have experienced moderate replacement (Fig. 3.6e and f) are dominated by pyrite, with pyrrhotite completely replaced. Primary textures such as chalcopyrite exsolution flames and pentlandite around the margins however are preserved but to varying degrees (Fig. 3.6e). Pyrite appears to predominantly replace pyrrhotite, chalcopyrite and the surrounding plagioclase and clinopyroxene. From Figure 3.6 it is evident that pyrite is not always seen to replace or overprint the paragenetically earlier pentlandite. Millerite is also present but forms only a minor phase and occurs as symplectic intergrowths within the pyrite. Where millerite is seen to replace pentlandite, it often retains the primary blocky texture of the latter. In addition, within moderately altered assemblages a close association is apparent between phlogopite and the sulfides. Quartz also commonly shows an affiliation to the sulfides which is observed throughout both the LMF and MANO. The quartz is typically developed around the margins of the sulfides (Fig. 3.5c) as coarse grains, and as fine grains within fractures which cross cut the sulfides. Both the quartz and phlogopite appear to coexist and do not appear to replace the pyrite. These textures are common throughout both the LMF and the MANO and are mostly observed in association with large ( $>1$  cm in length) blebs.

Where sulfide replacement is the most advanced (Fig. 3.6g and h), pre-existing primary textures, such as the chalcopyrite exsolution flames, are completely overprinted. These

sulfides are texturally the most complex and are overwhelmingly dominated by anhedral and euhedral pyrite that extensively replaced chalcopyrite, pyrrhotite and pentlandite (Fig. 3.6g and h). All these phases, including millerite, are observed throughout the pyrite as symplectic intergrowths. Quartz and phlogopite are spatially related to sulfide occurrences and often completely encase interstitial secondary sulfides (Fig. 3.5c). Magnetite and ilmenite are more common in areas where alteration has been extensive and typically exist along silicate-sulfide boundaries.

These textural observations are consistent with the replacement of pyrrhotite, chalcopyrite and pentlandite by pyrite and also pentlandite by millerite. Secondary silicate alteration is far more extensive than within primary sulfide assemblages and is not systematically related to the degree of sulfide replacement (Table 3.1). Within these secondary assemblages silicate alteration is generally restricted to the remnants of the primary chalcopyrite and pentlandite (Fig. 3.7b, c and d; Table 3.1). With increasing silicate alteration chalcopyrite and pentlandite become smaller and eventually only small relicts encased by actinolite, tremolite and chlorite exist. The original grain boundaries of these sulfide phases are often preserved as shown in Figure 3.7c. Where alteration of the secondary pyrite and millerite is present it is limited to around the margins. Within most assemblages however, pyrite appears to be in textural equilibrium with the secondary silicates (Fig. 3.7b) suggesting silicate alteration occurred simultaneously with the crystallization of pyrite. The close association of phlogopite and quartz with secondary sulfides suggests these phases also precipitated concurrently with pyrite and millerite.

In general, secondary textured sulfides are characterised by several key features, which include; (1) the presence of pyrite and millerite (2) affiliation of phlogopite with disseminated and blebby sulfides most apparent in the chromitites, and (3) also the association of intercumulus quartz with intergranular and blebby sulfides. In terms of PGE grade there is no notable difference between primary and secondary sulfides.

### **3.7.3 Footwall sulfide assemblages**

Within the Magaliesberg Quartzite Formation directly underlying the GNPA member in the eastern part of Grasvally, two texturally distinct sulfide assemblages are present. Neither assemblage is confined to veins, or restricted to clear horizons, but instead the mineralization appears disseminated in nature.

The most dominant assemblage is comprised only of pyrite. The pyrite is texturally distinct (Fig. 3.6i) and appears as polyphase aggregates or subhedral to irregular blebs which range in size from around 1 mm to >2 cm. The pyrite blebs are texturally unusual as they encompass resorbed quartz grains and are also characterised by straight boundaries (Fig. 3.6i). Small euhedral pyrite grains are observed disseminated within the quartzite where large blebs exist and the pyrite appears to be replacing/dissolving the quartz grains. Secondary silicates are not observed in association with this assemblage and the pyrite has not undergone any replacement. This assemblage also contains very minor chalcopyrite which is present either as tiny inclusions within the pyrite in association with very fine quartz or along fractures within the sulfide. The unusual texture of this pyrite is unique to the footwall rocks and has not been observed elsewhere in the GNPA member.

The second sulfide assemblage present in the footwall rocks is characterised by disseminated, intergranular sulfides which are comprised of either intergrown, anhedral pyrite with chalcopyrite and minor millerite or chalcopyrite which appears to be overprinted or surrounded by small, euhedral pyrite grains (Fig. 3.6i and j). Secondary chlorite appears to be developed in association with these sulfide assemblages. Within this assemblage the chalcopyrite is being replaced around the margins mostly by very small euhedral pyrite grains and minor millerite, with the original grain boundaries frequently preserved. The replacement textures imply that the pyrite formed after the chalcopyrite. Secondary silicates are also seen to replace chalcopyrite to varying degrees (Table 3.1). In contrast, the pyrite appears to have seen only minor replacement by secondary silicates.

The textural features potentially highlight three main sulfide phases developed in the footwall which include; 1) polyphase aggregates of pyrite, 2) relicts of primary intergranular chalcopyrite 3) late-stage, low temperature pyrite and millerite.

## **3.8 Discussion**

### **3.8.1 Regional context of the GNPA member**

McDonald et al. (2005) were the first to challenge and question the viability of the long held notion that the GNPA member corresponds to the Upper Critical Zone of the eastern and western limbs (e.g. van der Merwe 1976; 1978; Hulbert 1983). This correlation is based on the assumption that the zones of mineralization within the LMF and MANO correlate with the UG-2 chromitite and the Merensky Reef, even though to date very few demonstrable similarities have been documented (Maier et al. 2008). McDonald et al.

(2005) presented geochemical and mineralogical data highlighting the vast distinctions between the GNPA member and the Upper Critical Zone. Observations from this study reiterate some of these mineralogical differences and also demonstrate some fundamental differences in the style of PGE and BMS mineralization between the GNPA member and the Critical Zone.

This study has highlighted that mineralization in the GNPA member is not lithologically bounded and is distributed heterogeneously throughout the entire unit, unlike the Upper Critical Zone where mineralization is confined to discrete layers usually associated with chromitites. Furthermore, in contrast to the generally sulfide poor (<0.1 wt%) chromitites of the Upper Critical Zone where orthopyroxene prevails (Barnes and Maier 2002a), the sulfide rich (1 wt% S) GNPA chromitites are characterised by unique chromite-clinopyroxene-plagioclase cumulates, which have not been documented elsewhere in the complex. For these reasons we do not believe the chromitites of the Upper Critical Zone in the east and western limbs of the Bushveld can be correlated with those observed in the LMF of the GNPA member. Furthermore, throughout the GNPA member clinopyroxene is ubiquitous at between <10 to <30 modal % even where chromite is present, whereas in the Critical Zone it forms <10 modal % (Cameron 1982; Maier and Barnes 1998). In terms of PGE mineralization, the GNPA member contains notably lower PGE grades of <4 ppm (3PGE+Au) and Pt/Pd ratios (<1) than typical of the Upper Critical Zone where PGE grades range from 4 to 6 ppm (3PGE+Au; McDonald and Holwell 2011). To fully constrain the context of the GNPA member with the rest of the Bushveld Complex a detailed comparison of the PGE geochemistry and mineralogy is required and will be addressed in a companion paper (Smith et al. 2014; Chapter 4).

### **3.8.2 Sulfide mineralogy and distribution**

The most significant finding of this study is the extensive and widespread replacement style of primary magmatic sulfides to varying extents by low temperature pyrite and millerite; a feature which has not been observed elsewhere in the Bushveld Complex PGE deposits. The sulfide assemblage po-cpy-pn, and the textural relations between these three phases are considered typical of magmatic Ni-Cu-PGE deposits (Naldrett 2004). The sulfides termed primary are thus considered to represent the direct cooling product of a fractionating sulfide liquid, with pyrrhotite and pentlandite exsolved from high temperature monosulfide solid solution (mss) which crystallises at around 1000°C, and chalcopyrite exsolved from intermediate solid solution (iss) which forms at 900°C (Holwell and

McDonald 2010). This sulfide assemblage is thus interpreted to be purely magmatic in origin and so represent an initial primary style of mineralization within the GNPA member.

We propose that the secondary assemblages py–cpy–pn±po±mil and py–pn±mil formed by low temperature replacement of the primary sulfides, potentially related to late-stage magmatic fluids. The textural variability of these sulfides is resultant from the different degrees of alteration the primary assemblage experienced through the continuum illustrated in Figure 3.6.

Experimental studies carried out by Craig (1983) have also shown that the assemblage py–pn–mil, typical of the secondary sulfides throughout the GNPA member, is only stable at temperatures below 200°C. This therefore confirms that these texturally complex assemblages must be derived through low temperature alteration. This notion is further supported by the coexistence of pyrite and pentlandite which is commonly observed throughout the GNPA succession. Experimental work has shown that these two phases should not be able to co-exist above 212–230°C (Naldrett and Kullerud 1968; Naldrett et al. 1968; Craig 1983; Misra and Fleet 1984), therefore one of the phases must have crystallised at higher temperatures. The dominance of pentlandite within the primary assemblages and its coarse nature suggests that it exsolved from mss at high temperatures (from 650–230°C). Therefore the pyrite must have only been capable of crystallising at temperatures below 230°C (c.f. Dare et al. 2011). In addition the lack of zoning within the pyrite, which has been attributed as a primary texture (Dare et al. 2011), further supports that the pyrite present within the GNPA member is not of high temperature, magmatic origin.

Although not recorded within the Bushveld Complex, identical secondary sulfide assemblages have been documented within the PGE-bearing Lac des Iles Complex, Ontario (Djon and Barnes 2012), where such assemblages were generated through interaction with late magmatic fluids and the loss of Fe to actinolite and chlorite at temperatures below 213°C. Thus, it is plausible to suggest that within the GNPA member precipitation of pyrite and millerite occurred at comparable temperatures of around 200°C, and that the replacement of the sulfides was most likely concurrent with alteration by actinolite and chlorite. Furthermore, the close association of the secondary silicates actinolite, talc, tremolite, chlorite and serpentine with the secondary sulfides throughout the GNPA member suggests that both silicate and sulfide replacement occurred in relation to the same low temperature alteration event. The presence of sharp contacts between the

pyrite and altered amphiboles and the observed restriction of silicate replacement to the relicts of the primary chalcopyrite and pentlandite, further supports this notion. These observations also strongly suggest that the pyrite and secondary silicates crystallised concurrently.

An intriguing finding from this study is that although sulfide mineralization is distributed throughout the GNPA member in a discontinuous manner, a pattern exists in the distribution of secondary sulfides. Spatially, these secondary sulfides are more abundant to the east of the Grasvally Fault, where quartzites directly underlie the GNPA member (Table 3.1). Furthermore, within this region there is an apparent decrease in the degree of alteration by pyrite upwards through the succession into the MANO (Table 3.1), with only partial replacement of pyrrhotite by pyrite observed. We have demonstrated throughout the discussion that these sulfides were derived through low temperature alteration. The greater abundance of these sulfides and the higher degree of pyrite replacement towards the base of the GNPA member (where underlain by quartzites) strongly suggests a footwall influence over the development of these secondary sulfides. If this alteration occurred in response to the circulation of fluids then the spatial distribution of these sulfides is consistent with either; 1) the fluid being derived from the floor rocks through metamorphism or 2) the quartzite-LMF contact acting as a preferential fluid conduit.

It is important to highlight that although low temperature alteration within the northern limb of the Bushveld Complex is widespread, within the Platreef it has resulted only in the replacement of sulfides by secondary silicates (Armitage et al. 2002; Hutchinson and Kinnaird 2005; Holwell et al. 2006; Holwell and McDonald 2007; Yudovskaya et al. 2011). Within the GNPA member however it has also resulted in the extensive replacement of primary sulfides by pyrite and millerite. The reasons for this distinction between the Platreef and the GNPA member are currently unclear, although may include variations in fluid composition, floor rock composition and the amount of contamination. The effect of the significant thickness differences and thus cooling regimes needs to also be considered and explored.

Within magmatic sulfide systems the association of phlogopite with sulfides is common and in the Bushveld Complex has been noted in the Merensky Reef, the Platreef and the GNPA member. Ballhaus and Stumpfl (1986) concluded that within the Merensky Reef, phlogopite pre-dated sulfide solidification and proposed that this association resulted from the development of a Cl-rich fluid derived from the sulfide melt. In contrast to the

Merensky Reef, phlogopite does not occur as inclusions with the GNPA member sulfides and textural relations imply that its formation post-dates the crystallization of primary sulfides. Within the Platreef the majority of quartz is found in association with felsic veins, whereas in the GNPA member it is closely associated with secondary sulfides. The restriction of quartz to the secondary sulfides (Table 3.1) where it encases the sulfide grains implies that it precipitated during low temperature alteration of the sulfides which was potentially initiated by the circulation of hydrothermal fluids. The timing of quartz precipitation relative to that of the secondary silicates has not been constrained, but their close association with secondary sulfides suggests they all developed at comparable times to the formation of secondary sulfides.

A paragenetic sequence for the development of sulfides and secondary silicates for the GNPA member is provided in Figure 3.8. Between 650°C and 250°C pyrrhotite and pentlandite exsolved from mss, whereas chalcopyrite exsolved at similar temperatures from iss. On further cooling to below 230°C, low temperature alteration in some areas resulted in the precipitation of pyrite and millerite, replacing the original primary assemblage to varying degrees. Textural relations imply that the precipitation of secondary silicates and quartz occurred at similar times and temperatures to the precipitation of pyrite and are thus associated with the late-stage low temperature alteration. It is thought that the sulfides present within the footwall quartzites were transported via the downward migration of an immiscible sulfide melt.

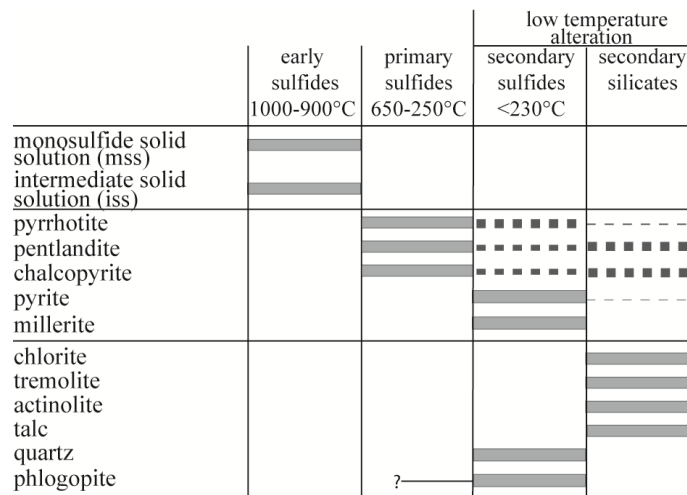


**Figure 3.8** Paragenetic sequence for sulfide and secondary silicate generation within the GNPA member. Thick, grey boxes represent phases crystallising, whereas dashed line indicates phases being replaced. Thickness of lines indicates degree of replacement, increasing with extent of replacement. Temperatures for the crystallization of mss, iss, pyrrhotite, pentlandite and chalcopyrite are taken from Holwell and McDonald (2011). Temperature estimations for the precipitation of pyrite and millerite are based on the experimental work by Naldrett and Kullerud (1968), Naldrett et al. (1968), Craig (1983) and Misra and Fleet (1984).

### 3.8.3 Implications for PGE mineralization

Throughout the GNPA member low temperature alteration has had a profound control over the mineralogy of the sulfides and this study has highlighted the possibility that late stage-low temperature hydrothermal fluids have interacted significantly with the unit. Economically, it is important to constrain the effect of fluids on the mineralogy and distribution of PGE and on ore grades throughout the GNPA member. At Turfspruit, Macalacaskop and Sandsloot, where fluids have interacted with the Platreef and metasedimentary rocks from the footwall, PGE are locally decoupled from BMS on a scale of microns to centimetres (Hutchinson and Kinnaird 2005; Kinnaird 2005; Kinnaird et al. 2005; Holwell et al. 2006). In comparison, on Rooipoort Maier et al. (2008) showed that within the GNPA member a positive correlation exists between PGE and BMS. Thus, unlike parts of the Platreef, where both the PGE mineralogy and distribution can be controlled by syn- or post-magmatic fluid activity, the GNPA member may be more comparable to the Lac des Iles Complex where low temperature alteration has changed only the mineralogy of the PGM and sulfides but had no control over the distribution of PGE. A more comprehensive study of the PGE mineralogy and geochemistry will be presented in a subsequent paper which will build on the identification of low temperature alteration in this study.

### 3.9 Conclusions

Within the northern limb of the Bushveld Complex, late-stage low temperature alteration is widespread in both the Platreef and the GNPA member however the development of secondary sulfides is restricted to the later. The initial style of BMS mineralization within the GNPA member is characterised by the primary sulfide assemblage po–pn–cpy which is magmatic in origin and represents the direct cooling product of a fractionating sulfide liquid. These phases exsolved from the high temperature monosulfide solid solution (mss) and intermediate solid solution (iss) at temperatures between 650°C and 250°C. Low temperature alteration has significantly altered much of the primary sulfide mineralogy, resulting in the development of the secondary assemblages py–cpy–pn±po±mil and py–pn±mil. Textural relations suggest pyrite and millerite crystallised at temperatures below 250°C. A close association is apparent between the secondary sulfides and the secondary silicates actinolite, tremolite and chlorite which crystallised at comparable times and thus temperatures. The greater abundance of secondary sulfides and the higher degree of pyrite and millerite replacement towards the base of the GNPA member, where underlain by

quartzites strongly suggests a footwall control over the low temperature alteration and thus the extent of the development of these secondary sulfide assemblages.

### **3.10 Acknowledgements**

The authors would like to thank Caledonia Mining Corporation and in particular Trevor Pearton, for allowing access to the drill core on the farms Rooipoort, Grasvally and Moorddrift, and giving permission to publish this work. Jennifer Smith's Ph.D. research is funded by the Natural Environment Research Council (NE/1528426/1). Constructive reviews by Judith Kinnaird and an anonymous referee helped improve the quality of the manuscript.

## Chapter Four

### Precious and base–metal geochemistry and mineralogy of the GNPA member: implications for a multistage emplacement model

#### **Chapter 4 is published within Mineralium Deposita**

Smith JW, Holwell DA, McDonald I (2014) Precious and base–metal geochemistry and mineralogy of the Grasvally Norite–Pyroxenite–Anorthosite (GNPA) member, northern Bushveld Complex, South Africa: implications for a multistage emplacement. *Mineralium Deposita*, 49:667–692.

I completed all sample collection, sample preparation, analysis using the SEM, figure production, data synthesis, data interpretation and I wrote the chapter. The authors assisted with data interpretation. Iain McDonald processed the LA-ICP-MS data and partially wrote the laser ablation technique.

## 4.1 Abstract

The Grasvally Norite–Pyroxenite–Anorthosite (GNPA) member within the northern limb of the Bushveld Complex is a mineralized, layered package of mafic cumulates developed to the south of the town of Mokopane, at a similar stratigraphic position to the Platreef. The concentration of platinum-group elements (PGE) in base metal sulfides (BMS) has been determined by laser ablation inductively coupled plasma-mass spectrometry. This data, coupled with whole rock PGE concentrations and a detailed account of the platinum-group mineralogy (PGM) provides an insight into the distribution of PGE and chalcophile elements within the GNPA member, during both primary magmatic and secondary hydrothermal alteration processes. Within the most unaltered sulfides, (containing pyrrhotite, pentlandite and chalcopyrite only), the majority of IPGE, Rh and some Pd occur in solid solution within pyrrhotite and pentlandite, with an associated Pt-As and Pd-Bi-Te dominated PGM assemblage. These observations in conjunction with the presence of good correlations between all bulk PGE and base metals throughout the GNPA member, indicates the presence and subsequent fractionation of a single PGE-rich sulfide liquid, which has not been significantly altered.

In places, the primary sulfides have been replaced to varying degrees by a low temperature assemblage of pyrite, millerite and chalcopyrite. These sulfides are associated with a PGM assemblage characterized by the presence of Pd antimonides and Pd arsenides, which are indicative of hydrothermal assemblages. The presence of appreciable quantities of IPGE, Pd and Rh within pyrite and to a lesser extent millerite, suggests these phases directly inherited PGE contents from the pyrrhotite and pentlandite that they replaced. The replacement of both the sulfides and PGM occurred *in situ*, thus preserving the originally strong spatial association between PGM and BMS, but altering the mineralogy. Precious metal geochemistry indicates that fluid redistribution of PGE is minimal with only Pd, Au and Cu being partially remobilised and decoupled from BMS. This is also indicated by the lower concentrations of Pd evident in both pyrite and millerite compared with the pentlandite being replaced.

The observations that the GNPA member was mineralized prior to intrusion of the Main Zone and that there was no local footwall control over the development of sulfide mineralization are inconsistent with genetic models involving the *in situ* development of a sulfide liquid through either depletion of an overlying magma column or *in situ* contamination of crustal S. We therefore believe that our observations are more compatible

with a multi-stage emplacement model, where pre-formed PGE-rich sulfides were emplaced into the GNPA member. Such a model explains the development and distribution of a single sulfide liquid throughout the entire 400-800 m thick succession. It is therefore envisaged that the GNPA member formed in a similar manner to its nearest analogue the Platreef. Notable differences however in PGE tenors indicate that the ore-forming process may have differed slightly within the staging chambers that supplied the Platreef and GNPA member.

## 4.2 Introduction

The Bushveld Complex, South Africa, is the world's largest repository of platinum–group elements (PGE). The Complex comprises a package of layered ultramafic and mafic cumulates named the Rustenburg Layered Suite; present in five geographically distinct limbs (Fig. 4.1) and divided into five stratigraphic units. The PGE reserves are present within three main deposits; the UG2 chromitite, the Merensky Reef and the Platreef. Within the eastern and western limbs of the intrusion, PGE mineralization is confined to thin, stratiform layers in association with sulfides or chromitites. The most important of these, the Merensky Reef and UG2 chromitite are located towards the top of the most economically important unit; the Critical Zone. Within the northern limb, Platreef mineralization is present within a 10–400 m thick basal unit, intruded as a series of sills (Kinnaird 2005) that rests directly on Palaeoproterozoic sediments and Archaean gneisses and granites and is overlain by Main Zone gabbronorites. Widespread contamination of the Platreef magma through assimilation of differing floor rocks along its strike length, largely accounts for the complexity of the deposit, which formed through the interaction of magmatic, metasomatic and hydrothermal processes (e.g. Harris and Chaumba 2001; Armitage et al. 2002; Manyeruke 2003; Hutchinson and Kinnaird 2005; Kinnaird 2005; Kinnaird et al. 2005; Manyeruke et al. 2005; Sharman-Harris et al. 2005; Holwell and McDonald 2006; Holwell et al. 2006; Holwell and McDonald 2007; Holwell et al. 2007; Hutchinson and McDonald 2008; McDonald et al. 2009; Holwell et al. 2011; Sharman et al. 2013).

The Platreef (*sensu-stricto*) is present only north of the Ysterberg-Planknek Fault (Kinnaird and McDonald 2005; Fig. 4.1), and represents a package of texturally heterogeneous and variably altered pyroxenitic lithologies which is irregularly mineralized with sulfide associated PGE, Ni and Cu (e.g. Armitage et al. 2002; Kinnaird 2005; Holwell et al. 2006; Holwell and McDonald 2006, Hutchinson and Kinnaird 2005; Hutchinson and McDonald 2008; Manyeruke et al. 2005; McDonald and Holwell 2011). To the south of Ysterberg-Planknek Fault a distinct layered package of PGE-bearing mafic cumulates termed the Grasvally Norite-Pyroxenite-Anorthosite (GNPA) member is developed (Hulbert 1983). The GNPA member is present at a similar stratigraphic position to the Platreef, being overlain by Main Zone gabbronorites and resting directly on both Lower Zone ultramafic/mafic cumulates and the Magaliesberg Quartzite Formation from the Palaeoproterozoic Transvaal Supergroup. In previous studies, the GNPA member has been assumed to correlate with the Platreef (e.g. von Gruenewaldt et al. 1989; van der Merwe,

1976; 2008; Maier et al. 2008) and possibly with the Critical Zone of the eastern and western limbs (von Gruenewaldt et al. 1989; van der Merwe 2008; Dunnett et al. 2012; Grobler et al. 2012). Since McDonald et al. (2005) challenged this proposed correlation the relationship of the GNPA member with the Platreef has been under review (see also McDonald and Holwell 2011).

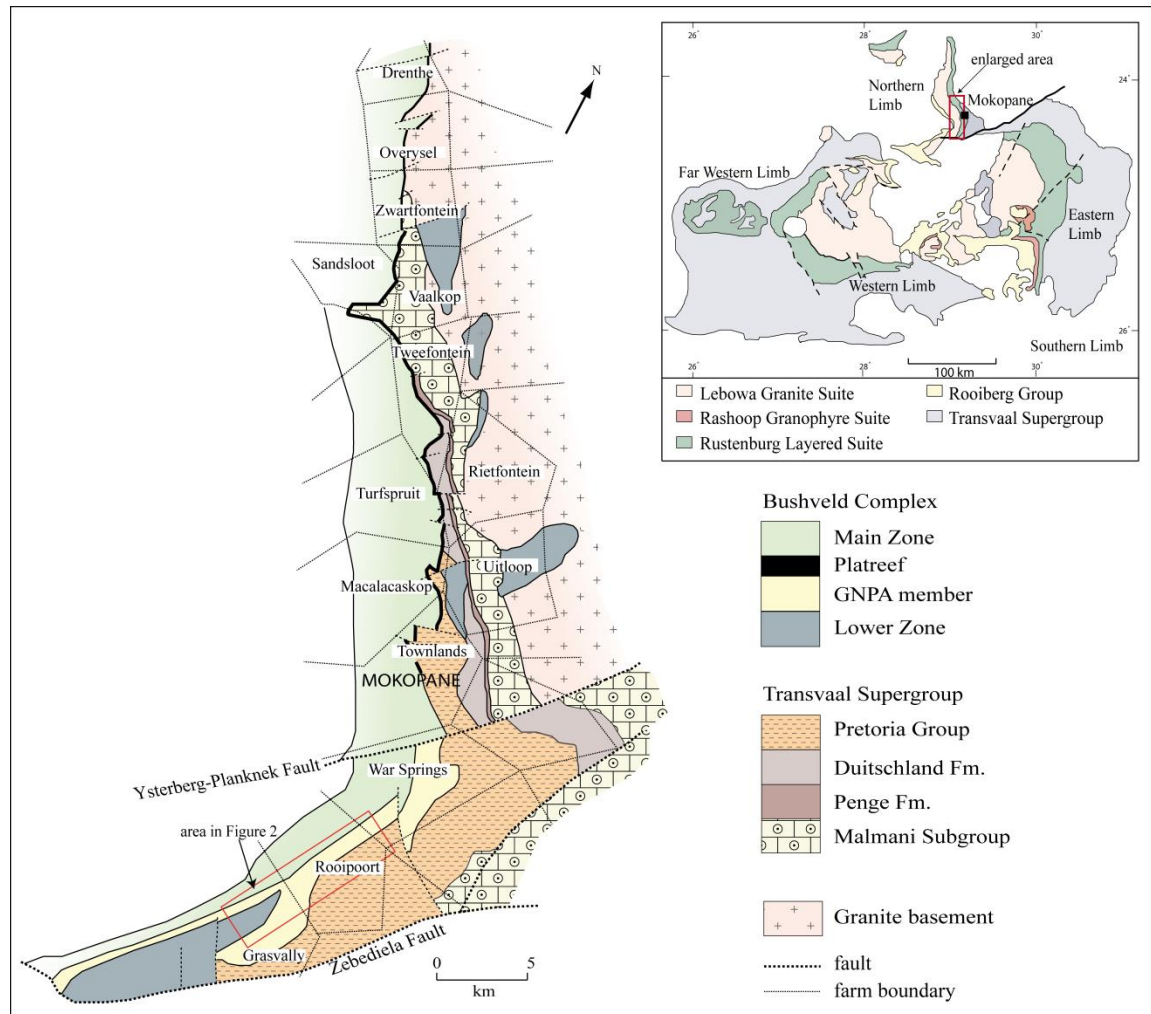


**Figure 4.1** Geological map of the northern limb of the Bushveld Complex, showing farms referred to in the text. Adapted from von Gruenewaldt et al. (1989). Inset map of the entire Bushveld Complex adapted from Eales and Cawthorn (1996).

A recent study by Smith et al. (2011; Chapter 3) concentrating on the sulfide mineralogy, concluded that the presence of two distinct sulfide assemblages reflects the involvement of both magmatic sulfide fractionation processes and low temperature fluid alteration (<230°C) in the development of sulfide mineralization within the GNPA member. At present the factors involved in ore genesis with regards to: the timing of S saturation relative to emplacement; the role of sulfides in concentrating PGE; and the effect of post-magmatic hydrothermal fluids are not well constrained.

Typically, contact-style PGE-Ni-Cu mineralization similar to that present within the GNPA member and Platreef is often attributed to the development of an immiscible sulfide liquid through in situ contamination by assimilation of crustal S (e.g. Duluth Complex; Mainwaring and Naldrett 1977; Ripley 1981; Ripley et al. 1986 and the Basal Series of the Stillwater Complex; Lambert et al. 1994; Lee 1996; McCallum 1996). Within the Platreef, it is now accepted that early contamination at depth induced S saturation, with localised contamination acting only as an ore-modifying process (Holwell et al. 2007; McDonald and Holwell 2007; Penniston-Dorland et al. 2008; Ihlenfeld and Keays 2011). The Platreef is also an example where hydrothermal fluids and contamination have had a significant influence over the resulting mineralogy and distribution of PGE (Hutchinson and Kinnaird 2005; Kinnaird 2005; Holwell and McDonald 2006; Holwell et al. 2006; Holwell and McDonald 2007; Hutchinson and McDonald 2008). The complexity of the Platreef highlights that in order to gain a full understanding of the ore genesis of any PGE-Ni-Cu deposit it is critical to assess in detail the effects of magmatic, contamination and hydrothermal processes. Considering the lesser known GNPA member, the presence of primary and secondary sulfide assemblages, strongly suggests that both magmatic and hydrothermal processes are the major factors involved in the generation and distribution of PGE and BMS mineralization. In this paper, we investigate the precise distribution and mineralogy of PGE within the GNPA member to establish: the role played by sulfide liquid in the concentration of PGE; and the effects of post-magmatic fluids on the mineralogy and distribution of PGE. We also explore the processes involved in ore genesis, with particular interest on constraining the timing of S saturation relative to emplacement, by comparing the GNPA mineralization with its nearest analogue the Platreef and more widely with the Merensky Reef (van der Merwe 1976; 1978, 2008; Hulbert 1983; Maier et al. 2008).

### **4.3 Regional Geological Setting**

The 2.06 Ga Bushveld Complex covers an area of ca. 65,000 km<sup>2</sup> and is the world's largest layered igneous intrusion. The complex comprises five limbs (Fig. 4.1): the near symmetrical western and eastern limbs; a southern limb, partially hidden by younger sediments; a heavily eroded far western limb; and a northern limb (Eales and Cawthorn 1996). The Bushveld Magmatic Province as a whole comprises the felsic volcanics of the Rooiberg Group (Twist 1985; Buchanan et al. 2002), the mafic-ultramafic layered rocks of the Rustenburg Layered Suite, the Rashedoop Granophyre Suite (Walraven 1985), the Lebowa Granite Suite (Walraven and Hattingh 1993) and a set of marginal pre- and syn-

Bushveld sills (Cawthorn et al. 1981) (Fig. 4.1). The Rustenburg Layered Suite consists of a 7–8 km thick layered package which is conventionally subdivided into five major stratigraphic zones; Marginal Zone norites, Lower Zone pyroxenites and harzburgites, Critical Zone chromitite-pyroxenite-norite cyclic units, Main Zone homogeneous gabbro-norites and Upper Zone anorthosites, ferrogabbros and magnetites. In the northern limb, the mafic succession deviates from the conventional Bushveld stratigraphy. The Platreef/GNPA member may represent the stratigraphic equivalent to the Critical Zone of the eastern and western limbs. Furthermore, Lower Zone cumulates are unusually thick (800–1600 m), compared to that in the other limbs (van der Merwe 1976).

The GNPA member, present south of the Ysterberg–Planknek Fault, comprises vari-textured gabbro-norites, norites, anorthosites, pyroxenites and a PGE-bearing chromitite. The 400–800 m thick succession differs from the pyroxenitic Platreef in that it can be subdivided into three distinct stratigraphic units (Fig. 4.2; de Klerk 2005); the Lower Mafic Unit (LMF); the Lower Gabbro-norite Unit (LGN); and the Mottled Anorthosite Unit (MANO). The LMF is distinguished from the homogeneous gabbro-norites of the LGN by an increase in melanocratic lithologies, the development of two chromitite layers and elevated bulk Cr values. The MANO is recognised by a substantial increase in plagioclase cumulates and the development of lithologies such as mottled and spotted anorthosites (Hulbert 1983; Smith et al. 2011b). To the east of the N-S trending Grasvally Fault (Fig. 4.2) the GNPA member forms a plunging syncline directly overlying interbedded quartzites and shales of the Magaliesberg Quartzite Formation (van der Merwe 2008). West of the Grasvally Fault Lower Zone cumulates underlie the GNPA member (Fig. 4.2). Northwards the base of the Rustenburg Layered Suite, represented by the Platreef, progressively transgresses downwards through interbedded quartzites and shales of the Magaliesberg Quartzite Formation, quartzites and shales of the Timeball Hill Formation, shales of the Deutschland Formation, the Penge banded iron formation, the Malmani Subgroup dolomites to rest on Archean basement granites and gneisses in the far north (e.g. Sharman-Harris et al. 2005; Holwell and McDonald 2006; van der Merwe 2008; Fig. 4.1).

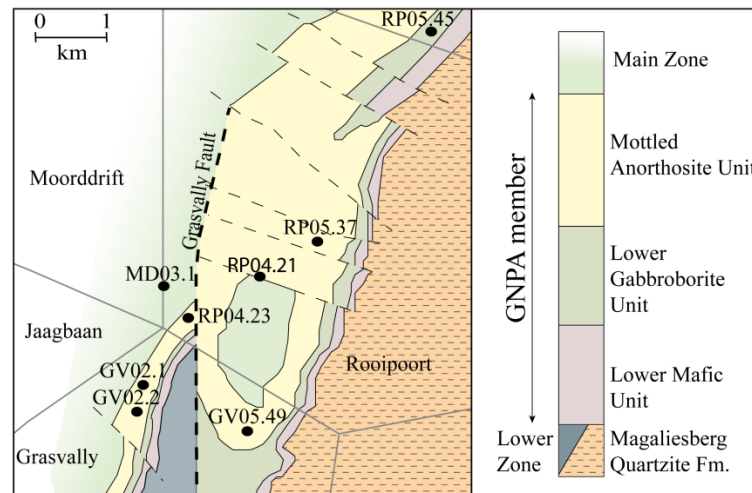


**Figure 4.2** Detailed map of the GNPA member in the Rooipoort-Grasvally region accompanied by stratigraphic column. Locality of boreholes sampled are also shown. Adapted from Maier et al. (2008).

Within the GNPA member, PGE and BMS mineralization is not lithologically bounded, with wide but irregular zones developed throughout the LMF and MANO units (Maier et al. 2008). Mineralization associated with a chromite layer positioned within the basal LMF unit, represents the only traceable horizon throughout the GNPA member in the Rooipoort and Grasvally region.

#### 4.4 Samples and methods

Samples of quarter core have been obtained from eight boreholes drilled by Falconbridge Ltd and Caledonia Mining on the farms Rooipoort, Grasvally and Moorddrift (Fig. 4.2) where the GNPA member overlies Lower Zone harzburgites and the Magaliesberg Quartzite Formation. A stratigraphic log of borehole RP04.23 provides a representative section of the entire GNPA member (Fig. 4.3), with the log of borehole RP05.45 showing differences in the succession where underlain by floor quartzites. These logs also highlight the position of mineralized zones identified by the presence of visible BMS and indications of PGE grades.

In total, 36 polished thin sections were analysed for platinum-group minerals (PGM) at the University of Leicester using a Hitachi S-3600N Environmental Scanning Electron Microscope, coupled to an Oxford Instruments INCA 350 energy dispersive X-ray analysis system.

Bulk concentrations of PGE and Au were determined at Cardiff University by Ni sulfide fire-assay with Te co-precipitation followed by ICP-MS procedure, following the methodology described by Huber et al. (2001) and McDonald and Viljoen (2006). The

proportions required for fusion of a 15 g sample were 6 g of Na<sub>2</sub>CO<sub>3</sub>, 12 g of borax, 0.9 g of sulfur, 1.08 g of carbonyl-purified Ni and 1 g of silica. The flux for samples containing >50% chromite contained 5 g of sample, 12 g of Na<sub>2</sub>CO<sub>3</sub>, 24 g of Li tetraborate, 0.9 g of sulfur, 1.08 g of carbonyl-purified Ni, 10 g of silica and 2.5 g of NaOH. All samples were fired in fire-clay crucibles at 1,050°C for 90 minutes. The sulfide buttons were dissolved in concentrated HCl. Noble metals that had entered the solution were co-precipitated with Te using SnCl<sub>2</sub> as a reductant. Finally, soluble PGE chloro-complex solutions were spiked with Tl, which acts as an internal standard, enabling instrumental drift to be monitored during ICP-MS.

Whole rock sulfur concentrations were determined by standard combustion iodometric procedures using a Laboratory Equipment Company (LECO) titrator at the University of Leicester. Depending on the sulfide content between 0.05 and 0.2 g of sample was combusted for each titration. The rerunning of blanks, standards and samples in triplicate ensured consistent results were obtained. The standard deviations of weight percent of sulfur ranged from 0.0005 to 0.2, indicating a high level of precision.

Sulfide analyses (given in Appendix 2) were carried out using a New Wave Research UP213 UV laser system coupled to a Thermo X Series 2 ICP-MS. The relative abundances of PGE and other elements were recorded in time-resolved analysis mode (time slices of 250 ms) as the laser beam followed a line designed to sample different sulfide or oxide phases. The beam diameter employed was 30 μm, with a frequency of 10 Hz and a power of ~ 6 J cm<sup>-2</sup>. The sample was moved at 6 μm sec<sup>-1</sup> relative to the laser along a pre-determined line pattern. Ablations were carried out under helium (flow ~0.7 L min<sup>-1</sup>) and the resulting vapour combined with argon (flow rate 0.65-0.75 L min<sup>-1</sup>) before delivery to the ICP-MS. Acquisitions lasted between 80 and 400 seconds, including a 20 second gas blank prior to the start of the analysis and a 10 second washout at the end. Signals within the time spectra that could be attributed to PGM included in the sulfides were not selected for integration so the data reflect concentrations in the sulfide minerals alone. Sulfur concentrations were measured prior to LA-ICP-MS using SEM and <sup>33</sup>S was used as internal standard as some sulfides did not contain Fe. Subtraction of gas blanks and internal standard corrections were performed using Thermo Plasmalab software.

Calibration was performed using a series of 5 synthetic Ni-Fe-S standards prepared from quenched sulfides. The standards incorporate S, Ni, Fe and Cu as major elements and Co, Zn, As, Se, Ru, Rh, Pd, Ag, Cd, Sb, Te, Re, Os, Ir, Pt, Au and Bi as trace elements and the

compositions of the 5 standards are given in Prichard et al (2013) and Appendix 2. The standards produce five point calibration curves for S, Ni and Fe and three point calibration curves for PGE, Ag, Cd, Re, Au and semi-metals. Standards 1-3 produce 3 point calibration curves for Cu, Co and Zn and reliable matrix-matched corrections for argide species ( $^{59}\text{Co}^{40}\text{Ar}$ ,  $^{61}\text{Ni}^{40}\text{Ar}$ ,  $^{63}\text{Cu}^{40}\text{Ar}$ ,  $^{65}\text{Cu}^{40}\text{Ar}$ ,  $^{66}\text{Zn}^{40}\text{Ar}$ ) that interfere with  $^{99}\text{Ru}$ ,  $^{101}\text{Ru}$ ,  $^{103}\text{Rh}$ ,  $^{105}\text{Pd}$  and  $^{106}\text{Pd}$ . Corrections for  $^{106}\text{Cd}$  on  $^{106}\text{Pd}$  and  $^{108}\text{Cd}$  on  $^{108}\text{Pd}$  were determined using Cd-bearing Standard 1 but Cd concentrations in the sulfides were <10 ppm, producing only very small corrections in most unknowns. Argide and isobaric-corrected data are indicated by asterisks beside  $^{101}\text{Ru}$ ,  $^{103}\text{Rh}$ ,  $^{105}\text{Pd}$ ,  $^{106}\text{Pd}$  and  $^{108}\text{Pd}$  in the relevant tables. Where independent corrections have been applied to different isotopes of the same element (e.g.  $^{66}\text{Zn}^{40}\text{Ar}$  and  $^{106}\text{Cd}$  on  $^{106}\text{Pd}$  and  $^{108}\text{Cd}$  on  $^{108}\text{Pd}$ ) the independently corrected values typically vary by less than 20% (and commonly <5%) indicating that the corrections are robust. The accuracy of the LA-ICP-MS procedure for PGE was checked by analysis of the Laflamme-Po724 standard run as an unknown against the Cardiff sulfide standards at the start and end of each day.

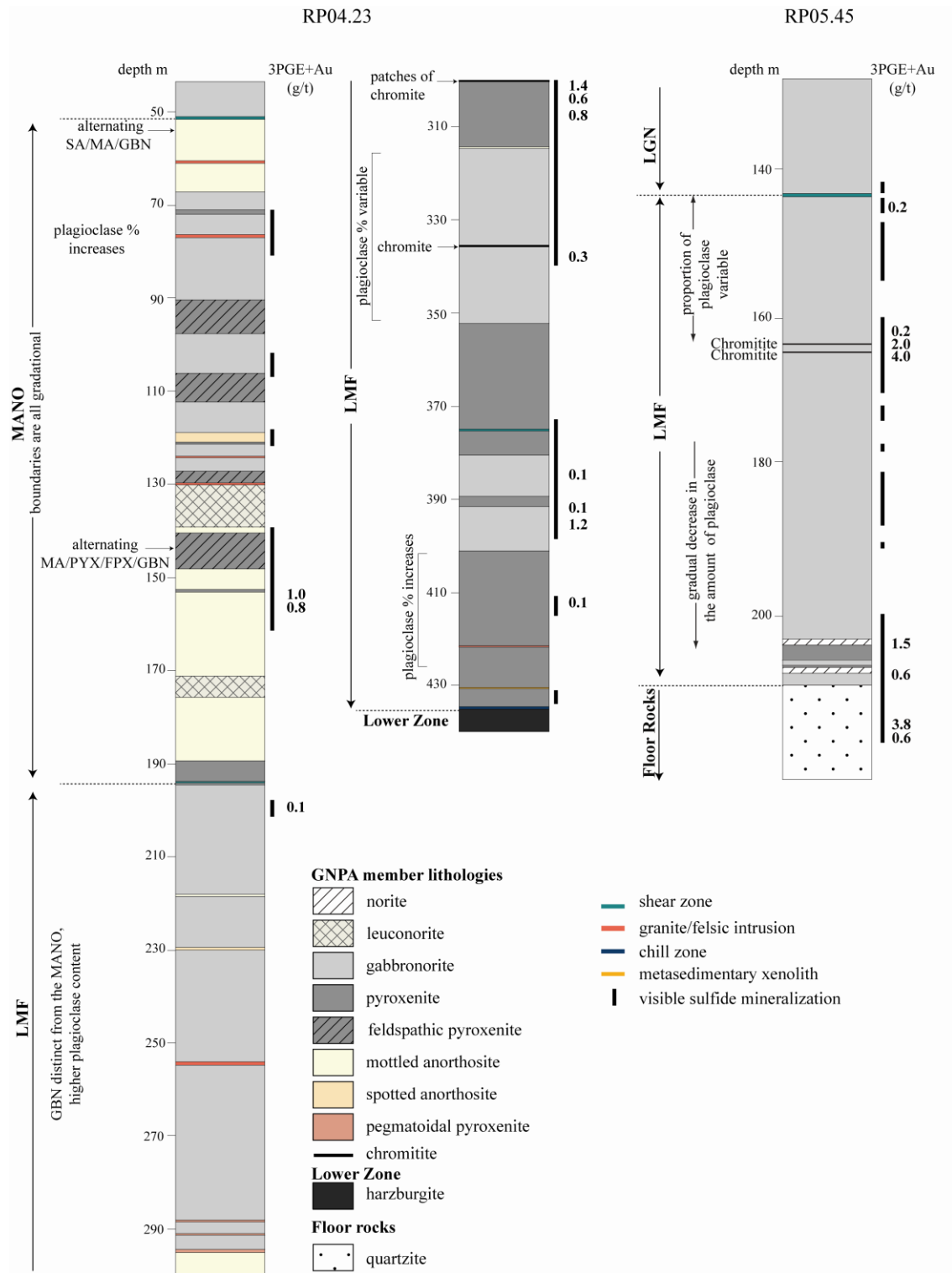


**Figure 4.3** Detailed stratigraphic logs of boreholes RP04.23 and RP05.45 of the Lower Mafic (LMF), Lower Gabbronorite (LGN) and Mottled Anorthosite (MANO) Units, highlighting zones of visible sulfide mineralization and indication of PGE grades. Lithological abbreviations SA spotted anorthosite, MA mottled anorthosite, GBN gabbronorite, PYX pyroxenite and FPX feldspathic pyroxenite.

## 4.5 Platinum–group mineralogy

Thirty-six polished thin sections from the quartzite floor rocks, LMF (including chromitites) and MANO units from boreholes RP04.23, RP05.45, MD03.1, RP04.21 and RP05.37 were examined for PGM. More than 800 individual PGM grains have been identified and are listed in Table 4.1. Each individual grain has been classified by its composition, size, rock type and associated BMS assemblage (primary or secondary). The relative proportions of the various PGM are based on an estimation of area (and by inference, volume) of each grain. This was calculated using the short- and long-axes of PGM, measured on the SEM. To prevent biases we present all data on PGM assemblages in percentage of total area of all PGM which reflects more accurately the relative proportions of each PGM type within an assemblage. Each occurrence was also classified by its association; enclosed in sulfide, attached to sulfide, enclosed by silicates, or attached/enclosed within chromite or oxide (Fig. 4.4).

### 4.5.1 PGM assemblage

Within the GNPA member the PGE mineralogy is dominated by Pt-As and Pd-Bi-Te-bearing PGM. Platinum and Pd-bearing phases constitute 53% and 35% (by area) respectively of all PGM classified. The identified PGM have been grouped into a total of eleven types (see Table 2). The five most abundant by area are (Table 4.2): (1) Pt arsenides (50%), (2) Pd bismuthotellurides (15%), (3) Pt-Pd tellurides (14%), (4) Pd antimonides (10%) and (5) Au-Ag minerals (8%). No PGM carriers of Os or Ir were observed within this study. In addition throughout the Rooipoort, Grasvally and Moorddrift area, PGE sulfides in the form of laurite, cooperite and braggite along with Pt-Pd-Fe alloys are rare forming <0.05% of the total assemblage by area (Table 4.1 and 4.2).

No noticeable differences exist between the PGM assemblages developed in the MANO unit, LMF unit and footwall rocks. Mineralization within the latter is interpreted to result from infiltration of the sulfide liquid into the footwall. With the exception of the chromitites (Table 4.1 and 4.2), the PGE mineralogy also does not vary considerably with lithology. The proportions of PGM types do however differ quite significantly between primary and secondary sulfides, indicating sulfide assemblage is the controlling factor on PGM assemblage (Table 4.1 and 4.2; Smith et al. 2011b). Thus, we regard sulfide mineral assemblage as the primary control on differing PGE mineralogies and the following sections are structured accordingly to this distinction.

Name	Ideal Formula	PGE- and Au-mineral categories	GNPA member and quartzite		Chromitite		Total
			primary sulfide	secondary sulfide	primary sulfide	secondary sulfide	
Michenerite	PdBiTe	Pd bismuthotelluride	98	32	7	49	186
Stibiopalladinite	Pd <sub>5+x</sub> Sb <sub>2-x</sub>	Pd antimonide	18	112		27	157
Sperrylite	PtAs <sub>2</sub>	Pt arsenide	8	75	3	23	109
Kotulskite	PdTe	Pd-telluride	26	51		18	95
Hessite	Ag <sub>2</sub> Te	Ag mineral	40	40			80
Moncheite	PtTe <sub>2</sub>	Pt telluride	2	14		14	30
Electrum	Au-Ag	Au mineral	4	15		5	24
Sudburyite	PdSb	Pd antimonide	24				24
Hollingworthite	RhAsS	PGE sulfarsenide	11	3	7	3	24
Isomertieite	Pd <sub>11</sub> Sb <sub>2</sub> As <sub>2</sub>	Pd antimonide		21			21
Testibiopalladite	PdSbTe	Pd antimonide	9	10		2	21
Merenskyite	PdTe <sub>2</sub>	Pd-telluride	7	13			20
Palladoarsenide	Pd <sub>2</sub> As	Pd arsenide		19			19
Telluropalladinite	Pd <sub>7</sub> Te <sub>4</sub>	Pd-telluride	14	1		1	16
Temagamite	Pd <sub>3</sub> HgTe <sub>3</sub>	Pd-telluride		12			12
Froodite	PdBi <sub>2</sub>	Pd bismuthide	6			1	7
Sobolevskite	PdBi	Pd bismuthide	2	1		1	4
Maslovite	PtBiTe	Pt bismuthide		4			4
Platarsite	PtAsS	PGE sulfarsenide			1	3	4
Telargpalite	(Pd,Ag) <sub>3+x</sub> Te	Pd Ag telluride		4			4
Stillwaterite	Pd <sub>8</sub> As <sub>3</sub>	Pd arsenide		3		1	4
Cherepanovite	RhAs	Rh arsenide				3	3
Sopcheite	Ag <sub>4</sub> Pd <sub>3</sub> Te <sub>4</sub>	Pd Ag telluride		1		1	2
Unconstrained	Pt-As-Sb	Pd antimonide				2	2
Unconstrained	Pd-Pt-Te-As	Pt-Pd telluride	1				1
Laurite	RuS <sub>2</sub>	Ru sulfide			1		1
Majakite	PdNiAs	Pd arsenide				1	1
Unconstrained	S-Te-Rh-Sb-As	PGE sulfarsenide	1				1
Unconstrained	Pd Ni	Pd alloy			1		1
Unconstrained	Pd-As-Rh	PGE sulfarsenide		1			1
Unconstrained	S-As-Pd	PGE sulfarsenide				1	1
Unconstrained	Pt-As-Te	Pt arsenide				1	1
Unconstrained	Pd-Bi-Sb	Pd bismuthide	1				1
Unconstrained	Pt-Pd-As	Pt-Pd arsenide	1				1

**Table 4-1** Name and ideal formulae of all occurrences of PGM and Au-Ag minerals identified in the GNPA member, for primary and secondary sulfide bearing samples in chromite-rich and chromite poor rocks

#### 4.5.1.1 Non chromitiferous rocks and quartzites

##### 4.5.1.1.1 Primary sulfide assemblages

The PGE mineralogy associated with the primary pyrrhotite–chalcopyrite–pentlandite sulfide assemblage is overwhelmingly dominated by Pt arsenides, specifically sperrylite (PtAs<sub>2</sub>), which forms around 70% of the total PGM assemblage (Table 4.2). Sperrylite, however represents only eight out of the 273 grains identified within primary sulfide-bearing samples (Table 4.1), thus a significant proportion of the area is contributed by a single grain with the dimensions 127 μm × 65 μm. Therefore the apparent dominance of sperrylite should be treated with caution on consideration of this potential nugget effect. The remaining assemblage consists primarily of the Pd bismuthotelluride michenerite (13%) and Pt-Pd tellurides (9%) with Au and Ag minerals such as electrum and hessite

constituting only 2%. It is important to highlight the rather low abundance of Sb-bearing PGM (3.6%) within the primary sulfide-bearing samples (Table 4.2).

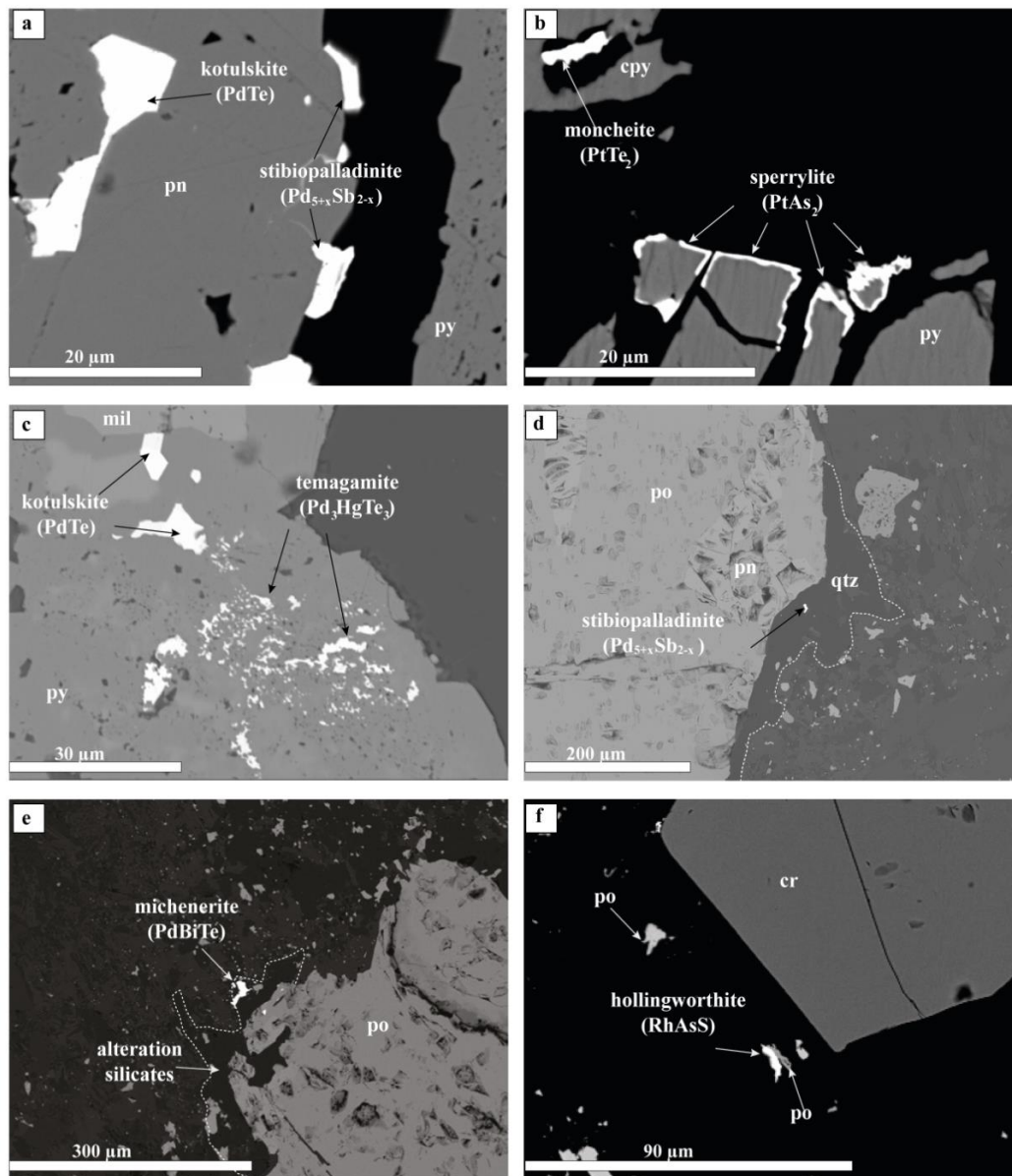


**Figure 4.4** Backscattered electron photomicrographs of PGM found within the GNPA member. (a-b) Pt/Pd-bearing phases found attached and enclosed within pentlandite (pn), chalcopyrite (cpy) and pyrite (py). (c) Cluster of PGM enclosed fully in pyrite and millerite (mil). (d-e) PGM residing in quartz and secondary silicates (e.g., actinolite, tremolite and chlorite), in close proximity to pyrrhotite (po) dominated sulfide blebs. (f) PGM within a chromitite showing association to sulfide over chromite (cr).

The PGM consistently appear to be closely associated with sulfide (e.g. Fig. 4) with 48% of PGM residing fully enclosed within sulfides (primarily pyrrhotite and pentlandite) or existing along the sulfide margins (Fig. 4.4a and b; Table 4.3). Although a significant proportion (51%) of PGM occur as satellite grains within secondary silicates, they remain spatially in close association with BMS (e.g. Fig. 4.4d and e).

<i>n</i>	GNPA member and quartzites		chromitites		total %
	primary sulfides 273	secondary sulfides 427	primary sulfides 20	secondary sulfides 153	
<b>PGM type</b>					
Pt/Pd arsenide	70.87	44.97	26.83	25.19	51.10
Pd bismuthotelluride	12.81	12.43	42.27	29.81	15.38
Pt/Pd telluride	8.97	14.54		24.52	13.94
Pd antimonide	3.58	12.35		15.88	9.66
Au/Ag minerals	2.39	14.77		2.05	8.35
PGE sulfarsenide	1.01	0.02	21.95	1.42	0.74
Pd Ag telluride		0.40		0.06	0.21
Pt/Pd bismuthide	0.37	0.51		0.02	0.38
Rh arsenide				1.01	0.21
Pd arsenide		0.42			0.2
PGE sulfide	0.01	0.01	7.32		0.02
Pd alloy			1.63	0.02	<0.1

**Table 4-2** Proportions of PGM type within primary and secondary sulfide-bearing samples in chromite-rich and chromite poor rocks in percentage of area of PGM.

Association	GNPA member and quartzites		chromitites	
	primary sulfides	secondary sulfides	primary sulfides	secondary sulfides
enclosed in sulfide	28.0	37.3	11.1	43.0
attached to sulfide	20.8	17.3	33.3	15.8
silicate	51.3	45.2	44.4	40.6
chromite			11.1	0.6
oxide		0.2		

**Table 4-3** Textural associations of PGM within the GNPA member, in percentage of grains.

#### 4.5.1.1.2 Secondary sulfide assemblages

In samples where primary sulfides are replaced to varying degrees by pyrite and millerite, the types and proportions of PGM vary from those discussed above (Table 4.1 and 4.2). Although sperrylite continues to dominate the assemblage, the proportion of Pt-bearing PGM is notably lower at around 44%. The most significant difference however is the increase in the proportion of Pd antimonides (12%) and the appearance of Pd arsenides, such as palladoarsenite ( $\text{Pd}_2\text{As}$ ; Table 4.1 and 4.2). The rest of the assemblage is, in general comparable to that described above, comprising Au and Ag minerals, Pt-Pd tellurides (each accounting for around 14%) and Pd bismuthotellurides (12%). More obscure phases identified that are unique to the secondary sulfides include sopcheite ( $\text{Ag}_4\text{Pd}_3\text{Te}_4$ ),

maslovite ( $\text{PtBiTe}$ ), isomerticite ( $\text{Pd}_{11}\text{Sb}_2\text{As}_2$ ) and temagamite ( $\text{Pd}_3\text{HgTe}_3$ ; Table 1; Fig. 4.4c). The latter is relatively rare within the northern limb, reported only once within the Platreef, at Tweefontein (McCutcheon and Kinnaird 2011). The associations of PGM are similar to those in the primary assemblages, with a strong relationship remaining between PGM and BMS with 45% of the PGM assemblage residing in alteration silicates (mainly chlorite, tremolite and actinolite) or quartz surrounding/replacing the sulfide bleb (Table 4.3; Fig. 4.4d and e). The rest of the assemblage (>50%) mainly exists in direct association with the sulfides, occurring both along the margins of and fully enclosed within sulfide minerals (Fig. 4.4c; Table 4.3). Pyrite and millerite are the dominant hosts of PGM inclusions, with few occurring within the relicts of primary pyrrhotite, pentlandite and chalcopyrite.

#### 4.5.1.2 *Chromitiferous rocks*

The PGM assemblage of the chromitites is broadly comparable to that of the chromite-poor rocks with Pt/Pd arsenides, Pd bismuthotellurides and Pt/Pd tellurides dominating. However, minor but highly significant differences do exist, including the appearance of PGE sulfides and the higher abundance of PGE sulfarsenides (Table 4.1 and 4.2). Within the chromitites, although the presence of chromite exerts a minor control over the platinum-group mineralogy it appears to be principally controlled by the sulfide assemblage developed along with the spinels (Table 4.2).

##### 4.5.1.2.1 *Primary sulfide assemblages*

Although the sample size is significantly lower than observed within the non chromitiferous rocks of the GNPA member, this study has still managed to reveal that while the PGM assemblage is dominated by Pd bismuthotellurides (42%) and Pt arsenides (27%) it is notably distinct due to the presence of laurite ( $\text{RuS}_2$ ) and the greater proportion of PGE sulfarsenides, principally hollingworthite ( $\text{RhAsS}$ ; Table 4.1 and 4.2; Fig. 4.4f).

The PGM exhibit a strong preference to BMS rather than chromite (Table 4.3). Overall 44% occur in direct association with sulfides, present either fully enclosed within pentlandite or along margins of sulfides (Fig. 4f). A comparable percentage of PGM were found within alteration silicates, as satellite grains surrounding BMS. The PGM are rarely found in association with the chromite grains with only 1 grain (11% of the assemblage) attached to chromite (Table 4.3). No PGM were found included within chromite grains.

#### 4.5.1.2.2 *Secondary sulfide assemblages*

Chromitites with secondary textured sulfides, have a PGM assemblage that is near comparable to other secondary sulfide-bearing rocks of the GNPA member (Table 4.2). The assemblage consists primarily of Pd bismuthotellurides (30%), Pt arsenides (25%) and Pt/Pd tellurides (24%), and shows considerably diversity in PGM type (Table 4.2). Further similarities include the rather high abundance of Pd antimonides which account for 16% of the assemblage. The platinum-group mineralogy within the GNPA member appears to therefore be more strongly controlled and/or related to the development of secondary sulfides than the presence of chromite.

As observed within the chromitites hosting primary textured sulfides, the PGM show greater preference to BMS than chromite (Table 4.3; Fig. 4.4f). A combined total of 58% were found in direct association with sulfides, thus situated fully enclosed or along the sulfide-silicate boundary (Table 4.3). Those enclosed in sulfide were generally hosted by pyrite and millerite. A high proportion of the PGM (40%) also reside within secondary silicates surrounding BMS. A close association between PGM and chromite is not observed within only one grain found attached to chromite (Table 4.3). No PGM were found as inclusions within the chromite.

## 4.6 PGE and base metal geochemistry

Throughout the GNPA member PGE and BMS mineralization is typically confined to irregular zones that range in thickness from a few metres to  $\geq 50$  m (Fig. 4.3), hosted by a range of rock types, including chromitites. Mineralization also extends for several metres into the underlying quartzites. Whole rock concentrations of S, Ni, Cu and PGE on Grasvally, Rooipoort and Moorddrift are listed in Table 4.4. The GNPA member is Pd-dominant, with Pt/Pd ratios of the non chromitiferous rocks ranging between 0.1 to 1.7 (mean 0.5) and Ni/Cu ratios of the mineralized samples (defined as samples with Cu >400 ppm; Ni >1000 ppm) between 0.4 and 4 (mean 1.6). The ore-body is characterized by variable PGE grades from sub economic (<0.1 ppm 3PGE+Au) to high grade (>4 ppm), with the latter associated primarily with the chromitites (Table 4.4). In general, high Cu (>400 ppm) and Ni (>1000 ppm) concentrations broadly correspond to high S contents and are also indicative of elevated PGE grades. This correlation is however less well defined within those samples hosting secondary sulfides.

In order to gain an insight into the controlling effects of magmatic and hydrothermal processes on the distribution of PGE it is important to assess in detail the relationship between PGE and BMS within those samples containing secondary sulfides (Fig. 4.5). In a similar manner to the approach used for the PGM assemblages, we address these relationships with relation to the primary and secondary sulfide assemblages.

**Table 4-4** indications of PGE grade (Ni-fire assay), Ni, Cu (determined by XRF) and S (LECO) contents of samples together with Ni/Cu, Pt/Pd, Pd/Ir and Rh/Ir ratios for primary (P) and secondary (S) sulfide bearing samples. Data is shown for the Mottled Anorthosite unit (MANO), Lower Gabbronorite unit (LGN), Lower Mafic unit (LMF) and the local floor rocks (FLR)

Sample	Rock type	Unit	Sulfide	Cu (ppm)	Ni (ppm)	S (ppm)	Ni/Cu	Os (ppb)	Ir (ppb)	Ru (ppb)	Rh (ppb)	Pt (ppb)	Pd (ppb)	Au (ppb)	3PGE + Au ppm	Pt/Pd	Pd/Ir	Rh/Ir	
<b>MD03.01</b>																			
552	OPX	MANO	S	3758	5133	9907	1.4	24.35	29.84	177.59	71.68	994.76	920.3	367.11	2.35	1.08	30.84	2.40	
553	OPX	MANO	S			2054		7.71	9.49	62.24	23.73	352.95	367.9	122.49	0.86	0.96	38.77	2.50	
569	OPX	MANO	S	2984	4051	7186	1.4	28.71	38.42	252.2	102.22	1564.1	1494.5	323.92	3.48	1.05	38.9	2.66	
582	NIR	MANO	S	657	1117	2501	1.7	21.11	27.89	218.44	63.72	648.84	377.28	47.75	1.14	1.72	13.53	2.28	
<b>GY02.1</b>																			
154	PYX	MANO	S			12260		0.92	1.38	6.66	6.6	113	400	8.5	0.52	0.28	290.46	4.78	
166	PYX	MANO	P			14684		3.99	5.8	27.7	34	400	1715	116	2.26	0.23	295.64	5.86	
206	PYX	MANO	S			5562		16	20	135	42.9	621	739	172	1.57	0.84	36.67	2.15	
476	PYX	LMF	S			18564		2.85	4.8	22.3	16.8	306	369	54.6	0.74	0.82	77	3.50	
487	GBN	LMF	S			10500		1.53	3.34	14	9	121	155	41	0.32	0.77	46.37	2.69	
504	FPYX	LMF	S			5790		0.5	0.88	3.86	3.1	44.2	64.5	11.9	0.12	0.68	73.2	3.52	
<b>RP05.37</b>																			
69	NIR	MANO	S	7218	4409	15014	0.6	8.26	8.78	47.57	76.98	665	3167	267.84	4.18	0.21	360.67	8.77	
71	PYX	MANO	S	995	4183	5491	4.2	5.79	7.24	31.76	55.5	473.03	3188	41.41	3.76	0.15	440.48	7.67	
127	GBN	MANO	S	3542	4384	16620	1.2	19.43	23.81	142	124	1148	1962	304.56	3.54	0.59	82.4	5.21	
<b>RP04.21</b>																			
448	MA	MANO	S	845	916	3786	1.1	4.17	5.44	22.58	38.45	339.68	724.77	42.54	1.15	0.47	133.27	7.07	
681	MA	MANO	S	584	904	3676	1.5	4.08	4.91	29.34	15.14	148.5	326.4	43.77	0.53	0.45	66.48	3.08	
690	GBN	MANO	P	796	2973	16500	3.7	9.68	12.62	117.12	32.58	253.22	1029	88.29	1.4	0.25	81.64	2.58	
693	GBN	MANO	S	894	1876	8076	2.1	8.54	11.9	74	37.85	371.55	677.09	56.4	1.14	0.55	56.88	3.18	

Sample	Rock type	Unit	Sulfide	Cu (ppm)	Ni (ppm)	S (ppm)	Ni/Cu	Os (ppb)	Ir (ppb)	Ru (ppb)	Rh (ppb)	Pt (ppb)	Pd (ppb)	Au (ppb)	3PGE + Au (ppm)	Pt/Pd	Pd/Ir	Rh/Ir	
<b>RR04.23</b>																			
157	MA	MANO	S	32	418	8060	13.06	1.24	2.42	10.27	10.8	146.12	786.25	104.28	1.04	0.19	324.9	4.46	
158	MA	MANO	S	2879	2463	2163	0.9	0.32	1.58	5.98	4.92	127.81	617.12	84.96	0.84	0.21	390.71	3.11	
162	MA	MANO	S	637	560	355	2.6												
185	MA	MANO	n.d	41	108		2.6												
188	MA	MANO	n.d	19	68		3.6												
192	PYX	MANO	P	15	641		42												
201	GBN	LGN	P			842		0.36	1.35	10.37	3.41	44.67	97.92	16.65	1.54	0.46	72.53	2.53	
300	CR	LMF	P	1778	1013	2656	0.5	12.94	16.51	84.59	42.57	667.73	310.38	337.26	1.35	2.15	18.8	2.58	
305	NR	LMF	P	4576	1950	7507	0.4	0.88	1.18	6.39	5.55	38.18	90.74	29.45	0.64	0.42	76.62	4.70	
307	CR	LMF	P	129	279	474	2.16	3.08	4.25	29.03	8.67	38.94	22.48	7.52	0.78	1.73	5.29	2.04	
315	GBN	LMF	P			317													
330	GBN	LMF	P	312	491	1986	1.5												
338	CPX	LMF	P	278	638	2923	2.2	9.43	20.42	94.52	27.37	204.51	76.83	9.58	0.31	2.66	3.76	1.34	
374	GBN	LMF	P	242	316	1157	1.3												
384	GBN	LMF	P	788	835	5123	1.1	1.42	1.51	18.11	4.85	43.03	117.99	26.63	7.16	0.36	78.35	3.21	
392	GBN	LMF	P	4517	2357	15933	0.5	1.9	3.17	15.73	15.72	278	800.57	141.8	23.24	0.35	252.68	4.96	
411	GBN	LMF	P	452	539	4336	1.19	0.27	0.4	2.7	1.4	17.49	67.56	18.75	5.74	0.26	167.27	3.50	
<b>RP05.45</b>																			
146	GBN	LMF	S			1227		0.66	1.53	7.01	4.55	40.57	98.57	14.49	1.16	0.41	64.58	2.97	

Sample	Rock type	Unit	Sulfide	Cu (ppm)	Ni (ppm)	S (ppm)	Ni/Cu	Os (ppb)	Ir (ppb)	Ru (ppb)	Rh (ppb)	Pt (ppb)	Pd (ppb)	3PGE + Au (ppm)	Pt/Pd	Pd/Ir	Rh/Ir	
149	GBN	LMF	S	87	213		2.4	0.38	0.65	2.52	2.59	38.05	56.84	0.11	0.67	86.83	3.98	
156	GBN	LMF	S	54	189	449	3.5											
165	GBN	LMF	S	170	317	1353	1.9	0.29	1.26	5.34	4.43	29.64	96.52	0.14	0.31	76.87	3.52	
166	CR	LMF	S	4389	3869	10267	0.9	22.99	33.55	214.83	101.27	642.4	1013.3	1.82	0.63	30.2	3.02	
167	CR	LMF	S	8477	4601	7350	0.5	58.79	104.2	743.76	193.14	1585.1	2017.8	4.04	0.79	19.35	1.85	
174	PYX	LMF	S	50	187	446	3.7											
183	GBN	LMF	nd	87	117		1.3											
195	GBN	LMF	nd	64	135		2.1											
205	NR	LMF	S	680	1371	3737	2.01	1.51	3.89	19.46	24.65	206.66	1247.8	1.56	0.17	321.07	6.34	
206	CPX	LMF	S	173	374	303	2.2	0.16	0.36	1.17	0.93	11.46	16.94	0.03	0.68	47.43	2.58	
208	NR	LMF	S	524	633	797	1.2	2.21	4.67	22.84	17.97	167.69	352.97	0.56	0.48	75.6	3.85	
210	QTZ	LMF	S	76	121		1.7											
214	QTZ	FLR	S			33400		5.1	9.29	45.65	214.1	946.33	2443.3	3.82	0.39	263.04	23.05	
215	QTZ	FLR	S	1417	2456	4280	1.4	0.68	1.36	6.71	20.93	125.09	635.06	0.59	0.2	467.8	15.39	
<b>GY02.2</b>																		
476	CR	LMF	S	1399	1045	7520	0.75	5.17	10.5	41.5	29.1	171	310	0.56	0.55	29.6	2.77	
477	CR	LMF	S	2364	2324	15797	0.98	37.6	88.7	406	189	577	727	1.57	0.79	8.19	2.13	
478	CR	LMF	S	837	784	2272	0.94	6.03	50.6	229	124	699	433	1.27	1.61	8.55	2.45	
480	PYX	LMF	S	205	283	2601	1.38	0.11	0.19	0.51	0.41	5.12	8	0.02	0.63	42.1	2.16	
<b>GY05.49</b>																		
127	CR	LMF	S	316	548	1714	1.73	47.8	87	513	166	870	243	1.3	3.57	2.79	1.91	
128	CR	LMF	S	499	1277	1634	2.56	65.4	113	701	289	1581	2251	4.3	0.7	19.91	2.56	

Lithological abbreviation's: CR chromitite, NR norite, GBN gabbro-norite, PYX pyroxenite, CPX clinopyroxenite, OPX orthopyroxenite, FPYX feldspathic pyroxenite, MA mottled anorthosite and QTZ quartzite.

#### 4.6.1 Non chromitiferous rocks and quartzites

##### 4.6.1.1 Primary sulfide assemblages

Selected PGE are plotted against each other in Figure 5 where a high degree of correlation is evident between the PGE in primary sulfide-bearing samples (Fig. 4.5a-f). The base metals (Cu and Ni) also correlate well with each other and with the PGE (Fig. 4.5i). Good correlations are also observed between PGE, Ni and Cu with S (Fig. 4.5j). Gold appears to also be strongly associated with PGE in the most unaltered GNPA member rocks (Fig. 5g and h). The Pt/Pd ratio of primary sulfides is well constrained ranging between 0.2 and 0.5 (mean 0.3; Table 4.4). The Ni/Cu ratio ranges from 0.4 to 3.7, with a mean of 1.4. The Pd/Ir and Rh/Ir ratios are consistent both between units and sulfide assemblages (Table 4.4; Fig. 4.6). The Pd/Ir ratio is rather variable ranging typically between 30 and 400. The Rh/Ir ratio varies between 2 and 8, with a mean of 3.8.

##### 4.6.1.2 Secondary sulfide assemblages

Strong positive correlations remain between the IPGEs, which is especially apparent between Ir and Ru (Fig. 4.5f). Both Rh and Pt correlate fairly well with the IPGEs and with each other (Fig. 4.5c and d), with only a slight scatter observed in the data set. In comparison, Pd, Au and to a lesser extent Cu exhibit noticeably poorer correlations with the other PGE and especially with those that are considered immobile under most conditions (Pt and Ir; Fig. 4.5a, b, e, g and k; Keays et al., 1982; Wood 2002). Interestingly, with the exception of two anomalous samples, Pd and Au continue to be strongly correlated with each other, even where alteration has occurred (Fig. 5h). Copper does not show any relationship with Au (Fig. 4.5l). Broad correlations are evident between Pd and Pt and also Rh, (Fig. 4.5a and b) although not as confined as those observed within the primary sulfide-bearing samples. No relationship is preserved between Pd and Ir (Fig. 4.5e). The base metals and PGE do not continue to be closely associated with S, with a much broader relationship evident (Fig. 4.5j). Copper and Ni do however remain generally well correlated with each other (Fig. 4.5i). Both the Pt/Pd ratio (mean of 0.6) and Ni/Cu ratio (mean of 1.8) are slightly elevated within the secondary sulfides in comparison to those samples hosting primary sulfides. All of these observations are consistent with the preferential remobilisation of Pd and Au over the rather more immobile Pt, IPGE and Rh (Wood 2002), by late-stage hydrothermal fluids.

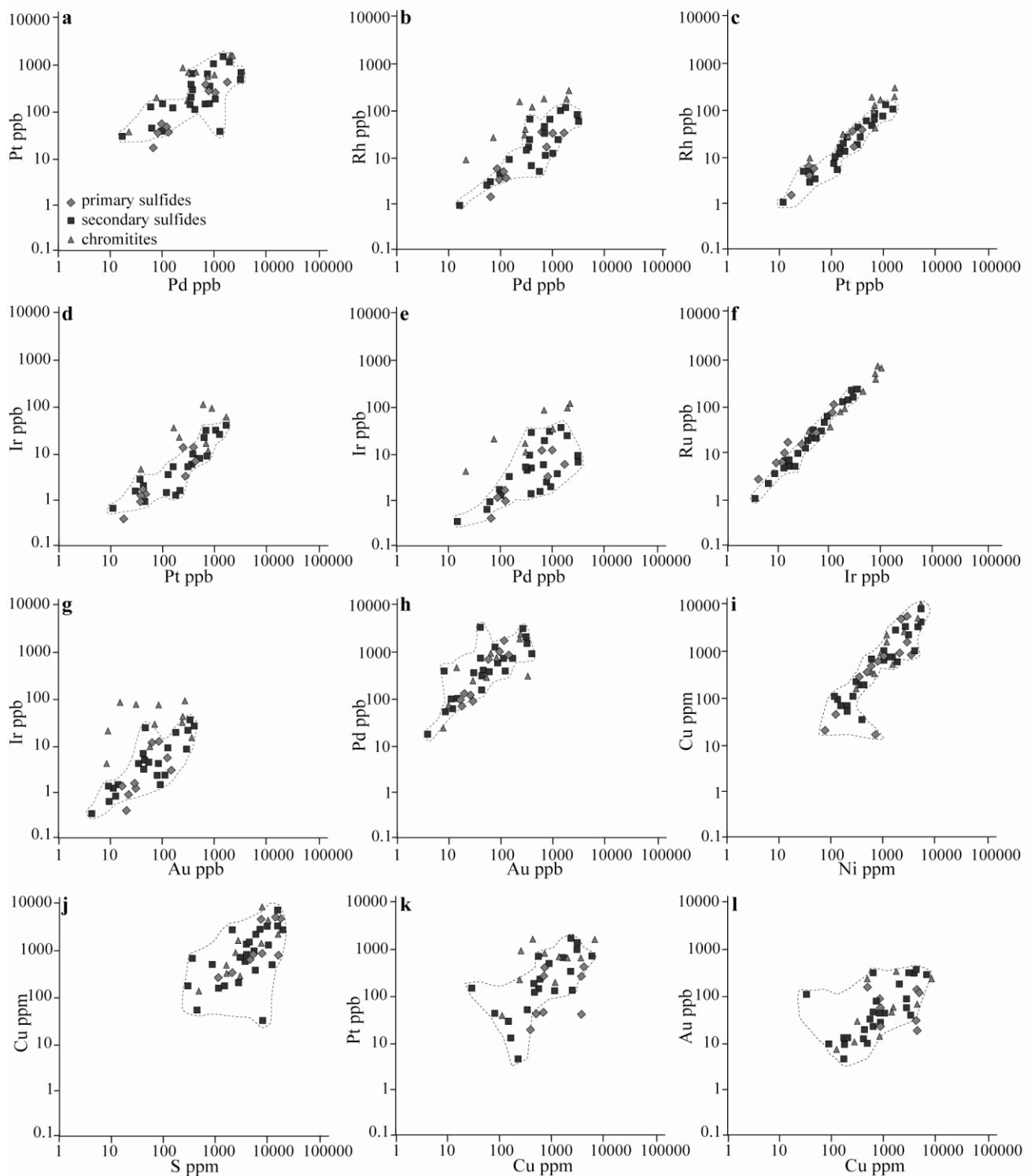


**Figure 4.5** Binary variation diagrams plotting bulk rock (a) Pt vs Pd, (b) Rh vs Pd, (c) Rh vs Pt, (d) Ir vs Pt, (e) Ir vs Pd, (f) Ru vs Ir, (g) Ir vs Au, (h) Pd vs Au, (i) Cu vs Ni, (j) Cu vs S (k) Cu vs Pt and (l) Cu vs Au

### 4.6.2 Chromitiferous rocks

It is noticeable from Figure 4.5, that the chromitites, which are both primary and secondary sulfide-bearing, in general contain elevated concentrations of certain PGE, especially Ir and Rh relative to the chromite-poor rocks of the GNPA member. A high degree of correlation is evident between Rh and Pt (Fig. 4.5c) and Ir and Ru (Fig. 4.5f). Broad positive correlations are identifiable between the remaining PGE (Fig. 4.5a, b, d and e). Gold shows no relationship with the PGE throughout the chromitites (Fig. 4.5g and h). Platinum-group elements, Ni and Cu in general correlate well with each other (Fig. 4.5a-f and i). The chromitiferous rocks containing significant sulfides ( $>0.7$  wt% S; Table 4), are also relatively Pd rich with Pt/Pd ratios confined between 0.5 and 0.8. Pt/Pd ratios associated with the sulfide-poor chromitites ( $<0.3$  wt% S; Table 4.4) are substantially higher ranging between 1.6 and 3.5 (e.g. Fig. 4.6a). The Pd/Ir (mean of 14) and Rh/Ir (mean of 2) ratios are notably lower in the chromitites than the non chromitiferous rocks.

#### 4.6.2.1 Variations with depth

In Figure 4.6, borehole RP04.23 provides representative depth profiles of Pt/Pd, Pd/Ir, Rh/Ir and Ni/Cu ratios within the GNPA member. There is no suggestion that the Pt/Pd, Pd/Ir and Rh/Ir ratios vary systematically with depth or significantly between the MANO and LMF units (Fig. 4.6a, b). In contrast, the Ni/Cu ratio decreases slightly with depth (Fig. 4.6c). This is also reflected in the overall average Ni/Cu ratio of 2 in the MANO unit and 1.2 in the LMF unit. It is important to highlight that the only noticeable variation in the Pt/Pd, Pd/Ir and Rh/Ir ratios with depth is in association with the chromitite layer (Fig. 4.6a and b; Table 4.4).

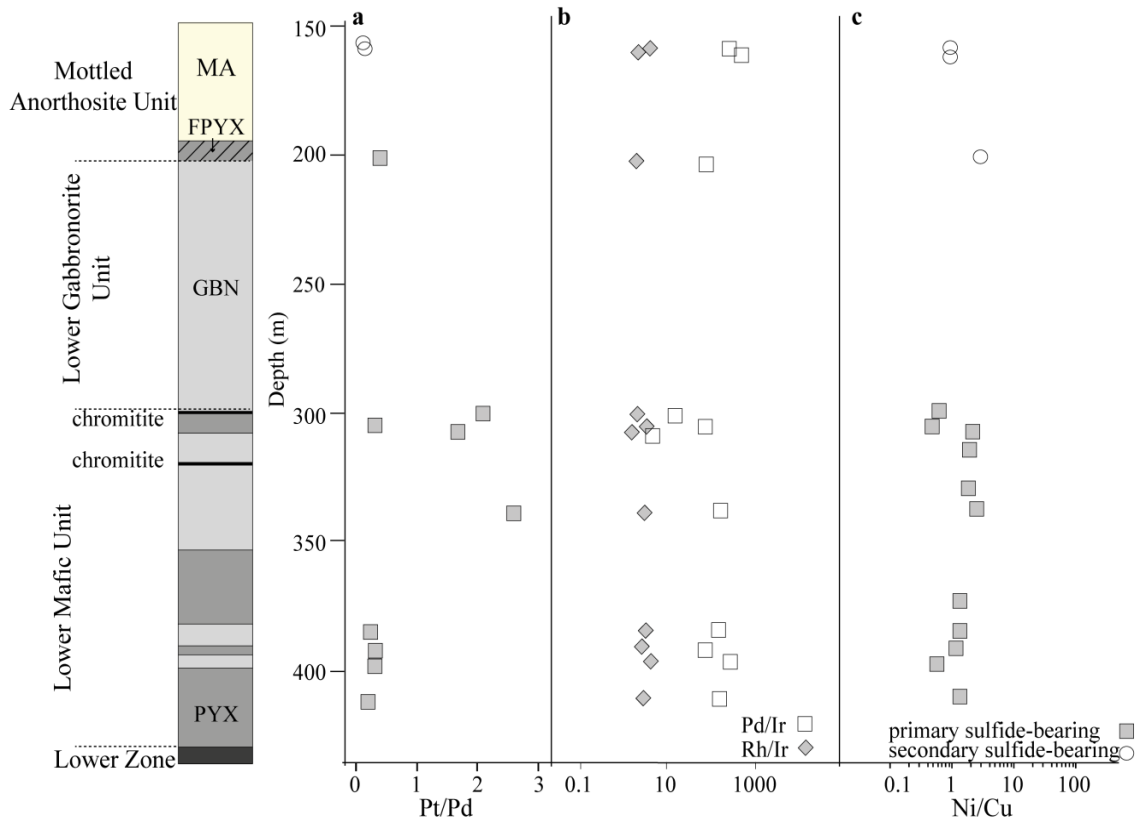


**Figure 4.6** Ratios with depth through borehole RP04.23 for primary and secondary sulfide-bearing rocks for a) Pt/Pd, b) Pd/Ir and Rh/Ir and c) Ni/Cu. *MA* mottled anorthosite, *FPYX* feldspathic pyroxenite, *GBN* gabbronorite and *PYX* pyroxenite.

#### 4.6.3 Chondrite normalized PGE patterns

Chondrite normalized PGE patterns for the chromitiferous and non chromitiferous rocks of the GNPA member are shown in Figure 4.7. The types of patterns observed are similar to those reported by Maier et al. (2008). The non-chromitiferous rocks (Fig. 4.7a) are characterized by relatively fractionated chondrite-normalized PGE profiles, which peak at Pd. In broad terms, those samples hosting primary and secondary sulfide assemblages exhibit similar shaped profiles; however, within the latter, the profiles are not parallel between Pt, Pd and Au, which is consistent with the geochemical plots presented in Figure 4.5 (a, e, g and h). The PGE profiles between the LMF and MANO units are indistinguishable.

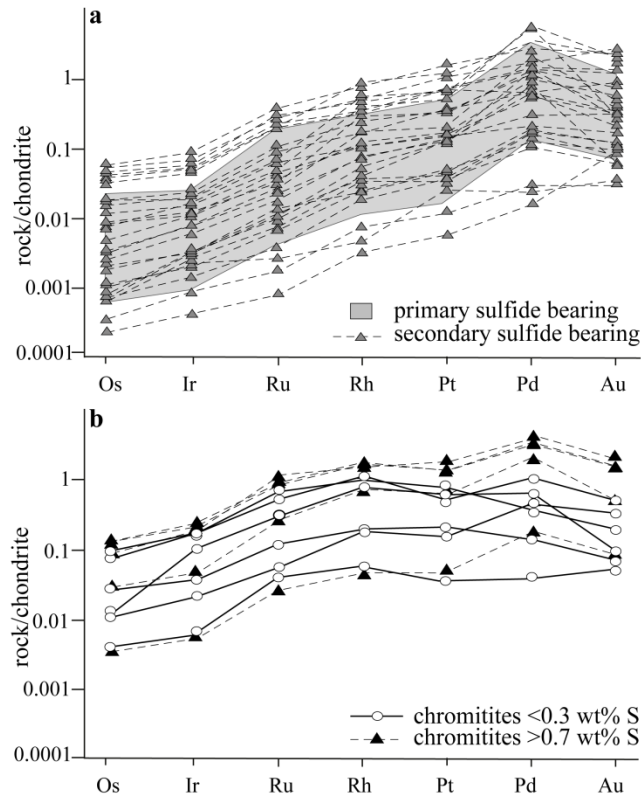


**Figure 4.7** Chondrite normalized PGE profiles for the GNPA member a) individual profiles for samples containing secondary-bearing sulfides, with the range of primary-bearing sulfide samples also shown b) chromitites separated into those containing <0.3 wt% S and those with S content >0.7 wt%. Normalisation factors from Lodders (2003).

The chromitiferous rocks of the GNPA member are characterized by less fractionated PGE profiles with lower PGE gradients than the non-chromitiferous rocks. Two PGE pattern types can be easily identified within the chromitites which appear to relate directly to sulfur content (Fig. 4.7b; Table 4.4). Those chromitites considered S poor (<0.3 wt %) form the characteristic arch-shaped pattern with a peak at Rh or Pt commonly associated with chromite-bearing rocks such as the Merensky Reef and UG2 chromitite (Barnes and Maier 2002a and b; Wilson and Chunnett 2006). These non-fractionated profiles peak at Rh and contain elevated quantities of IPGE but comparable PPGE concentrations to the non-chromitiferous rocks. The second PGE pattern, associated with chromitites containing >0.7 wt% S generally peaks at Pd and is more analogous to those associated with the non-chromitiferous rocks.

#### 4.7 PGE concentrations in BMS

Laser ablation-inductively coupled plasma-mass spectrometry (LA-ICP-MS), was utilized to determine the PGE contents of the primary sulfide phases pyrrhotite, pentlandite, chalcopyrite and secondary pyrite and millerite thus providing an insight into the behaviour of PGE during low temperature recrystallization and alteration. Results for the laser

ablation analysis of sulfides in the non-chromitiferous and chromitiferous rocks of the GNPA member are summarised in Table 4.5. Representative time resolved analysis (TRA) spectra for those major sulfide phases analysed; pentlandite, pyrrhotite, pyrite and millerite are shown in Figure 4.8. All phases carry detectable PGEs in solid solution. As concentrations are very low within chalcopyrite (Table 4.5), it is not regarded as a significant carrier of PGE within the GNPA member. In general, pyrrhotite, pentlandite, pyrite and millerite are the major carriers of IPGEs, whereas Rh and Pd reside mainly within pentlandite and pyrite, with very low Pt concentrations present in any sulfide phase. Sulfides commonly exhibit zoning of As and Co with elevated concentrations often confined to the boundary of adjacent phases, particularly between pentlandite and pyrite. Abundances of PGEs can be highly variable and erratic both within individual sulfide crystals and sulfide phases.

	Co (ppm)	Ni (wt%)	Cu (wt%)	Os (ppm)	Ir (ppm)	Ru (ppm)	Rh (ppm)	Pt (ppm)	Pd (ppm)	Au (ppm)
<b>Primary Assemblages- GNPA member</b>										
<b>Pyrrhotite (n= 35 )</b>										
Min	24.08	0.116	0	0.22	BDL	0.47	BDL	BDL	BDL	BDL
Max	2634	9.66	2.41	0.686	0.58	5.418	0.552	2.185	7.86	0.043
Mean	211	1.004	0.13	0.27	0.25	1.65	0.13	0.21	0.73	0.009
Std. Dev.	454	1.55	0.38	0.23	0.18	1.56	0.12	0.46	1.57	0.009
<b>Pentlandite (n= 12)</b>										
Min	4857	20.19	0.03	BDL	0.021	BDL	BDL	BDL	1.60	BDL
Max	15010	35.4	3.03	2.04	1.27	17.57	1.43	0.71	34.66	0.11
Mean	9530	30	0.51	0.58	0.25	4.6	0.38	0.08	13.11	0.03
Std. Dev.	3911	4.28	1.11	0.75	0.35	6.70	0.47	0.19	11.98	0.03
<b>Chalcopyrite (n= 4 )</b>										
Min	0.57	0.06	32.4	BDL						
Max	1.13	0.03	33.12	BDL	0.76	0.06	BDL	0.01	0.41	0.007
Mean	0.88	0.01	32.78	BDL	0.08	0.04	BDL	0.01	0.27	0.01
Std. Dev.	0.23	0.01	0.31	BDL	0.04	0.02	BDL	0.005	0.15	0.001
<b>Cubanite(n= 7)</b>										
Min	2.000	0.050	18.310	BDL						
Max	239.700	1.027	26.070	0.089	0.159	0.086	0.153	0.080	0.282	0.055
mean	79.727	0.359	21.725	0.042	0.059	0.061	0.072	0.034	0.137	0.026
STD	87.387	0.360	2.749	0.036	0.058	0.029	0.043	0.027	0.112	0.020
<b>Secondary Assemblages- GNPA member</b>										
<b>Pentlandite (n= 19)</b>										
Min	12	17.28	0.006	BDL	BDL	BDL	BDL	BDL	12.6	BDL
Max	9836	39.86	0.65	1.32	0.64	8.2	4.07	8.6	386	1.1
Mean	1995	32.86	0.12	0.3	0.23	1.95	1.2	0.8	141	0.1
Std. Dev.	2295	5.87	0.16	0.34	0.18	2.08	1.2	1.9	144	0.3
<b>Chalcopyrite (n= 1 )</b>										
Min										
Max	1.34	3.73	32.82	BDL	BDL	0.13	BDL	BDL	BDL	0.03
Mean										
Std. Dev.										
<b>Cubanite(n= 9)</b>										
Min	4.000	0.050	19.150	BDL						
Max	153.800	1.988	26.120	0.499	0.361	2.595	0.040	0.357	3.709	0.249
Mean	20.728	0.265	22.980	0.063	0.045	0.580	0.040	0.091	1.004	0.067
Std. Dev.	49.903	0.646	2.737	0.164	0.119	0.972	0.000	0.148	1.350	0.077
<b>Pyrite (n= 36)</b>										
Min	4	0.04	0	BDL						
Max	33370	2.8	3.9	0.8	0.89	9.5	29	4.9	60.8	1.9
Mean	5998	0.8	0.44	0.12	0.16	1.02	3.6	0.8	6.7	0.2
Std. Dev.	6773	0.9	0.72	0.2	0.23	2.11	7.01	1.2	12.2	0.44
<b>Footwall Pyrite (n= 14)</b>										
Min	5407	0.16	0	BDL						
Max	10480	0.35	0.1	0.3	0.48	2.7	1.9	2.2	0.3	0.3

Mean	8188	0.23	0.02	0.02	0.04	0.22	0.17	0.3	0.1	0.03
Std. Dev.	1525	0.06	0.03	0.07	0.12	0.71	0.49	0.6	0.9	0.07
<b>Millerite (n= 9)</b>										
Min	184	54.8	0	BDL	BDL	BDL	BDL	BDL	0.04	BDL
Max	565	62.95	1.8	0.18	0.35	1.23	5.3	0.035	50.18	0.06
Mean	306	59.19	0.28	0.06	0.15	0.5	1.67	0.008	7.3	0.01
Std. Dev.	146	2.49	0.5	0.06	0.13	0.47	1.7	0.01	16.42	0.02
<b>Chromitites</b>										
<b>Pyrite (n= 26)</b>										
Min	4	0.01	0	BDL	BDL	BDL	BDL	BDL	BDL	BDL
Max	18150	2.50	0.64	14	9.88	124.17	54	63	16.1	0.6
Mean	3230	1.03	1.4	1.5	1.3	12.7	5.2	3.6	2.8	0.1
Std. Dev.	4160	0.85	5.8	3.1	1.97	26.99	11.3	12.3	4.2	0.13
<b>Millerite (n= 10)</b>										
Min	33	45.21	0	BDL	BDL	BDL	BDL	BDL	BDL	BDL
Max	5818	63.26	4.5	1.09	3.2	2.7	2.8	1.3	4.3	0.2
Mean	2343	58.03	0.87	0.20	0.48	0.73	0.54	0.2	0.96	0.04
Std. Dev.	2150	5.1	1.4	0.33	0.96	0.91	0.93	0.47	1.24	0.06
<b>Pentlandite (n=10)</b>										
Min	59.44	30.28	0	BDL	0.01	BDL	0.485	BDL	0.94	BDL
Max	5178	45.1	1.43	0.73	1.58	4.84	5.35	9.50	192	0.09
Mean	3507	35.4	0.32	0.34	0.63	2.79	2.11	1.46	95	0.02
Std. Dev.	1910	16.8	0.58	0.24	0.56	1.51	1.38	2.89	72.1	0.03
<b>Chalcopyrite (n =8)</b>										
Min	0.016	0.001	30.36	BDL	BDL	BDL	BDL	BDL	BDL	BDL
Max	83.3	1.23	35.02	0.94	1.43	6.86	0.11	0.013	0.38	0.09
Mean	11.23	0.18	32.98	0.12	0.27	0.91	0.05	0.007	0.091	0.03
Std. Dev.	29.13	0.43	1.71	0.33	0.54	2.40	0.03	0.003	0.12	0.03
<b>Cubanite (n= 5)</b>										
Min	4.000	0.050	19.550	BDL	BDL	0.052	BDL	BDL	BDL	0.017
Max	202.900	6.130	23.530	0.054	0.040	0.381	0.040	0.059	0.316	0.107
Mean	52.602	2.175	20.850	0.016	0.012	0.178	0.040	0.026	0.103	0.059
Std.Dev.	85.236	2.711	1.558	0.021	0.016	0.134	0.000	0.029	0.119	0.038

**Table 4-5** Compositions of base metal sulfides from the GNPA member as determined by LA-ICP-MS analysis, for chromite rich and chromite poor rocks. Analysis BDL (below detection limit) were assigned a value of 50% of the detection limit to obtain the mean and standard deviations.

#### 4.7.1 Non chromitiferous rocks

##### 4.7.1.1 Primary sulfide assemblages

Within the primary assemblages, pyrrhotite and pentlandite were found to carry concentrations of Os (<2 ppm) and Ir (<2 ppm) and higher concentrations of Ru (<18 ppm) in solid solution (Fig. 4.8a and b). Pyrrhotite in particular shows a high degree of correlation between these elements (Fig. 4.9a and b). In most samples pentlandite is slightly more enriched in Os, Ir and Ru relative to coexisting pyrrhotite (Table 4.5). This is most apparent for Ru, where concentrations in pentlandite range from 0.05 to <18 ppm, in comparison to <6 ppm in pyrrhotite. Although the Ru content is variable in pentlandite between samples, it is consistent between individual pentlandites within samples. While comparable concentrations of Rh (<5 ppm) are present in pyrrhotite and pentlandite (Fig. 4.8b), the latter is the principle carrier of Pd with concentrations ranging from 2 to 35 ppm (Fig. 4.8a and b). Similar to Ru, although the Pd content is rather variable between samples, it is consistent within samples (Fig. 4.8a). Palladium and Rh show no relationship between one another or with the IPGEs (Fig. 4.9c and d). No PGE were present in solid solution or as discrete PGM within chalcopyrite or cubanite. In contrast to Pd, both Pt and Au are noticeably absent in all the sulfide phases (Table 4.5).

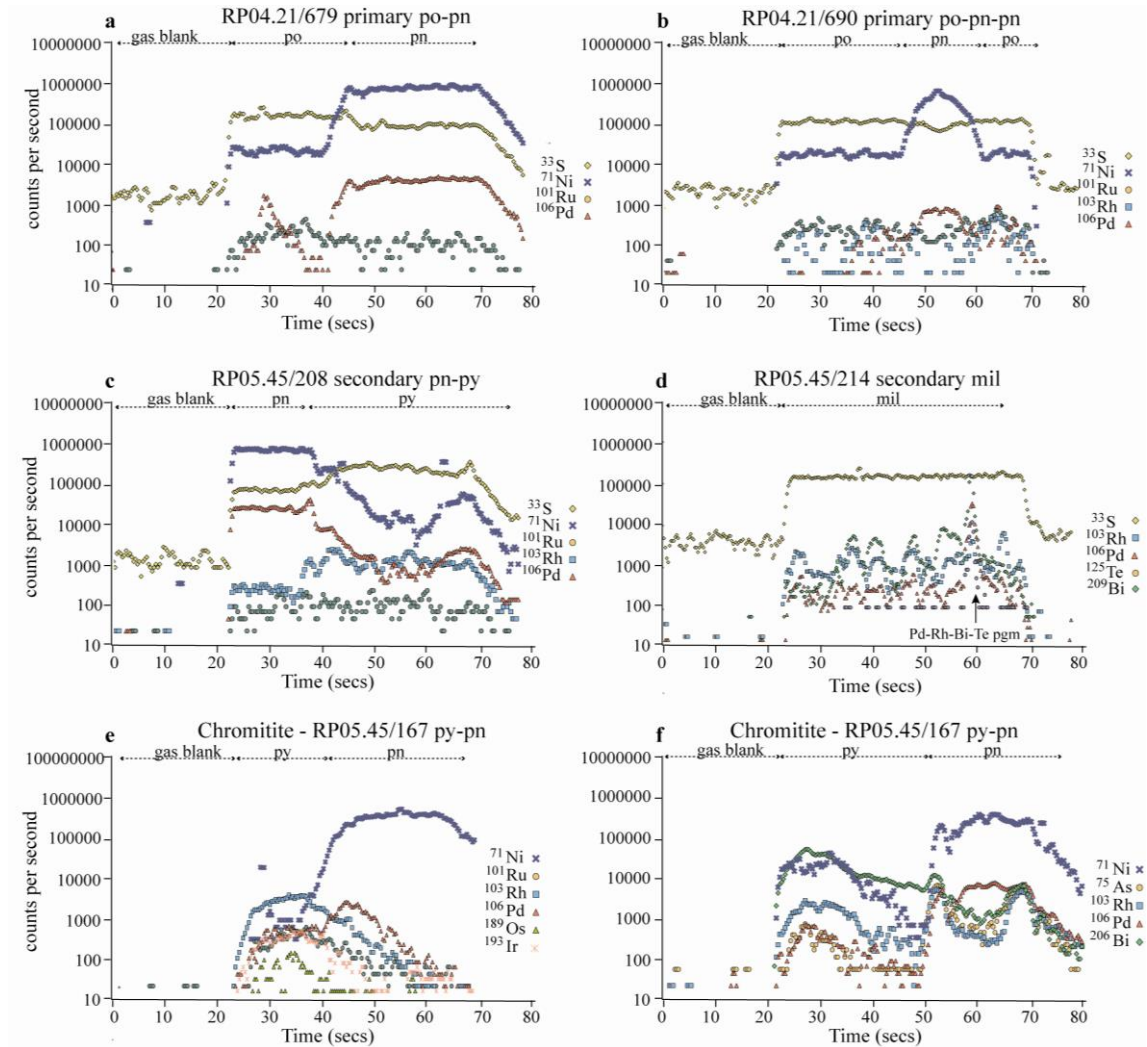


**Figure 4.8** Selected TRA spectra for a) and b) primary pyrrhotite and pentlandite, c) composite pentlandite and pyrite, d) millerite with PGM, (e) and (f) pyrite and pentlandite from the chromitite.

#### 4.7.1.2 Secondary sulfide assemblages

Relicts of primary pyrrhotite within the assemblage pyrite-pentlandite-chalcopyrite±pyrrhotite±millerite contain near comparable concentrations of IPGE (all at <1 ppm), Rh and Pd (both at <2 ppm) in solid solution as within the primary sulfide assemblages. Pentlandite present in secondary textured sulfides is also host to concentrations of Os (<2 ppm), Ir (<1 ppm) and Ru (<9 ppm) in solid solution (Fig. 4.8c). Ruthenium concentrations show greater variability both between and within samples ranging from below detection limit to 9 ppm (Table 4.5). Pentlandite remains the principal carrier of Pd and although its content is highly variable between samples (12 to <390 ppm) it is very consistent within samples (Fig. 4.8c; Table 4.5). Minor quantities of Rh (up to 4 ppm) remain present in solid solution within the pentlandite (Fig. 4.8c). No PGE were

present in solid solution within chalcopyrite or cubanite, with the exception of several analyses within the latter which detected Pd within solid solution up to 4 ppm (Table 4.5).

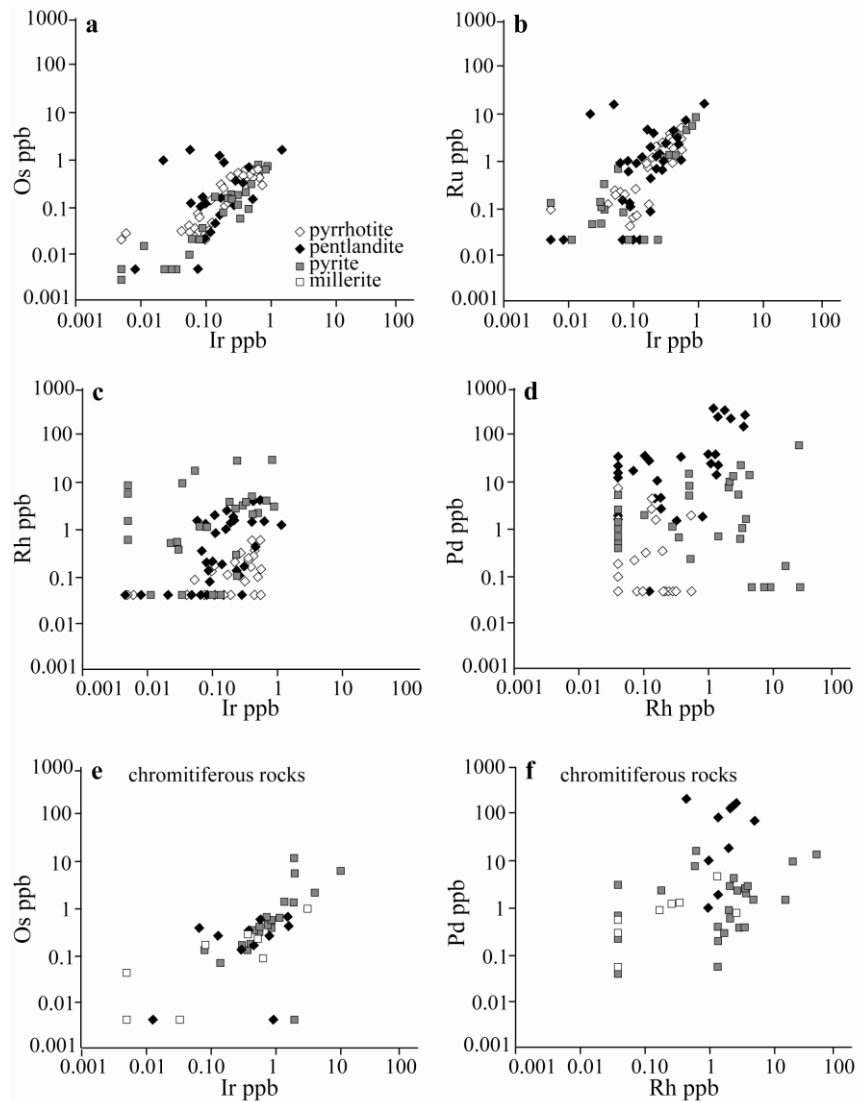


**Figure 4.9** PGE contents in individual pyrrhotite, pentlandite, pyrite and millerite grains plotted as a) Ir versus Os, b) Ir versus Ru, c) Ir versus Rh, d) Rh versus Pd, e) Ir versus Os for chromitites and f) Rh versus Pd for chromitites.

The most significant relationship found in the secondary sulfides is that pyrite and millerite were found to be important carriers of both Rh and Pd (Fig. 4.8c and d). Concentrations of both elements in solid solution are highly variable between and within samples (Fig. 4.8c and d). Palladium ranges from below detection limit to >50 ppm (mean 7 ppm) in pyrite and millerite (Table 4.5). Palladium also occurs as discrete PGM (typically Pd-Bi-Te) inclusions within the majority of sulfide phases (e.g. Fig. 4.8d). The Rh content is slightly elevated within the pyrite (<30 ppm, mean of 4 ppm) relative to coexisting millerite (mean 2 ppm; Table 4.5). Palladium and Rh show no relationship between one another or with

the IPGEs (Fig. 9c and d). Pyrite and millerite contain low concentrations of Os and Ir (all at <1 ppm) which, like in the primary phases, correlate well with each other (Fig. 4.9a). Ruthenium concentrations are slightly higher and more variable within pyrite (<10 ppm) relative to millerite, but a strong correlation with Ir is still preserved. Platinum, in contrast to Pd, is noticeably absent in the majority of phases only being detected in solid solution and as occasional PGM (Pt-Bi-Te) within several pyrite and pentlandite analyses (Fig. 4.8c; Table 4.5). Pyrite also contains gold in solid solution at concentrations of <2 ppm. These concentrations are notably higher than observed in the other sulfide phases within the GNPA member (Table 4.5).

#### **4.7.2 Chromitiferous rocks**

The chromitiferous rocks of the GNPA member contain significantly elevated concentrations of IPGE in comparison to the non-chromitiferous rocks (Table 4.4 and 4.5). Pyrite is the principal carrier of the IPGEs, where concentrations of Os (<14 ppm; mean 1.5 ppm), Ir (<10 ppm; mean 1 ppm) and Ru (<124 ppm; mean 13 ppm) are highly irregular between samples and within individual grains (Fig. 4.8e). The IPGEs are also found in solid solution within millerite, pentlandite and chalcopyrite but at lower and more consistent concentrations (Fig. 8e; Table 4.5). There is a high degree of correlation within all phases between the IPGEs (Fig. 4.9e).

Rhodium is hosted in solid solution principally by pyrite with lower concentrations identified within pentlandite and millerite (<5 ppm; Table 4.5; Fig. 4.8e and f). Interestingly, As and Bi exhibit parallel profiles to Rh (Fig. 4.8f), which may result from the zonation of these elements. Within pyrite, the Rh content is highly irregular reaching up to 54 ppm with a mean of only 5 ppm (Fig. 4.8f). Palladium was detected in all sulfide phases with the exception of chalcopyrite (Table 4.5). Pentlandite is the principal carrier of Pd (Fig. 8e and f), with concentrations being highly erratic (0.9 ppm to 192 ppm; mean 88 ppm) even within a single grain. Pyrite is also an important host, although concentrations are lower at <16 ppm and highly varied (mean 2 ppm; Fig. 4.8e and f). Millerite contains only minor quantities of Pd at <0.6 ppm (Fig. 4.8d). Correlations between Pd and Rh (Fig. 4.9f) and between Pd and IPGEs are poor. Similar to the non-chromitiferous rocks, Pt is generally absent from the majority of phases or present at very low concentrations in solid solution and as occasional PGM. Concentrations of Pt (up to 9ppm) were found in a few analyses of pyrite and pentlandite but the majority of analyses found no Pt above the limit of detection (Table 4.5).

## 4.8 Mass balance

For a semi-quantitative indication of the proportion of PGE present within BMS, and how these proportions change as the BMS assemblage changes we performed a mass balance, following similar methods to Huminicki et al. (2005) and Holwell and McDonald (2007) which are given in Appendix 3.

For the primary pyrrhotite-pentlandite-chalcopyrite sulfide assemblage we applied a similar approach to Holwell and McDonald (2007). As chalcopyrite contains virtually no PGE in solid solution, we recalculated the whole rock PGE contents to 100% pyrrhotite and pentlandite as these are the principal phases that contain PGE in solid solution. To determine the weight fraction of the sulfide phases present we utilized the Huminicki et al. (2005) method, using whole rock Cu, Ni and S data and stoichiometric mineral data. All whole-rock Cu was assigned to chalcopyrite and Ni was assigned to pentlandite, following a correction to account for trace amounts of Ni in pyrrhotite and silicates. The proportion of pyrrhotite was then obtained assuming that the remaining S, after subtracting the S required by pentlandite and chalcopyrite, corresponds to pyrrhotite.

Where the secondary pyrite-chalcopyrite-pentlandite±millerite±pyrrhotite assemblage is developed, the presence of pyrite and millerite was also taken into account. As no samples used in the calculation contained both millerite and pentlandite, we assigned all whole-rock Ni to the mineral present. The weight fraction of pyrite was then obtained assuming all remaining S corresponds to pyrite. This assumes no pyrrhotite, which is valid in this case as no pyrrhotite was observed in the samples used in the mass balance.

In Figure 4.10 we compare the average PGE contents of pyrrhotite, pentlandite, pyrite and millerite determined by LA-ICP-MS, normalized to chondrite, and the mean whole-rock concentrations of PGE and Au for the same samples, recalculated in 100% sulfide. This method is adapted from Ballhaus and Sylvester (2000), with the rationale that an element whose concentration within a sulfide is as high or higher than the recalculated whole rock contents indicates its presence in solid solution, whereas if it falls below, some of that element must be present as other discrete phases.

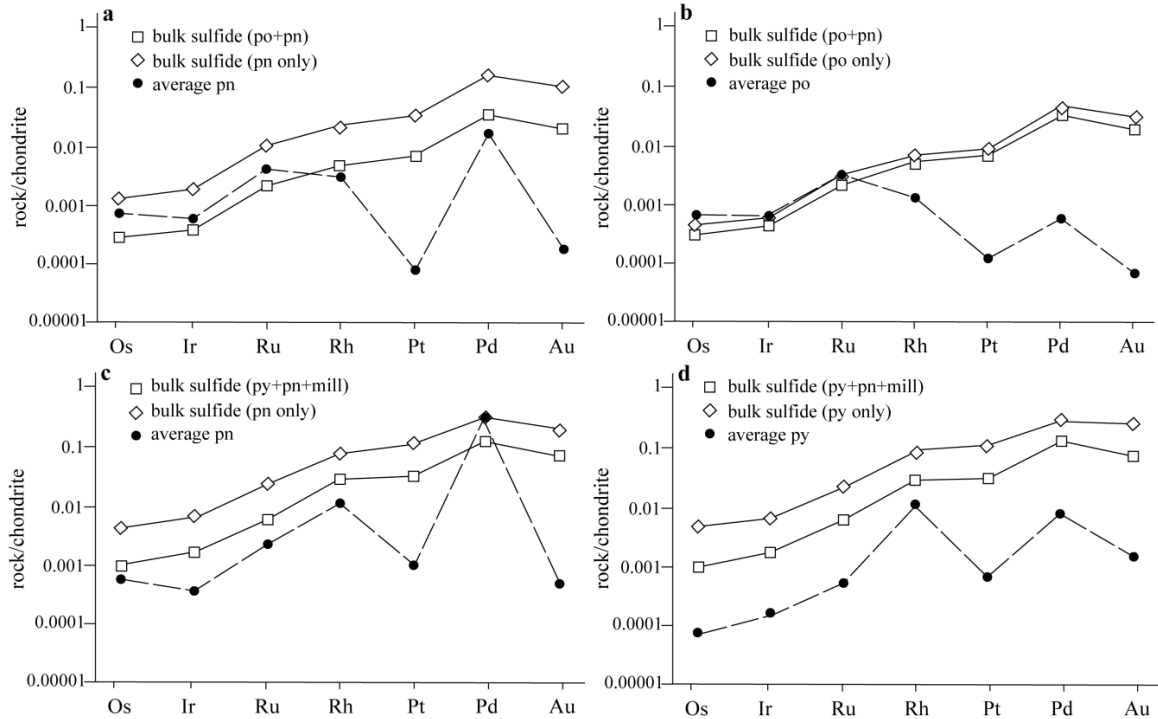


**Figure 4.10** Chondrite normalized diagrams of average PGE in a) pentlandite and bulk sulfide recalculated to 100% sulfide (po + pn and pn only) for primary sulfide-bearing rocks, b) pyrrhotite and bulk sulfide recalculated to 100% sulfide (po + pn and po only) for primary sulfide-bearing rocks, c) pentlandite and bulk sulfide in 100% sulfide (py + pn + mill and pn only) for secondary sulfide-bearing rocks and d) pyrite and bulk sulfide in 100% sulfide (py + pn + mill and py only) also for secondary sulfide-bearing rocks.

#### 4.8.1 Primary sulfide assemblages

The IPGE are accommodated comfortably in solid solution within pyrrhotite and pentlandite (Fig. 4.10a and b) as averaged IPGE concentration of both sulfide phases, plot higher than the recalculated bulk rock contents. The elevated concentration of IPGE in both phases, relative to whole rock indicates that these elements are present primarily within one phase (Fig. 4.10a and b). When whole rock is recalculated to 100% pentlandite (Fig. 4.10a) and 100% pyrrhotite (Fig. 4.10b) it is clear Ir and Ru are primarily present within pyrrhotite as whole rock Ir and Ru is almost identical to that in pyrrhotite (Fig. 4.10b). Rhodium and Pd both fall slightly below whole rock values indicating they must also be present as discrete PGM. The large negative anomalies in both Pt and Au show that these are the only metals to reside primarily as discrete phases with only a small fraction being held in solid solution. These results are in agreement with our PGM study which identified >70% of all PGM (by area) to be Pt phases, around 20% Pd, 2% Au and only 1% to be Rh phases.

### 4.8.2 Secondary sulfide assemblages

Large discrepancies exist between the observed data (both LA-ICP-MS and PGM studies) and that calculated by the mass balance as the averaged laser data is significantly lower, by an order of magnitude, to that recalculated from whole rock. The mass balance (Fig. 4.10c and d) suggests that Os, Ir and Ru occur primarily as discrete PGM phases where secondary sulfides exist. This seems highly implausible mainly because no Os, Ir or Ru-bearing PGM have been identified and the bulk PGE data (Fig. 4.5d and f) implies that these elements were not remobilized during alteration. Thus the IPGE are expected to remain hosted by BMS, as seen in the primary sulfide assemblage mass balance (Fig. 4.10a and b). According to the mass balance, Pd is fully accommodated within pentlandite however this is not consistent with our PGM study which identified 41% of all PGM by area to be Pd phases. There are a number of reasons why this mass balance may not be an accurate representation of the mineralization present. Firstly, the secondary sulfide assemblages are substantially more complex than portrayed in the calculation and vary significantly between samples. Furthermore, within fluid affected ore-bodies S-loss is common. Not correcting for this loss will effectively result in the PGE being greatly concentrated in the calculated sulfide fractions, thus resulting in a large discrepancy between the observed and calculated PGE contents as evident in Figure 4.10c and d.

Overall it is evident that our mass balance works well for samples hosting primary sulfides, and is thus in these instances an accurate representation of the mineralization present within the GNPA member prior to alteration. In contrast, due to the many variables and unknowns, our mass balance cannot be used with any degree of certainty for those samples hosting secondary sulfides.

## 4.9 Discussion

Our data shows that differences in the geochemical and mineralogical characteristics of PGE and BMS mineralization within the GNPA member correlate well with sulfide assemblage type, and are thus controlled by magmatic and hydrothermal processes. Significant features identified within this study include: (1) the strong correlation between PGE, S and base metals in primary sulfide assemblages; (2) variation of platinum-group mineralogy between sulfide assemblages; (3) the dominance of sulfide PGE patterns in sulfide-rich chromitites; (4) the presence of IPGE, Pd and Rh within pyrite and millerite; and (5) the lack of correlation between Pd and Au with Pt and Ir in fluid affected zones. In the following discussion we investigate the genetic implications of these features through

applying our data to the current suggested models for the potential correlative Platreef and Merensky Reef. We start therefore, to constrain the mechanisms involved in the development of GNPA mineralization and explore the behaviour of PGE during both initial sulfide fractionation and low temperature recrystallization.

#### **4.9.1 Primary magmatic signature**

The development of a primary sulfide liquid throughout the GNPA member is supported by the strong correlation evident between the chalcophile elements and S within the primary sulfide assemblage, which indicates the initial concentration of these elements, was governed by a single sulfide melt. This is further supported by the similarity of the associated, Bi-Te-As dominated PGM assemblage and the consistency of the Pt/Pd, Pd/Ir and Rh/Ir ratios throughout the entire GNPA stratigraphy (Fig. 4.6a, b; Table 4.4) as all imply crystallization from a compositionally similar PGE-rich sulfide liquid.

This study has also revealed that where primary sulfides exist: (1) all IPGE and Rh occur in solid solution within pyrrhotite and pentlandite (Fig. 4.10a); (2) pentlandite is a significant host of Pd with the rest occurring as PGM; (3) Pt resides primarily as discrete PGM; and (4) PGM are located in association with sulfides (Table 4.3). All these observations are consistent with the fractionation and crystallization of a magmatic sulfide liquid (Cabri and Laflamme 1976; Fleet et al. 1993; Li et al. 1996; Ballhaus et al. 2001; Mungall et al. 2005; Barnes et al. 2006; Holwell and McDonald 2010; McDonald and Holwell 2011). The presence of IPGE and Rh within pyrrhotite and pentlandite is consistent with the exsolution of these phases from early crystallizing monosulfide solid solution (mss), with which these elements are highly compatible with (Barnes et al. 2006). Platinum, Pd and Au are considered incompatible within both mss and intermediate solid solution (iss), which crystallizes from the residual fractionated sulfide liquid (Fleet et al. 1993; Li et al. 1996; Peregoedova 1998). These elements are therefore preferentially concentrated into a late-stage immiscible semimetal rich melt (Fleet et al. 1993; Helmy et al. 2007; Helmy et al. 2010; Tomkins 2010). Where semi-metals are in abundance (particularly Sb and As), through contamination at high temperatures (e.g. Platreef at Turfspruit), virtually all the Pt and Pd can be accommodated within the semimetal-rich melt, and thus reside as PGM (e.g. Hutchinson and McDonald 2008). In contrast, where semi-metals have been sourced directly from the magma and are thus limited (e.g. Platreef at Overysel) the late-stage melt preferentially scavenges Pt over Pd (Fleet et al. 1993; Helmy et al. 2007). This is observed within the GNPA member and thus provides evidence that prior to sulfide immiscibility,

the magma had not been significantly contaminated specifically with semi-metals. In this situation the presence of a high Pd:semimetal ratio results in excess Pd, that cannot be accommodated for within the semimetal melt, to partition into mss (Helmy et al. 2007). The presence of Pd in pentlandite is a feature also observed in the Platreef and many other Ni-Cu-PGE deposits (e.g. Cabri et al. 1984; Czamanske et al. 1992; Ballhaus and Ryan 1995; Godel et al. 2007; Holwell and McDonald 2007; Djon and Barnes 2012), where it is interpreted to result from Pd preferentially diffusing into pentlandite over pyrrhotite during recrystallization of mss. Within the GNPA member the primary sulfide associated Pt-As and Pd-Bi-Te dominated PGM assemblage (Table 4.1 and 4.2) crystallized around the margins of sulfides, as the semimetal melt was expelled to grain boundaries during crystallization of iss in the manner described by Holwell and McDonald (2010). Later replacement, around the margins of the sulfide blebs by secondary actinolite, tremolite and chlorite, (Smith et al. 2011b) isolates the PGMs as satellite grains within secondary silicates, which is a feature common throughout the GNPA member.

In addition to sulfide liquid, chromite precipitation is also known to effectively concentrate PGE, especially IPGE and Pt (see von Gruenewaldt 1989; Barnes and Maier 2002a and b; Prichard et al. 2004; Godel et al. 2007). Where this mechanism of PGE enrichment prevails, chromitites are characterized by: Pt/Pd >1; arched chondrite normalized PGE profiles; and an increase in PGE sulfides and sulfarsenides (Kinloch 1982; Kinloch and Peyerl 1990; Barnes and Maier 2002a and b; Wilson and Chunnnett 2006). Since chromitites within the GNPA are characterised by either a chromite or sulfide signature, we believe both mechanisms of PGE enrichment were in operation within the parental magma (Table 4.4; Fig.4.7). Based on the key observations that the chromite signature is confined to those chromitites considered S-poor (<0.3wt% S; Fig. 4.7b) and elevated grades occur in association with the S-rich chromitites (>0.7wt% S; Fig. 4.7b; Table 4.1, 4.2 and 4.4) we infer that where present sulfides were the main control over bulk PGE grades and relative element ratios within the GNPA member. Within the chromitites we believe PGE enrichment to have occurred in two stages: (1) some IPGE and Pt were concentrated during chromite precipitation, with the presence of PGE alloys in association with the chromite layer at War Springs (Fig. 4.1; Sutherland 2013) being indicative of such conditions; (2) with the remaining PGE collected by an immiscible sulfide liquid. It may be possible that if the chromite (and any associated Pt-rich PGM) had become mixed with any subsequent sulfide liquid the initial Pt-rich character may have been overprinted or lost if the ratio of sulfide to chromite was sufficiently high. Where sulfides did not significantly

interact with the chromitite layer, chromite was the principal mechanism by which PGE were concentrated thus high Pt/Pd ratios ( $>1$ ), reflecting the preferential fractionation of Pt over Pd by chromite (Barnes and Maier 2002b), and associated platinum-group mineralogy (Table 4.1, 4.2 and 4.4) are preserved. Our observations imply that within the GNPA member the magma (s) from which chromite crystallized had not been depleted of its PGE (in particular Pt, Rh, IPGE) contents prior to the formation of chromite.

#### 4.9.2 Hydrothermal interaction

The most striking difference between the PGM assemblages in the primary and secondary sulfides is the greater abundance of Sb-bearing PGM (e.g. stibiopalladinite and sudburyite) in association with the hydrothermally altered sulfides (Table 4.1 and 4.2). The occurrence of significant quantities of Pd antimonides and Pd arsenides, is considered indicative of either hydrothermal interaction (e.g. Cabri et al. 2005; McDonald et al. 2005; Holwell et al. 2006; Holwell et al. 2014), or contamination (e.g. Hutchinson and Kinnaird 2005; Hutchinson and McDonald 2008). Within the GNPA member, we believe that fluids interacted with the primary sulfide and associated PGM assemblage resulting in the direct alteration of the PGE and sulfide mineralogy. Although the mineralogy of some PGM has changed, they continue to reside in close association with the sulfides (Table 4.3), thus indicating recrystallization occurred *in situ* with minimal remobilisation of PGE. This could directly result from the high quantities of Sb, As, Bi and Te believed to have been present within the volatile phase, as these act to restrict the mobility of PGE rather than facilitate transportation of them (Mountain and Wood 1988).

Within the Platreef, volatile-rich fluids are thought to originate from metasedimentary crustal xenoliths and metamorphism of footwall dolomite and shale (Sharman-Harris et al. 2005; Holwell and McDonald 2006; Holwell et al. 2006; Pronost et al. 2008). Since the footwall to the GNPA member consists of quartzite and Lower Zone cumulates, we suggest that Sb-bearing fluids were derived from calc-silicate xenoliths, up to several metres in thickness, which have been identified along the footwall contact and within the GNPA member (Maier et al. 2008). Although dolomites do not form the immediate footwall to the GNPA member, the presence of calc-silicates may suggest that they were assimilated by the GNPA magma in a downdip direction (Maier et al. 2008).

#### 4.9.2.1 *The behaviour of PGE during low temperature alteration*

A major finding of this study is the presence of significant quantities of PGE held in solid solution within pyrite, a feature also documented within other Ni-Cu-PGE sulfide deposits (e.g. Oberthür et al. 1997; Barkov et al. 1997; Gervilla and Kojonen 2002; Cabri et al. 2002, 2008, 2010, Djon and Barnes 2012; Dare et al. 2011; Piña et al. 2012; 2013). Within the GNPA member, the pyrite is (1) host to comparable concentrations of IPGEs as pyrrhotite and pentlandite (Fig. 4.8b; Table 4.5); (2) significantly enriched in Rh ( $\geq 54$  ppm; Fig. 4.8b; Table 4.5); and (3) considerably lower in Pd contents than pentlandite (Fig. 4.8b; Table 4.5). These observations imply that the pyrite most likely directly inherited its PGE contents from the pyrrhotite and pentlandite it replaced during low temperature alteration, in a similar manner to that proposed by Dare et al. (2011) and Djon and Barnes (2012) for the McCreeley East and Lac des Iles deposits, respectively. The comparable concentrations of IPGE in pyrrhotite, pentlandite and pyrite, further highlights the immobile manner of these elements during sulfide replacement within the GNPA member. In contrast, the lower concentrations of Pd ( $< 100$  ppm) in pyrite than typical of pentlandite ( $> 100$  ppm) being directly replaced is consistent with the geochemical data, indicating Pd has experienced partial remobilization during low temperature alteration (Fig. 4.8b). Our data also highlights the ability of pyrite to host appreciable concentrations of Rh ( $\geq 54$  ppm; Table 4.5). The mechanisms by which Rh becomes concentrated within secondary pyrite are at present not well understood. Our study revealed that millerite also hosts PGE in solid solution. Although concentrations of Pd, Rh and IPGE are typically lower than within pyrite, we suggest that millerite also directly inherited its PGE contents from the phases it replaced.

#### 4.9.3 **Evaluation of ore forming processes**

In starting to constrain the mechanisms involved in the formation of the mineralization within the GNPA member, we explore two genetic models that are attributed to the generation of PGE mineralization within the Merensky Reef and the Platreef. These are, respectively:

- (i) sulfide saturation during emplacement - extraction of PGE from new magma influx
- (ii) sulfide saturation in a staging chamber, with emplacement of pre-formed PGE rich sulfides

In the following discussion we apply our data for the GNPA member to these two models, thus highlighting any potential common ore forming processes and providing new constraints on the timing of S saturation relative to emplacement.

#### 4.9.3.1 Sulfide saturation during emplacement

The Merensky Reef represents a stratiform type deposit, which is believed by many to have formed principally by the settling of a dense, immiscible sulfide liquid through a column of S-saturated magma (see Barnes and Maier 2002a, b and references therein; see Naldrett et al. 2009 for an alternative model which is not discussed here). Mixing of residual and primitive (Main Zone) magmas is thought to have initially induced S saturation, consequently depleting the magma of its metals (Maier and Barnes 1999; Li and Ripley 2005). The Main Zone within the eastern and western limbs of the Bushveld Complex is therefore depleted of PGE and is considered unprospective. In the case of the GNPA member, we strongly believe that this model is not applicable for the following reasons. In recent years, it has become apparent that the Main Zone within the northern limb is also host to PGE mineralization (Maier and Barnes 2010; McDonald and Harmer 2011; Lombard 2012; Kinnaird et al. 2012; Holwell et al. 2013). On the farm Moorddrift (Fig. 4.1 and 4.2), Holwell et al. (2013) describes the sulfide associated mineralization as stratiform type reefs which are magmatic in origin and thus unrelated to the underlying GNPA member or Platreef. These observations, in conjunction with the identification of a magmatic break between the intrusion of the Platreef and Main Zone (Holwell et al. 2005; Holwell and Jordaan 2006) suggests that the Main Zone was emplaced as a fertile magma with a separate PGE budget from the underlying deposits. In addition, within the GNPA member PGE and BMS mineralization is hosted only within the LMF and MANO units, with the separating LGN unit (Fig. 4.2) being completely barren. De Klerk (2005) proposed that the LGN unit represents a sill of Main Zone, if this is accepted then it would suggest that an immiscible sulfide liquid was developed within both the LMF and MANO units prior to intrusion of the Main Zone. All of the above evidence strongly implies that (1) the GNPA member did not source its PGE *in situ* from the overlying Main Zone and (2) that S saturation occurred prior to emplacement of Main Zone.

Another feasible mechanism by which S saturation can be reached during emplacement is through *in situ* contamination. The addition of crustal S through assimilation of S-bearing country rocks is considered by many as being an essential process in the generation of large magmatic ore deposits (Leshner and Groves 1986). Where contamination occurs *in situ*,

sulfide mineralization is typically developed along the basal parts of the intrusion (e.g. Duluth Complex; Mainwaring and Naldrett 1977; Ripley 1981; Ripley et al. 1986; and the Basal Series of the Stillwater Complex; Lee 1996; McCallum 1996). Within the GNPA member however, mineralization is not restricted along its basal margin, being observed throughout the entire 400-800m thick succession. In addition this genetic model becomes more unfeasible for the GNPA member when the local country rocks are considered (Fig. 4.1, 4.2 and 4.3). West of the Grasvally Fault, the footwall consists of 800–1600m succession of Lower Zone cumulates (Fig. 4.1 and 4.2), if contamination was local and *in situ* then sulfide mineralization would not be expected to be developed throughout the GNPA member within this area. Furthermore, east of this fault the GNPA member is underlain by quartzites from the Magaliesberg Quartzite Formation, which are an unlikely source of crustal S as they do not contain significant quantities of S (Smith et al. 2013).

In addition, the restriction of Sb-bearing PGM to those sulfides which have experienced hydrothermal alteration is also inconsistent with this model. Hutchinson and Kinnaird (2005) and Hutchinson and McDonald (2008) highlighted that along with S, semi-metals (particularly Sb) are also introduced into the magma and sulfide liquid during assimilation of local country rocks (e.g. Platreef at Turfspruit). Therefore within the GNPA member one would expect the primary sulfide associated PGM assemblage to also be abundant in Sb-bearing PGM. Finally, preliminary S isotopic results provide no indication that the GNPA member experienced local contamination during or post emplacement but does reveal that the magma was extensively contaminated with crustal S (Smith et al. 2012; 2013). In considering all the evidence presented, it appears highly implausible that the parental magma (s) of the GNPA member became S saturated during emplacement, thus a model which enables the magma to be both S saturated and PGE-rich at the time of emplacement is more favourable.

#### 4.9.3.2 *Staging chamber model*

It is generally accepted that the Platreef was emplaced as a number of sills that already contained a PGE-enriched sulfide liquid (e.g. Lee 1996; Kinnaird 2005; Holwell et al. 2007; McDonald and Holwell 2007). In the current model, early-stage contamination induced sulfide immiscibility at depth prior to emplacement (Ihlenfeld and Keays 2011). The early-formed sulfide liquid subsequently became progressively enriched in PGE, Ni and Cu through reacting with multiple batches of silicate magma at low R factors. Subsequent to further upgrading by partial dissolution (in the manner described by Kerr and Leitch 2005)

the sulfides were remobilized and emplaced into the Platreef (McDonald and Holwell 2011; McDonald et al. 2012).

The stratigraphic setting of the GNPA member is analogous to that of the adjacent Platreef. In the discussion above, we suggested that the GNPA member in essence, requires a genetic model comparable to that proposed for the Platreef. The Lower Zone cumulates that directly underlying the GNPA member are PGE, Ni and Cu depleted (McDonald and Holwell 2007), a feature considered to be consistent with the enrichment of sulfides through processing of pre-GNPA magma (s) within a deeper magmatic system (see also McDonald et al. 2009). This therefore implies that the GNPA member may have sourced its PGE content from the magma which was intruded to form the underlying Lower Zone. The involvement of a deeper chamber is further supported by the S isotope evidence which suggests the GNPA member was extensively contaminated with crustal S (Smith et al. 2012; 2013), a feature not indicative of the *in situ* assimilation of S-bearing country rocks. Due to the lack of local S-bearing country rocks, this must have occurred in a deeper magmatic system.

If the Platreef genetic model is applied to the GNPA member then the development of elevated PGE tenors only within the Platreef (Holwell and McDonald 2007) must be plausibly accounted for. The lower PGE tenors of sulfides obtained through our LA-ICP-MS data associated with the GNPA member are interpreted to be a primary feature, as the current study highlights that hydrothermal fluids have not significantly redistributed PGE from BMS. Consequently the presence of lower tenors in the GNPA member may be ascribed to: its generation from magma poorer in PGE; interaction of sulfides with a smaller volume of magma compared to the Platreef; or dilution of the PGE content within sulfide prior to emplacement. Additionally, within the Platreef staging chamber partial dissolution of sulfides contributed to the development of high PGE tenors (McDonald et al. 2012) that are comparable to those in the Merensky Reef (Godel et al. 2007). Therefore it is also possible that this process of upgrading was not in operation within the system which supplied the GNPA member, resulting in sulfides appearing poorer in PGE. Although these suggestions still enable the GNPA member to correspond with the Platreef, this discussion raises the possibility that: (1) the GNPA and Platreef were derived from magma differing slightly in composition, particularly in terms of PGE content; and/or (2) that the parental magmas and PGE-rich sulfides of the GNPA member and the

Platreef were supplied from a complex network of chambers and conduits, where the degree of sulfide dissolution and PGE enrichment was variable.

In summary, from the data currently available we propose that the GNPA member was emplaced in a similar manner to the Platreef involving the development of a sulfide liquid, enriched in PGE by equilibrating with a large volume of magma at depth in a conduit system. At present the importance of early-stage crustal contamination in driving S saturation can only be speculated, and will only be revealed through application of other techniques such as S isotopes and S/Se ratios. We envisage that the GNPA member most probably formed within the same conduit network as the Platreef, notable differences however in PGE tenor suggests that different ore forming processes operated north and south of the Ysterberg–Planknek Fault.

#### **4.10 Conclusions**

This study has revealed that the distribution of platinum-group and chalcophile elements within the GNPA member results from the complex behaviour of these elements during both magmatic and hydrothermal processes. The distribution of PGE within the primary sulfide assemblage and associated Pt-As and Pd-Bi-Te dominant PGM assemblage is consistent with the fractionation of a single sulfide liquid. Post emplacement fluid interaction has resulted in: the decoupling of Pd, Au and Cu from sulfides on a centimetre to decimetre scale; and the development of a more Sb-bearing PGM assemblage, characteristic of hydrothermal fluids. Recrystallization of PGM and sulfides occurred *in situ*, resulting in pyrite and millerite inheriting PGE directly from the pyrrhotite and pentlandite replaced. We reveal therefore that pyrite and millerite can be important carriers of IPGE, Rh and Pd.

In starting to constrain the ore genesis of sulfide and associated PGE mineralization within the GNPA member, we reject any model where sulfide immiscibility was induced during or post emplacement and thus through either *in situ* contamination or depletion of an overlying magma column by a settling sulfide liquid. We therefore favour a model similar to that proposed for the Platreef, where PGE-rich sulfides were formed at depth in a conduit system prior to emplacement. It is not yet clear how the GNPA member relates to the Platreef, although it is likely that they formed within the same conduit network. Notable differences in PGE tenor suggests that the processes involved in ore formation and PGE-

enrichment may have differed within the parental magmas of the GNPA member and the Platreef.

#### **4.11 Acknowledgements**

The authors would like to thank Caledonia Mining Corporation and in particular Trevor Pearton, for allowing access to the drillcore on the farms Rooipoort, Grasvally and Moorddrift, and giving permission to publish this work. Jennifer Smith's Ph.D. research is funded by the Natural Environment Research Council (NE/1528426/1). Louis Cabri and an anonymous reviewer are thanked for their constructive comments on improving the quality of the manuscript.

## Chapter Five

The use of S isotopes and S/Se ratios in determining ore-forming processes of magmatic Ni-Cu-PGE sulfide deposits: a case study from the northern Bushveld Complex

### **Chapter 5 is to be submitted to a peer-reviewed journal**

Smith JW, Holwell DA, McDonald I, AJ Boyce. The combined use of *in situ* S isotope and S/Se ratios in determining ore-forming processes of magmatic Ni-Cu-PGE sulfide deposits: a case study from the northern Bushveld Complex.

I completed all sample preparation, figure production, S isotope analysis, data synthesis, data interpretation and the chapter. The co-authors assisted in data interpretation and were involved in discussion during preparation of this manuscript. Iain McDonald processed LA-ICP-MS data.

## 5.1 Abstract

In the study of magmatic Ni-Cu-PGE sulfide deposits, S/Se ratios and S isotopes have long been used to trace the initial source of S and to constrain the role of crustal contamination in triggering S saturation. In recent years it has however, become increasingly apparent that the interpretation of both indicators may be fraught with uncertainties, implemented by the ability of syn- and post magmatic processes to modify the initial values of both indicators. For the first time, I present *in situ* mineral  $\delta^{34}\text{S}$  signatures and S/Se ratios combined with bulk S/Se ratios to investigate and assess their utility on a mineralogical versus bulk rock scale in constraining ore-forming processes and the source of S within magmatic sulfide deposits.

At least within the Grasvally Norite-Pyroxenite-Anorthosite (GNPA) member, S isotopes appear to be relatively robust in comparison to S/Se ratios to the effects of magmatic and low temperature processes, and are interpreted to be effective in retaining the initial isotope composition of the earliest forming sulfide liquid. Similar to many other magmatic sulfide deposits, the addition of crustal S through the assimilation of S-bearing country rocks is shown to be critical in the genesis of PGE mineralization throughout the GNPA member. With a crustal component evident in the primary sulfide assemblage regardless of footwall lithology, it is inferred that the parental magma(s) of the GNPA member was crustally contaminated, and thus S saturated at the time of emplacement. With no indication the degree of contamination systematically increases towards the metasediment footwall it can be further concluded that any interaction of the magma with the local footwall during emplacement did not introduce additional crustal S into the magmatic system and thus had no control over ore genesis.

Since S/Se ratios of both the primary and secondary sulfide assemblages are inconsistent with the  $\delta^{34}\text{S}$  signatures, it is believed that the initial crustal S/Se ratio of the sulfide liquid has been significantly modified by both magmatic and low temperature processes. Within the secondary assemblage, lowering of the S/Se ratio of the primary sulfide relicts to values below that of the mantle range are attributed to a loss in S rather than a gain in Se. The observed variability in the S/Se ratio of secondary pyrite (ranging from below mantle to crustal values), is largely related to the ability of pyrite to effectively inherit the primary distribution of Se. Although the greater susceptibility of the S/Se ratio to being modified provides a unique insight into the processes operating during ore-formation, which are not revealed by S isotopes, caution is required when considering the source of S as the inferred role of crustal contamination may differ according to the technique used.

Whilst it is acknowledged that *in situ* S/Se ratios provide detail previously masked by bulk S/Se ratios, especially when considering the effects of low temperature alteration on the mobility of Se and S, bulk ratios are believed to be more useful when tracing the overall effects of ore-modifying processes and in constraining the initial S source. Through determining the Se concentration of sulfides it has become apparent that the variable partitioning behaviour of Se during fractionation of a sulfide liquid at high temperatures, can result in large variations in the S/Se ratio both within and between individual sulfide minerals.

## 5.2 Introduction

Fundamental to the development of a magmatic Ni-Cu-PGE sulfide deposit is the process of sulfide saturation in the magma which results in the separation of an immiscible sulfide liquid from a silicate magma. The source of S responsible for sulfide saturation has been the subject of much debate, with many considering the addition of crustal S via assimilation of S-bearing country rocks critical in the generation of large magmatic ore deposits such as Noril'sk and the Bushveld Complex (e.g. Grinenko 1985; Lesher and Groves 1986; Naldrett 1999; Lesher and Burnham 2001; Lesher and Keays 2002; Li et al. 2002; Lightfoot and Keays 2005). In the study of magmatic Ni-Cu-PGE sulfide deposits, S/Se ratios and S isotopes have long been used to investigate the source of S and thus to constrain the role of crustal contamination in triggering S saturation (e.g. Eckstrand and Cogulu 1986; Eckstrand et al. 1989; Peck and Keays 1990; Ripley 1990; Thériault and Barnes 1998; Holwell et al. 2007; Ihlenfeld and Keays 2011; Sharman et al. 2013). The S/Se ratio of the mantle is well-constrained at 2850–4350 (Eckstrand and Hulbert 1987), with average values indicated by McDonough and Sun (1995) and Lorand et al. (2003) of 3333 and 3150, respectively. The mantle also exhibits a constrained  $\delta^{34}\text{S}$  signature of  $0\pm 2\text{‰}$  (Ohmoto and Rye 1979). In comparison, crustal rocks exhibit  $\delta^{34}\text{S}$  values in the range of  $<-40\text{‰}$  to  $>+30\text{‰}$  and mostly have S/Se ratios of 3500 to 100,000. Magmatic Ni-Cu-PGE deposits characterized by S/Se ratios and  $\delta^{34}\text{S}$  values within or close to the mantle range suggests the S responsible for ore formation was of mantle origin (e.g. Buchanan et al. 1981; Barnes et al. 2009). In contrast, S/Se ratios exceeding the mantle range or  $\delta^{34}\text{S}$  signatures distinct from that of mantle S signify a substantial contribution of externally derived S (e.g. Thériault and Barnes 1998; Lesher and Burnham 2001; Ihlenfeld and Keays 2011). Ultimately, through utilizing S isotopes and S/Se ratios as tracers of S, we are capable of tracing the fundamental triggers of S saturation, and thus also gain fundamental constraints on the relative timing of key ore-forming processes.

In recent years, however, it has become apparent that the interpretation of S/Se ratios and to a lesser extent S isotope signatures is fraught with uncertainties, implemented primarily by the ability of syn- and post-magmatic processes to modify the initial values of both indicators. Magmatic and low temperature processes thought to be capable of significantly altering the initial S/Se ratio of a sulfide liquid include: variations in the sulfide to silicate ratio (R-factor; Queffurus and Barnes 2014); segregation of a sulfide liquid; preferential retention of Se in the mantle during partial melting (Hattori et al. 2002); apparent

fractionation of Se between monosulfide solid solution and intermediate solid solution; and post-magmatic S-loss (Yamamoto 1976; Howard 1997). It has also been proposed that the S/Se ratio can also be significantly modified by a process termed ‘multistage-dissolution upgrading’ which involves partially dissolving sulfide at depth (e.g. Kerr and Leitch 2005; Holwell et al. 2011; McDonald et al. 2012; Holwell et al. 2014). In previous studies the effect of these processes on the S isotope composition of the initial sulfide liquid has not been explored in any detail. The intent of this paper is to combine detailed S isotope data with S/Se ratios to establish whether they are modified independently by different processes.

Until recently, the Se concentration of sulfides could not be determined accurately using *in situ* techniques, thus until very recently (e.g. Prichard et al. 2013; Dare et al. 2014) previous studies utilized S/Se ratios that were representative of bulk rock values (e.g. Ripley 1990; Thériault and Barnes 1998; Ripley et al. 2002; Hinchey and Hattori 2005; Ihlenfeld and Keays 2011; Holwell et al. 2014). In this paper I present a laser ablation-inductively coupled plasma-mass spectrometry (LA-ICP-MS) study into the Se contents of sulfides and for the first time, combine this with a detailed  $\delta^{34}\text{S}$  study in order to investigate and assess their utility on a mineralogical versus bulk rock scale in constraining ore-forming processes and the source of S. In this paper I present *in situ* mineral  $\delta^{34}\text{S}$  signatures and S/Se ratios, combined with bulk S/Se ratios from a deposit within the northern limb of the Bushveld Complex referred to as the Grasvally Norite-Pyroxenite-Anorthosite (GNPA) member (Fig. 5.1). The GNPA member represents an excellent testing ground for such a study as it has a very well defined primary sulfide assemblage, a low-temperature hydrothermal sulfide overprint, a lack of metamorphism, well-constrained S isotope values for the local sub lithospheric mantle and crustal rocks, and a number of possible emplacement mechanisms (Westerlund et al. 2004; McDonald et al. 2005; Maier et al. 2008; Smith et al. 2011b; Sharman et al. 2013). We therefore have well constrained end members, and a range of easily identifiable and well-constrained processes that have the potential to modify the initial S/Se ratio and determine the S isotope signatures.

Through utilizing the GNPA member as a case study, I intend to: (i) constrain the initial source of S for the GNPA member (ii) investigate the behaviour of Se during both sulfide fractionation and low temperature hydrothermal alteration; (iii) re-evaluate by detailed comparison, the application of  $\delta^{34}\text{S}$  signatures and S/Se ratios in the study of magmatic sulfide deposits through assessing the effects of each process on each indicator; (iv) assess if

*in situ* S/Se ratios provide greater detail on the processes involved in ore-formation; and (v) highlight the importance of using S/Se ratios in conjunction with S isotopes.

### 5.3 Processes determining and modifying S/Se ratio

Due to the chalcophile nature of elements such as Se and PGE, their concentration in sulfide is primarily dependent on the ability of the sulfide liquid to effectively interact with a large volume of silicate magma (i.e. the R-factor). Whilst the sulfide/silicate melt partition coefficient ( $D_{\text{sul/sil}}$ ) of PGEs range from 17,000 to 92,000 (Naldrett 2011 and references therein; Peach et al. 1990), the ( $D_{\text{sul/sil}}$ ) of Se is less certain with very different values of 1700 and  $323 \pm 41.7$  being determined by Peach et al. (1990) and Patten et al. (2013), respectively. Regardless of the uncertainty surrounding Se ( $D_{\text{sul/sil}}$ ), variations in R-factor will also have an effect on a sulfides Se concentration and thus S/Se ratio (e.g. Thériault and Barnes 1998; Ihlenfeld and Keays 2011). To illustrate, an increase in R-factor will further enrich the sulfide liquid in PGE and Se, thus producing sulfides characterized by high PGE tenors and low S/Se ratios (i.e. lower than the mantle range; Queffurus and Barnes 2014). Low S/Se ratios combined with high PGE tenors can also potentially be generated through a process termed ‘multistage-dissolution upgrading’ (Kerr and Leitch 2005). Kerr and Leitch (2005) showed that in conduit type-settings sulfides may be partially dissolved as multiple batches of S-undersaturated magma interact with sulfide liquid. This process is analogous to an increase in R-factor, upgrading metal tenors of elements with high sulfide/silicate melt partition coefficients ( $D_{\text{sul/sil}}$ ), including the PGE and Se. Conversely, elements with low partition coefficients such as Fe and S will be preferentially resorbed by the magma thus the highest PGE tenor sulfides will exhibit the lowest S/Se ratios. Consequently, variations in R-factor and sulfide dissolution may mask or reduce an initial crustal or even mantle signature (e.g. Platreef, McDonald et al. 2012; River Valley Intrusion, Ontario, Holwell et al. 2014).

In addition the Se contents of the initial silicate magma may also be modified during crystallization through early extraction of a sulfide liquid from the silicate magma. Due to the high ( $D_{\text{sul/sil}}$ ) of Se this effectively depletes the remaining silicate magma in Se, increasing the S/Se ratio to crustal like values in the overlying cumulates (Barnes et al. 2009). Furthermore, due to the apparent preferential retention of Se over S in the mantle the initial Se concentration and thus S/Se values of mantle derived magmas may also vary depending on the degree of partial melting and previous melting history of the mantle source (Hattori et al. 2002). Thus magmas derived through re-melting of the mantle are considered capable of

producing very low S/Se ratios (<1000) as the magma is depleted in S and enriched in Se (Hattori et al. 2002).

The S/Se ratio can be modified further by late stage- to post-magmatic processes including: low temperature hydrothermal alteration; supergene weathering; serpentinization and metamorphism. As S is relatively more mobile than Se in hydrothermal fluids below temperatures of around 500°C (Ewers 1977) and is thus preferentially incorporated into aqueous fluids (Yamamoto 1976; Howard 1977), all of these processes can result in preferential S-loss leading to a lowering of S/Se ratios (e.g. Peck and Keays 1990; Cawthorn and Meyer 1993; Maier and Barnes 1996; Ripley et al. 2002; Hinchey and Hattori 2005).

#### **5.4 Processes determining and modifying S isotope composition**

Within magmatic Ni-Cu-PGE sulfide deposits  $\delta^{34}\text{S}$  signatures which deviate from the  $\delta^{34}\text{S}$  composition of mantle S, are often attributed to the assimilation of S-bearing country rocks, and incorporation of crustal S into the magmatic system. The role of crustal contamination in triggering S saturation can however only be assessed if the isotopic composition of the country rock S is distinct from that of the local mantle. Since the bacterial processes (biologically mediated reduction of sulfate, e.g. Chambers and Trudinger 1979; Habicht and Canfield 1997) responsible for much of the S isotope fractionation found in sedimentary rocks were not established during the Archaean, most Archaean and some Proterozoic sediments are characterised by mantle like  $\delta^{34}\text{S}$  signatures (Ripley and Li 2003). In addition to the assimilation of S-bearing country rocks, S isotope variations in mafic magmas may also be caused by magma degassing associated with low pressure emplacement, changes in the redox state of the magma, fractionation by crystallization of sulfide at different temperatures (Ohmoto and Rye 1979) and S isotope exchange between the crustally contaminated sulfide liquid and mantle S (Ripley and Li 2003). Whilst the effects of the former three processes on  $\delta^{34}\text{S}$  values are considered negligible (up to 1‰ fractionation; Ohmoto and Rye 1979; Miyoshi et al. 1984; Ripley and Li 2003, and references therein), S isotope exchange is capable of masking or eliminating an initial crustal  $\delta^{34}\text{S}$  signature and thus evidence of the earliest stage of ore genesis (e.g. Platreef; Ihlenfeld and Keays 2011). This process is thought to be accompanied by the upgrading of a sulfides metal tenor via reaction with uncontaminated, S-undersaturated magma (Ripley and Li 2003; Kerr and Leitch 2005).

In deposits which have experienced multiple contamination events (pre-, syn- and post-emplacement), the initial isotope composition of the sulfide liquid may also be erased or

overprinted by later, localised contamination through the addition of crustal S that is distinct in its isotopic composition (e.g. Platreef; Holwell et al. 2007; Ihenfeld and Keays 2011; Sharman et al. 2013). Consequently, where a host magma is known to have locally assimilated S-bearing country rocks, it is critical during the development of a genetic model that the role of multiple contamination events on the isotope signatures are carefully considered.

### **5.5 Geological Setting of the GNPA member**

The 400–800 m thick GNPA member is developed in the northern limb of the Bushveld Complex, to the south of the Ysterberg–Planknek Fault and lies at the equivalent stratigraphic position to the Platreef, being overlain by Main Zone cumulates of the Rustenburg Layered Suite. The GNPA member is underlain by Lower Zone cumulates west of the Grasvalley Fault and Paleoproterozoic sediments comprised of the Magaliesberg Quartzite Formation to the east (Fig. 5.1). The GNPA member comprises vari-textured gabbro-norites, norites, anorthosites, pyroxenites and a PGE-bearing chromitite (Hulbert 1983; Smith et al. 2011b) and is typically sub-divided into three distinct stratigraphic units (de Klerk 2005): the Lower Mafic Unit (LMF); the Lower Gabbro-norite Unit (LGN); and the Mottled Anorthosite Unit (MANO). The LMF is distinguished from the homogeneous gabbro-norites of the LGN by an increase in melanocratic lithologies, the development of a chromitite layer and elevated bulk Cr values. The MANO is recognised by a substantial increase in plagioclase cumulates and the development of lithologies such as mottled and spotted anorthosites (Hulbert 1983; Smith et al. 2011b). The LGN unit, which is completely barren of PGE-bearing sulfides is thought to represent a sill of Main Zone rocks (de Klerk 2005). Detailed descriptions on the geology of the succession and associated PGE and BMS mineralization are provided in Hulbert (1983), McDonald et al. (2005), Maier et al. (2008) and Smith et al. (2011b, 2014).

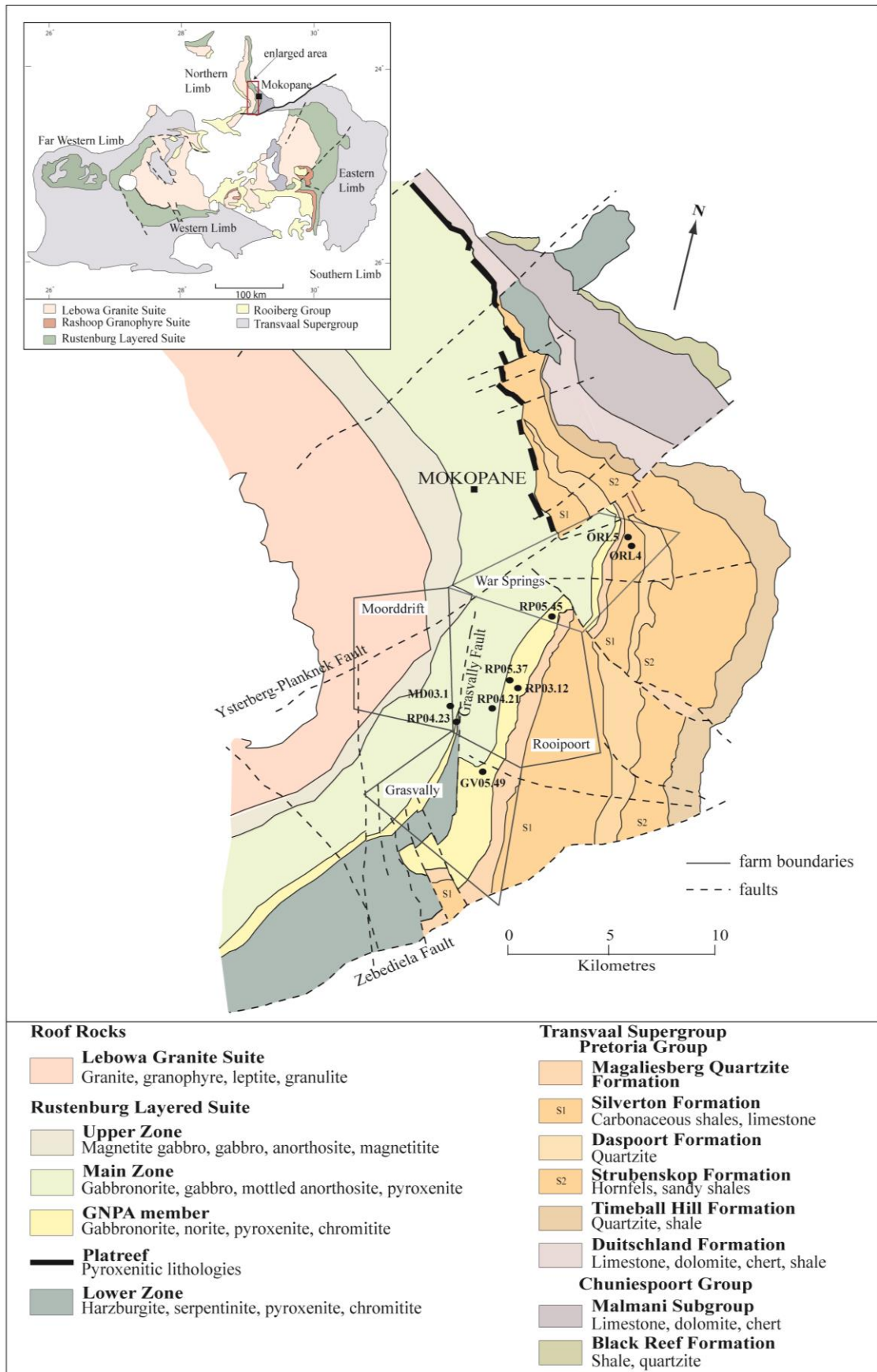


**Figure 5.1** Geological map of the northern limb of the Bushveld Complex showing locality of boreholes sampled and farms referred to in the text (adapted from van der Merwe 2008). Inset map of the entire Bushveld Complex modified from Eales and Cawthorn (1996).

### 5.5.1 Sulfide mineralogy

Within the GNPA member, the observed distribution and mineralogy of sulfides and PGE results from the interplay of both magmatic sulfide fractionation processes and low temperature (<230°C) fluid alteration (Fig. 5.2; Smith et al. 2011b; 2014). In places, a primary pyrrhotite–chalcopyrite–pentlandite sulfide assemblage (Fig. 5.2a) has been replaced to varying extents by a low temperature assemblage of pyrite, millerite and chalcopyrite (Fig. 5.2b and c). The degree of replacement varies significantly throughout the succession and can be viewed as a continuum from a purely magmatic sulfide assemblage to almost completely replaced sulfides (Fig. 5.2; Smith et al. 2011b). Remobilization and redistribution of PGE is limited, with sulfide associated platinum-group minerals recrystallized *in situ* and pyrite and millerite inheriting PGE contents of the phases replaced (Fig. 5.2; Chapter 4).

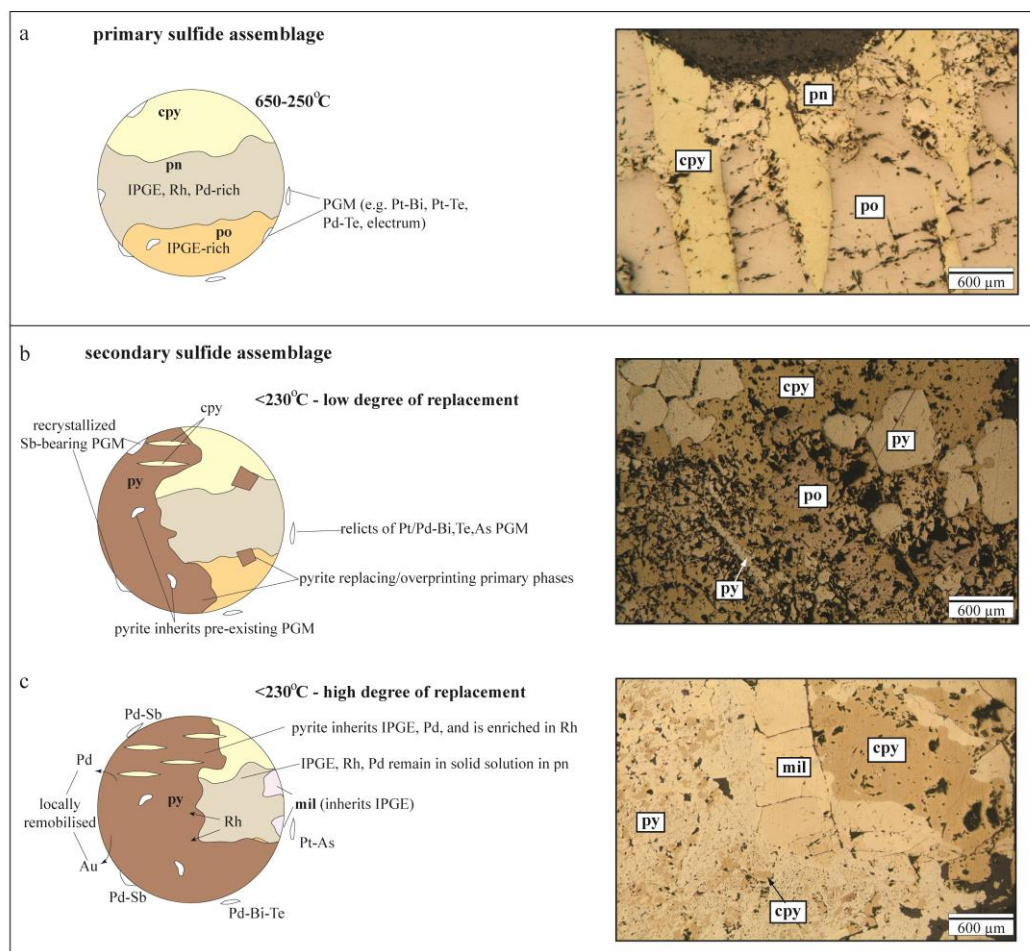


**Figure 5.2** Summary of the sulfide assemblages observed within the GNPA member showing the key mineralogical and textural changes observed during low temperature alteration of (a) a purely magmatic pyrrhotite (pn)-pentlandite (pn)-chalcopyrite (cpy) sulfide assemblage, (b) and (c) show variations in the extent of replacement by pyrite (py) and millerite (mil).

Within the Magaliesberg Quartzite Formation sulfides that are geochemically, texturally and mineralogically analogous to those developed within the GNPA member are interpreted to result from the infiltration of the magmatic sulfide liquid into the footwall (Smith et al. 2011b; Chapter 3). The quartzites which directly underlie the GNPA member east of the Grasvally Fault (Fig. 5.1) also contain some visible sedimentary pyrite, which is texturally distinct from the magmatic assemblage (Chapter 3; Fig. 3.6i and j). Sedimentary pyrite has only been observed in borehole RP05.45, GV05.49, ORL4 and ORL5. This pyrite is not host to PGE in solid solution or associated with a platinum-group mineral assemblage. Late-stage veins contain zones of abundant sulfides comprising chalcopyrite, pentlandite and galena which are PGE-poor.

### 5.5.2 Justification as a case study

The GNPA member was favourable as a case study for several reasons. Firstly the sulfide mineralization has been studied in detail, in terms of mineralogy, distribution and hydrothermal interaction (Smith et al. 2011b, 2014; Chapters 3 and 4), enabling the effects of any later alteration to be easily identified and thus considered in any interpretation. The well-defined primary sulfide assemblage and low temperature hydrothermal overprint provide a unique opportunity to assess in detail the partitioning behaviour of Se during sulfide fractionation and its mobility during low temperature alteration. Secondly, the isotopic composition of the local mantle and crustal rocks are well constrained providing reliable end members (Westerlund et al. 2004; Sharman et al. 2013). Additionally, the abundance of S isotope data available for the adjacent Platreef enables a direct comparison of the GNPA member with its nearest analogue (Manyeruke et al. 2005; Sharman-Harris et al. 2005; Holwell et al. 2007; Penniston-Dorland et al. 2008). Thirdly, as the GNPA member is underlain by Lower Zone cumulates and quartzites the effect, if any, of localised contamination and the *in situ* assimilation of country rocks should be easily recognized along with any related overprinting signatures. Finally, S/Se ratios and S isotope analyses have been obtained for the same samples and minerals, thus enabling a direct comparison of these two techniques.

## 5.6 Samples and Methods

Samples of quarter core were obtained from nine boreholes drilled by Falconbridge Ltd and Caledonia Mining on the farms Rooipoort, Grasvally, Moorddrift and War Springs (Fig. 5.1). In those drill cores sampled west of the Grasvally Fault, the footwall consists of Lower Zone harzburgites, whereas to the east quartzites from the Magaliesberg Quartzite Formation

underlie the GNPA member (Fig. 5.1). The sample suite covers a full range of GNPA member lithological units and mineralized zones, including areas identified by Smith et al. (2011b; 2014) that have experienced fluid interaction, and cover a strike length of around 15 km (Fig. 5.1).

The majority of the S isotope data (provided in Appendix 4) was determined utilizing the *in situ* laser ablation technique at SUERC within the NERC funded Isotope Community Support Facility (Table 5.1). This method was favoured over conventional analyses as textural inhomogeneities are easily identifiable, thus enabling the analysis of individual minerals within textually complex multi-phase sulfide aggregates. In addition it also allows analysis of sulfides that would be considered too small for conventional analysis. Polished blocks of 45 samples were placed into a sample chamber, which was evacuated and subsequently filled with an excess of oxygen gas. Sample areas, previously selected using reflected-light microscopy, were combusted using a SPECTRON LASERS 902Q CW Nd-YAG laser (1-W power), operating in TEM00 mode. Details of the system design, laser characteristics and experimental conditions are described in Kelley and Fallick (1990) and Wagner et al. (2002). The SO<sub>2</sub> gas produced by each laser combustion was cryogenically purified in a miniaturized glass extraction line using a CO<sub>2</sub>/acetone slush trap to remove water and a standard n-pentane trap to separate SO<sub>2</sub> from trace CO<sub>2</sub>. During the laser ablation technique there is a systematic fractionation of  $\delta^{34}\text{S}$  values of the resulting SO<sub>2</sub> gas compared to the mineral  $\delta^{34}\text{S}$  (Wagner et al. 2002). The fractionation factors used to correct the data are established for the SUERC facility and are as follows: pyrrhotite +0.4, pentlandite +1.9, chalcopyrite +0.7, pyrite +0.8 and millerite +1.9‰. Repeated analysis of individual sulfide phases revealed in general a reproducibility of  $\pm 0.2\%$ . Larger discrepancies (up to  $\pm 1\%$ ) however do exist between and within individual pyrite grains, revealing small-scale heterogeneity. All  $\delta^{34}\text{S}$  values were calculated relative to the Vienna-Canon-Diablo Troilite (V-CDT) standard and are reported in standard notation.

Several sulfide samples which exhibited textural and compositional homogeneity in reflected-light were selected for conventional analysis (see Appendix 4; Table 5.1). Individual sulfide phases were micro-drilled from nine polished blocks. Each analysis used 4-5 mg of sulfide which was subsequently converted to SO<sub>2</sub> for mass spectrometric analysis by combustion with 0.2 g of cuprous oxide, following the procedure of Robinson and Kusakabe (1975). Samples were combusted under vacuum at 1,070°C for 25 minutes and the SO<sub>2</sub> gas produced was purified prior to analysis in a VG SIRA II gas mass spectrometer in a glass

extraction line analogous to that used for laser analysis. Raw instrument  $\delta^{66}\text{SO}_2$  data were converted to  $\delta^{34}\text{S}$  values by calibration with international standards NBS-123 (+17.1‰) and AEA-S-3 (-31.5‰), as well as SUERC's internal lab standard CP-1 (-4.6‰).

Subsequent to  $\delta^{34}\text{S}$  analysis, Se concentrations of sulfides were determined *in-situ* by Laser Ablation-ICP-MS using a New Wave Research UP213 UV laser system coupled to a Thermo X Series 2 ICP-MS at Cardiff University. The relative abundances of PGE and other elements were recorded in time-resolved analyses mode (time slices of 250 ms) as the laser beam followed a line designed to sample different sulfide or oxide phases. The beam diameter employed was 30  $\mu\text{m}$ , with a frequency of 10 Hz and a power of  $\sim 6 \text{ J cm}^{-2}$ . The sample was moved at 6  $\mu\text{m sec}^{-1}$  relative to the laser along a pre-determined line pattern. Ablations were carried out under helium (flow  $\sim 0.7 \text{ L min}^{-1}$ ) and the resulting vapour combined with argon (flow rate 0.65-0.75  $\text{L min}^{-1}$ ) before delivery to the ICP-MS. Acquisitions lasted between 80 and 400 seconds, including a 20 second gas blank prior to the start of the analysis and a 10 second washout at the end. A detailed discussion on the errors associated with *in situ* determined Se concentrations is provided in Appendix 2 (pg 270). Counting errors averaged at 12% and 19% for standards containing 108 ppm Se and 57 ppm Se, respectively.

Sulfur concentrations were measured prior to LA-ICP-MS using the electron microprobe at the University of Leicester and  $^{33}\text{S}$  was used as internal standard as some sulfides did not contain Fe. Subtraction of gas blanks and internal standard corrections were performed using Thermo Plasmalab software. Calibration was performed using a series of 5 synthetic Ni-Fe-S standards prepared from quenched sulfides. The standards incorporate S, Ni, Fe and Cu as major elements and Co, Zn, As, Se, Ru, Rh, Pd, Ag, Cd, Sb, Te, Re, Os, Ir, Pt, Au and Bi as trace elements and the compositions of the 5 standards are given in Prichard et al (2013) and in Appendix 2. More detail on the standards used for calibration is provided in Prichard et al. (2013), Chapter 4 and Appendix 2.

In order to directly compare *in-situ* S isotopes with *in-situ* S/Se ratios, Se concentrations, where possible were obtained from the same grains but not the same spot as the  $\delta^{34}\text{S}$  analysis. In samples where the  $\delta^{34}\text{S}$  analysis resulted in combustion of the entire grain, Se was determined for adjacent grains. In the majority of samples *in situ* S/Se ratios utilize an average S content of either chalcopyrite, pyrite, pentlandite, pyrrhotite or millerite which

were determined by electron microprobe analysis prior to LA-ICP-MS (see Appendix 2). In samples where microprobe data was not available stoichiometric values of S were used.

Bulk rock S was determined by standard combustion procedures using a Laboratory Equipment Company C2320 (LECO) titrator at the University of Leicester. In total 23 samples were submitted to ALS Global Laboratories, Ireland, for determination of whole rock Se using Aqua Regia digest followed by ICP-MS and ICP-AES. The S content of sulfides analysed was obtained from a JEOL JXA-8600S electron microprobe at the University of Leicester using an accelerating voltage of 15 kV and a probe current of 30 nA with a focussed beam of <0.5 microns.

To recalculate whole rock Pt and Pd contents in 100% sulfide the formula provided by Barnes and Lightfoot (2005) was used:

$$C_{(100\%sul)} = C_{wr} \times 100 / (2.527 \times S + 0.3408 \times Cu + 0.4715 \times Ni)$$

Where  $C_{(100\%sul)}$  is the concentration of Pd or Pt in 100 % sulfide,  $C_{wr}$  is the concentration of the element in whole rock and  $S$ ,  $Cu$  and  $Ni$  is the concentration in wt % of these elements in whole rock.

## 5.7 Results

The  $\delta^{34}S$  signatures and S/Se ratios of samples representative of the entire GNPA member succession are provided in Figures 5.3, 5.5, 5.8 and in Tables 5.1 and 5.2. Throughout the GNPA member both the S/Se ratio and  $\delta^{34}S$  signature of the mineralized rocks does not vary systematically with stratigraphy (Table 5.1 and 5.2). Thus with the exception of the chromitites (Table 5.1) which are isotopically distinct from the rest of the succession, no evidence exists to suggest there is a depth or lithological control over the isotopic composition of the GNPA member. The S/Se ratio and/or  $\delta^{34}S$  signature do however show quite significant variations between and within primary and secondary sulfide assemblages. Within the following sections results are therefore presented in relation to this distinction.

**Table 5-1** Results of all conventional (c) and laser (l) S isotope analyses for GNPA member sulfides together with LA-ICP-MS determined S/Se ratios. See Figure 5.1 for location of boreholes. Lithological abbreviations: *MA* mottled anorthosite, *PYX* pyroxenite, *CPX* clinopyroxenite, *OPX* orthopyroxenite, *GBN* gabbro-norite, *NR* norite, *CR* chromitite, *QTZ* quartzite. Sulfide abbreviations *cpy* chalcopyrite, *cub* cubanite, *po* pyrrhotite, *pn* pentlandite, *py* pyrite, *mil* millerite, *py\** basement pyrite.

Borehole/depth	Lithology	Unit	Phase	Sulfide assemblage	$\delta^{34}\text{S}$ (‰ VCDT)	Technique	<i>in situ</i> S/Se
<b>RP04.23 – Rooipoort, Lower Zone footwall</b>							
157	MA	MANO	py	s	5	l	2318
191	PYX	MANO	pn	p	4	l	4148
191	PYX	MANO	pn	p	4	l	2147
191	PYX	MANO	cpy	p	2.8	l	
201	GBN	LGN	po	s	2.7	l	
305	NR	LMF	po	p	2.8	l	
330	GBN	LMF	po	p	2	c	
338	CPX	LMF	po	p	2.9	c	
384	GBN	LMF	po	p	3.5	c	
392	GBN	LMF	po	p	3.4	c	5297
392	GBN	LMF	po	p	3.5	c	4370
392	GBN	LMF	po	p	3.6	l	5335
392	GBN	LMF	cub	p	3.4	l	3289
392	GBN	LMF	cub	p			3156
392	GBN	LMF	cub	p			3466
392	GBN	LMF	pn	p	5.1	l	2613
392	GBN	LMF	pn	p	5.3	l	3621
396	GBN	LMF	po	p	3.3	c	
411	GBN	LMF	po	p	3.1	c	4800
411	GBN	LMF	po	p	3.2	l	2756
411	GBN	LMF	cub	p	4	l	4083
411	GBN	LMF	pn	p	5	l	4136
<b>RP05.45 – Rooipoort, quartzite footwall</b>							
146	GBN	LMF	py	s	6.8	l	3764
149	GBN	LMF	mil	s	3.9	l	
149	GBN	LMF	mil	s	3.6	l	
149	GBN	LMF	py	s	5	l	
149	GBN	LMF	py	s	4.2	l	
149	GBN	LMF	cpy	s	4.7	l	
165	GBN	LMF	cub	s	4.1	l	3535
165	GBN	LMF	cub	s	3.9	l	4776
165	GBN	LMF	py	s	3.9	l	4180
165	GBN	LMF	py	s	4.9	l	8267
165	GBN	LMF	py	s	4.9	l	4233
165	GBN	LMF	py	s		l	3948
165	GBN	LMF	mill	s	4.9	l	
166	CR	LMF	py	s	6.9	c	8611
166	CR	LMF	py	s	5.8	l	8546
166	CR	LMF	cub	s	5.3	l	5146
166	CR	LMF	cub	s			4116
166	CR	LMF	mil	s			2305
167*	CR	LMF	py	s	6.6	l	>8915 (min value as Se BDL)
167	CR	LMF	py	s	6.1	l	3364
167	CR	LMF	py	s	6.9	l	5183

167	CR	LMF	py	s	7.1	1	4863
167	CR	LMF	cub	s	5.4	1	1877
167	CR	LMF	cub	s	6.1	1	4096
167	CR	LMF	cub	s	4.4	1	4412
167	CR	LMF	cpy	s	4.4	1	
167	CR	LMF	cpy	s	2.8	1	
167	CR	LMF	pn	s	5.4	1	1919
167	CR	LMF	pn	s	5.6	1	2662
167	CR	LMF	pn	s	7.5	1	3015
167	CR	LMF	mill	s			2420
205	NR	LMF	py	s	4.1	1	
205	NR	LMF	py	s	4.3	1	
205	NR	LMF	mil	s	4.1	1	
205	NR	LMF	cpy	s	3.8	1	
206	CPX	LMF	cpy	s	3.9	1	
208	NR	LMF	py	s	5	1	8829
208	NR	LMF	py	s	4.9	1	3047
208	NR	LMF	py	s			5612
208	NR	LMF	pn	s	6	1	3695
208	NR	LMF	pn	s	5.8	1	2035
208	NR	LMF	pn	s			2325
208	NR	LMF	cub	s	5	1	2134
212	QTZ	FLR	py *	b	4.5	1	
212	QTZ	FLR	py *	b	4.1	1	
214	QTZ	FLR	py *	b	5.3	1	7731
214	QTZ	FLR	py *	b	5.6	1	8441
214	QTZ	FLR	py *	b	6.2	1	6916
214	QTZ	FLR	cub	s	3.6	1	3052
214	QTZ	FLR	cub	s	4.1	1	5917
214	QTZ	FLR	cub	s	4.5	1	
214	QTZ	FLR	mil	s	5.6	1	2217
214	QTZ	FLR	py	s	4.3	1	6476
215	QTZ	FLR	py *	b	4.1	c	6693
215	QTZ	FLR	py *	b	3.5	c	7875
215	QTZ	FLR	py *	b			5943
<b>RP04.21 – Rooipoort, quartzite footwall</b>							
448	MA	MANO	cpy	s	3.5	1	
448	MA	MANO	py	s	4.1	1	
448	MA	MANO	py+mil	s	3.6	1	
460	MA	MANO	po	p	2.3	1	
460	MA	MANO	po	p	2.5	1	
679	MA	MANO	py	s	3.5	1	8980
679	MA	MANO	py	s	3	1	3619
679	MA	MANO	py	s			5693
679	MA	MANO	po	s	1.7	1	2797
679	MA	MANO	po	s			3494
679	MA	MANO	po	s			2802
679	MA	MANO	pn	s	3.2	1	2126
679	MA	MANO	pn	s			2517
679	MA	MANO	cub	s	1.3	1	3328
679	MA	MANO	cub	s			2709
681	MA	MANO	cpy	s	2.8	1	

681	MA	MANO	pn+mil	s	2.4	1	
690	GBN	MANO	po	p	1.6	1	3564
690	GBN	MANO	po	p	1.9	1	3391
690	GBN	MANO	po	p	1.8	1	2592
690	GBN	MANO	po	p	2.9	1	3562
690	GBN	MANO	pn	p			2941
690	GBN	MANO	cpy	p			4004
693	GBN	MANO	po	p	2.6	1	4409
693	GBN	MANO	po	p	3.1	1	3922
693	GBN	MANO	po	p			3456
693	GBN	MANO	pn	p	4	1	2032
693	GBN	MANO	pn	p	4.7	1	3680
693	GBN	MANO	cpy	p	3.3	1	4008
<b>MD03.1 – Moorddrift, Lower Zone footwall</b>							
552	OPX	MANO	pn	s	3.5	1	2106
552	OPX	MANO	cub	s	2.4	1	2961
552	OPX	MANO	cub	s	2.9	1	2272
542	QTZ vein	MANO	cpy	s	8.1	c	
542	QTZ vein	MANO	cpy	s	8	c	
573	fracture fill	MANO	cpy	s	11.4	c	
573	fracture fill	MANO	cpy	s	11.9	c	
<b>RP05.37 – Rooipoort, quartzite footwall</b>							
106	GBN	MANO	py	s	4	1	
<b>RP03.12 – Rooipoort, quartzite footwall</b>							
140	GBN	LMF	py	s	2.3	1	
140	GBN	LMF	py	s	3.6	1	
144	PYX	LMF	py	s	4.5	1	
145	Cr	LMF	py	s	4.8	1	
<b>GV05.49 – Grasvally, quartzite footwall</b>							
127	Cr	LMF	py	s	4.3	1	
127	Cr	LMF	cpy	s	3.6	1	
128	Cr	LMF	py	s	6.3	1	
128	Cr	LMF	cpy	s	5.7	1	
128	Cr	LMF	pn	s	5.1	1	
140	GBN	LMF	po	s	4	1	
140	GBN	LMF	po	s	4.7	1	
140	GBN	LMF	cpy	s	3.2	1	
140	GBN	LMF	py	s	3.6	1	
214	QTZ	FLR	py*	b	10.5	1	
214	QTZ	FLR	py*	b	9.8	1	
<b>ORL 4 – War Springs, quartzite footwall</b>							
65	MA	MANO	py	s	3.5	1	
65	MA	MANO	pn	s	3.8	1	
65	MA	MANO	cpy	s	2.9	1	
221	PYX	LMF	cpy	s	1.9	1	
221	PYX	LMF	py	s	2.6	1	
221	PYX	LMF	py	s	2.4	1	
221	PYX	LMF	po	s	1.9	1	
221	PYX	LMF	po	s	0.9	1	
395	PYX	LMF	po	s	3.7	1	
395	PYX	LMF	po	s	4.2	1	
395	PYX	LMF	py	s	2.6	1	

395	PYX	LMF	pn	s	4.2	1
606	CR	LMF	po	s	5.5	1
606	CR	LMF	po	s	5.3	1
606	CR	LMF	po	s	5.8	1
606	CR	LMF	po	s	5.3	1
606	CR	LMF	cpy	s	5.1	1
606	CR	LMF	cpy	s	5.9	1
606	CR	LMF	po	s	4.6	1
<b>ORL5 – War Springs, quartzite footwall</b>						
97	MA	MANO	py	s	3.2	1
97	MA	MANO	py	s	3.2	1
108	GBN	LMF	py	s	2.6	1
108	GBN	LMF	cpy	s	2.6	1
597	PYX	LMF	py	s	5.1	1
597	PYX	LMF	py	s	5	1
597	PYX	LMF	pn	s	5.8	1

*S/Se ratios that are in italics represent the mean of several mineral analyses with comparable Se ratios*

### 5.7.1 Sulfur isotopes

I have performed the most comprehensive S isotope study to date on the area south of Mokopane, northern limb of the Bushveld Complex. The results of more than 130 analyses of sulfides from the GNPA member and associated country rocks on the farms War Springs, Rooipoort, Grasvally and Moorddrift (Fig. 5.1) are provided in Table 5.1. The isotopic composition of the mantle immediately beneath northern the Bushveld Complex has been inferred from sulfide inclusions within the Klipspringer kimberlite, 25 km east of Mokopane, which exhibits  $\delta^{34}\text{S}$  values of -1.8 to +2.4‰, with a mean of +1.0‰ (Westerlund et al. 2004). Previous studies into the isotopic composition of the Transvaal Supergroup have revealed that sulfide-bearing shales from the Deutschland Formation and Timeball Hill Formation have  $\delta^{34}\text{S}$  signatures ranging from -18‰ to +10‰ (Cameron 1982; Sharman-Harris et al. 2005; Sharman et al. 2013). Carbonates from the Deutschland Formation and Malmani Subgroup are isotopically distinct with  $\delta^{34}\text{S}$  signatures ranging from +10‰ to >+30‰ (Sharman et al. 2013).

#### 5.7.1.1 Non chromitiferous rocks

##### 5.7.1.1.1 Primary sulfide assemblages

The pyrrhotite-pentlandite-chalcopyrite assemblage (Fig. 5.2a) has a  $\delta^{34}\text{S}$  range of +1.6 to +4‰ with a mean of +2.8‰. The majority of analyses reveal signatures indicative of crustal derived S, with only five analyses, all of which were of pyrrhotite, residing within the local mantle range of -1.8 to +2.4‰ (Table 5.1). Even where the basal LMF unit is directly underlain by Lower Zone cumulates rather than metasediments of the Transvaal

Supergroup, all of the primary sulfides analysed reveal crustal  $\delta^{34}\text{S}$  signatures (Fig. 5.3a; Table 5.1).

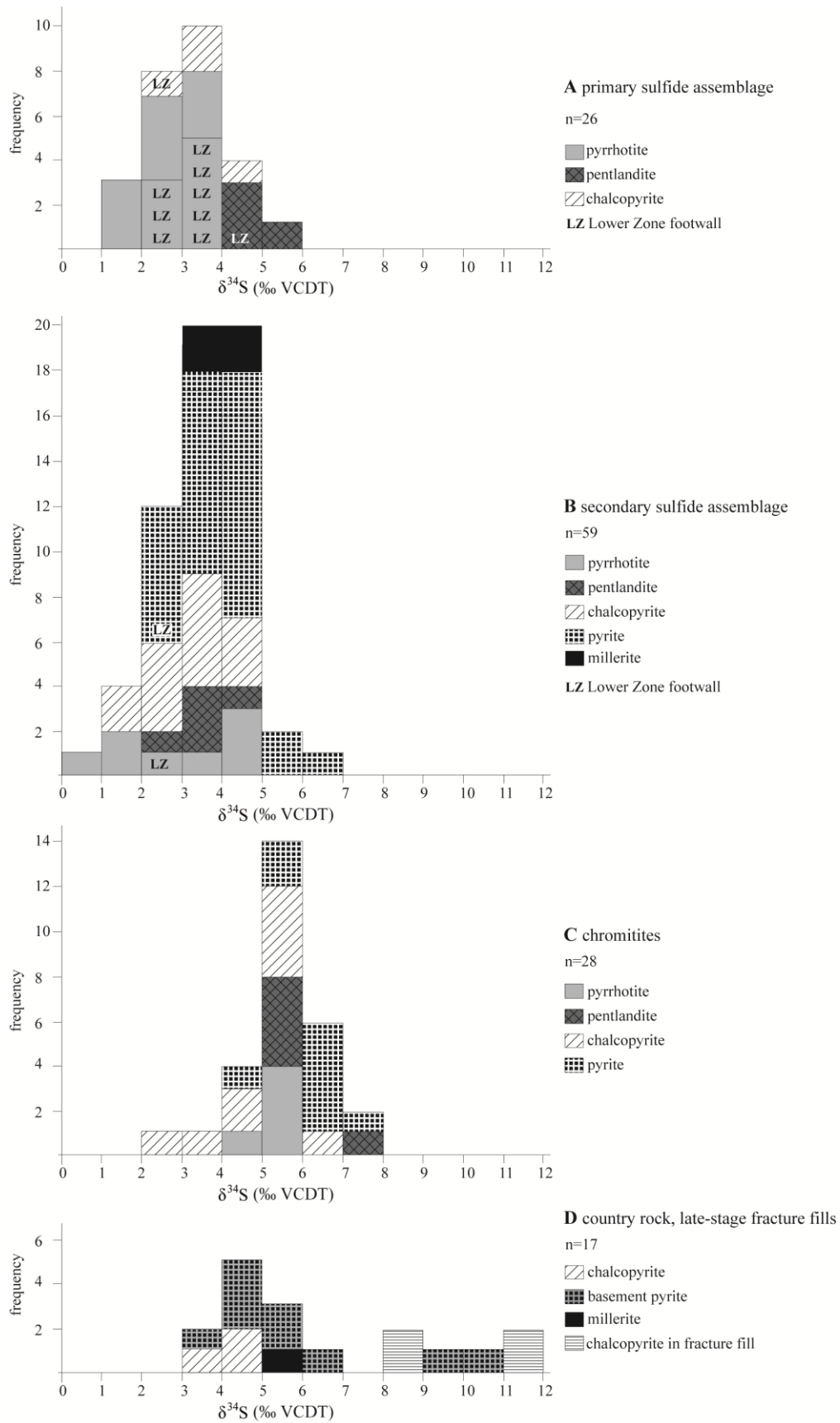


**Figure 5.3** Range in  $\delta^{34}\text{S}$  values for all observed sulfide phases within the GNPA member and its footwall for a) primary sulfide assemblage; b) secondary sulfide assemblage; c) sulfides developed within chromitites; and d) sulfides present within the local footwall and late-stage fracture fills. LZ indicates samples analysed with a Lower Zone footwall.

#### 5.7.1.1.2 *Secondary sulfide assemblages*

Where the primary sulfides have been replaced to varying degrees by pyrite and millerite (Fig. 5.2b and c), S isotope signatures of the 59 analyses range from  $\delta^{34}\text{S}$  +0.9 to +6.8‰ with a mean of +3.5‰. A strong crustal S component is evident within the majority of the early (pyrrhotite, chalcopyrite and pentlandite) and throughout the late (pyrite and millerite) forming sulfide phases with  $\delta^{34}\text{S}$  signatures ranging from +2.6 to +6.8‰ (Fig. 5.3b). However, relicts of primary pyrrhotite and chalcopyrite occasionally exhibit  $\delta^{34}\text{S}$  values consistent with local mantle S, whilst co-existing pentlandite and secondary pyrite have crustal  $\delta^{34}\text{S}$  signatures. Isotopic values consistent with mantle, ranging from  $\delta^{34}\text{S}$  +0.9 to +2.4‰ were only identified within ten analyses (Table 5.1). Within samples, sulfide phases are slightly heterogeneous in terms of their isotopic composition, with less than 2‰ variation observed (Table 5.1). There is no evidence of a stratigraphic control over the distribution/preservation of the mantle like signatures as they are distributed throughout the GNPA member, being observed within the basal LMF and upper MANO units and where underlain by Lower Zone cumulates and quartzites.

#### 5.7.1.2 *Chromitiferous rocks*

Throughout the Rooipoort and War Springs region the chromitites are isotopically distinct from the rest of the GNPA member, with  $\delta^{34}\text{S}$  values consistently 1 to 2‰ heavier than the primary and secondary sulfide assemblages (see Fig. 5.3c). The chromitites reveal a strong crustal S component with  $\delta^{34}\text{S}$  signatures ranging from +2.8 to +7.1‰ with a mean of +5.4‰ (Table 5.1; Fig. 5.3c).

#### 5.7.1.3 *Country rock and late-stage fracture fills*

Sulfides within the quartzite footwall, interpreted to have resulted from infiltration of the magmatic sulfide liquid into the footwall (Smith et al. 2011b; Chapter 3) and are thus fundamentally magmatic, are isotopically similar to those developed within the GNPA member, exhibiting a range from  $\delta^{34}\text{S}$  +3.6 to +5.6‰ (Table 5.1; represented by chalcopyrite and millerite in Fig. 5.3d). Conversely, sedimentary pyrite hosted within the Magaliesberg Quartzite Formation (Chapter 3) display greater variation in  $\delta^{34}\text{S}$  signatures and a very strong crustal component with values ranging from  $\delta^{34}\text{S}$  +3.5 to +10.5‰ (Table 5.1; represented by basement pyrite in Fig. 5.3d).

Chalcopyrite-bearing late stage fracture fills within the GNPA member have S isotope values that are significantly heavier than those associated with primary and secondary assemblages, with values around  $\delta^{34}\text{S} +8$  to  $+11\%$ , respectively (Fig. 5.3d; Table 5.1).

**Table 5-2** Whole rock S and Se for primary (p) and secondary (s) sulfide-bearing samples within the GNPA member together with PGE tenors (calculated using Barnes and Lightfoot 2005 formula). Abbreviations *FLR* floor rocks (quartzites), *LMF* Lower Mafic Unit, *MANO* Mottled Anorthosite Unit and *Cr* chromitite.

Borehole	Sample/ depth	Unit	Sulfide	Se ppm	S wt %	S/Se	Pt+Pd (ppb)	Pd in 100% sulfide ppm	Pt+Pd in 100% sulfide ppm
RP04.23	144	MANO	p	6.10	2.108	3456.23	1168	17	20
	157	MANO	s	3.00	0.806	2686.67	932	38	43
	201*	MANO	s	<0.20	0.084	4210.00*	143	41	61
	300	CR	p	1.50	0.266	1773.33	978	40	127
	305	LMF	p	3.50	0.751	2145.14	129	4	6
	338	LMF	p	0.70	0.292	4175.71	281	9	36
	384	LMF	p	0.70	0.406	5804.29	167	12	15
	392	LMF	p	0.90	0.512	5692.22	161	8	11
	411	LMF	p	0.70	0.434	6195.71	85	5	7
RP05.45	146	LMF	s	0.40	0.123	3067.50	139	34	49
	165	LMF	s	0.20	0.135	6765.00	126	27	36
	167	CR	s	2.10	0.735	3500.00	3603	85	153
	205	LMF	s	2.50	0.374	1494.80	1454	132	154
	208	LMF	s	0.50	0.080	1596.00	520	157	231
	215	FLR	s	1.20	0.428	3566.67	760	50	61
	214	FLR	s	8.30	3.340	4024.10	3389	26	36
	RP04.21	448	MANO	s	1.00	0.379	3786.00	1064	70
681	MANO	s	0.90	0.368	4083.33	474	33	48	
690	MANO	p	4.40	1.650	3750.00	1283	23	29	
693	MANO	p	2.00	0.808	4038.00	1048	31	48	
MD03.1	552	MANO	s	4.70	0.991	2107.87	1915	32	66
GV02.1	166	MANO	p	3.90	1.468	3765.13	2115	46	56
	476	LMF	s	3.20	1.856	5800.00	675	7	13

201\* S/Se ratio is a minimum value as detection limit is 0.2 for Se.

### 5.7.2 Bulk S/Se ratios

Mineralized rocks within the GNPA member typically contain 0.1 to 2 wt% S and Se concentrations of <0.2 (detection limit) to 6.1 ppm (Table 5.2). Due to the highly compatible nature of Se in sulfide a strong positive correlation exists between S and Se throughout the succession (Fig. 5.4). Sulfur/Se ratios are variable from 1495 to 6765, with the majority of samples residing within or below the mantle range of 2850–4350 (Eckstrand and Hulbert 1987; Table 5.2; Fig. 5.4). However, three primary and two secondary sulfides analysed, exhibiting ratios which exceed that of the mantle (Fig. 5.4; Table 5.1), are consistent with a crustal source of at least some of their S. These crustal signatures are associated with samples from the LMF unit, most of which were obtained west of the Grasvally Fault where Lower Zone cumulates underlie the GNPA member (Fig. 5.1; Table 5.2).

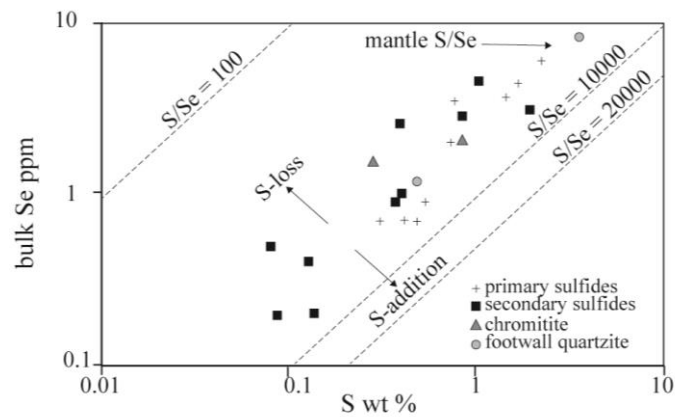


**Figure 5.4** Sulfur in wt% versus Se (ppm) for different sulfide assemblages hosted within the GNPA member.

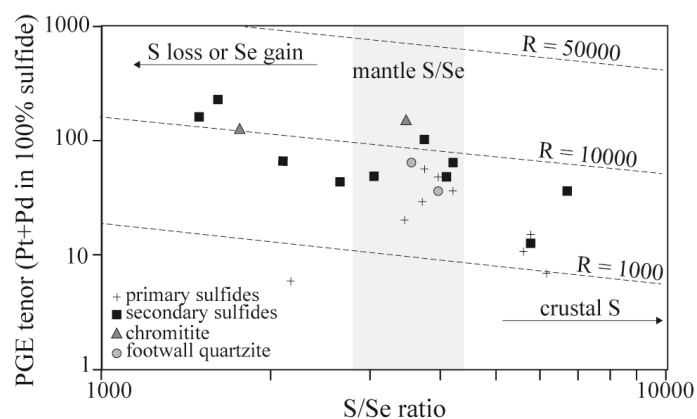


**Figure 5.5** PGE tenor (Pt + Pd in 100% sulfide), versus bulk S/Se ratio for samples within the GNPA member. Mantle S/Se range is taken from Eckstrand and Hulbert (1987). Data is overlain by different R-factor values which are taken from Queffurus and Barnes (2014).

From the broad negative correlation observed between PGE tenor (defined by Pt+Pd in 100% sulfide) and S/Se ratio, primary and secondary sulfides can be distinguished (Fig. 5.5). The former are in general, characterized by relatively low PGE tenors (typically between 6- <60 ppb, with the exception of the chromitite; Table 5.2), and S/Se ratios within or above the mantle range (3500-6500; Table 5.2). With the exception of one anomalous sample (RP04.23/305), primary sulfides show no evidence that they have experienced significant S-loss or addition of Se (Fig. 5.4 and 5.5). In comparison, secondary sulfides are characterized by notably lower S/Se ratios from 1495 to 4210 with only two samples residing within the crustal field (RP05.45/165, 6765; GV02.1/476, 5800), and higher PGE tenors (40 to <160 ppb with exception of GV02.1/476; Fig. 5.5; Table 5.2). Figure 5.5 illustrates clearly that as the S/Se ratio decreases to values lower than that of mantle, the PGE tenor progressively increases, signifying either S-loss or addition of Se and PGE. The Se content throughout the GNPA member increases relative to bulk PGE content (Pt+Pd; Fig. 5.6a), indicating that both are controlled relatively analogously by the presence of sulfide. A strong correlation also exists between PGE tenor and Se tenor throughout primary and secondary sulfides (Fig. 5.6b).

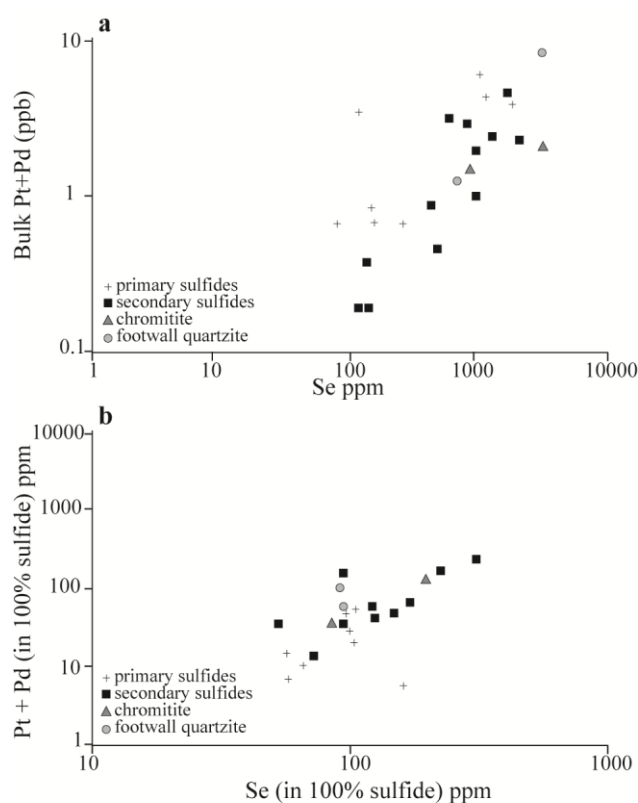


**Figure 5.6** Relationship between a) whole rock Se and PGE grade, and b) Pt+Pd tenor and Se tenor.

### 5.7.3 *In situ* S/Se ratios

The S/Se ratio of sulfides was calculated using Se concentrations from LA-ICP-MS analysis and S contents determined by electron microprobe (Appendix 2). The S values represent averages of the sulfide phase in each sample. Where microprobe data was not available, stoichiometric S values were utilized. The Se content of pyrrhotite, chalcopyrite, pentlandite, millerite and pyrite typically varies from the detection limit of 60 ppm up to 170 ppm (Table 5.3). Within the chromitites, concentrations of Se are noticeably elevated within pentlandite and millerite containing up to 220 ppm and 600 ppm, respectively. Representative time resolved analysis (TRA) spectra for the major sulfide phases analysed are provided in Figure 5.7. It is apparent that whilst all the magmatic sulfide phases contain detectable concentrations of Se in solid solution (Fig. 5.7a-g), the Se contents of crustal pyrite from the local footwall is noticeably lower at <68 ppm (Fig. 5.7h). Although the Se content of the individual sulfide phases varies slightly between samples, Se appears to be distributed uniformly within each sulfide phase. This is especially apparent within the primary pyrrhotite, pentlandite and chalcopyrite assemblage (Fig. 5.7a-d). Additionally, in comparison to elements such as Co and As which are clearly zoned within pyrite (Fig. 5.7g), there is no evidence that Se is zoned within any of the primary sulfide phases developed within the GNPA member (Fig. 5.7a-h).

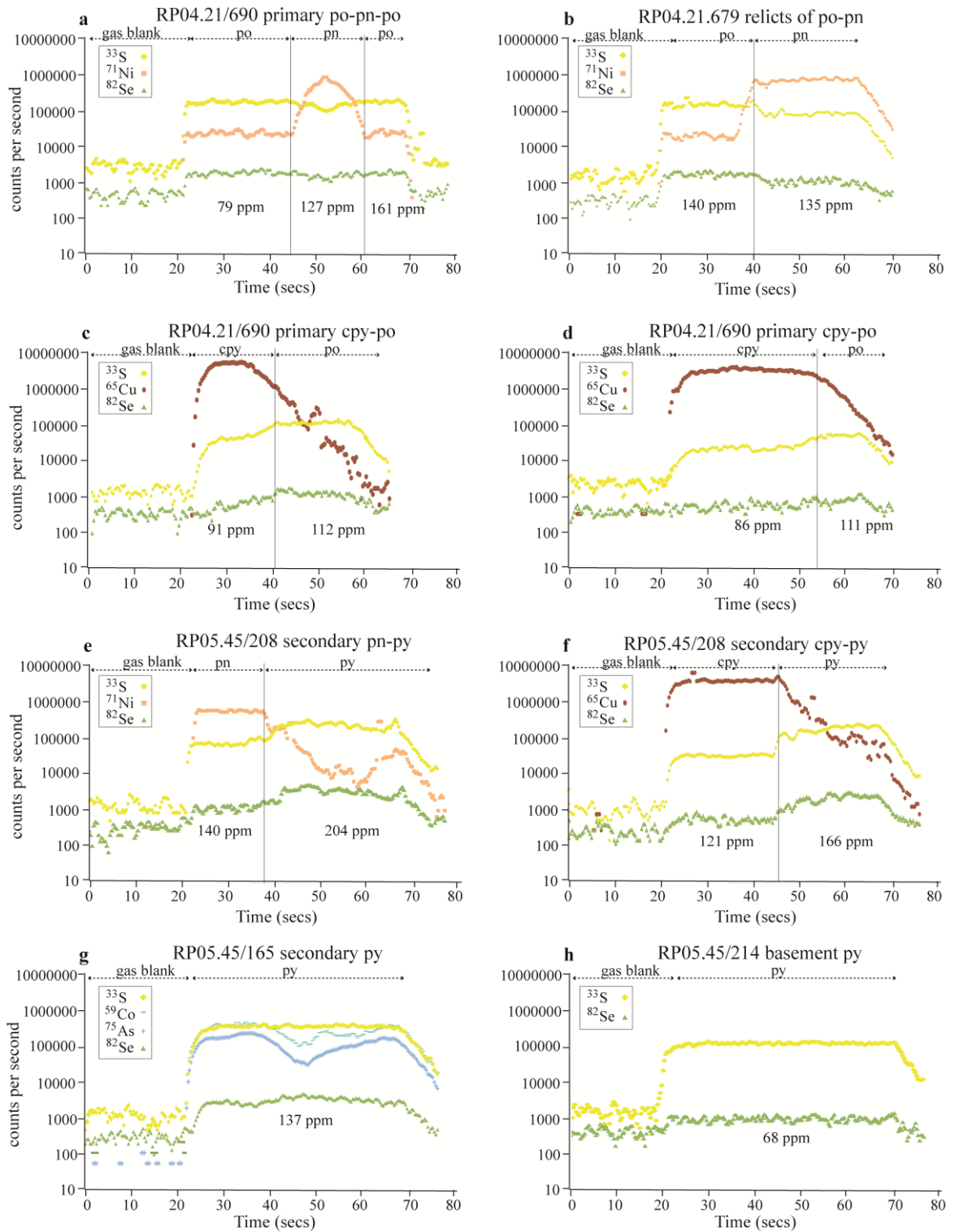


**Figure 5.7** Selected TRA spectra for a) and b) primary pyrrhotite and pentlandite, c) and d) primary chalcopyrite and pyrrhotite, e) pyrite replacing pentlandite, f) pyrite and chalcopyrite relicts, g) secondary pyrite developed within the GNPA member zoned in Co and As and h) pyrite from the Magaliesberg Quartzite Formation.

### 5.7.3.1 *Non chromitiferous rocks*

#### 5.7.3.1.1 *Primary sulfide assemblages*

Sulfur/Se ratios in chalcopyrite, pyrrhotite and pentlandite vary from 2032 to 5726 (Fig. 5.8a). Mantle S/Se ratios are widespread and are observed in all sulfide phases. Ratios lower than that of mantle are uncommon, occurring only in pyrrhotite from west of the Grasvally Fault, where Lower Zone underlies the GNPA member. Sulfur/Se ratios significantly lower than the mantle are also rare.

#### 5.7.3.1.2 *Secondary sulfide assemblages*

Relicts of primary pyrrhotite, chalcopyrite and pentlandite typically exhibit lower S/Se ratios than observed in the primary sulfide assemblage although the range in ratios is comparable at 2035 to 5917 (Table 5.1; Fig 5.8a and b). Most occurrences fall within the range of 2035 to 3695, which includes a significant proportion of pentlandite displaying S/Se ratios lower than mantle (Fig. 5.8b; Table 5.1). Pyrite and millerite are characterised by more variable S/Se ratios which fall within the range of 1975 to 8980 (Table 5.1). The S/Se ratio of pyrite within individual samples can be highly variable with mantle and crustal values commonly observed. Pyrite from the quartzite footwall exhibits crustal S/Se ratios in the crustal range of 5943–8455 (Fig. 5.8b; Table 5.1).

### 5.7.3.2 *Chromitiferous rocks*

Pyrite exhibits comparable S/Se ratios to that developed within the secondary sulfides, with crustal and mantle ratios observed (3364–8915; Table 5.1; Fig. 5.8b and c). Within the chromitites on Rooipoort and Grasvally, no pyrrhotite remains, however remnants of primary chalcopyrite and pentlandite have S/Se ratios within the range of 1544–5146, with several analyses revealing S/Se ratios significantly lower than the mantle range (Table 5.1; Fig. 5.8c).

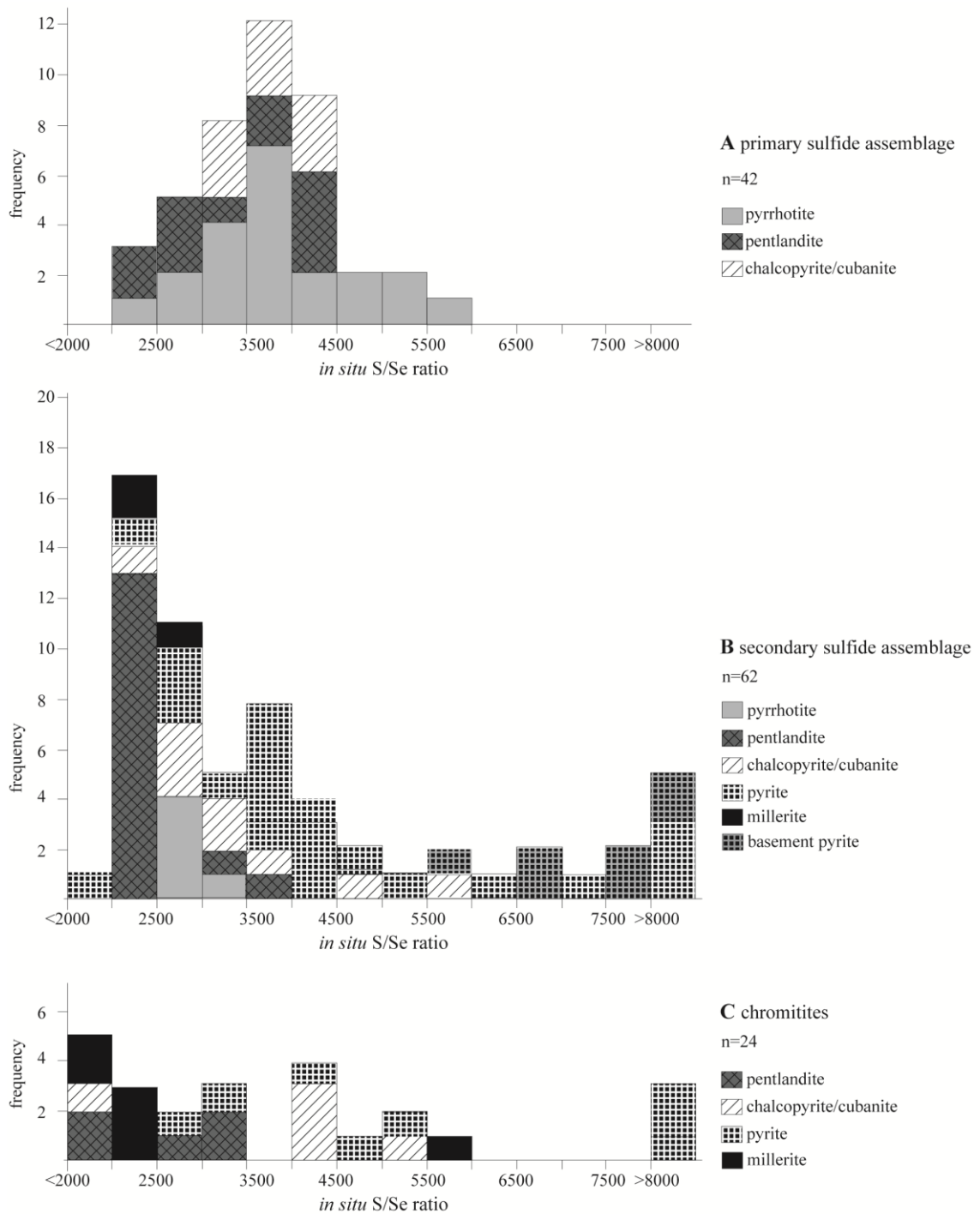


**Figure 5.8** Range in S/Se ratio for individual sulfide phases calculated from LA-ICP-MS for a) primary sulfide assemblage; b) secondary sulfide assemblage; c) sulfides developed within chromitites.

## 5.8 Comparison of S/Se ratios and S isotopes

The dominance of  $\delta^{34}\text{S}$  signatures distinct from that of mantle S, throughout the primary and secondary sulfide assemblages suggests a significant and extensive contribution of externally derived crustal S (Fig. 5.3). The results are in agreement with the limited (n=16)  $\delta^{34}\text{S}$  data previously presented by Maier et al. (2008) on the GNPA member which ranges from  $\delta^{34}\text{S}$

+1.8‰ to +5.1‰ with a mean of +3.7‰. Sulfur/Se ratios in comparison, are however more consistent with a mantle rather than a crustal S source, since the majority of bulk rock and *in situ* sulfide S/Se ratios reside within, close to, or below the mantle range of 2850–4350 (Eckstrand and Hulbert 1987). Without consideration for the many syn- and post- magmatic processes which can modify the initial ratio, the scarcity of S/Se ratios within the crustal range (Fig. 5.4 and 5.5) could be interpreted to indicate only a minimal input of crustal derived S, which is inconsistent with the  $\delta^{34}\text{S}$  data.

Although mineralized samples from the GNPA member are characterised by  $\delta^{34}\text{S}$  and S/Se ratios values that are indicative of both crustal and mantle S (i.e. neither indicator is confined to only mantle or crustal values), Figure 5.9 illustrates that within individual samples the  $\delta^{34}\text{S}$  signatures are rarely in agreement with the S/Se ratios. The notable lack of relationship between bulk rock S/Se ratios and S isotopes within the GNPA member is particularly apparent within the chromitites, which exhibit the most crustal  $\delta^{34}\text{S}$  signatures but are characterized by mantle S/Se ratios (Fig. 5.9). Disparities between the S/Se ratio and  $\delta^{34}\text{S}$  signature of the mineralized rocks (Figure 5.3, 5.5, 5.8, 5.9), suggest magmatic and/or low temperature processes have modified the S/Se ratio and/or the  $\delta^{34}\text{S}$  signature of the initial sulfide liquid. Although the *in situ* S/Se ratios show greater variability and complexity in comparison to bulk rock ratios, similar features and discrepancies with the  $\delta^{34}\text{S}$  signatures are also observed on a mineralogical scale throughout the GNPA member (see Figure 5.9 and 5.10).

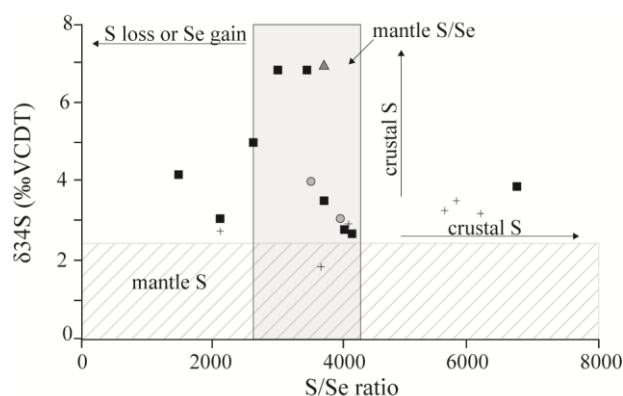


**Figure 5.9** Relationship between average  $\delta^{34}\text{S}$  signature of all the phases and the bulk S/Se ratio. See Figure 5.4 and 5.5 for symbol signs.

### 5.8.1 Primary sulfide assemblage

While the isotopic composition of coexisting pyrrhotite, pentlandite and chalcopyrite is rather consistent, the S/Se ratio shows greater variability both between and within the

individual sulfide phases (Fig. 5.10a; Table 5.1). Consequently, those samples exhibiting comparable crustal S/Se ratios and  $\delta^{34}\text{S}$  signatures (Fig. 5.9), on a more detailed scale, the individual phases have both a mantle and crustal component (see RP04.23/392 and 411 in Fig. 5.10a). In addition, whilst both the bulk rock and *in situ* sulfide S/Se ratios do not indicate values significantly below that of mantle, within two samples the *in situ* ratios are not representative of the bulk analysis. In both cases (RP04.23/392; 411; Fig. 5.10a), the bulk S/Se ratio is characterised by higher values than observed within the individual sulfide phases. Such disparities between the two analytical techniques could reflect a bias in the sulfide grains selected for LA-ICP-MS analysis.

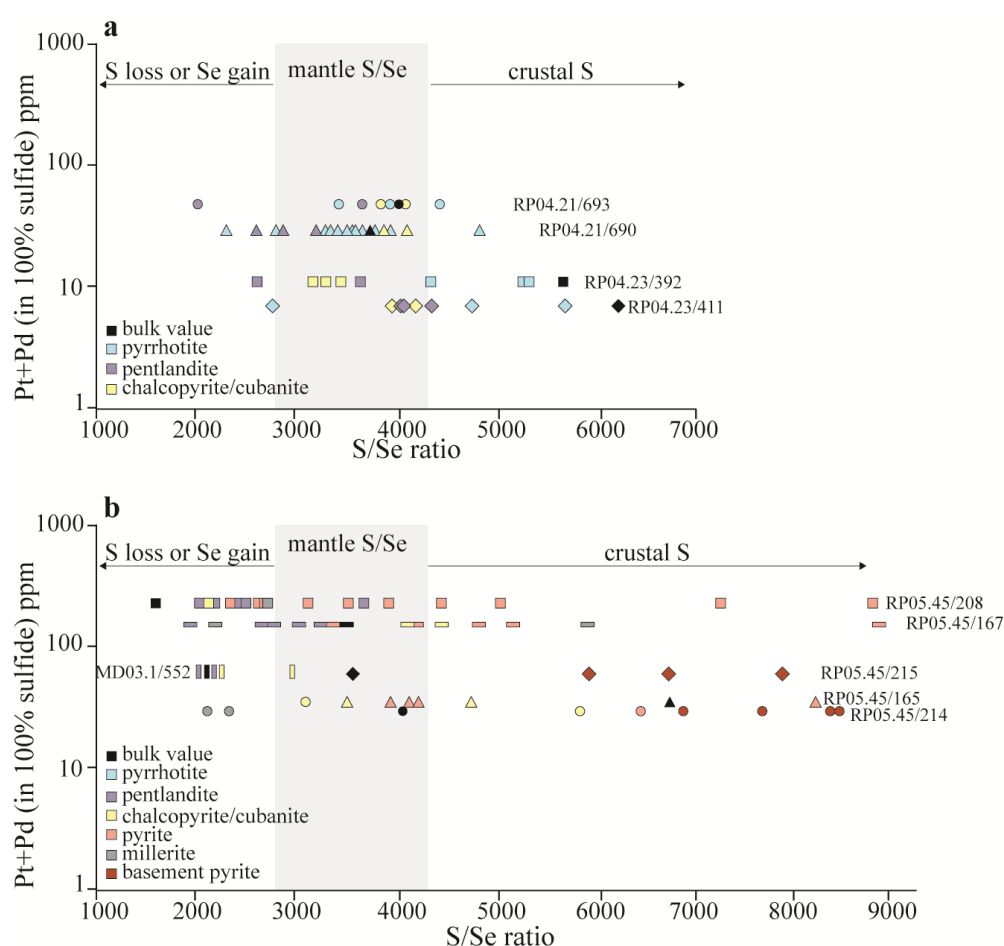


**Figure 5.10** Comparison of bulk S/Se ratios and the S/Se ratio of individual sulfide phases. All S/Se ratios are plotted against bulk Pt+Pd tenor for a) primary sulfide assemblages and b) secondary sulfide assemblages including footwall samples.

### 5.8.2 Secondary sulfide assemblage

The *in situ* analysis of secondary sulfides reveals that the S/Se ratio is more variable than within the unaltered sulfides, ranging from below mantle to crustal values within a single sample (Fig. 5.10b). With the exception of several chalcopyrite analyses which retain crustal

values, primary relicts are characterized by much lower S/Se ratios than typical of the unaltered samples being confined to within or below the mantle range (Fig. 5.10b). Such observations strongly imply that low temperature alteration modified the initial S/Se ratio, possibly in response to S-loss.

Throughout the secondary assemblages, the greatest variability in S/Se ratio is associated with the low temperature pyrite and millerite. The range in S/Se ratios is a true reflection on the variable Se contents of the pyrite, which is attributed to the extent to which the primary sulfide phases have been replaced and the ability of pyrite to inherit their Se contents. To illustrate, pyrite characterised by high concentrations of Se and thus low S/Se ratios that are comparable to the primary relicts indicates that the pyrite was effective in inheriting and/or scavenging Se from the primary sulfides being replaced. In comparison, individual pyrite grains with low Se contents and S/Se ratios consistent with a crustal origin could be indicative of pyrite which had minimal interaction with primary phases and/or did not inherit sufficient concentrations of Se from the primary phases (Fig. 5.10b).

Similar to the primary sulfides, it is apparent from Figure 5.10b that in many samples, *in situ* S/Se ratios are not representative of the significantly lower bulk values. Consequently, bulk signatures are rarely indicative of the elevated crustal signatures associated with much of the pyrite (e.g. RP05.45/165 Fig. 5.10b), possibly reflecting an analytical bias in terms of the grains selected for LA-ICP-MS analysis.

### **5.8.3 Footwall sulfide assemblages**

Within the quartzite footwall, represented by samples RP05.45/214 and RP05.45/215 in Figure 5.10b, the bulk S/Se ratio resides well within the mantle range. It is only through investigating on a mineralogical scale however that it becomes apparent that individual minerals actually exhibit ratios either within the crustal range close to that of the basement pyrite or significantly lower than that of mantle (Fig. 5.10b). In addition, the consistently high crustal S/Se ratios associated with the sedimentary pyrite confirms that it is unrelated to the magmatic sulfide liquid which has infiltrated into the footwall.

## **5.9 Discussion**

### **5.9.1 Primary partitioning behaviour and secondary mobility of Se in sulfides**

With the well-defined primary sulfide assemblage and a low-temperature hydrothermal sulfide overprint, the GNPA member provides an excellent opportunity to investigate both the partitioning behaviour of Se during magmatic sulfide fractionation processes and during

low temperature fluid alteration (<230°C) which has not been previously attempted. Since there is greater analytical error associated with Se concentrations that are close to the detection limit of 60 ppm (see Appendix 2), values <80 ppm have been excluded when considering the partitioning behaviour of Se.

#### 5.9.1.1 *Distribution and partitioning of selenium in primary sulfide*

The appreciable ( $80 \pm 9$  ppm– $164 \pm 19$  ppm) and broadly comparable concentrations of Se in solid solution within coexisting primary pyrrhotite, pentlandite and chalcopyrite/cubanite (average  $Se_{(po)}/Se_{(pn)}$ ,  $Se_{(po)}/Se_{(cpy)}$  and  $Se_{(pn)}/Se_{(cpy)}$  ratios of  $0.8 \pm 0.1$  to  $1.3 \pm 0.2$ ; Table 5.3), indicates that Se partitions readily into each magmatic sulfide phase and is thus compatible within both high temperature monosulfide solid solution (mss) and intermediate solid solution (iss). It can also be concluded from the ratios presented in Table 5.3 that the distribution of Se, at least within the GNPA member, is not affected significantly by the lower temperature recrystallization of po-pn-cpy, as these are generally all close to unity. Marginal differences in the Se contents however, are observed between the different primary sulfide phases (see Table 5.3; Fig. 5.7) implying that during sulfide fractionation Se is not consistently partitioned equally among the crystallizing phases. It is important to highlight that any interpretation from these small differences, in terms of the partitioning behaviour of Se, should be treated with caution since much of the variation can be accounted for by analytical error.

From the ratios presented in Table 5.3 it is evident that the highest concentrations of Se are typically associated with either pyrrhotite or pentlandite, which contain near comparable Se contents (e.g. samples RP04.21/679 and 690 with  $Se_{(po)}/Se_{(pn)}$  of  $1.0 \pm 0.1$ ). The Se content of the Cu-bearing phase is never seen to exceed that of both pyrrhotite and pentlandite within a sample. Whilst pentlandite contains either comparable or higher concentrations of Se to the Cu-bearing sulfide phase, pyrrhotite always has a higher Se content, with the exception of sample RP04.23/392.

From these observations it could be suggested that during recrystallization of mss (<650°C) Se is not preferentially concentrated into either pyrrhotite or pentlandite. In addition the ratios could also be interpreted to indicate that Se is not preferentially concentrated into iss over mss since the Cu-bearing sulfide phase present does not contain significantly more Se than the exsolution products of mss; pyrrhotite or pentlandite. Whilst comparable Se concentrations in pentlandite and chalcopyrite/cubanite could indicate that at high

temperatures Se is partitioned equally during the exsolution of mss and iss, the presence of  $Se_{(po)}/Se_{(cpy)}$  ratios  $>1$  could suggest that at lower temperatures (650–250°C) the distribution of Se is partially controlled by the exsolution of pyrrhotite, pentlandite and chalcopyrite/cubanite. To fully constrain and understand the partitioning behaviour of Se during sulfide fractionation a much larger study encompassing multiple deposits would be required.

**Table 5-3** Average LA-ICP-MS determined Se concentrations of pyrrhotite, pentlandite and chalcopyrite/cubanite in primary and secondary sulfide assemblages, together with low temperature pyrite and millerite. To reduce the error associated with the ratios all values  $<80$  ppm have been excluded. Note the detection limit for Se is 60 ppm. An indication of the analytical error is propagated from using the average 12% counting variation observed on the in house Cardiff standard which contains 108 ppm Se. For greater discussion on the errors see Appendix 2 (pg 270).

Sample	Se concentration in ppm					po:pn	po:cpy	pn:cpy	py:pn	py:cpy	py:mil
	po	pn	cpy/cub	py	mil						
<b>RP04.23/392</b>											
MIN		92	102								
MAX	88	128	112								
MEAN	88	110	107			0.8±0.1	0.8±0.1	1.0±0.1			
ERROR	11	13	13								
n	1	2	3								
<b>RP04.23/411</b>											
MIN	80		85								
MAX	139	83	89								
MEAN	109	83	87			1.3±0.2	1.3±0.2	1.0±0.1			
ERROR	13	10	10								
n	2	2	2								
<b>RP04.21/690</b>											
MIN	97	103	86								
MAX	161	127	91								
MEAN	114	115	89			1.0±0.1	1.3±0.2	1.3±0.2			
ERROR	14	14	11								
n	11	3	2								
<b>RP04.21/679</b>											
MIN	108	109	107	110							
MAX	140	156	131	148							
MEAN	129	135	119	135		1.0±0.1	1.1±0.1	1.1±0.2	1.0±0.1	1.1±0.2	
ERROR	16	16	14	16							
n	5	5	2	3							
<b>RP04.21/693</b>											
MIN	85	90									
MAX	109	164									
MEAN	97	127				0.8±0.1					
ERROR	12	15									
n	3	2									
<b>RP05.45/165</b>											
MIN				128							
MAX			100	137							
MEAN			100	131						1.3±0.2	
ERROR			12	16							
n			1	3							
<b>RP05.45/166-chromitite</b>											
MIN				152							
MAX				593							
MEAN		214	85	345							
ERROR		26	10	41							
n		1	1	4							
<b>RP05.45/167-chromitite</b>											
MIN		103	84	103	134						
MAX		173	183	159	162						
MEAN		127	134	125	148						
ERROR		15	16	15	18				1.0±0.1	1.0±0.1	0.9±0.1
n		4	2	5	2						0.8±0.1
<b>RP05.45/208</b>											
MIN		91		106							
MAX		164		229							
MEAN		140	121	165	131						
									1.2±0.2	1.2±0.2	1.4±0.2
											1.3±0.2

**Table 5-3 continued**

Sample	po	pn	cpy/cub	py	mil	po:pn	po:cpy	pn:cpy	py:pn	py:cpy	py:mil
ERROR		17	15	20	16						
n		8	1	8	1						
<b>RP05.45/214</b>											
MIN					153						
MAX					166						
MEAN			116		159						
ERROR			14		19						
n			1		2						
<b>MD03.1/552</b>											
MIN		120	161								
MAX		156	155								
MEAN		138	158					0.9±0.1			
ERROR		17	19								
n		2	2								

Through investigating the distribution of Se on a mineralogical scale it can be concluded that: (i) Se is compatible within both mss and iss (Fig. 5.10a; Fig 5.7a–d; Table 5.3); and (ii) pyrrhotite, pentlandite and chalcopyrite/cubanite contain near comparable quantities of Se. These features are not specific to the GNPA member or the Bushveld Complex, as LA-ICP-MS data available from the Jinchuan intrusion, China, presented in Table 5.4 (Prichard et al. 2013), reveals similarly appreciable quantities of Se in solid solution within chalcopyrite, pyrrhotite and pentlandite, with elevated concentrations also found to be typically restricted to the latter two sulfide minerals.

**Table 5-4** Average LA-ICP-MS determined Se concentrations of pyrrhotite, pentlandite and chalcopyrite for selected samples from the Jinchuan intrusion, China. Data obtained from Prichard et al. (2013).

sample	Se concentration			pn:cpy	po:pn	po:cpy
	po	pn	cpy			
JZ-04	113	115	135	0.85	0.98	0.84
JZ-02	134	147	126	1.17	0.91	1.06
JZ-26	171	191	120	1.59	0.90	1.43

Our findings, along with those from the Jinchuan intrusion, contrast with recent experimental work which constrained a  $D_{se}^{mss/sul}$  value of  $0.6 \pm 0.05$  (Helmy et al. 2010), indicating Se is slightly fractionated between mss and iss, through concentrating preferentially within the residual Cu-rich sulfide liquid. This is consistent with differences observed in the Se concentration (and S/Se ratio) between iss and mss fractions within a number of magmatic massive sulfide deposits (iss up to 330 ppm, 1005 to 3970; mss <90 ppm; >4350 to 10,000) which Queffurus and Barnes (2014) attributed to the enrichment of Se in iss relative to mss during formation of magmatic sulfide Ni-Cu-PGE deposits. Since Queffurus and Barnes (2014) considered only massive sulfide deposits such as Voisey's Bay, Sudbury and Noril'sk, the apparent disparities in the behaviour of Se during sulfide fractionation with observations from this study and Prichard et al. (2013) may relate to

different magmatic sulfide deposit types and modification of the Se contents post-fractionation of mss and iss.

Consequently, there are clearly some variable controls on the partitioning behaviour of Se in magmatic sulfides that are currently unclear. Although further studies are required to constrain and understand the apparent differences in the behaviour of Se at a mineralogical and deposit scale observations do imply however that either: (i) Se behaviour between mss and iss is apparently divergent in different deposits; or (ii) in massive sulfide deposits the high Se contents of iss (Queffurus and Barnes 2014) was obtained subsequent to fractionation of a sulfide liquid and segregation of iss from mss, thus it is not representative of the initial concentration Se in the sulfide phase.

#### *5.9.1.2 Mobility of selenium during fluid alteration*

Pyrite and millerite were found to also host significant concentrations of Se in solid solution (Table 5.3). With the exception of one sample the  $Se_{(py)}/Se_{(mil)}$  ratio varies from  $1.1 \pm 0.2$  to  $1.3 \pm 0.2$  (Table 5.3). Concentrations of Se particularly in pyrite appear broadly comparable or marginally elevated to those phases being replaced (Table 5.3). In many samples much of the apparent variation is within analytical error (e.g. RP05.45/208; RP05.45/165). Selenium largely remains uniformly distributed throughout the primary relicts (Fig. 5.7e and f) at comparable concentrations to the completely unaltered samples (Fig. 5.7a-d). In comparison, Se concentrations can be considerably more variable within the secondary pyrite and millerite (Fig. 5.7e and f; Table 5.3), with ranges of up to 106 to 230 ppm and 152 to 590 ppm observed within individual samples (Table 5.3), respectively.

In addition to sulfide fractionation processes, the presence of a secondary sulfide assemblage throughout the GNPA member provides an opportunity to explore the behaviour of Se during low temperature alteration. Prichard et al. (2013) recently concluded that the presence of PGE-selenide minerals isolated from sulfide minerals can be explained if Se behaves in a mobile manner only within saline, low pH, highly oxidizing fluids. Whilst similar conditions are required to dissolve and transport PGE (in particular Pt and Pd), these elements are capable of being remobilised under a variety of oxidation and pH states (Mountain and Wood 1988; Wood 2002). Consequently, the rarity of Se-bearing PGM worldwide is reflective of its mobility within only a very constricted range of fluid compositions. The highly oxidising conditions required to remobilise Se in low temperature fluids (100–300°C) are indicated in the Jinchuan intrusion by the association of Se-bearing minerals with a

magnetite–hematite alteration assemblage. Within the GNPA member the lack of acidic alteration and oxidized (e.g. magnetite, hematite) mineral assemblages in association with secondary pyrite and millerite, indicates that the fluid composition was not suitable for remobilisation of Se. This is supported by the complete absence of PGE-selenides throughout both the GNPA member and adjacent Platreef. In addition, the presence of Se in pyrite and millerite at concentrations near comparable to the pyrrhotite and pentlandite being replaced (Fig. 5.7e-g), suggests that during low temperature alteration Se is effectively inherited by the replacing secondary sulfide minerals. Consequently it appears that within the GNPA member, during interaction of sulfides with hydrothermal fluids Se behaves in an immobile manner, analogous to IPGEs, Pt and Rh (Smith et al. 2014; Chapter 4).

### **5.9.2 Implications for interpretation of S/Se ratios and S isotopes**

In deposits such as the GNPA member where sulfide mineralization results from the interplay of both sulfide fractionation and low temperature alteration processes, determining the contribution of crustal S in terms of ore genesis is complicated by the ability of syn- and post-magmatic processes to modify the initial composition of the sulfide liquid. This includes disparities between the S/Se ratio and  $\delta^{34}\text{S}$  signature both within and between the primary and secondary sulfide assemblage. In the GNPA member example, these differences indicate that the initial composition of the sulfide liquid has been modified by both magmatic and late-stage low temperature alteration processes. Such processes may include; variations in the R-factor; partial dissolution of sulfides at depth prior to emplacement; isotopic exchange between crustal and mantle S; and hydrothermal interaction (Yamamoto 1976; Howard 1997; Ripley and Li 2003; Kerr and Leitch 2005). Alternatively they may result from localised contamination and overprinting of the initial signatures. Through utilizing S isotopes and S/Se ratios on a mineralogical versus bulk rock scale I have gained a more detailed insight into the ore-forming processes involved in the genesis of the GNPA member. Key findings of this study include: (i) S isotopes record a strong and extensive contribution of crustal S, whilst S/Se ratios indicate minimal contamination; (ii) the S/Se ratio is highly variable within and between individual sulfide phases, whilst the  $\delta^{34}\text{S}$  signature remains consistent; (iii) the broad negative correlation between Pt+Pd tenor and S/Se ratio; and (iv) the restriction of S/Se ratios lower than mantle to the secondary sulfides.

In the following discussion I assess the implications of these features in terms of the utility and application of S/Se ratios and S isotopes in the study of magmatic sulfide deposits and for the genesis of the GNPA member.

### 5.9.2.1 Genetic implications for the GNPA member – as a case example

Where syn and/or post magmatic processes have significantly altered the initial composition of a sulfide liquid or sub-solidus assemblage, S/Se ratios need to be applied in conjunction with S isotopes as the inferred role of contamination in ore genesis may differ according to the technique utilized. Results for the GNPA member illustrate this clearly as S/Se ratios signify only a minimal input of crustal S, whilst  $\delta^{34}\text{S}$  signatures indicate a significant contribution of externally derived S. Thus used independently, there is a clear disparity in the possible interpretation and therefore any interpretation or genetic model developed may be fraught with uncertainties in such circumstances. Consequently, it is only through deciphering which indicator has been modified and by what process (es) that S isotopes and S/Se ratios are able to provide a truly reliable insight into the initial source of S.

#### 5.9.2.1.1 Contribution of crustal S to ore genesis in the GNPA member

With  $\delta^{34}\text{S}$  signatures revealing a distinct and consistent crustal component within both primary and secondary sulfides throughout the GNPA member, no evidence exists to suggest that the initial isotopic composition of the sulfide liquid has been modified significantly by magmatic or low temperature processes. The dominance of  $\delta^{34}\text{S}$  signatures greater than the local mantle range of -1.8 to +2.4‰ (Westerlund et al. 2004; Fig. 5.3a and b), therefore suggests that similarly to many other magmatic sulfide PGE-Ni-Cu deposits (e.g. Lesher and Groves 1986; Lesher and Burnham 2001; Li et al. 2002; Ripley and Li 2003; Ihlenfeld and Keays 2011) the addition of crustal S through assimilation of S-bearing country rocks was critical in the genesis of mineralization within the GNPA member.

Typically, contact-type PGE deposits are characterized by *in situ* contamination by local S-bearing country rocks, which can either be responsible for ore formation (e.g. Duluth Complex; Mainwaring and Naldrett 1977; Ripley 1981; Ripley et al. 1986 and the Basal Series of the Stillwater Complex; Lambert et al. 1994; Lee 1996; McCallum 1996) or simply overprint or modify an early developed crustal signature (e.g. Platreef; Holwell et al. 2007; McDonald and Holwell 2007; Penniston-Dorland et al. 2008; Ihlenfeld and Keays 2011). Whilst Maier et al. (2008) inferred a local control over the  $\delta^{34}\text{S}$  composition of sulfides within the GNPA member, the data in this study is inconsistent with the contribution of S from the local footwall as: (i) a crustal component is evident in sulfides developed east and west of the Grasvally Fault where underlain by quartzites and Lower Zone cumulates; and (ii) there is no evidence that the degree of contamination increases towards the footwall contact which is a feature commonly observed within the Platreef where the magma has sufficiently interacted

with the local footwall (Sharman-Harris et al. 2005; Holwell et al. 2007). In addition, the quartzites which underlie the GNPA member are themselves an unlikely source of S as although sufficiently high  $\delta^{34}\text{S}$  values are found in pyrite (+3.5 up to +10‰; Table 5.1; Fig. 5.3), S-bearing minerals are relatively scarce throughout the Magaliesberg Quartzite Formation. As these findings are therefore inconsistent with any model which involves the *in situ* development of a sulfide liquid, but yet are characterised by some crustal S, it is concluded that the magma from which the GNPA member crystallized was contaminated and saturated in S prior to emplacement. These observations combined with geochemical data presented in Smith et al. (2014; Chapter 4) are in agreement with a multi-stage emplacement model similar to that proposed for the GNPA members nearest analogue the Platreef where pre-formed PGE-rich sulfides were developed at depth in response to assimilation of S-bearing country rocks (see Lee 1996; Kinnaird 2005; Holwell et al. 2007; McDonald and Holwell 2007; Ihlenfeld and Keays 2011; McDonald and Holwell 2011).

In a recent study, Sharman et al. (2013) demonstrated through the application of multiple S isotope data that the crustal S present within the Platreef originated from a restricted stratigraphic horizon within the Duitschland Formation, characterized by  $\delta^{34}\text{S}$  signatures in the range of +2‰ to +20‰. Although, in places, the Duitschland Formation directly underlies the Platreef, Sharman et al. (2013) concluded that the Platreef magmas assimilated carbonates and shales of the Duitschland Formation at depth prior to emplacement. Although the GNPA member intruded the Transvaal Supergroup at a higher stratigraphic position than the adjacent Platreef, the GNPA magma likely interacted with sediments lower in the Transvaal succession, which form the footwall to the Platreef, at depth prior to emplacement. Thus, it is plausible to suggest that crustal S in the GNPA member may also have been sourced from the Duitschland Formation.

Although the majority of the S/Se data is not representative of the initial source of S due to lowering of ratios by syn and/or post magmatic processes (Fig. 5.5; Table 5.1 and 5.2), preservation of crustal S/Se ratios within part of the primary sulfide assemblage provides further evidence of an early contribution of crustal S. As these high S/Se ratios which range from 5629 to 6196 (Fig. 5.5; Table 5.2) are only preserved where the succession is underlain by Lower Zone cumulates, they also indicate that the GNPA magma was emplaced saturated in S. Thus our S/Se data is also in support of a single contamination event, which occurred at depth prior to emplacement of the GNPA member.

*5.9.2.1.2 Insight into ore-modifying processes in the GNPA member*

In contrast to the S isotopes which retain the initial composition of the sulfide liquid and thus source of S, S/Se ratios, at least within the GNPA member, reveal details and constraints on subsequent ore-forming/modifying processes operating within the magmatic system. Notable variations in the S/Se ratio both within and between primary and secondary sulfides and the general absence of ratios consistent with the S isotope data, confirms that within the GNPA member the S/Se ratio has been modified significantly by both pre-emplacment magmatic and low temperature hydrothermal processes.

An initial crustal S/Se ratio, which is only preserved within several unaltered samples within the GNPA member (Figs. 5.5 and 5.8), can be effectively erased by a variety of processes. Those relevant to this study include: (i) post-emplacment S-loss through low temperature alteration (Yamamoto 1976; Howard 1977); (ii) syn- or pre-emplacment partial dissolution of sulfides by the process ‘multistage-dissolution upgrading’ (Kerr and Leitch 2005); and (iii) an increase in the R-factor and/or greater interaction of the sulfide with the silicate melt (Queffurus and Barnes 2014). Whilst the former two processes are capable of generating S/Se ratios lower than that of mantle (2850 to 4350; Eckstrand and Hulbert 1987), McDonald et al. (2012) highlights that although the latter acts to further enrich sulfides in PGE and Se (e.g. Ihlenfeld and Keays 2011) variations in R-factor cannot alone, produce S/Se ratios lower than the mafic end member, which must be equal to or greater than the mantle ratio.

From the data presented it is apparent that S/Se ratios significantly lower than mantle are, in general, restricted to those samples hosting secondary sulfides (Figs. 5.5, 5.9 and 5.10). This observed association is interpreted to be strongly suggestive that lowering of the S/Se ratio to values less than 2500 (Figs. 5.4 and 5.5; Table 5.2) occurred post-emplacment in association with low temperature hydrothermal alteration and thus due to S-loss rather than a gain in Se. The data however, also shows that the initial crustal component of the sulfide liquid (revealed by S isotopes) had been largely erased prior to emplacment as much of the completely unaltered primary sulfide assemblage reveals S/Se ratios that are consistent with mantle rather than crustal S. I interpret this possible early reduction in the S/Se ratio to be associated with pre-emplacment upgrading of the sulfides metal content (particularly of those elements with high partition coefficients, such as PGE and Se; Kerr and Leitch 2005) and thus to result from either an increase in the R-factor or partial dissolution of a low PGE tenor sulfide with an initially crustal S component. Lowering of the S/Se ratio in association

with enrichment of sulfides in PGE and Se by either process is further supported by; the broad negative relationship observed in the data between PGE tenor and S/Se ratio (Fig. 5.5); and the positive correlation evident between PGE and Se tenor (Fig. 5.6). The variation in PGE tenor and its relationship with S/Se ratio is considered to be a primary feature of the earliest sulfide liquid carried by the GNPA magma, a feature also noted in the Platreef (Ihlenfeld and Keays 2011). Therefore the observed PGE and Se tenors of sulfides are believed to have been largely attained prior to the development of a secondary sulfide assemblage, with localised S-loss related to post-emplacement hydrothermal alteration further exaggerating the pre-existing association of the lowest S/Se ratios with the highest PGE tenors (Fig. 5.4 and 5.5).

The chromitites in the GNPA member are distinct in terms of their  $\delta^{34}\text{S}$  composition (Fig. 5.3). Since the  $\delta^{34}\text{S}$  signatures are notably heavier (by around 2‰) within both the primary and secondary sulfides (Fig. 5.3a), then it is likely that  $\delta^{34}\text{S}$  was fractionated during the formation of the chromitites. Although this fractionation is poorly understood, it is speculated whether it might result from changes in the magmatic conditions which are known to occur during chromite formation or be indicative that the magma(s) from which the chromite crystallized were more contaminated with crustal S than those which formed the rest of the GNPA member. At present this however remains unconstrained.

#### 5.9.2.2 *A genetic model for the GNPA member PGE mineralization*

Smith et al. (2014; Chapter 4) concluded that the observed geochemistry and mineralogy of PGE mineralization within the GNPA member was inconsistent with any genetic model involving the *in situ* development of a sulfide liquid. Consequently, Smith et al. (2014) proposed that their data was more compatible with a multi-stage emplacement model, whereby PGE enrichment of sulfides happened at depth in a subchamber or conduit system, prior to emplacement; and later emplaced into the main chamber. Although the data presented in this study is consistent with such a model, key observations provide further constraints on the genesis of mineralization within GNPA member. A schematic summary of the proposed multi-stage model for the formation of mineralization within the GNPA member is provided in Figure 5.11 and can be summarised as follows:

1. At depth in a staging chamber shales and carbonates from the Deutschland Formation contaminate the magma passing through the chamber (possibly Lower Zone magma) extensively with crustal S (Fig. 5.11a).

2. The contaminant is well homogenised with the magma, inducing sulfide saturation and development of an immiscible sulfide liquid (Fig. 5.11a). The strong crustal component of the sulfide was initially evident in both the  $\delta^{34}\text{S}$  signature ( $>2.4\text{‰}$  to  $<7\text{‰}$ ) and S/Se ratio (values up to 6196 observed).
3. Sulfides become enriched in PGE, Ni, Cu and semi-metals through interaction and processing of pre-GNPA magma (s) (Fig. 5.11a). It is possible that like the Platreef, the GNPA member sourced its PGE content from the magma which was intruded to form the Lower Zone (McDonald and Holwell 2007; McDonald et al. 2009; McDonald and Holwell 2011).
4. Upgrading of metal tenors within the sulfide (and a reduction of S/Se ratios) via either dissolution of sulfide or an increase in R-factor.
5. Due to its density the PGE-rich sulfide liquid settles to the floor of the staging chamber (Fig. 5.11a).
6. A major influx of new magma (GNPA magma) entrains the PGE-bearing sulfides and transports them out of the staging chamber into the GNPA member (Fig. 5.11b).
7. During emplacement, the local quartzites do not contaminate the GNPA magma further, with the sulfide retaining its initial crustal  $\delta^{34}\text{S}$  signature. PGE-bearing sulfides are distributed throughout the 400–800m crystallizing succession (Fig. 5.11b).
8. Hydrothermal alteration remobilises Pd and Au on a minor scale, and replaces the primary sulfide and PGE mineralogy (Smith et al. 2011b; 2014). Low temperature alteration is associated with S-loss, which lowers the S/Se ratio of some sulfides to values below the mantle range (Fig. 5.11b). Crystallization of pyrite at low temperatures ( $<250^\circ\text{C}$ ) fractionates  $\delta^{34}\text{S}$  by around  $1.5\text{‰}$  (Ohmoto and Rye 1979), causing the secondary sulfide assemblage to appear around  $1\text{‰}$  heavier than characteristic of the primary assemblage (Table 5.1; Fig. 5.3).

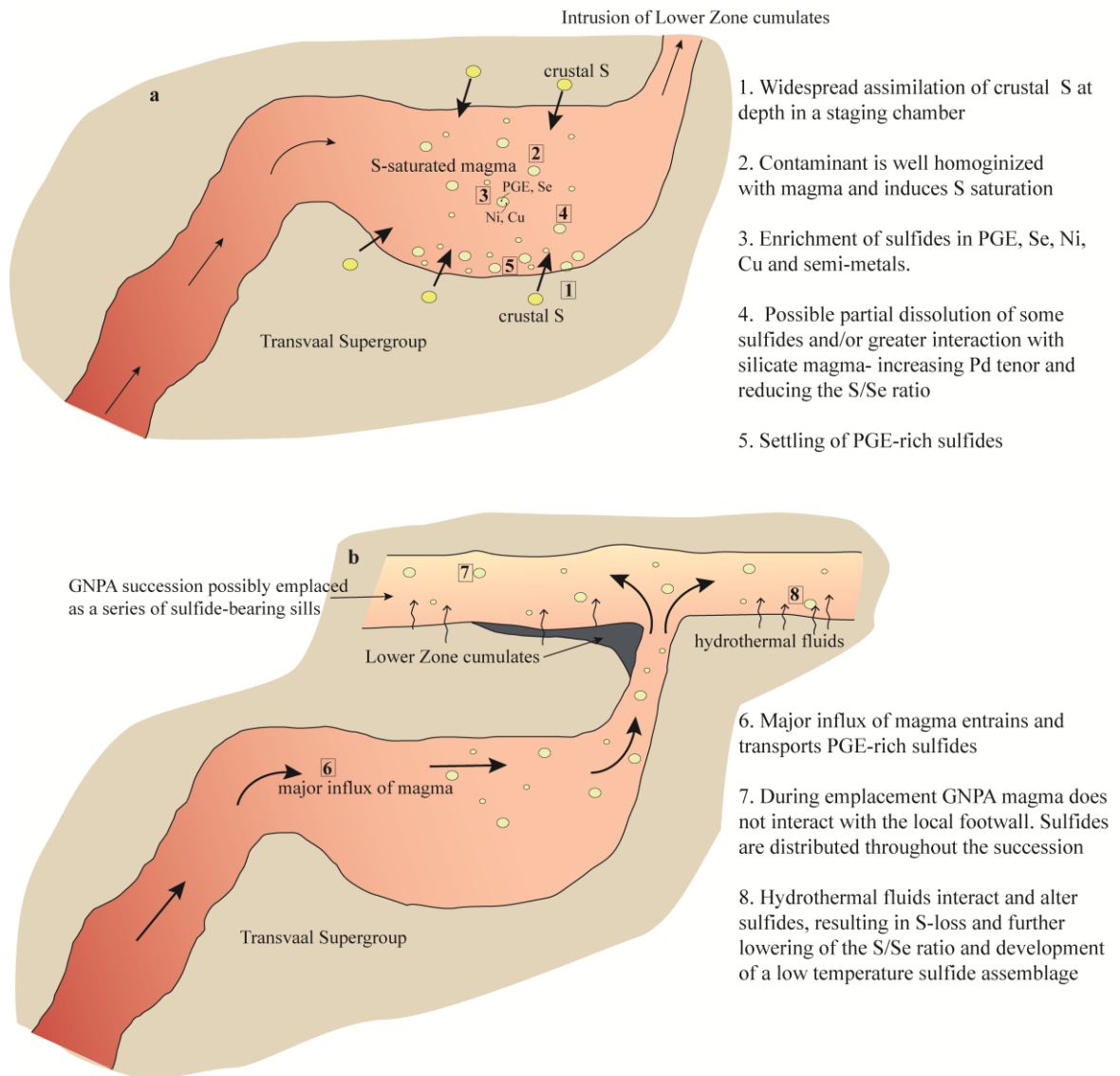


**Figure 5.11** Schematic model of the formation of the GNPA member. See text for explanation of the numbered stages.

### 5.9.2.3 Implications for the application of S isotopes and S/Se ratios

It can be concluded that S isotopes and S/Se ratios have the ability to act as independent tracers of the initial source of S. When care is taken in the analysis and interpretation of such data, variations in the  $\delta^{34}\text{S}$  signature and/or S/Se ratio can reveal an incredible amount of additional detail on the genetic history of a Ni-Cu-PGE deposit, providing constraints on both the timing and effect of ore-forming and ore-modifying processes. It is believed that both S isotopes and S/Se ratios, when used independently, can be effective in constraining the initial characteristics of an immiscible sulfide liquid, so long as the processes by which they can be modified are identified and considered. It is, however apparent from this study that when S isotopes are used in conjunction with S/Se ratios, less uncertainty surrounds any

interpretation and a greater insight into the ore genesis of a deposit is gained. Since the S/Se ratio is most susceptible to being modified by syn- and post-magmatic processes this indicator has the ability to preserve detail on a variety of processes including: partial dissolution, variations in R-factor, hydrothermal alteration and post-magmatic S-loss. Although in comparison S isotopes are relatively more robust, the effects of localised contamination are commonly imprinted and thus retained within the isotope composition of sulfides (e.g. Leshner 1986; Arcuri et al. 1998; Ripley et al. 1999; 2002; Holwell et al. 2007; 2012).

It is evident from the present study that utilizing both bulk and *in situ* methods to determine the S/Se ratio and thus source of S is beneficial for several reasons. Firstly, *in situ* analyses reveal detail previously masked by bulk ratios, including local variations in S/Se ratio between and within sulfide assemblages, which may aid in the elimination of processes responsible for modifying ratios (i.e. high temperature magmatic or post-magmatic S-loss). Furthermore, it also reveals if S/Se ratios both within and between sulfide phases are homogenous or heterogeneous, and thus whether bulk values are representative of the individual phases. It is important to note however that the variable partitioning behaviour of Se during fractionation of a sulfide liquid at high temperatures can result in large variations in the S/Se ratio both within and between individual minerals to the point where a bulk S/Se value is more useful. Finally, determining the concentration of Se in the sulfide phases provides an opportunity to investigate the partitioning behaviour and mobility of Se during magmatic sulfide fractionation processes, which are apparently variable from one deposit to the next; and also the effects of low temperature fluid alteration.

### **5.10 Acknowledgements**

The authors would like to thank Caledonia Mining Corporation and in particular Trevor Pearton, for allowing access to the drillcore on the farms Rooipoort, Grasvally and Moorddrift, and giving permission to publish this work. Jennifer Smith's Ph.D. research is funded by the Natural Environment Research Council (NE/1528426/1). The S isotope work was carried out via a NERC Facilities grant (IP/1280/1111) awarded to DAH at the Isotope Community Support Facility at SUERC. SUERC is supported by NERC and the Scottish Universities consortium.

## **Chapter Six**

### Geochemical characteristics of the GNPA member

## 6.1 Abstract

In constraining the genesis of PGE mineralization within the Grasvally Norite-Pyroxenite-Anorthosite (GNPA) member, geochemical variations offer an insight into the magmatic history of the parental magma(s), providing further constraints on: the magmatic lineage; the nature of emplacement; and the timing and degree of contamination experienced. Evidence that the GNPA member formed from multiple influxes of magma is best preserved within the orthopyroxene and plagioclase compositions, with compositional breaks defining three distinct mafic packages, which in part, correspond to the main stratigraphic units which constitute the GNPA member. Compositional breaks at the contact between the Lower Mafic (LMF) and Mottled Anorthosite (MANO) units are supported by subtle reversals observed in the major and trace element chemistry (e.g. Sr, V, bulk Mg#).

The geochemical characteristics of the GNPA are consistent with previous work which suggest the parental magmas were of a mixed composition containing both B1 (Lower Zone) and B2/B3 (Main Zone) magma components. In this chapter it is constrained that mixing of these compositionally distinct magmas occurred prior to emplacement of the GNPA member in response to the rising of an early pulse of Main Zone type magma into an established Lower Zone staging-chamber system, which contained resident B1 type magma. Since geochemically the GNPA member is analogous to the Platreef (e.g. REE signatures, Pd-dominant, mineral compositions, element ratios), they are viewed to have formed from compositionally similar or related magmas. The *in situ* mixing of new and residual fractionated hybrid magma during emplacement is interpreted to result in the crystallization from pyroxenites and chromite in the basal LMF, to gabbronorites in the upper LMF, and finally anorthosites and gabbronorites in the MANO unit. Similarities in element ratios, pyroxene compositions and REE signatures between the Lower Gabbronorite unit (LGN) and Main Zone rocks indicate that in comparison to the LMF and MANO units, the gabbronorites of the LGN crystallized from an unmixed B2/B3 magma, which was intruded subsequent to significant cooling and solidification of the LMF and MANO units.

Trace element signatures and variations reveal that the parental magma of the GNPA member experienced at least two stages of crustal contamination. Evidence of an early pre-emplacement contamination event, through the assimilation of S-bearing country rocks is preserved throughout the entire GNPA member, and is considered responsible for

triggering S saturation at depth. The second contamination event resulted from the interaction of the GNPA magma with the local footwall country rocks at the time of emplacement. This event did not introduce additional S into the system and thus had no control over genesis of PGE mineralization within the GNPA member.

## 6.2 Introduction

Within the eastern and western limbs of the Bushveld Complex, the main stratigraphic units (Lower, Critical, Main and Upper zones) are readily distinguished by their major, trace element, mineral chemistry and Sr isotope composition (Eales and Cawthorn 1996; Cawthorn and Walraven 1998; Maier and Barnes 1998; Kruger 2005; Seabrook et al. 2005). Through studying the geochemical characteristics of a mafic layered intrusion one can thus gain an insight into its magmatic history, including the: magmatic lineage; the nature of emplacement; the timing and degree of contamination; and thus essential aspects of the development of any magmatic deposits hosted therein.

Within the northern limb of the Bushveld Complex, whilst the gabbro-norites overlying the Platreef and GNPA member are correlated with the Main Zone elsewhere in the complex, there is no consensus of opinion on the correlation of the Platreef/GNPA member with the succession in other limbs and in particular with the Critical Zone of the eastern and western limbs. The GNPA member, based primarily on the development of a UG2-‘like’ chromitite, has been regarded by both Hulbert (1983) and van der Merwe (1978; 2008) as an upper Critical Zone equivalent and is considered by many to form part of the same succession as the Platreef (Wagner 1929; McDonald et al. 2005). Whilst Maier et al. (2008) and van der Merwe (2008) believe that the GNPA member merges laterally with the Platreef, van der Merwe (1978) previously positioned the Platreef at the base of the Main Zone thus equating the GNPA member with the Upper Critical Zone. The latter is favoured by Kruger (2005) and Wagner (1929) who consider the Platreef to represent a time equivalent of the Merensky Reef. The correlation of the GNPA/Platreef with the Upper Critical Zone has, however been contested due to key geochemical differences highlighted by McDonald et al. (2005).

In this chapter, the geochemical characteristics of the GNPA member are studied in detail, with the aim of placing constraints on the genesis of the PGE mineralization and its relationship with the Platreef and Upper Critical Zone. Here the effects of local and regional contamination processes on the geochemistry of the GNPA member are also explored.

## 6.3 Samples and Methods

Samples used in this study were obtained from eight boreholes drilled by Falconbridge Ltd and Caledonia Mining on the farms Rooipoort, Grasvally and Moorddrift (see Fig. 4.2). X-

ray Fluorescence for bulk geochemistry was undertaken at the University of Leicester on 78 samples. Bulk major elements were determined by fusion beads produced by mixing milled powders (ignited to 950°C to determine loss on ignition) with Johnson-Matthey spectroflux JM100B (80% Lithium Metaborate, 20% Lithium Tetraborate) and then fired in a platinum crucible. Trace elements were measured from 32 mm diameter pressed pellets which contained 7 g of fine ground sample powder combined with 12-15 drops of a 7% PVA binding agent, pressed at 10 tons per square inch. All samples were analysed using a PANalytical Axios-Advanced XRF spectrometer. The major and trace element data produced during this study is provided in Appendix 1.

Selected samples (48 in total), representative of the main stratigraphic units of the GNPA member (LMF 15 samples, LGN 13 samples and MANO 20 samples) and the local metasediments (4 samples), were also analysed for trace and rare earth elements (REE; see Appendix 1) at Cardiff University using a JY Horiba Ultima 2 inductively coupled plasma optical emission spectrometer (ICP-OES) and Thermo X7 series inductively coupled plasma mass spectrometer (ICP-MS). This was done to obtain data on REE which is not possible using XRF. Ignited powders were fused with Li metaborate on a Claisse Fluxy automated fusion system to produce a melt that could be dissolved in 2% HNO<sub>3</sub> for analysis. Full details of the standard ICP analysis procedures and the instrumental parameters are given in McDonald and Viljoen (2006).

Mineral analysis was carried out at the Open University using a Cameca SX100 electron microprobe. An operating voltage of 20 kV and probe current of 20 nA (measured on a Faraday cage) with a 10 micron beam diameter were used for quantitative analysis. The composition of cumulus and intercumulus orthopyroxene, clinopyroxene and plagioclase was determined at regular intervals (roughly 10 m) over 400 m of the succession throughout borehole RP04.23 (see Chapter 4, Fig. 4.3 for stratigraphic log). This borehole was selected to investigate variations in mineral compositions as in this region the GNPA member has an unreactive Lower Zone footwall thus it can be assumed that there is minimal crustal influence over the mineral chemistry, as may be the case where the GNPA member directly overlies quartzite and calc-silicate floor rocks.

#### **6.4 Major element geochemistry**

Whole rock analyses are given in Appendix 1. The major element chemistry of GNPA lithologies (pyroxenites, gabbronorites, norites and anorthosites) can be easily modelled as

a function of the proportions of orthopyroxene, clinopyroxene and plagioclase (Fig. 6.1). Thus similar to the Platreef (McDonald and Holwell 2011; Manyeruke et al. 2005), there is little evidence for the addition of a crustal component. It should be noted samples that plot significantly outside the compositional field in Figure 6.1b have a substantial chromite component.

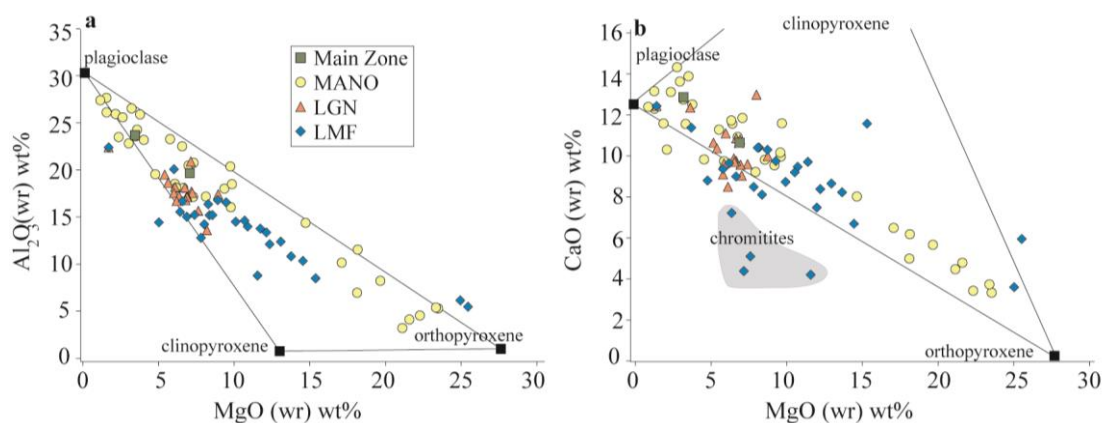


**Figure 6.1** Major element plots of the GNPA member showing the composition of the Lower Mafic (LMF), Lower Gabbronorite (LGN) and Mottled Anorthosite (MANO) units compared to different end-member minerals.

#### 6.4.1 Geochemical variations with depth

Within this study, borehole RP04.23 has been used to represent a section of the GNPA succession where there is no evident local footwall influence or significant late-stage alteration as indicated in Chapters 3, 4 and 5. Although the LGN unit is present within other boreholes sampled for bulk analysis, it is believed to be absent within RP04.23, with the 100 m thick succession of gabbronorites (see stratigraphic log in Fig. 4.3; Fig. 6.2) interpreted to represent a more felsic portion of the LMF. This is based on the observations that the upper and lower contacts of the gabbronorites are not represented by chilled zones or characterised by geochemical compositional breaks.

Depth profiles of selected major and trace elements throughout drill core RP04.23 are provided in Figure. 6.2 and 6.3, respectively. From the base of the succession there is an overriding upward decreasing trend in the  $\text{SiO}_2/\text{Al}_2\text{O}_3$  content of the GNPA member (Fig. 6.2a), which is, in general, mirrored by a notable increase in the  $\text{Al}_2\text{O}_3$  and CaO content, although a slight upward decrease through the MANO unit is possibly observed in  $\text{Al}_2\text{O}_3$  profile (Fig. 6.2b and c). Whilst bulk Mg#, MgO and  $\text{Fe}_2\text{O}_3$  contents show an overall upward decrease (Fig. 6.2d-f), discrete trends are observed in the Mg# and  $\text{Fe}_2\text{O}_3$ . Within the LMF unit, a subtle upward decrease to around 350 m is observed in the Mg# (Fig.

6.2d). Above this the Mg# increases up to the LMF-MANO contact, and then begins to decrease with height through the MANO unit (Fi. 6.2d). In comparison the Fe<sub>2</sub>O<sub>3</sub> content remains relatively constant throughout the lower section of the LMF unit, until immediately above the upper chromitite where it begins to decrease through into the MANO unit (Fig. 6.2e).

Many of the trends/variations observed within bulk geochemistry (e.g. Al<sub>2</sub>O<sub>3</sub>, CaO, MgO and to a lesser extent Fe<sub>2</sub>O<sub>3</sub>) coincide with lithological changes and are thus reflective of the overall varying proportions of plagioclase and pyroxene throughout the succession and the observed increase in plagioclase cumulates and decrease in modal pyroxene between the LMF and MANO units. Figure 6.2 shows clearly that whilst these major element trends are well defined within the LMF, they are noticeably less apparent within the MANO unit. This is interpreted to be indicative of the greater lithological variations observed within the MANO and thus the presence of both mottled anorthosites and more mafic lithologies (pyroxenites, gabbro-norites) since an increase in the MgO and Fe<sub>2</sub>O<sub>3</sub> content (Fig. 6.2e-f) coincides with changes in the mineral proportions (i.e. increase in pyroxene). In comparison to the other major elements shown in Figure 6.2, TiO<sub>2</sub> (Fig. 6.2g) does not appear to show as much variation with depth, with only a very subtle upward decrease and increase observed in the LMF and MANO units, respectively. Although the TiO<sub>2</sub> content is variable within each unit these do not seem to be controlled as much by lithology as is observed in Fe<sub>2</sub>O<sub>3</sub>, MgO, and Al<sub>2</sub>O<sub>3</sub> (Fig. 6.a, b, e and g).

The CaO/Al<sub>2</sub>O<sub>3</sub> ratio throughout the GNPA member is relatively constant with most samples in borehole RP04.23 (Fig. 6.2h) residing within the small range of 0.5–0.7, which is consistent with the CaO/Al<sub>2</sub>O<sub>3</sub> ratio of plagioclase (0.6; Kinnaird 2005). Similar ratios are also observed where the LMF unit has a metasediment footwall (data in Appendix 1). These findings provide confirmation that in the studied area the succession has not been contaminated extensively by calc-silicates as CaO/Al<sub>2</sub>O<sub>3</sub> ratios >1 would be expected in contaminated regions (Kinnaird 2005).

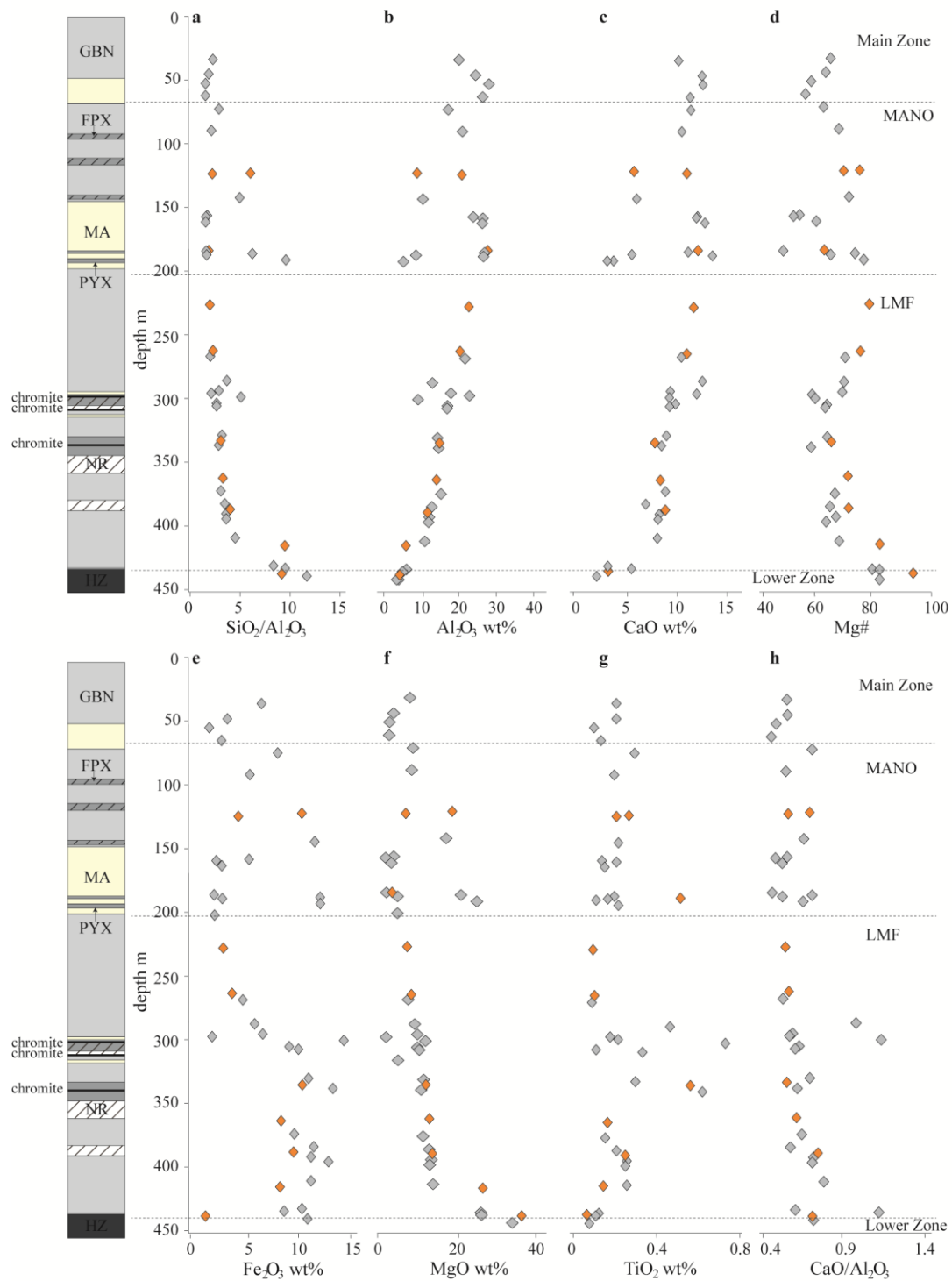


**Figure 6.2** Major element geochemical variations with depth in borehole RP04.23. a)  $\text{SiO}_2/\text{Al}_2\text{O}_3$ , b)  $\text{Al}_2\text{O}_3$  wt%, c)  $\text{CaO}$  wt%, d)  $\text{Mg}\#$ , e)  $\text{Fe}_2\text{O}_3$  wt%, f)  $\text{MgO}$  wt%, g)  $\text{TiO}_2$  wt% and h)  $\text{CaO}/\text{Al}_2\text{O}_3$ . Orange symbols represent data obtained from Maier et al. (2008). Lithological abbreviations: *GBN* gabbronorite, *NR* norite, *FPX* feldspathic pyroxenite, *PYX* pyroxenite, *MA* mottled anorthosite and *HZ* harzburgite.

The Cr content of the GNPA member decreases systematically with height, as the overall modal abundance of plagioclase increases (Fig. 6.3a). The appearance of cumulus chromite is indicated by the abnormally high Cr contents (>16000 ppm) of several samples within the upper section of the LMF unit. With the exception of one anomalous sample at 157m, the Cr content within the MANO increases in association with an increase in the modal abundance of pyroxene (Fig. 6.3a). Although the Zr content within each unit varies independently of lithological changes, it is relatively constant throughout the LMF unit, with a broad increase only evident within the MANO unit which continues to the Main Zone contact (Fig. 6.3b).

Two distinct trends are noticeable within the Sr depth profile which corresponds to the LMF and MANO units. Within the LMF unit an upward increase is observed up to the contact with the MANO unit where a reversal occurs. The MANO-Main Zone contact is marked by a clear shift in Sr (Fig. 6.3c). Vanadium is seen to mirror the Sr depth profile, decreasing upwards through the LMF, with a subtle increase observed in the MANO unit up to the contact with Main Zone (Fig. 6.3d) rocks where a significant decrease occurs.

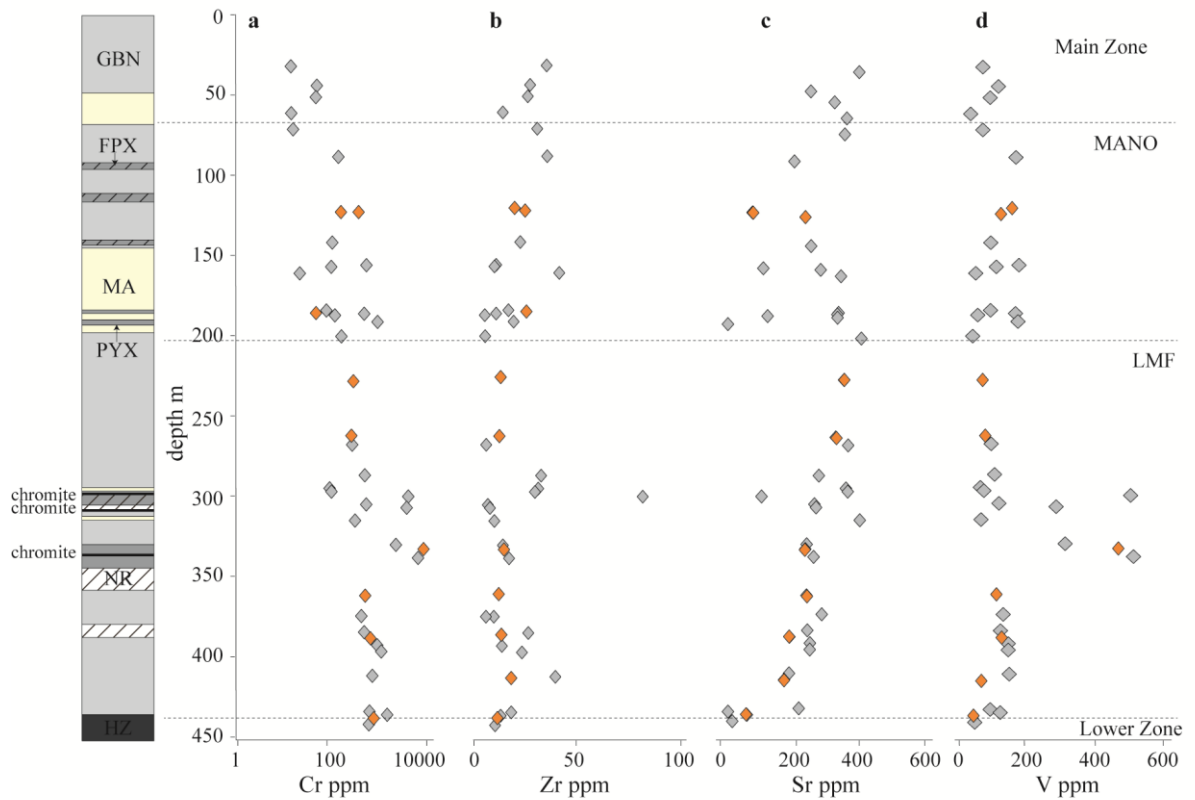


**Figure 6.3** Trace element geochemical variations with depth in borehole RP04.23. a) Cr ppm, b) Zr ppm, c) Sr ppm and d) V ppm. Lithological abbreviations are the same as in Figure 6.2.

#### 6.4.2 Cr/MgO ratios

The Cr/MgO ratio of Bushveld rocks are often used to distinguish Critical Zone (Cr/MgO >100) and Main Zone (Cr/MgO <60) rocks (Seabrook et al. 2005; Fig. 6.4; Table 6.1). The main stratigraphic units of the GNPA member and overlying Main Zone rocks, define distinct compositional fields in terms of their whole rock Cr and MgO contents, although some overlap between units is observed (Fig. 6.4; Table 6.1). The highest Cr content is associated with the LMF unit (typically 200-5000 ppm throughout the succession and 16,810–142,890 ppm in the chromitite layers), which is also characterised by a high and restricted MgO content ranging between 5 and 15 wt%, with the exception of one anomalous samples which contains 2 wt% (Fig. 6.4). Throughout most of the LMF unit Cr/MgO ratios (typically >80) are consistent with values considered indicative of the Critical Zone in the eastern and western limbs of the Bushveld Complex (Fig. 6.4). Several LMF samples do however exhibit Main Zone values (Table 6.1; Fig. 6.4).

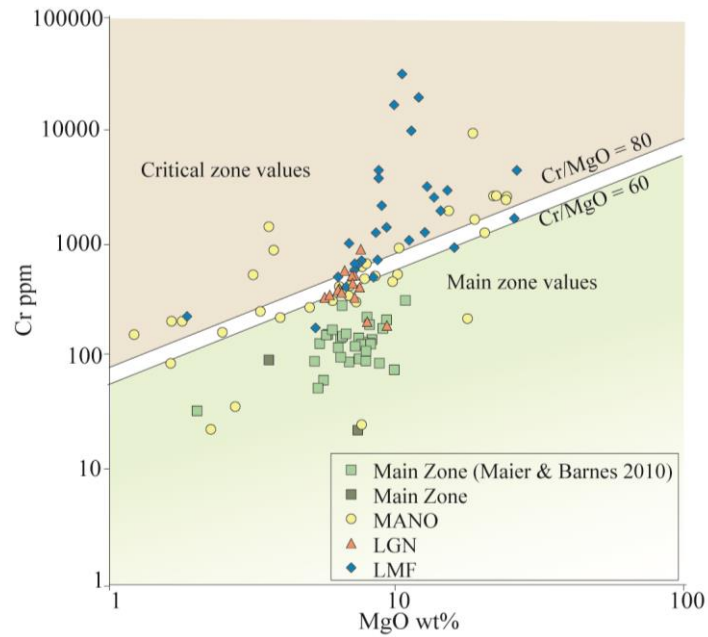


**Figure 6.4** Whole rock Cr (ppm) and MgO (wt%) contents of the Lower Mafic, Lower Gabbroonorite, and Mottled Anorthosite units. The Main Zone data represented by green squares has been taken from Maier and Barnes (2010). Solid lines indicate Cr/MgO ratios of 80 and 60, showing Critical and Main Zone fields (Seabrook et al. 2005). Analyses were taken from boreholes RP04.23, RP04.21, RP05.45, RP05.37, MD03.1, GV05.49 and GV05.50.

The MgO and Cr content are most variable within the MANO unit, which is characterised by a significant increase in plagioclase cumulates relative to the underlying LGN and LMF units. A broad positive correlation, reflecting lithological variations, is evident throughout the MANO. Samples with very low whole rock MgO contents correspond to the plagioclase rich cumulates and lithologies such as mottled and spotted anorthosites (Fig. 6.2). Higher MgO and Cr contents, comparable to that observed within the LMF unit, are associated with the more mafic lithologies (pyroxenite and gabbroonorite) developed within the MANO unit (Fig. 6.2 and 6.3). From Figure 6.4 it is apparent that Cr/MgO ratios of the MANO unit overlap with both Critical and Main Zone values (Table 6.1).

	Cr/MgO	Ce/Sm
<b>Main Zone</b>		
northern limb (Moorddrift)	20–30	6–11
northern limb (Sandsloot)	55–76	5–9
eastern and western limbs	40–60	5–12
<b>GNPA member</b>		
MANO	3–558	6–13
LMF (excluding chromitites)	20–255	
LMF (including chromitities)	20–19310	5–15
LGN	47–89	9–11
Quartzite		11–18
Platreef	14–160	4–13
Upper Critical Zone	>80	9–22

**Table 6-1** Summary of major and trace element ratios for the GNPA member compared to those associated with the Platreef, Main Zone and Upper Critical Zone (from Seabrook et al. 2005; Maier and Barnes 2010; McDonald and Holwell 2011, and references therein).

In comparison to the rest of the GNPA member the LGN defines a relatively small compositional field in Figure 6.4, indicating a very limited range in Cr and MgO contents. The lack of any significant variation most likely reflects the presence of only gabbro-norites within this unit. Although samples from the LGN and Main Zone (in the Moorddrift region) exhibit comparable MgO contents (Table 6.1), the former contains Cr abundances consistent with the lower limit of the LMF unit (Fig. 6.4). The Cr/MgO ratio of the LGN unit is also generally higher than characteristic of the Main Zone within the northern limb with values (Cr/MgO 47–89) being comparable to many LMF and MANO samples (Table 6.1; Fig. 6.4). The majority of samples however reside within the more confined range of 47–65, and are thus consistent with Seabrook et al. (2005) Main Zone values (Fig. 6.4).

From Figure 6.4 it is evident that the Main Zone in the Moorddrift region is distinct in terms of Cr/MgO ratios from the underlying GNPA member. Main Zone values (Cr/MgO <30; Maier and Barnes 2010) within the northern limb are however significantly lower than typically observed within the Main Zone above the Platreef (55-76) and within the eastern and western limbs of the Bushveld Complex (Cr/MgO 40–60; Table 6.1; Seabrook et al. 2005).

## 6.5 Trace element geochemistry

### 6.5.1 Rare earth element geochemistry

Chondrite-normalized rare earth element (REE) patterns for the GNPA member and its local footwall are provided in Figure 6.5. Overall the LMF, LGN and MANO units are characterised by: (i) relatively fractionated REE patterns, enriched in the light rare earth elements (LREE;  $\text{La}/\text{Lu}_N$  1.6–14; Fig. 6.5); (ii) almost no fractionation of the HREE ( $\text{Tb}/\text{Yb}_N$  1.1); and (iii) a pronounced Eu anomaly when normalised to chondrite ( $\text{Eu}/\text{Eu}^*$  0.8–3.6). The GNPA member shows notable similarities to both the Platreef and Upper Critical Zone (Fig. 6.6).

The most fractionated profiles ( $\text{La}/\text{Lu}_N$  5–12) within the GNPA member are associated with samples obtained from the MANO and LMF units east of the Grasvally Fault, where the succession overlies metasediments (Fig. 6.5a and d). Here the rocks show strong enrichment in LREE ( $\text{Ce}/\text{Sm}_N$  2.1–3.6) and almost no fractionation of the HREE (average  $\text{Tb}/\text{Yb}_N$  of 1). These observations support Maier et al. (2008) earlier findings (Fig. 6.5a and d) and are analogous to the Lower Platreef at Townlands which is characterised by  $\text{La}/\text{La}_N$  ratios between 4.8–5.4 and  $\text{Ce}/\text{Sm}_N$  ratios of 2.7–3.1 (Manyeruke et al. 2005; Fig. 6.6b). Although the individual profiles of samples from borehole RP05.45 do not appear to become progressively enriched in REE with depth and thus proximity to the quartzite footwall, REE concentrations are noticeably elevated within the basal LMF unit (Fig. 6.5d).

In contrast, where Lower Zone cumulates underlie the GNPA member REE concentrations are comparable between the LMF and MANO units (Fig. 6.b and e). Here, REE profiles are fractionated and LREE enriched but less so than observed east of the Grasvally Fault (Fig. 6.a-b, d-e), also showing no fractionation of HREE ( $\text{Tb}/\text{Yb}_N$  0.9). Most samples reveal lower  $\text{La}/\text{Lu}_N$  (1.6–4.8) and  $\text{Ce}/\text{Sm}_N$  (1.3–2) ratios, which are directly comparable to the Upper Platreef at Townlands (Fig. 6.6b; Manyeruke et al. 2005) where  $\text{La}/\text{Lu}_N$  and  $\text{Ce}/\text{Sm}_N$  ratios vary from 2.2–4.3 and 1.9–2.5, respectively. Additionally, these REE patterns also show broad similarities to the Platreef at both Overysel and Sandsloot (Fig. 6.6c; McDonald et al. 2005; Holwell and McDonald 2006). The LGN unit, which has previously been suggested to represent a sill of Main Zone (de Klerk 2005), is notably fairly homogeneous in its REE contents and geochemistry in comparison to the overlying MANO unit and underlying LMF unit, (Fig. 6.5b). The restricted set of normalised patterns observed (Fig. 6.5c) are well fractionated ( $\text{La}/\text{Lu}_N$  6.0–10.8), LREE enriched ( $\text{Ce}/\text{Sm}$  2.4) and reside comfortably within the Main Zone field (shown in Fig. 6.6a).

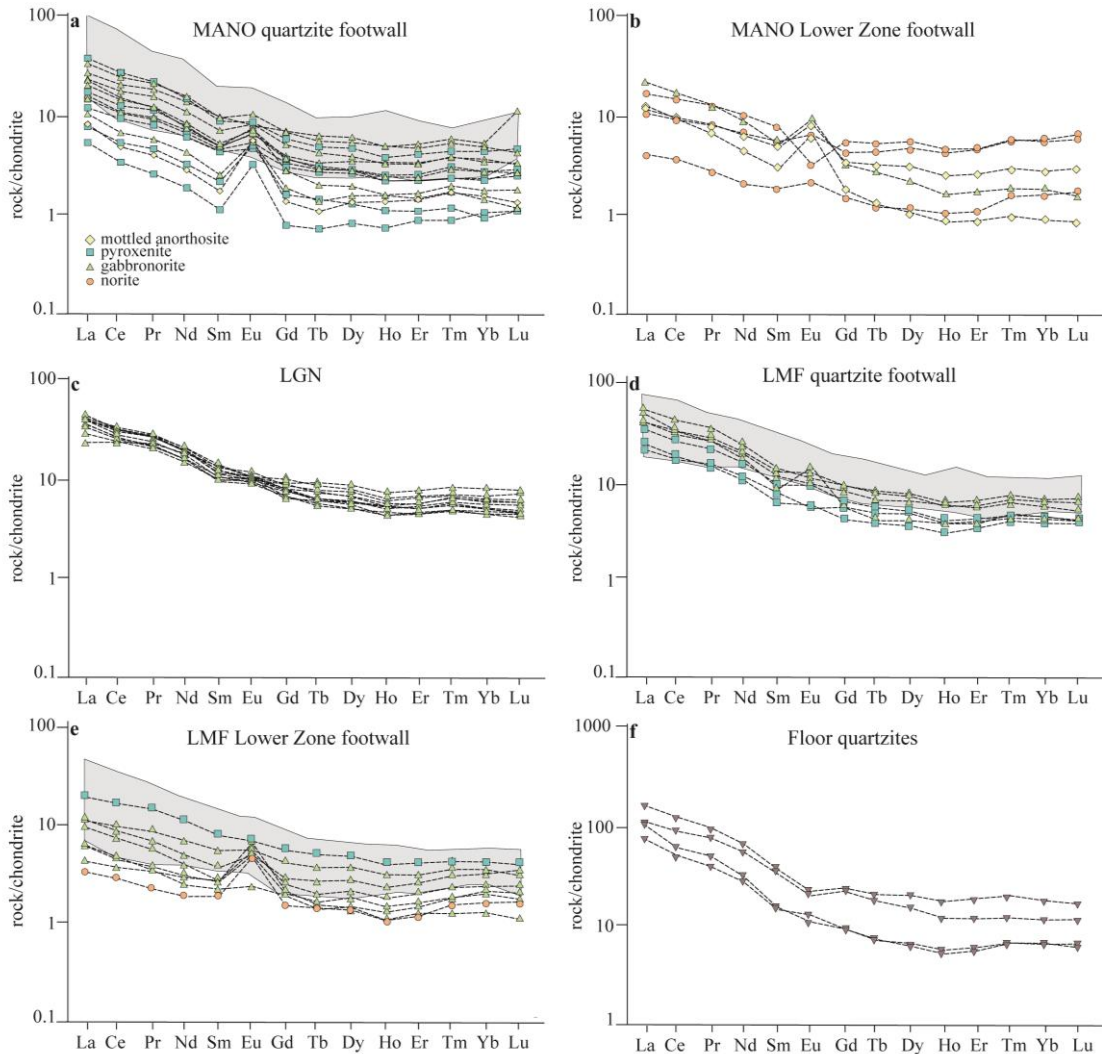


**Figure 6.5** Chondrite normalized rare earth element plots for a) the mottled anorthosite unit where underlain by quartzites, b) the mottled anorthosite unit where underlain by Lower Zone, c) the Lower Gabbronorite unit, d) the Lower Mafic unit where underlain by quartzites, e) the Lower Mafic unit where underlain by Lower Zone and e) footwall quartzites from the Magaliesberg Quartzite Formation. Shaded fields represent data from Maier et al. (2008).

The GNPA member, like the Upper Critical Zone (Fig. 6.6a), is also characterised by a moderately positive Eu anomaly ( $\text{Eu}/\text{Eu}^*$  1.01–2.76) which is most pronounced within the plagioclase rich MANO unit ( $\text{Eu}/\text{Eu}^*$  1.1–3.6). The LGN unit is characterised by the smallest positive Eu anomaly ( $\text{Eu}/\text{Eu}^*$  1.02–1.2) which is noticeably lower than considered typical of Main Zone rocks ( $\text{Eu}/\text{Eu}^*$  2.1; Maier and Barnes 1998). Small negative Eu anomalies ( $\text{Eu}/\text{Eu}^*$  0.4–0.9), comparable to those within the Platreef at Sandsloot ( $\text{Eu}/\text{Eu}^*$  0.72–0.93; McDonald et al. 2005) are uncommon within the GNPA member (Fig. 6.5 and Fig. 6.6c).

The Magaliesberg Quartzite Formation which, east and north of the Grasvally Fault, directly underlies the GNPA member exhibits highly fractionated REE patterns ( $\text{La}/\text{Lu}_N$  11–19) that are significantly more enriched than those of the GNPA lithologies (Fig. 6.5f). In addition, the footwall generally reveals a small negative Eu anomaly ( $\text{Eu}/\text{Eu}^*$  0.7–0.9).

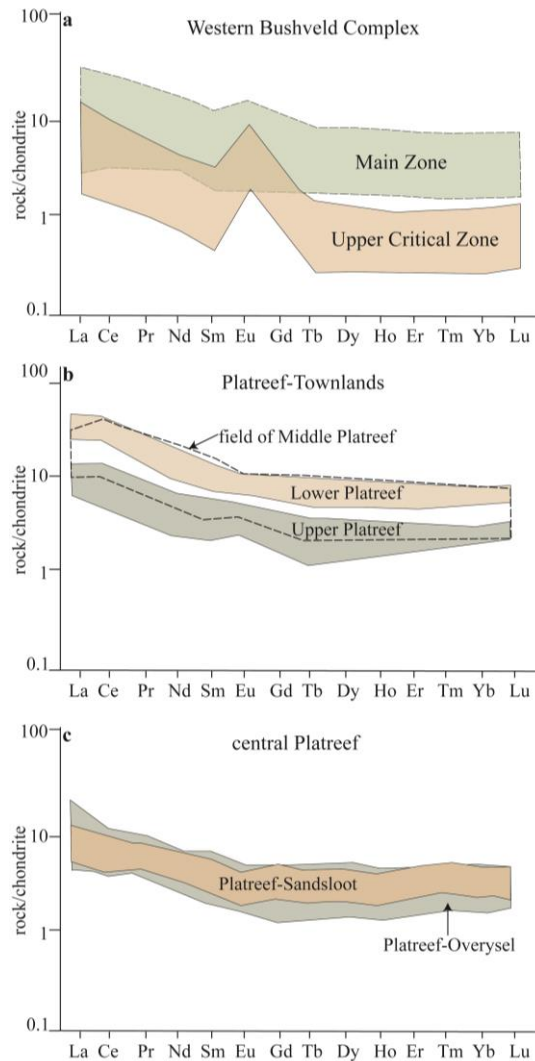


**Figure 6.6** Chondrite normalized rare earth element fields for a) The Main Zone and Upper Critical Zone from the western Bushveld Complex (from Maier and Barnes 1998), b) the Upper, Middle and Lower Platreef rocks from Townlands (from Manyeruke et al. 2005) and c) the central sector of the Platreef at Sandsloot and Overysel (from Holwell and McDonald 2006)

#### 6.5.1.1 Variations in $\text{Ce}/\text{Sm}$ ratios

The binary variation diagrams in Figure 6.7 provide some constraints on the magmatic lineage of the GNPA member. Within the eastern and western limbs of the Bushveld Complex the  $\text{Ce}/\text{Sm}$  ratio typically increases with depth (Maier and Barnes 1998; Table 6.1), a feature that is also observed within the Platreef (Manyeruke et al. 2005). The Main Zone has an average  $\text{Ce}/\text{Sm}$  ratio of 8.97 (Maier and Barnes 1998), whilst rocks of the

Upper Critical Zone have an average Ce/Sm ratio of 13.6. Overall the GNPA member exhibits a similar range in Ce/Sm ratios to the Platreef (Table 6.1). Within the GNPA member the Ce/Sm ratio ranges from 6–13 in the MANO unit, 9–11 in the LGN unit and 5–15 in the LMF unit (Fig. 6.7a and b; Table 6.1). It should be noted that although the Ce/Sm ratios of the LGN are consistent and comparable to Main Zone values (data from Moorddrift; Maier and Barnes 2010), the former is noticeably more enriched in the incompatible trace elements (Fig. 6.7a and c), which is a feature not apparent from analysis of the REE profiles (Fig. 6.5).

With each stratigraphic unit averaging between 9.6 and 10.4 the GNPA member is most comparable to the Main Zone in terms of Ce/Sm ratios, although the data does scatter between the liquid lines of B1 (Lower/Lower Critical Zone) and B2/B3 (Upper Critical Zone/Main Zone) type magmas (Fig. 6.7). Although these findings could be interpreted to indicate that the GNPA member formed through mixing of B1 with B2/B3 magma it could also be accounted for through the assimilation of footwall shales or quartzites which have similar Ce/Sm ratios to B1 magma (Table 6.7a and b). Where the footwall consists of metasediments, there is a significant increase in the trace element content of the GNPA member (Fig. 6.5a, d, Fig. 6.7b), and thus a strong localised crustal component. The high concentration of incompatible trace elements within the shales and quartzites which directly underlie the GNPA member makes them the most likely contaminant (Fig. 6.7a and b; Klein and Beukes 1989).

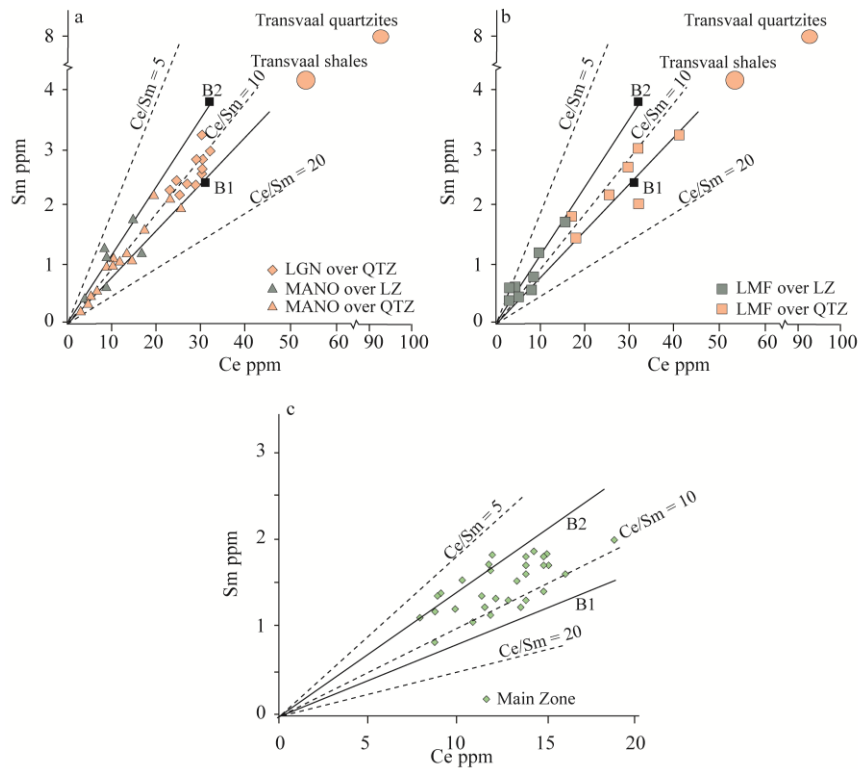


**Figure 6.7** Binary variation diagrams of Ce vs Sm showing data from a) the Mottled Anorthosite unit and Lower Gabbro unit, b) the Lower Mafic unit with a quartzites and Lower Zone footwall, and c) Main Zone on Moorddrift (from Maier and Barnes 2010). Solid lines indicate Ce/Sm ratio of B2/B3 and B1 magmas (from Curl 2001). Compositional fields of the Transvaal shales (from Klein and Beukes 1989) and the immediate underlying quartzites (own data) are also shown.

### 6.5.2 Spidergrams

Primitive mantle-normalized, multi-element spider diagrams of representative samples from the GNPA member and its local quartzite footwall are presented in Figure 6.8. Throughout the succession, trace element signatures are consistent, characterised by pronounced negative Nb, Sr and Ti anomalies and strong enrichment in LILE (Fig. 6.8a-c). Whilst the MANO and LMF units exhibit variations in absolute trace element concentrations, the LGN unit exhibits an extremely restricted range in its trace element content and geochemistry (Fig. 6.8a-c).

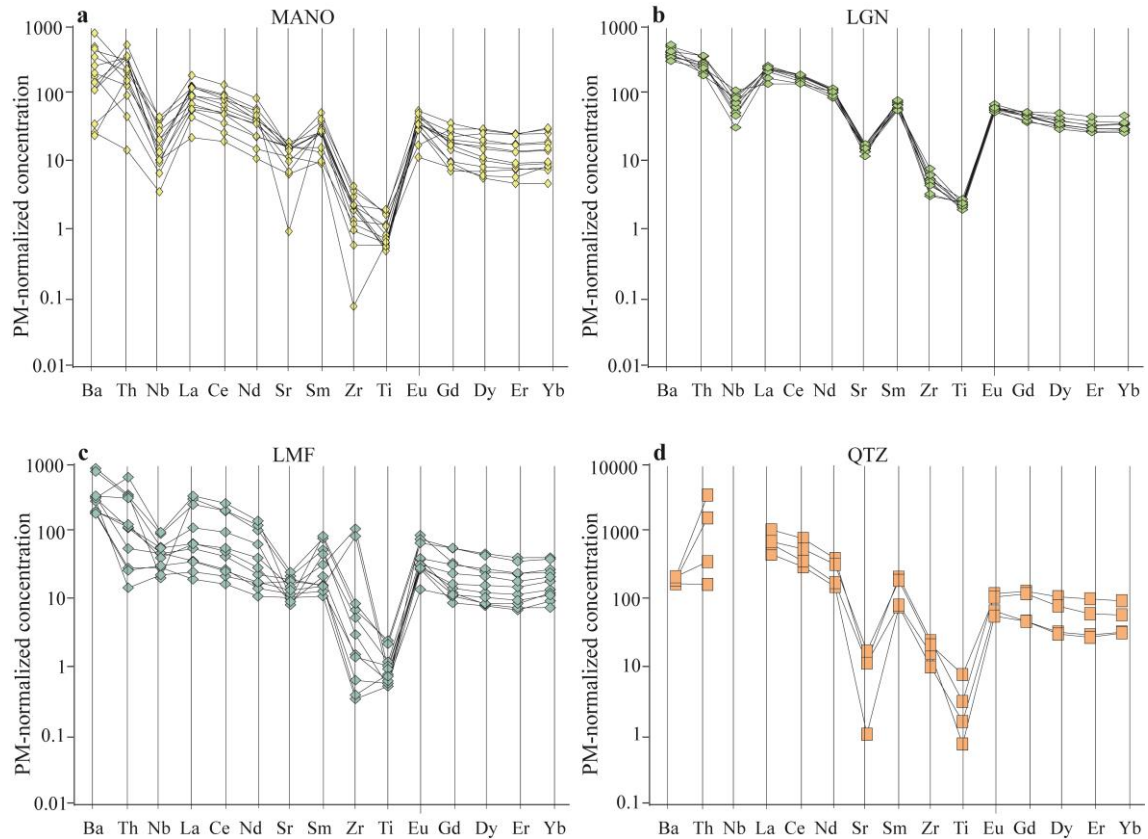


**Figure 6.8** primitive mantle-normalized trace element patterns for samples from a) the Mottled Anorthosite unit (MANO), b) the Lower Gabbro unit (LGN), c) the Lower Mafic unit (LMF) and d) quartzites from the Magaliesberg Quartzite Formation.

The majority of samples within the GNPA member exhibit low  $(\text{Nb}/\text{Th})_{\text{PM}}$  ratios (less than 0.4) and elevated  $(\text{Th}/\text{Yb})_{\text{PM}}$  ratios (1 to 24), thus defining a relatively tight trend (similar to that observed in the Platreef; Ihlenfeld and Keays 2011) on the  $(\text{Nb}/\text{Th})_{\text{PM}}$  vs.  $(\text{Th}/\text{Yb})_{\text{PM}}$  plot presented in Figure 6.9. With  $(\text{Nb}/\text{Th})_{\text{PM}}$  ratios  $<1$  and  $(\text{Th}/\text{Yb})_{\text{PM}}$  ratios  $>5$  considered indicative of a crustally contaminated mantle derived magma (Lightfoot and Hawkesworth 1988; Lightfoot et al. 1990; Ihlenfeld and Keays 2011), a crustal influence is noticeable throughout the GNPA member with few samples residing within the purely magmatic range (Fig. 6.9a). From Figure 6.8 and 6.9 however, it is evident that the degree of contamination is not a function of proximity to local footwall metasediments as the basal LMF unit exhibits a similar range in  $(\text{Nb}/\text{Th})_{\text{PM}}$  and  $(\text{Th}/\text{Yb})_{\text{PM}}$  ratios to the LGN and MANO units.

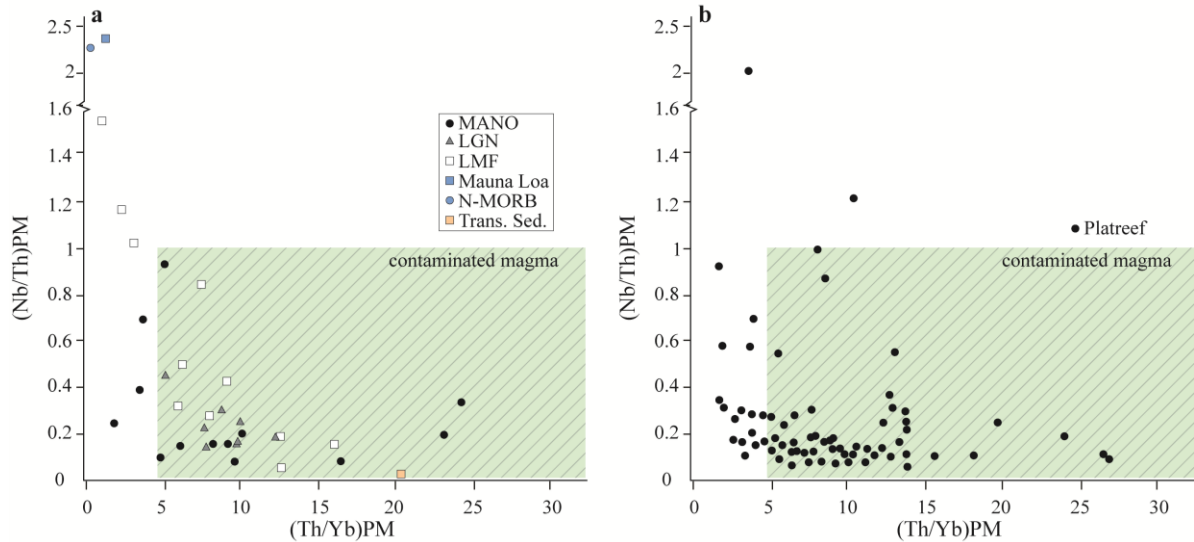


**Figure 6.9** a) Plot of  $(\text{Nb}/\text{Th})_{\text{PM}}$  vs  $(\text{Th}/\text{Yb})_{\text{PM}}$  for samples from the GNPA member. Average compositions of N-MORB, Hawaiian (Mauna Loa) tholeiites and Transvaal sediments are also shown for reference. b) comparison with  $(\text{Nb}/\text{Th})_{\text{PM}}$  and  $(\text{Th}/\text{Yb})_{\text{PM}}$  ratios observed in the Platreef (Ihlenfeld and Keays 2011).

## 6.6 Mineral Chemistry

The composition of orthopyroxene, clinopyroxene and plagioclase for the GNPA member is summarised in Table 6.2. Data of all mineral analyses obtained during this study is provided in Appendix 5.

	Orthopyroxene		Clinopyroxene	Plagioclase
<b>Main Zone</b>				
Rooipoort	Mg# <sub>66-67</sub>	En <sub>63-65</sub>	Wo <sub>41-46</sub>	An <sub>60-73</sub>
Overysel	Mg# <sub>60-63</sub>			An <sub>71-82</sub>
<b>GNPA member</b>	Mg# <sub>60-83</sub>	En <sub>58-82</sub>	Wo <sub>32-49</sub>	An <sub>62-80</sub>
LMF	Mg# <sub>66-83</sub>	En <sub>61-82</sub>	Wo <sub>35-48</sub>	An <sub>63-78</sub>
LGN	Mg# <sub>60-63</sub>	En <sub>58-61</sub>	Wo <sub>43-46</sub>	An <sub>71-80</sub>
MANO	Mg# <sub>63-74</sub>	En <sub>60-72</sub>	Wo <sub>32-49</sub>	An <sub>62-76</sub>
Platreef	Mg# <sub>68-80</sub>	En <sub>71-74</sub>		An <sub>70-85</sub>
Upper Critical Zone	Mg# <sub>78-84</sub>			An <sub>68-85</sub>

**Table 6-2** Mineral compositions for the GNPA member. Data for the LGN unit taken from analysis by Iain McDonald (personal communication). Data for other Bushveld rocks are from McDonald and Holwell (2011) and references therein.

### 6.6.1 Plagioclase composition

The An content of plagioclase within the GNPA member is variable with a range of An<sub>62-80</sub> observed throughout the succession. The plagioclase composition of the LMF and MANO units (An<sub>62-78</sub>) overlaps with the Platreef and Upper Critical Zone values, although not with

the upper part of the range (Table 6.2; Cameron 1982; Kruger and Marsh 1985; Naldrett et al. 1986; Maier and Eales 1994; McDonald et al. 2005; Holwell 2006). In comparison the gabbro-norites of the LGN unit reveal compositions consistent with the Main Zone on Overysel (Table 6.2).

It is evident from the representative drill core section (RP04.23) shown in Figure 6.10 that the An content of plagioclase is not constant throughout the succession. Notable variations in the averaged plagioclase composition define four distinct rock packages, which in part, correspond to the LMF, MANO and Main Zone. The base of each unit is characterised by a significant shift or reversal in the An content. The lower section of the LMF unit (from 400–338m) displays an upward decrease in An content, from values of An<sub>71</sub> at the base to An<sub>64</sub>. Above this plagioclase becomes progressively more calcic with height (Fig. 6.10). The reversal in composition which must occur between 338m and 315m coincides with the appearance of chromite, which is first observed at a depth of 338m (Fig. 6.10). This trend of upward increasing An content continues for over 200m, until the LMF-MANO contact where the highest An contents (An<sub>76</sub>) of the entire succession are observed. The base of the MANO unit is characterised by a reversal in plagioclase composition. In the overlying plagioclase rich cumulates an upward decrease in An content is observed from values of An<sub>73</sub> at the base to An<sub>66</sub> near the Main Zone contact. The Main Zone is marked by a significant shift in plagioclase composition, from An<sub>66</sub> at the upper contact of the MANO unit to An<sub>71</sub> at the base of the Main Zone (Fig. 6.10).

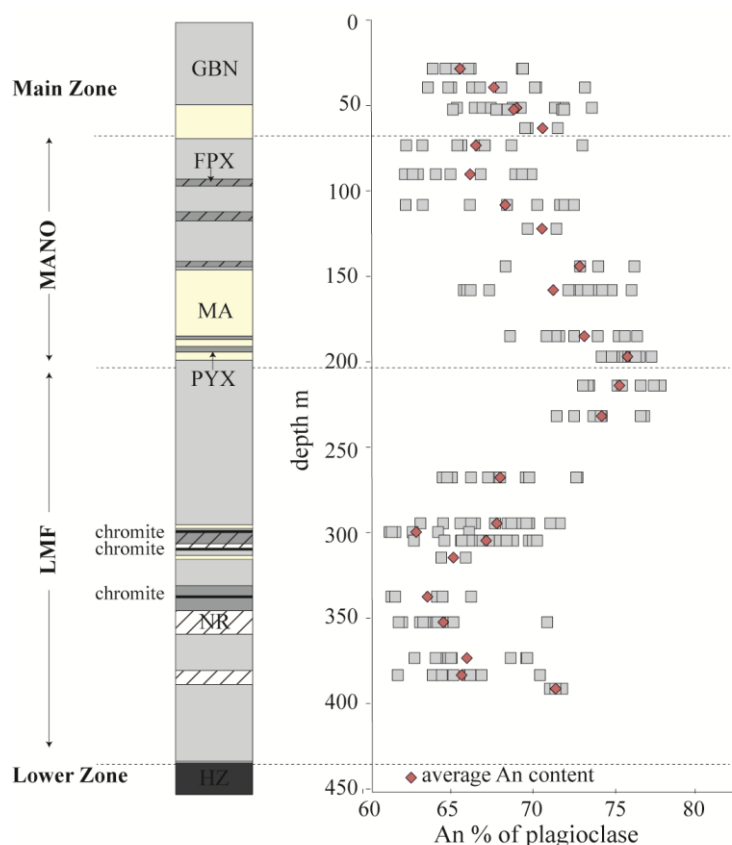


**Figure 6.10** Variations of the An content of plagioclase with height throughout the GNPA member in borehole RP04.23. Lithological abbreviations are the same as in Figure 6.2.

### 6.6.2 Pyroxene composition

Pyroxene compositions in the GNPA member are seen to vary both between and within the three main stratigraphic units (Table 6.2). Although overall the pyroxene composition ranges between  $Mg\#_{60-83}$  the bulk of the data resides within the composition of  $Mg\#_{66-74}$  (Fig 6.11a; Table 6.2). Near comparable orthopyroxene and clinopyroxene compositions are evident within the MANO and LMF units ( $Mg\#_{63-74}$  and  $Mg\#_{66-83}$ , respectively). Although these compositions overlap with that of the few Main Zone gabbro-norites analysed within the Rooipoort region (Table 6.2, Fig. 6.11a), they are noticeably distinct in their composition to the Main Zone gabbro-norites developed above the Platreef further north on Overysel ( $Mg\#_{60-63}$ ; Table 6.2). Orthopyroxenes hosted within the LMF and MANO units are compositionally similar to those within the adjacent Platreef which also has a main population between  $Mg\#_{ca.66-80}$  (Fig. 6.11; 6.12; Table 6.2; McDonald et al. 2005; Armitage 2011). Therefore like the Platreef, orthopyroxenes within the GNPA member are generally more Fe-rich than within the Upper Critical Zone of the eastern and western limbs, although some overlap is observed ( $Mg\#_{78-84}$ ; Table 6.2; Fig. 6.12; Eales and

Cawthorn 1996; Maier and Eales 1994). These observations are consistent with data obtained from other sources on the GNPA member (Fig 6.11.a and b).

From Figure 6.11b it is apparent that the LGN orthopyroxenes differ in composition to those developed within the LMF and MANO units. The LGN is characterised by a lower population of less variable Mg numbers ( $Mg\#_{60-63}$ ) that are consistent with Main Zone compositions above the Platreef (Table 6.2; Fig. 6.11b). Such findings support the notion proposed by de Klerk (2005) that the geochemically homogenous LGN unit represents a chilled sill of Main Zone magma, intruded between the LMF and MANO units.

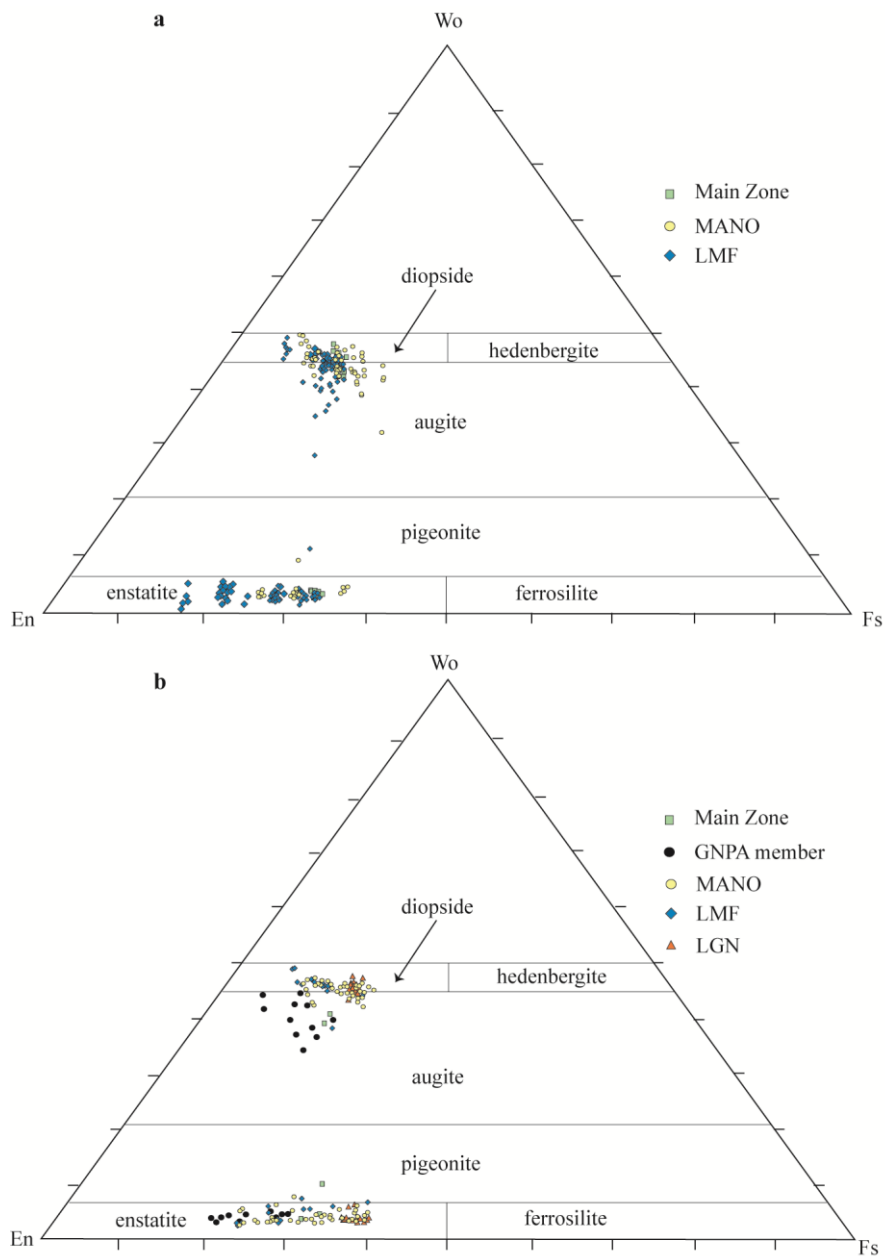


**Figure 6.11** Compositions of pyroxenes from the GNPA member and overlying Main Zone. a) represents data collected in this study from borehole RP04.23, b) data from various boreholes within the Rooipoort region from Hulbert (1983; GNPA member and Main Zone analysis) and through personal communication with Iain McDonald (MANO, LGN, LMF).

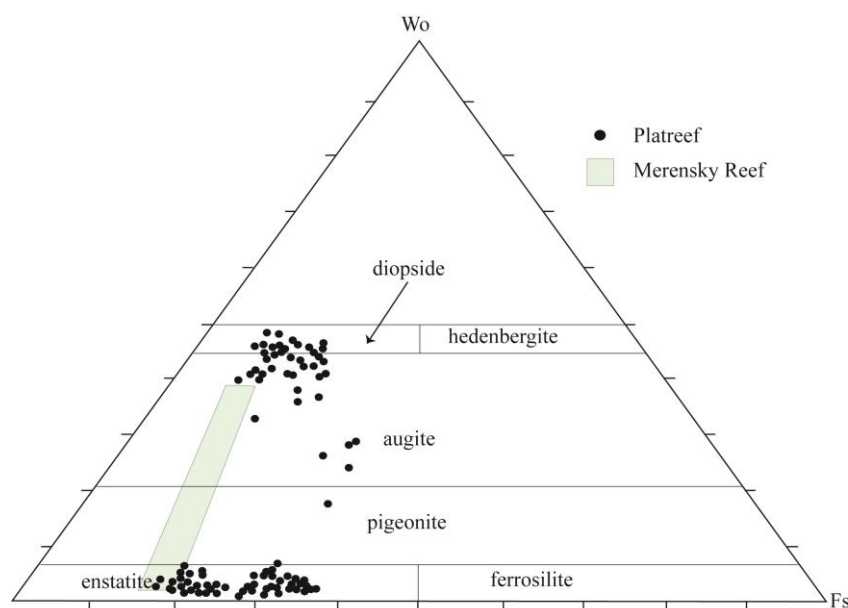


**Figure 6.12** Pyroxene compositions within the Platreef (from McDonald et al. 2005), shaded area shows the range of typical Merensky Reef pyroxenes (from Buchanan et al. 1981; Cawthorn et al. 1985).

#### 6.6.2.1 Variations in pyroxene composition with depth

Figure 6.13 provides a depth profile of pyroxene compositions through borehole RP04.23. The composition of orthopyroxene, like that of plagioclase, is not constant throughout the succession, with trends defining at least four distinct mafic packages (Fig. 6.13a and b). As observed with the An content of plagioclase (section 6.6.1), significant shifts/reversals in orthopyroxene composition in places, correspond to boundaries between stratigraphic units (Fig. 6.13a, b). Within the lower portion of the LMF unit (from 433–370 m), orthopyroxenes reveal an upwards enrichment in Fe. Above this there is a noticeable shift in the composition of orthopyroxene which towards the top of the LMF unit continues to become more Mg-rich up to the LMF-MANO contact. Although data is limited within the MANO unit, a reversal in composition must occur between 130 and 190 m, above which the orthopyroxenes become increasingly more Fe-rich with proximity to the MANO-Main Zone contact. The Main Zone is marked by a significant shift in the orthopyroxene composition. Variations in the orthopyroxene composition parallel trends observed within the An content of plagioclase (Fig. 6.10; Fig. 6.13.a and b).

In contrast to the orthopyroxenes, the clinopyroxene composition is constant throughout the succession (Fig. 6.13c) with average compositions generally resided between  $Wo_{43-44}$ , with an overall range of  $Wo_{38-46}$  observed (Table 6.2).

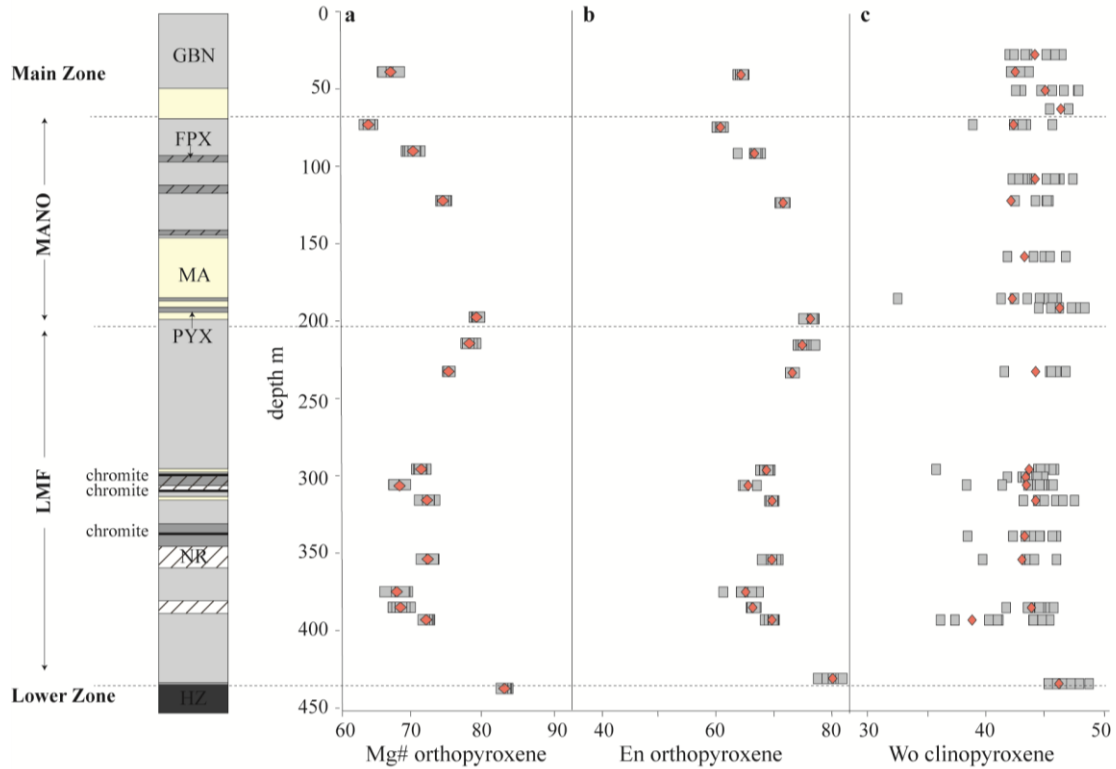


**Figure 6.13** Variations in pyroxene composition with depth in borehole RP04.23 a) Mg# orthopyroxene, b) En content of orthopyroxene and c) Wo content of clinopyroxene. Average compositions are shown in red. Lithological abbreviations are the same as in Figure 6.2.

### 6.6.3 Comparison of mineral and whole rock chemistry

Within borehole RP04.23, variations in both the whole rock and mineral chemistry are observed throughout the succession. Whilst elements such as  $\text{Al}_2\text{O}_3$ ,  $\text{CaO}$ ,  $\text{MgO}$  and  $\text{Cr}$  and  $\text{SiO}_2/\text{Al}_2\text{O}_3$  and  $\text{CaO}/\text{Al}_2\text{O}_3$  ratios all vary systematically with depth (Fig. 6.2a-c, f, g), reflecting the gradual increase in modal plagioclase upwards through the succession, trace element profiles of  $\text{Zr}$ ,  $\text{Sr}$  and  $\text{V}$  define two distinct compositional trends. Reversals observed in the trace elements at the LMF-MANO contact coincide with a strong reversal in the orthopyroxene and plagioclase composition, which also show evidence of an earlier reversal within the LMF unit (Fig. 6.3b-c; 6.10; 6.13a and b). The sharp reversals and shifts in Mg# (opx), En and An content, which define at least three discrete packages within the GNPA member, are also observed/indicated within the bulk Mg# (Fig. 6.2d).

## 6.7 Discussion

### 6.7.1 Crustal contamination

Through utilizing S isotopes and S/Se ratios as tracers of S, in Chapter 5, I recognised that the parental magma (s) of the GNPA member was strongly crustally contaminated (at least in terms of S) at the time of emplacement. Evidence of this early, pre-emplacement contamination event along with a later localised, *in situ* contamination event are preserved within the trace element chemistry of the succession.

#### 6.7.1.1 First contamination event

The consistency of the primitive mantle-normalized spidergrams presented in Figure. 6.8 demonstrate that the GNPA magma (s) was characterised by pronounced negative Nb and Ti anomalies and LILE enrichment, features also reflected in the low  $(\text{Nb}/\text{Th})_{\text{PM}}$  ratios and high  $(\text{Th}/\text{Yb})_{\text{PM}}$  ratios shown in Figure. 6.9. Since these geochemical signatures are characteristic of crustal rocks (Lightfoot and Hawkesworth 1988; 1997), and thus considered indicative of crustal contamination of a mantle derived magma (Lightfoot and Hawkesworth 1988; Lightfoot et al. 1990; Ihlenfeld and Keays 2011), it is inferred that the parental magma of the GNPA member was strongly contaminated by crustal rocks. With a pronounced crustal component being observed throughout the LMF and MANO units, regardless of footwall lithology (Lower Zone and quartzites), it is concluded that the contamination signature evident throughout the succession is the product of an early contamination event, which occurred at depth prior to emplacement, in support of the earlier findings from the S/Se and S isotope evidence (Chapter 5).

From the rather uniform degree of contamination apparent from: (i) the consistency of the  $\delta^{34}\text{S}$  signature throughout the succession (see Chapter 5) and (ii) the relatively tight trend defined by samples in Figure 6.9, it can be inferred that the contaminant was well homogenized with the GNPA magma. Since such features are not consistent with the *in situ* assimilation of crustal rocks, I believe them to be indicative of regional contamination processes which enable the contaminant to easily equilibrate with all of the parental magma (s). From the trace element data it can therefore be concluded that the magma from which the GNPA crystallised attained its crustal signature prior to emplacement. These findings consequently support the genetic model presented in Chapter 5, where based on S isotope signatures, I proposed that the GNPA magma was saturated in S prior to emplacement in response to widespread contamination by S-bearing crustal rocks. Although it can be constrained from the trace element data presented that this first crustal contaminant was

enriched in LILE and characterised by elevated Th/Yb ratios ( $>15$ ), its exact nature and origin remains speculative. In a recent study, Sharman et al. (2013) demonstrated that the crustal S present within the Platreef originated from shales or carbonates from the Duitschland Formation. On the basis of S isotope signatures, Smith et al. (2014) postulated a similar source of crustal contaminant for the GNPA member.

#### 6.7.1.2 *Second contamination event*

In contrast to the first contamination event the effects of later assimilation of crustal rocks are localised, preserved only where a metasedimentary footwall exists. Evidence of this second contamination event is only gained through analysis of variations in the abundance of incompatible elements. To the east of the Grasvally Fault (see geological map Fig. 4.2), where the GNPA member is in contact with the Magaliesberg Quartzite Formation, a local footwall control over the REE signatures of the succession is observed (Fig. 6.5). Here, the LMF and MANO units are characterised by: (i) elevated absolute concentrations of REE; (ii) enrichment in the incompatible elements (illustrated by Ce and Sm in Figure 6.7a, b); and (iii) fractionation of LREE. With these features becoming more pronounced with proximity to the footwall (i.e. in the LMF unit; Fig. 6.5a, d; Fig. 6.7), it is concluded that the second contamination event resulted from the interaction of the GNPA magma with local footwall rocks at the time of emplacement.

In PGE-Ni-Cu deposits developed in contact-type settings, the effects of localised assimilation of country rocks at the time of emplacement are often recorded within the S isotope composition of sulfides (e.g. Duluth Complex; Mainwaring and Naldrett 1977; Ripley 1981; Ripley et al. 1986 and the Basal Series of the Stillwater Complex; Lambert et al. 1994; Lee 1996; McCallum 1996). Where syn- or post-emplacement contamination represents a secondary S assimilation event,  $\delta^{34}\text{S}$  signatures consistent with the local footwall are seen to overprint and obscure an initial crustal or mantle  $\delta^{34}\text{S}$  signature (e.g. Platreef; Manyeruke et al. 2005; Sharman-Harris et al. 2005; Holwell et al. 2007; Ihlenfeld and Keays 2011). Within the GNPA member however, S isotopes are only indicative of a single, pre-emplacement primary S assimilation event (Smith et al. 2014; see Chapter 5), with: (i) no variations in  $\delta^{34}\text{S}$  composition observed with changing footwall lithology west and east of the Grasvally Fault (Lower Zone harzburgite and quartzites, respectively; Fig. 4.2; Fig 5.1); and (ii) no evidence the degree of contamination increases towards the metasediment footwall contact (Smith et al. 2014; Chapter 5). Since these observations are inconsistent with the assimilation of S-bearing country rocks, it is concluded that the

second contamination event did not introduce additional crustal S into the magmatic system (unlike at Turfspruit) at the time of emplacement and thus did not have any control over the genesis of sulfide mineralization within the GNPA member. The crustal  $\delta^{34}\text{S}$  component observed throughout the succession is thus indicative of the initial source of S (Chapter 5).

### **6.7.2 Emplacement of the GNPA member**

Within layered intrusions such as the Bushveld Complex, compositional breaks in major, trace element and mineral chemistry are often considered indicative of the addition of a new pulse of magma, which is compositionally similar or distinct from that which formed the preceding cumulates. The boundaries between the main stratigraphic units of the Bushveld Complex have thus been inferred from geochemical along with mineralogical and petrological breaks (Cameron 1982; Kruger 1994; Kruger 2005; Eales and Cawthorn 1996). It is important to be aware however that not all geochemical breaks (especially in Mg#) coincide with the addition of magma, and are instead occasionally attributed to the trapped liquid shift effect (see Barnes 1986, Cawthorn et al. 1992; Cawthorn 1996).

Within the GNPA member, disparities between the whole rock and mineral chemistry of the succession (Fig. 6.2; 6.3; 6.10; 6.13), can be accounted for by the lithological control observed on major and trace element geochemistry. The continued fractionation trend of many of the major and trace elements (Fig. 6.2; 6.3a) is thus reflective of the overall upward decrease in the modal abundance of pyroxene, which consequently masks evidence of magma replenishment as indicated from variations in mineral compositions. The major and trace depth profiles (e.g.  $\text{SiO}_2/\text{Al}_2\text{O}_3$ , CaO, MgO, Cr) however do demonstrate that the LMF and MANO units of the GNPA member were derived from compositionally similar magmas, that were distinct from the parental magmas of the Lower Zone and Main Zone.

Sharp reversals in the composition of both plagioclase and orthopyroxene, at the base of the MANO unit, (also observed in bulk Mg#, Zr, Sr, and V; Fig. 6.2d, 6.3b-d), and within the basal section of the LMF unit (Fig. 6.10 and 6.13a, b), are interpreted to indicate new influxes of compositionally similar magma. The interpretation that the GNPA member thus represents a series of separate magma influxes into a single chamber rather than a single intrusive phase is also consistent with the compositional breaks identified within the GNPA member developed further north on War Springs. Here Sutherland (2013) noted multiple changes in the upward trends of  $\text{TiO}_2$  and  $\text{SiO}_2/\text{Al}_2\text{O}_3$ , (similar to those identified

within the Platreef by Kinnaird 2005) which were not consistent with lithological variations and thus considered indicative of influxes of magma. Within the Critical Zone of the eastern and western limbs, the appearance of chromitite layers and anorthosites are generally attributed to the mixing of residual fractionated magma with more primitive magma (Irvine 1977; Kruger and Marsh 1982; Campbell et al. 1983; Irvine et al. 1983; Kinnaird et al. 2002; Kruger 2005). Evidence of magma replenishment within the GNPA member is therefore also indicated by the lower and upper mineral reversals coinciding with the appearance of cumulus chromite and plagioclase, respectively. McDonald et al. (2005) also suggested such a mechanism for chromite formation and attributed the unique orthopyroxene-clinopyroxene-chromite cumulates observed within the chromitites (Hulbert 1983; Chapter 3) to mixing of magmas. Such an interpretation also places constraints on the timing of chromite formation, and implies chromite precipitated *in situ*. This is consistent with the lateral continuity of the chromitite layers throughout the Rooipoort and Grasvally region.

With evidence of only a single sulfide liquid distributed throughout the LMF and MANO units (Smith et al. 2014; Chapter 4), it can be concluded that either: (i) the sulfides were entrained and transported within each batch of magma that was intruded into the GNPA member; or (ii) all the sulfide droplets were intruded with the final magma influx and subsequently infiltrated through the entire crystal pile.

Through identifying the GNPA member consists of at least three discrete rock packages (Fig. 6.10; 6.13) it is concluded that crystallization from pyroxenites in the basal LMF, to gabbronorites in the upper LMF, and finally gabbronorites and anorthosites in the MANO unit resulted from the progressive mixing of new and residual fractionated magmas. Although the multiple magma pulses which form the GNPA member are unable to be confidently correlated with those identified in the Platreef (Kinnaird 2005), in terms of REE signatures comparisons can be drawn with the Platreef sills on Townlands (Manyeruke et al. 2005). Consequently this study highlights that the emplacement mechanism is analogous north and south of the Ysterberg-Planknek Fault (Kinnaird 2005; Nyama et al. 2005).

#### 6.7.2.1 *Timing of S saturation and chromite formation*

In the current genetic model, presented in Chapter 5, PGE-rich sulfides are thought to have formed at depth prior to emplacement of the GNPA member. Although it can be

inferred from the data presented that the parental magma was saturated in S at the time of chromite formation, this is inconsistent with the PGE characteristics of the chromitite layers, which indicate crystallization from a S-undersaturated magma and the effective concentration of IPGE, Rh and Pt over Pd prior to interaction with sulfide liquid (Smith et al. 2014, Chapter 4; see von Gruenewaldt 1989; Barnes and Maier 2002a and b; Prichard et al. 2004; Godel et al. 2007). Within magmatic sulfide deposits the concentration of Os, Ir, Ru, Rh and Pt by chromite is generally attributed to either: (i) the direct crystallization of Pt-Os-Ir alloys and laurite from the parental magmas (Keays and Campbell 1981; Tredoux et al. 1985; Cawthorn 1999); or (ii) the presence of IPGE and Pt-rich clusters in the silicate magma (Tredoux et al. 1995). Where the cluster model is favoured, it is thought Ru and Rh partition into chromite. The crystallization of chromite also destabilizes the PGE clusters resulting in the precipitation of the clusters as Pt, Os and Ir rich PGM (Barnes and Maier 2002b).

If it is accepted that chromite formed *in situ*, then the ability of chromite to effectively scavenge Pt, Rh and IPGE over Pd, subsequent to sulfide immiscibility may be indicative that the parental magma (s) of the GNPA member had not been completely depleted of its PGE content prior to emplacement. This could potentially result from having either a large volume of magma present within the chamber or limited interaction between the sulfide droplets and magma. The low PGE tenors of the GNPA member, in comparison to those characteristic of the Platreef, may also indicate that the sulfide liquid observed within the GNPA member was not completely effective at scavenging all PGE at depth prior to emplacement. Alternatively, if a model similar to that proposed for the Platreef is envisaged for the GNPA member then sulfides acquired their PGE contents through interaction with multiple batches of Lower Zone magmas prior to intrusion (McDonald and Holwell 2007). Since such a model only requires the parental magmas of the GNPA/Platreef to entrain and transport sulfides and not to enrich them in PGE, then it is feasible that chromite sourced and concentrated Pt, Rh and IPGE from the largely un-depleted magmas which ultimately formed the GNPA member. Both scenarios could potentially account for the apparent *in situ* concentration of PGE by chromite within S saturated conditions. As highlighted by Smith et al. 2014 (Chapter 4) in areas where chromite interacted with an earlier formed sulfide liquid (e.g. east of the Grasvally Fault) evidence of PGE enrichment through chromite precipitation (e.g. Pt/Pd >1) is completely erased, being overprinted by typically sulfide concentrated PGE signatures (e.g. Pt/Pd <1).

### 6.7.3 Magmatic lineage of the GNPA member

When the effects of localised contamination are removed it is evident that geochemically the GNPA member is analogous to the Platreef with comparable REE signatures (Fig. 6.5; 6.6), orthopyroxene and plagioclase compositions, major and trace element ratios (Table 6.1; 6.2) and Pt/Pd ratios observed (McDonald et al. 2005; Maier et al. 2008; McDonald and Holwell 2011; Smith et al. 2014). The data presented here is therefore consistent with the notion that the GNPA member and Platreef were derived from compositionally similar or related magmas, merging laterally into the other (von Gruenewaldt et al. 1989; McDonald et al. 2005; Maier et al. 2008; Naldrett 2008; van der Merwe 2008).

Within the northern limb, constraints on the composition of the parental magmas to the Platreef and GNPA member are limited, primarily due to the effects of localised contamination. A chilled marginal member identified at the base of the GNPA member however, provides some insight into the initial composition of the GNPA member (Hulbert 1983). Although the chilled rocks were shown to be of tholeiitic composition, Hulbert (1983) and McDonald et al. (2005) have both argued that certain characteristics of the LMF rocks (particularly in the chromitites) can only be accounted for through the mixing of tholeiitic magma with basaltic (B1) compositions (Hulbert 1983; McDonald et al. 2005). Consequently, whilst I believe the relationship observed between Ce and Sm is in part attributed to *in situ* mixing of a local contaminant with parental magma (i.e. where underlain by quartzites; Fig. 6.7b; see section 6.5.1.1), I interpret the B1 and B2/B3 components of the GNPA member rocks (Fig. 6.7a) to result largely from the mixing of these two magma types, rather than mixing of one with a contaminant. Thus Hulbert (1983) and McDonald et al. (2005) proposal is consistent with major and trace element data (Cr/MgO and Ce/Sm ratios) indicating components of both B1 and B2/B3 magmas throughout the LMF and MANO units (Table 6.1; Fig. 6.4; 6.7). McDonald et al. (2005) proposed that a hybrid magma was produced through mixing of B2/B3 type magma with residual Lower Zone (B1) type magma crystallizing olivine, orthopyroxene and chromite. This proposal however is inconsistent with evidence that suggests the Lower Zone cumulates were consolidated, significantly cooled and tilted prior to the intrusion of GNPA/Platreef magma (s) (van der Merwe 1978; Kinnaird et al. 2005).

To account for the observed tholeiitic and ultramafic type components throughout the LMF and MANO units, we propose that the hybrid magma from which the GNPA member crystallized was developed at depth through the mixing of residual B1 magma

(LZ) with an early phase of Main Zone magma (B2/B3). This is in accordance with McDonald and Holwell (2007) Platreef model, where it is believed the established Lower Zone plumbing system was invaded by a compositionally distinct magma which ultimately resulted in the emplacement of the Platreef (also see McDonald and Holwell 2011). Since the findings of this study suggest the parental magma to the GNPA member was emplaced as a series of magmatic pulses, it is believed that each influx of magma mixed with residual hybrid magma rather than LZ magma (B1) as proposed by McDonald et al. (2005). A schematic summary of the proposed multiphase emplacement model for the GNPA member is provided in Figure 6.14.

Whilst the Upper Critical zone is also considered to result from the mixing of B1 and B2/B3 magmas (e.g. Eales et al. 1990; Barnes and Maier 2002b), key differences in Pt/Pd ratios, crystallization sequence and orthopyroxene compositions (Fig. 6.11; 6.12) may suggest that the starting compositions of the B1 type magma differed in the northern limb to that present within the eastern and western limbs of the Bushveld Complex and/or differed in the proportions of each magma mixed. Observations throughout Chapter 4 and 6 are consistent with the suggestion that both the GNPA member and Platreef formed from a magma poorer in Mg, richer in Ca and Fe and Pd dominant relative to the magma (s) that formed the Upper Critical Zone (McDonald et al. 2005; 2009).

The similarity of Cr/MgO, Ce/Sm ratios, pyroxene compositions and REE signatures of the LGN unit to those typical of Main Zone rocks (Table 6.1; 6.2; Fig. 6.5; 6.6), strongly suggests that in comparison to the LMF and MANO units, the gabbro-norites of the LGN crystallized from an unmixed B2/B3 type magma (Fig. 6.14c). I therefore concur with the previous suggestions that the LGN represents a sill of Main Zone magma intruded subsequent to the emplacement of LMF and MANO units as illustrated in Figure 6.14 (de Klerk 2005).

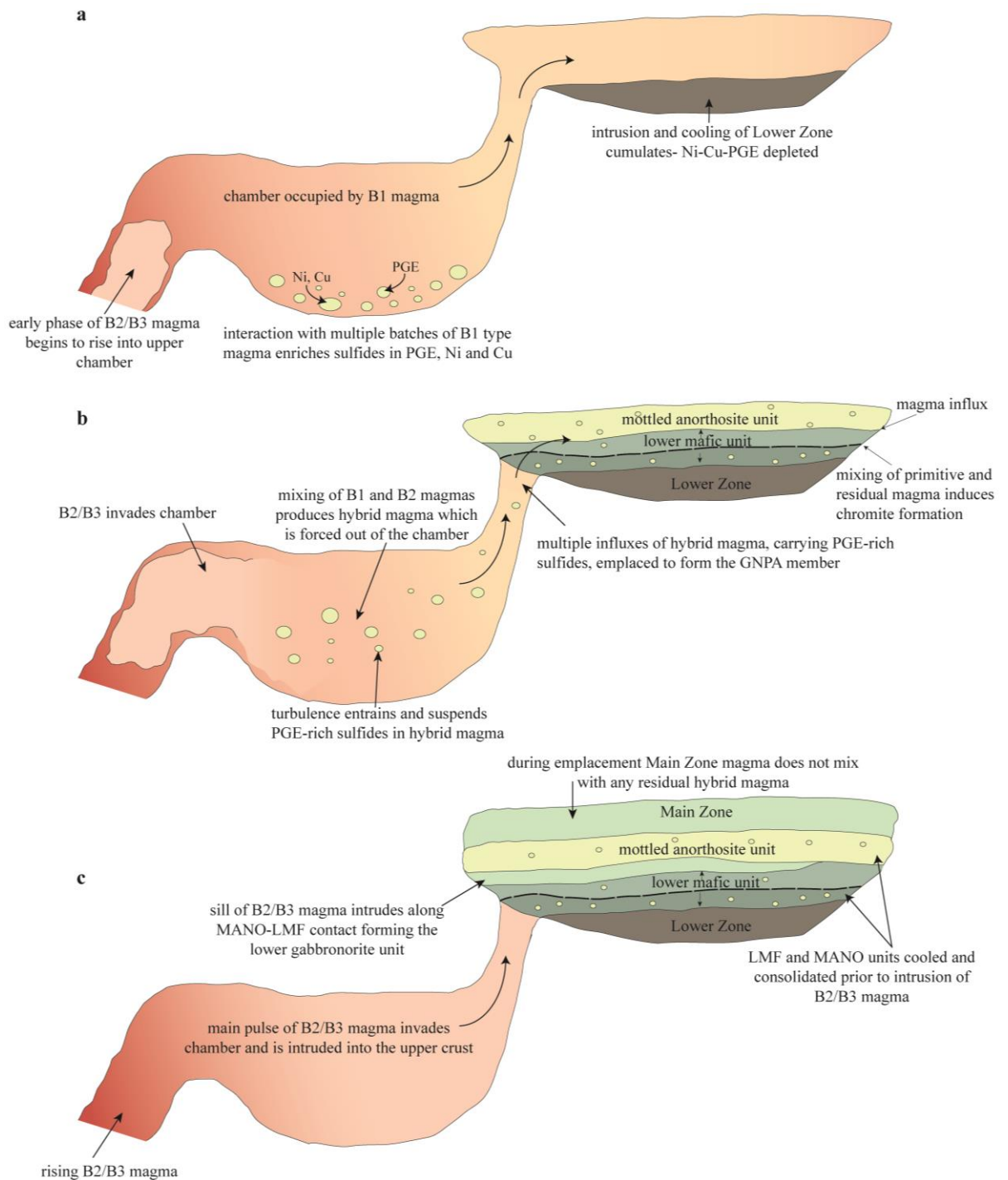


**Figure 6.14** Schematic model of the formation of the GNPA member. **a)** sulfides interact with batches of B1 type magma in a staging chamber, becoming increasingly Ni, Cu PGE rich, producing Ni-Cu-PGE depleted Lower Zone cumulates. **b)** an early pulse of B2/B3 (Main Zone) magma invades the chamber, mixing with residual B1 magma that was not emplaced into the Lower Zone to produce a hybrid magma. Due to turbulence of the new magma entering the chamber, PGE-rich sulfides are entrained and subsequently transported within the hybrid magma. Multiple influxes of the hybrid magma crystallize to form the GNPA member. Mixing between primitive and residual hybrid magma results in chromite formation. There is no interaction of the hybrid magma with residual B1 magma as Lower Zone cumulates have been sufficiently cooled and consolidated. **c)** The main pulse of B2/B3 type magma enters the established plumbing system and is intruded into the upper crust. During emplacement magma intrudes along the LMF-MANO contact, forming a sill of Main Zone known as the Lower Gabbro-norite Unit. The LMF and MANO units were cooled sufficiently prior to emplacement of B2/B3 magma.

## 6.8 Conclusions

Geochemical variations reveal that the parental magma (s) of the GNPA member experienced at least two stages of crustal contamination. The first contamination event occurred prior to emplacement, at depth through the assimilation of S-bearing country rocks. This event was essential for triggering S saturation and the development of an immiscible sulfide liquid and is preserved throughout the GNPA member within both the  $\delta^{34}\text{S}$  and trace element signatures. The second contamination event resulted from the interaction of the GNPA magma with local footwall rocks at the time of emplacement. The *in situ* assimilation of the Magaliesberg Quartzite Formation did not introduce additional crustal S into the magmatic system, consequently having no control on the genesis of sulfide mineralization within the GNPA member.

Geochemical characteristics also indicate that the GNPA member, like the Upper Critical zone, crystallized from a 'hybrid' magma with components of B1 (basaltic) and B2/B3 (tholeiitic) magma. Constraints on the timing of emplacement relative to consolidation of the Lower Zone cumulates, indicates that the hybrid magma was produced at depth, prior to emplacement through mixing of residual Lower Zone magma (B1) with an early phase of Main Zone magma (B2/B3). From the data presented it is concluded that the GNPA formed by successive pulses of more primitive magma interacting with residual hybrid magma during emplacement.

# Chapter Seven

## Conclusions

## 7.1 Conclusions

### 7.1.1 Chapters 3 and 4

Within the GNPA member, the observed distribution and mineralogy of sulfides and PGE results from both magmatic sulfide fractionation processes and low temperature (<230°C) fluid alteration. The distribution of PGE within the primary sulfide assemblage and associated Pt-As and Pd-Bi-Te dominant PGM assemblage is consistent with the fractionation of a single primary sulfide liquid. In places, the primary pyrrhotite–chalcopyrite–pentlandite sulfide assemblage has been replaced to varying extents by a low temperature assemblage of pyrite, millerite and chalcopyrite. The degree of replacement is seen to vary throughout the succession and can be viewed as a continuum from a purely magmatic sulfide assemblage to almost completely replaced sulfides. Post-emplacment fluid interaction has resulted in: some decoupling of Pd, Au and Cu from sulfides on a centimetre to decimetre scale; and the development of a more Sb-bearing PGM assemblage, which is considered indicative of interaction with hydrothermal fluids. Recrystallization of PGM and sulfides occurred *in situ*, resulting in pyrite and millerite inheriting PGE directly from the pyrrhotite and pentlandite replaced. It is revealed therefore that pyrite and millerite can be important carriers of IPGE, Rh and Pd, which could have implications for the recovery of ore within the northern limb of the Bushveld Complex.

### 7.1.2 Chapter 5

Through utilizing S isotopes combined with bulk rock and *in situ* sulfide S/Se ratios to constrain the sources of S, it is demonstrated that the addition of crustal S was critical in the genesis of mineralization throughout the GNPA member. At least within the GNPA member, S isotopes appear to be more robust than S/Se ratios as an indicator of the initial composition of the earliest forming sulfide liquid. With little evidence the S isotope signature has been significantly modified by magmatic and hydrothermal processes the crustal component observed throughout the primary and secondary sulfide assemblage is interpreted to be representative of the initial source of S. It is thought that like the Platreef, the GNPA magma (s) sourced crustal S from the Transvaal Supergroup, possibly through the assimilation of S-bearing carbonates and shales from the Deutschland Formation. With a crustal component evident in the primary sulfide assemblage regardless of footwall lithology, it is constrained that that the parental magma (s) of the GNPA member was crustally contaminated, and also S saturated at the time of emplacement.

Since S/Se ratios of both the primary and secondary sulfide assemblages are inconsistent with the  $\delta^{34}\text{S}$  signatures, it is believed that the initial crustal S/Se ratio of the sulfide liquid has been significantly modified by both magmatic (partial dissolution of sulfides and/or variations in R-factor) and low temperature processes (post-magmatic, hydrothermal S-loss). Although the greater susceptibility of the S/Se ratio to modification provides insight into the processes operating during ore-formation, it should be highlighted that caution is required when considering the source of S as the inferred role of crustal contamination may differ according to the technique used. Furthermore it is emphasized that to remove any uncertainty surrounding the interpretation of both indicators and thus a genetic model it is essential to use S isotopes in conjunction with S/Se ratios.

Whilst it is acknowledged that *in situ* S/Se ratios provide detail previously masked by bulk S/Se ratios, especially when considering the effects of low temperature alteration on the mobility of Se and S, I believe bulk ratios to be more useful when tracing the overall effects of ore-modifying processes and in constraining the initial S source. This is believed since large variations can be observed in the S/Se ratio both within and between individual sulfide minerals which have been attributed to the variable partitioning behaviour of Se during sulfide fractionation. Determining the Se concentration of individual sulfides does however provide an opportunity to investigate both the partitioning behaviour of Se during magmatic sulfide fractionation processes and its mobility during low temperature fluid alteration (<230°C). It is concluded that: (i) Se is compatible within both mss and iss; (ii) Se is fractionated slightly more into mss over iss; and (iii) pyrite and millerite are capable of hosting appreciable quantities of Se, which within the GNPA member behaves in a relatively immobile manner during fluid interaction.

### 7.1.3 Chapter 6

Sharp reversals in the orthopyroxene and plagioclase compositions of cumulates (and to a lesser extent trace elements such as V, Sr and Zr) provide the first convincing evidence that the GNPA member, like the Upper Critical Zone, formed from multiple influxes of magma. Within the GNPA member, the addition of compositionally similar magma is represented by the appearance of cumulus chromite and plagioclase, which is attributed to the *in situ* mixing of new and residual fractionated magmas. Although the parental magma (s) of the GNPA member, like those of the Upper Critical Zone, reveal components of both B1 and B2/B3 type magmas, geochemically the GNPA member is most similar to its nearest analogue, the Platreef. From the constraints on the timing of emplacement and

consolidation of the GNPA member and Platreef relative to solidification of the preceding Lower Zone and intrusion of the Main Zone, it can be inferred that mixing of magma types occurred prior to emplacement possibly within an established Lower Zone conduit network.

Trace element signatures reveal that parental magma (s) of the GNPA member experienced at least two stages of crustal contamination. Evidence of an early pre-emplacement contamination event, through the assimilation of S-bearing and LILE enriched country rocks is preserved throughout the entire GNPA member, and is considered responsible for triggering S saturation at depth (Chapter 5). The second contamination event resulted from the interaction of the GNPA magma with the local footwall country rocks at the time of emplacement. This event did not introduce additional S into the system and thus had no control over genesis of PGE mineralization within the GNPA member.

## **7.2 Implications for our understanding of the northern limb**

### **7.2.1 Formation of the GNPA member**

Within the northern limb of the Bushveld Complex, the Rustenburg Layered Suite has been disturbed by several phases of faulting, all of which are thought to post-date emplacement and consolidation of the intrusion (Truter 1947; van Rooyen 1954; de Villiers 1967; van der Merwe 1978; Hulbert 1983). Although the relationship between the Platreef and GNPA member is masked by the NE trending Ysterberg-Planknek Fault, which marks the final episode of faulting within the southern sector of the limb, they are considered by many, primarily on the basis that they lie at the equivalent stratigraphic position (Fig. 7.1), to represent parts of the same succession (McDonald et al. 2005; Maier et al. 2008; van der Merwe 2008; Grobler et al. 2012).

On the basis of several key observations that are presented and/or discussed in the foregoing chapters it is envisaged that the GNPA member formed simultaneous to and in an analogous manner to the Platreef as is illustrated in Figure 7.1. Evidence supporting this include firstly that the parental magma (s) to the GNPA member were analogous in composition to those which crystallized to form the Platreef, as noted in Chapter 6 (Fig. 7.1). Secondly, both deposits reveal similar constraints on the timing of emplacement and enrichment in PGE relative to intrusion of Lower and Main Zone magmas (Figure 7.1), as indicated by field relations (Chapter 3; Chapter 4; Hulbert 1983; Holwell et al. 2005; Holwell and Jordaan 2006), and the S isotope composition and S/Se ratio of the initial

sulfide liquid (Chapter 5; Ihlenfeld and Keays 2011; McDonald and Holwell 2007; 2009; 2011). From these observations it can be inferred that both the Platreef and GNPA parental magmas were emplaced saturated in S (Chapter 5) onto consolidated Lower Zone cumulates (van der Merwe 1978; Kinnaird et al. 2005) and were significantly cooled prior to intrusion of Main Zone magma, which throughout the northern limb was emplaced as a fertile magma with a separate PGE budget to the underlying PGE-Ni-Cu sulfide deposits (Holwell and Jordaan 2006; Maier and Barnes 2010; McDonald and Harmer 2011; Lombard 2012; Kinnaird et al. 2012; Holwell et al. 2013).

The many findings of this study, which are summarised in section 7.1, can be used to generate an outline model for the formation of the GNPA member and its relationship with the adjacent Platreef. A schematic summary of the proposed multi-stage model is provided in Figure 7.1 and is discussed in detail in the following section.

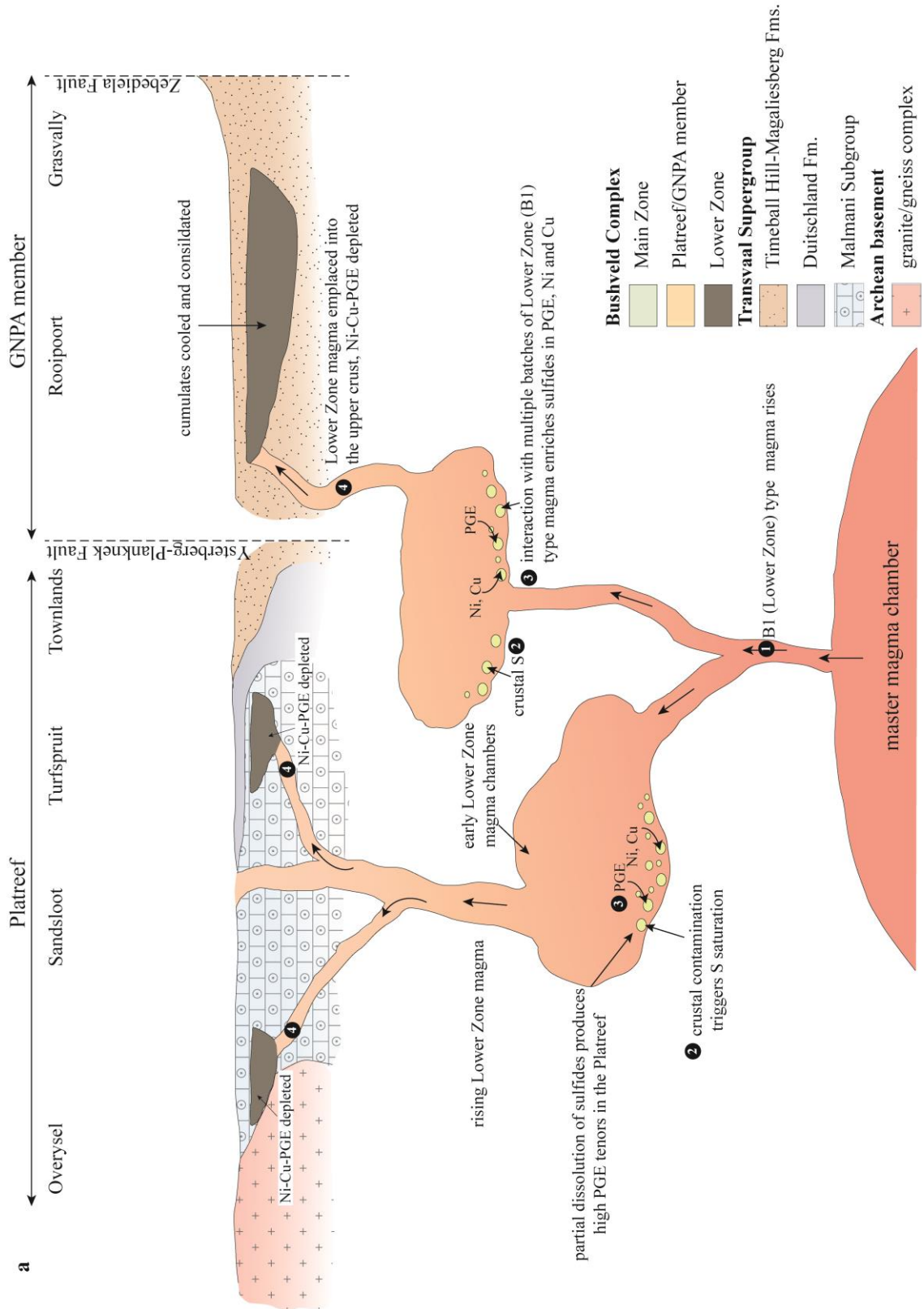


**Figure 7.1a** Genetic model looking east, for the intrusion and mineralization in the GNPA member relative to the Platreef. Sulfide immiscibility occurs in an intermediate staging chamber. The passage of Lower Zone magma over sulfides may have contributed to enrichment of sulfides in PGE

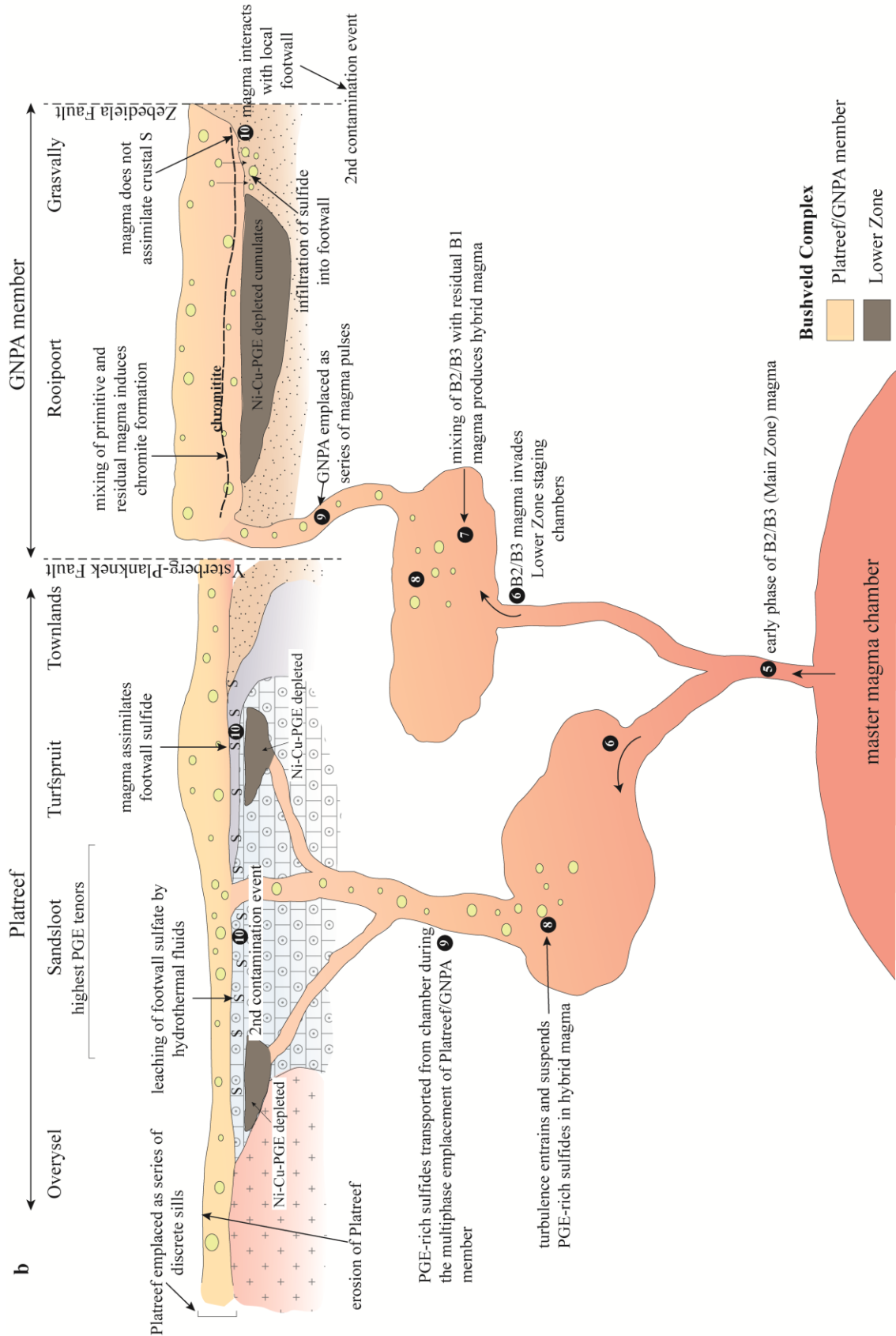


**Figure 7.1b** An early phase of Main Zone type magma invades the established chamber system. Mixing of magma produces a ‘hybrid’ composition which entrains PGE-rich sulfides and is intruded as a series of sills into the Transvaal Supergroup to form the GNPA member. During emplacement magma interacts with the local footwall.

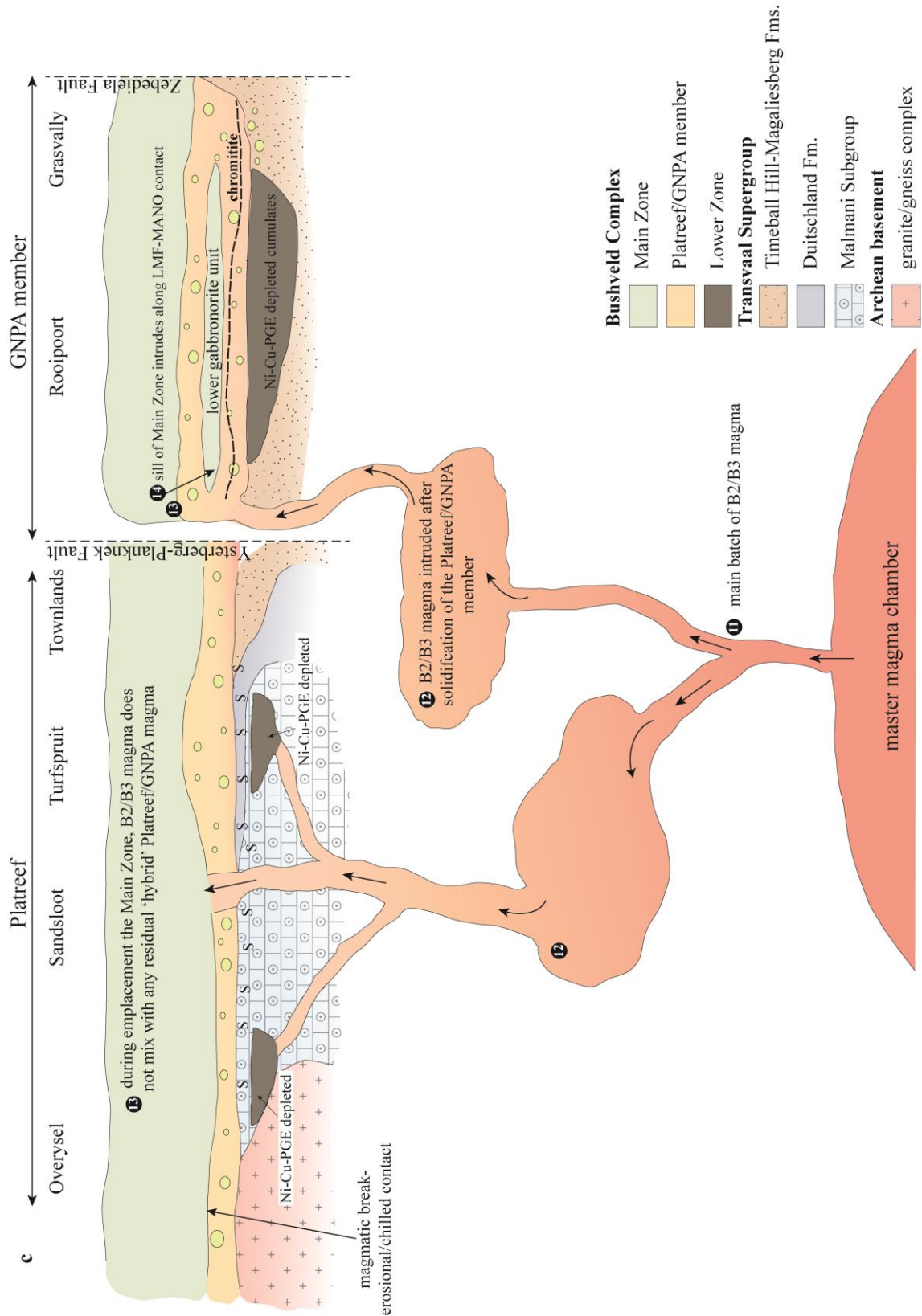


**Figure 7.1c** Intrusion of the bulk of the Main Zone magma occurs after solidification of the GNPA member and Platreef. The Main Zone magma chills against, partially erodes the Platreef and intrudes into the GNPA member.

### 7.2.2 Ore genesis

It has been demonstrated throughout the preceding chapters that mineralogical, geochemical and isotopic observations are inconsistent with any model which invokes the development of a sulfide liquid during or post-emplacement through either *in situ* contamination or depletion of an overlying magma column (e.g. Main Zone). Rather the findings of this thesis are more consistent with a model similar to that envisaged for the Platreef where PGE-rich sulfides were formed at depth in a conduit system prior to emplacement (Fig. 7.1; Lee 1996; McDonald and Holwell 2007; 2011), in response to the assimilation of crustal S (Chapter 5 and 6).

The proposed model can be summarised as follows:

1. At depth in a staging chamber, magma passing through (possibly of Lower Zone (B1) composition) assimilates S-bearing and LILE enriched country rocks (Chapter 5; stages 1 and 2 Fig. 7.1a). Crustal S is likely derived from shales and carbonates of the Duitschland Formation and possibly other units of the Transvaal Supergroup. The contaminant is well homogenised with the magma, inducing sulfide saturation and development of an immiscible sulfide liquid (stage 2). Although the strong crustal component was initially evident in both the  $\delta^{34}\text{S}$  signature ( $>+2.4\text{‰}$  up to  $+7\text{‰}$ ) and S/Se ratio ( $>4000$ ) of the initial sulfide liquid it is now preserved only within the S isotope composition of primary and secondary sulfides.
2. Sulfide droplets become enriched in PGE, Ni, Cu and semi-metals through interaction and processing of pre-GNPA magma (s) (Fig. 7.1a stage 3). It is possible that like the Platreef, the GNPA member sourced its PGE content from the B1 type magma which was intruded to form the Lower Zone (McDonald and Holwell 2007; McDonald et al. 2009; McDonald and Holwell 2011).
3. An early pulse of new magma (B2/B3 in composition) invades previously established staging chambers, mixing with residual Lower Zone (B1) to produce magma of a hybrid composition (Fig. 7.1b. stages 5-7). This represents the parental magma to the GNPA member and possibly the Platreef. The hybrid magma then entrained and transported the PGE-rich sulfides being intruded into the Transvaal Supergroup to form the GNPA member (Fig. 7.1b. stages 8-9).
4. Multiple influxes of hybrid magma intruded into the Transvaal Supergroup to form the GNPA member. The addition of compositionally similar magma is represented by the appearance of cumulus chromite and plagioclase, which is attributed to the *in situ* mixing of new and residual fractionated magmas (Fig. 7.1b). Since our

observations imply: (i) that the chromitite layers formed *in situ*; and (ii) crystallization of chromite effectively concentrated Pt, Os, Ir, Ru and Rh, it is believed that the parental magmas (s) had not been fully depleted of their PGE contents at depth by the sulfide liquid, prior to the formation of chromite.

5. During emplacement the magma interacts with the local footwall quartzites. In contrast to the Platreef at Turfspruit and Sandsloot, this second contamination event did not introduce additional crustal S into the system (Fig. 7.1b stage 10), with primary sulfides retaining their initial crustal  $\delta^{34}\text{S}$  signature. This event therefore had no control over ore genesis within the GNPA member.
6. Subsequent to emplacement hydrothermal fluids, possibly derived from xenoliths of calc-silicates within the GNPA member (Chapter 4), altered much of the primary sulfide and PGE mineralogy (Chapter 3 and 4). This low temperature alteration (<250°C) resulted in: (i) S-loss, lowering the S/Se ratio to below the mantle range (Table 5.1 and 5.2); (ii)  $\delta^{34}\text{S}$  to fractionate by +1.58‰ during pyrite formation (Ohmoto and Rye 1979; Chapter 5; Fig. 5.3); (iii) the decoupling and remobilization of Pd, Au and to a lesser extent Cu from sulfides on a centimetre to decimetre scale (Chapter 4; Fig. 4.5); and (iv) the alteration of sulfide margins by tremolite, actinolite, chlorite and talc (Chapter 3).
7. Following the emplacement of the GNPA member and the Platreef a significant period of crystallization and cooling occurred (Fig. 7.1b).
8. The rest of the B2/B3 (Main Zone) magma was then intruded as a PGE fertile magma (Fig. 7.1c stages 11-13). This magma exploited the contact between the Lower Mafic and Mottled Anorthosite units to produce a sill of Main Zone, represented by the Lower Gabbro unit (Fig. 7.1c stage 14).

Whilst the GNPA member and Platreef are geochemically analogous (Chapter 6), believed to be derived from compositionally similar/related magmas (Fig. 7.1), noticeable variations in the PGE tenor of sulfides are observed north and south of the Ysterberg-Planknek Fault. Sulfides within the central sector of the Platreef are believed to have acquired their very high PGE tenors and low S/Se ratios (<2500) at depth by the process ‘multistage-dissolution upgrading’ (Kerr and Leitch 2005; McDonald and Holwell 2007, 2011; McDonald et al. 2012; Jones 2013; see also Chapter 5 section 5.2). During this process sulfide is partially dissolved through interacting with multiple batches of S-undersaturated magma at relatively low R-factors within a conduit setting, which effectively upgrades the metal contents of elements with high partition coefficients such as PGE and Se (Kerr and

Leitch 2005). In the case of the Platreef, upgrading of a sulfides PGE content is also accompanied by a reduction in  $\delta^{34}\text{S}$  via S isotope exchange between an initially crustal contaminated sulfide liquid and mantle S (Ripley and Li 2003; Ihlenfeld and Keays 2011). The entire Platreef however is not characterised by such high PGE tenors, with a recent study by Jones (2013) proposing sulfide inclusions characterised by low PGE tenors and high S/Se ratios within the Platreef were derived from a staging chamber which had undergone fewer cycles of enrichment and dissolution to that which supplied the high PGE tenor sulfides to the central sector. This interpretation in conjunction with the low PGE tenors, high S/Se ratios and crustal  $\delta^{34}\text{S}$  signatures typical of primary sulfides within the GNPA member favours a model which envisages that the parental magmas and PGE rich-sulfides of the GNPA member and Platreef were supplied from a complex network of chambers and conduits, as is alluded to in Figure 7.1, where ore forming processes differed significantly within the conduit system. Alternatively, significant variations in PGE tenor between and within the Platreef and GNPA member may also be attributed to different mixing proportions of an early PGE enriched sulfide liquid with later batches of magma carrying low PGE tenor sulfide droplets (Jones 2013). If this is accepted then it is possible that both deposits were derived from a common conduit such as that presented within McDonald and Holwell (2007) conceptual model.

### **7.2.3 Relationship of the GNPA member with the Platreef**

Although it has been demonstrated that the GNPA member and Platreef formed concurrently from compositionally similar/related magma, due to faulting within the region, the lateral relationship between the GNPA member and Platreef still remains unclear. At present, there are two plausible competing theories (discussed below), which will remain possibilities until our understanding of how these deposits exist at depth (seismic data and deep drilling downdip from the Platreef; McDonald and Holwell 2011) and the structural setting of the northern limb is improved (see section 7.4). Considering the findings of this thesis, the constraints placed on ore genesis of the GNPA member and associated mineralization (summarised in section 7.2.2), are consistent with a model which envisages the GNPA member and Platreef to be emplaced as two discrete intrusions derived from separate staging chambers as is illustrated schematically in Figure 7.1. Such a model may suggest that the GNPA member and Platreef do not merge laterally which opposes with a number of previous studies (McDonald et al. 2005; Maier et al. 2008 van der Merwe 2008).

This notion however, that the GNPA member and Platreef do not represent part of the same intrusion is inconsistent with the recent discovery, from deep drilling programs on Turfspruit and Sandsloot, that at depth the Platreef changes from steeply west-dipping to flat-lying, with the latter referred to as the Flatreef (Fig. 7.2; Myeni and Muzondo 2011; Grobler et al. 2012). Detailed logging carried out by Ivanplats has led to the recent discovery that a Merensky Reef-like cyclic unit (referred to as the Turfspruit cyclic unit; Fig. 7.2) is developed throughout Turfspruit, with a corresponding UG2-like cyclic unit observed at depth within the Flatreef, where the deposit is underlain by Lower Zone cumulates (Fig. 7.2; Dunnett et al. 2012; Grobler et al. 2012). Identification of these cyclic units provides the first convincing stratigraphic correlations between the Platreef/GNPA member with the Upper Critical Zone of the eastern and western limbs. At present the exact relationship of the GNPA member/Platreef with the Upper Critical Zone does however remain speculative, since important differences in the composition of parental magmas (Chapter 6; McDonald et al. 2005) and the relationship with the overlying Main Zone (Holwell et al. 2005; Seabrook 2005; Holwell and Jordaan 2006) are currently unexplained and poorly understood. Regardless of these disparities, the presence of Upper Critical zone equivalent units within the Platreef at depth is consistent with the ‘pudding basin’ model (Fig. 7.3a) proposed by Naldrett et al. (2008), where the Platreef is considered to represent sulfide-rich magma which escaped up the margins of the northern limb chamber, being exposed/preserved only in this limb due to lower levels of erosion (Fig. 7.3a).

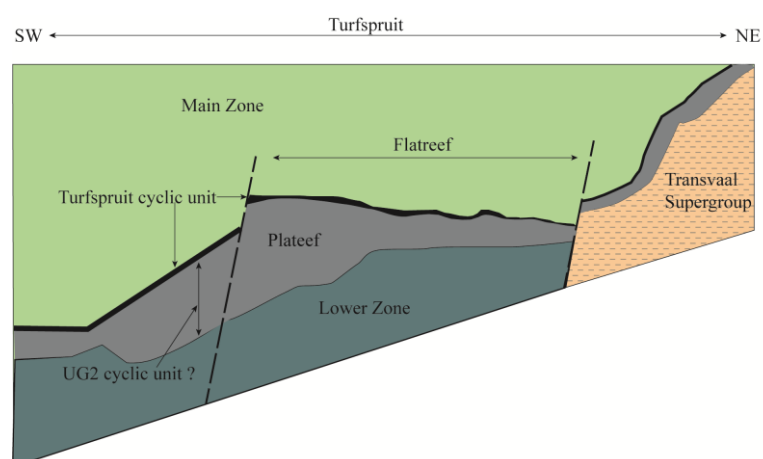


**Figure 7.2** Cross sectional view of the Platreef on Turfspruit (modified from Grobler et al. 2012).

If such a model is accepted then it is predicted that downdip the Platreef will progressively transform towards the centre of the limb, into a layered succession that resembles a UG2-Merensky sequence. Since such a sequence is known to occur at depth (Fig. 7.2; Dunn et al. 2012; Grobler et al. 2012), it could be proposed that the layered GNPA member, which has previously been regarded as an Upper Critical Zone equivalent (Hulbert 1983; van der Merwe 1978; Maier et al. 2008; van der Merwe 2008), may be representative of the Platreef at depth (Fig. 7.3b). Consequently as is illustrated in Figure 7.3b the Platreef would be viewed as a marginal facies of the GNPA member. Due to the lack of deep drilling and seismic data, it is however not yet clear whether the GNPA member is developed downdip into a more complete Critical Zone sequence as is observed in the eastern and western limbs (Fig. 7.3a).

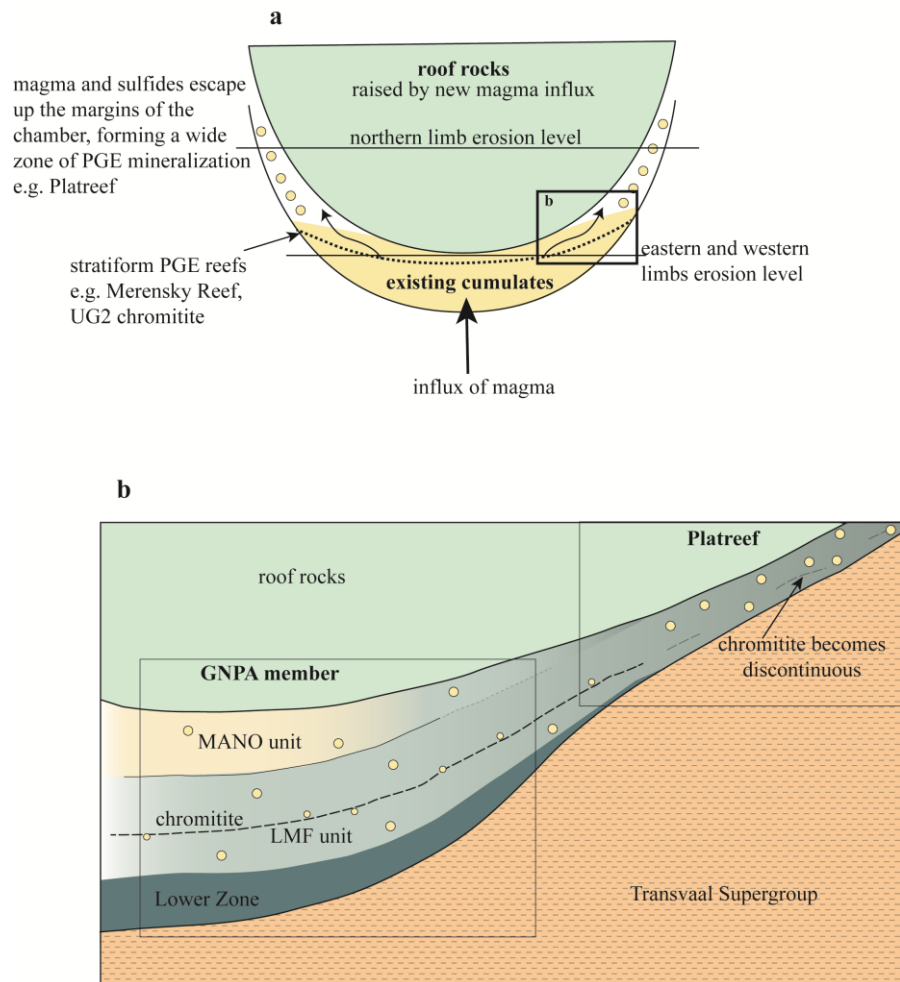


**Figure 7.3** a) 'Pudding basin' model after Naldrett et al. (2008) showing the concept of nested pudding bowls to represent the floor and roof of the Bushveld chamber. New injections of magma raise the roof and/or squeeze up along the margins. Contrasting levels of erosion determine whether the marginal deposits are exposed. b) the proposed relationship between the Platreef and GNPA member, where the former progressively transforms with depth into a thicker layered succession, which is underlain by Lower Zone cumulates and contains laterally continuous chromitites.

If it is accepted that the Platreef transforms with depth into a layered succession characteristic of the GNPA member, which is supported by the many geochemical similarities discussed in Chapter 6, then exposure of the GNPA member south of the Ysterberg-Planknek Fault may be attributed to post-emplacement faulting and the subsequent erosion of the Platreef thus appearing absent in the Grasvally-Rooipoort sector of the limb. This suggestion however remains unproven due to the lack of any real constraints on the timing and direction of movement on the Ysterberg-Planknek Fault.

### **7.3 Summary**

Through adopting a multi-disciplinary approach this thesis investigates in detail the nature and origin of PGE mineralization within the GNPA member, which has implications not only for our understanding of the magmatic history of the northern limb (GNPA member and Platreef) but also for the relationship of the Platreef/GNPA member with the Upper Critical Zone of the eastern and western limbs of the Bushveld Complex. Overall it has been demonstrated within the foregoing chapters that magmatic, contamination and hydrothermal processes all played important roles in the development of the GNPA member and associated base metal sulfide and PGE mineralization. To summarise, the main conclusions of this study are:

- Parental magmas of the GNPA member were of a 'hybrid' composition containing B1 and B2/B3 magma components which were strongly crustally contaminated and S saturated at the time of emplacement.
- The assimilation of S-bearing country rocks at depth was critical for ore genesis. Interaction with the local (Magaliesberg Quartzite Formation) did not introduce additional S into the magmatic system.
- A single sulfide liquid enriched in PGE, Ni, Cu and semi-metals was distributed throughout the succession during multiphase emplacement of the GNPA member.
- The distribution and mineralogy of platinum-group and chalcophile elements results from the complex behaviour of these elements during sulfide fractionation and hydrothermal processes.

- The GNPA member and the Platreef crystallized from compositionally similar magmas which experienced different degrees of PGE enrichment. These were possibly supplied from a complex network of chambers and conduits.
- It is possible that the Platreef progressively transforms with depth into the GNPA member and presents sulfide-rich magma which escaped up the margins of the northern limb chamber.

#### 7.4 Recommendations for future work

- Although hydrothermal fluids have partially controlled the distribution and mineralogy of base metal sulfide and PGE mineralization throughout the GNPA member, the source (s) of these fluids have not been explored in any detail. Whilst possible origins of these fluids was speculated in Chapter 4 (section 4.9.2), a detailed fluid inclusion study integrated with O and H isotope studies could provide insight into the composition of the fluids and also may elucidate potential fluid sources (s).
- Since Chapter 5 is one of the few studies which investigates the utility of S isotopes and S/Se ratios as indicators of the initial source of S a more widespread study, possibly incorporating different magmatic Ni-Cu-PGE sulfide deposit types, is required to fully appreciate their ability to be used independently with confidence when considering the role of crustal contamination in triggering S saturation. In addition, if such a study also included *in situ* analyses of Se (by LA-ICP-MS), then it would be possible to constrain further all the factors which control the behaviour of Se during sulfide fractionation and hydrothermal processes. If this was then combined with experimental studies into the partition coefficients of Se, the capability of *in situ* S/Se ratios of sulfides as tracers of S would be able to be assessed fully.
- Whilst this thesis attempts to place constraints on the relationship of the northern limb with the rest of the Bushveld Complex, one of the outstanding questions regarding the formation of the Platreef, GNPA member and Upper Critical Zone is whether they were derived from a common magma. As long as this question remains, key geochemical differences highlighted by McDonald et al. (2005) and McDonald and Holwell (2011) between the northern limb deposits and the Upper

Critical Zone (e.g. Pt/Pd ratio, Mg#, Cr/MgO and Ce/Sm ratios, timing of intrusion of Main Zone relative to solidification of underlying cumulates, style of mineralization) will continue to be unexplained and poorly understood. Consequently, models attempting to account for at least some of these differences (e.g. the ‘pudding basin’ model proposed by Naldrett et al. (2008)) will remain speculative and unproven.

- A structural study focussing on the timing, movement and displacement of faults within the northern limb, especially that of the Ysterberg-Planknek Fault (which masks the field relationship between the Platreef and GNPA member) could provide a more detailed understanding of the lateral relationship between the GNPA member and the Platreef, and thus provide confirmation that, as proposed in this thesis, the Platreef represents a marginal facies of the GNPA member. A regional study on fault movement within the northern limb could also provide constraints on: the location of feeders; whether certain phases of faulting facilitated or prevented magma movement; and the control these structures had on the magmatic stratigraphy of the Platreef and GNPA member. From answering these one might gain an understanding of key lithological differences between the Platreef and the GNPA member (e.g. the absence of plagioclase-rich cumulates north of the Ysterberg-Planknek Fault).

# References

- Arcuri T, Ripley EM, Hauck SA (1998) Sulfur and oxygen isotope studies of the interaction between pelitic xenoliths and basaltic magma at the Babbitt and Serpentine Cu-Ni deposits, Duluth Complex, Minnesota. *Economic Geology* 93:1063–1075.
- Armitage PEB (2011) Development of the Platreef in the northern limb of the Bushveld Complex at Sandsloot, Mokopane District, South Africa. PhD thesis, University of Greenwich.
- Armitage PEB, McDonald I, Edwards SJ, Manby CM (2002) Platinum-group element mineralization in the Platreef and calc-silicate footwall at Sandsloot, Potgietersrus district, South Africa. *Applied Earth Science (Transactions of the Institute of Mining and Metallurgy B)* 111:B36–B45.
- Armitage PEB, McDonald I, Tredoux M (2007) A geological investigation of the Waterberg hydrothermal platinum deposit, Mookgophong, Limpopo Province, South Africa. *Applied Earth Science (Transactions of the Institute of Mining and Metallurgy B)* 116:B113–129.
- Arndt NT, Leshar CM, Czamanske GK (2005) Mantle-Derived Magmas and Magmatic Ni-Cu-(PGE) Deposits. *Economic Geology 100th Anniversary Volume* pp. 5–23.
- Ashwall LD, Webb SJ, Knopper MW (2005) Magmatic stratigraphy in the Bushveld Northern Lobe: continuous geophysical and mineralogical data from the 2950 m Bellevue drillcore. *South African Journal of Geology* 108:199–232.
- Ballhaus C, Ryan CG (1995) Platinum-group elements in the Merensky Reef. I. PGE in solid solution in base metal sulfides and the down-temperature equilibration history of Merensky ores. *Contribution to Mineralogy and Petrology* 122:241–251.
- Ballhaus CG, Stumpfl EF (1986) Sulfide and platinum mineralization in the Merensky Reef: evidence from hydrous silicates and fluid inclusions. *Contributions to Mineralogy and Petrology* 94:193–204.
- Ballhaus C, Sylvester P (2000) Noble metal enrichment processes in the Merensky Reef, Bushveld Complex. *Journal of Petrology* 41:545–561.

- 
- Ballhaus C, Tredoux M, Spath A (2001) Phase relations in the Fe–Ni–Cu–PGE–S system at magmatic temperature and application to massive sulphide ores of the Sudbury Igneous Complex. *Journal of Petrology* 42:1911–1926.
- Barkov AY, Halkoaho TAA, Laajoki KVO, Alapieti TT, Peura RA (1997) Ruthenian pyrite and nickeloan malanite from the Imandra layered complex, northwestern Russia. *Canadian Mineralogist* 35:887–897.
- Barnes S J (1986) The effect of trapped liquid crystallization on cumulus mineral compositions in layered intrusions. *Contributions to Mineralogy and Petrology* 93:524–531.
- Barnes S-J, Maier WD (2002a) Platinum-group element distributions in the Rustenburg Layered Suite of the Bushveld Complex, South Africa. *Canadian Institute of Mining, Metallurgy and Petroleum Special Volume* 54:553–580.
- Barnes S-J, Maier WD (2002b), Platinum-group elements and microstructures of normal Merensky Reef from Impala Platinum Mines, Bushveld Complex. *Journal of Petrology* 43:103–128.
- Barnes S-J, Lightfoot PC (2005) Formation of magmatic nickel-sulfide ore deposits and processes affecting their copper and platinum-group element contents. In: Hedenquist JW, Thompson, JFH, Goldfarb RJ, Richards JP (eds.) *Economic Geology 100<sup>th</sup> Anniversary Volume* 179–213.
- Barnes S-J, Acterberg E, Makovicky E, Li C (2001) Proton probe results for partitioning of platinum-group elements between monosulphide solid solution and sulphide liquid. *South African Journal of Geology* 104:275–286.
- Barnes S-J, Cox RA, Zeintek ML (2006) Platinum-group element, gold, silver and base metal distribution in compositionally zoned sulfide droplets from the Medvezky Creek Mine, Noril'sk, Russia. *Contribution to Mineralogy and Petrology* 152:187–200.
- Barnes S-J, Makovicky E, Makovicky M, Rose Hansen J, Karup Moller S (1997) Partition coefficients for Ni, Cu, Pd, Pt, Rh and Ir between monosulfide solid solution and sulfide liquid and the formation of compositionally zoned Ni–Cu sulfide bodies by
-

- 
- fractional crystallization of a sulfide liquid. *Canadian Journal of Earth Science* 34:366–374.
- Barnes S-J, Savard D, Bédard P, Maier WD (2009) Selenium and sulfur concentrations in the Bushveld Complex of South Africa and implications for formation of the platinum-group element deposits. *Mineralium Deposita* 44:647–663.
- Bekker A, Kaufman AJ, Karhu JA, Beukes NJ, Swart QD, Coetzee LL, Eriksson KA (2001) Chemostratigraphy of the Paleoproterozoic Duitschland Formation, South Africa: Implications for coupled climate change and carbon cycling. *American Journal of Science* 30:261–285.
- Bekker A, Holland HD, Wang P-L, Rumble III D, Stein HJ, Hannah JL, Coetzee LL, Beukes NJ (2004) Dating the rise of atmospheric oxygen. *Nature* 427:117–120.
- Boudreau AE, McCallum IS (1992) Concentration of Platinum-Group elements by Magmatic Fluids in Layered Intrusions. *Economic Geology* 87:1830–1848.
- Boudreau AE, Meurer WP (1999) Chromatographic separation of the platinum-group elements, gold, base metals and sulfur during degassing of a compacting and solidifying crystal pile. *Contributions to Mineralogy and Petrology* 134:174–185.
- Buick IS, Maas R, Gibson R (2001) Precise U–Pb titanite age constraints on the emplacement of the Bushveld Complex, South Africa. *Journal of the Geological Society* 158:3–6.
- Buchanan DL, Nolan J (1979) Solubility of sulfur and sulfide immiscibility in synthetic tholeiitic melts and their relevance to Bushveld Complex rocks. *Canadian Mineralogist* 17:483–494.
- Buchanan DL, Nolan J, Suddaby P, Rouse JE, Viljoen MJ, Davenport JWJ (1981) the genesis of sulfide mineralization in a portion of the Potgietersrus Limb of the Bushveld Complex. *Economic Geology* 76:568–579.
- Buchanan PC, Reimold WU, Koeberl C, Kruger FJ (2002) Geochemistry of intermediate to siliceous volcanic rocks of the Rooiberg Group Bushveld Magmatic Province South Africa. *Contributions to Mineralogy and Petrology* 144:131–143.
-

- 
- Butler J (2011) *Platinum 2011*, Johnson Matthey, Royston.
- Cabri LJ, Laflamme JHG (1976) The mineralogy of the platinum-group elements from some copper-nickel deposits of the Sudbury area, Ontario. *Economic Geology* 71:1159–1195.
- Cabri LJ, Bank H, El Goresy A, Laflamme JHG, Nobiling R, Sizgoric MB, Traxel K (1984) Quantitative trace-element analyses of sulfides from Sudbury and Stillwater by proton microprobe. *The Canadian Mineralogist* 22:521–542.
- Cabri LJ, Choi Y, Nelson M, Tubrett M, Sylvester PJ (2010) Advances in precious metal trace element analyses for deportment using LAM-ICP-MS. In: *Proceedings of the 42<sup>nd</sup> Annual Canadian Mineral Processors Conference*, pp 181–196.
- Cabri, LJ, McDonald AM, Stanley CJ, Rudashevsky NS, Poirier G, Durham BR, Mungall JE, Rudashevsky VN (2005) Naldrettite, Pd<sub>2</sub>Sb, a new palladium antimonide from the Mesamax Northwest deposit, Ungava region, Québec, Canada. *Mineralogical Magazine* 69: 89–97.
- Cabri LJ, Rudashevsky NS, Rudashevsky VN (2008) Current approaches for the process mineralogy of platinum-group element ores and tailings. In: *Ninth international congress for Applied Mineralogy ICAM 2008*. The Australasian Institute of Mining and Metallurgy, publication series no 8/2008, pp 9–17.
- Cabri LJ, Wilson JMD, Distler VV, Kingston D, Nejedly Z, Sluzheniken SF (2002) Mineralogical distribution of trace platinum-group elements in the disseminated sulphide ores of Norilsk 1 layered intrusion. *Transactions of the Institute of Mining and Metallurgy B (Australasian Institute of Mining and Metallurgy Proceedings)*, *Applied Earth Science* 111:B15–B22.
- Cameron EN (1977) Chromite in the central sector of the eastern Bushveld Complex, South Africa. *American Mineralogist* 62:1082–1096.
- Cameron EN (1982) The Upper Critical Zone of the Eastern Bushveld Complex—Precursor of the Merensky Reef. *Economic Geology* 77:1307–1327.
- Cameron EM (1982) Sulphate and sulphate reduction in early Precambrian oceans. *Nature* 296:145–148.
-

- Campbell IH, Naldrett AJ, Barnes SJ (1983) A model for the origin of the platinum-rich sulfide horizons in the Bushveld and Stillwater Complexes. *Journal of Petrology* 24:133–165.
- Cawthorn RG (1996) Re-evaluation of magma compositions and processes in the uppermost Critical Zone of the Bushveld Complex. *Mineralogical Magazine*, 60:131–148.
- Cawthorn RG (1999) Platinum-group element mineralization in the Bushveld Complex--a critical reassessment of geochemical models. *South African Journal of Geology* 102:268–281.
- Cawthorn RG (2005) Pressure fluctuations and formation of the PGE-rich Merensky and chromitite reefs, Bushveld Complex. *Mineralium Deposita* 40:231–235
- Cawthorn RG, Meyer FM (1993) Petrochemistry of the Okiep copper district basic intrusive bodies, northwestern Cape province, South Africa. *Economic Geology* 88:590–605.
- Cawthorn RG, Walraven F (1998) Emplacement and crystallization time for the Bushveld Complex. *Journal of Petrology* 39:1669–1687.
- Cawthorn RG, Barton JM, Viljoen MJ (1985) Interaction of floor rocks with the Platreef on Overysel, Potgietersrus, northern Transvaal. *Economic Geology* 80:988–1006.
- Cawthorn RG, Davies G, Clubley-Armstrong A, McCarthy TS (1981) Sills associated with the Bushveld Complex. *Lithos* 14:1–15.
- Cawthorn RG, Meyer PS, Kruger FJ (1991) Major addition of magma at the Pyroxenite Marker in the western Bushveld Complex, South Africa. *Journal of Petrology* 32:739–763.
- Cawthorn RG, Merkle RKW, Viljoen MJ (2002) Platinum-group elements in the Bushveld Complex. *Canadian Institute of Mining, Metallurgy and Petroleum Special volume* 54:389–430.

- 
- Cawthorn RG, Sander BK, Jones IM (1992) Evidence for the trapped liquid shift effect in the Mount Ayliff Intrusion, South Africa. *Contributions to Mineralogy and Petrology* 111:194–202.
- Cawthorn RG, Webb SJ (2001) Connectivity between the western and eastern limbs of the Bushveld Complex. *Tectonophysics* 330:195–209.
- Chambers LA, Trudinger PA (1979) Microbiological fractionation of stable sulfur isotopes: A review and critique. *Journal of Geomicrobiology* 1:249–293.
- Cousins CA (1959) The structure of the mafic portion of the Bushveld Igneous Complex. *Transactions of the Geological Society of South Africa* 62:174–189.
- Cousins CA, Feringa G, (1964) The chromite deposits of the western belt of the Bushveld Complex. *The geology of some ore deposits in Southern Africa* 2:183–202.
- Craig JR (1983) Pyrite-Pentlandite Assemblages and Other Low Temperature relations in the Fe–Ni–S System. *American Journal of Science* 283-A:496–510.
- Curl EA (2001) Parental magmas of the Bushveld Complex, South Africa. PhD thesis, Department of Earth Sciences, Monash University, Australia pp. 140.
- Czamanske GK, Kunilov VE, Zientek ML, Cabri LJ, Likhachev AP, Calk LC, Oscarson RL (1992) A proton-microprobe study of magmatic sulfide ores from the Noril'sk-Talnakh district, Siberia. *The Canadian Mineralogist* 30:249–287.
- Dare SAS, Barnes S-J, Prichard HM, Fisher PC (2011) Chalcophile and platinum-group element (PGE) concentrations in the sulfide minerals from the McCreedy East deposit, Sudbury, Canada, and the origin of PGE in pyrite. *Mineralium Deposita* 46:381–407.
- Dare SA, Barnes SJ, Prichard HM, Fisher PC (2014) Mineralogy and Geochemistry of Cu-Rich Ores from the McCreedy East Ni-Cu-PGE Deposit (Sudbury, Canada): Implications for the Behaviour of Platinum Group and Chalcophile Elements at the End of Crystallization of a Sulfide Liquid. *Economic Geology* 109:343–366.
- de Klerk L (2005) Bushveld Stratigraphy on Rooipoort, Potgietersrus Limb [abs.]. Platreef Workshop, 2<sup>nd</sup>, Mokopane, South Africa, 28<sup>th</sup> – 30<sup>th</sup> October 2005, Abstracts.
-

- 
- de Villiers (1967) The geology of the area south of Potgietersrus, with special reference to the chromite deposits. Ph.D. thesis, University of the Witwatersrand, pp. 124.
- Djon MLN, Barnes S-J (2012) Changes in sulphides and platinum-group minerals with the degree of alteration in the Roby, Twilight, and High Grade Zones of the Lac des Iles Complex, Ontario, Canada. *Mineralium Deposita* 47:875–896.
- Dunnett T, Grobler DF, Simmonotti NMEM, Mapeka JM (2012) Lithological variations within Upper Critical Zone stratigraphy, Turfspruit 241KR, northern limb, Bushveld Complex [abs.]. Platreef Workshop, 5th, Mokopane, South Africa, 9<sup>th</sup> – 11<sup>th</sup> November 2012, Abstracts.
- Eales HV, Cawthorn RG (1996) The Bushveld Complex. In: Cawthorn RG, (ed) *Layered Intrusions*. Elsevier Science, pp 181–230.
- Eales HV, de Klerk WJ, Teigler B (1990) Evidence for magma mixing processes within the Critical and Lower Zones of the Northwestern Bushveld Complex, South Africa. *Chemical Geology* 88:261–278.
- Eckstrand OR, Cogolu E (1986) Se/S evidence relating to genesis of sulphides in the Crystal Lake gabbro, Thunder Bay, Ontario. Geological Association of Canada – Abstract Program 11, 66.
- Eckstrand OR, Grinenko LN, Krouse HR, Paktunc AD, Schwann PL, Scoates RF (1989) Preliminary data on sulphur isotopes and Se/S ratios, and the source of sulphur in magmatic sulphides from the Foz River Sill, Molson Dykes and Thompson nickel deposits, northern Manitoba. *Current Research, Part C. Geological Survey of Canada Paper* 235–242.
- Eckstrand OR, Hulbert LJ (1987) Selenium and the source of sulfur in magmatic nickel and platinum deposits (abs): Geological Association of Canada–Mineralogical Association Canada Program with Abstracts 12:40.
- Ewers GR (1977) Experimental hot water-rock interactions and their significance to natural hydrothermal systems in New Zealand. *Geochimica et Cosmochimica Acta* 41:143–150.

- 
- Fleet ME, Chryssoulis SL, Stone WE, Weisener CG (1993) Partitioning of platinum-group elements and Au in the Fe–Ni–Cu–S system: experiments on the fractional crystallization of sulfide melt. *Contribution to Mineralogy and Petrology* 115:36–44.
- Gervilla F, Kojonen K (2002) The platinum-group minerals in the upper section of the Keivitsansarvi Ni–Cu–PGE deposit, northern Finland. *Canadian Mineralogist* 40:377–394.
- Godel B, Barnes S-J, Maier WM (2007) Platinum-group elements in sulfide minerals, platinum-group minerals, and whole-rocks of the Merensky Reef (Bushveld Complex, South Africa) Implications for the formation of the reef. *Journal of Petrology* 48:1569–1604.
- Good N, de Wit MJ (1997) The Thabazimbi-Murchison lineament of the Kaapvaal craton, South Africa: 2700 Ma of episodic deformation. *Journal of the Geological Society* 154:93–97.
- Grinenko LI (1985) Sources of sulfur of the nickeliferous and barren gabbro-dolerite intrusions of the northwest Siberian platform. *International Geology Review* 27:695–708.
- Grobler DF, Nielsen SA, Broughton DW (2012) Upper Critical Zone (Merensky Reef) correlates within the Platreef on Turfspruit 241KR, northern limb, Bushveld Complex [abs.]. Platreef Workshop, 5th, Mokopane, South Africa, 9<sup>th</sup> – 11<sup>th</sup> November 2012, Abstracts.
- Habicht K, Canfield DE (1997) Sulfur isotope fractionation during bacterial sulfate reduction in organic-rich sediments. *Geochimica et Cosmochimica Acta* 61:5351–5361.
- Hall AL (1932) The Bushveld Igneous Complex of the Central Transvaal. *Geological Society of South Africa Memoir* 28, pp. 544.
- Hannah JL, Bekker A, Stein HJ, Markey RJ, Holland HD (2004) Primitive Os and 2316 Ma age for marine shale: implications for Paleoproterozoic glacial events and the rise of atmospheric oxygen. *Earth and Planetary Science Letters* 225:43–52.
- Harmer RE, Sharpe M R (1985) Field relations and strontium isotope systematics of the marginal rocks of the Eastern Bushveld Complex. *Economic Geology* 80:813–837.
-

- 
- Harris C, Chaumba JB (2001) Crustal contamination and fluid-rock interaction during the formation of the Platreef, northern lobe of the Bushveld Complex, South Africa. *Journal of Petrology* 42:1321–1347.
- Hatton CJ, von Gruenewaldt G (1987) The geological setting and petrogenesis of the Bushveld chromitite layers. In Stow CW (ed) *Chromite deposits through time*. International Geological Congress, Washington 109–142.
- Hattori KH, Arai S, Clarke DB (2002) Selenium, tellurium, arsenic and antimony contents of primary mantle sulfides. *Canadian Mineralogist* 40:637–650.
- Haughton DR, Roeder PL, Skinner BJ (1974) The solubility of sulfur in mafic magmas. *Economic Geology* 69:451–462.
- Helmy HM, Ballhaus C, Berndt J, Bockrath C, Wohlgemuth-Ueberwasser C (2007) Formation of Pt, Pd and Ni tellurides; experiments in sulfide-telluride systems. *Contributions to Mineralogy and Petrology* 153:577–591.
- Helmy HM, Ballhaus C, Wohlgemuth-Ueberwasser C, Fonseca ROC, Laurenz V (2010) Partitioning of Se, As, Sb, Te and Bi between monosulfide solid solution and sulfide melt- Application to magmatic sulfide deposits. *Geochimica et Cosmochimica Acta* 74:6174–6179.
- Henderson P, Suddaby P (1971) The Nature and Origin of the Chrome-Spinel of the Rhum Layered Intrusion. *Contributions to Mineralogy and Petrology* 33:21–31.
- Hinchey JG, Hattori KH (2005) Magmatic mineralization and hydrothermal enrichment of the High Grade Zone at the Lac des Iles palladium mine, northern Ontario, Canada. *Mineralium Deposita* 40:13–23.
- Holwell DA (2006) The role of magmatism, contamination and hydrothermal processes in the development of Platreef mineralization, Bushveld Complex, South Africa. Unpublished Ph.D thesis, Wales, Cardiff University, p. 285.
- Holwell DA, Keays RR (2014) The Formation of Low-Volume, High-Tenor Magmatic PGE-Au Sulfide Mineralization in Closed Systems: Evidence from Precious and Base Metal Geochemistry of the Platinova Reef, Skaergaard Intrusion, East Greenland. *Economic Geology* 109:387–406.
-

- 
- Holwell DA, Jordaan A (2006) Three-dimensional mapping of the Platreef at the Zwartfontein South mine: implications for the timing of magmatic events in the northern limb of the Bushveld Complex, South Africa. *Applied Earth Science (Transactions of the Institute of Mining and Metallurgy B)* 115:B41–B48.
- Holwell DA, McDonald I (2006) Petrology, geochemistry and the mechanisms determining the distribution of platinum-group element and base metal sulfide mineralization in the Platreef at Overysel, northern Bushveld Complex, South Africa. *Mineralium Deposita* 41:575–598.
- Holwell DA, McDonald I (2007) Distributions of platinum-group elements in the Platreef at Overysel, northern Bushveld Complex: a combined PGM and LA-ICP-MS study. *Contributions to Mineralogy and Petrology* 154:171–190.
- Holwell DA, McDonald I (2010) A review of the behaviours of platinum-group elements within natural magmatic sulfide ore systems. *Platinum Metals Review* 54:26–36.
- Holwell DA, Abraham-James T, Keays RR, Boyce AJ (2012) The nature and genesis of marginal Cu–PGE–Au sulphide mineralisation in Paleogene Macrodykes of the Kangerlussuaq region, East Greenland. *Mineralium Deposita* 47:3–21.
- Holwell DA, Armitage PEB, McDonald I (2005) Observations on the relationship between the Platreef and its hangingwall. *Applied Earth Science (Transactions of the Institute of Mining and Metallurgy B)* 114:B225–B241.
- Holwell DA, Boyce AJ, McDonald I (2007) Sulfur isotope variations within the Platreef Ni–Cu–PGE deposit: Genetic Implications for the origin of sulfide mineralization. *Economic Geology* 102:1091–1110.
- Holwell DA, Jones A, Smith JW, Boyce AJ (2013) New mineralogical and isotopic constraints on Main Zone-hosted PGE mineralisation at Moorddrift, northern Bushveld Complex. *Mineralium Deposita* 48:675–686.
- Holwell DA, Keays RR, Firth EA, Findlay J (2014) Geochemistry and mineralogy of platinum-group element mineralization in the River Valley intrusion, Ontario, Canada: a model for early stage S saturation and multi-stage emplacement and the implications for ‘contact-type’ Ni–Cu–PGE mineralization. *Economic Geology* 109:689–712.
-

- Holwell DA, McDonald I, Armitage PEB (2006) Platinum-group mineral assemblages in the Platreef at the Sandsloot Mine, northern Bushveld Complex, South Africa. *Mineralogical Magazine* 70:83–101.
- Holwell DA, McDonald I, Butler IB (2011) Precious metal enrichment in the Platreef, Bushveld Complex, South Africa: evidence from homogenized magmatic sulfide melt inclusions. *Mineralium Deposita* 161:1011–1026.
- Howard JH (1977) Geochemistry of selenium: formation of ferroselite and selenium behavior in the vicinity of oxidizing sulfide and uranium deposits. *Geochimica et Cosmochimica Acta* 41:1665–1678.
- Huber H, Koeberl C, McDonald I, Reimold WU (2001) Geochemistry and petrology of Witwatersrand and Dwyka diamictites from South Africa: search for an extra-terrestrial component. *Geochimica et Cosmochimica Acta* 65:2007–2016.
- Hulbert LJ (1983) A petrographical investigation of the Rustenburg Layered Suite and associated mineralization south of Potgietersrus. Unpublished D.Sc. dissertation, Pretoria, South Africa, The University of Pretoria.
- Hulbert LJ, von Gruenewaldt G (1982) Nickel, copper, and platinum mineralization in the Lower Zone of the Bushveld Complex, south of Potgietersrus. *Economic Geology* 77:1296–1306.
- Hulbert LJ, von Gruenewaldt G (1985) Textural and compositional features of chromite in the lower and critical zones of the Bushveld Complex south of Potgietersrus. *Economic Geology* 80:872–895.
- Huminicki MAE, Sylvester PJ, Cabri LJ, Lesher CM, Tubrett M (2005) Quantitative mass balance of platinum group elements in the Kelly Lake Ni-Cu-PGE deposit, Copper Cliff offset, Sudbury. *Economic Geology* 100:1631–1646.
- Hutchinson D, Kinnaird JA (2005) Complex multistage genesis for the Ni-Cu-PGE mineralization in the southern region of the Platreef, Bushveld Complex, South Africa. *Applied Earth Science (Transactions of the Institute of Mining and Metallurgy B)* 114:B208–B223.

- 
- Hutchinson D, McDonald I (2008) Laser ablation ICP-MS study of platinum-group elements in sulfides from the Platreef at Turfspruit, northern limb of the Bushveld Complex, South Africa. *Mineralium Deposita* 43:695–711.
- Hutchinson D, Kinnaird JA, Schurmann (2004) Complex multi-stage mineralisation history in the southern sector of the Platreef, Bushveld Complex, South Africa., Abstract Volume Geoscience Africa, University of the Witwatersrand, South Africa
- Ihlenfeld C, Keays R (2011) Crustal contamination and PGE mineralization in the Platreef, Bushveld Complex, South Africa: evidence for multiple contamination events and transport of magmatic sulfides. *Mineralium Deposita* 46:813–832.
- Irvine TN (1975) Crystallization sequences in the Muskox intrusion and other layered intrusions—II. Origin of chromitite layers and similar deposits of other magmatic ores. *Geochimica et Cosmochimica Acta* 39:991–1020.
- Irvine TN (1977) Origin of chromitite layers in the Muskox intrusion and other stratiform intrusions: a new interpretation. *Geology* 5:273–7.
- Irvine TN, Keith DW, Todd SG (1983) The JM platinum-palladium reef of the Stillwater Complex, Montana; II, Origin by double-diffusive convective magma mixing and implications for the Bushveld Complex. *Economic Geology* 78:1287-1334.
- Irvine TN, Sharpe MR (1986) Magma mixing and the origin of stratiform oxide ore zones in the Bushveld and Stillwater Complexes. In: Gallagher M G, Ixer R A, Neary C R, et al. (eds.), *Metallogeny of Basic and Ultrabasic Rocks*. Institute of Mining Metal, London. p. 183–198.
- Jones EJ (2013) Petrological and geochemical study of Platreef chromitites, northern Bushveld, South Africa. PhD thesis, Cardiff University pp. 240–248.
- Keays RR (1995) The role of komatiite and picritic magmatism and S-saturation in the formation of ore deposits. *Lithos* 34:1–18.
- Keays RR, Campbell IH (1981) Precious metals in the Jimberlana Intrusion, Western Australia; implications for the genesis of platiniferous ores in layered intrusions. *Economic Geology* 76:1118–1141.
-

- 
- Keays RR, Nickel EH, Groves DI, McGoldrick PJ (1982) Iridium and palladium as discriminants of volcanic exhalative, hydrothermal and magmatic nickel sulfide mineralization. *Economic Geology* 77:1535–1547.
- Kelley SP, Fallick AE (1990) High precision spatially resolved analysis of  $\delta^{34}\text{S}$  in sulfides using a laser extraction system. *Geochimica et Cosmochimica Acta* 54:883–888.
- Kerr A, Leitch AM (2005) Self destructive sulfide segregation systems and the formation of high-grade magmatic ore deposits. *Economic Geology* 100:311–332.
- Kinloch ED (1982) Regional trends in the platinum-group mineralogy of the critical zone of the Bushveld Complex, South Africa. *Economic Geology* 77:1328–1347.
- Kinloch ED, Peyerl W (1990) Platinum-group minerals in various rock types of the Merensky Reef: Genetic implications. *Economic Geology* 85:537–555.
- Kinnaird JA (2005) Geochemical evidence for multiphase emplacement in the southern Platreef. *Applied Earth Science (Transactions of the Institute of Mining and Metallurgy B)* 114:B225–B241.
- Kinnaird J. A, Kruger FJ, Nex PAM, Cawthorn RG (2002) Chromitite formation—a key to understanding processes of platinum enrichment. *Applied Earth Science (Transactions of the Institute of Mining and Metallurgy B)* 111:23–35.
- Kinnaird JA, McDonald I (2005) An introduction to mineralisation in the northern limb of the Bushveld Complex. *Applied Earth Science (Transactions of the Institute of Mining and Metallurgy B)* 114:B194–B198.
- Kinnaird JA, Hutchinson D, Schurmann L, Nex PAM, de Lange R (2005) Petrology and mineralization of the southern Platreef: Northern limb of the Bushveld Complex, South Africa. *Mineralium Deposita* 40:576–597.
- Kinnaird JA, Yudovskaya M, Naldrett AJ, Botha MJ, Chunnnett GK (2012) PGE mineralisation in the Main Zone of the northern limb of the Bushveld Complex. In: 12th International Ni–Cu–(PGE) Symposium, Guiyang, China. Abstracts 73–76.

- 
- Klein C, Beukes NJ (1989) Geochemistry and sedimentology of a facies transition from limestone to iron-formation deposition in the early Proterozoic Transvaal Supergroup, South Africa. *Economic Geology* 84:1733–1774.
- Kruger FJ (1994) The Sr-isotopic stratigraphy of the Western Bushveld Complex. *South African Journal of Geology* 97:393–398.
- Kruger FJ (1992) The origin of the Merensky cyclic unit: isotopic and mineralogical evidence for an alternative orthomagmatic model. *Australian Journal of Earth Science* 39:255–261.
- Kruger FJ (1999) The Bushveld Complex unconformity related ore deposits: an isotopic perspective. In: Stanley et al (eds) *Mineral Deposits: Processes to Processing*. Balkema Rotterdam, pp.737–738.
- Kruger FJ (2003) Filling the Bushveld Complex magma chamber: intrachamber magma dynamics and the generation of giant chromitite and PGE deposits. *Applied Earth Science (Transactions of the Institute of Mining and Metallurgy B)* 112:B208–B209.
- Kruger FJ (2005) Filling the Bushveld Complex magma chamber: lateral expansion, roof and floor interaction, magmatic unconformities, and the formation of giant chromitite, PGE and Ti-V-magnetitite deposits. *Mineralium Deposita* 40:451–472.
- Kruger FJ, Marsh JS (1982) Significance of  $^{87}\text{Sr}/^{86}\text{Sr}$  ratios in the Merensky cyclic unit of the Western Bushveld Complex. *Nature* 298:53–55.
- Kruger FJ, Marsh JS (1985) The mineralogy, petrology and origin of the Merensky cyclic unit in the Western Bushveld Complex. *Economic Geology* 80:958–974.
- Kruger FJ, Cawthorn RG, Meyer PS, Walsh KL (1986) Sr-isotopic, chemical and mineralogical variations across the pyroxenites marker and in the Upper Zone of the western Bushveld Complex. In: ‘Geocongress’ 86, 21<sup>st</sup>, Johannesburg. Geological Society of South Africa, extended abstracts p. 609–612.
- Lambert DD, Walker RJ, Morgan JW, Shirey SB, Carlson RW, Zientek ML, Lipin BR, Koski MS, Cooper RL (1994) Re—Os and Sm—Nd Isotope Geochemistry of the Stillwater Complex, Montana: Implications for the Petrogenesis of the J-M Reef. *Journal of Petrology* 35:1717–1753.
-

- 
- Lee CA (1996) A review of mineralization in the Bushveld Complex and some other layered mafic intrusions. In: Cawthorn RG (ed) Layered intrusions. Elsevier Science, pp.103–146.
- Lee CA, Parry SJ (1988) Platinum-group element geochemistry of the lower and middle group chromitites of the eastern Bushveld Complex. *Economic Geology* 83:1127–1139.
- Leeb-du Toit A (1986) The Impala Platinum mines. In: Anhaeusser CR, Maske S (eds) Mineral Deposits of South Africa. Johannesburg, Geological Society of South Africa, pp. 1091–1106.
- Leshner CM (1989) Komatiite-associated nickel sulfide deposits. In: Whitney JA, Naldrett AJ (eds) Ore deposition associated with magmas. *Reviews in Economic Geology, Society of Economic Geologists* pp.45–102.
- Leshner CM, Burnham OM (2001) Multicomponent elemental and isotopic mixing in Ni-Cu-(PGE) ores at Kambalda, Western Australia. *Canadian Mineralogist* 39:421–446.
- Leshner CM, Groves DG (1986) Controls on the formation of komatiite-associated nickel-copper sulphide deposits. In: Friedrich GH et al. (eds) *Geology and Metallogeny of Copper Deposits*. Springer, Berlin, pp. 43–62.
- Leshner CM, Keays RR (2002) Komatiite-associated Ni-Cu-(PGE) deposits: Geology, mineralogy, geochemistry and genesis. *Canadian Institute of Mining, Metallurgy and Petroleum, Special Volume* 54:579–618.
- Li C, Naldrett AJ (1993) Sulfide capacity of magma: A quantitative model and its application to the formation of the sulfide ores at Sudbury. *Economic Geology* 88:1253–1260.
- Li C, Ripley EM (2005) Empirical equations to predict the sulfur content of mafic magmas at sulfide saturation and applications to magmatic sulfide deposits. *Mineralium Deposita* 40:218–230.
- Li C, Barnes S-J, Makovicky E, Rose-Hansen J, Makovicky M (1996) Partitioning of nickel, copper, iridium, rhenium, platinum, and palladium between monosulfide solid solution and sulfide liquid: Effects of composition and temperature. *Geochimica et Cosmochimica Acta* 60:1231–1996.
-

- 
- Li C, Maier WD, de Waal SA (2001). The role of magma mixing in the genesis of PGE mineralization in the Bushveld Complex: Thermodynamic calculations and new interpretations. *Economic Geology* 96:653–662.
- Li C, Ripley EM, Maier WD, Gomwe TES (2002) Olivine and S isotopic compositions of the Uitkomst Ni-Cu sulfide ore-bearing complex, South Africa: Evidence for S contamination and multiple magma emplacements. *Chemical Geology* 188:149–159.
- Li C, Ripley EM, Merino E, Maier WD (2004) Replacement of base metal sulfides by actinolite, epidote, calcite and magnetite in the UG2 and Merensky Reef of the Bushveld Complex, South Africa. *Economic Geology* 99:183–184.
- Li C, Ripley EM, Oberthur T, Miller JD, Joslin GD (2008) Textural, mineralogical and stable isotope studies of hydrothermal alteration in the main sulfide zone of the Great Dyke, Zimbabwe and the precious metals zone of the Sonju Lake Intrusion, Minnesota, USA. *Mineralium Deposita* 43:98–110.
- Lightfoot PC, Hawkesworth CJ (1988) Origin of Deccan Trap lavas: evidence from combined trace element and Sr-, Nd-and Pb-isotope studies. *Earth and Planetary Science Letters* 91:89–104.
- Lightfoot PC, Hawkesworth CJ (1997) Flood basalts and magmatic Ni, Cu, and PGE sulphide mineralization: comparative geochemistry of the Noril'sk (Siberian Traps) and West Greenland sequences. In: Mahoney J (ed) *Large igneous provinces: continental, oceanic and planetary flood volcanism*. 100:357–380.
- Lightfoot PC, Hawkesworth CJ, Devey CW, Rogers NW, Van Calsteren PWC (1990) Source and differentiation of Deccan Trap Lavas: implications of geochemical and mineral chemical variations. *Journal of Petrology* 31:1165–1200.
- Lodders K (2003) Solar system abundances and condensation temperatures of the elements. *Astrophysical Journal* 591:1220–1247.
- Lombard K (2012) Exploration results and mineral resource estimate for the Waterberg Platinum Project. Coffey Mining, South Africa, p. 89.

- 
- Lorand JP, Alard O, Luguët A, Keays RR (2003) Sulfur and selenium systematics of the subcontinental lithospheric mantle: inferences from the Massif Central xenolith suite (France). *Geochimica et Cosmochimica Acta* 67:4137–4151.
- Maier WD (2005) Platinum-group element (PGE) deposits and occurrences: Mineralization styles, genetic concepts, and exploration criteria. *Journal of African Earth Sciences* 41:165–191.
- Maier WD, Barnes S-J (1996) Unusually high concentrations of magnetite at Caraiba and other Cu-sulfide deposits in the Curaca Valley, Bahia, Brazil. *Canadian Mineralogist* 34:717–731.
- Maier WD, Barnes SJ, (1998) Concentrations of rare earth elements in silicate rocks of the Lower, Critical and Main Zones of the Bushveld Complex. *Chemical Geology* 150:85–103.
- Maier WD, Barnes S-J (1999) Platinum-group elements in silicate rocks of the Lower, Critical, and Main zones at Union section, western Bushveld Complex. *Journal of Petrology* 40:1647–1671.
- Maier WD, Barnes S-J (2010) The petrogenesis of platinum-group element reefs in the Upper Main Zone of the Northern Lobe of the Bushveld Complex on the farm Moorddrift, South Africa. *Economic Geology* 105:841–854.
- Maier WD, Eales HV (1994) A facies model for the interval between the UG2 and Merensky Reef, Western Bushveld Complex: *Applied Earth Science (Transactions of the Institute of Mining and Metallurgy B)* 103:22–30.
- Maier WD, de Klerk L, Blaine J, Manyeruke T, Barnes S-J, Stevens MVA, Mavrogenes JA (2008) Petrogenesis of contact-style PGE mineralization in the northern lobe in the Bushveld Complex: comparison of data from the farms Rooipoort, Townlands, Drenthe and Nonnenweth. *Mineralium Deposita* 43:255–280.
- Mainwaring PR, Naldrett AJ (1977) Country-rock assimilation and the genesis of Cu-No sulfides in the Waterhen intrusion, Duluth Complex, Minnesota. *Economic Geology* 72:1269–1284.
-

- 
- Manyeruke TD (2003) The petrology and geochemistry of the Platreef on the farms Townlands, near Potgietersrus, northern Bushveld Complex. Unpublished M.Sc. thesis, Pretoria, South Africa, The University of Pretoria.
- Manyeruke TD, Maier WD, Barnes S-J (2005) Major and Trace Element Geochemistry of the Platreef on the farm Townlands, northern Bushveld Complex. *South African Journal of Geology* 108:381–396.
- Mavrogenes JA, O'Neill HSC (1999) The relative effects of pressure temperature and oxygen fugacity on the solubility of sulfide in mafic magmas. *Geochimica et Cosmochimica Acta* 63:1173–1180.
- McCallum IS (1996) The Stillwater Complex. In: Cawthorn RG, (ed) *Layered Intrusions*. Elsevier Science, pp. 441–484.
- McCallum ME, Loucks RR, Carlson RR, Cooley EF, Doerge TA (1976) Platinum metals associated with hydrothermal copper ores of the New Rambler mine, Medicine Bow Mountains, Wyoming. *Economic Geology* 71:1429–1450.
- McCutcheon SC, Kinnaird JA (2011) Platinum-group mineral assemblages in the Platreef at Tweefontein [abs.]. Platreef Workshop, 4<sup>th</sup>, Mokopane, South Africa, 14<sup>th</sup>-16<sup>th</sup> January 2011, Abstracts.
- McDonald I, Harmer RE (2011) Cu–Ni–PGE mineralisation at Aurora is not Platreef, so where does it fit in? [abs.]. Platreef Workshop, 4<sup>th</sup>, Mokopane, South Africa, 14<sup>th</sup>-16<sup>th</sup> January 2011, Abstracts.
- McDonald I, Holwell DA (2007) Did lower zone magma conduits store PGE-rich sulphides that were later supplied to the Platreef? *South African Journal of Geology* 110:611–616.
- McDonald I, Holwell DA (2011) Geology of the northern Bushveld Complex and the setting and genesis of the Platreef Ni-Cu-PGE Deposit. *Reviews in Economic Geology* 17:297–327.
- McDonald I, Viljoen (2006) Platinum-group element geochemistry of mantle eclogites: a reconnaissance study of xenoliths from Orapa kimberlite, Botswana. *Applied Earth Science (Transactions of the Institute of Mining and Metallurgy B)* 115:81–93.
-

- McDonald AM, Cabri LJ, Stanley CJ, Rudashevsky NS, Poirier G, Mungall JE, Ross KC, Durham BR, Rudashevsky VN (2005) Ungavaite, Pd<sub>4</sub>Sb<sub>3</sub>, a new intermetallic mineral species from the Mesamax Northwest deposit, Ungava region, Quebec, Canada: description and genetic implications. *The Canadian Mineralogist* 43:1735–1744.
- McDonald I, Holwell DA, Armitage PEB (2005) Geochemistry and mineralogy of the Platreef and ‘Critical Zone’ of the northern lobe of the Bushveld Complex, South Africa: implications for Bushveld stratigraphy and the development of PGE mineralization. *Mineralium Deposita* 40:526–549.
- McDonald I, Holwell DA, Wesley B (2009) Assessing the potential involvement of an early magma staging chamber in the generation of the Platreef Ni–Cu–PGE deposit in the northern limb of the Bushveld Complex: a pilot study of the Lower Zone Complex at Zwartfontein. *Applied Earth Science (Transactions of the Institute of Mining and Metallurgy B)* 118:5–20.
- McDonald I, Jones RE, Holwell DA, Butler IB (2012) Platinum-group element tenors and S/Se ratios of Platreef sulphide melt inclusions [abs.]. Platreef Workshop, 5<sup>th</sup>, Mokopane, South Africa, 9<sup>th</sup>-12<sup>th</sup> January 2012, Abstracts.
- McDonald I, Ohnenstetter S, Rowe JP, Tredoux M, Pattrick RAD, Vaughand DJ (1999) Platinum precipitation in the Waterberg deposit, Naboomspruit, South Africa. *South African Journal of Geology* 102:184–191.
- McDonald I, Vaughand DJ, Tredoux M (1995) Platinum mineralization in quartz veins near Naboomspruit, central Transvaal. *South African Journal of Geology* 98:168–175.
- McDonough WF, Sun SS (1995) The composition of the earth. *Chemical Geology* 120:223–253.
- Meyer R, de Beer H (1987) Structure of the Bushveld Complex from resistivity measurements. *Nature* 325:610–612.
- Misra KC (2000) Understanding mineral deposits. Kluwer Academic Publishers, Dordrecht, p.845.
- Misra KC, Fleet ME (1984) Chemical composition and stability of violarite. *Economic Geology* 59:391–403.

- 
- Miyoshi T, Sakai H, Chiba H (1984) Experimental study of sulfur isotope fractionation factors between sulfate and sulfide in high temperature melts. *Geochemistry Journal* 18:75–84.
- Mountain BW, Wood SA (1988) Chemical controls on the solubility, transport, and deposition of platinum and palladium in hydrothermal solutions: a thermodynamic approach. *Economic Geology* 83:492–510.
- Muller C (2008). Platinum Group Metals Ltd 43-101 on Oorlogfontein 45KS.
- Mungall JE, Andrews DRA, Cabri LJ, Sylvester PJ, Tubrett M (2005) Partitioning of Cu, Ni, Au, and platinum-group elements between monosulfide solid solution and sulfide melt under oxygen and sulfur fugacities. *Geochimica et Cosmochimica Acta* 69:4349–4360.
- Myeni P, Muzondo T (2011) Economic implications of geological structures at Mogalakwena platinum mine [abs.]. Platreef Workshop, 4th, Mokopane, South Africa, 14<sup>th</sup> – 16<sup>th</sup> January 2011, Abstracts.
- Naldrett AJ (2004) *Magmatic Sulfide Deposits: Geology, Geochemistry and Exploration*. Springer, Heidelberg, pp. 728.
- Naldrett AJ (2011) Fundamentals of Magmatic Sulfide Deposits. *Reviews in Economic Geology* 17:1–50.
- Naldrett AJ, Barnes S.-J (1986) The behaviour of platinum group elements during fractional crystallization and partial melting with special reference to the composition of magmatic sulfide ores. *Fortschritte der Mineralogie* 74:113–133.
- Naldrett AJ, Kullerud G (1968) A study of the Strathcona mine and its bearing on the origin of the nickel-copper ore of the Sudbury District, Ontario. *Journal of Petrology* 8:453–531.
- Naldrett AJ, von Gruenewaldt G (1989) Association of platinum-group elements with chromitite in layered intrusions and ophiolite complexes. *Economic Geology* 84:180–187.

- 
- Naldrett AJ, Asif M, Krstic S, Li C (2000) The composition of mineralization at the Voisey's Bay Ni-Cu sulfide deposit, with special reference to platinum-group elements. *Economic Geology* 95:845–866.
- Naldrett AJ, Craig JR, Kullerud G (1968) The central portion of the Fe–Ni–S system and its bearing on pentlandite exsolution in iron-nickel sulfide ores. *Economic Geology* 62:826–848.
- Naldrett AJ, Fedorenko VA, Asif M, Lin S, Kunilov VE, Stekhin AI, Lightfoot PC, Gorbachev NS (1996) Controls on the composition of Ni-Cu sulfide deposits as illustrated by those at Noril'sk, Siberia. *Economic Geology* 91:751–773.
- Naldrett A, Gasparini EC, Barnes S-J, von Gruenewaldt G, Sharpe MR (1986) The Upper Critical Zone of the Bushveld Complex and the origin of Merensky-type ores. *Economic Geology* 105:669–688.
- Naldrett A, Kinnaird J, Wilson A, Chunnet G (2008) Concentration of PGE in the Earth's crust with special reference to the Bushveld Complex. *Earth Science Frontiers* 15:264–297.
- Naldrett AJ, Wilson A, Kinnaird J, Chunnett G (2009) PGE Tenor and Metal Ratios within and below the Merensky Reef, Bushveld Complex: Implications for its Genesis. *Journal of Petrology* 50:625–659.
- Naldrett AJ, Wilson A, Kinnaird J, Yudovskaya M, Chunnett G (2012) The origin of chromitites and related PGE mineralization in the Bushveld Complex: new mineralogical and petrological constraints. *Mineralium Deposita* 47:209–232.
- Nyama N, Nex P, Yao (2005) Preliminary Petrological Studies of the Platreef on Tweefontein Hill, Bushveld Igneous Complex, South Africa. *International Platinum Symposium, 10<sup>th</sup>*, University of Oulu, Extended Abstracts p. 505–508.
- Oberthür T, Cabri LJ, Weiser TW, McMahon G, Müller P (1997) Pt, Pd and other trace elements in sulfides of the main sulphide zone, great dyke, Zimbabwe: a reconnaissance study. *Canadian Mineralogist* 35:597–609.
-

- Ohmoto H, Rye RO (1979) Isotopes of sulfur and carbon. In: Barnes HL (ed) *Geochemistry of hydrothermal ore deposits*, 2<sup>nd</sup> edition: London, Wiley and Sons, pp. 509–567.
- Patten C, Barnes S J, Mathez EA, Jenner FE (2013) Partition coefficients of chalcophile elements between sulfide and silicate melts and the early crystallization history of sulfide liquid: LA-ICP-MS analysis of MORB sulfide droplets. *Chemical Geology* 358:176–188.
- Peach CL, Mathez EA, Keays RR (1990) Sulfide melt-silicate melt distribution coefficients for the noble metals and other chalcophile metals as deduced from MORB: Implications for partial melting. *Geochimica et Cosmochimica Acta* 54:3379–3389.
- Peck DC, Keays RR (1990) Insights into the behaviour of precious metals in primitive, S-undersaturated magmas; evidence from the Heazlewood River Complex, Tasmania. *Canadian Mineralogist* 28:553–577
- Penniston-Dorland SC, Wing BA, Nex PAM, Kinnaird JA, Farquhar J, Brown M, Sharman ER (2008) Multiple sulfur isotopes reveal a magmatic origin for the Platreef platinum group element deposit, Bushveld Complex, South Africa. *Geology* 36:979–982.
- Peregoedova AV (1998) The experimental study of the Pt–Pd–partitioning between monosulfide solid solution and Cu–Ni–sulfide melt at 900–840°C. In: 8th International Platinum Symposium abstracts. Geological Society of South Africa and South African Institute of Minerals and Metallurgy, Symposium Series S18:325–373.
- Piña R, Gervilla F, Barnes S-J, Ortega L, Lunar (2012) Distribution of platinum-group and chalcophile elements in the Aguablanca Ni-Cu sulfide deposit (SW Spain): Evidence from a LA-ICP-MS study. *Chemical Geology* 302–303:61–75.
- Piña R, Gervilla F, Barnes S-J, Ortega L, Lunar (2013) Platinum-group elements-bearing pyrite from the Aguablanca Ni-Cu sulfide deposit (SW Spain): a LA-ICP-MS study. *European Journal of Mineralogy* 25-2:241–252.
- Prichard HM, Barnes S-J, Maier WD, Fisher PC (2004) Variations in the nature of the platinum-group minerals in a cross-section through the Merensky Reef at Impala Platinum: implications for the mode of formation of the reef. *The Canadian Mineralogist* 42:423–437.

- 
- Prichard HM, Knight RD, Fisher PC, McDonald I, Mei-Fu Zhou, Wang CY (2013) Distribution of platinum-group elements in magmatic and altered ores in the Jinchuan intrusion, China: an example of selenium remobilization by post magmatic fluids. *Mineralium Deposita* 48:767–786.
- Pronost J, Harris C, Pin C (2008) Relationship between footwall composition, crustal contamination, and fluid–rock interaction in the Platreef, Bushveld Complex, South Africa. *Mineralium Deposita* 43:825–848.
- Queffurus M, Barnes S-J (in review 2014) Processes affecting the sulfur to selenium ratio in magmatic nickel-copper and platinum-group element deposits. *Ore Geology Reviews*.
- Rehkämper M, Halliday AN, Fitton JG, Lee DC, Wieneke M, Arndt NT (1999) Ir, Ru, Pt, and Pd in basalts and komatiites: New constraints for the geochemical behavior of the platinum-group elements in the mantle. *Geochimica et Cosmochimica Acta* 63:3915–3934.
- Ripley EM (1981) Sulfur isotopic abundances of the Dunka Road Cu-Ni deposit, Duluth Complex, Minnesota. *Economic Geology* 76:619–620.
- Ripley EM (1990) Se/S ratios of the Virginia Formation and Cu-Ni mineralization in the Babbitt area, Duluth Complex, Minnesota. *Economic Geology* 85:1935–1940.
- Ripley EM, Li C (2003) Sulfur isotope exchange and metal enrichment in the formation of magmatic Cu-Ni-(PGE) deposits. *Economic Geology* 98:635–641.
- Ripley EM, Lambert DD, Frick LR (1986) Re-Os, Sm-Nd, and Pd isotopic constraints on mantle and crustal contributions to magmatic sulfide mineralization in the Duluth Complex. *Geochimica et Cosmochimica Acta* 62:3349–3365.
- Ripley EM, Li C, Shin D (2002) Paragenesis assimilation in the genesis of magmatic Ni–Cu–Co sulfide mineralization at Voisey’s Bay, Labrador:  $\delta^{34}\text{S}$ ,  $\delta^{13}\text{C}$  and Se/S evidence. *Economic Geology* 97:1307–1318.
- Ripley EM, Park YR, Li C, Naldrett AJ (1999) Sulfur and oxygen isotopic evidence of country rock contamination in the Voisey's Bay Ni–Cu–Co deposit, Labrador, Canada. *Lithos* 47:53–68.
-

- Robinson BW, Kusakabe M (1975) Quantitative preparation of sulfur dioxide for  $^{34}\text{S}/^{32}\text{S}$  analyses from sulfides by combustion with cuprous oxide: *Analytical Chemistry* 47:1179–1181.
- Scoate JS, Friedman RM (2008) Precise age of the platiniferous Merensky Reef, Bushveld Complex, South Africa, but the U-Pb zircon chemical abrasion ID-TIMS technique. *Economic Geology* 103:465–471.
- Scoon RN, Teigler B (1994) Platinum-group element mineralization in the critical zone of the western Bushveld Complex; I, Sulfide poor-chromitites below the UG-2. *Economic Geology* 89:1094–1121.
- Seabrook CL, Cawthorn RG, Kruger FJ (2005) The Merensky Reef, Bushveld Complex: mixing of minerals not mixing of magmas. *Economic Geology* 100:1191–1206.
- Sharman-Harris E, Kinnaird JA, Harris C, Horstmann UE, Wing B (2005) A new look at sulfide mineralization of the northern limb, Bushveld Complex: A stable isotope study. *Applied Earth Science (Transactions of the Institute of Mining and Metallurgy B)* 114:B252–B263.
- Sharman ER, Penniston-Dorland SC, Kinnaird JA, Nex PAM, Brown M, Wing BA (2013) Primary origin of marginal Ni-Cu-(PGE) mineralization in layered intrusions:  $\Delta^{33}\text{S}$  evidence from the Platreef, Bushveld, South Africa. *Economic Geology* 108:365–377.
- Shima H, Naldrett AJ (1975) Solubility of sulfur in an ultramafic melt and the relevance of the system Fe–S–O. *Economic Geology* 70:960–967.
- Sinyakova EF, Kosyakov VI, Kolonin GR (2001) Behaviour of PGE on the cross-section of melts in the system Fe-Ni-S ( $\text{Fe}_x\text{Ni}_{0.49-x}\text{S}_{0.51}$ ). *Russian Journal of Geology and Geophysics* 42:1287–1304.
- Smith JW, Holwell DA, McDonald I, Pearton T (2010) Platinum-group mineralogy within the GNPA member in the Rooipoort area, Northern Limb, Bushveld Complex, South Africa. *Applied Earth Science (Trans. Inst. Min. Metall. B)* 119:114, Abstracts.
- Smith JW, Holwell DA, McDonald I (2011a) New observations on the nature and setting of PGE mineralization in the northern Bushveld Complex, south of Mokopane, South

- 
- Africa. In: Barra F, et al. (eds) LETS TALK ORE DEPOSITS. Proceedings of the 11<sup>th</sup> Biennial Meeting, Antofagasta, Chile, 2, 654–656
- Smith JW, Holwell DA, McDonald I (2011b) The mineralogy and petrology of platinum-group element-bearing sulfide mineralization within the Grasvalley Norite–Pyroxenite–Anorthosite (GNPA) member, south of Mokopane, northern Bushveld Complex, South Africa. *Applied Earth Science (Transactions of the Institute of Mining and Metallurgy B)* 120:B158–B174.
- Smith JW, Holwell DA, McDonald I (2012) An overview of PGE and BMS mineralization within the GNPA member [abs.]. Platreef Workshop, 5<sup>th</sup>, Mokopane, South Africa, 9<sup>th</sup> – 11<sup>th</sup> November 2012, Abstracts.
- Smith JW, Holwell DA, McDonald I (2014) Precious and base–metal geochemistry and mineralogy of the Grasvalley–Norite–Pyroxenite–Anorthosite (GNPA) member, northern Bushveld Complex, South Africa: implications for a multistage emplacement. *Mineralium Deposita* 49:667–692.
- Smith JW, Holwell DA, McDonald I, Boyce AJ (2013) The emplacement and relative timing of PGE mineralisation within the northern Bushveld Complex. In: Jonsson et al. (eds) Mineral deposit research for a high-tech world. Proceedings of the 12th Biennial Meeting, Uppsala, Sweden 2:1061–1064.
- Sutherland, A-J (2013) The nature and genesis of PGE-rich sulphide horizons on the farm War Springs, northern Bushveld Complex, South Africa, MGeol thesis (unpublished), England, University of Leicester.
- Teigler B, Eales HV (1993) Correlation between chromite composition and PGE mineralization in the Critical Zone of the western Bushveld Complex. *Mineralium Deposita* 28:291–302.
- Thériault RM, Barnes S-J (1998) Compositional variations in Cu–Ni–PGE sulfides of the Dunka Road deposit, Duluth Complex, Minnesota: the importance of combined assimilation and magmatic processes. *Canadian Mineralogist* 36:869–886.
- Tomkins AG (2010) Wetting facilitates late-stage segregation of precious metal-enriched sulfosalt melt in magmatic sulfide systems. *Geology* 38:951–954.
-

- 
- Tredoux M, Sellschop JF, Davies G, de Wit MJ (1985) The behaviour of the PGE and Au during partial melting and fractional crystallization: evidence from magmas on the Kaapvaal Craton. *Canadian Mineralogist* 23:317–318.
- Tredoux M, Lindsay NM, Davies G, McDonald I (1995) The fractionation of platinum-group elements in magmatic systems, with the suggestion of a novel causal mechanism. *South African Journal of Geology* 98:157–167.
- Truter FC (1947) A remarkable transcurrent fault near Potgietersrust, Transvaal. *Geological Society of South Africa* 50:1–15.
- Twist D (1985) Geochemical evolution of the Rooiberg silicic lavas in the Loskop Dam area; Southeastern Bushveld. *Economic Geology* 80:1153–1165.
- van der Merwe MJ (1976) The layered sequence of the Potgietersrus limb of the Bushveld Complex. *Economic Geology* 71:1337–1351.
- van der Merwe M.J (1978) The geology of the basic and ultramafic rocks of the Potgietersrus limb of the Busveld Complex, Ph.D. thesis (unpublished), South Africa, University of the Witwatersrand.
- van der Merwe MJ (2008) The geology and structure of the Rustenburg Layered Suite in the Potgietersrus/Mokopane area of the Bushveld Complex, South Africa. *Mineralium Deposita* 43:405–419.
- Van Rooyen (1954) Die geologie van .n gedeelte van gebied 7 (Potgietersrus). *Geological Survey of South Africa, Pretoria*, pp. 116.
- Verbeek J, Lomberg J (2005) Rooipoort PGE, Mokopane, Limpopo province, South Africa, Qualified persons report by RSG Global for Caledonia Mining Corporation.
- von Gruenewaldt G, Hulbert LJ, Naldrett AJ (1989) Contrasting platinum group element concentration patterns in cumulates of the Bushveld Complex. *Mineralium Deposita* 24:219–229.
- Wagner PA (1929) The platinum deposits and mines of South Africa. Oliver and Boyd, Edinburgh, pp. 326.
-

- 
- Wagner T, Boyce AJ, Fallick AE (2002) Laser combustion analysis of  $\delta^{34}\text{S}$  of sulfosalt minerals: Determination of the fractionation systematics and some crystal-chemical considerations. *Geochimica et Cosmochimica Acta* 66:2855–2863.
- Wallace P, Carmichael ISE (1992) Sulfur in basaltic magmas. *Geochimica et Cosmochimica Acta* 56:1863–1874
- Walraven F (1985) Genetic aspects of the granophyric rocks of the Bushveld Complex. *Economic Geology* 80:1166–1180.
- Walraven F (1997) Geochronology of the Rooiberg Group, Transvaal Supergroup, South Africa. *Economic Geology Research Unit Information Circular, University of the Witwatersrand, Johannesburg* 316, p. 21.
- Walraven F, Hattingh E (1993) Geochronology of the Nebo Granite Bushveld Complex. *South Africa Journal of Geology* 96:31–41.
- Walraven F, Armstrong RA, Kruger FJ (1990) A chronostratigraphic framework for the north-central Kaapvaal Craton, the Bushveld Complex and Vredefort structure. *Tectonophysics* 171:23–48.
- Webb SJ, Nguuri T, Cawthorn RG, James D (2004) Gravity modelling of Bushveld Complex connectivity supported by southern African seismic experiment result. *South African Journal of Geology* 107:207–218.
- Weise S, Yudovskaya M, Kinnaird J (2008) Geological observations on the Main Zone–Platreef contact on the farms Tweefontein, Vaalkop, Zwartfontein and Overysel, [abs.], 3<sup>rd</sup> Platreef Workshop, Mokopane, South Africa, 11<sup>th</sup>-13<sup>th</sup> July 2008, Abstracts.
- Wendlandt RF (1982) Sulfide saturation of basalt and andesite melts at high pressures and temperatures. *American Mineralogist* 67:877–885.
- Westerlund KJ, Gurney JJ, Carlson RW, Shirey SB, Hauri EH, Richardson SH (2004) A metasomatic origin for late Archean eclogitic diamonds: Implications from internal morphology of diamonds and Re-Os and S isotope characteristics of their sulfide inclusions from the Late Jurassic Klipspringer kimberlites. *South African Journal of Geology* 107:119–130.
-

- Wilmore CC, Boudreau AE, Kruger FJ (2000) The halogen geochemistry of the Bushveld Complex, Republic of South Africa: Implications for chalcophile element distribution in the Lower and Critical Zones. *Journal of Petrology* 41:1517–1590.
- Wilson A, Chunnnett G (2006) Trace Element and Platinum Group Element Distributions and the Genesis of the Merensky Reef, Western Bushveld Complex, South Africa. *Journal of Petrology* 47: 2369–2403.
- Wood SA (2002) The aqueous geochemistry of the platinum–group elements with applications to ore deposits. In: Cabri LJ (ed) *The Geology, Geochemistry, Mineralogy and Mineral Beneficiation of Platinum–Group Elements*. Canadian Institute of Mining, Metallurgy and Petroleum, Special Volume 54 pp. 211–249.
- Yamamoto M (1976) Relationship between Se/S and sulfur isotope ratios of hydrothermal sulfide minerals. *Mineralium Deposita* 11:197–209.
- Yudovskaya M, Kinnaird J, Naldrett AJ, Mokhov AV, McDonald I, Reinke C (2011) Facies variation in PGE mineralization in the Central Platreef of the Bushveld Complex, South Africa. *Canadian Mineralogist* 49:1349–1384.
- Yudovskaya M, Kinnaird JA, Sobolev A, Kuzmin D, Wilson A (2012) The Lower Zone Beneath the Platreef in the Northern Limb of the Bushveld Complex [abs.], Ni–PGE Worksop, Cardiff, 6<sup>th</sup> January 2012, Abstracts.

# Appendix 1

## Whole Rock Geochemistry

**Lithological abbreviations:** GBN gabbro-norite, NR norite, MA mottled anorthosite, PYX pyroxenite, CPX clinopyroxenite, CR chromitite, CZ chill zone, HZ harzburgite.

Data for whole rock XRF (major and trace elements) and Ni-sulfide Fire Assay which was followed by ICP-MS (for platinum-group elements). Methodologies are provided in Chapter 6 and 4, respectively. Analysis with unreasonable totals (<96wt % or >103wt %) have been omitted from thesis.

Borehole	RP04.23										
SAMPLE	34	46	53	63	73	90	143	157	158	162	185
Lithology	GBN	GBN	MA	MA	GBN	GBN	PYX	MA	MA	MA	MA
SiO <sub>2</sub>	52.06	51.33	50.44	51.68	51.6	51.71	52.47	48.7	51.27	50.04	50.81
TiO <sub>2</sub>	0.2	0.2	0.1	0.12	0.29	0.2	0.2	0.13	0.19	0.14	0.51
Al <sub>2</sub> O <sub>3</sub>	19.65	23.68	27.64	25.92	17.12	20.45	10.14	23.53	26.09	25.58	27.38
Fe <sub>2</sub> O <sub>3</sub>	6.75	3.64	2.05	3.08	7.94	5.79	11.93	5.67	2.82	3.3	2.49
MnO	0.126	0.069	0.032	0.046	0.155	0.104	0.223	0.073	0.055	0.059	0.053
MgO	7.08	3.46	1.57	2.17	7.3	6.99	17.12	3.46	1.58	2.64	1.17
CaO	10.66	12.91	13.2	11.62	11.89	10.96	6.53	12.79	12.34	13.16	12.43
Na <sub>2</sub> O	2.49	2.84	2.93	3.39	2.02	2.49	1.06	2.52	3.23	2.79	3.25
K <sub>2</sub> O	0.436	0.699	0.703	0.634	0.358	0.356	0.084	0.311	0.608	0.469	0.875
P <sub>2</sub> O <sub>5</sub>	0.021	0.026	0.02	<0.001	0.032	0.008	0.004	0.001	0.01	<0.001	0.009
SO <sub>3</sub>	<0.002	<0.002	0.003	<0.002	0.019	<0.002	0.004	0.196	0.184	<0.002	<0.002
Cr <sub>2</sub> O <sub>3</sub>	0.011	0.01	0.01	0.002	0.041	0.033	0.16	0.027	0.003	0.021	0.022
NiO	0.016	0.006	0.017	0.001	0.021	0.016	0.049	0.337	0.077	0.01	0.01
LOI	0.58	1.15	1.34	1.13	1.04	0.95	0.24	1.81	1.39	1.2	1.02
Total	100.09	100.02	100.03	99.79	99.81	100.05	100.22	99.56	99.84	99.4	99.99
<b>ppm</b>											
Rb	36	11.9	23	25.3	22	9.7	7.4	2.6	8.6	19.9	14.7
Sr	415.4	271.1	342.1	378	372.3	221.8	271.7	129	300.2	360.6	353.6
Y	5.4	7.5	7	2.3	5.5	11.5	7.2	6.1	6.8	5.1	5.8
Zr	36.7	25.1	23.8	13.4	29.5	37.2	22.6	10.2	9.8	38.6	15.2
Nb	4.1	1.7	1.9	0.7	1.1	1.9	2	0.7	0.4	3.1	1.5
Mo	0.8	1.2	1.1	0.6	0.8	1.3	0.9	1.2	1.2	1	0.7
Pb	4.3	17.9	11.9	2.8	6.8	37.2	2.6	2	11.5	9.6	31.7
Th	1.5	1.7	1	1	2.1	2	0.7	<0.6	0.6	2.1	1
U	0.5	0.9	<0.4	<0.4	1.1	1	0.7	1	<0.4	0.7	0.5
Ga	20.7	15.9	19.7	19.9	19.6	14.3	17.4	8.7	17.2	19.4	18.6
Zn	31.2	65.8	43	21	32.8	143.5	45.3	85.5	39.2	42.1	52.1
Cu	12.4	25.7	18	7.8	25.6	48.4	13.8	32.5	2879.6	637.6	41.3
Ni	27	144.3	70.2	32.8	36.1	168.8	145.2	418.9	2463.9	560.5	108.4
Co	9.2	41.6	17.6	11.5	14.7	42.9	32.6	94.1	64.9	20.7	17.2
Cr	21.5	90.5	84.7	21.9	24.1	296.5	211.3	1390.8	200	34.9	152.2
V	70.6	104.1	84.6	32.8	62	161	91.7	173.6	105	48.5	79.8
Sc	11.1	25	18.9	11.8	16.1	32	17.8	38.3	21.8	12	19.5
Ba	187.2	150	167	152.2	157.8	116.3	117.2	48.3	266	184.9	148.2
La	7.1	7.3	6.7	6.6	7.1	6.4	6.3	<2.3	4.9	7.7	5.8
Ce	15	10.9	13.1	6.8	9.4	11.8	10	7.2	<6.1	14.1	11.6
Nd	8.6	4.6	8	6.6	9.2	8.2	7.7	3.5	6.3	10.2	11.9
Cs	<1.7	<1.8	<1.8	<1.7	4.4	<1.8	<1.6	<1.9	<1.8	1.9	<1.8
As	2.4	7.9	6.2	1.3	2.9	17.7	<0.5	<0.6	1	1	2.1
Sb	<1.0	<1.0	<1.0	<1.0	<1.0	<1.0	<1.0	<1.1	<1.1	<1.0	1.3
Se	<0.5	<0.6	<0.6	0.6	<0.5	<0.6	<0.6	<0.7	2.3	1.4	<0.6
Sn	<0.8	<0.9	<0.9	<0.8	<0.8	<0.9	<0.9	<1.0	<0.9	<0.8	<0.9
W	<1.0	<1.1	<1.0	<0.9	<1.0	<1.2	<1.1	<1.3	<1.2	<1.0	<1.0
<b>ppb</b>											
Os								1.24	0.32		
Ir								2.42	1.58		
Ru								10.3	5.98		
Rh								10.8	4.92		
Pt								146	128		
Pd								786	617		
Au								104	85		



Appendix 1. Whole rock data

Borehole	RP04.23									
SAMPLE	187	188	192	268	287	295	297	300	305	307
Lithology	PYX	MA	CPX	GBN	GBN	PYX	MA	CR	NR	CR
SiO <sub>2</sub>	52.76	50.08	50.98	50.89	53.11	52.51	52.6	47.59	50.17	49.37
TiO <sub>2</sub>	0.16	0.1	0.2	0.1	0.45	0.18	0.21	0.72	0.1	0.32
Al <sub>2</sub> O <sub>3</sub>	8.21	26.51	5.27	20.88	13.59	17.39	22.37	8.78	16.78	16.54
Fe <sub>2</sub> O <sub>3</sub>	12.33	3.15	12.4	5.33	6.25	7.01	2.22	14.24	9.24	10.06
MnO	0.23	0.059	0.225	0.099	0.129	0.135	0.061	0.232	0.15	0.167
MgO	19.67	3.23	23.49	7.15	8.22	8.95	1.72	11.56	8.93	9.48
CaO	5.7	13.67	3.37	10.83	13.03	10.03	12.47	9.75	10.34	9.79
Na <sub>2</sub> O	0.56	2.54	0.2	2.43	2.04	2.24	3.44	1.13	2.1	1.94
K <sub>2</sub> O	0.082	0.285	0.057	0.692	0.886	0.333	1.507	0.317	0.366	0.196
P <sub>2</sub> O <sub>5</sub>	<0.001	<0.001	<0.001	<0.001	0.055	0.009	0.038	0.065	<0.001	0.004
SO <sub>3</sub>	0.004	0.004	0.004	<0.002	0.003	0.002	<0.002	0.077	0.26	<0.002
Cr <sub>2</sub> O <sub>3</sub>	0.158	0.034	0.305	0.087	0.116	0.166	0.027	2.722	0.187	2.457
NiO	0.075	0.005	0.075	0.017	0.036	0.032	0.007	0.127	0.247	0.038
LOI	0.22	0.3	3.23	1.36	1.61	0.57	2.72	1.04	0.63	0.18
Total	100.18	99.98	99.79	99.87	99.53	99.56	99.4	98.35	99.5	100.55
ppm										
Rb	3.8	6.1	4.6	27.2	10.6	86.4	87.7	15.7	13.8	5.7
Sr	142.2	350.2	24.1	381.6	294.6	375.4	380.4	124	281.6	285.9
Y	5.2	3.6	6.9	2.7	6.9	10.3	10.1	24	3.2	4.8
Zr	11.5	3.8	17.2	5	32.3	30.2	28	83.6	3.4	5.8
Nb	0.8	0.6	0.8	0.6	1.3	2.8	2.7	2.3	2	0.6
Mo	1.3	0.9	1.5	0.9	1.3	1.2	1	2.6	1.7	1.4
Pb	22.2	3.1	7.8	0.8	4.8	4.6	4.6	24.7	10.9	1.9
Th	1.6	<0.5	0.9	<0.5	1.1	2	1.7	2.8	0.7	0.6
U	0.7	0.6	0.8	<0.4	0.5	1.3	1.1	<0.5	<0.5	1
Ga	7.5	18.4	6	16.2	15.2	19.6	19.4	14.3	14.7	16.4
Zn	97.3	26	89.3	35.7	53.9	18.4	17.6	146.9	71.2	80.8
Cu	26.6	19.4	15.1	12.7	91.9	18.2	19.4	1778.8	4576	129.1
Ni	624.4	68.2	641.4	146.9	212.1	39.3	40.1	1013.8	1950.9	279.4
Co	99.5	17.2	89.4	37.9	52	9	7.9	93.5	89.6	64.4
Cr	1229.6	245.4	2566.4	636.2	1276.2	183.1	201.8	18623	1369.2	16810
V	159.4	58.2	169	86.6	100.8	50.8	55.6	483.1	105.3	277.3
Sc	28.1	16.4	29.9	20.8	25.4	14.7	16.1	43.6	24	24.2
Ba	32.1	102.4	2.4	154.8	108.5	207.9	220.4	90.8	90.3	78
La	2.5	1.9	4.4	3.1	5.4	12.1	11.5	11.4	2.6	4.8
Ce	<7.2	6.2	<7.4	<6.1	9	18.5	22.3	<7.3	<6.5	<6.7
Nd	3.3	9	3.3	3.9	6.8	11.2	13	11.9	<2.9	3.7
Cs	<1.7	<1.8	2	<1.7	<1.8	<1.7	<1.8	2.1	<1.8	<1.7
As	<0.5	<0.5	<0.5	0.6	<0.5	1.3	1.5	0.8	<0.6	<0.6
Sb	<1.1	<1.0	<1.1	<1.0	<1.1	<1.0	<1.0	<1.3	<1.1	<1.1
Se	<0.7	<0.6	<0.6	<0.6	<0.6	<0.5	<0.6	2.3	3.4	<0.7
Sn	<1.0	<0.9	<1.0	<0.9	<0.9	<0.8	<0.8	<1.1	<1.0	<1.0
W	<1.3	<1.0	<1.2	<1.1	<1.1	<0.9	<1.0	<1.5	<1.4	<1.3
ppb										
Os								12.9	0.88	3.08
Ir								16.5	1.18	4.25
Ru								84.6	6.39	29
Rh								42.6	5.55	8.7
Pt								668	38.2	38.9
Pd								310	90.7	22.5
Au								337	29.4	7.52

Appendix 1. Whole rock data

Borehole	RP04.23									
SAMPLE	330	338	374	384	392	396	411	433	435	441
Lithology	GBN	PYX CR	GBN	NR	GBN	GBN	GBN	GBN	CZ	HZ
SiO <sub>2</sub>	49.79	46.32	50.27	52.2	50.55	49.62	51.93	52.19	51.71	41.84
TiO <sub>2</sub>	0.28	0.61	0.15	0.19	0.25	0.24	0.25	0.12	0.11	0.06
Al <sub>2</sub> O <sub>3</sub>	13.98	14.48	14.61	13.35	12.37	12.11	10.82	6.14	5.46	3.54
Fe <sub>2</sub> O <sub>3</sub>	11.21	13.22	9.48	11.6	11.38	12.96	11.37	10.51	8.99	10.93
MnO	0.175	0.178	0.169	0.185	0.193	0.183	0.197	0.199	0.179	0.157
MgO	10.9	10.11	10.71	12.14	13.09	12.36	13.78	24.96	25.46	32.65
CaO	9.51	8.77	9.24	7.52	8.69	8.42	8.27	3.64	5.99	2.49
Na <sub>2</sub> O	1.72	1.79	1.83	1.58	1.34	1.39	1.15	0.16	-0.03	-0.03
K <sub>2</sub> O	0.265	0.34	0.645	0.496	0.709	0.453	0.51	0.564	0.011	0.056
P <sub>2</sub> O <sub>5</sub>	0.003	0.006	<0.001	0.004	0.008	0.027	0.008	0.008	<0.001	0.007
SO <sub>3</sub>	0.009	0.012	0.009	0.077	0.09	0.161	0.059	<0.002	<0.002	0.004
Cr <sub>2</sub> O <sub>3</sub>	1.37	4.633	0.145	0.164	0.34	0.422	0.233	0.208	0.511	0.256
NiO	0.068	0.092	0.044	0.096	0.121	0.339	0.076	0.13	0.088	0.214
LOI	0.17	0.39	0.51	0.38	0.46	0.79	1.09	1.18	1.29	7.4
Total	99.45	100.95	97.8	99.98	99.58	99.48	99.75	100.01	99.77	99.57
ppm										
Rb	8.3	13.6	30.2	21.5	39.2	20.2	25.6	33.3	3.4	5.5
Sr	258.5	278.7	303.1	260.3	268.3	267.7	205.8	234.9	24.2	36.8
Y	6.7	7.5	5.2	5.6	8.4	7.8	9.3	3.7	3.5	2.5
Zr	11.9	13.7	3.9	25.5	13.1	22.1	39.7	15.3	10	8.8
Nb	0.7	1.2	0.3	1.8	0.9	1.5	1.4	0.9	0.3	0.4
Mo	1.6	1.8	1.4	1.4	1.3	1.7	1.8	1	1.4	1.3
Pb	5.3	8.6	3.3	12	12.6	40.1	13.8	13.4	11.1	3.6
Th	0.8	1	<0.6	2.1	0.7	2	1.6	1.5	<0.5	<0.5
U	<0.5	0.9	0.5	0.7	<0.5	<0.5	1.1	0.7	<0.4	<0.4
Ga	15.6	18.7	15.1	12.6	13	12.8	11.9	6.1	4.3	2.9
Zn	81.6	105	64.9	82.3	78.1	81.1	78.5	100.1	89.7	77.5
Cu	312.7	278.8	242.3	577.2	788.7	4517.4	452.1	28.5	19.3	13.4
Ni	491.5	638.7	316.6	684.3	835.1	2357.8	539.1	1064.8	747.5	1882.7
Co	69.9	82.3	64.4	80.7	83.3	118	73.1	97.2	83.9	123.9
Cr	9373	31698	1048.4	1236.3	2523.9	3151.4	1923.7	1649.1	4396.8	1590.7
V	304.5	486.4	117.3	109.4	132.9	132.7	136.3	74.3	95.4	36.2
Sc	28.9	26.4	28.6	24.5	27.6	27	35.8	22.1	23.6	17
Ba	94.7	104.1	149.3	117.1	185.7	121.4	147.1	184.2	4.7	-1.2
La	5.2	6	<2.0	3.2	2.3	4	3.3	2	<1.9	1.8
Ce	<6.8	<7.2	<6.4	7.6	<6.7	7.1	8	<7.3	<6.9	<7.0
Nd	5.4	<3.1	<2.8	3.5	2.9	4.4	4.2	<2.8	3	<2.6
Cs	<1.7	<1.7	<1.7	<1.7	<1.7	<1.7	<1.7	<1.6	<1.6	<1.5
As	<0.6	<0.6	<0.5	<0.6	<0.6	<0.6	<0.6	<0.5	<0.5	<0.5
Sb	<1.2	<1.2	<1.1	<1.1	<1.1	<1.2	<1.1	<1.1	<1.0	<1.0
Se	1.4	1	<0.7	<0.7	<0.7	3.1	<0.7	<0.6	<0.6	<0.6
Sn	<1.0	<1.1	<1.0	<1.0	<1.0	<1.0	<1.0	<0.9	<0.9	<0.9
W	<1.3	<1.4	<1.2	<1.3	<1.3	<1.5	<1.3	<1.2	<1.2	<1.2
ppb										
Os		9.43		0.55	1.42	1.9	0.27			0.27
Ir		20.4		0.91	1.51	3.17	0.4			0.4
Ru		94.5		7	18.1	15.7	2.7			2.7
Rh		27.4		3.7	4.85	15.7	1.4			1.4
Pt		205		37.7	43.0	278	17.5			17.5
Pd		76.8		129	118	801	67.6			67.6
Au		9.58		21.7	26.6	142	18.8			18.8

Borehole	RP05.45								
SAMPLE	47	94	144	149	156	158	165	166	167a
Lithology	GBN	GBN	GBN	GBN	NR	GBN	PYX	CR	CR
SiO <sub>2</sub>	52.12	52.5	53.04	53.73	51.73	60.33	54.16	36.48	27.72
TiO <sub>2</sub>	0.39	0.52	0.56	0.46	0.41	0.10	0.48	0.93	0.8
Al <sub>2</sub> O <sub>3</sub>	18.17	17.53	17.2	17.53	15.17	16.67	15.19	12.77	15.22
Fe <sub>2</sub> O <sub>3</sub>	8.13	8.29	8.42	7.11	8.53	1.60	9.28	17.16	18.94
MnO	0.14	0.14	0.134	0.126	0.142	0.11	0.15	0.213	0.191
MgO	6.11	6.04	6.37	7.25	8.38	6.60	8.58	7.82	7.4
CaO	9.67	9.13	8.53	9.08	10.45	7.25	8.15	5.14	4.42
Na <sub>2</sub> O	2.62	2.78	2.27	2.24	1.86	2.08	2.12	1.44	1.23
K <sub>2</sub> O	0.731	1.036	1.161	0.691	0.702	0.38	0.792	0.627	0.425
P <sub>2</sub> O <sub>5</sub>	0.051	0.09	0.092	0.08	0.057	0.02	0.076	0.078	0.074
SO <sub>3</sub>	0.01	0.017	0.022	0.009	<0.002		0.045	0.199	0.118
Cr <sub>2</sub> O <sub>3</sub>	0.056	0.054	0.073	0.121	0.608	0.14	0.304	13.919	20.886
NiO	0.016	0.011	0.014	0.025	0.021	0.019	0.039	0.391	0.438
LOI	1.45	1.89	2.04	1.72	1.96	1.02	0.7	1.66	0.57
Total	99.65	100.04	99.92	100.17	100.02	96.33	100.06	98.82	98.43
ppm									
Rb	22.3	32.5	38.3	19.9	23.5	2.7	25.2	29.8	22.4
Sr	331.9	359.7	279.6	270.4	225.7	414.7	282.9	184.8	189.8
Y	13.9	15.9	19.4	11.7	13.4	10.1	14.6	14.3	13.4
Zr	46.6	53.2	45.7	105.7	61.8	30.8	84.7	42.5	77.2
Nb	2.7	3.7	4	3.9	3.2	1.28	4	3.4	4.7
Mo	1.7	1.5	1.5	1.4	1.7		1.7	3.8	3.3
Pb	4.4	6	8	5.8	3.6		8.2	17.6	19
Th	1.9	2.8	3.9	3.1	2.2	2.59	2.7	3.5	2.8
U	0.7	1.5	1	1.5	0.7	0.72	0.6	1.9	0.4
Ga	17.7	16.7	16.6	14.8	14.7	15.9	15.7	27.4	41.2
Zn	63.4	62.5	64	50.8	76.4	33.0	67.7	313.5	328.6
Cu	47.8	44.7	59.4	87.3	54.4	39.4	170.9	4389.1	8477.6
Ni	142.9	108	135.7	213.1	189.5	149.2	317.7	3869.3	4601.5
Co	36.4	38.5	37.4	42.2	47.7	30.1	55.5	156.6	207.7
Cr	393.3	381	565.2	876.1	4418.2	984.9	2134.2	95231	142898
V	133.8	138.8	168.2	135	211.7	70.7	154.7	746.2	1086.3
Sc	22.1	20.9	26.1	21.6	29.6	15.4	23.9	21.8	17.5
Ba	265	350.2	424.8	251.5	248.6	525.9	245.2	142.3	190.7
La	11.7	16.6	17.7	13.7	12.4	18.32	15.2	15.4	19.4
Ce	22	32.2	37.5	26	16.5	31.43	26.4	<8.8	<9.8
Nd	11	16.8	19.4	12.6	11.4	12.19	11.3	<3.4	<3.7
Cs	<1.7	<1.8	<1.7	<1.7	<1.8		<1.7	1.7	<1.6
As	<0.5	2	4.2	3.1	3.4		4.9	14	1.7
Sb	<1.1	<1.1	<1.1	<1.0	<1.1		<1.1	<1.4	<1.5
Se	<0.6	<0.6	<0.6	<0.6	<0.6		<0.6	2.8	2
Sn	<0.9	<0.9	<1.0	<0.9	<1.0		<1.0	<1.3	<1.4
W	<1.2	<1.2	<1.2	<1.1	<1.2		<1.2	<2.0	<2.4
ppb									
Os				0.38			0.29	23	58.8
Ir				0.65			1.26	33.6	104
Ru				2.52			5.34	215	744
Rh				2.59			4.43	101	193
Pt				38			29.6	642	1585
Pd				56			96.5	1013	2018
Au				8			11.3	68.9	248

Appendix 1. Whole rock data

Borehole	RP05.45									
SAMPLE	167b	167c	174	183	195	207	207.5	208	210	215
Lithology	CR	CR	PYX	GBN	GBN	GBN	PYX	NR	GBN	QTZ
SiO <sub>2</sub>	39.27	52.04	52.59	53.95	53.83	55.66	51.89	53.44	59.68	71.17
TiO <sub>2</sub>	0.61	0.42	0.34	0.47	0.57	0.49	0.3	0.43	0.42	0.23
Al <sub>2</sub> O <sub>3</sub>	13.75	20.06	16.35	15.53	15.01	14.21	8.49	10.32	14.42	12.44
Fe <sub>2</sub> O <sub>3</sub>	17.73	6.29	7.57	9.83	10.49	8.49	8.97	11.44	7.55	4.27
MnO	0.19	0.1	0.137	0.165	0.164	0.172	0.19	0.207	0.147	0.132
MgO	11.74	6.04	8.3	6.44	6.89	8.04	15.4	14.56	5.04	1.34
CaO	4.24	9.4	10.44	9.68	9.04	8.53	11.61	6.73	8.84	4.98
Na <sub>2</sub> O	1.19	2.25	2.17	2.51	2.4	1.9	0.9	1.38	0.91	1.45
K <sub>2</sub> O	0.56	0.48	0.715	0.819	1.068	0.73	0.44	0.66	0.741	0.981
P <sub>2</sub> O <sub>5</sub>	0.03	0.06	0.042	0.058	0.089	0.075	0.04	0.055	0.068	0.028
SO <sub>3</sub>			<0.002	<0.002	0.009	0.028		0.033	0.091	0.506
Cr <sub>2</sub> O <sub>3</sub>	10.97	0.07	0.092	0.049	0.079	0.066	0.13	0.397	0.021	<0.01
NiO	0.38	0.05	0.021	0.012	0.015	0.016	0.047	0.077	0.013	0.354
LOI	0.92	2.49	1.18	0.58	0.53	1.53	0.88	0.39	2.17	1.38
Total	101.21	99.71	99.95	100.09	100.18	99.94	99.24	100.11	100.12	99.26
ppm										
Rb	14.4015	7.57338	23.6	24.7	30.2	22.1	8.36960	26	29	42.3
Sr	182.7	315	302.9	332.3	289.5	256.1	125.9	176.5	211.2	279.2
Y	11.2	13.2	11.8	15.4	21.2	17	13.1	13.8	17.5	14.9
Zr	74	77.5	39	69.1	54.9	49.4	41.1	58.6	86.7	216.5
Nb			2.2	3.2	4.4	3.9		3.2	4.6	4.1
Mo			1.7	1.7	1.6	1.7		1.8	1.5	1.3
Pb			5.3	4.8	7.4	14.1		6.7	10.4	25.6
Th	3.02	2.25	1.9	2.6	3.2	3.6	1.78	3.9	5.2	10.9
U	1.03	0.71	1	0.6	1.4	1.4	0.51	2.1	1.8	1.3
Ga	26.9109	17.7783	15.4	16.9	16.8	13.5	8.90673	12.1	15.8	18
Zn	353.8	33	54.5	67.5	78.6	105.7	68.3	93.8	59.2	108.4
Cu	879.6	134.9	50.9	87.2	64.5	181.4	173.4	524.9	76.4	1417.7
Ni	3010.2	388.3	187.2	117.2	135.7	149.5	374	633.5	121.7	2456
Co	142.5	45.5	45.3	49	49.2	46.7	46	75.7	34	19.5
Cr	75151.8	495.9	703	404.1	572.8	493.1	906	2919.4	174.4	16.7
V	798.1	89.8	153.1	185.4	181.8	141.4	113.6	162.2	136.6	24.5
Sc	18.3	18.7	28.8	29.3	26	27.5	28.6	27.5	25.4	6.2
Ba	75.4	88.6	234.8	322.1	399.3	479.9	49	198.9	406.2	377.5
La	9.17	12.9	10.2	14.6	19.1	16.9	8.05	13.8	21.7	42.8
Ce	17.54	24.95	18.7	23.6	38.9	32.8	16.51	20.9	42.3	72.1
Nd	7.51	11.23	11.8	11.7	18.8	15.7	8.24	12.7	19.4	26.9
Cs			<1.7	<1.8	<1.8	<1.7		<1.7	<1.7	<1.6
As			<0.5	<0.6	0.8	1.7		1	<0.5	0.9
Sb			<1.1	<1.1	<1.1	<1.1		<1.1	<1.0	<0.9
Se			<0.6	<0.7	<0.7	<0.6		<0.7	<0.6	0.9
Sn			<0.9	<1.0	<1.0	<0.9		<1.0	0.9	<0.8
W			<1.2	<1.2	<1.3	<1.2		<1.3	<1.1	<1.1
ppb										
Os	56.2	1.66			0.43		0.16	2.21		0.68
Ir	97.5	2.51			1.11		0.36	4.67		1.36
Ru	705	18.1			1.77		1.17	22.8		6.71
Rh	178	6.51			0.64		0.93	18		20.9
Pt	1498	49.3			25		11.5	168		125
Pd	1873	115			13.4		16.9	353		635
Au	233	13.0			4.74		4.14	29.2		31.9

Appendix 1. Whole rock data

Borehole	RP05.45	RP05.45	RP05.45	MD03.1	MD03.1	MD03.1	MD03.1	MD03.1	GV05.49	GV05.49
SAMPLE	215.5	215.8	216	552	553	565	569	582	25	30a
Lithology	QTZ	QTZ	QTZ	Peg OPX	PYX	PYX	PYX	Peg PYX	NR	GBN
SiO <sub>2</sub>	56.91	71.73	48.72	53.8	54.27	53.99	53.15	50.59	52.86	52.27
TiO <sub>2</sub>	0.67	0.16	1.66	0.34	0.28	0.2	0.22	0.15	0.43	0.41
Al <sub>2</sub> O <sub>3</sub>	19.86	11.78	17.63	3.19	4.1	5.38	4.53	11.53	18.51	18.06
Fe <sub>2</sub> O <sub>3</sub>	4.33	5.75	15.77	13.54	12.42	11.69	12.7	10.04	8.02	8.58
MnO	0.14	0.16	0.2	0.219	0.219	0.213	0.212	0.179	0.13	0.17
MgO	3.84	1.68	5.69	21.13	21.59	23.35	22.29	18.18	6.1	6.65
CaO	4.82	4.96	6.41	4.51	4.83	3.77	3.46	6.22	9.78	11.61
Na <sub>2</sub> O	5.76	1.69	2.45	0.29	0.41	0.49	0.27	0.85	2.48	2.13
K <sub>2</sub> O	1.2	0.59	0.42	0.263	0.144	0.095	0.098	0.153	0.759	0.47
P <sub>2</sub> O <sub>5</sub>	0.08	0.02	0.36	0.006	0.037	0.011	0.012	0.006	0.076	0.04
SO <sub>3</sub>				0.086	0.122	0.038	0.154	0.034	0.026	
Cr <sub>2</sub> O <sub>3</sub>	0.01	0.01	0.01	0.325	0.328	0.3	0.295	1.484	0.06	0.06
NiO	0.002	0.003	0.015	0.771	0.275	0.105	0.596	0.162	0.026	0.017
LOI	2.08	1.06	0.73	1.34	0.87	0.86	1.71	0.41	0.48	0.44
Total	99.71	99.59	100.06	99.8	99.9	100.48	99.7	99.98	99.73	100.85
ppm										
Rb	19.8058	17.1366	4.11965	17.1	10.2	6.8	8.5	7.6	25	10.33
Sr	253.8	242.4	361.4	23.2	41.6	67.4	32.6	156.5	325.1	304.8
Y	57.2	16	35.1	12.8	11.1	5.7	6.8	3.6	13.2	15.8
Zr	271	176.5	235.8	46.3	31	20.1	28	12.9	47.4	52.7
Nb				2.8	1.9	1.1	2.8	0.7	2.5	
Mo				2.1	1.4	1.5	1.5	1.3	1.2	
Pb				11.1	11.2	11.1	22.6	5.8	6	
Th	27.64	12.83	2.94	2.9	1.7	1.9	1.8	0.8	1.7	
U	5.7	3.33	1.09	1.7	0.9	1	0.8	<0.5	0.6	
Ga	20.9474	18.3684	40.2182	6.4	5.3	6.6	5.7	9.8	16.8	16.55
Zn	124.8	113.3	128.8	93.1	102.3	97.8	97	79.1	59	94.8
Cu	93.7	21.2	86.3	3758.9	782.4	164.4	2984.8	657.6	155.5	178.0
Ni	16.5	26.7	118.3	5133.6	1966.2	793.3	4051.8	1117.1	183.1	129.9
Co	10	9.3	54.1	121	103.4	98.5	141.8	89	40.8	39.8
Cr	50.2	19.1	50.2	2604.5	2615.4	2409.6	2316.7	10153	407.4	414.7
V	96.2	103.3	235.1	208.7	202.1	156.5	160	152.7	116	101.7
Sc	11.5	3	28.5	33.1	31.2	25.5	25.6	22.3	20.7	29.3
Ba	146.9	132.4	147.4	50.6	43.3	35.2	17.5	44.8	269.6	54.7
La	70.27	43.78	47.08	6.8	7.4	4.1	4.8	3	16.2	9.66
Ce	134.84	63.07	94.74	8	8.3	<7.3	7.5	<7.0	24.6	19.02
Nd	51.39	22.91	42.01	7.1	6.6	3	3.1	<2.8	11.4	9.45
Cs				<1.6	<1.6	<1.5	<1.5	<1.6	<1.7	
As				7.2	6.8	5.3	12.8	2.4	3.8	
Sb				<1.2	<1.1	<1.1	<1.1	<1.1	1.1	
Se				5	1.2	0.9	3.6	0.8	<0.6	
Sn				<1.1	<1.0	<1.0	<1.0	<1.0	<1.0	
W				<1.6	<1.3	<1.2	<1.4	<1.3	<1.2	
ppb										
Os				24.35	7.71		28.71	21		
Ir				29.84	9.49		38.42	27		
Ru				177.59	62		252	218		
Rh				71.68	23.73		102.22	62.72		
Pt				994	352		1564	648		
Pd				920	367		1494	377		
Au				367	122		323	47		

Appendix 1. Whole rock data

Borehole	GV05.49	GV05.49	GV05.49	GV05.49	RP05.37	RP05.37	RP05.37	RP05.37	RP04.21
SAMPLE	30b	40	45	45b	69	71	73	127	415a
Lithology	MA	GBN	GBN	GBN	NR	PYX	GBN	GBN	PYX
SiO <sub>2</sub>	54.34	53.74	54.14	54.16	48.72	51.92	51.45	49.11	50.91
TiO <sub>2</sub>	0.45	0.41	0.34	0.51	0.17	0.36	0.14	0.16	0.08
Al <sub>2</sub> O <sub>3</sub>	19.53	17.24	19.49	16.70	17.15	6.94	14.37	20.74	20.36
Fe <sub>2</sub> O <sub>3</sub>	7.42	8.39	7.27	8.56	11.42	13.21	9.39	7.22	6.44
MnO	0.13	0.15	0.12	0.15	0.157	0.214	0.168	0.087	0.16
MgO	4.80	6.90	5.42	6.22	8.14	18.14	14.73	7.33	9.76
CaO	9.87	10.90	10.68	11.14	9.26	5.03	8.06	10.89	10.21
Na <sub>2</sub> O	1.97	2.02	2.09	1.92	1.83	0.5	1.08	1.98	1.57
K <sub>2</sub> O	0.56	0.39	0.55	0.41	0.426	0.239	0.243	0.218	0.14
P <sub>2</sub> O <sub>5</sub>	0.04	0.06	0.06	0.07	0.008	0.057	0.012	0.013	0.00
SO <sub>3</sub>					0.285	0.255	0.036	0.069	
Cr <sub>2</sub> O <sub>3</sub>	0.03	0.04	0.04	0.05	0.073	0.2	0.245	0.085	0.15
NiO	0.01	0.01	0.01	0.01	0.639	0.658	0.112	0.729	0.03
LOI	1.00	0.30	0.48	0.32	0.63	1.91	0.38	1.11	0.39
Total	100.10	100.50	100.65	100.16	98.91	99.63	100.42	99.76	100.00
ppm									
Rb	11.467	7.7222	11.570	6.9550	14.9	13.5	10.1	5.5	2.2417
Sr	349.8	301.9	339.3	294.0	247.7	59.9	191.9	330.1	244.7
Y	11.7	15.7	13.4	19.9	6	12.5	4.8	5	3.4
Zr	91.6	66.4	69.7	79.2	19.6	69.4	20.1	18.8	19.4
Nb					1	3.1	0.9	1.1	
Mo					1.4	1.7	1.5	1.5	
Pb					23.6	4.8	1.7	6.8	
Th					1.5	4	<0.6	<0.6	
U					0.8	1.2	<0.5	<0.5	
Ga	17.302	16.094	17.072	16.548	15.9	8.5	10.9	15.9	13.980
Zn	36.8	67.4	34.1	59.4	72	78.4	64.3	36.1	38.0
Cu	43.0	87.3	29.7	43.8	7218.3	995.3	233	3542.9	33.6
Ni	113.1	145.6	89.3	125.7	4409.3	4183.1	743.1	4384.1	241.9
Co	28.1	36.8	30.0	38.5	98.6	144.8	71.8	79.1	33.5
Cr	266.3	325.3	327.0	360.7	505.5	1609.7	1921.8	612	524.5
V	95.5	109.3	97.2	140.0	84.8	176.9	119.3	60.6	88.2
Sc	18.0	28.5	20.6	33.7	19.6	32.4	22.7	16.8	16.5
Ba	97.1	68.2	71.1	64.0	121.4	44.4	68.7	91.3	13.9
La	13.59	12.26	13.10	14.71	3.5	9.7	4.5	6.4	1.91
Ce	25.16	23.85	24.93	29.75	9.1	20.5	<6.6	<6.0	3.12
Nd	10.16	11.30	11.12	14.65	4.1	7.8	3	4	1.28
Cs					<1.7	<1.6	<1.6	<1.7	
As					<0.6	1.3	<0.5	<0.5	
Sb					<1.2	<1.1	<1.1	1.5	
Se					6	2	<0.6	7	
Sn					<1.1	<1.1	<1.0	<1.0	
W					<1.5	<1.5	<1.2	<1.4	
ppb									
Os					8.26	5.79		19	
Ir					8.78	7.24		23	
Ru					47	34		142	
Rh					76	55		124	
Pt					665	473		1148	
Pd					3167	3188		1962	
Au					267	41		304	

Appendix 1. Whole rock data

Borehole	RP04.21	GV05.50							
SAMPLE	415b	418	448	538	681	693	690a	690b	342
Lithology	GBN	PYX	Ma	MA	Ma	NR	GBN	GBN	GBN
SiO <sub>2</sub>	51.79	50.92	49.77	50.72	50.49	50.23	45.95	40.57	53.84
TiO <sub>2</sub>	0.15	0.11	0.11	0.17	0.19	0.21	0.17	0.07	0.11
Al <sub>2</sub> O <sub>3</sub>	22.49	23.25	25.87	23.17	18	24.26	18.48	22.8	23.47
Fe <sub>2</sub> O <sub>3</sub>	5.35	4.89	3.51	1.67	8.8	5.28	9.78	12.6	1.61
MnO	0.12	0.106	0.057	0.08	0.119	0.082	0.12	0.06	0.05
MgO	6.57	5.78	3.79	4.04	9.37	3.6	9.86	3.05	2.38
CaO	11.76	11.32	13.92	12.55	9.58	11.6	11.63	14.36	10.35
Na <sub>2</sub> O	1.83	2.35	2.32	2.40	1.84	2.36	1.53	1.56	3.07
K <sub>2</sub> O	0.32	0.613	0.433	0.47	0.202	0.89	0.23	0.8	1.13
P <sub>2</sub> O <sub>5</sub>	0.01	0.006	0.007	0.06	0.008	0.025	0.01	0.01	0.01
SO <sub>3</sub>		0.015	0.082		0.177	0.091			
Cr <sub>2</sub> O <sub>3</sub>	0.045	0.044	0.074	0.02	0.108	0.027	0.13	0.08	0.02
NiO	0.02	0.029	0.146	0.009	0.293	0.133	0.13	0.08	0.0008
LOI	0.58	0.73	1.06	0.80	0.75	1.08	1.26	2.82	2.10
Total	100.99	100.17	101.16	96.17	99.93	99.88	99.16	98.79	98.14
ppm									
Rb	7.4555	25.8	39	14.7	12.2	6.3	4.5552	19.864	65.6
Sr	295.0	313.3	366.4	330.4	387.8	272.5	294.6	269.3	389.8
Y	7.4	3.4	7.4	9.2	4.5	5.7	7.4	4.8	4.2
Zr	35.4	12.2	30.8	32.5	11.5	19.7	51.4	19.2	20.6
Nb		0.7	2	1.03	0.6	1.5			0.92
Mo		0.9	1.2		1	1.4			
Pb		6.1	10.9		20.2	6.9			
Th		<0.5	1.6	1.39	<0.5	<0.5	0.78	0.03	1.23
U		0.7	1.1	0.36	0.6	<0.5	0.27	0.07	0.38
Ga	16.5483	16.4	18.7	17.4	17.9	14.3			16.7
Zn	24.2	36.1	58.6	61.0	26.5	60.7	104.2	72	52.5
Cu	71.9	133.9	845.3	62.5	584.6	894.2	796.8	2584.8	214.6
Ni	161.8	217.8	916.8	73.2	904.4	1876.6	2973.5	4847.5	6.6
Co	24.9	30.4	40.4	26.9	29.9	90.8	115.9	232.6	14.2
Cr	339.6	305.3	216	165.5	450	859.3	896.6	518.4	160.0
V	92.9	55	98.4	100.3	52.9	106.2	86.7	96.5	86.3
Sc	17.0	15.5	18	16.1	14.5	20.7	20.7	13	10.1
Ba	30.2	122.9	233.9	159.3	132.4	86.2	34	82.8	324.5
La	5.25	6	9.4	8.37	3.8	7	4.29	2.77	8.15
Ce	9.77	<5.9	19.6	16.30	<5.7	<6.5	8.64	4.93	13.97
Nd	4.55	4.7	12.3	7.51	5.8	4.2	4.16	2.22	5.15
Cs		<1.7	<1.8		<1.6	<1.8			
As		<0.5	1.6		<0.5	<0.5			
Sb		<1.0	<1.0		<1.0	<1.1			
Se		<0.6	0.8		1.2	1.8			
Sn		<0.9	<0.9		<0.9	<1.0			
W		<1.0	<1.1		<1.1	<1.2			
ppb									
Os			4.17		4	8.54	9.68	2.86	
Ir			5.44		4	11	12	3.46	
Ru			22		29	74	117	31.6	
Rh			38		15	37	32	11	
Pt			339		148	371	253	120	
Pd			724		326	677	1030	334	
Au			42		43	56	88.3	62	

## Major element results for international reference material

Reference Material	SiO <sub>2</sub> wt%	TiO <sub>2</sub> wt%	Al <sub>2</sub> O <sub>3</sub> wt%	Fe <sub>2</sub> O <sub>3</sub> wt%	MnO wt%	MgO wt%	CaO wt%	Na <sub>2</sub> O wt%	K <sub>2</sub> O wt%	P <sub>2</sub> O <sub>5</sub> wt%	SO <sub>3</sub> wt%
BH-1	68.62	0.41	14.58	5.78	0.13	2.63	3.56	3.86	0.85	0.08	0.12
BH-1	68.76	0.4	14.52	5.7	0.13	2.62	3.56	3.83	0.85	0.08	0.1
BH-1	68.44	0.41	14.43	5.73	0.13	2.65	3.51	3.73	0.93	0.07	0.08
Average	68.61	0.4	14.51	5.74	0.13	2.64	3.54	3.81	0.88	0.07	0.1
Stdv	0.16	0	0.07	0.04	0	0.01	0.03	0.07	0.04	0.01	0.02
Rstdv	0.23	0	0.48	0.7	0	0.38	0.85	1.84	4.55	14.29	20
BH-1 cert	68.07	0.43	14.35	5.81	0.14	2.50	3.53	3.94	0.87	0.07	
accuracy	0.79	-7.83	1.10	-1.15	-4.00	5.46	0.31	-3.29	1.03	1.84	
WS-1	51.50	2.53	13.97	13.60	0.18	5.29	8.80	2.82	1.30	0.31	0.10
WS-1	51.46	2.52	13.92	13.40	0.18	5.29	8.79	2.83	1.31	0.31	0.10
WS-1	51.15	2.50	13.86	13.51	0.18	5.23	8.74	2.78	1.34	0.30	0.05
Average	51.37	2.52	13.91	13.50	0.18	5.27	8.78	2.81	1.32	0.30	0.08
Stdv	0.19	0.01	0.06	0.10	0.00	0.03	0.03	0.02	0.02	0.01	0.03
Rstdv	0.37	0.40	0.43	0.74	0.00	0.57	0.34	0.71	1.52	3.33	37.50
WS-1 cert	51.31	2.54	14.04	13.51	0.18	5.31	8.87	3.10	1.36	0.30	
accuracy	0.11	-0.63	-0.91	-0.11	-0.07	-0.81	-0.97	-9.34	-3.19	-1.61	
BCS375	67.42	0.38	20.29	0.11	0.00	0.06	0.83	10.72	0.77	0.03	0.09
BCS375	67.36	0.38	20.24	0.10	0.00	0.05	0.83	10.68	0.77	0.03	0.10
BCS375	67.07	0.37	20.09	0.10	0.00	0.02	0.85	10.42	0.77	0.02	0.04
Average	67.28	0.38	20.21	0.10	0.00	0.04	0.84	10.61	0.77	0.03	0.08
Stdv	0.19	0.01	0.10	0.00	0.00	0.02	0.01	0.16	0.00	0.01	0.03
Rstdv	0.28	2.63	0.49	0.00		50.00	1.19	1.51	0.00	33.33	37.50
BCS375-cert	67.10	0.38	19.80	0.12	0.00	0.50	0.89	10.40	0.79		
accuracy	0.27	0.00	2.07	-16.67		-92.00	-5.62	2.02	-2.53		
MRG-1	39.27	3.86	8.47	18.15	0.17	13.33	14.92	0.75	0.21	0.07	0.18
MRG-1	39.31	3.85	8.47	18.16	0.17	13.52	15.04	0.72	0.21	0.05	0.15
MRG-1	39.31	3.84	8.46	17.89	0.17	13.33	14.89	0.73	0.21	0.07	0.18
Average	39.29	3.85	8.47	18.07	0.17	13.39	14.95	0.74	0.21	0.06	0.17
Stdv	0.02	0.01	0.01	0.15	0.00	0.11	0.08	0.02	0.00	0.01	0.02
Rstdv	0.05	0.26	0.12	0.83	0.00	0.82	0.54	2.70	0.00	16.67	11.76
MRG-1-cert	39.59	3.82	8.57	18.16	0.17	13.72	14.90	0.75	0.18	0.08	
accuracy	0.77	-0.82	1.15	0.50	1.27	2.44	-0.34	1.27	-15.18	25.95	
NIM-D	38.54	0.02	0.18	16.99	0.22	43.07	0.26	-0.06	0.00	0.00	0.01
NIM-D	38.55	0.02	0.19	17.04	0.22	43.05	0.27	-0.07	0.00	0.00	0.02
NIM-D	38.57	0.02	0.19	17.00	0.21	43.06	0.26	-0.07	0.00	0.00	0.02
Average	38.55	0.02	0.19	17.01	0.22	43.06	0.27	-0.06	0.00	0.00	0.02
Stdv	0.02	0.00	0.01	0.03	0.00	0.01	0.00	0.00	0.00	0.00	0.00
Rstdv	0.05	0.00	5.26	0.18	0.00	0.02	0.00	0.00			0.00
NIM-D-cert	38.60	0.02	0.30	16.80	0.22	43.11	0.28	0.04			
accuracy	-0.13	0.94	-36.07	1.23	0.94	-0.11	-2.67				

\*high relative standard deviations are indicative of larger errors.

## Trace element results for international reference material

Reference Material	Ga	Zn	Cu	Ni	Co	Cr	V	Sc	Ba	La	Ce	Nd	Cs
	ppm	ppm	ppm	ppm	ppm	ppm	ppm	ppm	ppm	ppm	ppm	ppm	ppm
NIM-G	27.22	53.12	22.39	6.64	0.25	11.90	0.51	1.06	102.78	111.51	202.25	76.74	6.86
	27.72	52.31	16.32	6.41	0.52	13.77	0.08	0.93	107.04	111.59	204.68	77.02	6.18
	28.38	54.08	16.26	7.30	1.57	11.73	0.33	0.73	109.97	108.66	204.56	76.35	4.43
Average	27.77	53.17	18.32	6.78	0.78	12.47	0.30	0.91	106.60	110.58	203.83	76.70	5.82
Stdv	0.58	0.89	3.52	0.46	0.69	1.13	0.22	0.17	3.62	1.67	1.37	0.33	1.25
Rstdv	2.09	1.67	19.21	6.78	88.46	9.06	73.33	18.68	3.40	1.51	0.67	0.43	21.48
NIM-G-cert	27.00	50.00	12.00	8.00	4.00	12.00	2.00	1.00	120.00	109.00	195.00	72.00	1.00
accuracy	2.85	6.34	52.67	-15.25	-80.50	3.92	-85.00	-9.00	-11.17	1.45	4.53	6.53	482.00
MRG-1	17.48	217.69	145.54	195.32	84.67	465.31	549.56	58.27	51.85	8.67	36.02	17.82	3.15
	17.71	214.90	139.32	196.12	85.30	461.81	549.47	57.99	51.53	6.74	33.21	20.50	2.42
	17.68	214.31	137.61	194.51	82.00	459.02	538.86	57.84	51.85	9.12	34.02	18.61	3.19
Average	17.62	215.63	140.82	195.32	83.99	462.05	545.97	58.03	51.75	8.17	34.42	18.98	2.92
Stdv	0.13	1.81	4.17	0.81	1.75	3.16	6.15	0.22	0.18	1.27	1.45	1.38	0.43
Rstdv	0.74	0.84	2.96	0.41	2.08	0.68	1.13	0.38	0.35	15.54	4.21	7.27	14.73
MRG-1-cert	17.00	191.00	134.00	193.00	87.00	430.00	526.00	55.00	61.00	9.80	28.00	19.20	0.57
accuracy	3.65	12.90	5.09	1.20	-3.46	7.45	3.80	5.51	-15.16	-16.63	22.93	-1.15	412.28
BE-N	17.15	118.95	82.96	275.37	59.16	335.08	232.81	25.72	1119.74	81.56	152.78	66.79	-1.25
	16.75	115.93	77.74	276.19	61.19	339.97	234.49	26.43	1121.87	79.72	152.78	68.53	0.03
	16.97	118.81	75.73	274.64	62.01	358.11	239.04	25.71	1151.23	87.37	152.85	67.31	1.13
Average	16.96	117.90	78.81	275.40	60.79	344.39	235.45	25.95	1130.94	82.88	152.80	67.54	-0.03
Stdv	0.20	1.70	3.73	0.78	1.47	12.13	3.23	0.41	17.60	4.00	0.04	0.90	1.19
Rstdv	1.18	1.44	4.73	0.28	2.42	3.52	1.37	1.58	1.56	4.83	0.03	1.33	-3966.67
BE-N-cert	17.00	120.00	72.00	267.00	60.00	360.00	235.00	22.00	1025.00	82.00	152.00	70.00	0.80
accuracy	-0.24	-1.75	9.46	3.15	1.32	-4.34	0.19	17.95	10.34	1.07	0.53	-3.51	-103.75

Trace element results for international reference material (cont.)

Reference Material	As	Pb	Sb	Se	Sn	W	Zn	Rb	Sr	Y	Zr	Nb	Mo	Pb	Th	U
	ppm	ppm	ppm	ppm	ppm	ppm	ppm	ppm	ppm	ppm	ppm	ppm	ppm	ppm	ppm	ppm
NIM-G	12.83	38.72	1.36	-0.73	5.57	7.55	53.89	318.65	13.04	143.68	285.59	55.90	0.99	38.04	51.66	16.07
	13.05	38.43	1.10	0.03	6.94	6.05	54.04	319.29	13.01	143.82	284.28	55.75	1.31	37.73	51.18	16.50
	13.83	38.91	0.28	-0.13	4.45	6.89	56.08	319.55	13.54	144.29	284.17	55.97	1.10	37.94	51.80	15.90
Average	13.24	38.69	0.91	-0.28	5.66	6.83	54.67	319.16	13.20	143.93	284.68	55.87	1.13	37.90	51.55	16.15
Stdv	0.53	0.24	0.56	0.40	1.25	0.75	1.23	0.46	0.30	0.32	0.79	0.11	0.17	0.16	0.33	0.31
Rstdv	4.00	0.62	61.54	-142.86	22.08	10.98	2.25	0.14	2.27	0.22	0.28	0.20	15.04	0.42	0.64	1.92
NIM-G-cert accuracy	15.00	40.00	0.60		4.00		50.00	320.00	10.00	143.00	300.00	53.00	3.00		51.00	15.00
	-11.73	-3.28	51.67		41.50		9.34	-0.26	32.00	0.65	-5.11	5.42	-62.33		1.08	7.67
MRG-1	1.38	4.13	-0.06	-0.21	2.79	-2.66	222.77	8.48	273.84	14.27	110.99	21.31	2.76	4.43	0.56	-0.20
	0.76	4.82	2.22	-0.11	4.97	-1.14	227.52	8.95	274.88	14.30	112.31	21.50	2.56	6.47	-0.12	0.66
	1.28	3.62	-0.53	-0.30	2.98	-1.21	224.74	8.68	275.19	14.31	112.62	21.50	3.05	6.53	1.23	0.89
Average	1.14	4.19	0.54	-0.21	3.58	-1.67	225.01	8.70	274.64	14.29	111.97	21.44	2.79	5.81	0.56	0.45
Stdv	0.33	0.61	1.47	0.10	1.21	0.86	2.38	0.24	0.71	0.02	0.87	0.11	0.24	1.19	0.67	0.57
Rstdv	28.95	14.56	272.22	-47.62	33.80	-51.50	1.06	2.76	0.26	0.14	0.78	0.51	8.60	20.48	119.64	126.67
MRG-1-cert accuracy	0.73	10.00	0.86	0.19	3.62	0.30	191.00	8.50	266.00	14.00	108.00	20.00	0.87		0.93	0.24
	56.16	-58.10	-37.21	-208.25		-656.67	17.81	2.35	3.25	2.07	3.68	7.20	220.69		-39.78	87.50
BE-N	4.71	-0.78	0.52	-0.64	0.58	28.12	121.82	44.70	1374.07	29.38	266.36	112.73	1.98	3.93	10.87	2.14
	3.95	0.54	-1.28	0.01	0.99	26.63	122.27	44.62	1375.68	29.88	268.74	112.55	2.19	4.00	10.41	2.39
	4.99	-1.81	-2.37	0.22	-0.22	27.56	122.88	44.73	1376.59	29.80	268.48	112.67	1.78	4.02	10.42	2.40
Average	4.55	-0.68	-1.05	-0.14	0.45	27.44	122.32	44.68	1375.45	29.69	267.86	112.65	1.99	3.98	10.57	2.31
Stdv	0.54	1.18	1.46	0.45	0.62	0.75	0.53	0.06	1.27	0.27	1.30	0.09	0.21	0.05	0.26	0.15
Rstdv	11.87	-173.53	-139.05	-321.43	137.78	2.73	0.43	0.13	0.09	0.91	0.49	0.08	10.55	1.26	2.46	6.49
BE-N-cert accuracy	1.80	4.00	0.26		2.00	29.00	120.00	47.00	1370.00	30.00	265.00	100.00	2.60		10.40	2.40
	152.78	-117.00	-503.85		-77.50	-5.38	1.93	-4.94	0.40	-1.03	1.08	12.65	-23.46		1.63	-3.75
N1007	17.68	17.35	1.16	9.31	2.83	1.59	120.38									
	17.39	16.99	0.35	9.57	3.29	1.75	119.62									
Average	17.54	17.17	0.75	9.44	3.06	1.67	120.00									
Stdv	0.21	0.26	0.57	0.18	0.32	0.12	0.54									
Rstdv	1.20	1.51	76.00	1.91	10.46	7.19	0.45									

## PGE standards

	<b>Os</b>	<b>Ir</b>	<b>Ru</b>	<b>Rh</b>	<b>Pt</b>	<b>Pd</b>	<b>Au</b>
	ppb	ppb	ppb	ppb	ppb	ppb	ppb
TDB1	0.1	0.11	0.23	0.56	5.33	25	7.25
TDB1	0.15	0.23	0.59	0.62	3.62	12.3	3.39
TDB1 avg	0.125	0.17	0.41	0.59	4.475	18.65	5.32
TDB1 cert	0.1	0.15	0.3	0.7	5.8 +/- 1.1	22.4 +/- 1.4	6.3 +/- 1.0
<i>Stdv</i>	<i>0.04</i>	<i>0.08</i>	<i>0.25</i>	<i>0.04</i>	<i>1.21</i>	<i>8.98</i>	<i>2.73</i>
<i>Rstdv %</i>	<i>32</i>	<i>47.1</i>	<i>61</i>	<i>6.8</i>	<i>27</i>	<i>48.2</i>	<i>51.3</i>
<i>Accuracy</i>	<i>25</i>	<i>13.33</i>	<i>36.67</i>	<i>-15.71</i>	<i>-22.84</i>	<i>-16.74</i>	<i>-15.56</i>
WMG1	22.3	50	33.5	24.8	753	367	96.7
WMG1	21.7	47.8	33.2	24.8	761	389	92.8
WMG1 avg	22	48.9	33.35	24.8	757	378	94.75
WMG1 cert	24	46	35	26	731	382	110
<i>Stdv</i>	<i>0.42</i>	<i>1.56</i>	<i>0.21</i>	<i>0</i>	<i>5.66</i>	<i>15.56</i>	<i>2.76</i>
<i>Rstdv %</i>	<i>1.9</i>	<i>3.2</i>	<i>0.6</i>	<i>0</i>	<i>0.7</i>	<i>4.1</i>	<i>2.9</i>
<i>Accuracy</i>	<i>-8.33</i>	<i>6.30</i>	<i>-4.71</i>	<i>-4.62</i>	<i>3.56</i>	<i>-1.05</i>	<i>-13.86</i>

## Duplicates

	<b>Os</b>	<b>Ir</b>	<b>Ru</b>	<b>Rh</b>	<b>Pt</b>	<b>Pd</b>	<b>Au</b>
RP04.23/305	0.88	1.18	6.39	5.55	38.2	90.7	29.4
RP04.23/305B	0.70	1.07	6.55	5.30	41.3	81.1	28.7
<i>Stdv</i>	<i>0.13</i>	<i>0.08</i>	<i>0.12</i>	<i>0.18</i>	<i>2.23</i>	<i>6.84</i>	<i>0.50</i>
RP04.23/392	1.42	1.51	18.1	4.85	43.0	118	26.6
RP04.23/392B	1.49	1.60	19.2	4.65	40.2	117	22.7
<i>Stdv</i>	<i>0.05</i>	<i>0.07</i>	<i>0.74</i>	<i>0.14</i>	<i>1.98</i>	<i>0.44</i>	<i>2.75</i>
RP04.23/396	1.90	3.17	15.7	15.7	278	801	142
RP04.23/396B	1.82	3.02	15.9	15.3	188	804	109
<i>Stdv</i>	<i>0.06</i>	<i>0.11</i>	<i>0.15</i>	<i>0.27</i>	<i>63.37</i>	<i>2.11</i>	<i>23.40</i>

Sulfur content – determined using LECO. The methodology of this technique is provided in Chapter 4.

Borehole	Sample depth	S wt%	Mean	STDEV	RSTDEV %	S ppm
<b>RP05.45</b>	146	0.1180	0.1227	0.0072	5.9	1227
		0.1190				
	156	0.1310	0.0450	0.0014	3.0	450
		0.0434				
	165	0.0459	0.1353	0.0097	7.2	1353
		0.0456				
	166	0.1270	1.0267	0.0289	2.8	10267
		0.1330				
	167a	0.1460	0.7350	0.0092	1.2	7350
		1.0100				
	167b	1.0600	0.3203	0.0038	1.2	3203
		0.7430				
	167c	0.7250	0.1880	0.0101	5.4	1880
		0.7370				
	174	0.3160	0.0446	0.0055	12.3	446
		0.3230				
	195	0.3220	0.0518	0.0024	4.7	518
		0.1990				
	205	0.1860	0.3737	0.0091	2.4	3737
		0.1790				
	208	0.0392	0.0798	0.0022	2.8	798
		0.0502				
	207	0.0444	0.0303	0.0010	3.3	303
		0.0505				
	214	0.0546	3.3400	0.0917	2.7	33400
		0.0503				
	215a	0.3750	0.4280	0.0095	2.2	4280
		0.3640				
	215b	0.3820	0.0270	0.0055	20.5	270
		0.0772				
	215c	0.0811	0.0296	0.0034	11.5	296
		0.0810				
	215d	0.0300	0.0210	0.0016	7.4	210
0.0295						
<b>RP04.23</b>	53	0.0314	0.0222	0.0014	6.2	222
		3.2600				
	63	3.3200	0.0309	0.0025	8.1	309
		3.4400				
	144	0.4170	2.1083	3.7	21083	
		0.4330				
	157	0.4340	0.8060	0.0098	1.2	8060
		0.0327				
	158	0.0265	0.2163	0.0110	5.1	2163
		0.0217				
	162	0.0332	0.0355	0.0012	3.5	355
		0.0290				
	201	0.0265	0.0842	0.0015	1.8	842
		0.0192				
	268	0.0192	0.0241	0.0045	18.5	241
		0.0216				
			0.0221			

		0.0284				
295		0.0388				
		0.0383	0.0419	0.0058	13.7	419
		0.0485				
300		0.2640				
		0.2680	0.2657	0.0021	0.8	2657
		0.2650				
305		0.7500				
		0.7500	0.7508	0.0038	0.5	7508
		0.7470				
		0.7560				
307		0.0471				
		0.0487	0.0474	0.0012	2.5	474
		0.0464				
315		0.0246				
		0.0342	0.0317	0.0062	19.7	317
		0.0363				
330		0.1900				
		0.2020	0.1987	0.0076	3.8	1987
		0.2040				
338		0.2770				
		0.3090	0.2923	0.0160	5.5	2923
		0.2910				
374		0.0939				
		0.1200	0.1157	0.0246	21.3	1157
		0.1490				
		0.1000				
384		0.3950				
		0.4070	0.4063	0.0110	2.7	4063
		0.4170				
392		0.5090				
		0.5200	0.5123	0.0067	1.3	5123
		0.5080				
396		1.6700				
		1.5700	1.5933	0.0681	4.3	15933
		1.5400				
411		0.4410				
		0.4300	0.4337	0.0064	1.5	4337
		0.4300				
441		0.0564				
		0.0644	0.0628	0.0058	9.2	628
		0.0676				
<b>RP04.21</b>	415	0.0160				
		0.0189	0.0173	0.0015	8.6	173
		0.0169				
	415	0.0308				
		0.0279	0.0270	0.0043	15.8	270
		0.0224				
	448*		0.3786		1.3	3786
	681*		0.3676		2.4	3676
	690a	1.8100				
		1.3800	1.6500	0.2352	14.3	16500
		1.7600				
	690b					
		5.1600	5.1667	0.058	0.1	52525
		5.1700				
		5.1700				
	693*		0.8076		1.8	8076
<b>GV05.49</b>	30	0.0048				
		0.0114				
		0.0078	0.0125	0.0095	75.7	125
		0.0262				
	30	0.0077				
		0.0238				
		0.0251	0.0240	0.0010	4.0	240
		0.0232				
	35	0.0263	0.0228	0.0064	27.8	228
		0.0155				
		0.0267				
	45	0.0259				
		0.0253	0.0259	0.0006	2.3	259
		0.0264				
	45	0.0283				
		0.0307	0.0294	0.0012	4.1	294
		0.0293				
	127a*		0.0395		7.3	395
	127b*		0.1714		2.1	1714

	128*		0.1634		1.7	1634
<b>RP05.37</b>	69*		1.5014		7.7	15014
	71*		0.5491		2.2	5491
	127*		1.6620		1.7	16620
<b>GV02.1</b>	154*		1.2360		2.4	12360
	166*		1.4684		3.1	14684
	206*		0.5562		2.3	5562
	476*		1.8560		2.8	18560
	487*		1.0500		1.2	10500
	504*		0.5790		1.2	5790
<b>GV02.2</b>	476*		0.7520		0.6	7520
	477*		1.5797		0.2	15797
	478*		0.2272		0.8	2272
	479*		0.3089		1.7	3089
	480*		0.2601		2.4	2601
<b>MD03.1</b>	552*		0.9967		3.4	9967
	553*		0.2054		0.9	2054
	542	5.8100				
		5.2500	5.5833	0.2948	5.3	55833
		5.6900				
	569*		0.7186		1.0	7186
	582*		0.2501		2.5	2501

Relative and standard deviations of samples marked with \* are derived from triplicate runs of each sample

Limit of detection	(3x std dev on blank)	0.018
Limit of determination	(10 x std dev on blank)	0.059
Not detected	<0.018	
Less than limit of determination	>0.018 <0.06	

Whole rock semi-metals and trace elements analysed at ALS global using Aqua Regia digest followed by ICP-MS and ICP-AES. See Chapter 5.

		RP05.45	RP04.23	RP04.23	RP04.23	RP04.23							
		146	146	165	167	205	208	215	214	144	157	201	300
Ag	ppm	0.21	0.18	0.11	1.84	0.86	0.31	0.43	2.18	0.89	0.72	0.14	0.59
Al	%	4.3	4.24	3.5	2.27	1.47	2.19	2.93	2.56	5.79	9.95	11.65	2.48
As	ppm	2.4	3.1	2.5	1.4	4.4	0.7	1.2	13.4	2.8	2.2	0.3	0.7
Au	ppm	<0.2	<0.2	<0.2	0.3	<0.2	<0.2	<0.2	0.3	<0.2	<0.2	<0.2	0.2
B	ppm	<10	<10	<10	<10	<10	<10	<10	<10	<10	<10	<10	<10
Ba	ppm	80	80	40	40	20	30	110	70	80	150	60	40
Be	ppm	0.22	0.2	0.22	0.21	0.09	0.15	1.2	1.39	0.24	0.23	0.18	0.14
Bi	ppm	0.14	0.15	0.09	1.36	0.7	0.2	0.44	1.32	0.92	0.6	0.07	0.62
Ca	%	2.02	1.95	2.03	1.21	0.98	1.17	2.06	2.02	3.47	5.6	7.28	1.22
Cd	ppm	0.04	0.04	0.04	0.31	0.17	0.04	0.12	0.4	0.08	0.09	0.04	0.18
Ce	ppm	12.85	11.85	15.55	13.8	9.85	12.75	51.5	37.8	3.5	4.61	3.14	11.05
Co	ppm	42	42.9	22.7	82	35.5	17.4	26.2	179	141.5	66.9	7.3	44
Cr	ppm	365	365	249	618	169	255	13	18	2	62	26	519
Cs	ppm	1.14	1.1	0.73	1.26	0.72	1.13	0.8	0.88	0.54	0.3	0.36	0.63
Cu	ppm	260	260	201	3430	747	546	1460	8750	2650	2370	167.5	1480
Fe	%	3.88	3.88	1.81	1.71	1.65	1.22	2.33	3.81	2.91	2.96	0.45	2.52
Ga	ppm	8.33	8.17	6.31	3.34	3.06	4.23	9.99	8.64	8.75	14.2	16.3	5.15
Ge	ppm	<0.05	0.07	0.06	0.08	0.07	0.05	0.13	0.11	0.06	0.07	<0.05	0.06
Hf	ppm	0.06	0.06	0.08	0.13	0.12	0.08	0.09	0.13	0.02	0.04	<0.02	0.08
Hg	ppm	<0.01	0.01	<0.01	<0.01	0.22	<0.01	<0.01	0.07	<0.01	<0.01	<0.01	<0.01
In	ppm	0.009	0.013	<0.005	0.037	0.005	0.005	0.015	0.075	0.029	0.022	<0.005	0.02
K	%	0.1	0.1	0.17	0.12	0.07	0.22	0.09	0.14	0.07	0.1	0.14	0.14
La	ppm	6.3	5.9	7.9	6.2	5.9	6.9	26.1	20.7	1.9	2.6	1.8	5.5
Li	ppm	21.3	21.3	8.4	11.7	8.9	8.3	10.9	13.8	24.9	29.8	11.2	28.5
Mg	%	2.66	2.67	0.99	1.34	1.16	1.01	0.61	0.67	0.4	1	0.22	1.71
Mn	ppm	474	474	155	121	170	149	530	767	191	298	55	273
Mo	ppm	0.32	0.36	0.4	0.33	0.28	0.19	0.34	0.9	0.49	0.23	0.05	0.56
Na	%	0.46	0.44	0.48	0.23	0.18	0.31	0.21	0.12	0.72	1.18	1.38	0.3
Nb	ppm	<0.05	<0.05	0.09	0.17	0.1	0.1	0.34	0.34	<0.05	<0.05	0.05	0.05
Ni	ppm	356	358	184	2920	1020	223	2560	>10000	4820	2470	253	628
P	ppm	320	310	360	260	250	270	140	120	50	30	30	300
Pb	ppm	3.9	4.1	5.6	12.9	4.4	4.1	25	32.9	15.1	11.5	39.6	21.7
Rb	ppm	5.6	5.5	9.6	8.4	4.4	15.7	4.9	8.6	1.9	1.5	3.2	9.9
Re	ppm	0.001	0.001	<0.001	0.008	0.002	0.001	0.002	0.023	0.01	0.009	<0.001	0.002
S	%	0.09	0.1	0.14	0.81	0.41	0.06	0.45	3.21	2.14	0.89	0.06	0.28
Sb	ppm	<0.05	0.08	0.1	0.47	0.16	0.23	0.25	0.66	1.3	0.4	0.05	0.33
Sc	ppm	2.1	2	1.9	3.2	1.8	1.6	2	2.4	0.2	4.4	0.4	3.2
Se	ppm	0.3	0.4	0.2	2.1	2.5	0.5	1.2	8.3	6.1	3	<0.2	1.5
Sn	ppm	0.3	0.3	0.5	0.4	0.3	0.3	0.8	0.8	0.6	0.3	0.6	0.3
Sr	ppm	114.5	111	100.5	47.4	29.7	60.4	75.2	55.2	150	227	348	62.7
Ta	ppm	<0.01	<0.01	<0.01	<0.01	<0.01	<0.01	<0.01	0.01	<0.01	<0.01	<0.01	<0.01
Te	ppm	0.04	0.03	0.07	0.48	1.22	0.06	0.08	0.54	0.7	0.25	0.04	0.73
Th	ppm	2.3	2.1	2.6	3	1.9	2.9	10.8	9.4	0.3	0.3	0.2	1.8
Ti	%	0.08	0.076	0.099	0.062	0.071	0.096	0.044	0.046	0.009	0.028	0.007	0.074
Tl	ppm	0.03	0.03	0.05	0.16	0.06	0.1	0.04	0.08	0.22	0.12	0.07	0.24
U	ppm	0.61	0.51	0.64	0.48	0.52	1.09	1.18	1.26	0.06	0.06	0.05	0.4
V	ppm	54	54	50	18	23	29	18	25	5	33	4	31
W	ppm	0.14	0.12	0.19	0.05	0.24	0.18	2.55	1.35	0.07	0.05	<0.05	0.25
Y	ppm	3.41	3.23	3.03	5.19	1.61	1.52	6.91	6.09	0.48	1.16	0.31	3.15
Zn	ppm	39	40	12	3	32	12	103	294	24	30	9	19
Zr	ppm	1.9	1.8	2	2.9	3.7	2.5	2.2	3.5	0.8	1.1	0.7	2.2

Appendix 1. Whole rock data

		RP04.23	RP04.23	RP04.23	RP04.23	RP04.23	GV02.1	GV02.1	RP04.21	RP04.21	RP04.21	RP04.21	MD03.1
		305	338	384	392	411	166	476	448	681	690	693	552
Ag	ppm	1.33	0.17	0.37	0.44	0.29	1.14	0.76	0.58	0.56	0.78	0.26	1.67
Al	%	4.95	2.13	3.02	3.03	3.09	6.13	2.84	6.39	8.72	5.47	5.36	0.94
As	ppm	0.5	0.5	0.1	0.1	0.3	0.9	0.7	2.2	0.5	0.4	0.6	2.8
Au	ppm	<0.2	<0.2	<0.2	<0.2	<0.2	0.2	<0.2	<0.2	<0.2	<0.2	<0.2	0.5
B	ppm	<10	<10	<10	<10	<10	<10	<10	<10	<10	<10	<10	<10
Ba	ppm	40	20	30	30	50	50	30	50	50	40	40	40
Be	ppm	0.12	0.11	0.16	0.15	0.2	0.2	0.21	0.31	0.17	0.11	0.17	0.05
Bi	ppm	0.84	0.35	0.32	0.54	0.34	0.75	0.72	0.4	0.37	1.68	0.34	0.91
Ca	%	3.43	1.23	1.81	1.85	1.64	4.02	1.82	3.93	5.42	3.38	3.17	0.33
Cd	ppm	0.22	0.05	0.08	0.05	0.11	0.14	0.15	0.07	0.07	0.14	0.07	0.16
Ce	ppm	1.36	1.69	2.92	2.61	2.98	4.19	6.05	9.02	4.33	3.66	4.29	3.15
Co	ppm	53.4	23.3	32.4	35.5	38.5	87.2	93.6	25.9	25.7	121.5	70.8	84.3
Cr	ppm	78	162	100	113	382	14	130	44	51	74	110	365
Cs	ppm	0.37	0.32	0.36	0.58	0.97	0.5	0.62	0.62	0.23	0.37	0.45	0.8
Cu	ppm	3320	262	654	809	514	4030	2460	958	718	1880	986	2980
Fe	%	1.55	1.01	1.21	1.2	2.35	2.59	3.11	1.44	0.89	2.8	2	2.17
Ga	ppm	8.18	3.81	4.66	5.06	6.05	9.44	5.39	9.74	12.3	8.05	8.41	2.63
Ge	ppm	<0.05	<0.05	<0.05	<0.05	<0.05	0.06	0.05	0.05	<0.05	<0.05	0.05	0.07
Hf	ppm	<0.02	0.03	0.05	<0.02	0.04	0.04	0.1	0.07	0.02	0.03	0.03	0.05
Hg	ppm	<0.01	<0.01	<0.01	<0.01	<0.01	<0.01	<0.01	<0.01	<0.01	<0.01	<0.01	<0.01
In	ppm	0.023	<0.005	<0.005	<0.005	0.005	0.023	0.012	<0.005	<0.005	0.011	0.005	0.012
K	%	0.09	0.05	0.07	0.06	0.13	0.08	0.12	0.1	0.1	0.06	0.07	0.19
La	ppm	0.8	1	1.7	1.6	1.8	2.3	3.1	4.7	2.4	1.9	2.3	1.8
Li	ppm	12.5	12.1	7.2	6.3	17.9	21.8	16	6.2	3.1	5.3	7.3	12.6
Mg	%	0.44	0.45	0.4	0.33	1.19	0.37	0.4	0.37	0.3	0.55	0.8	1.45
Mn	ppm	127	78	62	48	214	143	90	85	60	90	130	159
Mo	ppm	0.07	0.05	0.1	0.09	0.29	0.31	0.39	0.17	0.14	0.19	0.17	0.47
Na	%	0.71	0.31	0.43	0.41	0.37	0.73	0.38	0.76	1.01	0.62	0.67	0.05
Nb	ppm	0.11	0.05	0.11	0.05	<0.05	<0.05	0.14	0.07	<0.05	0.07	<0.05	0.08
Ni	ppm	1700	434	571	681	432	3690	1850	848	954	2540	1890	4790
P	ppm	20	30	50	50	60	20	130	130	50	70	60	50
Pb	ppm	9.9	3.7	7.9	7.3	11.2	15.1	6.6	7.5	19	11.1	4.5	8.7
Rb	ppm	2.7	2.1	4.2	3.3	9.1	2.1	9.7	4.6	1.5	1.7	2.7	14.3
Re	ppm	0.007	0.002	0.001	0.001	0.001	0.011	0.003	0.003	0.002	0.008	0.005	0.016
S	%	0.81	0.3	0.45	0.5	0.45	1.38	1.62	0.39	0.34	1.62	0.76	1
Sb	ppm	0.06	0.13	0.05	<0.05	<0.05	0.71	0.19	0.22	0.16	0.22	0.3	0.4
Sc	ppm	0.7	0.7	0.6	0.5	1.5	1.8	1	1	0.6	0.8	1	2.2
Se	ppm	3.5	0.7	0.7	0.9	0.7	3.9	3.2	1	0.9	4.4	2	4.7
Sn	ppm	0.2	0.2	0.3	0.2	0.2	0.4	0.3	0.3	0.2	0.2	0.2	0.5
Sr	ppm	152.5	63.4	99.6	106.5	89.5	137	78	163	264	148	155	9.1
Ta	ppm	<0.01	<0.01	<0.01	<0.01	<0.01	<0.01	<0.01	<0.01	<0.01	<0.01	<0.01	<0.01
Te	ppm	0.18	0.04	0.14	0.11	0.08	0.39	0.69	0.14	0.15	1.08	0.38	1.3
Th	ppm	<0.2	0.3	1.1	0.3	1.2	0.8	2	1.4	0.2	0.5	0.6	2.2
Ti	%	0.006	0.02	0.019	0.016	0.053	0.017	0.032	0.023	0.012	0.015	0.026	0.081
Tl	ppm	0.2	0.05	0.05	0.07	0.25	0.08	0.18	0.05	0.04	0.13	0.11	0.34
U	ppm	<0.05	0.06	0.26	0.07	0.18	0.13	0.4	0.29	0.06	0.1	0.13	0.46
V	ppm	7	9	12	7	32	24	19	41	9	8	15	37
W	ppm	<0.05	0.07	0.05	<0.05	0.1	0.05	0.12	0.07	<0.05	0.11	0.14	0.14
Y	ppm	0.18	0.27	0.37	0.28	0.63	1.02	1.07	1.5	0.42	0.47	0.64	0.82
Zn	ppm	25	6	7	3	11	43	23	19	9	15	23	27
Zr	ppm	<0.5	0.9	1.7	0.7	1.5	1.5	3.3	2.9	1	1.9	1.3	1.5

## ALS standards

		BLANK	GN05	GN05 -Duplicate	Average	Stdv	MRGeo08 target range			GBM908-5 target range		
							MRGeo08	lower	upper	GBM908-5	lower	upper
Ag	ppm	<0.01	1.33	1.34	1.335	0.01	4.67	4	4.92	58.6	52.4	64
Al	%	<0.01	4.95	5.12	5.035	0.12	2.72	2.44	3	1.12	1.02	1.26
As	ppm	<0.1	0.5	0.2	0.35	0.21	32	28.9	35.5	6.3	5.8	7.4
Au	ppm	<0.2	<0.2	<0.2			<0.2	<0.2	0.6	<0.2	<0.2	0.6
B	ppm	<10	<10	<10			<10	<10	20	<10	<10	30
Ba	ppm	<10	40	40	40	0.00	430	370	530	190	160	230
Be	ppm	<0.05	0.12	0.1	0.11	0.01	0.92	0.66	0.94	0.41	0.3	0.54
Bi	ppm	<0.01	0.84	0.8	0.82	0.03	0.73	0.62	0.78	0.87	0.79	0.98
Ca	%	<0.01	3.43	3.33	3.38	0.07	1.09	1	1.24	0.71	0.63	0.79
Cd	ppm	<0.01	0.22	0.22	0.22	0.00	2.14	2.01	2.47	0.12	0.12	0.17
Ce	ppm	<0.02	1.36	1.37	1.365	0.01	71.8	66.7	81.5	184.5	170.5	208
Co	ppm	<0.1	53.4	52.7	53.05	0.49	21.4	17.5	21.6	11.2	10.7	133
Cr	ppm	<1	78	73	75.5	3.54	91	81	102	19	15	20
Cs	ppm	<0.05	0.37	0.38	0.375	0.01	10.55	9.85	12.15	1.1	0.98	1.31
Cu	ppm	<0.2	3320	3150	3235	120.21	632	587	675	501	465	535
Fe	%	<0.01	1.55	1.59	1.57	0.03	3.58	3.22	3.96	2.33	2.13	2.62
Ga	ppm	<0.05	8.18	8.25	8.215	0.05	10.05	8.89	10.95	5.77	5.31	6.6
Ge	ppm	<0.05	<0.05	0.05	0.05		0.15	0.1	0.32	0.16	0.08	0.3
Hf	ppm	<0.02	<0.02	<0.02			0.79	0.67	0.87	0.34	0.29	0.41
Hg	ppm	<0.01	<0.01	<0.01			0.06	0.04	0.1	0.01	<0.01	0.05
In	ppm	<0.005	0.023	0.016	0.0195	0.00	0.16	0.142	0.184	0.005	<0.005	0.026
K	%	<0.01	0.09	0.08	0.085	0.01	1.22	1.12	1.4	0.82	0.73	0.91
La	ppm	<0.2	0.8	0.9	0.85	0.07	34.7	33.2	41	102	91.9	112.5
Li	ppm	<0.1	12.5	12.6	12.55	0.07	33.2	30.2	37.2	9.8	9.4	11.7
Mg	%	<0.01	0.44	0.45	0.445	0.01	1.15	1.03	1.29	0.77	0.68	0.86
Mn	ppm	<5	127	120	123.5	4.95	416	378	473	352	315	396
Mo	ppm	<0.05	0.07	0.07	0.07	0.00	14.5	13.1	16.1	51.6	49.5	60.6
Na	%	<0.01	0.71	0.73	0.72	0.01	0.35	0.3	0.39	0.03	0.02	0.06
Nb	ppm	<0.05	0.11	0.06	0.085	0.04	0.98	0.79	1.09	0.79	0.89	1.2
Ni	ppm	<0.2	1700	1690	1695	7.07	699	622	760	427	381	466
P	ppm	<10	20	10	15	7.07	1010	900	1130	1260	1140	1410
Pb	ppm	<0.2	9.9	9.6	9.75	0.21	1070	959	1175	375	345	422
Rb	ppm	<0.1	2.7	2.7	2.7	0.00	143.5	132	162	58.1	50.8	62.3
Re	ppm	<0.001	0.007	0.008	0.0075	0.00	0.007	0.0007	0.011	<0.001	<0.001	0.003
S	%	<0.01	0.81	0.82	0.815	0.01	0.3	0.27	0.36	0.15	0.14	0.2
Sb	ppm	<0.05	0.06	0.05	0.055	0.01	3.31	2.8	3.9	0.08	<0.05	0.25
Sc	ppm	<0.1	0.7	0.7	0.7	0.00	7.4	6.8	8.6	1.4	1.3	1.9
Se	ppm	0.2	3.5	3.2	3.35	0.21	1.3	0.9	1.9	0.6	0.3	1.1
Sn	ppm	<0.2	0.2	0.2	0.2	0.00	3.2	2.8	4	1.5	1.1	2
Sr	ppm	<0.2	152.5	157.5	155	3.54	82.9	73.2	89.9	49	47.3	58.2
Ta	ppm	<0.01	<0.01	0.01	0.01		0.02	<0.01	0.04	<0.01	<0.01	0.03
Te	ppm	0.02	0.18	0.21	0.195	0.02	<0.01	<0.01	0.04	0.03	0.02	0.07
Th	ppm	<0.2	<0.2	<0.2			21.3	19.5	24.3	39.1	34.4	42.4
Ti	%	<0.005	0.006	0.006	0.006	0.00	0.39	0.35	0.439	0.167	0.146	0.189
Tl	ppm	<0.02	0.2	0.19	0.195	0.01	0.82	0.66	0.94	0.42	0.31	0.47
U	ppm	<0.05	<0.05	<0.05			5.55	4.99	6.21	2.75	2.64	3.34
V	ppm	<1	7	7	7	0.00	101	90	112	26	22	29
W	ppm	<0.05	<0.05	0.05	0.05		2.96	2.44	3.42	2.24	1.75	2.48
Y	ppm	<0.05	0.18	0.18	0.18	0.00	18.7	17.85	21.9	26.2	25.45	31.1
Zn	ppm	<2	25	25	25	0.00	796	708	870	235	214	266
Zr	ppm	<0.5	<0.5	<0.5			20.6	18.1	25.7	7.9	6.8	10.5

Bulk S/Se ratios presented in Chapter 5 use S concentrations determined by LECO. This technique was favourable for S as it generally derives data with a higher degree of precision. LECO S values were also utilised to ensure consistency throughout the thesis.

Rare Earth Elements – All data was obtained using fusions which were analysed using ICP-OES and ICP-MS. Details on the methodology used is provided in Chapter 6.

ppm	La	Ce	Pr	Nd	Sm	Eu	Gd	Tb	Dy	Ho	Er	Tm	Yb	Lu	Hf	Ta	Pb	Th	U
<b>Mottled Anorthosite unit</b>																			
RP04.21/326	2.9	4.5	0.5	1.9	0.4	0.5	0.4	0.1	0.5	0.1	0.3	0.1	0.4	0.0	0.1	0.0		0.1	0.0
RP04.21/326	5.7	10.0	1.3	4.9	1.1	0.5	1.2	0.2	1.3	0.3	0.8	0.1	0.9	0.1	0.5	0.1		0.8	0.2
RP04.21/415	1.9	3.1	0.3	1.3	0.3	0.3	0.2	0.0	0.3	0.1	0.2	0.0	0.3	0.0	0.2	0.0	16	0.1	0.0
RP04.21/415	5.3	9.8	1.2	4.6	1.0	0.5	1.0	0.2	1.0	0.2	0.5	0.1	0.6	0.1	0.6	0.1	10.6	0.9	0.2
RP04.21/538	8.4	16.3	2.1	7.5	1.6	0.7	1.5	0.2	1.4	0.3	0.8	0.1	0.8	0.1	0.8	0.1		1.4	0.4
RP04.21/690	4.3	8.6	1.1	4.2	1.0	0.4	0.9	0.2	1.0	0.2	0.5	0.1	0.5	0.1	0.6	0.1	17	0.8	0.3
RP04.21/690	2.8	4.9	0.6	2.2	0.5	0.4	0.5	0.1	0.5	0.1	0.3	0.0	0.2	0.0	0.2	0.0	38	0.0	0.1
GV05.49/30	9.7	19.0	2.4	9.5	2.2	0.7	2.1	0.4	2.2	0.4	1.2	0.2	1.3	0.4	1.3	0.1	13	1.2	0.3
GV05.49/30	13.6	25.2	2.9	10.2	2.0	0.7	1.7	0.3	1.7	0.3	1.0	0.2	1.0	0.2	2.4	0.3	10	3.6	1.0
RP05.40/80	3.7	6.2	0.8	2.9	0.6	0.5	0.6	0.1	0.6	0.1	0.4	0.1	0.3	0.0	0.2	0.0		0.4	0.1
RP05.40/255	12.0	22.5	2.8	10.7	2.1	0.9	2.0	0.3	2.0	0.4	1.1	0.2	1.2	0.2	1.0	0.2		1.7	0.5
GV05.50/264	6.2	11.6	1.5	5.4	1.1	0.6	1.1	0.2	1.0	0.2	0.6	0.1	0.6	0.1	0.7	0.1		1.0	0.3
GV05.50/342	8.1	14.0	1.6	5.2	1.1	0.6	0.8	0.1	0.7	0.1	0.4	0.1	0.4	0.1	0.6	0.1		1.2	0.4
GV05.50/343	7.3	13.3	1.6	5.7	1.2	0.6	1.1	0.2	1.0	0.2	0.6	0.1	0.6	0.1	0.6	0.1		1.4	0.4
RP04.23/5	4.6	8.5	0.9	3.0	0.7	0.6	0.5	0.1	0.4	0.1	0.2	0.0	0.2	0.0	0.4	0.1	3.5	0.9	0.2
RP04.23/15	4.2	8.9	1.1	4.3	1.1	0.7	1.0	0.2	1.1	0.2	0.6	0.1	0.7	0.1	0.4	0.1	12	0.4	0.1
MD03.1/552	6.0	13.7	1.7	7.0	1.7	0.3	1.7	0.3	2.1	0.4	1.1	0.2	1.3	0.2	1.6	0.2	9.2	2.4	0.7
MD03.1/582	1.5	3.3	0.4	1.4	0.4	0.2	0.4	0.1	0.4	0.1	0.3	0.1	0.4	0.1	0.6	0.1	4.6	0.3	0.1
GV02.1/154	3.8	8.4	1.1	4.6	1.2	0.5	1.3	0.2	1.8	0.3	1.1	0.2	1.4	0.2	0.6	0.1	4.7	0.9	0.2
GV02.1/172	7.9	15.6	1.7	6.0	1.2	0.8	1.0	0.1	0.8	0.1	0.4	0.1	0.4	0.1	0.7	0.2	13	1.8	0.5
<b>Lower Mafic Unit</b>																			
RP05.45/158	18.3	31.4	3.6	12.2	2.1	1.3	1.7	0.2	1.6	0.3	1.0	0.2	1.1	0.2	0.8	0.1		2.6	0.7
RP05.45/167	9.2	17.5	2.0	7.5	1.5	0.5	1.3	0.2	1.4	0.3	0.9	0.2	1.0	0.2	1.9	0.2	57	3.0	1.0
RP05.45/167	12.9	25.0	3.0	11.2	2.2	0.8	2.0	0.3	2.0	0.4	1.1	0.2	1.2	0.2	2.0	0.2	10	2.3	0.7
RP05.45/183	15.2	31.8	3.9	14.4	3.0	1.1	2.9	0.5	3.0	0.5	1.7	0.3	1.7	0.3	2.1	0.3	6.3	2.5	0.7
RP05.45/191	15.2	29.3	3.6	13.7	2.7	0.9	2.5	0.4	2.5	0.5	1.4	0.2	1.5	0.2	1.8	0.3		3.2	0.9
RP05.45/206	8.1	16.5	2.1	8.2	1.9	0.5	1.8	0.3	1.9	0.3	1.0	0.2	1.1	0.2	0.9	0.1	10	1.8	0.5
RP05.45/210	20.3	40.8	4.9	16.7	3.3	1.0	2.9	0.5	2.8	0.5	1.5	0.2	1.6	0.2	2.5	0.3	9.3	4.7	1.7
RP04.23/305	1.2	2.6	0.3	1.3	0.4	0.4	0.5	0.1	0.5	0.1	0.3	0.1	0.4	0.1	0.4	0.1	7.8	0.2	0.1
RP04.23/315	3.4	6.7	0.8	2.7	0.6	0.6	0.6	0.1	0.5	0.1	0.3	0.0	0.3	0.0	0.5	0.1	3.3	0.4	0.1
RP04.23/374	1.5	3.5	0.5	2.0	0.6	0.5	0.7	0.1	0.8	0.1	0.5	0.1	0.6	0.1	0.5	0.1	2.9	0.1	0.1
RP04.23/433	2.2	4.4	0.5	1.7	0.5	0.2	0.6	0.1	0.6	0.1	0.4	0.1	0.5	0.1	0.6	0.2	10	0.8	0.3
GV02.1/433	2.2	4.1	0.5	2.1	0.6	0.4	0.6	0.1	0.7	0.1	0.4	0.1	0.5	0.1	0.6	0.1	1.2	0.2	0.1
GV02.1/476	6.9	15.3	1.9	7.6	1.8	0.6	1.7	0.3	1.8	0.3	1.0	0.1	1.0	0.1	1.4	0.1	8.4	2.3	0.7
GV02.1/487	4.0	8.0	0.9	3.4	0.8	0.4	0.9	0.2	1.0	0.2	0.6	0.1	0.8	0.1	1.0	0.2	11	0.9	0.2
GV02.1/503	4.0	8.9	1.1	4.8	1.2	0.5	1.2	0.2	1.4	0.3	0.8	0.1	0.9	0.1	0.8	0.1	12	1.0	0.2
<b>Lower Gabbroic unit</b>																			
GV05.49/40	12.3	23.9	2.9	11.3	2.5	0.8	2.3	0.4	2.3	0.4	1.3	0.2	1.4	0.2	1.7	0.2	14	1.6	0.5
GV05.49/45	13.1	24.9	3.0	11.1	2.2	0.9	2.1	0.3	1.9	0.4	1.1	0.2	1.1	0.2	1.7	0.2	15	2.6	0.7
GV05.49/45	14.7	29.8	3.8	14.7	3.2	0.9	3.1	0.5	3.0	0.6	1.7	0.3	1.7	0.3	2.0	0.3	13	2.4	0.7
GV05.50/415	14.4	26.5	3.3	12.3	2.4	0.9	2.4	0.4	2.2	0.4	1.3	0.2	1.3	0.2	1.8	0.2		2.2	0.6

Appendix 1. Whole rock data

GV05.50/415	16.1	30.0	3.7	13.4	2.7	0.9	2.5	0.4	2.2	0.5	1.3	0.2	1.2	0.2	0.9	0.2	2.2	0.6	
GV05.50/499	14.6	28.6	3.7	13.4	2.8	0.9	2.7	0.4	2.6	0.5	1.4	0.2	1.5	0.2	1.5	0.2	2.0	0.5	
RP05.45/47	10.6	22.7	2.8	10.4	2.3	0.8	2.0	0.4	2.1	0.4	1.2	0.2	1.2	0.2	1.9	0.2	4.4	1.9	0.5
ppm	La	Ce	Pr	Nd	Sm	Eu	Gd	Tb	Dy	Ho	Er	Tm	Yb	Lu	Hf	Ta	Pb	Th	U
RP05.45/94	14.6	30.4	3.7	13.8	2.8	0.9	2.5	0.4	2.5	0.5	1.4	0.2	1.5	0.2	1.8	0.3	6.8	2.8	0.6
RP05.45/135	15.2	31.5	3.9	14.5	3.0	1.0	2.7	0.4	2.8	0.5	1.6	0.2	1.6	0.2	1.3	0.3	5.0	1.4	0.3
RP05.45/146	13.3	24.6	3.0	11.2	2.2	0.8	2.1	0.3	1.9	0.4	1.1	0.2	1.1	0.2	1.2	0.2	1.5	0.4	
RP05.45/148	16.2	29.7	3.6	13.5	2.6	0.9	2.4	0.4	2.3	0.5	1.3	0.2	1.3	0.2	1.6	0.3	2.8	0.8	
RP04.23/201	1.8	3.5	0.4	1.3	0.4	0.4	0.3	0.0	0.2	0.0	0.1	0.0	0.1	0.0	0.3	0.3	33.	0.3	0.1
RP04.23/287	8.7	22.6	3.1	12.8	3.1	0.9	2.8	0.5	3.3	0.6	1.9	0.3	2.0	0.3	8.1	0.3	30	1.8	0.7
<b>Floor rocks</b>																			
RP05.45/217a	70.3	134.8	14.9	51.4	8.9	1.9	7.4	1.2	7.6	1.5	4.6	0.7	4.4	0.6	8.6	1.3	33.7	27	5.7
RP05.45.217b	30.7	52.1	5.7	20.0	3.3	1.1	2.7	0.4	2.3	0.4	1.4	0.2	1.5	0.2	3.0	0.3	26.4	1.4	0.6
RP05.45/217c	43.8	63.1	7.4	22.9	3.5	0.9	2.7	0.4	2.2	0.4	1.3	0.2	1.5	0.2	5.1	0.4	20.5	12	3.3
RP05.45/219	47.1	94.7	11.5	42.0	8.0	1.7	6.8	1.0	5.6	1.0	2.8	0.4	2.7	0.4	6.0	0.7	17.3	2.9	1.1

	La	Ce	Pr	Nd	Sm	Eu	Gd	Tb	Dy	Ho	Er	Tm	Yb	Lu	Hf	Ta	Pb	Th	U
ppm																			
JB1a	36.37	65.80	7.37	25.71	5.02	1.48	4.52	0.70	4.15	0.74	2.09	0.33	2.07	0.31	3.51	1.69	7.33	8.76	1.56
JB1a	37.01	64.49	7.21	25.55	4.97	1.41	4.53	0.69	3.97	0.70	2.06	0.32	2.05	0.30	2.99	1.56	15.75	8.61	1.69
Average	36.69	65.15	7.29	25.63	4.99	1.45	4.53	0.70	4.06	0.72	2.07	0.32	2.06	0.31	3.25	1.62	11.54	8.69	1.62
Stdv	0.45	0.93	0.12	0.11	0.03	0.05	0.01	0.01	0.12	0.02	0.02	0.01	0.01	0.01	0.36	0.09	5.96	0.11	0.09
%Stdv	1.23	1.42	1.58	0.42	0.66	3.62	0.12	1.26	3.05	3.17	0.91	3.36	0.63	3.74	11.22	5.42	51.62	1.24	5.59

# Appendix 2

LA-ICP-MS data

Methodology of LA-ICP-MS technique is provided in Chapter 4

Composition of quenched sulfide standards used for LA-ICP-MS

		Std-1	Std-2	Std-3	Std-4	Std-5
S	wt%	29.50	30.1	28.60	31.60	30.1
Fe	wt%	5.18	7.3	4.15	9.47	10.6
Ni	wt%	62.37	51.7	46.90	59.03	58.3
Cu	wt%		11	19.81		
Co	ppm	36	4,850	15,000		
Zn	ppm	100	3,000	4,600		
As	ppm				57	108
Se	ppm				140	264
Ru	ppm				51	160
Rh	ppm				51	160
Pd	ppm				50	120
Ag	ppm				147	152
Cd	ppm	143				
Sb	ppm				52	108
Te	ppm				210	644
Re	ppm				61	127
Os	ppm				50	160
Ir	ppm				55	160
Pt	ppm				50	125
Au	ppm				44	125
Bi	ppm	6	6.5	5	146	263

The accuracy of the LA-ICP-MS procedure for PGE was checked by analysis of the Laflamme-Po724 standard run as an unknown against the Cardiff sulfide standards. Results for accuracy and precision are shown below

		Certified	Run-1	Run-2	Run-3	Run-4	Run-5	average	Stdv	Rstdv	Accuracy % Max	Accuracy % Min
S	wt%	38.1			38	38	38	38	0	0	0.00	
Fe	wt%	n/a			61.07	60.8	61.32	61.06	0.2601	0.43		
Ni	wt%	n/a	0	0	<0.05	<0.05	<0.05	0	0			
Cu	wt%	n/a	0	0	<0.03	<0.03	<0.03	0	0			
Co	ppm	n/a	9	9	7	6	6	7.4	1.5166	20.49		
Zn	ppm	n/a	0.8	1.2	12	12	11	7.4	5.8583	79.17		
As	ppm	n/a	<5	<5	<5	<5	<5					
Se	ppm	n/a			<60	<60	<60					
Ru	ppm	37.00±1.00	37.78	35.35	35.87	39.16	37.23	37.078	1.5245	4.11	5.84	2.11
Rh	ppm	37.00±1.70	36.12	35.91	36.02	47.28	34.78	38.022	5.2035	13.69	27.78	2.38
Pd	ppm	45.00±0.80	43.59	47.94	45.57	48.2	42.53	45.566	2.5345	5.56	7.11	1.27
Ag	ppm				<0.1	0.19	<0.1					
Cd	ppm	n/a			<0.9	<0.9	<0.9					
Sb	ppm	n/a	0.21	0.19	0.82	<0.8	<0.8	0.41	0.3581	87.34		
Te	ppm	n/a	0.1	0.11	1.12	<0.9	<0.9	0.44	0.586	133.18		
Re	ppm	n/a			<0.02	<0.02	<0.02					
Os	ppm	35.20±1.90	33.88	34.12	38.85	36.67	38.79	36.462	2.4144	6.62	10.37	3.07
Ir	ppm	36.2±0.5	36.03	36.99	38.92	35.45	39.15	37.308	1.6717	4.48	8.15	0.47
Pt	ppm	35.9±0.7	36.34	35.97	40.81	38.16	38.67	37.99	1.9523	5.14	13.68	1.95
Au	ppm	47.3±2.4	42.24	43.01	40.61	42.91	45.52	42.858	1.7711	4.13	-14.14	3.76
Bi	ppm	n/a	<0.04	<0.04	<0.05	<0.05	<0.05					

Lower limit of detection for PGE

Os	Is	Ru	Rh	Pt	Pd	Au	Ni	Cu	Co	As	Se	Sb	Te	Bi
0.01	0.01	0.05	0.08	0.01	0.1	0.01	0.05	0.03	4	5	60	0.8	0.9	0.05

LA-ICP-MS analysis of sulfides – pyrrhotite . Green shading corresponds to those used in Table 5.1.

sample	RP04.23/157				RP04.23/384				RP04.23/392				RP04.23/411				RR04.21/690			
	run	po1	po2	po3	po4	po5	po1	po2	po3	po4	po1	po2	Po-Pn1	po1	po2	pn-po1	po-pn1	po1	po2	
Co	ppm	184	140	154	2634	112	68	61	51	62	25	117	317	30	24	1165	183	135	156	
Ni	%	0.12	0.87	1.08	9.67	0.80	0.47	0.45	0.39	0.48	0.29	0.64	1.21	0.21	0.17	2.72	0.86	0.52	0.78	
Cu	%	0.88	0.00	0.00	0.02	0.00	0.09	0.06	0.41	0.00	<0.03	<0.03	<0.03	<0.03	<0.03	<0.03	<0.03	2.14	<0.03	
Zn	ppm	23.1	1.1	0.4	0.8	0.7	1.4	2.2	23.4	1.0	10	3	24	10	25	52	16	411	5	
As	ppm	<5	7	<5	14	<5	<5	<5	<5	<5	<5	<5	<5	<5	<5	<5	<5	<5	<5	
Se	ppm										73	88	72	80	67	139	79	107	106	
Ru	ppm	0.21	0.14	0.28	<0.05	0.21	0.21	0.25	0.21	0.23	0.07	0.08	0.05	<0.05	0.12	0.13	3.11	1.28	3.91	
Rh	ppm	<0.08	<0.08	<0.08	<0.08	<0.08	0.08	<0.08	<0.08	<0.08	0.12	0.16	0.13	0.12	0.12	0.10	0.13	<0.1	0.32	
Pd	ppm	1.78	<0.1	0.11	7.86	<0.1	<0.1	1.70	0.19	<0.1	<0.15	1.59	<0.15	<0.15	<0.15	0.33	<0.15	<0.15	<0.15	
Sb	ppm	3.35	0.09	0.04	0.46	0.06	0.04	0.27	0.15	0.03	0.83	<0.8	0.95	<0.8	0.98	1.48	0.71	1.02	<0.8	
Te	ppm	1.02	0.23	0.15	0.52	0.26	0.30	1.94	0.64	0.31	1.36	3.20	2.23	1.20	1.07	2.40	0.90	<0.9	<0.9	
Re	ppm	0.20	0.08	0.23	0.29	0.22	0.09	0.12	0.11	0.11	0.29	0.21	0.11	0.16	0.18	0.14	0.21	0.10	0.34	
Os	ppm	0.07	0.03	0.14	0.03	0.03	0.03	0.04	0.06	0.03	0.03	0.05	0.03	0.03	0.02	0.11	0.50	0.13	0.59	
Ir	ppm	0.07	0.04	0.11	0.01	0.07	0.05	0.05	0.07	0.06	0.10	0.12	0.09	0.10	0.09	0.18	0.57	0.20	0.46	
Pt	ppm	<0.01	<0.01	<0.01	<0.01	<0.01	<0.01	<0.01	<0.01	<0.01	0.03	0.12	0.21	0.03	<0.02	<0.02	0.32	0.05	0.23	
Au	ppm	0.04	<0.01	<0.01	0.01	<0.01	<0.01	<0.01	<0.01	<0.01	<0.01	0.02	0.01	0.02	0.02	0.04	<0.01	0.01	<0.01	
Bi	ppm	7.35	0.20	0.45	3.48	0.37	0.30	6.23	0.83	0.33	0.37	4.10	0.99	0.14	0.23	0.46	0.36	0.24	0.23	

sample	RP04.21/690 cont.							RP04.23/693							RP04.21/679							
	po3	po4	po5	po6	po7	po-pn-po	pn-po2	cpy-po	po1	po2	po3	po1	po2	po3	po1	po2	po3	po1	po2	po3	po-pn3	py-po
run	112	126	110	111	121	143	169	132	119	81	80	99	42	82	77	81	194					
ppm	0.57	0.65	0.53	0.54	0.62	0.73	0.74	0.65	0.60	0.78	1.08	0.94	0.77	1.18	1.12	1.30	0.62					
%	<0.03	<0.03	<0.03	<0.03	<0.03	<0.03	<0.03	<0.03	0.28	<0.03	<0.03	<0.03	<0.03	<0.03	<0.03	<0.03	<0.03					
%																						
Zn	4	27	12	19	17	8	20	35	100	55	27	38	26	39	40	51	50					
ppm	<5	<5	<5	<5	<5	<5	<5	<5	<5	<5	<5	<5	<5	<5	<5	<5	<5					
As	111	100	97	104	115	107	161	133	112	109	85	96	108	135	126	140	139					
ppm	4.00	2.54	2.21	2.66	5.42	3.18	4.21	3.09	0.10	0.81	3.35	2.36	3.17	2.09	1.00	1.84	0.95					
Ru	0.22	0.07	0.19	0.29	0.55	0.20	0.54	0.25	<0.1	<0.1	0.10	<0.1	<0.1	0.14	0.14	<0.1	0.04					
ppm	<0.15	0.22	<0.15	<0.15	<0.15	0.35	2.05	<0.15	<0.15	<0.15	<0.15	<0.15	<0.15	4.39	2.71	2.06	<0.15					
Pd	<0.8	<0.8	<0.8	<0.8	<0.8	<0.8	0.83	<0.8	<0.8	<0.8	<0.8	<0.8	<0.8	<0.8	<0.8	<0.8	<0.8					
Sb	<0.9	0.95	<0.9	<0.9	<0.9	0.95	4.73	<0.9	<0.9	<0.9	<0.9	<0.9	<0.9	9.26	4.66	3.20	1.08					
ppm	0.19	0.13	0.22	0.30	0.31	0.27	0.15	0.21	0.16	0.42	0.58	0.55	0.28	0.90	0.47	0.41	0.18					
Re	0.62	0.43	0.42	0.55	0.69	0.39	0.41	0.53	0.02	0.24	0.51	0.68	0.41	0.44	0.40	0.43	0.30					
ppm	0.38	0.34	0.23	0.29	0.57	0.37	0.42	0.43	<0.02	0.17	0.54	0.45	0.47	0.42	0.41	0.58	0.16					
Os	0.16	0.04	0.04	0.13	0.64	0.11	0.37	0.21	<0.02	0.02	<0.02	<0.02	0.28	2.19	1.72	0.65	0.05					
ppm	0.01	<0.01	<0.01	0.01	0.01	0.01	<0.01	<0.01	0.01	<0.01	<0.01	<0.01	<0.01	<0.01	<0.01	<0.01	<0.01					
Au	7.35	0.20	0.45	0.44	0.55	0.25	0.22	0.22	0.72	0.20	0.15	0.31	1.49	4.13	1.99	1.49	0.8					
ppm																						

## LA-ICP-MS analysis of sulfides – chalcopyrite and cubanite

sample	RP04.23/157				RP04.23/384				RP04.23/392				RP04.23/411				RP04.21/693				RP04.21/679	
	run	cpy3	cpy1	cpy2	cpy3	cpy4	cpy1	cpy2	cpy3	cpy4	cub	cub	cub	cub1	cub2	cub	cub1	cub	cub1	cub	cub1	cub2
Co	ppm	1	1	1	1	1	1	1	1	<4	<4	<4	<4	<4	<4	240	29	154	<4	<4	<4	<4
Ni	%	3.73	0.01	0.01	0.03	0.01	0.03	0.01	0.01	<0.05	<0.05	<0.05	<0.05	<0.05	0.14	1.03	0.14	1.99	0.14	1.99	<0.05	<0.05
Cu	%	32.82	32.67	32.94	32.40	33.12	32.40	32.94	33.12	26.07	24.80	26.05	25.04	25.68	18.31	23.51	18.31	25.90	18.31	25.90	26.12	26.12
Zn	ppm	396.8	303.9	278.8	370.3	326.7	370.3	278.8	326.7	3062	2624	3152	2134	1596	2477	5763	2477	2930	2477	2930	6820	6820
As	ppm	<5	<5	<5	<5	<5	<5	<5	<5	<5	<5	<5	<5	<5	<5	<5	<5	<5	<5	<5	<5	<5
Se	ppm									107	112	102	89	85	91	86	91	131	91	131	107	107
Ru	ppm	0.13	0.06	<0.05	<0.05	0.05	<0.05	<0.05	0.05	<0.05	<0.05	<0.05	0.07	<0.05	0.09	0.08	0.09	2.59	0.09	2.59	0.14	0.14
Rh	ppm	<0.08	<0.08	<0.08	<0.08	<0.08	<0.08	<0.08	<0.08	<0.1	0.15	<0.1	<0.1	<0.1	<0.1	<0.1	<0.1	<0.1	<0.1	<0.1	<0.1	<0.1
Pd	ppm	<0.1	0.41	0.31	<0.1	0.31	<0.1	0.31	0.31	0.28	<0.15	0.24	0.28	<0.15	0.22	0.22	<0.15	2.69	<0.15	2.69	<0.15	<0.15
Sb	ppm	0.26	0.09	0.19	0.13	0.17	0.13	0.19	0.17	1.17	1.37	2.04	1.05	<0.8	<0.8	<0.8	<0.8	0.89	<0.8	0.89	<0.8	<0.8
Te	ppm	1.14	0.28	0.31	0.15	0.39	0.15	0.31	0.39	6.20	<0.9	3.98	<0.9	2.12	0.98	0.95	0.98	1.79	0.98	1.79	0.96	0.96
Re	ppm	0.00	0.01	0.05	0.09	0.00	0.09	0.05	0.00	0.07	0.02	0.03	<0.02	0.02	0.09	0.05	0.09	0.94	0.09	0.94	0.02	0.02
Os	ppm	<0.01	0.01	<0.01	<0.01	<0.01	<0.01	<0.01	<0.01	0.09	0.07	<0.02	<0.02	<0.02	0.04	<0.02	0.04	0.50	<0.02	0.50	<0.02	<0.02
Ir	ppm	<0.01	<0.01	<0.01	0.08	<0.01	0.08	<0.01	<0.01	0.16	0.14	0.04	0.03	0.07	0.04	0.04	<0.02	0.36	<0.02	0.36	<0.02	<0.02
Pt	ppm	<0.01	0.01	<0.01	<0.01	<0.01	<0.01	<0.01	<0.01	0.04	<0.02	0.08	0.05	0.02	0.02	<0.02	0.02	0.05	<0.02	0.05	<0.02	<0.02
Au	ppm	0.03	<0.01	<0.01	0.01	0.01	0.01	<0.01	0.01	0.05	0.06	<0.01	0.03	0.02	0.02	<0.01	<0.01	0.02	<0.01	0.02	<0.01	<0.01
Bi	ppm	0.21	0.16	0.25	0.69	0.31	0.69	0.25	0.31	0.32	0.37	0.35	0.21	0.06	0.13	0.13	1.86	1.36	1.86	1.36	0.81	0.81

sample	RP04.21/690		RP05.45/165		RP05.45/208		RP05.45/214		MD03.1	
	cub	cub	cub 1	cub2	cub1	cub 2	cub 1	cub 2	cub 1	cub 2
run										
Co   ppm	29	240	<4	<4	5	<4	<4	<4	<4	<4
Ni   %	0.14	1.03	<0.05	<0.05	<0.05	<0.05	<0.05	<0.05	<0.05	<0.05
Cu   %	18.31	23.51	24.74	23.90	25.21	21.00	19.15	21.00	21.01	19.79
Zn   ppm	2477	5763	751	620	1647	281	476	281	5907	6235
As   ppm	<5	<5	<5	<5	<5	<5	<5	<5	<5	<5
Se   ppm	91	86	100	74	166	116	<60	116	156	120
Ru   ppm	0.09	0.08	0.10	0.13	1.94	0.24	<0.05	0.24	<0.05	<0.05
Rh   ppm	<0.1	<0.1	<0.1	<0.1	<0.1	<0.1	<0.1	<0.1	<0.1	<0.1
Pd   ppm	<0.15	0.22	0.30	0.51	0.17	<0.15	<0.15	<0.15	1.51	3.71
Sb   ppm	<0.8	<0.8	<0.9	<0.9	<0.8	<0.8	<0.8	<0.8	<0.8	<0.8
Te   ppm	0.98	0.95	3.12	4.69	14.05	1.56	1.04	1.56	3.27	5.19
Re   ppm	0.09	0.05	<0.02	0.02	0.04	0.02	0.03	0.02	<0.02	<0.02
Os   ppm	0.04	<0.02	<0.02	<0.02	<0.02	<0.02	<0.02	<0.02	0.02	0.02
Ir   ppm	<0.02	0.04	<0.02	<0.02	<0.02	<0.02	<0.02	<0.02	<0.02	<0.02
Pt   ppm	0.02	<0.02	<0.02	<0.02	<0.02	<0.02	0.05	<0.02	0.34	0.36
Au   ppm	0.02	<0.01	0.11	0.25	0.02	0.07	0.07	0.07	0.04	0.02
Bi   ppm	1.86	0.13	0.06	0.15	0.33	1.98	2.63	1.98	0.78	2.41

## LA-ICP-MS analysis of sulfides – pentlandite

sample	PR04.24/157				RP04.23/191			RP04.23/392			RP04.23/411			RP04.23/690		
	run	Pn1	Pn2	Pn3	Pn4	Pn1	Pn2	Pn1	Po-Pn1	pn2	pn3	pn-po1	po-pn 1	pn-po2	po-pn-po	
Co	ppm	80	12	38	9836	10850	11900	10740	7935	15010	14870	14430	6321	5355	4857	
Ni	%	31.16	36.01	36.57	23.47	33.05	31.26	35.42	27.47	31.36	28.93	30.47	20.19	28.76	26.43	
Cu	%	0.02	0.38	0.01	0.65	3.03	0.06	<0.03	2.72	<0.03	<0.03	<0.03	<0.03	<0.03	<0.03	
Zn	ppm	41.9	56.8	1.7	4.4	667	759	36	398	5	48	31	83	38	29	
As	ppm	<5	<5	<5	21	23	25	<5	<5	<5	<5	<5	<5	<5	<5	
Se	ppm					80	155	92	128	76	83	83	127	103	115	
Ru	ppm	<0.05	<0.05	0.62	<0.05	10.88	17.27	<0.05	0.16	<0.05	0.14	<0.05	1.35	4.49	2.73	
Rh	ppm	<0.08	<0.08	<0.08	0.08	<0.1	<0.1	0.80	0.32	0.18	0.18	<0.1	0.16	1.43	0.15	
Pd	ppm	12.68	16.80	17.66	18.56	23.07	34.66	1.96	1.60	2.78	4.94	2.10	11.14	17.29	4.63	
Sb	ppm	2.02	0.15	2.73	2.16	4.64	8.09	<0.8	1.42	1.04	4.05	1.03	1.42	<0.8	<0.8	
Te	ppm	1.57	0.80	1.38	6.27	50.36	32.38	3.74	6.70	8.63	9.99	1.97	1.70	<0.9	2.15	
Re	ppm	0.02	0.00	0.04	0.15	2.78	2.95	0.31	0.12	0.23	0.20	0.14	0.07	0.25	0.15	
Os	ppm	<0.01	<0.01	0.03	0.17	1.17	2.04	0.05	<0.02	0.03	0.02	<0.02	0.07	0.76	0.38	
Ir	ppm	0.01	<0.01	0.08	0.09	0.02	0.05	0.12	0.07	0.10	0.09	0.07	0.14	0.42	0.33	
Pt	ppm	0.01	<0.01	<0.01	<0.01	0.05	0.06	<0.02	<0.02	<0.02	<0.02	<0.02	0.07	0.71	0.07	
Au	ppm	0.02	0.01	0.01	0.38	0.02	0.11	0.01	0.03	0.02	0.05	0.04	0.01	0.01	0.01	
Bi	ppm	1.57	0.08	1.69	29.86	4.01	3.18	0.42	0.79	1.21	5.08	7.76	0.88	0.49	0.94	

sample	RP04.23/693				RP04.21/679				RP05.45/208				MD03.1/552			
	pn1	pn2	po-pn1	po-pn2	po-pn3	py-pn1	pn1	pn2	pn3	pn4	pn5	pn-py1	pn-py2	py-pn3	pn1	pn2
run	6595	5507	3990	2234	2416	2926	2399	433	277	357	1017	625	744	1498	2608	2653
Co ppm	25.65	35.01	30.66	32.72	32.20	27.62	26.28	36.89	39.64	39.86	35.58	36.17	33.75	32.31	37.56	38.67
Ni %	<0.03	<0.03	0.12	<0.03	<0.03	<0.03	0.31	0.08	0.07	<0.03	0.28	<0.03	<0.03	<0.03	<0.03	<0.03
Cu %	310	125	50	89	58	62	244	189	297	6	157	202	45	584	37	50
Zn ppm	20	<5	47	<5	<5	36	283	33	24	6	204	74	53	82	<5	<5
As ppm	164	90	109	133	135	139	91	135	158	164	140	141	140	153	161	155
Se ppm	17.58	1.62	8.25	0.72	1.17	3.01	1.17	1.04	2.19	1.07	2.30	1.40	1.00	0.77	4.33	5.24
Ru ppm	1.13	0.12	1.53	0.11	<0.1	0.40	4.07	1.99	2.43	1.30	3.86	1.85	1.51	1.47	1.36	1.03
Rh ppm	24.65	28.54	24.59	37.98	37.16	35.22	296.09	341.98	252.47	383.49	173.79	386.78	269.69	285.17	38.67	42.56
Pd ppm	7.55	<0.8	<0.8	<0.8	<0.8	1.48	30.02	22.77	2.09	<0.8	12.86	6.85	5.44	19.04	<0.8	<0.8
Sb ppm	5.68	<0.9	7.75	4.26	2.30	9.70	5.91	2.68	5.50	<0.9	3.48	2.48	3.08	4.41	20.55	1.01
Te ppm	0.76	0.45	0.30	0.14	0.25	0.14	0.51	0.36	0.42	0.27	0.48	0.73	0.63	0.46	0.47	0.66
Re ppm	2.04	0.42	0.67	0.12	0.35	0.37	0.17	0.14	0.16	0.11	0.35	0.18	0.14	0.14	0.95	1.33
Os ppm	1.28	0.26	0.64	0.26	0.28	0.46	0.53	0.11	0.17	0.08	0.44	0.21	0.06	0.22	0.19	0.16
Ir ppm	<0.02	<0.02	0.85	0.12	0.14	0.56	8.60	1.01	0.74	0.01	1.70	0.92	0.15	0.14	0.02	<0.02
Pt ppm	0.07	0.02	1.09	<0.01	<0.01	<0.01	0.08	0.07	0.01	<0.01	0.24	0.11	0.03	0.02	<0.01	<0.01
Au ppm	21.71	0.90	17.53	1.06	1.48	16.93	4.68	0.18	0.15	<0.05	2.66	0.94	0.29	0.66	<0.05	0.05
Bi ppm																

## LA-ICP-MS analysis of sulfides – pyrite and millerite

sample	RP04.23/157							RP04.21/679							RR05.45/165						
	py1	py2	py3	py4	py5	py6	py7	py1	py2	py3	py-pn1	py-pn2	py1	py2	py3	py4	py1	py2	py3	py4	
Co	13400	1676	1815	19540	16030	33370	716	7252	6753	7022	6085	11470	322	787	402	194	322	787	402	194	
Ni	0.11	2.13	0.56	1.90	2.20	0.17	0.08	<0.05	<0.05	0.06	0.26	0.53	2.28	2.35	2.27	0.13	2.28	2.35	2.27	0.13	
Cu	0.20	0.58	0.15	0.36	0.60	0.25	3.92	0.12	0.19	0.20	0.32	0.51	0.55	0.37	0.15	<0.03	0.55	0.37	0.15	<0.03	
Zn	1.0	45.9	39.2	2.7	2.5	15.4	35.5	119	53	46	1098	112	44	71	84	61	44	71	84	61	
As	457	6	4	<5	49	72	5	10	<5	8	279	113	642	496	794	270	642	496	794	270	
Se	271	201						78	73	60	148	146	129	137	128	65	129	137	128	65	
Ru	0.74	0.11	<0.05	<0.05	<0.05	<0.05	<0.05	6.39	<0.05	<0.05	9.53	5.40	0.05	0.12	0.05	<0.05	0.05	0.12	0.05	<0.05	
Rh	27.87	<0.08	<0.08	<0.08	0.11	0.27	<0.08	29.21	5.07	8.16	3.10	4.05	0.51	0.54	0.55	<0.1	0.51	0.54	0.55	<0.1	
Pd	60.84	1.46	1.82	5.24	1.89	1.12	0.82	<0.15	<0.15	<0.15	0.56	1.62	15.32	5.17	8.05	2.22	15.32	5.17	8.05	2.22	
Sb	84.34	1.30	2.96	7.07	1.35	5.90	2.70	<0.8	<0.8	<0.8	<0.8	<0.8	23.86	15.25	14.27	7.28	23.86	15.25	14.27	7.28	
Te	17.75	1.39	0.99	10.64	3.64	5.61	1.28	<0.9	<0.9	1.26	5.75	9.44	5.28	2.86	5.77	<0.9	5.28	2.86	5.77	<0.9	
Re	0.27	0.03	0.28	0.24	0.33	0.25	0.19	0.25	<0.02	<0.02	0.12	0.40	0.27	0.34	0.21	<0.02	0.27	0.34	0.21	<0.02	
Os	0.16	<0.01	0.02	0.18	0.21	0.18	0.04	0.69	<0.02	<0.02	0.84	0.82	<0.02	<0.02	<0.02	<0.02	<0.02	<0.02	<0.02	<0.02	
Ir	0.24	0.03	0.01	0.14	0.24	0.23	0.09	0.81	<0.02	<0.02	0.89	0.65	0.02	0.03	0.03	<0.02	0.02	0.03	0.03	<0.02	
Pt	<0.01	<0.01	<0.01	<0.01	<0.01	<0.01	<0.01	0.21	0.03	0.24	1.81	1.80	1.21	0.25	1.53	<0.02	1.21	0.25	1.53	<0.02	
Au	0.07	0.10	0.02	0.10	0.11	0.40	0.02	0.02	<0.01	<0.01	0.03	0.06	0.73	0.50	0.61	0.03	0.73	0.50	0.61	0.03	
Bi	33.87	7.90	9.28	38.15	24.39	54.40	18.98	2.23	3.61	1.78	31.91	21.01	1.79	3.15	5.88	0.58	1.79	3.15	5.88	0.58	

sample	RP05.45/208							RP05.45/214							RP05.45/146						
	py-pn	py1	py2	py3	py4	py5	py6	py7	pn-py1	mill	py2	py1	py2	py3	py4	py5	py	Py			
run																					
Co	ppm	8699	566	49	<4	468	9831	9988	21	4897	335	3812	8472	5515	7017	7972	1699	2170			
Ni	%	0.65	0.05	<0.05	0.05	0.46	2.86	0.30	<0.05	0.89	57.56	1.99	0.25	0.19	0.18	0.25	2.59	2.18			
Cu	%	0.22	0.42	0.09	<0.03	1.67	0.80	0.69	0.11	0.38	<0.03	0.25	0.00	0.00	0.01	1.38	0.09	0.15			
Zn	ppm	59	36	35	23	5670	130	53	46	57	41	99	0.5	1.3	4.0	1087.0	4.8	6.6			
As	ppm	54	51	45	<5	208	219	20	<5	150	34	142	351	288	206	141	447	543			
Se	ppm	172	137	61	106	121	201	152	74	229	131	204	83				155	131			
Ru	ppm	1.56	0.16	<0.05	<0.05	<0.05	1.87	1.41	<0.05	1.37	<0.05	0.99	0.34	0.82	0.79	0.14	0.10	<0.05			
Rh	ppm	2.23	0.36	<0.1	<0.1	<0.1	4.74	3.24	<0.1	3.44	<0.1	2.56	9.37	3.36	17.17	1.48	1.14	1.17			
Pd	ppm	8.24	0.64	0.50	<0.15	0.72	14.12	5.37	0.75	23.61	0.22	13.07	<0.1	0.96	0.15	0.64	26.01	30.39			
Sb	ppm	0.67	<0.8	2.78	<0.8	0.88	5.59	1.55	<0.8	5.96	<0.8	3.32	0.16	0.17	0.23	0.31	8.37	11.12			
Te	ppm	4.87	2.14	1.06	<0.9	<0.9	8.08	8.71	2.97	10.59	1.71	8.78	0.11	0.20	0.14	0.08	4.79	3.41			
Re	ppm	0.68	<0.02	<0.02	<0.02	<0.02	0.82	0.53	<0.02	0.44	0.03	0.39	0.04	0.09	0.12	<b>0.04</b>	<b>0.19</b>	<b>0.29</b>			
Os	ppm	0.10	<0.02	<0.02	0.00	<0.02	0.23	0.20	<0.02	0.13	<0.02	0.17	0.01	0.09	0.01	<0.01	0.02	0.02			
Ir	ppm	0.44	0.03	<0.02	<0.02	<0.02	0.41	0.30	<0.02	0.32	<0.02	0.22	0.03	0.19	0.06	<0.01	0.07	0.08			
Pt	ppm	1.76	0.14	<0.02	<0.02	<0.02	4.31	2.59	0.04	1.31	0.04	0.80	1.09	0.01	0.41	0.29	3.69	0.30			
Au	ppm	0.03	<0.01	0.01	<0.01	0.09	1.21	0.16	0.02	0.10	<0.01	0.09	<0.01	0.01	<0.01	0.03	1.49	1.90			
Bi	ppm	1.72	0.55	0.83	0.02	4.44	10.76	7.07	0.76	5.10	0.07	3.38	0.96	3.17	2.88	40.67	18.99	28.45			

## LA-ICP-MS analysis of sulfides – footwall pyrite and millerite

sample	RP05.45/214							RP05.45/215							RP05.45/214			
	run	py1	py2	py3	py4	py5	py6	py7	py8	py9	py10	py11	py1	py2	py3	mil1	mil2	mil1
Co	ppm	9793	9501	8695	7182	7161	9452	10480	5407	9651	7114	8302	5829	8279	7792	566	542	209
Ni	%	0.17	0.16	0.17	0.21	0.19	0.36	0.20	0.20	0.26	0.26	0.28	0.34	0.22	0.20	62.64	59.46	58.12
Cu	%	0.01	0.00	0.04	0.00	0.00	0.00	0.00	0.10	<0.03	0.03	<0.03	<0.03	<0.03	<0.03	0.00	0.00	0.38
Zn	ppm	0.4	0.4	2.3	0.7	0.7	0.8	4.5	80	55	43	69	52	94	47	0.9	0.3	132
As	ppm	243	194	219	397	161	550	224	288	404	423	437	691	122	131	<5	3	25
Se	ppm								78	64	64	70	91	68	80			166
Ru	ppm	<0.05	<0.05	<0.05	<0.05	<0.05	<0.05	<0.05	0.15	<0.05	2.71	<0.05	<0.05	<0.05	<0.05	<0.05	<0.05	0.45
Rh	ppm	<0.08	<0.08	<0.08	<0.08	<0.08	<0.08	<0.08	1.90	<0.1	<0.1	<0.1	<0.1	<0.1	<0.1	<0.08	<0.08	5.33
Pd	ppm	0.14	<0.1	<0.1	0.10	0.14	<0.1	0.35	0.27	<0.15	<0.15	<0.15	<0.15	<0.15	<0.15	<0.1	<0.1	10.70
Sb	ppm	0.23	0.15	0.19	0.19	0.34	0.16	0.26	<0.8	<0.8	<0.8	<0.8	<0.8	<0.8	<0.8	0.09	0.02	2.81
Te	ppm	0.12	0.08	0.14	0.11	0.09	0.06	0.17	<0.9	<0.9	<0.9	<0.9	<0.9	<0.9	<0.9	0.24	0.32	5.68
Re	ppm	0.06	0.13	0.06	0.01	0.00	0.03	0.02	0.44	0.08	0.40	0.06	0.03	0.03	0.23	0.01	0.00	0.75
Os	ppm	<0.01	<0.01	<0.01	<0.01	<0.01	<0.01	<0.01	<0.02	<0.02	0.30	<0.02	<0.02	<0.02	<0.02	<0.01	<0.01	<0.02
Ir	ppm	<0.01	<0.01	<0.01	<0.01	<0.01	<0.01	<0.01	0.04	<0.02	0.48	<0.02	<0.02	<0.02	<0.02	<0.01	<0.01	0.33
Pt	ppm	2.22	0.12	0.97	<0.01	0.04	<0.01	<0.01	0.07	0.03	<0.02	<0.02	<0.02	0.04	1.07	<0.01	<0.01	<0.02
Au	ppm	0.28	<0.01	<0.01	0.01	0.01	<0.01	0.01	0.01	<0.01	0.02	<0.01	<0.01	0.01	<0.01	<0.01	<0.01	0.03
Bi	ppm	17.89	1.85	2.51	1.76	22.87	0.34	12.91	14.96	3.59	1.93	1.08	0.31	1.19	1.06	0.38	0.22	12.16

sample		RP05.45/214							
	run	mil2	mil3	mil4	mil5	mil6	mil7	mil8	
Co	ppm	185	235	221	216	218	250	252	
Ni	%	62.95	59.03	54.84	58.44	61.66	59.97	59.71	
Cu	%	0.09	0.07	0.06	1.85	0.02	0.16	0.10	
Zn	ppm	199	1.2	1.6	11.4	1.7	1.9	0.8	
As	ppm	36	23	<5	15	18	15	29	
Se	ppm	153							
Ru	ppm	0.62	0.87	1.23	0.44	1.15	0.97	1.16	
Rh	ppm	2.07	1.83	2.80	0.24	5.37	3.55	2.64	
Pd	ppm	50.18	1.17	0.55	1.19	160.89	15.76	1.69	
Sb	ppm	<0.8	0.07	0.20	0.23	2.44	0.30	0.19	
Te	ppm	29.07	0.46	0.27	0.39	108.88	9.01	0.47	
Re	ppm	0.79	0.24	0.22	0.16	0.28	0.26	0.24	
Os	ppm	0.18	0.09	0.13	0.03	0.03	0.19	0.07	
Ir	ppm	0.22	0.20	0.35	0.11	0.25	0.23	0.21	
Pt	ppm	<0.02	<0.01	<0.01	<0.01	<0.01	0.01	<0.01	
Au	ppm	0.01	0.01	0.06	<0.01	<0.01	0.02	0.02	
Bi	ppm	27.36	2.10	3.84	6.76	187.20	19.13	2.96	

## LA-ICP-MS analysis of sulfides in chromitites

sample	RP05.4														RP05.45/167		
	run	py2	py3	py4	py5	py6	py7	py8	py9	py10	py11	py12	py13	py14	py1	py2	py3
Co	ppm	11	32	4185	3299	2108	6266	5303	4654	1349	624	2909	1390	5	163	56	757
Ni	%	0.01	0.03	2.20	2.32	2.50	1.82	2.06	2.08	1.66	0.77	1.93	1.20	<0.05	0.11	<0.05	1.29
Cu	%	0.00	0.00	0.00	0.00	0.00	0.01	0.00	0.00	0.00	0.00	0.00	0.00	<0.03	0.21	0.05	0.55
Zn	ppm	0.8	1.1	1.1	4.4	1.3	1.0	0.8	1.2	3.6	5.9	1.2	1.2	35	1.0	67	237
As	ppm	<5	<5	378	1140	1052	485	974	368	720	488	771	428	23	<5	<5	<5
Se	ppm													62	128	<60	
Ru	ppm	<0.05	<0.05	0.93	55.23	0.59	6.00	1.39	16.56	51.31	124.17	<0.05	<0.05	<0.05	1.54	18.66	6.07
Rh	ppm	<0.08	<0.08	0.63	5.09	<0.08	0.63	0.19	2.21	23.35	54.45	<0.08	<0.08	<0.1	1.53	15.87	4.06
Pd	ppm	<0.1	<0.1	7.38	1.45	0.23	16.13	2.27	0.78	9.52	13.22	2.65	0.58	<0.15	0.38	1.39	2.04
Sb	ppm	0.14	0.19	7.10	1.04	0.07	13.73	1.02	0.60	1.47	1.40	1.31	1.74	<0.8	0.22	<0.8	4.46
Tc	ppm	0.59	0.21	1.40	2.47	0.34	4.35	0.94	1.58	1.52	2.07	2.66	0.48	2.19	0.72	92.55	7.24
Re	ppm	0.00	0.00	0.16	2.80	0.05	0.94	0.26	0.64	3.18	7.30	0.00	0.00	<0.02	0.08	2.24	1.61
Os	ppm	<0.01	<0.01	0.72	6.96	0.08	1.57	0.39	1.54	6.21	13.98	<0.01	<0.01	<0.02	0.15	2.50	0.70
Ir	ppm	<0.01	<0.01	0.76	9.88	0.14	1.40	0.49	1.95	1.95	1.95	1.95	1.95	<0.02	0.37	4.07	1.11
Pt	ppm	<0.01	<0.01	<0.01	<0.01	<0.01	<0.01	<0.01	<0.01	<0.01	0.01	<0.01	<0.01	<0.02	0.35	63.06	1.53
Au	ppm	0.02	<0.01	0.03	0.09	<0.01	0.08	0.02	0.04	0.04	0.10	0.02	0.01	0.01	0.05	0.03	0.25
Bi	ppm	0.29	3.45	14.49	119.50	1.98	33.95	8.22	38.06	145.80	241.40	7.44	3.54	<0.05	10.41	52.95	26.15

sample	RP05.45/166												RP05.45/167				
	py4	py5	py6	py7	py8	py9	py10	py11	py12	mil1	mil2	mil3	mil4	mil1	mil2	mil3	mil4
run	5949	4972	348	8816	471	1312	9944	905	18150	106	120	51	34	3704	4212	4229	5818
Co ppm	0.97	0.91	1.73	0.32	0.53	0.15	1.06	0.07	0.81	60.21	55.96	60.33	58.42	58.31	63.26	62.72	59.48
Ni %	0.56	0.69	0.39	0.74	0.96	0.09	0.44	0.09	0.64	0.71	0.28	0.05	0.07	0.54	0.00	0.00	0.74
Cu %	62	63	55	1.0	2.0	0.8	0.9	0.7	1.3	178	101	175	53	0.9	0.8	0.6	95
Zn ppm	8	24	6	18	31	<5	13	8	<5	67	30	42	32	25	19	21	15
As ppm	159	103	110	2.65	2.37	1.78	2.27	1.39	4.04	593	152	156	481	<0.05	<0.05	<0.05	1.00
Se ppm	2.64	3.63	4.32	3.13	2.37	1.89	2.38	1.50	4.28	1.49	<0.1	0.18	1.04	<0.08	<0.08	<0.08	1.48
Ru ppm	2.55	2.98	3.76	0.38	0.61	0.28	2.84	0.19	2.66	0.28	0.26	0.83	1.19	<0.1	0.55	0.28	4.33
Rh ppm	4.00	2.32	2.21	1.37	1.00	0.41	1.80	0.28	4.58	1.26	<0.8	<0.8	<0.8	0.03	0.16	0.14	<0.8
Pd ppm	1.20	2.95	5.26	1.51	1.55	1.48	5.18	5.77	8.78	2.30	1.71	<0.9	<0.9	0.37	0.84	0.65	1.43
Sb ppm	5.36	8.47	5.04	0.16	0.10	0.10	0.11	0.08	0.21	0.63	0.03	0.72	0.51	0.00	0.00	0.00	0.33
Te ppm	0.25	0.42	0.59	0.37	0.28	0.20	0.27	0.17	0.45	0.10	<0.02	0.33	0.19	<0.01	<0.01	<0.01	0.26
Re ppm	0.47	0.51	0.63	0.57	0.50	0.41	0.48	0.31	0.85	0.65	0.03	0.38	0.08	<0.01	<0.01	<0.01	0.52
Os ppm	0.59	0.80	0.92	0.58	0.63	0.69	1.55	7.84	4.01	0.13	<0.02	<0.02	<0.02	0.01	<0.01	0.01	0.89
Ir ppm	4.00	4.47	3.84	0.14	0.13	0.06	0.22	0.04	0.59	0.11	<0.01	0.02	0.01	<0.01	<0.01	<0.01	<0.01
Pt ppm	0.20	0.24	0.27	0.14	0.13	0.06	0.22	0.04	0.59	0.11	<0.01	0.02	0.01	<0.01	<0.01	<0.01	<0.01
Au ppm	34.37	50.49	17.07	25.76	33.97	11.81	70.44	13.20	130.60	12.97	5.03	5.74	10.34	0.49	3.41	2.91	3.16
Bi ppm																	

sample	RP05.45/166						RP05.45/167					RP05.45/166						
	run	mil5	mil6	cub1	cub2		cpy3	cpy4	cpy5	cpy1	cpy2	cpy3	cpy4	cpy5	cub	c cub	pn1	pn2
Co	ppm	2499	2658	13	<4		1	2	2	83	0	0	0	0	<4	39	59	198
Ni	%	56.40	45.21	6.13	<0.05		0.02	0.00	0.22	1.23	0.00	0.01	0.00	<0.05	3.85	0.79	34.75	30.28
Cu	%	1.82	4.55	20.08	20.72		31.29	30.36	31.77	32.94	34.82	35.02	33.38	23.53	20.37	19.55	0.02	1.43
Zn	ppm	52	71	524	631		69.2	75.7	54.3	9.4	11.0	10.5	11.7	181	94	237	1.1	6
As	ppm	5	15	<5	<5		<5	<5	<5	24	21	17	22	<5	<5	<5	<5	144
Se	ppm	<60	162	68	85									78	84	183		214
Ru	ppm	<0.05	2.80	0.05	0.09		<0.05	6.86	0.07	<0.05	0.06	0.13	<0.05	0.24	0.38	0.12	4.84	4.07
Rh	ppm	<0.1	2.90	<0.1	<0.1		<0.08	0.11	<0.08	<0.08	<0.08	<0.08	<0.08	<0.1	<0.1	<0.1	1.45	1.08
Pd	ppm	0.27	0.73	0.32	<0.15		<0.1	<0.1	0.38	<0.1	<0.1	<0.1	<0.1	<0.15	<0.15	<0.15	1.76	0.94
Sb	ppm	<0.8	<0.8	<0.8	<0.8		0.14	0.09	0.02	0.01	0.20	0.23	0.08	<0.8	<0.8	0.94	0.02	<0.8
Te	ppm	1.60	2.03	<0.9	<0.9		0.18	0.27	0.01	0.17	0.08	0.08	0.23	<0.9	<0.9	<0.9	3.01	2.63
Re	ppm	0.03	0.20	0.03	0.03		0.66	0.44	0.92	0.00	0.01	0.00	0.00	0.04	0.02	<0.02	0.19	0.52
Os	ppm	0.05	1.09	0.05	<0.02		<0.01	0.94	0.02	<0.01	<0.01	<0.01	<0.01	<0.02	0.01	<0.02	0.65	0.69
Ir	ppm	<0.02	3.15	<0.02	<0.02		<0.01	1.43	0.75	<0.01	<0.01	<0.01	<0.01	<0.02	0.04	<0.02	0.57	0.91
Pt	ppm	<0.02	1.34	<0.02	0.06		<0.01	<0.01	<0.01	0.01	<0.01	<0.01	0.01	<0.02	<0.02	0.06	<0.01	<0.02
Au	ppm	<0.01	0.18	0.08	0.03		0.09	0.04	0.07	<0.01	0.02	<0.01	0.02	0.02	0.07	0.11	0.01	0.02
Bi	ppm	0.88	6.35	2.43	0.62		5.09	5.34	11.09	2.39	0.60	1.47	2.05	0.73	0.97	0.86	17.91	18.10

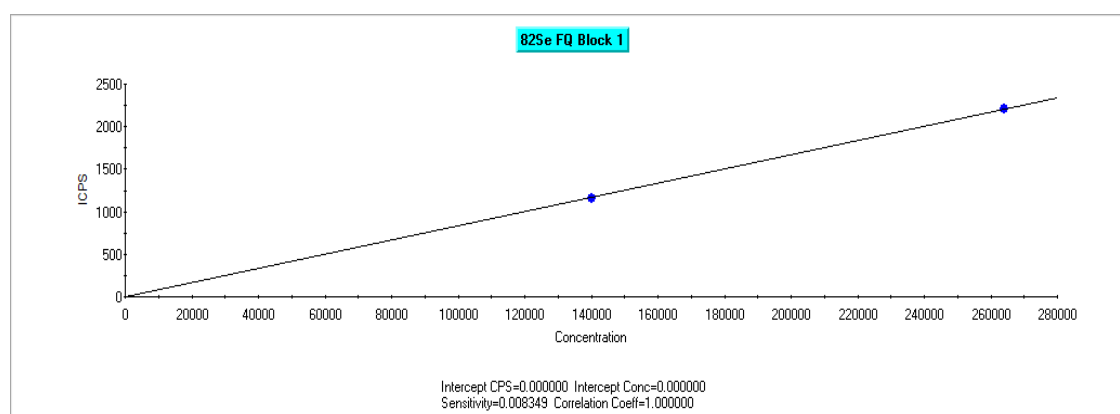
sample		RP05.45/167									
run	pn1	pn2	pn3	pn5	pn6	pn8	pn9	pn10			
Co	ppm	4874	4875	5050	4241	5178	4891	4078	3090		
Ni	%	41.22	42.77	45.14	39.14	38.18	31.65	38.89	38.03		
Cu	%	0.00	0.00	0.00	0.01	0.01	<0.03	0.26	1.37		
Zn	ppm	0.6	0.8	0.7	1.1	0.2	94	33	109		
As	ppm	15	13	13	15	19	7	32	19		
Se	ppm						103	120	110		
Ru	ppm	3.02	3.13	2.67	2.60	<0.05	1.99	0.94	4.43		
Rh	ppm	2.65	2.43	2.68	2.52	0.49	2.38	1.02	1.51		
Pd	ppm	152.30	155.20	162.20	141.60	192.50	138.10	10.07	81.11		
Sb	ppm	0.24	0.34	0.05	0.17	0.20	<0.8	<0.8	<0.8		
Te	ppm	1.74	26.94	0.77	1.58	0.08	2.61	2.64	2.07		
Re	ppm	0.18	0.15	0.11	0.21	0.01	0.39	0.47	0.57		
Os	ppm	0.37	0.40	0.44	0.31	<0.01	0.31	0.15	0.73		
Ir	ppm	0.38	0.43	0.07	0.13	0.01	0.83	0.30	1.48		
Pt	ppm	0.64	34.34	0.20	1.10	0.06	0.68	2.03	0.42		
Au	ppm	<0.01	0.01	<0.01	<0.01	<0.01	0.03	0.01	0.09		
Bi	ppm	0.29	12.44	0.19	0.74	0.13	2.58	10.75	12.45		

S/Se ratios (see Table 5.1) were calculated using average S wt% determined by electron microprobe analysis. Where microprobe data was not available stoichiometric values were used.

Sample	Mineral	Average S wt% (microprobe)	STDV
RP04.23/191	Pn	33.25	0.14
RP04.23392	Po	38.63	0.18
	Cpy	35.27	0.13
	Pn	33.38	0.15
RP04.23/411	Po	38.21	0.10
	Cpy	35.50	0.12
	Pn	33.43	0.13
RP05.45/165	Cpy	35.49	0.12
	Py	53.97	0.14
RP05.45/166	Py	53.74	0.21
	Cpy	34.95	0.06
	Mill	35.41	0.25
RP05.45/167	Py	53.49	0.26
	Cpy	34.34	0.09
	Pn	33.25	0.16
	Mill	35.54	0.26
RP05.45/208	Py	53.82	0.28
	Pn	33.46	0.26
	Mill	35.53	0.36
RP05.45/214	Py*	53.80	0.27
	Cpy	35.5	0.21
	Mil	35.30	0.22
	Py	53.75	0.07
RP05.45/215	Py*	53.80	0.18

#### Potential sources of errors associated with selenium concentrations determined by LA-ICP-MS

The error associated with the *in situ* S/Se ratios presented in Chapter 5 will include an analytical error from both the S and Se concentrations utilised. The Se calibration line presented below demonstrates that the lines utilised during acquisition of the Se data were very well constrained and are therefore considered to be a very minor source of uncertainty.



From personal communication with Ian McDonald it appears that the most significant source of uncertainty is from the signal variation during ablation which shows greater variation when approaching the detection limit of Se (60 ppm). This is reflected in the counting errors of the two Se-bearing standards, which are summarised below.

---

Se bearing standards	Se concentration	Average counts (of three runs)	Stdv (counts)	Rstdv % (from counts)
STD-4	57 ppm	1064	202	19%
STD-5	108 ppm	2078	242	12%

Due to the greater uncertainty and error associated with Se ratios close to detection limit, all concentrations <80 ppm have been disregarded from Table 5.3. The errors propagated through to the Se ratios between phases presented in Table 5.3 were derived from the calculated 12% counting variation on each Se analysis. These ratios have an associated error of  $\pm 0.1$  to  $\pm 0.2$ .

Utilising the 12% counting error on the Se data presented in Table 5.3, shows that much of the large variations observed within a single phase are real, although the minor variations are within the calculated analytical error and may reflect this uncertainty. Selenium is in many samples, heterogeneously distributed within each sulfide phase. The variations in counts observed on each run (Figure 5.7) therefore includes both analytical and natural error (i.e. heterogeneity).

The in situ S/Se ratios include data <80 ppm. In Chapter 5 it is important to be aware that a larger error will be associated with those S/Se ratios which utilise data <80 ppm. These typically have higher S/Se ratios compared to the rest of the data. Some of the variability in S/Se ratios within a sample e.g. RP04.23/392 pyrrhotite (Figure 5.10) will result from the analytical error.

# Appendix 3

Mass Balance calculations and data

For our mass balance in Chapter 4, our calculations are based on those of Huminicki et al. 2005.

Our calculations require: (i) concentration of each element in the whole rock (Appendix 1); (ii) the weight fraction (in wt.%) of each sulfide phase (Table 1 and 2), as determined from whole rock geochemistry below; and (iii) the average concentration of each element in each sulfide phase, determined by microprobe analysis (given below).

The weight fraction (X) of chalcopyrite (Ccp), pyrrhotite (Po) and pentlandite (Pn) was calculated for each sample using whole rock (wr) Cu, Ni and S and stoichiometric values for the sulfides.

Note: CuCcp(avg) = 34.63 wt %; SCcp (avg) = 34.94 wt %; FeCcp (avg) = 30.43 wt %; NiPn (avg) = 34.21 wt %; SPn (avg) = 33.23 wt %; FePn (avg) = 32.56 wt %; SPo (avg) = 37.67 wt %; FePo (avg) = 62.33 wt %; NiPo (avg) = 0.92 wt%; Ni in silicate (0.01).

The amount of chalcopyrite present is:

$$\begin{aligned}XC_{cp} &= C_{usamp}/Cu_{Ccp} \text{ (avg)} \\SC_{cp} &= XC_{cp} * SC_{cp} \text{ (avg)} \\Fe_{Ccp} &= XC_{cp} * Fe_{Ccp} \text{ (avg)}\end{aligned}$$

The amount of pentlandite present is:

$$\begin{aligned}XP_n \text{ (1)} &= (N_{isamp}-N_{isilicate})/Ni_{Pn} \text{ (avg)} \\SP_n \text{ (1)} &= XP_n \text{ (1)} * SP_n \text{ (avg)} \\Fe_{Pn} \text{ (1)} &= XP_n \text{ (1)} * Fe_{Pn} \text{ (avg)}\end{aligned}$$

The amount of pyrrhotite present is:

$$\begin{aligned}XP_o \text{ (1)} &= (S_{samp} - SC_{cp} - SP_n \text{ (1)})/SP_o \text{ (avg)} \\Fe_{Po} \text{ (1)} &= XP_o \text{ (1)} * Fe_{Po} \text{ (avg)} \\Ni_{Po} \text{ (1)} &= XP_o \text{ (1)} * Ni_{Po} \text{ (avg)}\end{aligned}$$

The contribution of Ni in pyrrhotite is taken into consideration:

The amount of pentlandite present is:

$$\begin{aligned}XP_n \text{ (2)} &= (N_{isamp}-Ni_{Po} \text{ (1)})/Ni_{Pn} \text{ (avg)} \\SP_n \text{ (2)} &= XP_n \text{ (2)} * SP_n \text{ (avg)} \\Fe_{Pn} \text{ (2)} &= XP_n \text{ (2)} * Fe_{Pn} \text{ (avg)}\end{aligned}$$

The amount of pyrrhotite present is:

$$\begin{aligned}XP_o \text{ (2)} &= (S_{samp}-SC_{cp}-SP_n \text{ (2)})/SP_o \text{ (avg)} \\Fe_{Po} \text{ (2)} &= XP_o \text{ (2)} * Fe_{Po} \text{ (avg)} \\Ni_{Po} \text{ (2)} &= XP_o \text{ (2)} * Ni_{Po} \text{ (avg)}\end{aligned}$$

$$X_{sul} = XC_{cp} + XP_n \text{ (2)} + XP_o \text{ (2)}$$

Remove cpy as barren of PGE so  $X_{sul} = X_{po} + X_{pn}$

The metal content of sulfides was then determined semi-quantitatively by: whole rock concentration of element in whole rock/wt fraction of sulfide

**Table 1:** Primary sulfide assemblages

borehole /depth	calculated sulfide fraction (wt%)			PGE in sulfide recalculated to 100%						
	cpy	pn	po	Os	Ir	Ru	Rh	Pt	Pd	Au
RP04.21/690a	0.0075	0.0139	0.0255							
	bulk sulfide po+pn			0.254	0.331	3.076	0.856	6.651	27.050	2.319
	bulk sulfide po only			0.383	0.499	4.630	1.288	10.010	40.711	3.490
	bulk sulfide pn only			0.758	0.987	9.167	2.550	19.820	80.610	6.910
690b	0.0023	0.0084	0.1301							
	bulk sulfide po+pn			0.021	0.025	0.231	0.084	0.880	2.445	0.458
	bulk sulfide po only			0.022	0.026	0.240	0.087	0.912	2.537	0.475
	bulk sulfide pn only			0.582	0.703	6.424	2.332	24.428	67.907	12.718
693	0.0017	0.0017	0.0078							
	bulk sulfide po+pn			0.060	0.099	0.761	0.403	4.096	14.080	2.361
	bulk sulfide po only			0.074	0.122	0.934	0.494	5.022	17.267	2.896
	bulk sulfide pn only			0.327	0.537	4.126	2.181	22.195	76.304	12.796
RP04.23/384	0.0023	0.0021	0.0098							
	bulk sulfide po+pn			0.123	0.130	1.565	0.419	3.718	10.195	2.301
	bulk sulfide po only			0.149	0.158	1.905	0.510	4.525	12.407	2.800
	bulk sulfide pn only			0.687	0.730	8.780	2.350	20.858	57.190	12.907
392a	0.0130	0.0066	0.0259							
	bulk sulfide po+pn			0.062	0.104	0.515	0.515	9.102	26.210	4.642
	bulk sulfide po only			0.077	0.128	0.637	0.637	11.267	32.446	5.747
	bulk sulfide pn only			0.325	0.540	2.679	2.678	47.357	136.377	24.155
392b	0.0013	0.0013	0.0092							
	bulk sulfide po+pn			0.027	0.039	0.263	0.136	1.704	6.582	1.827
	bulk sulfide po only			0.030	0.045	0.300	0.155	1.942	7.501	2.082
	bulk sulfide pn only			0.217	0.321	2.149	1.111	13.902	53.709	14.908
396a	0.0023	0.0021	0.0098							
	bulk sulfide po+pn			0.129	0.138	1.656	0.401	3.476	10.142	1.965
	bulk sulfide po only			0.157	0.168	2.015	0.488	4.231	12.342	2.392
	bulk sulfide pn only			0.723	0.775	9.288	2.252	19.501	56.889	11.025
396b	0.0130	0.0066	0.0259							
	bulk sulfide po+pn			0.060	0.099	0.522	0.502	6.167	26.308	3.559
	bulk sulfide po only			0.074	0.122	0.646	0.621	7.635	32.567	4.405
	bulk sulfide pn only			0.310	0.514	2.716	2.612	32.090	136.886	18.516
411	0.0026	0.0052	0.0148							
	bulk sulfide po+pn			0.438	0.610	3.792	1.940	19.041	34.700	2.890
	bulk sulfide po only			0.581	0.810	5.036	2.576	25.285	46.079	3.838
	bulk sulfide pn only			1.773	2.470	15.358	7.855	77.108	140.517	11.704

**Table 2:** Secondary sulfide assemblages

borehole /depth	calculated sulfide fraction (wt%)			PGE in sulfide recalculated to 100%						
	mill	pn	py	Os	Ir	Ru	Rh	Pt	Pd	Au
RP045.45/146	0.0009		0.0009							
	bulk sulfide py+mil			0.359	0.828	3.802	2.466	22.013	53.481	7.864
	bulk sulfide py only			0.701	1.616	7.417	4.811	42.943	104.331	15.342
165	0.000367		0.002							
	bulk sulfide py+mil			0.13	0.57	2.418	2.01	13.42	43.709	5.118
	bulk sulfide py only			0.16	0.68	2.901	2.41	16.1	52.445	6.141
214	0.025635		0.011							
	bulk sulfide py+mil			0.14	0.25	1.247	5.85	25.85	66.735	5.899
	bulk sulfide py only			0.46	0.85	4.159	19.5	86.21	222.59	19.68
215			0.005							
	bulk sulfide py only			0.13	0.27	1.333	4.15	24.83	126.06	6.332
MD03.1/552		0.01320	0.003							
	bulk sulfide py+pn			1.51	1.86	11.04	4.46	61.87	57.237	22.83
	bulk sulfide py only			8.47	10.4	61.74	24.9	345.9	319.97	127.6
	bulk sulfide pn only			1.84	2.26	13.45	5.43	75.34	69.706	27.81

# Appendix 4

## Sulfur Isotopes

Sulfur Isotope analysis using laser technique at SUERC  
 Samples from Rooipoort

Sample	Mineral	Pent	CO <sub>2</sub>	SO <sub>2</sub>	$\delta^{66}\text{S}$	$\delta^{34}\text{S}_{\text{raw}}$	$\delta^{34}\text{S}_{\text{true}}$
RP04.21							
448	cpy	4.6	0.09	0.5	-6.25	2.8	3.5
	py +mil	4.2	0.06	0.4	-5.72	3.4	4.1
	py	4.2	0.05	0.5	-6.227	2.8	3.6
460	po	3.8	0.8	4.5	-6.478	1.9	2.3
	po	4	0.2	4.1	-6.311	2.1	2.5
679	py	4.2	1.4	1	-6.315	2.7	3.5
	py	5	0.1		-6.500	2.2	3
	po	4.4	0.08	3	-7.605	1.3	1.7
	cpy	4.4	0.04	6	-8.253	0.6	1.3
	pn	4.4	0.06	2.3	-7.582	1.3	3.2
681	cpy	4.6	0.07	3	-6.854	2.1	2.8
	py+pn	4.6	0.08	2.2	-7.375	1.6	2.4
690	po	4.6	0.09	2.1	-7.683	1.2	1.6
	po	5	0.07	1	-6.227	2.8	3.6
	po	5	1	2.6	-7.505	1.4	1.8
693	po	4.1	0.06	2.5	-6.501	2.5	2.9
	po	4.2	0.07	1.2	-6.751	2.2	2.6
	pn	4.4	0.07	2	-6.869	2.1	4.0
	pn	5.1	0.09		-6.023	2.8	4.7
	po	4.8	0.04	1.7	-6.370	2.7	3.1
	cpy	5	0.06		-6.141	2.6	3.3
RP05.45							
146	py	4.2	0.04	0.6	-3.043	6.0	6.8
149	mil	5.8	0.07	0.3	-7.233	1.7	3.6
	py	5	1	1.2	-5.761	3.4	4.2
	mil	4.6	0.07	1	-7.0	2	3.9
	py	4.2	0.07	0.6	-5.05	4.2	5.0
	cpy	4	0.06	3	-5.174	4	4.7
165	cpy	5	0.05	1.4	-5.744	3.4	4.1
	cpy	5.1	0.04	2.1	-5.915	3.2	3.9
	py	5.2	0.07	1.3	-5.970	3.1	3.9
	py	5.2	0.04	1.1	-5.058	4.1	4.9
	py	4.9	0.1		-4.870	4.1	4.9
	mil	5.2	0.05	1	-6.088	3.0	4.9
166	cpy	4.5	0.1		-4.363	4.6	5.3
167	cpy	5.2	0.1	3	-5.415	3.7	4.4
	cpy	6.0	0.1	3.5	-5.512	3.7	4.4
	py	5.6	0.1	0.9	-5.115	6.3	7.1
	py	4.2	0.03	0.6	-2.950	6.1	6.9
	pn	4.2	0.03	0.85	-3.59	5.6	7.5
	pn	5.6	0.04	1	-5.604	3.6	5.4
	cpy	4	0.05	0.96	-3.547	5.4	6.1
	cpy	5.2	0.05	0.8	-6.853	2.1	2.3
	py	5.6	0.04	0.8	-3.575	5.8	6.6
	cpy	5.3	0.04	1.4	-4.577	4.7	5.4
	pn	5.2	0.07	2.8	-5.447	3.7	5.6
	py	5.2	0.05	1.1	-4.084	5.3	6.1
	py	5	0.1		-4.043	5	5.8
205	py	4.2	0.08	1	-5.53	3.5	4.1
	py	4.7	0.07	0.8	-5.663	3.5	4.3
	mil	5.4	0.06	0.4	-6.814	2.2	4.1
	cpy	5.2	0.04	1.1	-6.014	1.7	3.6
206	cpy	5.2	0.06	3.1	-5.953	3.2	3.9
208	py	5	0.05	1.13	-4.735	4.2	5
	py	5.2	0.06	2.4	-4.833	4.1	4.9
	cpy	5	0.06		-4.670	4.3	5
	pn	5.2	0.1		-4.673	4.9	6.8
212	py	5.4	0.08	1.2	-5.475	3.7	4.5
	py	5.2	0.1	1.1	-5.813	3.3	4.1
	cpy+mil	5.2	0.05	0.6	-9.253	-0.6	0.1
214	py	5.4	0.09	0.6	-4.763	4.5	5.3
	py	5.2	0.09	1.2	-4.511	4.8	5.6
	cpy	5.4	0.1	2	-6.177	2.9	3.6
	cpy	5.2	0.02	1.7	-5.847	3.3	4.1
	mil	4.6	0.06	2.6	-6.907	2.1	2.8
	py	4.2	0.05	0.8	-3.547	5.4	6.2
	cpy	4	0.09	1.86	-5.063	3.8	4.5
	py	4.2	0.06	0.7	-5.324	3.5	4.3
RP04.23							
158	py	5.2	0.03	0.33	-4.628	4.2	5.0
191	pn	4.8	0.06	1.1	-6.919	2.1	4.0

201	cpy	4.6	0.08	1.7	-6.892	2.1	2.8
	po	4.4	0.07	0.53	-0.392	2.3	2.7
305	po	4	0.05	1.13	-6.372	2.3	2.8
392	cpy	5	0.1	2.1	-6.091	2.7	3.4
	pn	5	0.1		-5.477	3.4	5.3
	po	5	0.1		-5.614	3.2	3.6
411	cpy	4.8	0.1		-5.552	3.3	4
	pn	4.9	0.1		-6.720	3.1	5
	po	4.7	0.1		-5.951	2.8	3.2
RP03.12							
140	py	4	0.1	2.1	-6.778	1.5	2.3
	py	4	0.05	1	-5.701	2.8	3.6
144	py	4	1	3.1	-4.872	3.7	4.5
145	py	3.8	0.07	6	-5.329	4.0	4.8
RP05.37							
106	py	4	0.08	6.8	-5.311	3.2	4.0

## Samples from Grasvally and Moorddrift

Sample	Mineral	Pent	Co <sub>2</sub>	SO <sub>2</sub>	$\delta^{66}\text{S}$	$\delta^{34}\text{S}_{\text{raw}}$	$\delta^{34}\text{S}_{\text{true}}$
GV05.49							
128	py	4.4	0.07	2	-3.323	5.5	6.3
	cpy	4.2	0.07	3.8	-3.733	5.0	5.7
	pn	4	0.05	1.6	-5.336	3.2	5.1
127	py	4	0.1	3.2	-5.083	3.5	4.3
	cpy	4.1	0.05	1.7	-5.597	2.9	3.6
140	po	4	0.05	2.5	-4.958	3.6	4.0
	po	4.2	0.1	1.1	-4.332	4.3	4.7
	cpy	3.8	0.08	6	-5.929	2.5	3.2
	py	4	0.1	2.8	-5.69	2.8	3.6
214	py	4.6	0.1	1	0.395	9.7	10.5
	py	4.4	0.1	3.1	-0.221	9.0	9.8
MD03.1							
552	pn	4.8	0.09	2	-7.296	1.6	3.5
	cpy	4.8	0.08	2.5	-7.213	1.7	2.4
	py	4.8	0.07	0.8	-7.065	2.1	2.9

## Samples from War Springs

Sample	Mineral	Pent	Co <sub>2</sub>	SO <sub>2</sub>	$\delta^{66}\text{S}$	$\delta^{34}\text{S}_{\text{raw}}$	$\delta^{34}\text{S}_{\text{true}}$
ORL4							
65	py	4	0.05	2	-5.752	2.7	3.5
	pn	3.8	0.06	3.6	-6.44	1.9	3.8
	cpy	4	0.07	2.1	-6.183	2.2	2.9
395	po	3.8	0.05	2.8	-5.339	3.3	3.7
	po	3.8	0.3	5.1	-4.742	3.8	4.2
	py	3.8	0.22	6.9	-6.488	1.8	2.6
	pn	3.8	0.1	4.7	-6.125	2.3	4.2
606a2	po	3.8	0.14	4.7	-3.349	5.4	5.8
	po	3.9	0.2	5.4	-3.799	4.9	5.3
	cpy	3.9	0.1	4	-4.232	4.4	5.1
606a1	po	4	0.1	2.6	-3.615	5.1	5.5
	po	4	0.14	2.5	-3.85	4.9	5.3
606b	po	3.8	0.13	3.2	-4.401	4.2	4.6
	cpy	4	0.1	1.3	-3.57	5.2	5.9
221	cpy	3.8	0.1	2.6	-7.02	1.2	1.9
	py	3.8	0.09	3.7	-6.53	1.8	2.6
	po	3.6	0.1	4	-6.823	1.5	1.9
	py	3.6	0.1	8.6	-6.714	1.6	2.4
	po	3.6	0.13	3.2	-7.704	0.5	0.9
ORL5							
597	py	3.6	0.13	4.3	-4.364	4.3	5.1
	pn	3.7	0.12	1.8	-4.714	3.9	5.8
	py	3.6	0.06	3.1	-4.405	4.2	5.0
97	cpy	4	0.06	2.8	-6.019	2.4	3.2
	py	4	0.1	2.2	-6.037	2.4	3.2
108	py	4	0.1	5	-6.53	1.8	2.6
	cpy	4	0.1	1.1	-6.578	1.7	2.4
	py	3.8	0.06	3.7			2.5

Fractionation factors: pyrrhotite +0.4, pentlandite +0.9, chalcopyrite +0.7, pyrite +0.8 and millerite +1.9 ‰. Repeated analysis of individual sulfide phases revealed in general a reproducibility of  $\pm 0.2$  ‰ (repeats include samples RP04.21 460 po, 679 py, RP05.45 165, cpy, 208 py, 214 py and ORL 65 pn).

## Sulfur Isotope analysis using conventional technique at SUERC

Sample	Mineral		$\delta^{66}\text{SO}_2$	$\alpha$	$\delta^{34}\text{S}$
CP1	cpy	STD	-10.455	0.050	-4.6
NBS-123	sp	STD	10.268	.010	17.1
IAEA-S-3	Ag <sub>2</sub> S	STD	-36.236	.033	-31.5
RP04.23					
338	po		-3.351	.012	2.9
384			-2.752	.007	3.5
392			-2.725	.012	3.5
411			-3.161	.031	3.1
RP05.45					
215	py		-2.191	.010	4.1
RP04.21					
542	cpy		1.591	.015	8.0

# Appendix 5

## Electron Microprobe data

Microprobe data utilized in Chapter 6 has been filtered to exclude any analysis with unsuitably low totals of <97 wt %. Lithological abbreviations are the same as in Appendix 1.

## Microprobe analysis of orthopyroxene

Depth	Rock type	Unit	SiO <sub>2</sub>	TiO <sub>2</sub>	Al <sub>2</sub> O <sub>3</sub>	Cr <sub>2</sub> O <sub>3</sub>	MgO	CaO	MnO	FeO	Na <sub>2</sub> O	K <sub>2</sub> O	Total	En	Wo	Fs
39	GBN	MZ	53.74	0.14	0.81	0.04	22.77	1.97	0.41	20.31	0.05	0.00	100.24	63.99	3.98	32.03
39	GBN	MZ	53.68	0.19	0.78	0.00	22.99	1.71	0.38	21.03	0.03	0.00	100.80	63.82	3.42	32.76
39	GBN	MZ	53.76	0.17	0.78	0.05	22.88	1.54	0.40	20.34	0.06	0.00	99.99	64.64	3.13	32.24
39	GBN	MZ	53.54	0.23	0.67	0.05	22.90	1.59	0.41	20.65	0.06	0.00	100.10	64.27	3.21	32.52
39	GBN	MZ	53.04	0.19	0.66	0.01	22.66	1.73	0.39	20.66	0.03	0.00	99.37	63.83	3.51	32.67
39	GBN	MZ	53.61	0.19	0.65	0.03	23.12	1.47	0.38	20.28	0.02	0.00	99.75	65.03	2.97	32.00
39	GBN	MZ	53.71	0.17	0.71	0.00	22.93	1.97	0.39	20.20	0.04	0.00	100.13	64.27	3.97	31.77
39	GBN	MZ	53.64	0.26	0.63	0.06	23.13	1.94	0.38	19.89	0.02	0.00	99.94	64.81	3.91	31.28
39	GBN	MZ	53.87	0.18	0.69	0.02	23.20	2.07	0.38	20.06	0.03	0.00	100.50	64.55	4.14	31.32
39	GBN	MZ	53.57	0.21	0.72	0.04	23.13	1.95	0.37	19.76	0.03	0.00	99.78	64.93	3.94	31.13
73	GBN	MANO	52.60	0.38	0.76	0.04	21.36	2.27	0.39	22.26	0.05	0.00	100.10	60.20	4.59	35.21
73	GBN	MANO	53.05	0.37	0.72	0.08	21.42	2.13	0.43	21.89	0.04	0.00	100.11	60.79	4.35	34.86
73	GBN	MANO	53.40	0.20	0.62	0.08	21.56	1.75	0.42	21.83	0.03	0.00	99.89	61.48	3.59	34.92
73	GBN	MANO	53.23	0.28	0.72	0.08	21.55	1.94	0.41	22.07	0.02	0.00	100.29	61.00	3.94	35.06
90	GBN	MANO	53.95	0.27	0.65	0.11	24.00	1.96	0.37	18.72	0.04	0.00	100.07	66.82	3.93	29.25
90	GBN	MANO	53.96	0.24	0.56	0.07	24.34	1.55	0.37	18.95	0.04	0.00	100.07	67.44	3.10	29.46
90	GBN	MANO	53.88	0.31	0.67	0.09	22.82	4.59	0.35	17.14	0.03	0.00	99.87	63.85	9.23	26.92
90	GBN	MANO	53.44	0.28	0.59	0.10	24.38	1.54	0.36	18.57	0.03	0.00	99.29	67.89	3.09	29.02
90	GBN	MANO	53.52	0.21	0.62	0.05	23.38	1.58	0.37	18.83	0.04	0.00	98.60	66.64	3.24	30.12
90	GBN	MANO	53.95	0.32	0.58	0.09	23.95	1.75	0.37	19.01	0.02	0.00	100.03	66.75	3.51	29.73
90	GBN	MANO	53.86	0.33	0.60	0.08	23.87	2.15	0.37	18.54	0.03	0.00	99.82	66.64	4.32	29.05
90	GBN	MANO	54.02	0.30	0.65	0.04	24.04	1.51	0.38	18.88	0.05	0.00	99.85	67.31	3.03	29.66
90	GBN	MANO	53.58	0.37	0.61	0.08	23.81	1.55	0.35	18.99	0.05	0.00	99.38	66.91	3.13	29.96
90	GBN	MANO	53.76	0.35	0.56	0.05	24.09	1.74	0.38	19.08	0.00	0.00	100.01	66.82	3.47	29.71
90	GBN	MANO	53.61	0.32	0.56	0.09	24.01	1.78	0.36	18.73	0.02	0.00	99.48	67.07	3.57	29.36
122	NR	MANO	52.78	0.25	0.63	0.18	25.47	1.82	0.32	15.73	0.03	0.00	97.20	71.54	3.67	24.78
122	NR	MANO	52.28	0.32	0.61	0.15	25.19	1.75	0.34	15.71	0.03	0.00	96.38	71.43	3.58	25.00
122	NR	MANO	52.73	0.30	0.57	0.16	25.50	1.40	0.32	15.98	0.01	0.00	96.96	71.89	2.83	25.28
122	NR	MANO	52.80	0.29	0.61	0.19	25.42	1.79	0.29	15.65	0.05	0.00	97.09	71.63	3.62	24.74
122	NR	MANO	52.58	0.17	0.84	0.18	25.62	1.38	0.30	16.13	0.02	0.00	97.22	71.85	2.78	25.37
122	NR	MANO	52.88	0.20	0.75	0.16	25.20	2.01	0.29	15.71	0.03	0.00	97.22	71.07	4.07	24.86
197	GBN	MANO	54.45	0.15	0.97	0.33	28.22	1.54	0.30	13.26	0.01	0.00	99.21	76.74	3.02	20.24
197	GBN	MANO	54.21	0.17	1.00	0.37	28.38	1.33	0.29	13.24	0.02	0.00	99.01	77.19	2.61	20.20
197	GBN	MANO	54.00	0.06	1.09	0.36	28.22	1.72	0.26	13.22	0.03	0.00	98.95	76.53	3.35	20.12
197	GBN	MANO	54.01	0.13	1.07	0.43	27.94	2.15	0.31	13.07	0.04	0.00	99.12	75.89	4.19	19.92
197	GBN	MANO	54.38	0.24	0.81	0.36	28.46	1.45	0.29	13.38	0.02	0.00	99.38	76.89	2.82	20.29
197	GBN	MANO	54.82	0.27	0.79	0.33	28.37	1.32	0.29	13.37	0.01	0.00	99.57	77.05	2.58	20.38
197	GBN	MANO	54.58	0.09	1.07	0.42	28.01	1.94	0.27	13.01	0.03	0.00	99.42	76.31	3.81	19.89
197	GBN	MANO	54.37	0.11	1.00	0.41	27.72	2.41	0.29	12.85	0.03	0.00	99.18	75.61	4.72	19.67
197	GBN	MANO	54.27	0.18	0.84	0.32	28.36	1.64	0.28	13.15	0.02	0.00	99.06	76.81	3.20	19.99
197	GBN	MANO	54.21	0.13	1.03	0.38	27.60	2.78	0.28	12.71	0.03	0.00	99.14	75.13	5.45	19.42
214	GBN	LMF	53.82	0.18	0.64	0.22	28.14	1.16	0.30	14.06	0.02	0.00	98.54	76.33	2.27	21.40
214	GBN	LMF	53.59	0.18	0.76	0.26	27.49	2.53	0.32	13.78	0.02	0.00	98.92	74.21	4.91	20.88
214	GBN	LMF	53.96	0.26	0.68	0.23	27.95	1.34	0.32	13.89	0.03	0.00	98.65	76.15	2.63	21.23

Appendix 5: Microprobe data

Depth	Rock type	Unit	SiO <sub>2</sub>	TiO <sub>2</sub>	Al <sub>2</sub> O <sub>3</sub>	Cr <sub>2</sub> O <sub>3</sub>	MgO	CaO	MnO	FeO	Na <sub>2</sub> O	K <sub>2</sub> O	Total	En	Wo	Fs
214	GBN	LMF	54.48	0.14	0.87	0.33	28.15	1.13	0.31	14.21	0.03	0.00	99.64	76.21	2.20	21.59
214	GBN	LMF	54.96	0.10	0.59	0.27	28.44	0.82	0.28	13.84	0.02	0.00	99.33	77.28	1.61	21.11
214	GBN	LMF	53.55	0.12	0.81	0.29	27.60	2.35	0.29	13.64	0.03	0.00	98.68	74.71	4.57	20.73
214	GBN	LMF	52.26	0.13	1.97	0.27	26.74	2.25	0.27	12.70	0.06	0.02	96.65	75.36	4.55	20.09
214	GBN	LMF	54.57	0.14	0.80	0.25	27.83	2.03	0.29	13.58	0.01	0.00	99.49	75.41	3.95	20.64
214	GBN	LMF	54.83	0.14	0.97	0.33	27.67	2.05	0.30	13.76	0.04	0.00	100.09	75.06	4.00	20.94
232	GBN	LMF	53.94	0.18	0.83	0.32	26.28	1.65	0.30	15.35	0.08	0.01	98.93	72.83	3.29	23.88
232	GBN	LMF	54.18	0.25	0.68	0.28	26.79	1.10	0.34	15.58	0.09	0.01	99.29	73.75	2.18	24.07
232	GBN	LMF	54.18	0.25	0.68	0.28	26.79	1.10	0.34	15.58	0.09	0.01	99.29	73.75	2.18	24.07
295	GBN	LMF	52.83	0.24	0.81	0.35	25.00	1.49	0.37	18.09	0.05	0.01	99.24	69.01	2.96	28.03
295	GBN	LMF	53.64	0.22	0.79	0.28	24.72	1.28	0.38	17.70	0.02	0.00	99.04	69.49	2.59	27.92
295	GBN	LMF	53.40	0.19	0.93	0.33	24.69	1.46	0.39	18.10	0.05	0.00	99.54	68.78	2.92	28.29
295	GBN	LMF	53.44	0.17	0.96	0.31	24.18	2.74	0.33	17.00	0.14	0.11	99.39	67.74	5.53	26.73
295	GBN	LMF	52.86	0.25	0.88	0.34	25.21	1.43	0.40	17.81	0.04	0.00	99.22	69.57	2.84	27.59
295	GBN	LMF	53.36	0.25	0.90	0.33	24.78	2.38	0.36	17.39	0.05	0.00	99.80	68.36	4.72	26.93
295	GBN	LMF	53.77	0.22	0.77	0.30	24.70	2.30	0.38	17.37	0.03	0.00	99.83	68.41	4.58	27.00
295	GBN	LMF	53.83	0.26	0.87	0.29	24.84	1.40	0.38	18.04	0.04	0.00	99.96	69.06	2.80	28.14
295	GBN	LMF	53.84	0.28	0.89	0.37	24.90	1.38	0.35	17.93	0.03	0.00	99.96	69.26	2.75	27.99
295	GBN	LMF	53.80	0.30	1.00	0.30	24.95	1.51	0.38	18.04	0.03	0.00	100.32	69.01	3.00	27.99
295	GBN	LMF	53.78	0.27	0.79	0.25	24.98	1.36	0.36	18.05	0.07	0.00	99.92	69.22	2.71	28.07
305	NR	LMF	53.51	0.11	0.77	0.21	23.01	1.80	0.40	20.03	0.03	0.00	99.87	64.73	3.64	31.62
305	NR	LMF	53.66	0.15	0.79	0.23	23.17	1.57	0.39	20.16	0.03	0.00	100.16	65.06	3.17	31.77
305	NR	LMF	53.84	0.17	0.77	0.30	24.00	1.42	0.37	19.08	0.02	0.00	99.97	67.17	2.86	29.97
315	GBN	LMF	52.89	0.15	0.97	0.39	24.40	1.63	0.32	16.66	0.02	0.00	97.44	69.86	3.36	26.77
315	GBN	LMF	53.16	0.16	1.04	0.39	24.25	1.96	0.33	16.53	0.03	0.00	97.85	69.41	4.04	26.55
315	GBN	LMF	53.31	0.21	0.80	0.33	24.45	1.48	0.34	16.95	0.01	0.00	97.88	69.80	3.04	27.16
315	GBN	LMF	52.54	0.25	0.77	0.38	24.39	1.35	0.34	17.41	0.01	0.00	97.44	69.42	2.76	27.82
315	GBN	LMF	52.40	0.24	0.71	0.26	24.23	1.25	0.35	17.54	0.02	0.00	97.00	69.28	2.58	28.14
315	GBN	LMF	53.13	0.30	0.74	0.27	24.42	1.46	0.33	16.77	0.03	0.00	97.46	70.01	3.02	26.98
315	GBN	LMF	52.82	0.16	0.91	0.46	24.10	1.78	0.32	16.56	0.03	0.00	97.13	69.51	3.69	26.80
353	NR	LMF	52.97	0.21	0.95	0.40	24.29	1.74	0.30	16.82	0.02	0.00	97.71	69.43	3.58	26.98
353	NR	LMF	52.70	0.25	0.82	0.35	24.38	1.75	0.32	16.93	0.03	0.00	97.52	69.38	3.58	27.04
353	NR	LMF	52.61	0.33	0.84	0.34	24.33	1.36	0.29	17.26	0.02	0.00	97.38	69.52	2.80	27.68
353	NR	LMF	52.93	0.21	0.98	0.31	24.77	1.31	0.31	16.74	0.05	0.00	97.61	70.56	2.68	26.77
353	NR	LMF	52.84	0.16	0.73	0.31	24.65	1.84	0.29	16.61	0.04	0.00	97.46	69.84	3.75	26.41
374	GBN	LMF	53.18	0.17	0.86	0.17	22.83	1.76	0.38	20.27	0.03	0.00	99.63	64.37	3.56	32.07
374	GBN	LMF	52.86	0.25	0.87	0.20	23.05	1.55	0.39	20.16	0.02	0.00	99.34	64.98	3.14	31.88
374	GBN	LMF	51.59	0.25	0.93	0.23	23.08	1.42	0.36	20.00	0.03	0.00	97.89	65.35	2.89	31.76
374	GBN	LMF	51.77	0.22	0.80	0.22	23.30	1.29	0.37	20.53	0.03	0.00	98.51	65.18	2.59	32.23
374	GBN	LMF	51.20	0.18	0.75	0.17	23.11	1.40	0.36	20.86	0.02	0.00	98.05	64.51	2.80	32.69
374	GBN	LMF	51.84	0.28	0.79	0.15	22.97	1.63	0.39	20.56	0.02	0.00	98.63	64.39	3.28	32.33
374	GBN	LMF	52.29	0.25	0.83	0.18	23.64	1.42	0.34	19.66	0.01	0.00	98.61	66.23	2.86	30.91
374	GBN	LMF	52.52	0.20	0.72	0.23	23.50	1.63	0.38	19.65	0.01	0.00	98.83	65.82	3.28	30.89
374	GBN	LMF	52.47	0.21	0.75	0.31	21.79	5.64	0.32	17.22	0.08	0.00	98.79	61.37	11.43	27.21
374	GBN	LMF	52.52	0.25	0.83	0.23	23.54	1.58	0.36	19.53	0.03	0.00	98.86	66.07	3.19	30.75

Appendix 5: Microprobe data

Depth	Rock type	Unit	SiO <sub>2</sub>	TiO <sub>2</sub>	Al <sub>2</sub> O <sub>3</sub>	Cr <sub>2</sub> O <sub>3</sub>	MgO	CaO	MnO	FeO	Na <sub>2</sub> O	K <sub>2</sub> O	Total	En	Wo	Fs
374	GBN	LMF	52.45	0.14	0.66	0.15	24.19	0.79	0.36	19.71	0.01	0.00	98.46	67.54	1.58	30.89
374	GBN	LMF	53.15	0.21	0.98	0.19	23.47	1.63	0.36	19.36	0.04	0.00	99.39	66.11	3.29	30.60
374	GBN	LMF	52.99	0.22	0.79	0.20	23.67	1.37	0.35	19.61	0.02	0.00	99.21	66.38	2.75	30.86
384	NR	LMF	51.75	0.07	1.02	0.40	23.70	2.19	0.35	18.66	0.03	0.00	98.16	66.30	4.40	29.29
384	NR	LMF	51.80	0.13	1.13	0.36	23.54	1.93	0.35	19.04	0.04	0.00	98.32	66.10	3.90	30.00
384	NR	LMF	51.86	0.10	1.35	0.41	23.63	1.72	0.35	19.37	0.04	0.00	98.82	66.13	3.45	30.42
384	NR	LMF	51.19	0.24	0.84	0.13	23.81	1.14	0.36	19.31	0.03	0.00	97.03	67.14	2.30	30.56
384	NR	LMF	51.24	0.15	0.98	0.20	23.61	1.87	0.39	19.04	0.02	0.00	97.50	66.24	3.78	29.98
384	NR	LMF	52.25	0.29	0.64	0.14	23.52	1.16	0.38	19.87	0.02	0.00	98.26	66.25	2.34	31.41
384	NR	LMF	53.09	0.26	0.87	0.15	23.67	1.27	0.39	19.59	0.02	0.00	99.31	66.53	2.57	30.90
384	NR	LMF	53.15	0.29	0.83	0.14	23.73	1.29	0.40	19.61	0.02	0.00	99.45	66.53	2.60	30.86
384	NR	LMF	53.05	0.35	0.69	0.12	23.59	1.44	0.40	19.58	0.03	0.00	99.23	66.24	2.90	30.86
384	NR	LMF	53.24	0.28	0.75	0.16	23.82	1.14	0.39	19.48	0.01	0.00	99.26	66.97	2.30	30.73
392	GBN	LMF	53.88	0.24	1.06	0.30	24.59	2.41	0.33	17.04	0.05	0.00	99.88	68.54	4.82	26.64
392	GBN	LMF	53.99	0.17	1.14	0.27	24.84	1.54	0.36	17.29	0.03	0.00	99.63	69.68	3.11	27.21
392	GBN	LMF	53.90	0.15	1.17	0.37	24.84	2.08	0.35	17.04	0.05	0.00	99.96	69.20	4.16	26.64
392	GBN	LMF	54.20	0.25	0.80	0.23	25.26	1.44	0.37	17.35	0.03	0.01	99.93	70.12	2.87	27.02
392	GBN	LMF	54.23	0.20	0.70	0.16	25.23	1.21	0.36	17.44	0.05	0.00	99.57	70.30	2.43	27.27
392	GBN	LMF	53.86	0.25	0.74	0.19	25.19	1.37	0.33	17.59	0.03	0.00	99.55	69.89	2.73	27.38
392	GBN	LMF	53.99	0.22	0.76	0.20	25.32	1.26	0.34	17.64	0.03	0.00	99.74	70.10	2.50	27.41
392	GBN	LMF	53.65	0.25	0.96	0.25	24.99	1.24	0.37	17.33	0.01	0.00	99.06	70.18	2.51	27.32
392	GBN	LMF	53.95	0.17	0.82	0.31	25.18	1.20	0.36	17.70	0.01	0.00	99.69	69.98	2.40	27.62
433	CPX	LMF	55.78	0.20	0.55	0.21	29.40	1.16	0.23	11.04	0.02	0.00	98.58	80.70	2.29	17.01
433	CPX	LMF	55.95	0.20	0.72	0.20	29.37	1.34	0.21	10.69	0.04	0.00	98.74	80.83	2.66	16.51
433	CPX	LMF	54.74	0.08	0.74	0.21	28.68	2.92	0.21	10.01	0.07	0.00	97.66	78.79	5.78	15.43
433	CPX	LMF	54.92	0.15	0.73	0.19	29.52	1.42	0.21	10.88	0.05	0.01	98.06	80.55	2.79	16.66
433	CPX	LMF	55.34	0.08	0.30	0.15	30.20	0.59	0.21	10.93	0.02	0.00	97.82	82.17	1.15	16.68
433	CPX	LMF	55.11	0.16	0.73	0.16	29.35	1.43	0.21	10.66	0.05	0.00	97.85	80.72	2.83	16.46
433	CPX	LMF	54.75	0.23	0.57	0.21	29.30	1.09	0.23	11.03	0.03	0.00	97.44	80.78	2.16	17.06
433	CPX	LMF	55.92	0.12	0.88	0.24	29.70	1.07	0.20	10.63	0.03	0.00	98.79	81.51	2.12	16.37
433	CPX	LMF	55.41	0.18	0.78	0.19	29.43	1.78	0.20	10.66	0.03	0.01	98.65	80.22	3.48	16.30
433	CPX	LMF	54.81	0.11	0.75	0.24	29.68	1.05	0.22	10.91	0.02	0.00	97.77	81.20	2.06	16.75

## Microprobe analysis of clinopyroxene

Depth	Rock type	Unit	SiO <sub>2</sub>	TiO <sub>2</sub>	Al <sub>2</sub> O <sub>3</sub>	Cr <sub>2</sub> O <sub>3</sub>	MgO	CaO	MnO	FeO	Na <sub>2</sub> O	K <sub>2</sub> O	Total	En	Wo	Fs
28	GBN	MZ	51.05	0.67	1.50	0.11	14.03	21.87	0.22	9.17	0.22	0.00	98.84	40.21	45.06	14.74
28	GBN	MZ	51.44	0.74	1.44	0.06	14.10	21.88	0.21	8.45	0.24	0.01	98.56	40.78	45.50	13.71
28	GBN	MZ	52.51	0.58	1.34	0.07	14.20	22.21	0.20	8.58	0.21	0.00	99.88	40.59	45.64	13.76
28	GBN	MZ	52.00	0.52	1.34	0.12	14.83	22.02	0.21	8.74	0.21	0.00	99.98	41.70	44.51	13.80
28	GBN	MZ	52.49	0.53	1.06	0.02	15.10	20.49	0.24	10.36	0.23	0.00	100.51	42.36	41.33	16.31
28	GBN	MZ	52.11	0.59	1.54	0.06	14.59	20.96	0.23	9.76	0.21	0.00	100.06	41.52	42.88	15.59
28	GBN	MZ	52.37	0.66	1.52	0.09	14.59	21.07	0.24	9.89	0.22	0.00	100.64	41.34	42.93	15.73
28	GBN	MZ	52.29	0.57	1.46	0.08	14.28	22.42	0.21	8.50	0.23	0.00	100.05	40.60	45.84	13.56
28	GBN	MZ	52.47	0.52	1.56	0.05	14.42	22.20	0.21	8.70	0.24	0.00	100.38	40.90	45.26	13.85
28	GBN	MZ	52.12	0.52	1.50	0.08	14.75	20.41	0.24	10.20	0.21	0.00	100.05	41.96	41.75	16.29
28	GBN	MZ	51.92	0.51	1.54	0.13	14.58	20.82	0.24	9.86	0.20	0.00	99.79	41.55	42.68	15.77
39	GBN	MZ	52.68	0.47	1.47	0.07	14.76	20.21	0.25	10.28	0.21	0.00	100.39	42.09	41.46	16.45
39	GBN	MZ	52.41	0.38	1.59	0.06	14.61	21.03	0.24	9.64	0.25	0.00	100.22	41.58	43.03	15.39
39	GBN	MZ	52.50	0.46	1.45	0.08	14.71	20.74	0.26	10.03	0.25	0.00	100.48	41.74	42.29	15.97
51	GBN	MZ	51.41	0.54	1.61	0.10	14.24	21.60	0.19	8.42	0.23	0.00	98.35	41.28	45.01	13.70
51	GBN	MZ	50.81	0.49	1.75	0.07	14.10	21.96	0.20	7.89	0.22	0.00	97.49	41.09	46.01	12.90
51	GBN	MZ	51.67	0.54	1.27	0.07	14.44	21.21	0.21	8.77	0.23	0.00	98.42	41.73	44.05	14.22
51	GBN	MZ	52.12	0.36	3.01	0.09	13.84	22.37	0.19	7.41	0.56	0.00	99.95	40.60	47.19	12.20
51	GBN	MZ	50.42	0.44	1.30	0.12	14.73	20.54	0.22	9.53	0.22	0.00	97.52	42.28	42.37	15.35
51	GBN	MZ	50.76	0.44	1.26	0.08	14.76	20.20	0.23	9.60	0.22	0.00	97.53	42.57	41.89	15.54
51	GBN	MZ	50.62	0.47	1.40	0.15	13.97	22.66	0.22	7.48	0.26	0.00	97.24	40.54	47.27	12.19
63	MA	MANO	50.32	0.45	1.38	0.06	12.89	21.82	0.22	10.03	0.21	0.00	97.37	37.69	45.86	16.46
63	MA	MANO	51.21	0.32	1.40	0.07	13.22	22.47	0.20	9.10	0.22	0.00	98.22	38.34	46.85	14.81
73	GBN	MANO	52.27	0.38	1.56	0.25	14.00	20.35	0.25	10.75	0.19	0.00	99.99	40.38	42.21	17.41
73	GBN	MANO	51.33	0.49	1.62	0.11	14.02	20.16	0.21	11.11	0.19	0.00	99.25	40.34	41.72	17.94
73	GBN	MANO	51.08	0.45	1.62	0.11	14.52	18.51	0.27	12.47	0.23	0.00	99.26	41.70	38.21	20.09
73	GBN	MANO	52.07	0.47	1.29	0.12	14.18	20.62	0.27	10.71	0.23	0.00	99.97	40.49	42.34	17.17
73	GBN	MANO	50.37	0.46	2.15	0.17	14.04	20.59	0.31	10.27	0.19	0.00	98.55	40.57	42.78	16.65
73	GBN	MANO	51.49	0.49	1.79	0.17	14.00	20.22	0.28	10.71	0.25	0.01	99.41	40.53	42.08	17.39
73	GBN	MANO	51.72	0.56	1.45	0.15	14.01	20.55	0.24	10.73	0.31	0.00	99.72	40.25	42.45	17.30
73	GBN	MANO	51.75	0.55	1.40	0.17	13.62	21.80	0.24	9.84	0.27	0.00	99.64	39.11	45.02	15.87
108	GBN	MANO	52.05	0.50	1.45	0.17	14.34	21.94	0.23	8.72	0.24	0.00	99.63	40.97	45.06	13.97
108	GBN	MANO	52.07	0.56	1.39	0.17	14.67	21.00	0.22	9.25	0.21	0.00	99.54	41.97	43.18	14.84
108	GBN	MANO	52.15	0.52	1.07	0.20	14.15	22.82	0.22	8.04	0.24	0.00	99.40	40.35	46.79	12.87
108	GBN	MANO	52.29	0.55	1.05	0.13	14.33	22.37	0.23	8.57	0.23	0.00	99.75	40.67	45.67	13.66
108	GBN	MANO	50.10	0.45	1.38	0.23	14.67	20.88	0.22	9.48	0.23	0.00	97.64	41.91	42.89	15.20
108	GBN	MANO	51.15	0.40	1.44	0.21	14.79	20.94	0.22	9.60	0.24	0.00	98.99	41.97	42.74	15.28
108	GBN	MANO	51.29	0.56	1.21	0.18	14.44	21.86	0.25	9.17	0.24	0.00	99.19	40.91	44.52	14.57
108	GBN	MANO	51.88	0.38	0.91	0.11	14.39	22.22	0.23	8.73	0.22	0.00	99.06	40.81	45.31	13.89
108	GBN	MANO	51.63	0.61	1.39	0.15	14.84	20.17	0.25	9.81	0.24	0.00	99.09	42.59	41.60	15.80
108	GBN	MANO	51.66	0.38	1.04	0.15	14.68	22.33	0.24	8.49	0.26	0.01	99.22	41.35	45.23	13.42
108	GBN	MANO	51.23	0.69	1.39	0.15	14.86	20.75	0.21	9.45	0.29	0.02	99.04	42.36	42.52	15.12
108	GBN	MANO	51.17	0.59	1.31	0.14	15.17	20.78	0.24	9.47	0.25	0.00	99.12	42.82	42.17	15.01
122	NR	MANO	51.95	0.32	1.64	0.31	15.33	21.48	0.19	6.89	0.26	0.00	98.36	44.26	44.58	11.16

Appendix 5: Microprobe data

Depth	Rock type	Unit	SiO <sub>2</sub>	TiO <sub>2</sub>	Al <sub>2</sub> O <sub>3</sub>	Cr <sub>2</sub> O <sub>3</sub>	MgO	CaO	MnO	FeO	Na <sub>2</sub> O	K <sub>2</sub> O	Total	En	Wo	Fs
122	NR	MANO	51.72	0.37	1.58	0.31	15.12	21.76	0.19	6.75	0.27	0.00	98.08	43.75	45.29	10.96
122	NR	MANO	52.14	0.51	1.57	0.34	15.70	21.13	0.19	7.08	0.29	0.01	98.97	45.02	43.58	11.40
122	NR	MANO	51.61	0.38	1.54	0.30	15.74	20.06	0.21	7.71	0.24	0.00	97.78	45.63	41.83	12.54
158	MA	MANO	51.60	0.58	1.40	0.03	12.49	20.75	0.28	12.41	0.25	0.00	99.79	36.33	43.41	20.26
158	MA	MANO	51.31	0.53	1.53	0.04	12.85	19.71	0.30	13.18	0.25	0.00	99.70	37.33	41.18	21.49
158	MA	MANO	51.88	0.45	1.47	0.14	13.41	21.52	0.26	10.74	0.23	0.01	100.11	38.41	44.32	17.26
158	MA	MANO	51.77	0.44	1.50	0.15	13.59	21.60	0.23	9.85	0.22	0.00	99.36	39.22	44.83	15.95
158	MA	MANO	51.93	0.39	1.35	0.17	13.94	22.56	0.21	8.86	0.22	0.00	99.62	39.67	46.17	14.15
185	MA	MANO	50.60	0.47	1.37	0.11	13.45	20.57	0.22	11.13	0.22	0.00	98.13	39.01	42.88	18.12
185	MA	MANO	49.97	0.51	1.40	0.10	12.98	21.65	0.23	10.17	0.23	0.00	97.24	37.89	45.44	16.67
185	MA	MANO	49.85	0.49	1.37	0.11	13.19	21.21	0.24	10.60	0.20	0.00	97.27	38.36	44.34	17.30
185	MA	MANO	49.91	0.51	1.16	0.06	13.22	20.99	0.23	10.78	0.21	0.00	97.07	38.48	43.92	17.60
185	MA	MANO	51.78	0.48	1.20	0.08	14.41	15.06	0.32	15.75	0.18	0.00	99.25	42.28	31.77	25.94
185	MA	MANO	51.53	0.54	2.01	0.03	13.55	18.72	0.22	10.90	0.32	0.00	97.81	40.91	40.63	18.47
185	MA	MANO	51.36	0.46	1.60	0.12	13.09	21.40	0.23	10.12	0.23	0.00	98.60	38.32	45.05	16.63
185	MA	MANO	50.69	0.58	1.35	0.13	13.49	19.88	0.22	11.47	0.20	0.00	98.00	39.42	41.77	18.81
191	PYX	MANO	53.15	0.20	1.01	0.48	15.71	23.21	0.16	5.19	0.31	0.01	99.43	44.49	47.26	8.25
191	PYX	MANO	53.73	0.07	0.51	0.18	15.81	24.45	0.18	4.82	0.15	0.00	99.91	43.81	48.70	7.50
191	PYX	MANO	51.37	0.39	1.96	0.73	15.26	22.58	0.16	5.87	0.30	0.02	98.65	43.87	46.67	9.46
191	PYX	MANO	52.15	0.38	2.23	0.75	15.50	21.99	0.18	6.11	0.30	0.00	99.58	44.62	45.51	9.86
191	PYX	MANO	52.88	0.32	1.58	0.48	15.44	23.54	0.18	5.41	0.22	0.00	100.06	43.62	47.81	8.57
191	PYX	MANO	52.28	0.43	1.84	0.76	16.12	21.45	0.17	6.44	0.30	0.01	99.78	45.85	43.87	10.28
191	PYX	MANO	52.58	0.41	1.97	0.78	15.90	22.11	0.17	6.35	0.32	0.00	100.59	44.96	44.96	10.08
191	PYX	MANO	52.39	0.36	1.88	0.69	15.56	22.10	0.19	6.04	0.31	0.00	99.52	44.66	45.61	9.72
191	PYX	MANO	52.73	0.38	1.94	0.71	15.76	22.27	0.19	6.28	0.30	0.00	100.56	44.66	45.36	9.98
191	PYX	MANO	52.09	0.38	2.07	0.68	15.86	21.91	0.18	6.20	0.27	0.00	99.64	45.19	44.90	9.91
232	GBN	LMF	51.34	0.26	1.92	0.70	15.46	21.75	0.20	6.78	0.29	0.00	98.69	44.30	44.80	10.90
232	GBN	LMF	51.08	0.22	1.95	0.70	15.25	21.94	0.16	6.79	0.31	0.00	98.40	43.78	45.28	10.94
232	GBN	LMF	51.96	0.37	1.50	0.74	15.54	22.21	0.18	6.59	0.26	0.00	99.34	44.13	45.36	10.51
232	GBN	LMF	51.91	0.34	1.95	0.70	15.15	22.46	0.17	6.56	0.28	0.00	99.52	43.31	46.17	10.52
232	GBN	LMF	52.83	0.21	1.95	0.62	15.96	19.21	0.17	7.09	0.26	0.00	98.30	47.28	40.93	11.79
232	GBN	LMF	50.83	0.30	1.68	0.70	15.37	21.91	0.18	7.03	0.27	0.00	98.27	43.83	44.92	11.25
268	GBN	LMF	52.40	0.37	1.65	0.55	14.95	22.73	0.17	6.67	0.25	0.01	99.74	42.66	46.65	10.69
268	GBN	LMF	51.06	0.35	2.81	0.72	15.63	19.77	0.20	7.86	0.28	0.03	98.68	45.63	41.50	12.87
268	GBN	LMF	50.02	0.28	3.16	0.46	15.97	19.42	0.19	8.28	0.25	0.01	98.03	46.19	40.38	13.44
268	GBN	LMF	51.92	0.34	1.70	0.49	15.21	21.48	0.20	7.51	0.27	0.00	99.12	43.62	44.30	12.08
268	GBN	LMF	52.62	0.36	1.59	0.45	15.27	22.19	0.20	7.35	0.28	0.00	100.31	43.20	45.13	11.67
268	GBN	LMF	51.26	0.39	1.53	0.43	15.37	21.29	0.20	7.72	0.24	0.00	98.42	43.90	43.72	12.38
268	GBN	LMF	52.18	0.31	1.49	0.47	15.08	21.81	0.18	7.43	0.28	0.00	99.24	43.17	44.90	11.94
268	GBN	LMF	52.10	0.36	1.64	0.51	14.95	21.58	0.19	7.18	0.29	0.01	98.80	43.34	44.98	11.68
295	GBN	LMF	52.44	0.28	1.80	0.52	17.09	17.09	0.22	9.96	0.23	0.00	99.62	48.88	35.14	15.99
295	GBN	LMF	52.20	0.42	1.81	0.77	14.79	21.42	0.20	7.99	0.32	0.01	99.93	42.65	44.43	12.93
295	GBN	LMF	52.19	0.33	1.77	0.72	14.86	21.84	0.22	7.88	0.31	0.00	100.13	42.47	44.89	12.64
295	GBN	LMF	52.24	0.38	1.95	0.88	14.60	21.75	0.20	7.75	0.30	0.00	100.04	42.21	45.21	12.57
295	GBN	LMF	52.05	0.46	1.79	0.80	14.75	21.74	0.21	7.80	0.31	0.00	99.91	42.43	44.97	12.60

Appendix 5: Microprobe data

Depth	Rock type	Unit	SiO <sub>2</sub>	TiO <sub>2</sub>	Al <sub>2</sub> O <sub>3</sub>	Cr <sub>2</sub> O <sub>3</sub>	MgO	CaO	MnO	FeO	Na <sub>2</sub> O	K <sub>2</sub> O	Total	En	Wo	Fs
295	GBN	LMF	52.23	0.30	1.92	0.78	14.85	21.19	0.21	8.38	0.33	0.00	100.18	42.69	43.79	13.51
295	GBN	LMF	52.33	0.25	1.83	0.78	14.79	21.47	0.21	8.11	0.33	0.00	100.10	42.52	44.39	13.09
295	GBN	LMF	52.37	0.32	1.85	0.74	14.92	21.34	0.21	8.22	0.29	0.01	100.26	42.77	44.00	13.23
300	Cr	LMF	52.37	0.30	2.09	0.54	14.97	21.18	0.22	8.41	0.29	0.00	100.37	42.89	43.61	13.51
300	Cr	LMF	51.20	0.25	2.28	0.51	16.11	20.42	0.22	8.65	0.26	0.01	99.90	45.19	41.18	13.62
300	Cr	LMF	52.17	0.27	2.08	0.90	14.71	21.33	0.22	8.32	0.33	0.00	100.32	42.37	44.18	13.45
300	Cr	LMF	52.19	0.29	2.16	0.92	14.74	21.36	0.22	8.18	0.34	0.00	100.39	42.49	44.28	13.23
300	Cr	LMF	52.20	0.31	2.11	0.91	14.84	20.99	0.24	8.12	0.31	0.00	100.02	43.04	43.75	13.22
300	Cr	LMF	52.43	0.36	1.78	0.77	15.39	20.53	0.23	8.25	0.31	0.00	100.06	44.25	42.44	13.31
300	Cr	LMF	51.75	0.33	2.03	0.97	15.14	20.54	0.25	8.32	0.33	0.00	99.65	43.79	42.70	13.51
305	NR	LMF	51.79	0.25	2.08	0.85	14.34	21.72	0.22	8.57	0.30	0.00	100.11	41.24	44.92	13.84
305	NR	LMF	51.80	0.31	2.06	0.87	14.37	21.58	0.22	8.84	0.30	0.00	100.33	41.23	44.53	14.24
305	NR	LMF	52.04	0.30	1.70	0.79	14.30	21.65	0.22	8.54	0.29	0.00	99.83	41.25	44.92	13.82
305	NR	LMF	51.77	0.25	2.06	0.79	15.59	18.24	0.22	10.87	0.22	0.01	100.01	44.80	37.67	17.53
305	NR	LMF	52.51	0.23	1.59	0.75	14.69	20.99	0.22	8.85	0.29	0.01	100.12	42.28	43.43	14.29
305	NR	LMF	52.15	0.31	1.60	0.76	14.62	21.25	0.24	8.72	0.27	0.00	99.91	42.01	43.93	14.06
305	NR	LMF	52.45	0.25	1.60	0.74	14.79	20.89	0.23	9.20	0.24	0.00	100.37	42.28	42.95	14.77
305	NR	LMF	52.15	0.31	1.88	0.88	14.49	21.22	0.24	8.88	0.28	0.00	100.33	41.72	43.93	14.35
305	NR	LMF	52.29	0.30	1.69	0.77	14.44	21.87	0.24	8.40	0.27	0.00	100.27	41.41	45.09	13.51
305	NR	LMF	52.26	0.31	1.61	0.80	15.16	19.80	0.23	9.91	0.24	0.00	100.31	43.37	40.73	15.90
315	GBN	LMF	50.95	0.41	1.82	0.86	14.60	21.63	0.19	7.41	0.33	0.00	98.19	42.56	45.33	12.12
315	GBN	LMF	51.04	0.33	2.02	0.94	14.87	21.06	0.19	7.57	0.30	0.00	98.31	43.39	44.21	12.40
315	GBN	LMF	50.68	0.36	1.37	0.76	14.78	22.02	0.16	6.87	0.29	0.00	97.30	42.89	45.93	11.18
315	GBN	LMF	51.01	0.39	1.62	0.73	15.26	20.33	0.19	7.99	0.27	0.00	97.80	44.41	42.54	13.05
315	GBN	LMF	50.65	0.30	2.04	0.90	14.71	20.91	0.22	7.81	0.32	0.00	97.87	43.11	44.05	12.84
315	GBN	LMF	49.81	0.28	1.97	0.99	14.75	20.78	0.21	7.91	0.32	0.00	97.00	43.22	43.77	13.00
315	GBN	LMF	50.84	0.35	1.94	0.90	14.62	21.05	0.20	7.83	0.29	0.00	98.02	42.82	44.32	12.86
338	CPX	LMF	52.08	0.33	2.13	0.79	14.58	20.76	0.22	8.86	0.28	0.00	100.04	42.27	43.30	14.43
338	CPX	LMF	52.16	0.31	1.85	0.69	14.82	20.05	0.26	9.58	0.26	0.00	99.97	42.82	41.65	15.53
338	CPX	LMF	52.19	0.37	1.91	0.73	14.93	20.08	0.23	9.41	0.27	0.00	100.11	43.10	41.66	15.24
338	CPX	LMF	51.97	0.40	1.98	0.76	14.27	21.79	0.22	8.41	0.29	0.00	100.09	41.18	45.20	13.62
338	CPX	LMF	52.14	0.38	1.98	0.72	14.46	21.23	0.22	8.88	0.34	0.00	100.33	41.66	43.98	14.35
338	CPX	LMF	51.88	0.39	2.19	0.65	15.44	18.10	0.26	10.69	0.29	0.00	99.88	44.81	37.77	17.42
338	CPX	LMF	51.85	0.40	2.17	0.74	14.42	21.18	0.23	8.91	0.28	0.00	100.18	41.63	43.95	14.42
338	CPX	LMF	52.32	0.29	1.64	0.61	14.19	22.01	0.25	8.67	0.35	0.00	100.33	40.67	45.38	13.95
338	CPX	LMF	52.27	0.24	1.41	0.59	14.99	20.69	0.18	8.86	0.26	0.00	99.49	43.02	42.71	14.27
338	CPX	LMF	52.03	0.33	2.25	0.84	14.29	21.63	0.20	8.37	0.31	0.01	100.26	41.38	45.03	13.59
353	NR	LMF	49.94	0.41	1.68	0.65	15.96	18.77	0.20	9.09	0.21	0.00	96.91	46.19	39.05	14.76
353	NR	LMF	50.67	0.31	1.65	0.70	14.82	21.84	0.16	7.28	0.29	0.00	97.72	42.83	45.38	11.80
353	NR	LMF	50.12	0.31	1.64	0.77	15.18	20.62	0.17	7.88	0.28	0.00	96.97	44.09	43.06	12.85
353	NR	LMF	49.14	0.27	1.84	0.66	14.91	20.74	0.17	7.98	0.30	0.00	96.01	43.47	43.48	13.06
384	NR	LMF	50.91	0.40	2.06	0.48	14.41	20.80	0.23	9.78	0.32	0.00	99.40	41.35	42.90	15.75
384	NR	LMF	50.47	0.39	1.92	0.44	14.24	21.08	0.19	9.43	0.27	0.00	98.42	41.06	43.69	15.25
384	NR	LMF	50.47	0.53	1.69	0.38	14.45	21.26	0.22	9.11	0.28	0.00	98.38	41.46	43.87	14.67
384	NR	LMF	50.87	0.47	1.71	0.38	14.31	21.57	0.22	8.86	0.29	0.00	98.66	41.13	44.58	14.30

Appendix 5: Microprobe data

Depth	Rock type	Unit	SiO <sub>2</sub>	TiO <sub>2</sub>	Al <sub>2</sub> O <sub>3</sub>	Cr <sub>2</sub> O <sub>3</sub>	MgO	CaO	MnO	FeO	Na <sub>2</sub> O	K <sub>2</sub> O	Total	En	Wo	Fs
384	NR	LMF	50.74	0.43	1.86	0.44	14.22	22.03	0.22	8.94	0.28	0.00	99.16	40.54	45.16	14.30
384	NR	LMF	50.92	0.42	1.87	0.41	14.72	19.90	0.24	10.34	0.27	0.00	99.09	42.27	41.08	16.65
384	NR	LMF	51.75	0.43	1.76	0.48	14.40	21.33	0.22	9.02	0.29	0.00	99.67	41.38	44.07	14.55
384	NR	LMF	51.68	0.43	1.77	0.42	14.32	21.24	0.22	9.25	0.31	0.00	99.64	41.18	43.90	14.92
392	GBN	LMF	51.54	0.34	2.06	0.59	14.68	20.79	0.21	8.63	0.29	0.01	99.14	42.59	43.37	14.04
392	GBN	LMF	51.60	0.37	1.90	0.58	15.44	19.58	0.26	9.45	0.29	0.00	99.47	44.33	40.44	15.23
392	GBN	LMF	51.38	0.43	1.89	0.53	14.84	20.97	0.21	8.61	0.28	0.00	99.14	42.70	43.40	13.90
392	GBN	LMF	52.03	0.50	1.82	0.51	14.75	21.80	0.20	8.13	0.27	0.01	100.03	42.16	44.80	13.04
392	GBN	LMF	51.88	0.47	1.74	0.46	14.84	21.49	0.21	8.41	0.26	0.00	99.76	42.38	44.14	13.48
392	GBN	LMF	50.95	0.50	1.92	0.60	15.41	19.38	0.23	9.30	0.33	0.00	98.62	44.58	40.32	15.10
392	GBN	LMF	51.40	0.44	1.75	0.51	16.61	17.32	0.27	10.81	0.24	0.00	99.35	47.29	35.45	17.27
392	GBN	LMF	51.25	0.46	1.87	0.51	16.12	17.74	0.24	10.50	0.25	0.00	98.94	46.38	36.68	16.94
392	GBN	LMF	51.45	0.36	1.94	0.68	15.80	18.98	0.24	8.97	0.29	0.01	98.72	45.82	39.58	14.60
433	CPX	LMF	52.22	0.31	1.40	0.36	16.61	22.11	0.12	4.58	0.35	0.00	98.05	47.35	45.32	7.33
433	CPX	LMF	52.35	0.30	1.13	0.48	16.32	22.39	0.13	4.53	0.31	0.00	97.95	46.68	46.05	7.27
433	CPX	LMF	51.44	0.32	1.28	0.52	16.84	21.81	0.12	4.62	0.33	0.00	97.27	47.95	44.66	7.38
433	CPX	LMF	53.37	0.17	0.71	0.30	16.44	23.31	0.10	3.92	0.30	0.01	98.61	46.43	47.35	6.22
433	CPX	LMF	53.37	0.15	0.55	0.29	16.36	23.95	0.09	3.87	0.30	0.00	98.94	45.76	48.16	6.08
433	CPX	LMF	53.90	0.36	0.87	0.44	16.42	22.80	0.10	4.19	0.37	0.00	99.46	46.70	46.61	6.69

## Microprobe analysis of plagioclase

Depth	Rock type	Unit	SiO <sub>2</sub>	TiO <sub>2</sub>	Al <sub>2</sub> O <sub>3</sub>	Cr <sub>2</sub> O <sub>3</sub>	MgO	CaO	MnO	FeO	N <sub>2</sub> O	K <sub>2</sub> O	Total	An
28	GBN	MZ	51.85	0.07	30.29	0.02	0.03	13.29	0.00	0.27	3.96	0.29	100.08	64.97
28	GBN	MZ	51.52	0.01	30.40	0.01	0.04	13.58	0.00	0.30	3.96	0.28	100.10	65.44
28	GBN	MZ	51.59	0.01	30.22	0.02	0.03	13.65	0.01	0.29	3.83	0.27	99.90	66.34
28	GBN	MZ	50.84	0.07	29.83	0.01	0.04	13.18	0.00	0.26	3.95	0.28	98.47	64.83
28	GBN	MZ	51.95	0.03	29.87	0.00	0.04	13.15	0.01	0.28	4.08	0.24	99.64	64.05
28	GBN	MZ	51.77	0.06	30.44	0.02	0.04	13.45	0.00	0.30	3.80	0.27	100.14	66.20
28	GBN	MZ	51.03	0.06	30.97	0.00	0.03	14.34	0.00	0.35	3.49	0.24	100.51	69.42
28	GBN	MZ	50.87	0.04	30.78	0.03	0.04	14.28	0.00	0.31	3.46	0.19	100.00	69.51
39	GBN	MZ	52.00	0.03	30.27	0.03	0.04	13.47	0.00	0.36	3.76	0.34	100.29	66.44
39	GBN	MZ	51.92	0.06	29.93	0.00	0.03	13.75	0.00	0.36	3.76	0.26	100.07	66.90
39	GBN	MZ	49.91	0.02	31.11	0.00	0.04	14.41	0.00	0.34	3.36	0.26	99.46	70.30
39	GBN	MZ	48.36	0.03	31.67	0.01	0.04	14.92	0.00	0.32	3.01	0.24	98.61	73.25
39	GBN	MZ	48.84	0.04	30.90	0.02	0.04	14.04	0.02	0.38	3.62	0.24	98.14	68.17
39	GBN	MZ	49.43	0.03	29.75	0.00	0.04	13.25	0.01	0.41	3.91	0.31	97.13	65.17
39	GBN	MZ	50.45	0.04	30.87	0.00	0.03	14.41	0.00	0.42	3.38	0.20	99.80	70.21
39	GBN	MZ	51.01	0.02	30.54	0.00	0.04	14.23	0.00	0.36	3.67	0.24	100.11	68.19
39	GBN	MZ	50.53	0.01	30.42	0.02	0.03	13.24	0.00	0.33	3.94	0.27	98.81	64.99
39	GBN	MZ	46.67	0.02	29.34	0.02	0.03	12.88	0.00	0.29	4.04	0.25	93.54	63.77
51	GBN	MZ	50.49	0.07	28.90	0.00	0.05	13.48	0.02	0.38	3.74	0.26	97.38	66.58
51	GBN	MZ	50.97	0.07	29.29	0.01	0.06	13.60	0.00	0.36	3.69	0.27	98.32	67.07
51	GBN	MZ	49.80	0.07	28.55	0.01	0.03	13.65	0.00	0.41	3.62	0.22	96.36	67.55
51	GBN	MZ	48.10	0.02	29.51	0.00	0.04	14.76	0.00	0.47	3.18	0.22	96.29	71.95
51	GBN	MZ	48.48	0.05	29.69	0.00	0.04	14.80	0.01	0.39	3.27	0.18	96.90	71.42
51	GBN	MZ	49.70	0.04	29.70	0.00	0.03	14.23	0.01	0.36	3.47	0.21	97.74	69.36
51	GBN	MZ	49.62	0.04	28.62	0.04	0.05	13.49	0.00	0.48	3.92	0.23	96.49	65.52
51	GBN	MZ	48.69	0.06	30.16	0.01	0.03	14.94	0.01	0.44	2.95	0.18	97.47	73.65
51	GBN	MZ	50.46	0.00	29.85	0.00	0.04	14.10	0.00	0.40	3.52	0.19	98.56	68.87
52	MA	MANO	51.08	0.08	30.52	0.00	0.04	14.05	0.01	0.48	3.64	0.20	100.09	68.10
52	MA	MANO	51.41	0.02	30.33	0.01	0.07	12.26	0.00	0.50	3.60	1.27	99.47	65.27
52	MA	MANO	51.12	0.04	30.20	0.00	0.04	13.99	0.00	0.45	3.66	0.23	99.72	67.90
52	MA	MANO	50.10	0.03	30.90	0.00	0.04	14.74	0.00	0.56	3.19	0.18	99.75	71.87
52	MA	MANO	51.07	0.00	30.43	0.00	0.07	14.10	0.01	0.43	3.57	0.18	99.85	68.57
52	MA	MANO	50.03	0.00	31.17	0.00	0.05	14.99	0.00	0.51	3.23	0.16	100.15	71.97
63	MA	MANO	49.27	0.04	29.92	0.01	0.05	14.55	0.01	0.52	3.19	0.20	97.76	71.59
63	MA	MANO	50.35	0.00	30.23	0.02	0.03	14.23	0.00	0.46	3.41	0.18	98.90	69.78
63	MA	MANO	50.03	0.06	29.62	0.00	0.04	14.19	0.00	0.46	3.42	0.20	98.03	69.64
73	GBN	MANO	50.05	0.02	31.58	0.04	0.03	14.92	0.00	0.45	3.04	0.20	100.32	73.09
73	GBN	MANO	52.14	0.03	30.18	0.04	0.05	13.57	0.00	0.42	3.90	0.31	100.65	65.79
73	GBN	MANO	52.88	0.02	29.99	0.00	0.07	12.61	0.00	0.54	4.19	0.54	100.85	62.45
73	GBN	MANO	51.88	0.13	29.87	0.01	0.04	13.02	0.00	0.58	3.78	0.60	99.89	65.54
73	GBN	MANO	51.80	0.04	30.72	0.00	0.02	13.67	0.00	0.41	3.73	0.23	100.63	66.94
73	GBN	MANO	51.64	0.00	30.57	0.01	0.03	13.83	0.00	0.48	3.73	0.27	100.56	67.19
73	GBN	MANO	51.14	0.02	30.19	0.01	0.05	13.92	0.00	0.45	3.49	0.28	99.55	68.81
73	GBN	MANO	51.92	0.04	29.35	0.00	0.06	12.24	0.02	0.43	3.90	1.07	99.01	63.43

Appendix 5: Microprobe data

Depth	Rock type	Unit	SiO <sub>2</sub>	TiO <sub>2</sub>	Al <sub>2</sub> O <sub>3</sub>	Cr <sub>2</sub> O <sub>3</sub>	MgO	CaO	MnO	FeO	N <sub>2</sub> O	K <sub>2</sub> O	Total	An
90	GBN	MANO	51.91	0.05	29.41	0.01	0.04	13.03	0.01	0.34	4.01	0.23	99.03	64.24
90	GBN	MANO	52.60	0.04	29.53	0.01	0.04	12.72	0.00	0.35	4.24	0.31	99.82	62.38
90	GBN	MANO	51.04	0.07	30.63	0.00	0.03	14.15	0.00	0.33	3.51	0.20	99.96	69.04
90	GBN	MANO	51.15	0.05	30.97	0.00	0.03	14.22	0.00	0.43	3.38	0.18	100.41	69.93
90	GBN	MANO	50.77	0.04	30.90	0.00	0.06	14.51	0.00	0.41	3.44	0.21	100.35	70.01
90	GBN	MANO	51.12	0.01	30.56	0.00	0.03	14.20	0.00	0.37	3.45	0.22	99.96	69.44
90	GBN	MANO	51.74	0.06	30.64	0.02	0.03	13.36	0.01	0.31	3.96	0.19	100.32	65.12
90	GBN	MANO	52.09	0.02	30.27	0.01	0.03	13.06	0.00	0.28	4.21	0.19	100.15	63.16
90	GBN	MANO	51.03	0.04	30.57	0.03	0.03	13.71	0.00	0.38	3.74	0.15	99.67	66.95
90	GBN	MANO	52.19	0.08	29.43	0.00	0.02	12.91	0.00	0.33	4.22	0.24	99.42	62.85
108	GBN	MANO	48.49	0.02	30.08	0.00	0.04	14.68	0.00	0.42	3.20	0.20	97.13	71.75
108	GBN	MANO	48.66	0.06	29.95	0.01	0.03	14.75	0.01	0.36	3.17	0.17	97.16	72.01
108	GBN	MANO	50.31	0.03	29.56	0.02	0.04	14.00	0.01	0.41	3.55	0.21	98.14	68.54
108	GBN	MANO	51.34	0.08	28.72	0.02	0.05	12.97	0.01	0.44	4.13	0.34	98.09	63.45
108	GBN	MANO	50.94	0.05	29.21	0.04	0.04	13.72	0.00	0.37	3.85	0.24	98.46	66.30
108	GBN	MANO	51.98	0.05	28.67	0.01	0.04	12.84	0.00	0.31	4.27	0.26	98.42	62.43
108	GBN	MANO	49.86	0.06	29.87	0.02	0.05	14.32	0.01	0.41	3.34	0.23	98.17	70.35
108	GBN	MANO	49.16	0.05	30.30	0.04	0.05	14.71	0.00	0.40	3.07	0.19	97.99	72.58
122	NR	MANO	49.57	0.05	29.95	0.00	0.03	14.44	0.00	0.40	3.18	0.20	97.80	71.51
122	NR	MANO	50.53	0.06	29.96	0.02	0.05	14.25	0.01	0.32	3.41	0.23	98.83	69.78
144	AN	MANO	48.79	0.06	30.95	0.03	0.04	15.39	0.00	0.49	2.65	0.17	98.57	76.21
144	AN	MANO	48.96	0.01	30.55	0.00	0.03	15.18	0.00	0.51	2.94	0.19	98.37	74.05
144	AN	MANO	49.32	0.02	30.42	0.02	0.04	14.70	0.00	0.48	3.01	0.23	98.23	72.95
144	AN	MANO	50.95	0.02	29.78	0.03	0.05	13.80	0.01	0.43	3.52	0.25	98.84	68.45
158	MA	MANO	51.89	0.08	30.12	0.00	0.02	13.57	0.00	0.53	3.87	0.26	100.34	65.94
158	MA	MANO	50.02	0.02	31.48	0.00	0.04	14.92	0.01	0.52	3.08	0.23	100.31	72.81
158	MA	MANO	51.95	0.06	30.17	0.00	0.05	13.41	0.00	0.47	3.80	0.31	100.21	66.13
158	MA	MANO	49.88	0.04	31.87	0.03	0.04	15.26	0.01	0.45	2.83	0.22	100.63	74.85
158	MA	MANO	49.85	0.01	31.28	0.04	0.06	15.05	0.00	0.53	2.92	0.22	99.95	74.05
158	MA	MANO	51.49	0.07	29.98	0.02	0.05	13.42	0.00	0.51	3.76	0.38	99.67	66.34
158	MA	MANO	49.16	0.01	31.79	0.00	0.04	15.60	0.01	0.45	2.71	0.19	99.97	76.05
158	MA	MANO	49.75	0.05	31.53	0.00	0.05	15.21	0.01	0.49	2.91	0.22	100.23	74.28
158	MA	MANO	50.00	0.06	31.06	0.00	0.06	15.12	0.00	0.55	3.03	0.20	100.08	73.42
158	MA	MANO	50.54	0.07	31.31	0.00	0.04	14.80	0.00	0.57	3.13	0.20	100.67	72.33
158	MA	MANO	49.84	0.03	31.32	0.01	0.05	14.68	0.00	0.55	3.12	0.22	99.82	72.23
158	MA	MANO	51.23	0.02	30.19	0.00	0.03	13.91	0.00	0.51	3.71	0.29	99.89	67.47
185	MA	MANO	48.44	0.03	30.53	0.00	0.05	15.41	0.00	0.46	2.80	0.18	97.89	75.28
185	MA	MANO	48.34	0.00	30.86	0.02	0.05	15.75	0.00	0.48	2.69	0.17	98.36	76.38
185	MA	MANO	49.21	0.05	29.76	0.02	0.06	14.51	0.00	0.48	3.17	0.30	97.56	71.68
185	MA	MANO	49.15	0.00	29.56	0.00	0.04	14.41	0.01	0.41	3.18	0.30	97.05	71.46
185	MA	MANO	50.02	0.00	31.41	0.00	0.04	14.86	0.00	0.41	3.10	0.17	100.01	72.59
185	MA	MANO	49.29	0.01	30.63	0.00	0.05	15.20	0.01	0.52	2.95	0.18	98.85	74.01
185	MA	MANO	49.12	0.03	31.03	0.00	0.05	15.38	0.00	0.51	2.79	0.16	99.07	75.27
185	MA	MANO	48.96	0.01	31.40	0.00	0.03	15.50	0.00	0.37	2.76	0.16	99.19	75.64
185	MA	MANO	49.38	0.03	29.60	0.03	0.03	14.56	0.00	0.44	3.30	0.20	97.57	70.92

Appendix 5: Microprobe data

Depth	Rock type	Unit	SiO <sub>2</sub>	TiO <sub>2</sub>	Al <sub>2</sub> O <sub>3</sub>	Cr <sub>2</sub> O <sub>3</sub>	MgO	CaO	MnO	FeO	Na <sub>2</sub> O	K <sub>2</sub> O	Total	An
185	MA	MANO	49.74	0.02	29.33	0.00	0.04	14.10	0.00	0.43	3.55	0.26	97.47	68.72
197	GBN	MANO	48.55	0.04	30.66	0.02	0.04	15.24	0.00	0.38	2.92	0.21	98.06	74.25
197	GBN	MANO	48.89	0.01	31.12	0.02	0.10	15.28	0.00	0.35	2.79	0.18	98.75	75.20
197	GBN	MANO	48.63	0.06	31.18	0.00	0.06	15.55	0.01	0.28	2.76	0.17	98.70	75.67
197	GBN	MANO	48.53	0.03	30.77	0.00	0.16	15.41	0.00	0.35	2.86	0.16	98.27	74.86
197	GBN	MANO	48.24	0.03	30.74	0.02	0.06	15.60	0.00	0.34	2.78	0.16	97.96	75.64
197	GBN	MANO	48.83	0.01	30.77	0.01	0.53	15.30	0.00	0.59	2.69	0.13	98.86	75.85
197	GBN	MANO	48.11	0.01	30.40	0.00	0.07	15.49	0.00	0.37	2.70	0.19	97.34	76.02
197	GBN	MANO	48.50	0.05	31.26	0.00	0.07	15.68	0.00	0.38	2.66	0.15	98.74	76.53
197	GBN	MANO	48.70	0.02	31.42	0.00	0.07	15.72	0.00	0.38	2.71	0.17	99.19	76.25
197	GBN	MANO	48.64	0.02	31.46	0.00	0.07	15.74	0.00	0.44	2.56	0.14	99.06	77.26
197	GBN	MANO	48.86	0.00	31.42	0.03	0.06	15.76	0.00	0.38	2.71	0.14	99.36	76.29
214	GBN	LMF	47.77	0.03	31.47	0.01	0.05	15.79	0.00	0.29	2.49	0.15	98.05	77.80
214	GBN	LMF	47.46	0.04	31.21	0.03	0.05	15.87	0.00	0.25	2.56	0.15	97.63	77.39
214	GBN	LMF	48.42	0.07	30.98	0.00	0.06	15.40	0.00	0.25	2.81	0.16	98.14	75.20
214	GBN	LMF	49.26	0.01	30.56	0.02	0.07	14.99	0.01	0.37	2.99	0.22	98.49	73.50
214	GBN	LMF	49.42	0.02	30.91	0.00	0.08	14.90	0.00	0.36	2.98	0.22	98.88	73.42
214	GBN	LMF	48.61	0.01	31.16	0.00	0.08	15.75	0.00	0.36	2.66	0.16	98.78	76.61
214	GBN	LMF	47.83	0.00	30.48	0.00	0.08	15.55	0.00	0.39	2.79	0.19	97.31	75.47
214	GBN	LMF	49.49	0.00	30.56	0.00	0.09	14.70	0.00	0.35	2.99	0.21	98.38	73.12
232	GBN	LMF	48.41	0.03	30.00	0.00	0.05	15.08	0.00	0.47	2.97	0.22	97.23	73.74
232	GBN	LMF	48.57	0.05	29.99	0.01	0.07	14.76	0.01	0.44	3.08	0.22	97.21	72.58
232	GBN	LMF	48.04	0.01	29.93	0.00	0.05	15.91	0.01	0.35	2.66	0.23	97.17	76.80
232	GBN	LMF	48.60	0.01	30.52	0.01	0.05	15.21	0.00	0.42	2.92	0.21	97.95	74.24
232	GBN	LMF	49.14	0.05	31.59	0.00	0.04	15.69	0.00	0.42	2.65	0.20	99.78	76.61
232	GBN	LMF	49.46	0.08	31.20	0.00	0.05	15.30	0.01	0.47	2.94	0.22	99.74	74.19
232	GBN	LMF	50.02	0.07	30.34	0.03	0.05	14.67	0.01	0.44	3.23	0.21	99.06	71.53
268	GBN	LMF	50.20	0.08	31.52	0.01	0.04	14.97	0.00	0.41	3.09	0.22	100.54	72.78
268	GBN	LMF	51.33	0.02	30.52	0.00	0.03	13.94	0.01	0.39	3.62	0.28	100.13	68.02
268	GBN	LMF	52.14	0.05	30.09	0.00	0.06	13.22	0.00	0.34	3.99	0.27	100.16	64.66
268	GBN	LMF	51.63	0.04	30.62	0.00	0.07	13.57	0.00	0.40	3.58	0.28	100.19	67.71
268	GBN	LMF	51.90	0.00	30.27	0.00	0.05	13.32	0.00	0.38	3.93	0.30	100.15	65.21
268	GBN	LMF	51.55	0.04	30.76	0.00	0.05	13.67	0.00	0.36	3.66	0.29	100.37	67.39
268	GBN	LMF	51.84	0.01	30.78	0.03	0.05	12.69	0.00	0.39	3.79	0.75	100.34	64.92
268	GBN	LMF	50.50	0.01	31.09	0.00	0.05	14.29	0.00	0.48	3.44	0.21	100.07	69.66
268	GBN	LMF	51.12	0.04	30.12	0.02	0.03	13.47	0.00	0.38	3.77	0.28	99.23	66.36
268	GBN	LMF	50.98	0.04	30.50	0.00	0.06	14.23	0.01	0.40	3.39	0.25	99.86	69.88
268	GBN	LMF	50.88	0.00	30.72	0.00	0.05	13.90	0.00	0.45	3.60	0.28	99.88	68.12
268	GBN	LMF	50.07	0.07	31.38	0.01	0.04	14.73	0.00	0.36	3.06	0.24	99.96	72.71
295	GBN	LMF	49.84	0.02	31.26	0.01	0.04	14.66	0.00	0.47	3.19	0.23	99.73	71.72
295	GBN	LMF	51.99	0.03	29.78	0.00	0.06	12.97	0.00	0.37	4.15	0.42	99.78	63.32
295	GBN	LMF	50.86	0.00	30.47	0.01	0.07	14.01	0.00	0.43	3.55	0.32	99.72	68.56
295	GBN	LMF	51.31	0.05	30.17	0.00	0.06	13.38	0.01	0.45	3.71	0.30	99.44	66.60
295	GBN	LMF	52.25	0.03	30.01	0.00	0.05	13.12	0.00	0.42	3.96	0.33	100.17	64.68
295	GBN	LMF	51.78	0.03	30.13	0.00	0.06	13.58	0.00	0.42	3.90	0.33	100.22	65.83

Appendix 5: Microprobe data

Depth	Rock type	Unit	SiO <sub>2</sub>	TiO <sub>2</sub>	Al <sub>2</sub> O <sub>3</sub>	Cr <sub>2</sub> O <sub>3</sub>	MgO	CaO	MnO	FeO	Na <sub>2</sub> O	K <sub>2</sub> O	Total	An
295	GBN	LMF	50.99	0.02	30.76	0.00	0.06	14.15	0.00	0.47	3.45	0.26	100.17	69.39
295	GBN	LMF	50.49	0.02	30.90	0.00	0.06	14.64	0.00	0.42	3.28	0.23	100.04	71.14
295	GBN	LMF	50.78	0.02	30.78	0.00	0.03	14.36	0.01	0.38	3.42	0.24	100.03	69.87
295	GBN	LMF	51.16	0.00	30.44	0.00	0.06	14.18	0.01	0.42	3.47	0.26	100.00	69.33
295	GBN	LMF	51.93	0.04	30.12	0.00	0.06	13.50	0.00	0.42	3.89	0.31	100.26	65.73
295	GBN	LMF	51.29	0.04	30.34	0.04	0.04	14.06	0.00	0.34	3.69	0.26	100.11	67.81
295	GBN	LMF	51.92	0.00	30.01	0.01	0.08	13.78	0.00	0.39	3.86	0.31	100.36	66.38
295	GBN	LMF	51.00	0.02	30.63	0.00	0.06	14.12	0.00	0.42	3.54	0.29	100.07	68.81
295	GBN	LMF	50.45	0.05	30.83	0.00	0.06	14.24	0.00	0.39	3.42	0.36	99.81	69.70
300	Cr	LMF	53.05	0.04	29.41	0.00	0.06	12.51	0.00	0.34	4.33	0.23	99.97	61.46
300	Cr	LMF	52.75	0.04	29.50	0.00	0.05	12.62	0.01	0.43	4.31	0.27	99.96	61.81
300	Cr	LMF	52.66	0.03	29.64	0.03	0.07	12.96	0.00	0.34	4.23	0.23	100.19	62.85
300	Cr	LMF	52.91	0.05	29.45	0.00	0.03	12.60	0.00	0.31	4.34	0.20	99.89	61.60
300	Cr	LMF	51.97	0.04	30.14	0.02	0.04	13.20	0.00	0.39	4.04	0.25	100.09	64.38
300	Cr	LMF	51.91	0.01	30.05	0.00	0.03	13.54	0.00	0.41	3.81	0.24	99.99	66.25
305	NR	LMF	50.69	0.04	30.52	0.00	0.05	14.51	0.00	0.45	3.46	0.21	99.94	69.86
305	NR	LMF	51.58	0.05	30.38	0.00	0.05	13.84	0.01	0.35	3.66	0.27	100.18	67.63
305	NR	LMF	51.33	0.02	30.34	0.00	0.05	13.76	0.01	0.35	3.56	0.25	99.67	68.10
305	NR	LMF	50.63	0.00	30.98	0.00	0.05	14.43	0.00	0.44	3.40	0.21	100.14	70.09
305	NR	LMF	51.46	0.05	30.34	0.00	0.05	13.85	0.00	0.44	3.76	0.24	100.20	67.06
305	NR	LMF	51.55	0.00	30.19	0.01	0.05	13.77	0.00	0.45	3.78	0.26	100.06	66.81
305	NR	LMF	52.19	0.04	30.14	0.02	0.05	13.49	0.00	0.41	3.88	0.28	100.50	65.75
305	NR	LMF	50.84	0.00	30.80	0.01	0.03	14.39	0.00	0.45	3.35	0.21	100.09	70.34
305	NR	LMF	52.03	0.04	30.42	0.00	0.06	13.64	0.01	0.47	3.81	0.26	100.74	66.40
305	NR	LMF	52.19	0.04	29.77	0.01	0.05	13.32	0.01	0.42	4.01	0.27	100.08	64.76
305	NR	LMF	51.03	0.02	30.68	0.01	0.04	14.15	0.00	0.44	3.53	0.22	100.13	68.90
305	NR	LMF	51.05	0.01	30.24	0.00	0.05	14.10	0.00	0.40	3.58	0.25	99.68	68.51
305	NR	LMF	51.85	0.02	29.83	0.00	0.06	13.56	0.02	0.42	3.82	0.27	99.85	66.25
305	NR	LMF	52.55	0.00	29.31	0.00	0.04	13.00	0.00	0.42	4.23	0.24	99.80	62.92
305	NR	LMF	51.86	0.02	29.73	0.00	0.05	13.45	0.00	0.39	3.86	0.25	99.63	65.80
315	GBN	LMF	51.95	0.04	29.65	0.00	0.03	13.54	0.00	0.35	3.85	0.27	99.68	66.05
315	GBN	LMF	51.42	0.03	28.77	0.02	0.03	13.13	0.00	0.30	3.98	0.32	98.00	64.57
338	CPX	LMF	53.22	0.02	29.31	0.03	0.03	12.46	0.00	0.27	4.30	0.37	100.01	61.57
338	CPX	LMF	52.32	0.00	29.72	0.00	0.04	13.12	0.00	0.34	4.02	0.40	99.96	64.31
338	CPX	LMF	52.05	0.02	30.04	0.01	0.05	13.44	0.00	0.35	3.76	0.30	100.01	66.38
338	CPX	LMF	53.02	0.02	29.44	0.00	0.03	12.62	0.00	0.28	4.31	0.29	100.02	61.79
338	CPX	LMF	52.19	0.03	30.05	0.03	0.05	13.21	0.00	0.34	3.99	0.31	100.21	64.65
353	NR	LMF	51.25	0.05	28.15	0.00	0.06	12.69	0.00	0.33	4.26	0.32	97.10	62.22
353	NR	LMF	52.22	0.03	28.73	0.03	0.05	12.72	0.01	0.29	4.08	0.33	98.47	63.29
353	NR	LMF	51.22	0.03	28.45	0.00	0.05	13.07	0.00	0.30	3.95	0.31	97.36	64.66
353	NR	LMF	52.18	0.03	28.29	0.01	0.04	12.66	0.00	0.24	4.29	0.32	98.07	62.00
353	NR	LMF	52.02	0.03	28.89	0.00	0.06	12.92	0.00	0.27	4.11	0.29	98.58	63.49
353	NR	LMF	51.73	0.01	29.50	0.03	0.03	13.06	0.00	0.27	4.04	0.24	98.92	64.12
353	NR	LMF	51.64	0.00	28.90	0.00	0.05	13.08	0.00	0.25	4.02	0.24	98.16	64.27
353	NR	LMF	50.72	0.05	28.69	0.03	0.05	13.08	0.00	0.27	3.98	0.29	97.16	64.51

Appendix 5: Microprobe data

Depth	Rock type	Unit	SiO <sub>2</sub>	TiO <sub>2</sub>	Al <sub>2</sub> O <sub>3</sub>	Cr <sub>2</sub> O <sub>3</sub>	MgO	CaO	MnO	FeO	Na <sub>2</sub> O	K <sub>2</sub> O	Total	An
353	NR	LMF	50.92	0.00	28.28	0.03	0.05	13.27	0.01	0.29	3.90	0.30	97.04	65.31
353	NR	LMF	49.35	0.00	29.80	0.03	0.05	14.43	0.01	0.30	3.26	0.23	97.46	70.96
353	NR	LMF	51.49	0.04	28.58	0.00	0.05	13.04	0.01	0.28	3.99	0.31	97.79	64.35
374	GBN	LMF	51.30	0.02	29.04	0.01	0.05	13.11	0.01	0.45	3.92	0.30	98.20	64.91
374	GBN	LMF	51.29	0.03	28.94	0.00	0.04	13.26	0.01	0.46	3.91	0.30	98.24	65.20
374	GBN	LMF	50.90	0.05	28.71	0.00	0.03	13.15	0.00	0.43	4.03	0.29	97.57	64.33
374	GBN	LMF	51.16	0.02	28.81	0.03	0.04	13.37	0.00	0.41	3.95	0.29	98.08	65.16
374	GBN	LMF	49.26	0.04	29.28	0.00	0.04	14.23	0.00	0.57	3.42	0.21	97.05	69.69
374	GBN	LMF	50.86	0.00	28.75	0.01	0.06	13.06	0.00	0.43	4.02	0.25	97.43	64.24
374	GBN	LMF	49.56	0.04	29.51	0.00	0.04	14.16	0.00	0.47	3.39	0.20	97.37	69.75
374	GBN	LMF	50.12	0.04	29.43	0.00	0.03	13.72	0.01	0.47	3.45	0.42	97.68	68.76
374	GBN	LMF	51.68	0.04	28.73	0.02	0.06	12.86	0.00	0.50	4.18	0.29	98.34	62.96
384	NR	LMF	50.18	0.05	30.31	0.01	0.04	14.33	0.00	0.51	3.31	0.21	98.95	70.52
384	NR	LMF	50.98	0.01	29.64	0.02	0.04	13.66	0.00	0.58	3.72	0.29	98.94	66.99
384	NR	LMF	51.09	0.04	28.92	0.00	0.04	13.45	0.01	0.55	3.95	0.29	98.33	65.30
384	NR	LMF	51.14	0.04	28.60	0.00	0.04	13.06	0.00	0.47	4.05	0.28	97.67	64.05
384	NR	LMF	51.41	0.02	28.41	0.01	0.03	12.87	0.01	0.42	4.37	0.28	97.83	61.95
384	NR	LMF	50.61	0.02	28.66	0.03	0.06	13.43	0.01	0.59	3.80	0.33	97.51	66.16
384	NR	LMF	51.59	0.04	28.94	0.00	0.05	13.21	0.00	0.56	4.00	0.30	98.69	64.60
384	NR	LMF	51.50	0.03	29.63	0.05	0.05	13.47	0.01	0.53	3.78	0.33	99.38	66.30
384	NR	LMF	51.51	0.05	29.52	0.00	0.06	13.62	0.00	0.55	3.82	0.32	99.44	66.32
392	GBN	LMF	49.61	0.01	29.72	0.00	0.05	14.66	0.00	0.46	3.26	0.28	98.04	71.34
392	GBN	LMF	49.46	0.05	29.72	0.00	0.05	14.59	0.00	0.43	3.20	0.23	97.73	71.60
392	GBN	LMF	49.36	0.05	30.16	0.00	0.04	14.68	0.00	0.49	3.18	0.23	98.19	71.86
392	GBN	LMF	49.81	0.01	30.05	0.00	0.05	14.89	0.00	0.47	3.34	0.23	98.84	71.12
392	GBN	LMF	50.07	0.00	30.26	0.00	0.04	14.60	0.00	0.54	3.23	0.25	99.00	71.45

$$En = 100 * (MgO / 40.32) / ((MgO / 40.32) + (CaO / 56.08) + (FeO / 71.85))$$

$$Fs = 100 * (FeO / 71.85) / ((MgO / 40.32) + (CaO / 56.08) + (FeO / 71.85))$$

$$Wo = 100 * (CaO / 56.08) / ((MgO / 40.32) + (CaO / 56.08) + (FeO / 71.85))$$

$$Mg\# = 100 * (MgO / 40.32) / ((MgO / 40.32) + (FeO / 71.85))$$

$$An = 100 * (CaO / 56.08) / ((CaO / 56.08) + 2 * (Na_2O / 61.98))$$